Universidad de Granada

Tesis doctoral

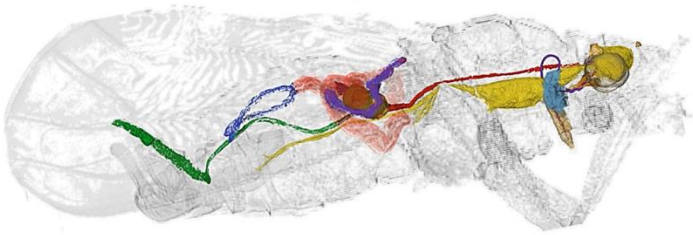

ESTUDIO MICROTOMOGRÁFICO DE LA ANATOMÍA FUNCIONAL DE DOS ESPECIES DE INSECTOS PLAGA, EL PSÍLIDO ASIÁTICO DE LOS CÍTRICOS, *Diaphorina citri* (Hemiptera, Liviidae) Y LA BROCA DEL CAFÉ, *Hypothenemus hampei* (Coleoptera, Curculionidae)

Presentada por:
Ignacio Alba Alejandre

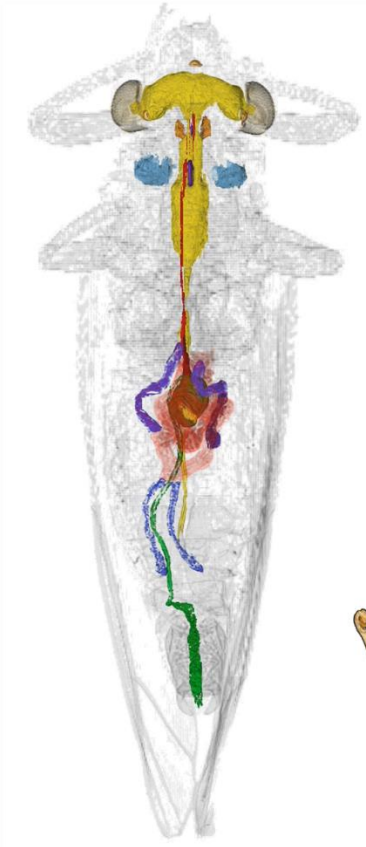

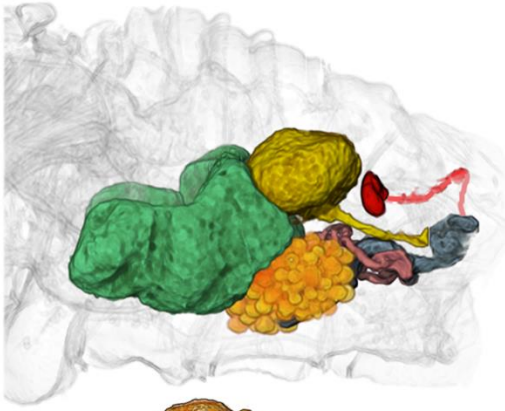

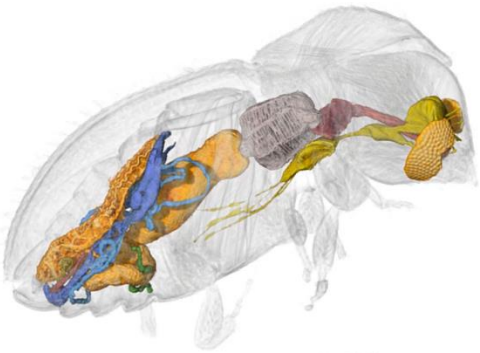

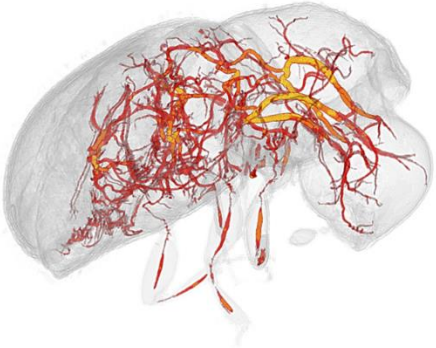

Dirigida por: Javier Alba Tercedor

Departamento de Zoología
Programa de Doctorado en Biología Fundamental y de Sistemas

2020

Editor: Universidad de Granada
Autor: Ignacio Alba-Alejandre
ISBN: 9788413067032
URI: http://hdl.handle.net/10481/65057

Esta tesis se ha subvencionado con el subproyecto-contrato S15192.01 realizado entre la "Kansas State University (KSU)" y la Universidad de Granada (UGR), como parte del proyecto "Developing an Infrastructure and Product Test Pipeline to Deliver Novel Therapies for Citrus Greening Disease". (USDA-NIFA Award 2014-70016-23028: 2015-2020) coordinado por Susan J. Brown (KSU), (www.citrusgreening.org).

This PhD thesis benefitted from a sub-award agreement S15192.01 between the Kansas State University (KSU) and the University of Granada, as part of the USDA-NIFA Award 2014-70016-23028 to Susan J. Brown (KSU), 'Developing an Infrastructure and Product Test Pipeline to Deliver Novel Therapies for Citrus Greening Disease' (2015–2020). (www.citrusgreening.org).

Como citar esta tesis/How to cite this thesis:

ALBA-ALEJANDRE, I., 2020. Estudio microtomográfico de la anatomía funcional de dos especies de insectos plaga, el psílido asiático de los cítricos, *Diaphorina citri* (Hemiptera: Liviidae) y la broca del café, *Hypothenemus hampei* (Coleoptera, Curculionidae). Tesis doctoral. Universidad de Granada. España. ISBN: 9788413067032. http://hdl.handle.net/10481/65057

ALBA-ALEJANDRE, I., 2020.- Micro-CT study of the functional anatomy of two pest insects species, the Asian citrus psyllid, *Diaphorina citri* (Hemiptera: Liviidae) and the coffee berry borer, *Hypothenemus hampei* (Coleoptera, Curculionidae). Doctoral thesis. University of Granada. Spain. . ISBN: 9788413067032. http://hdl.handle.net/10481/65057

- Impresa/Printed Noviembre/November 2020 -

Universidad de Granada
Tesis doctoral

ESTUDIO MICROTOMOGRÁFICO DE LA ANATOMÍA FUNCIONAL DE DOS ESPECIES DE INSECTOS PLAGA, EL PSÍLIDO ASIÁTICO DE LOS CÍTRICOS, *Diaphorina citri* (Hemiptera, Liviidae) Y LA BROCA DEL CAFÉ, *Hypothenemus hampei* (Coleoptera, Curculionidae)

Presentada por:
Ignacio Alba Alejandre

Dirigida por: Javier Alba Tercedor

Departamento de Zoología
Programa de Doctorado en Biología Fundamental y de Sistemas

2020

A mis padres, a Miriam y Diana

AGRADECIMIENTOS

A mi madre por conseguir saber cuándo estaba estresado de más y hacer lo posible para paliarlo. Dicen que madre no hay más que una, pero yo tengo la suerte de tener una madre excepcional.

A mi mujer Miriam y mi pequeña Diana, siento las horas que no os he podido dedicar por tener que dedicarlas a mirar "bichos" pero prometo poder dedicaros el tiempo que os merecéis a partir de ahora.

Quiero agradecer a mi padre, amigo, jefe y director de tesis, su ayuda, ánimos y apoyo incondicional durante todo el desarrollo de esta tesis, pero al mismo tiempo exigirme para poder dar lo mejor de mí y sin el cual, literalmente, no estaría aquí.

A los profesores Felipe Pascual Torres (mi tutor académico) y a José Manuel Tierno de Figueroa su paciencia respondiendo a mis dudas, preguntas y demás cuestiones académico-burocráticas.

A Wayne Hunter (USDA, Fort Pierce, Florida., USA) y Fernando Vega (USDA, Beltsville, Maryland, USA), que nos involucraron en el estudio del psílido asiático de los cítricos y la broca del café, respectivamente. A Xavier Bellés (Inst. de Biología Evolutiva, CSIC, UPF) por su inestimable ayuda identificando la especie no descrita de *Ptinus* s. str. (Ptinidae). *A José Maria Gil Sánchez por su ayuda en el análisis estadístico del estudio de la broca del café dentro de la baya*.

Gracias a mis amigos Sergio, Fergu, Milín y Jesús por ayudarme a desconectar cuando lo he necesitado. Una vez que la situación se normalice en este extraño año que nos ha tocado vivir, queda pendiente una celebración como Dios manda, sin tanta distancia de seguridad y con una copa en las manos.

A los "compis" del laboratorio: Ángel (futuro campeón de España de bici) por la buena energía que transmite, siempre con una sonrisa en los labios y Guillermo y nuestras charlas frikis sobre videojuegos.

A Antonio Romero Sanchiz, persona endiabladamente inteligente y enérgica, sé que te habría encantado poder asistir a la lectura de la tesis. Allá donde estés, que sepas que parte de esta tesis es gracias a ti.

A las mil personas más que seguro me olvido, si eres uno de ellos, mil gracias de corazón, no es que no os agradezca vuestra ayuda, es solo mi mala cabeza.

Tabla de contenidos

1.- RESUMEN / ABSTRACT

1.1.- RESUMEN

Tradicionalmente, el estudio de la anatomía interna en los insectos, se ha basado en técnicas de disección con las limitaciones propias de la misma. La microtomografía computarizada (micro-CT), es una técnica relativamente nueva que se basa en la obtención de imágenes de rayos X que tras ser procesadas permite reconstruir la anatomía externa e interna y del espécimen. Así como separar con diferente color las estructuras. Pudiendo observarlas en su posición anatómica desde cualquier perspectiva y sin necesidad de realizar disecciones y por tanto sin las deformaciones y destrucción que estas implican. Todo ello ha abierto un abanico de posibilidades inimaginables antes, e imposibles, con los métodos clásicos de disección y/o con las técnicas de microscopia.

El objetivo principal de esta tesis doctoral ha sido realizar un estudio microtomográfico detallado (con imágenes 3D de alta resolución y vídeos) de la anatomía externa e interna de dos especies de insectos plaga: el psílido asiático de los cítricos (*Diaphorina citri* Kuwayama, 1908) y la broca del café (*Hypothenemus hampei* Ferrari, 1867), de gran importancia a nivel mundial por los enormes daños y pérdidas económicas que provocan. Adicionalmente, durante la realización del estudio de la actividad de *H. hampei* en el interior de la cereza del café, encontramos especímenes del gorgojo del grano de café (*Araecerus fasciculatus* De Geer en 1775) emergiendo de las cerezas del café, este descubrimiento motivó un estudio del mismo y su actividad dentro de la cereza del café, que fue objeto de una publicación adicional al respecto y que se incluye como material adicional.

Los resultados aquí obtenidos, junto con los del trabajo previo (Alba-Tercedor & Alba-Alejandre, 2019) (en que realizamos un estudio microtomográfico de la abeja de la miel y comparamos los resultados con la publicación clásica de Snodgrass (Snodgrass, 1910) sobre la anatomía de la especie), confirman que las técnicas de micro-CT constituyen una excelente alternativa a los métodos tradicionales basados en la disección. Al ser una técnica no destructiva que permite observar las estructuras (externas e internas) en su posición anatómica real, desde cualquier perspectiva, tantas veces como se requiera, sin riesgo de deformarlas o romperlas, y sin los inconvenientes de

las deformaciones producidas durante las manipulaciones que requiere la disección. Asimismo, durante el estudio microtomográfico de ambas especies se ha podido completar detalles de estructuras ya descritas por otros autores y al mismo tiempo se han descubierto otras que nunca habían sido descritas, y que de no ser por la micro-CT difícilmente podrían haberse puesto de manifiesto. Los resultados obtenidos, en su mayor parte ya publicados, de una forma resumida han sido los siguientes:

1.1.1.- El psílido asiático de los cítricos (*Diaphorina citri*)

1.1.1.1.- Anatomía externa:

- La cabeza (con descripción detallada de las estructuras, incluidos el aparato bucal, ojos, antenas).
- El tórax (morfología de los diferentes segmentos, patas, escleritos, distribución de los espiráculos, y las alas).
- El abdomen (segmentos, distribución de los espiráculos, y terminalia de ambos sexos).

1.1.1.2.- Anatomía interna:

- Digestivo (faringe, esófago, cámara filtradora, intestino medio, e intestino posterior y ano).
- Sistema excretor (las estructuras tubulares, apéndices, del intestino medio, consideradas clásicamente como túbulos de Malpigio, se describen y comparan con otras de otros insectos)
- Estructuras internas de la cámara cibarial (bomba precibarial -salivar-, bomba cibarial, conos maxilares y mandibulares y los músculos asociados).
- Disposición de los estiletes.
- Glándulas (salivares, coxales y antenales). Las glándulas coxales y antenales se describen y citan por vez primera en Psylloidea, discutiéndose su posible función como productoras de feromonas sexuales.

- Sistema traqueal (espiráculos, y disposición de los tubos traqueales abdominales).
- Sistema circulatorio (vaso dorsal, aorta y músculos aliformes).
- Sistema nervioso (cerebro, cadena nerviosa ganglionar ventral y nervios). Se describen por vez primera en Psylloidea la existencia de diferencias sexuales en la conformación del cerebro y ganglios de la cadena nerviosa ventral.
- Sistema reproductor masculino (testículos, vesículas seminales, glándulas accesorias, bomba espermática, conductos de conexión y edeago).
- Sistema reproductor femenino (ovarios, glándulas accesorias, espermateca, glándula coleterial (=cementante), conductos de conexión y el ovipositor). La anatomía funcional de la espermateca se describe y analiza por primera vez en Psylloidea.
- Bacterioma (situación, organización externa e interna). Siendo la primera reconstrucción tridimensional del mismo.
- Diferentes detalles de la musculatura.

1.1.1.3.- Aspectos anatómico-morfológicos y funcionales derivados de la alimentación picadora-chupadora:

- Estructuras implicadas.
- Punto de perforación.
- Los estiletes dentro de los vasos de la planta.
- Vainas salivares.

1.1.2.- La broca del café (*Hypothenemus hampei*)

1.1.2.1.- Estudio de la actividad vital de *H. hampei* en el interior de la baya del café

Se observó, un patrón comportamental en el que la hembra se coloca con el abdomen dirigido al exterior, taponando la entrada de los túneles. Asimismo, la construcción de túneles presenta un trazado en zig-zag que dificulta la penetración de posibles parasitoides. Por otro lado el aprovechamiento de los recursos alimenticios de la cereza del café se maximiza gracias a la secuencia constructora de los túneles y cámaras de oviposición. Que de forma secuencial comienza en la periferia semilla y se mueve hacia el interior.

1.1.2.2.- Anatomía externa:

- La cabeza (estructuras y diferencias sexuales en número y disposición de omatidios).
- El tórax (diferentes segmentos, espiráculos respiratorios y primera observación sobre las diferencias sexuales en la morfología del pronoto).
- El abdomen (espiráculos respiratorios, y diferencias sexuales en el número de segmentos).

1.1.2.3.- Anatomía interna:

- Aparato digestivo (esófago, buche, proventrículo, intestino medio (ventrículo), intestino posterior, ciegos gástricos, ampolla rectal y ano. Se describen por primera vez diferencias sexuales en la conformación y número de circunvoluciones del intestino medio).
- Sistema excretor (número y disposición de los túbulos de Malpigio).
- Sistema reproductor masculino (testículos, glándulas accesorias, vesículas seminales, bomba espermática, conducto eyaculador y primera descripción del edeago).

- Sistema reproductor femenino: ovarios, oviductos laterales, glándula accesoria, espermateca, glándula espermática, oviducto común y gonoporo.
- Sistema respiratorio (con un detallado estudio de los espiráculos respiratorios; se describen por vez primera, en detalle, los sistemas de filtración que presentan, y se reconstruye por vez primera todo el sistema de tubos traqueales, nombrándose las diferentes ramas, algunas nunca antes descritas. Habiéndose calculado la longitud total de tubos y estudiado la distribución por tamaños de la luz interna.
- Aparato circulatorio (vaso dorsal y aorta).
- Sistema nervioso (cerebro, ganglios de la cadena nerviosa ventral y nervios). Se describen por vez primera diferencias sexuales en el tamaño y conformación del cerebro.

La musculatura. Señalando por vez primera una reducción de los músculos implicados en el vuelo en los machos.

1.1.3.- El gorgojo del grano de café (*Araecerus fasciculatus*)

La especie fue descrita en 1775 como *Curculio fasciculatus*, y es la primera vez en los dos siglos y medio transcurridos en que gracias a las modernas técnicas de microtomografía se ha podido "congelar" la actividad del insecto en el interior de una baya de café y estudiarla en detalle. Este estudio ha revelado aspectos interesantes de la biología del gorgojo del café dentro de la baya del café. Habiéndose reconstruido larvas de 5º estadio y hembras dentro de la cereza del café.

Además, durante el estudio se descubrió un ejemplar macho de una especie no descrita de coleóptero de la familia Ptinidae (*Ptinus* s.tr. sp.)

1.2.- ABSTRACT

Traditionally, the study of the internal anatomy of insects has been based on dissection techniques with their own limitations. The computerized microtomography (micro-CT), is a relatively new technique that is based on obtaining X-ray images that after being processed allows to reconstruct the external and internal anatomy and the specimen, as well as to separate with different color the structures. Being able to observe them in their anatomical position from any perspective and without the need for dissections and therefore without the deformations and destruction that these imply. All this has opened up a range of possibilities previously unimaginable, and impossible, with the classic methods of dissection and/or microscopy techniques.

The main objective of this doctoral thesis has been to carry out a detailed microtomographic study (with high resolution 3D images and videos,) of the external and internal anatomy of two species of insect pests: the Asian citrus psyllid (*Diaphorina citri* Kuwayama, 1908) and the coffee berry borer (*Hypothenemus hampei* Ferrari, 1867), of great importance worldwide due to the enormous damage and economic losses they cause. Additionally, during the study of *H. hampei's* activity within the coffee cherry, we found specimens of the coffee bean weevil (*Araecerus fasciculatus* De Geer in 1775) emerging from coffee cherries. This discovery motivated a study of the bean weevil and its activity within the coffee berry, which was the object of an additional publication on the subject and which is included as additional material.

The results obtained here, together with those of our previous work(Alba-Tercedor & Alba-Alejandre, 2019) (in which we carried out a microtomographic study of the honey bee and compared the results with the classic publication of Snodgrass (Snodgrass, 1910) on the anatomy of the species), confirm that the micro-CT techniques constitute an excellent alternative to the traditional methods based on dissection. As it is a non-destructive technique that allows to observe the structures (external and internal) in their real anatomical position, from any perspective, as many times as required, without the risk of deforming or breaking them. And without the inconvenience of the deformations produced during the manipulations required for dissection. Likewise, during the microtomographic study of both species it has been possible to corroborate structures already

described by other authors and at the same time others have been discovered, never described before, which if it were not for the micro-CT could hardly have been made evident. The results obtained, for the most part already published, in a summarized form, have been the following:

1.2.1.- The Asian Citrus Psyllid (*Diaphorina citri)*

1.2.1.1.- External anatomy:

- The head (with detailed description of the structures, including the mouth, eyes, antennae).
- The thorax (morphology of the different segments, legs, sclerites, distribution of the spiracles, and the wings).
- The abdomen (segments, distribution of the spiracles, and terminalia of both sexes).

1.2.1.2.- Internal anatomy:

- Digestive (pharynx, esophagus, filtering chamber, midgut, hindgut and anus).
- Excretory system (the tubular structures, appendages, of the middle intestine, classically considered as Malpighian tubules, are described and compared with other ones in insects)
- Internal structures of the cybarial chamber (precibarial -salivary - pump, cybarial pump, maxillary and mandibular cones and associated muscles).
- Disposition of the stylets bundle.
- Glands (salivary, coxal and antennal). The coxal and antenal glands are described and cited for the first time in Pylloidea, discussing their possible function as producers of sex pheromones.
- Tracheal system (spiracles, and arrangement of abdominal tracheal tubes).
- Circulatory system (dorsal vessel, aorta and alary muscles).

- Nervous system (brain, ventral ganglion cord and nerves). For the first time in Psylloidea, the existence of sexual differences in the conformation of the brain and ventral nerve chain nodes is described
- Male reproductive system (testicles, seminal vesicles, accessory glands, sperm pump, connecting tubes and aedeagus).
- Female reproductive system (ovaries, accessory glands, spermatheca, colleterial (=cement) gland connecting ducts and ovipositor). The functional anatomy of the sperm pump is described and analyzed for the first time in Psylloidea.
- Bacteriome (location, and external and internal organization). Being the first three-dimensional reconstruction of this organ.
- Different details of the Musculature.

1.2.1.3.- Anatomical-morphological and functional aspects derived from the piercing-sucker feeding:

- Structures involved.
- Penetration point.
- Stylets bundle into the plant vessels
- Salivary sheaths.

1.2.2.- The coffee berry borer (*Hypothenemus hampei*)

1.2.2.1.- Study of the vital activity of *H. hampei* inside the coffee berry

It was observed a behavioral pattern in which the female is placed with the abdomen directed to the outside, blocking the entrance of the tunnels. Likewise, the construction of tunnels presents a zig-zag pattern that difficult the penetration of possible parasitoids. On the other hand, the use of the food resources of the coffee cherry is maximized thanks to the construction sequence of the tunnels and oviposition

chambers (beginning in the seed periphery and moving towards the interior).

1.2.2.2.- External anatomy:

- The Head (structures and sexual differences in number and disposition of ommatidia).
- The Thorax (different segments, respiratory spiracles and first observation on sexual differences in the morphology of the pronotum).
- The Abdomen (respiratory spiracles, and sexual differences in the number of segments).

1.2.2.3.- Internal anatomy:

- Digestive system (esophagus, crop, proventricle, midgut, hindgut, gastric ceca, rectal ampulla and anus. For the first time, sexual differences in the conformation and number of circumvolutions of the midgut are described).
- Excretory system (number and disposition of the Malpigian tubules).
- Male reproductive system (testicles, accessory glands, seminal vesicles, spermatic pump, ejaculatory duct and first description of the aedeagus)
- Female reproductive system (ovaries, lateral oviducts, accessory gland, spermatheca, spermatic gland, common oviduct and gonopore).
- Respiratory system (with a detailed study of the respiratory spiracles; for the first time the filtration systems are described in detail, and the entire system of tracheal tubes is reconstructed in Psylloidea for the first time, the different branches are named, introducing new terms for some which have never had been described. Moreover, the total length of tubes has been calculated and the distribution size of the internal lumen of tubes is analyzed.
- Circulatory system (dorsal vessel and aorta).

- Nervous system (brain, ventral ganglion cord, and nerves). Sexual differences in the size and shape of the brain are described for the first time.
- The musculature. Pointing for the first time the reduction of the muscles involved in flight in males.

1.2.3.- The coffee bean weevil (*Araecerus fasciculatus*)

The species was described in 1775 as *Curculio fasciculatus*, and it is the first time in the two and a half centuries that thanks to modern microtomography techniques it has been possible to "freeze" the activity of the insect inside a coffee berry and study it in detail. This study has revealed interesting aspects of the biology of the bark beetle inside the coffee berry. Having reconstructed 5th instar larvae and females inside the coffee berry.

In addition, during the study a male specimen of an undescribed species of beetles of the family Ptinidae (*Ptinus* s.tr. sp.) was discovered.

2.- INTRODUCCIÓN

2.1.- Organización de esta memoria

Dado que la presente tesis se defiende por la modalidad de recopilación de trabajos ya publicados en revistas recogidas en el “Journal of Citation Reports” (JCR), hemos seguido la normativa de la Escuela de Postgrado de la Universidad de Granada que textualmente dice: “no debe utilizar el pdf generado por la revista dado que podría resultar en violación de derechos de copyright. En su lugar debe utilizar el manuscrito enviado a la revista (puede distribuir las figuras y tablas a lo largo del texto)”. Por tanto, en el apartado de “Resultados y Discusión” se incluyen los textos, las referencias, y las figuras correspondientes en el orden en que aparecen en los artículos. De tal modo que la numeración de las figuras se ha mantenido, y, por tanto, ésta no es correlativa desde el comienzo de la memoria, sino que en cada apartado (correspondiente a una publicación) las figuras (y tablas en su caso) se numeran comenzando por el número uno, y así sucesivamente, hasta el comienzo de un nuevo apartado (una nueva publicación) en que se comienza nuevamente con el número uno.

Por ello, la introducción, material y métodos, resultados, discusión y bibliografía, son específicas para cada una de las publicaciones que en conjunto agrupamos bajo la sección de Resultados y Discusión de esta memoria de tesis. Del mismo modo, siguiendo las exigencias específicas de la Comisión Académica del programa de doctorado hemos incluido un apartado de Discusión General en castellano que recoge los aspectos más relevantes, discutidos en los capítulos anteriores.

2.2.- La microtomografía computarizada

La microtomografía computarizada (también denominada micro-CT o μCT) es una técnica relativamente nueva, cuyo origen se remonta a 1972 cuando el ingeniero electrónico inglés Godfrey Newbold Hounsfield (1919-2004) inventó la primera máquina de tomografía computarizada o TC, invento que le valió junto al físico Allan McLeod Cormack (1924-1998), que había presentado entre 1964 y 1965 la base matemática para la reconstrucción de imágenes de TC, el Premio Nobel de Fisiología o Medicina en 1979. Actualmente, como homenaje a

Hounsfield, para medir la radiodensidad de la TC, se utilizan las denominadas unidades Hounsfield, que van desde -1000 hasta +1000, siendo -1000 el aire (muy baja densidad, se ve de color negro), cero el agua (densidad media, se ve de color gris) y +1000 el hueso (alta densidad, se ve de color blanco). En cualquier caso, no sería hasta 1994 cuando aparece el primer escáner comercial micro-CT, el cual se usaba para el estudio de los huesos.

La micro-CT es básicamente en una imagen de rayos X en 3D y utiliza el mismo método utilizado en la tomografía computarizada en medicina pero a pequeña escala con una resolución enormemente aumentada, de manera que, si bien en la TC se trabaja en resoluciones de milímetros, en micro-CT, se obtienen resoluciones de alrededor de 0,5 µm. Los nuevos nano-CT están aumentando considerablemente la resolución y posibilidades de esta tecnología. La micro-CT representa fundamentalmente la microscopía 3D, donde la estructura interna de objetos a escala muy pequeña se captura de manera no destructiva. No se requiere realizar cortes finos, ni un tratamiento complejo previo: un solo escaneo genera una imagen de la estructura 3D interna completa de la muestra en alta resolución, dejando la muestra intacta para posteriores tratamientos.

El funcionamiento consiste en una fuente de rayos X con microenfoque que ilumina el objeto y un detector de rayos X plano que recoge imágenes de proyección ampliadas. Basado en cientos de vistas angulares adquiridas mientras el objeto gira, un ordenador sintetiza un conjunto de cortes de sección transversal virtual a través de la muestra. Posteriormente es posible desplazarse por las secciones transversales, interpolando secciones a lo largo de los diferentes planos, para inspeccionar la estructura interna deseada. La reconstrucción volumétrica (*volume rendering*, en inglés) permite la visualización tridimensional de la muestra, la cual está formada por voxels (unidad cúbica que compone un objeto tridimensional, equivalente al pixel en un objeto bidimensional). La micro-CT permite medir parámetros morfométricos 3D e incluso crear modelos visuales realistas que permiten hacer viajes virtuales al interior de la muestra, así como modelos que se pueden visualizar en dispositivos móviles (teléfonos inteligentes y tabletas) que resultan de gran utilidad en investigación y como ayudas docentes.

2.3.- El psílido asiático de los cítricos (*Diaphorina citri*, Hemiptera, Liviidae)

2.3.1.- *Un poco de historia*

Diaphorina citri, fue descubierto en Shinchiku (Taiwan) en 1907 (Kuwayama, 1907) y en la actualidad posee una enorme importancia a nivel mundial por ser un vector de una enfermedad que afecta a los cítricos denominada "Huanglonbing" (HLB, palabra china que significa literalmente enfermedad del dragón amarillo) también llamada enfermedad de enverdecimiento de los cítricos o "citrus greening disease" en inglés. Desde 1995 se propuso que el nombre oficial de la enfermedad fuese huanglongbing (HLB), en homenaje a Lin Kung Hsiang quien le dio ese nombre tras hacer un estudio sistemático de la enfermedad en China desde 1941-1955, donde inicialmente, en 1919, no se le daba demasiada importancia, se pensaba que eran unos síntomas producidos por falta de agua o nutrientes y se le llamaba enfermedad de los brotes amarillos pero que en 1936 se había extendido convirtiéndose en un grave problema. Lin tras llevar a cabo diferentes experimentos comprobó que se trataba una enfermedad infecciosa ya que los árboles sanos se infectaban al hacerle injertos de árboles enfermos, pero al mismo tiempo asumió que existía la transmisión a través de un vector al infectarse árboles que no había injertado.

En 1928 se observó una enfermedad parecida a HLB en Transvaal, Sudáfrica, que denominaban "brotes amarillos" si bien su naturaleza era aún desconocida no siendo hasta 1965 cuando se demostró que era una enfermedad trasmisible tanto por inoculación por injerto (McClean & Oberholzer, 1965a) como a través del vector *Trioza erytreae* o psílido africano de los cítricos (McClean & Oberholzer, 1965b). En 1967 Filipinas demostró, que la HLB, la enfermedad que denominaban "hoja moteada" y que inicialmente se pensó que era debida a falta de zinc, era una enfermedad que podía ser transmitida por el psílido asiático de los cítricos, *D. citri* (Martínez & Wallace, 1967)

En 1970, la microscopía electrónica de unas hojas de naranjas infectadas en Sudáfrica permitió la identificación y confirmación de las bacterias responsables del HLB (Laflèche & Bové, 1970) si bien en ese momento se creía que eran micoplasma. Organismos similares se vieron por microscopía electrónica en

hojas de la India, Taiwán y Filipinas. En 1984 quedó finalmente demostrado que no era una micoplasma sino una bacteria Gram negativa (Garnier & Bove, 1984a, b).

Toda esta labor de investigación a lo largo de los años, ha permitido que en la actualidad se conozca que la enfermedad HLB, es una enfermedad que afecta a los cítricos (limones, limas, naranjas, pomelos, mandarinas y kumquats), que se transmite cuando los vectores (*D. citri* o *T. erytreae)* que están infectados se alimentan del floema de las hojas y al hacerlo inoculan una α-proteobacteria Gram negativa no cultivable en laboratorio y limitada al floema, del género *Candidatus* Liberibacter spp. de la que actualmente se conocen 3 especies responsables de HLB: *Candidatus* Liberibacter asiaticus (CLas, que afecta a países asiáticos y también a Brasil y EEUU, Florida fundamentalmente), *Candidatus* Liberibacter americanus (CLam, presente de momento únicamente en Brasil) y *Candidatus* Liberibacter africanus (CLaf, presente en países africanos).

D. citri transmite CLas y CLam mientras que *T. erytreae* transmite CLaf. Si bien esta tesis se centra en el psílido asiático de los cítricos, *D. citri*, es necesario señalar que el psílido africano de los cítricos, *Trioza erytreae*, se detectó en España en las Islas Canarias en 2002 en Tenerife, La Palma y La Gomera, actualmente está presente en todas las islas del archipiélago menos en Fuerteventura. En la España peninsular se encuentra en Galicia (Pérez-Otero *et al.*, 2015), principalmente en las provincias de Pontevedra y La Coruña, y en áreas restringidas de Lugo y Orense. Por el momento, España está libre de HLB al no estar presente ninguna de las tres especies de la bacteria *Candidatus* Liberibacter spp. causantes del HLB ni el insecto vector *Diaphorina citri*.

2.3.2.- ***Importancia y distribución***

El Huanglonbing (HLB) está considerada, a nivel mundial, como la enfermedad de los cítricos más devastadora (Bové, 2006; Brlansky & Rogers, 2007; Farnsworth *et al.*, 2014). La enfermedad se encuentra en más de 40 países diferentes en Asia, Oceanía, Norteamérica y Sudamérica (Halbert & Manjunath, 2004; Shen *et al.*, 2013). Los 5 principales productores de cítricos a nivel mundial, ordenados del primero al quinto (España es el sexto): Brasil, China,

Estados Unidos, México e India, están especialmente amenazados por el HLB. Sólo en Florida se estima que el HLB supone un coste anual de alrededor de 1000 millones de dólares y unas pérdidas de entre 5000-8000 empleos al año (Farnsworth *et al.*, 2014)

A continuación, se muestran unos mapas de distribución mundial del vector *D. citri* y de los patógenos CLas y CLam, indicando en color naranja la distribución de cada uno (modificado a partir de www.cabi.org).

Distribución mundial del psílido asiático de los cítricos

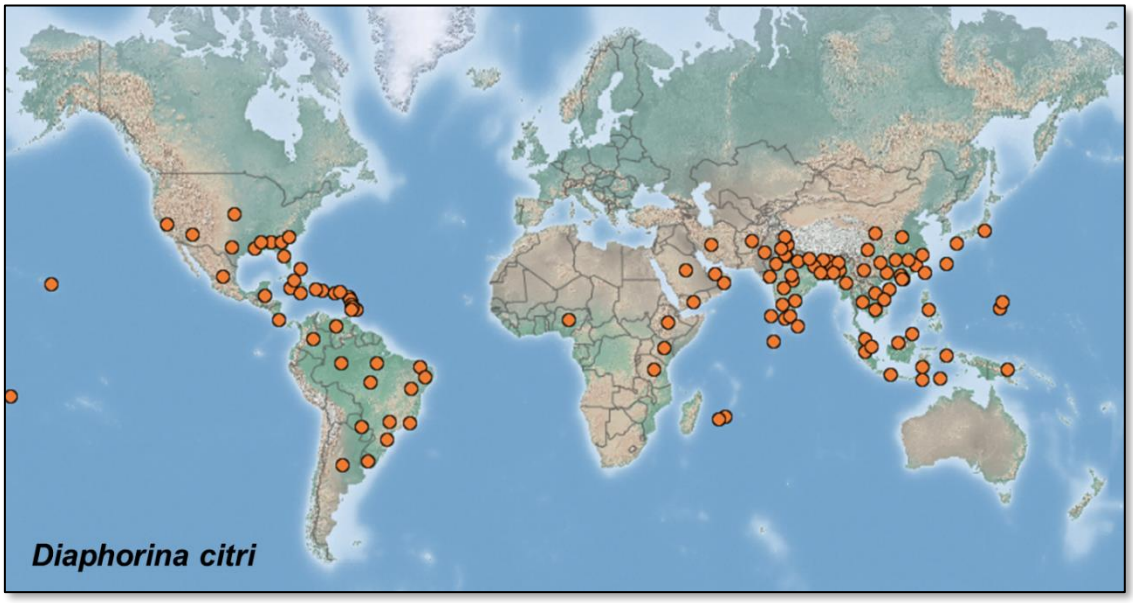

Distribución mundial de las bacterias que transmite *D.* citri y que causan la enfermedad "Huanglongbing" a los cítricos

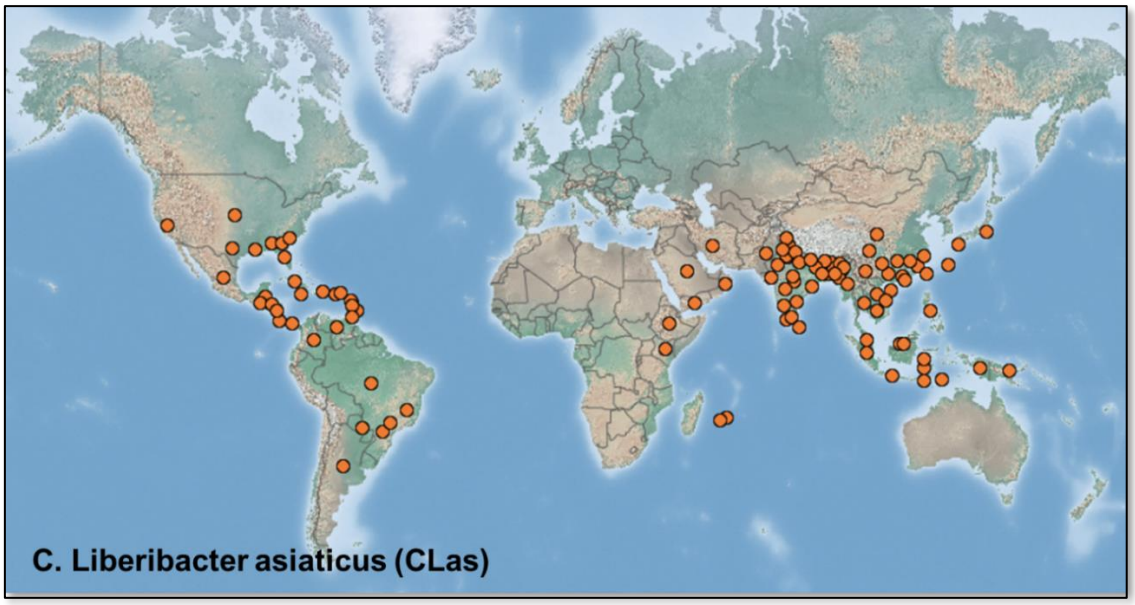

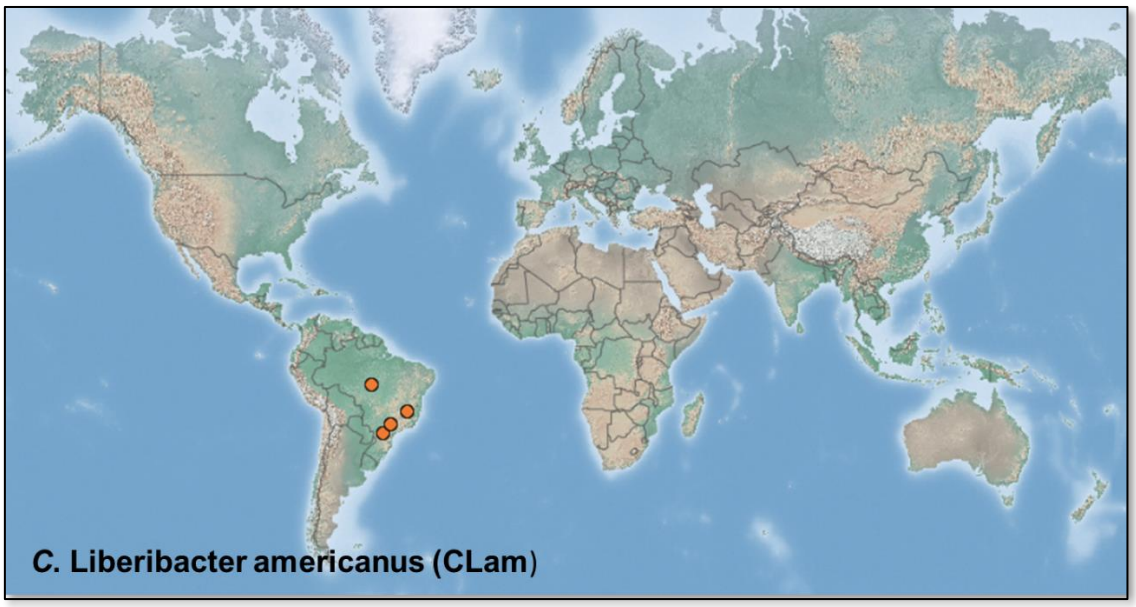

2.3.3.- *Ciclo de vida del psílido asiático de los cítricos*

El ciclo de vida completo de *D. citri* requiere de entre 15 a 47 días, dependiendo de las condiciones ambientales. Las hembras depositan los huevos en las puntas de los brotes en crecimiento o entre las hojas desplegadas de los cítricos, pudiendo poner cerca de 800 huevos durante su vida a una temperatura de 28ºC. El patógeno *Candidatus* Liberibacter spp. es transmitido a *D. citri* al alimentarse este de cítricos infectados durante el estado de ninfa (*D. citri* posee 5 estadíos ninfales) donde tras la ingesta, el patógeno aumenta su concentración entre 25-360 veces lo que permite que cuando de adulto se alimente de otros cítricos los infecte transmitiendo el patógeno, de lo contrario, si no es hasta la etapa adulta cuando *D. citri* se alimenta de una planta infectada, la concentración apenas aumenta lo que se traduce en que no es capaz de trasmitirlo (Inoue *et al.*, 2009). Un reciente estudio demuestra que el desarrollo de varias generaciones alimentándose de cítricos infectados, aumenta el % de adultos infectados del 42% al 100% en la cuarta generación aumentando también la población bacteriana entre generaciones (de Souza Pacheco *et al.*, 2020)

La vida media de los adultos es inversamente proporcional a la temperatura, siempre que esta no baje de los 15ºC, pudiendo variar desde 117 días a 51 días a 15 y 31ºC respectivamente, si bien la temperatura óptima de crecimiento es de 25-28ºC (Liu & Tsai, 2000). Las hembras adultas son más grandes que los machos siendo la longitud media de 3,3 mm y 2,7 mm respectivamente. Al año se producen de nueve a diez generaciones; aunque han llegado a observarse hasta 16 generaciones en condiciones experimentales.

2.3.4.- *Monitorización de la enfermedad HLB*

Se están utilizando técnicas moleculares como la PCR para la identificación de la enfermedad HLB y se están investigando técnicas espectroscópicas y de imagen, haciendo perfiles de los compuestos orgánicos volátiles de las plantas y amplificación isotérmica (Arredondo Valdes *et al.*, 2016). En cualquier caso, el mecanismo más utilizado en primera instancia para monitorear HLB es la exploración directa de los cítricos. La detección de la enfermedad puede ser difícil ya que puede tardar de uno a varios años en producir síntomas, y los síntomas pueden confundirse con otras enfermedades y/o con la deficiencia de

nutrientes de la planta, lo cual dificulta el control de la enfermedad. Los primeros síntomas aparecen como pequeños puntos amarillentos en las hojas que posteriormente pasan a ser un moteado difuso asimétrico. Los árboles sintomáticos muestran una acumulación excesiva de almidón en las partes aéreas de la planta (tallo y hojas), el cual no se degrada, que junto a una alteración en el metabolismo de carbohidratos, resulta en la inanición de las raíces, el deterioro grave de la salud y la muerte de los árboles (Etxeberria *et al.*, 2009; Fan *et al.*, 2010). Del mismo modo el HLB da lugar a fruta de tamaño pequeño, colores de maduración invertidos, aborto de semillas y sabor amargo y desagradable (Dala-Paula *et al.*, 2019).

2.4.- La broca del café (*Hypothenemus hampei*, Coleoptera, Curculionidae)

2.4.1.- *Un poco de historia*

El barrenador del café, comúnmente llamado “la broca del café” (*Hypothenemus hampei*), fue descrita en Austria en 1867 por Johann Angelo Ferrari quien lo denominó *Cryphalus hampei* a partir de semillas de café importadas a Francia de origen desconocido, el nombre *hampei* proviene del Dr. Clemens Hampe, quien le proporcionó las muestras. El género *Hypothenemus* (del griego *hypo*: bajo y *thenemus*: boca, hace referencia a la posición de la boca hacia abajo) comprende 181 especies, siendo *H. hampei* la más estudiada con diferencia por las pérdidas de rendimiento y de calidad que produce en el café.

2.4.2.- *Importancia y distribución*

Si bien se han descrito muchas especies de insectos que atacan a las plantas de café (Waller *et al.*, 2007), solo la broca del café (*Hypothenemus hampei*), se ha especializado en consumir y reproducirse dentro de la baya del café, lo que la convierte en la plaga de insectos del café más importante económicamente en todo el mundo (Damon, 2000). El consumo que hace *H. hampei* del café es posible gracias a una microbiota de hasta 13 especies de bacterias que degradan la cafeína que de no ser por ellas sería tóxica para *H. hampei* (Ceja-Navarro *et al.*, 2012).

El cultivo de café se realiza en alrededor de 80 países, se estima que supone más de 10 millones de hectáreas de cultivo y más de 20 millones de familias dependen del mismo para su subsistencia, teniendo la industria del café un valor estimado en 2012 de 173,4 mil millones de dólares (Vega *et al.*, 2015). Actualmente, la broca del café está presente en la mayoría de los países productores de café (Vega *et al.*, 2015) y las pérdidas mundiales anuales probablemente superen los 500 millones de dólares, con pérdidas anuales sólo en Brasil estimadas de 215–358 millones de dólares (Oliveira *et al.*, 2013). Todo esto da una idea de los esfuerzos que se están realizando con el fin de poder controlar esta plaga. En cualquier caso, la realidad es que, debido a su ciclo de vida críptico dentro de la baya de café, el control de la plaga es complejo.

A continuación, se muestra un mapa de la distribución mundial de la broca del café (modificado a partir de www.cabi.org)

Distribución mundial de la broca del café

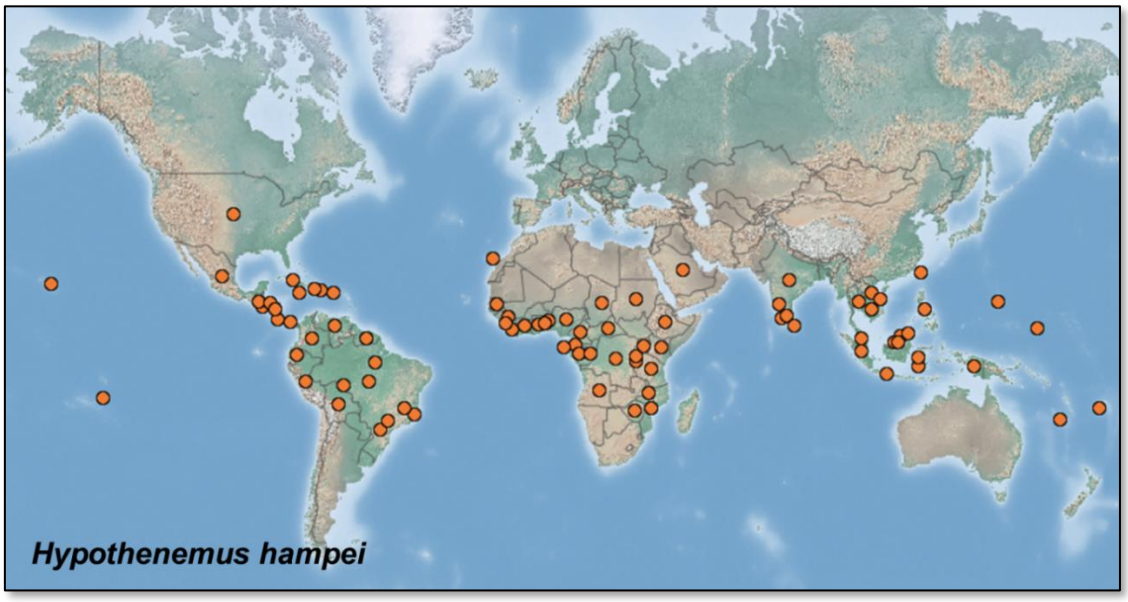

2.4.3.- *Ciclo de vida de la broca del café*

El ciclo de vida completo (huevo, larva, pupa y adulto, las hembras poseen dos estadíos larvales) dura aproximadamente un mes, si bien dependiendo de las condiciones ambientales puede variar de 21 hasta 63 días. El ciclo comienza cuando una hembra adulta, denominada hembra colonizadora, emerge de una baya de café infestada, pudiendo volar hasta 300-400 m (Leroy, 1936) si fuese

necesario para buscar otra baya de café donde perfora un agujero, generalmente a través del área conocida como disco, siendo este entre 0,6-1 mm de diámetro (Varón *et al.*, 2004; Wilkinson, 1928). La hembra entra en la baya y construye galerías (Alba-Alejandre *et al.*, 2018), donde ovoposita una media de 35-50 huevos en un periodo de 11-15 días, pudiendo ovopositar hasta 119 huevos. Dichos huevos eclosionarán en una proporción de unas 10 hembras por cada macho, esta proporción sesgada que favorece a las hembras parece ser debida a la presencia de *Wolbachia* (Vega *et al.,* 2002). Las larvas emergentes consumen la semilla y una vez que las hembras alcanzan la etapa adulta, unos 3-4 días después, se aparean con sus hermanos (Vega *et al.*, 2015). Los machos alcanzan la etapa adulta antes que las hembras para estar maduros sexualmente cuando las hembras sean adultas. Del mismo modo, puesto que la proporción de hembras es mayor que la de machos, un solo macho puede aparearse con múltiples hembras, habiéndose registrado un único macho inseminando a más de 120 hembras (Giordanengo, 1992). Las hembras pasan la mayor parte de su ciclo de vida dentro de la baya de café y los machos nacen y mueren dentro de la baya, siendo su principal papel el apareamiento. Los machos adultos son más pequeños (1-1,3 mm de longitud) que las hembras (1,6-1,9 mm de longitud), no pueden volar y poseen ojos rudimentarios (Vega *et al.*, 2014). Igualmente la vida media de los machos es menor que la de las hembras, siendo la vida media de los machos de entre 40-80 días y las hembras entre 130-155 días (Vega *et al.*, 2015).

El número de generaciones al año es dependiente de las condiciones ambientales pudiendo tener entre 9 hasta 13 generaciones al año en Costa de Marfil, si bien, lo más frecuente son de 3 a 5 generaciones al año (Damon, 2000).

2.4.4.- ***Monitorización de la presencia de la broca del café***

El mecanismo más utilizado para monitorizar la presencia de la broca consiste en la inspección visual de las bayas de café en busca de pequeños orificios inferiores a 1 mm de diámetro, generalmente en la zona del disco, indicativos de que la broca del café ha perforado un agujero en la misma.

3.- ANTECEDENTES Y OBJETIVOS

3.1.- Antecedentes

3.1.1.-Estudios sobre aspectos no anatómicos

Los estudios previos de estas especies plaga se han centrado fundamentalmente en:

- El control químico (Boina & Onagbola, 2009; Boina *et al.*, 2010; Gatineau *et al.*, 2010; Qureshi *et al.*, 2014; Sponagel, 1994; Tiwari *et al.*, 2012; Waterhouse & Norris, 1989; Zaka *et al.*, 2010)
- Control biológico (Bistline-East *et al.*, 2015; Chen *et al.*, 2017; Chen & Stansly, 2014; Chien & Chu, 1996; Étienne *et al.*, 2001; Etienne & Aubert, 1980; K. H. Ibarra-Cortés *et al.*, 2017; Ibarra-Cortés *et al.*, 2017; Michaud, 2002; Moore & Prior, 1988; Palomares-Pérez *et al.*, 2015)
- Estudios genéticos (Kuznetsova *et al.*, 1997; Macharashvili & Kuznetsova, 1997; Maryańska-Nadachowska *et al.*, 1996; Valencia *et al.*, 1994; Wang *et al.*, 2017; Wu *et al.*, 2016).

3.1.2.- Estudios anatómicos

Aldrovandi (Aldrovandi, 1602) y Malpigio (Malpighi, 1669), hace más de 400 años realizaron los primeros estudios anatómicos y publicaron magníficas ilustraciones de la anatomía de insectos, para lo cual realizaron disecciones de los mismos. Desde entonces, y hasta la actualidad, en la gran mayoría de trabajos anatómicos las ilustraciones y descripciones están basadas en disecciones de los especímenes. Aunque estas técnicas han resultado extremadamente útiles, inevitablemente distorsionan, al menos, la disposición espacial de las estructuras internas, si no dañan a las mismas.

Las técnicas de micro-CT han demostrado ser unas herramientas muy poderosas y útiles para estudios detallados en la visualización de estructuras internas de animales/insectos(i.e.: Jiang *et al.*, 2019; Kypke & Solodovnikov, 2018; Li *et al.*, 2011; Schambach *et al.*, 2010; Shaha *et al.*, 2013; Smith *et al.*, 2016). Los resultados han sido validados comparándolos con metodologías clásicas basadas en disecciones (Alba-Tercedor & Alba-Alejandre, 2019; Wipfler *et al.*, 2016).

3.1.2.1.- Estudios anatómicos sobre *D. citri*

Partiendo del trabajo pionero de Witlaczil de finales del siglo XIX (Macloskie, 1886; Witlaczil, 1885) diferentes estudios habían descrito aspectos de la anatomía de diferentes especies de psílidos (Ammar *et al.*, 2015; Arras *et al.*, 2012; Barcellos *et al.*, 2017; Bitsch, 1979; Blowers & Moran, 1967; Brittain, 1922; Brown *et al.*, 2016; Cicero *et al.*, 2015, 2018; Cicero, 2017, 2020; Cicero & Brown, 2009; Cicero & Stansly, 2019; Dossi & Cônsoli, 2014; Dossi & Cônsoli, 2010; Drohojowska *et al.*, 2013; Garzo *et al.*, 2012; George *et al.*, 2017; Ghanim *et al.*, 2016; E. Głowacka & Maryańska-Nadachowska, 1993, 1998; Elzbieta Głowacka *et al.*, 1995; Grove, 1919; Hall *et al.*, 2013; Heslop-Harrison, 1952; Kruse *et al.*, 2017; Kuznetsova *et al.*, 2012; Liang *et al.*, 2013; Macharashvili & Kuznetsova, 1997; Mally, 1894; Marchini *et al.*, 2012; Matsuda, 1970, 1976b, 1976a; Morgan *et al.*, 2013; Muir, 1930; Onagbola *et al.*, 2008; Ossiannilsson, 1992; Ouvrard *et al.*, 2002; Pesson, 1951; Prophetou-Athanasiadou & Tzanakakis, 1998; Saunders, 1921; Schlee, 1969; Snodgrass, 1935; Stockton *et al.*, 2017; Weber, 1929; Yen & Burckhardt, 2017; Zheng *et al.*, 2020; Zucht, 1972). Además de una publicación preliminar sobre las oportunidades que la microtomografía ofrece para el estudio de la anatomía del psílido asiático de los cítricos (Alba-Tercedor *et al.*, 2017).

3.1.2.2.- Estudios anatómicos sobre *H. hampei*

Aunque se han publicado más de 1.800 trabajos sobre la broca de café (Pérez *et al.*, 2015), hasta ahora el conocimiento de su anatomía interna se restringía a aspectos parciales, basados en técnicas de disección (Constantino *et al.*, 2011; López-Guillén *et al.*, 2011; Román-Ruiz *et al.*, 2017; Rubio-Gómez *et al.*, 2007; Rubio G. *et al.*, 2008).

3.1.3.- Bibliografía

Alba-Alejandre, I., Alba-Tercedor, J., & Vega, F. E. (2018). Observing the devastating coffee berry borer (Hypothenemus hampei) inside the coffee berry using micro-computed tomography. *Scientific Reports*, *8*(1), 17033. https://doi.org/10.1038/s41598-018-35324-4

Alba-Tercedor, J., & Alba-Alejandre, I. (2019). Comparing micro-CT results of insects with classical anatomical studies: The European honey bee (*Apis mellifera* Linnaeus, 1758) as a benchmark (Insecta: Hymenoptera, Apidae). *Microscopy and Analysis*, *3*(1), 12-15 EU. https://microscopy-analysis.com/article/january_19/comparing_classical_anatomical_studies_of_insects

Alba-Tercedor, J., Hunter, W. B., Cicero, J. M., & Sáinz-Bariáin, M. (2017). Use of micro-CT to elucidate details of the anatomy and feeding of the Asian Citrus Psyllid *Diaphorina citri* Kuwayama , 1908 (Insecta : Hemiptera , Lividae). In *Bruker Micro-CT Users Meeting 2017* (pp. 270–285). Bruker micro-CT-Skyscan. http://bruker-microct.com/company/UM2017/AbstractBook2017.pdf

Ammar, E.-D., Hall, D. G., & Shatters, R. G. (2015). Ultrastructure and Development of the New Stylets Inside Pre-molting First Instar Nymphs of the Asian Citrus Psyllid *Diaphorina citri* (Hemiptera: Liviidae). *Florida Entomologist* —, *98*(1). https://doi.org/10.1653/024.098.0163

Arras, J., Hunter, W., & Bextine, B. (2012). Comparative analysis of antennae sensory arrays in Asian citrus psyllid, *Diaphorina citri*, and potato psyllid, *Bactericera cockerelli* (Hemiptera). *Southwestern Entomologist*. https://doi.org/http://dx.doi.org/10.3958/059.037.0101

Arredondo Valdés, R., Delgado Ortiz, J. C., Beltrán Beache, M., Anguiano Cabello, J., Cerna Chávez, E., Rodríguez Pagaza, Y., & Ochoa Fuentes, Y. M. (2016). A review of techniques for detecting Huanglongbing (greening) in citrus. *Canadian journal of microbiology*, 62(10), 803-811.

Barcellos, M. S., Fernanda, J., Cossolin, S., Dias, G., & Lino-Neto, J. (2017). Sperm morphology of the leafhopper *Diaphorina citri* Kuwayama (Hemiptera: Sternorrhyncha: Psylloidea: Liviidae). *Micron*, *99*, 49–55. https://doi.org/10.1016/j.micron.2017.03.017

Bitsch, J. (1979). Morphologie Abdominale des Insectes. Ordre des Homoptères, B.-Psylles. In P.-P. Grassé (Ed.), *Traité de Zoologie. Anatomie, Systématique, Biologie. T. VIII, Insectes Thorax, Abdomen. Fasc. II* (pp. 420–429). Masson et Cie.

Blowers, J. R., & Moran, V. C. (1967). Notes on the female reproductive system of the South African Citrus Psylla, *Trioza erytreae* (Del Guercio) (Homoptera : Psyllidae). *Journal of the Entomological Society of Southern Africa*, *30*(1), 75–81. http://journals.co.za/docserver/fulltext/JESSA/30/1/2701.pdf?expires=1506671192&id=id&accname=guest&checksum=3A2E414A6D93326F9DCB5EE541F23E2A

Brittain, W. H. (1922). The morphology and synonymy of *Psylla mali* Schmidberger. *Proceeding Acadian Entomological Society (Fredericton)*, *8*, 23–51.

Brown, J. K., Cicero, J. M., & Fisher, T. W. (2016). Psyllid-Transmitted Candidatus Liberibacter Species Infecting Citrus and Solanaceous Hosts. In J. K. Brown (Ed.), *Vector-Mediated Transmission of Plant Pathogens* (pp. 399–422). The American Phytopathological Society. https://doi.org/10.1094/9780890545355.028

Cicero, J. M. (2017). Stylet biogenesis in *Bactericera cockerelli* (Hemiptera: Triozidae). *Arthropod Structure & Development*, *46*(4), 644–661.

https://doi.org/10.1016/j.asd.2016.12.007

Cicero, J. M. (2020). Functional Anatomy of the Asian Citrus Psyllid. In J. A. Qureshi & P. A. Stansly (Eds.), *Asian Citrus Psyllid: Biology, Ecology and Management of the Huanglongbing Vector* (pp. 12–29). CABI.

Cicero, J. M., Alba-Tercedor, J., Hunter, W. B., Cano, L. M., Saha, S., Mueller, L. A., & Brown, S. J. (2018). Asian citrus psyllid stylet morphology and applicability to the model for inter-instar stylet replacement in the potato psyllid. *Arthropod Structure & Development*, *47*(5), 542–551. https://doi.org/10.1016/j.asd.2018.06.007

Cicero, J. M., & Brown, J. (2009). The digestive system of *Diaphorina citri* and *Bactericera cockerelli* (Hemiptera: Psyllidae). *Entomological Society of America*, *102*(4), 650–665. http://aesa.oxfordjournals.org/content/102/4/650.abstract

Cicero, J. M., & Stansly, P. A. (2019). New Anatomical Evidence from the Male Asian Citrus Psyllid (Hemiptera: Liviidae) Invokes Controversy Over the Accepted Function of Some Male Reproductive Organs in Psylloidea. *Journal of Insect Science*, *19*(3). https://doi.org/10.1093/jisesa/iez048

Cicero, J. M., Stansly, P. A., & Brown, J. K. (2015). Functional anatomy of the oral region of the potato psyllid (Hemiptera: Psylloidea: Triozidae). *Annals of the Entomological Society of America*, *108*(5), 743–761. https://doi.org/10.1093/aesa/sav059

Dala-Paula, B. M., Plotto, A., Bai, J., Manthey, J. A., Baldwin, E. A., Ferrarezi, R. S., & Gloria, M. B. A. (2019). Effect of Huanglongbing or Greening Disease on Orange Juice Quality, a Review. *Frontiers in Plant Science*, *9*. https://doi.org/10.3389/fpls.2018.01976

Dossi, Fabio C. A., & Cônsoli, F. L. F. (2014). Gross morphology and ultrastructure of the female reproductive system of *Diaphorina citri* (Hemiptera: Liviidae). *Zoologia*, *31*(2), 162–169. https://doi.org/10.1590/S1984-46702014000200007

Dossi, Fábio C A, & Cônsoli, F. L. (2010). Desenvolvimento ovariano e influência da cópula na maturação dos ovários de *Diaphorina citri* Kuwayama (Hemiptera: Psyllidae). *Neotropical Entomology*, *39*(3), 414–419. https://doi.org/10.1590/S1519-566X2010000300015

Drohojowska, J., Kalandyk-Kołodziejczyk, M., & Simon, E. (2013). Thorax morphology of selected species of the genus Cacopsylla (Hemiptera, Psylloidea). *ZooKeys*, *319*, 27–35. https://doi.org/10.3897/zookeys.319.4218

Etxeberria, E., Gonzalez, P., Achor, D., & Albrigo, G. (2009). Anatomical distribution of abnormally high levels of starch in HLB-affected Valencia orange trees. *Physiological and Molecular …*. http://www.sciencedirect.com/science/article/pii/S0885576509000617

Fan, J., Chen, C., Brlansky, R. H., Gmitter Jr., F. G., & Li, Z.-G. (2010). Changes in carbohydrate metabolism in Citrus sinensis infected with 'Candidatus Liberibacter asiaticus.' *Plant Pathology*, *59*(6), 1037–1043. https://doi.org/10.1111/j.1365-3059.2010.02328.x

Farnsworth, D., Grogan, K. A., Bruggen, A. H. C. van, & Moss, C. B. (2014). The Potential Economic Cost and Response to Greening in Florida Citrus. In *Choices* (Vol. 29, pp. 1–6). Agricultural & Applied Economics Association. https://doi.org/10.2307/choices.29.3.11

Garzo, E., Bonani, J. P., Lopes, J. R. S., & Fereres, A. (2012). Morphological description of the mouthparts of the Asian citrus psyllid, *Diaphorina citri* Kuwayama (Hemiptera: Psyllidae). *Arthropod Structure & Development*, *41*(1), 79–86. https://doi.org/10.1016/j.asd.2011.07.005

George, J., Ammar, E. D., Hall, D. G., & Lapointe, S. L. (2017). Sclerenchymatous ring as a barrier to phloem feeding by Asian citrus psyllid: Evidence from electrical penetration graph and visualization of stylet pathways. *PLoS ONE*. https://doi.org/10.1371/journal.pone.0173520

Ghanim, M., Fattah-Hosseini, S., Levy, A., & Cilia, M. (2016). Morphological abnormalities and cell death in the Asian citrus psyllid (*Diaphorina citri*) midgut associated with Candidatus Liberibacter asiaticus. *Scientific Reports*, *6*(1), 33418. https://doi.org/10.1038/srep33418

Głowacka, E., & Maryańska-Nadachowska, A. (1993). Anatomy of male reproductive system of the Psylla Geoffr. s. 1.(Homoptera, Psyllodea)-Validity for the systematic relations within the Genus. *Folia Biologica (Kraków)*, *41*(3–4), 55–64. https://books.google.es/books?id=c3296OYP72UC&pg=PA55&lpg=PA55&dq=Anatomy+of+Male+Reproductive+System+of+the+Psylla+Geoffr.+s.+1.(Homoptera,+Psyllodea)-Validity+for+the+Systematic+Relations+within+the+Genus&source=bl&ots=3AYvVsTdTJ&sig=OL8ufud_a_jGrMxOUrx

Głowacka, E., & Maryańska-Nadachowska, A. (1998). Male reproductive system and karyotype of *Mycopsylla fici* (Tryon) (Homoptera, Psylloidea). *Folia Biologica (Kraków)*, *46*(1–2), 17–21.

Głowacka, Elzbieta, Kuznetsova, V. G., & Maryańska-Nadachowska, A. (1995). Testis follicle number in Psyllids (Psylloidea, Homoptera) as an anatomical feature in studies of systematic relations within the group. *Folia Biologica (Kraków)*, *43*(3–4), 115–124.

Grove, A. J. (1919). The anatomy of the head and mouth parts of *Psylla mali*, the Apple sucker, with some remarks on the function of the labium. *Parasitology*, *11*(3–4), 456–488. https://doi.org/https://doi.org/10.1017/S0031182000004388

Halbert, S. S. E. S., & Manjunath, K. K. L. (2004). Asian Citrus Psyllids (Sternorrhyncha: Psyllidae) and Greening Disease of Citrus: a Literature Review and Assessment of Risk in Florida. *Florida Entomologist*, *87*(3), 330–353. https://doi.org/10.1653/0015-4040(2004)087[0330:ACPSPA]2.0.CO;2

Hall, D. G., Richardson, M. L., Ammar, E.-D., & Halbert, S. E. (2013). Asian citrus psyllid, *Diaphorina citri*, vector of citrus huanglongbing disease. *Entomologia Experimentalis et Applicata*, *146*(2), 207–223. https://doi.org/10.1111/eea.12025

Heslop-Harrison, G. (1952). XXVII.—The number and distribution of the spiracles of the adult psyllid. *Annals and Magazine of Natural History*, *5*(51), 248-260 + plates XIV-XVI. https://doi.org/10.1080/00222935208654288

Inoue, H., Ohnishi, J., Ito, T., Tomimura, K., Miyata, S., Iwanami, T., & Ashihara, W. (2009). Enhanced proliferation and efficient transmission of Candidatus Liberibacter asiaticus by adult Diaphorina citri after acquisition feeding in the nymphal stage. *Annals of Applied Biology*, *155*(1), 29–36. http://onlinelibrary.wiley.com/doi/10.1111/j.1744-7348.2009.00317.x/full

Kruse, A., Fattah-Hosseini, S., Saha, S., Johnson, R., Warwick, E., Sturgeon, K., Mueller, L., MacCoss, M. J., Shatters, R. G., & Cilia Heck, M. (2017). Combining 'omics and microscopy to visualize interactions between the Asian citrus psyllid vector and the Huanglongbing pathogen Candidatus Liberibacter asiaticus in the insect gut. *PLOS ONE*, *12*(6), e0179531. https://doi.org/10.1371/journal.pone.0179531

Kuwayama, S. (1907). Die Psylliden Japanese. *Transactions of the Sapporo Natural History Society*, *2*, 149-189. (D. citri: p. 160-161, Plate III,Fig. 16).

https://www.hemiptera-databases.org/psyllespdf/25.pdf

Kuznetsova, V. G., Labina, E. S., Shapoval, N. A., Maryańska-Nadachowska, A., & Lukhtanov, V. A. (2012). *Cacopsylla fraudatrix* sp.n. (Hemiptera: Psylloidea) recognised from testis structure and mitochondrial gene COI. *Zootaxa*, *63*(3547), 55–63.

Liang, X., Zhang, C., Li, Z., Xu, L., & Dai, W. (2013). Fine structure and sensory apparatus of the mouthparts of the pear psyllid, *Cacopsylla chinensis* (Yang et Li)(Hemiptera: Psyllidae). *Arthropod Structure & Development*, *42*(6), 495–506. http://www.sciencedirect.com/science/article/pii/S1467803913000765

Macharashvili, I. D., & Kuznetsova, V. G. (1997). Karyotypes, Spermatogenesis, and Morphology of the Internal Reproductive System in Males of Some Psyllid Species (Homoptera, Psylloidea) of the Fauna of Georgia: I. Karyotypes and Spermatogonial Meiosis. *Entomological Review*, *77*(1), 12–20. https://s3.amazonaws.com/academia.edu.documents/39487107/Karyotypes_spermatogenesis_and_morpholog20151028-28433-1pw66oj.pdf?AWSAccessKeyId=AKIAIWOWYYGZ2Y53UL3A&Expires=1508150605&Signature=CzdGVvNgbta89lAvwfvbqYpcBBA%3D&response-content-disposition=inline

Macloskie, G. (1886). Entomology. Witlaczil on Psyllidae. *American Naturalist*, *20*(3), 283–287.

Mally, C. W. (1894). Psyllidae found at Ames. *Proceedings of the Iowa Academy of Science*, *2*(1), 152–171.

Marchini, D., Del Bene, G., Viscuso, R., & Dallai, R. (2012). Sperm Storage by Spermatodoses in the Spermatheca of *Trioza alacris* (Flor, 1861) Hemiptera, Psylloidea, Triozidae: A Structural and Ultrastructural Study. *Journal of Morphology*, *273*, 195–210.

Matsuda, R. (1970). Morphology and evolution of the insect throrax. *Memoirs of the Entomological Society of Canada*, *102*(S76), 5–431. https://doi.org/10.4039/entm10276fv

Matsuda, R. (1976a). The female efferent duct and associated structures. In *Morphology and Evolution of the Insect Abdomen* (pp. 97–104). Pergamon Press Ltd. https://doi.org/10.1016/B978-0-08-018753-2.50018-6

Matsuda, R. (1976b). The Homoptera. In *Morphology and Evolution of the Insect Abdomen* (pp. 280–299). Pergamon Press Ltd. https://doi.org/10.1016/B978-0-08-018753-2.50040-X

Morgan, J. K., Luzio, G. A., Ammar, E.-D., Hunter, W. B., Hall, D. G., & Shatters Jr, R. G. (2013). Formation of Stylet Sheaths in āere (in air) from Eight Species of Phytophagous Hemipterans from Six Families (Suborders: Auchenorrhyncha and Sternorrhyncha). *PLoS ONE*, *8*(4), e62444. https://doi.org/10.1371/journal.pone.0062444

Muir, F. (1930). LIII.—Notes on certain controversial points of morphology of the abdomen and genitalia of Psyllidæ. *Annals and Magazine of Natural History, Series 10*, *5*(29), 545–552. https://doi.org/10.1080/00222933008673163

Oliveira, C. M., Auad, A. M., Mendes, S. M., & Frizzas, M. R. (2013). Economic impact of exotic insect pests in Brazilian agriculture. *Journal of Applied Entomology*, *137*(1–2), 1–15. https://doi.org/10.1111/jen.12018

Onagbola, E. O. E., Meyer, W. W. L., Boina, R., Stelinski, L. L., Boina, D., & Stelinski, L. L. (2008). Morphological characterization of the antennal sensilla of the Asian citrus

psyllid, *Diaphorina citri* Kuwayama (Hemiptera: Psyllidae), with reference to their probable. *Micron*, *39*, 1184–1191. https://doi.org/10.1016/j.micron.2008.05.002

Ossiannilsson, F. (1992). *The Psylloidea (Homoptera) of Fennoscandia and Demark*. E.J. Brill. https://books.google.es/books?id=X_fgWnvLS2gC&pg=PA7&lpg=PA7&dq=ossiannilson+psylloidea+fennoscandian&source=bl&ots=4V0spLX1n1&sig=ACfU3U3D5VxM6vzpdIdJy7VIf5s11DGSrw&hl=es&sa=X&ved=2ahUKEwiumePoq5HlAhVOAWMBHVwbCKgQ6AEwCnoECAgQAQ#v=onepage&q&f=false

Ouvrard, D., Bourgoin, T., & Campbell, B. C. (2002). Comparative Morphological Assessment of the Psyllid Pleuron (Insecta, Hemiptera, Sternorrhyncha). *J. Morphol*, *252*, 276–290. https://doi.org/10.1002/jmor.1105

Pérez-Otero, R., Mansilla, J., & del Estal, P. (2015). Detección de la psila africana de los cítricos, Trioza erytreae (Del Gercio, 1918) (Hemiptera: Psylloidea; Triozidae), en la Península Ibérica. *Arquivos Entomolóxicos*, *13*, 119–122.

Pesson, P. (1951). Ordre des Homoptères (Homoptera Leach, 1815). In P.-P. Grassé (Ed.), *Traité de zoologie. Anatomie, systématique, biologie. Tome X. Fascicule II. Insectes supérieurs et Hémipteróides* (Editions M, pp. 1390–1656). Masson et Cie.

Prophetou-Athanasiadou, D. A., & Tzanakakis, M. E. (1998). The Reproductive System and Ovarian Development of the Adult Olive Psylla *Euphyllura phillyreae* Foerster (Homoptera: Aphalaridae). *Entomologia Hellenica*, *12*, 37–45. https://doi.org/http://dx.doi.org/10.12681/eh.14018

Saunders, L. G. (1921). *The Anatomy of* Psyllia mali *Schmidberger. Manuscript Thesis (M. Sc.) McGill University. Montreal.*

Schlee, D. (1969). Sperma-übertragung (und andere merkmale) in ihrer bedeutung für das phylogenetische system der sternorrhyncha (insecta, hemiptera) Phylogenetische studien an hemiptera I. psylliformes (psyllina und aleyrodina) als monophyletische gruppe. *Z. Morph. Tiere*, *64*, 95–138. https://doi.org/https://doi.org/10.1007/BF00391783

Shen, W., Halbert, S. E., Dickstein, E., Manjunath, K. L., Shimwela, M. M., & Bruggen, A. H. C. van. (2013). Occurrence and in-grove distribution of citrus huanglongbing in north Central Florida. In *Journal of Plant Pathology* (Vol. 95, pp. 361–371). Società Italiana di Patologia Vegetale (SIPaV). https://doi.org/10.2307/23721526

Snodgrass, R. E. (1910). Anatomy of the Honeybee. In *U.S. Department o Agriculture. Bureau of Entomology. technical Series* (Vol. 18). Government Printing Office. https://doi.org/10.1080/00368121.1977.9955353

Snodgrass, R. E. (1935). *Principles of Insect Morphology*. McGraw-Hill Book Company, Inc. https://doi.org/0801428831

Stockton, D. G., Pescitelli, L. E., Martini, X., & Stelinski, L. L. (2017). Female mate preference in an invasive phytopathogen vector: how learning may influence mate choice and fecundity in Diaphorina citri. *Entomologia Experimentalis et Applicata*, *164*(1), 16–26. https://doi.org/10.1111/eea.12590

Vega, F. E., Infante, F., & Johnson, A. J. (2015). The genus Hypothenemus, with emphasis on H. hampei, the coffee berry borer. In *Bark Beetles* (pp. 427–494). Elsevier. https://doi.org/10.1016/B978-0-12-417156-5.00011-3

Vega, F. E., Simpkins, A., Bauchan, G., Infante, F., Kramer, M., & Land, M. F. (2014). On the eyes of male coffee berry borers as rudimentary organs. *PloS One*, *9*(1), e85860. https://doi.org/10.1371/journal.pone.0085860

Weber, H. (1929). Kopf und thorax von *Psylla mali* Schmidb. (Hemiptera-Homoptera). Eine morphogenetische studie. *Z. Morph. Ökol. Tiere*, *14*, 59–165. https://link.springer.com/content/pdf/10.1007/BF00419345.pdf

Wipfler, B., Pohl, H., Yavorskaya, M. I., & Beutel, R. G. (2016). A review of methods for analysing insect structures — the role of morphology in the age of phylogenomics. *Current Opinion in Insect Science*, *18*, 60–68. https://doi.org/10.1016/j.cois.2016.09.004

Witlaczil, E. (1885). Die Anatomie der Psylloden. *Zeitschrift Für Wissenschaftliche Zoologie*, *42*, 569-638 + 3 tafeln. https://archive.org/details/zeitschriftfurwi4218unse/page/624/mode/2up?q=psyll

Yen, A., & Burckhardt, D. (2017). *Diagnostic protocol for the detection of the tomato potato Psyllid,* Bactericera cockerelli *(Šulc) prepared for the Subcommittee on Plant Health Diagnostic Standards (SPHDS)*. http://plantbiosecuritydiagnostics.net.au/resource-hub/priority-pest-diagnostic-resources/

Zheng, L., Liang, Q., Yu, M., Cao, Y., & Chen, W. (2020). Morphological characterization of antennae and antennal sensilla of *Diaphorina citri* Kuwayama (Hemiptera: Liviidae) nymphs. *PLOS ONE*, *15*(6), e0234030. https://doi.org/10.1371/journal.pone.0234030

Zucht, B. (1972). Bau und Entwicklung der äußeren Genitalorgane bei Psyllinen (Homopteren). *Zool. Jb. Anat. Bd.*, *231*, 167–231.

3.2.- Objetivos

Los objetivos planteados en la presente tesis doctoral consisten en un estudio en detalle (usando técnicas microtomográficas), de la anatomía funcional (externa e interna) de *Diaphorina citri* e *Hypothenemus hampei* (ambas especies plaga, de gran importancia económica), para evidenciar las diferentes estructuras en su posición natural, y así obtener imágenes y videos 3D que conformen un atlas anatómico singular. Para completar las lagunas de conocimiento existentes. Lo cual incluye la reconstrucción de las estructuras externas y órganos internos. Además de visualizar aspectos de la actividad "secreta" en el interior de las cerezas del café (en el caso de *H. hampei)* y de aspectos funcionales de la alimentación, en el caso de *D. citri.*

En su conjunto, a partir de los trabajos resultantes, disponer de unas bases de datos de imágenes que sirvan de base para la creación de modelos tridimensionales digitales que pueden volver a ser inspeccionados y valorados si así se desea para futuras revisiones y trabajos científicos.

Además, las imágenes, videos y modelos 3d, susceptibles de usar con dispositivos móviles (teléfonos inteligentes y tabletas), podrán ser de gran utilidad en tareas didácticas y de divulgación.

4.- METODOLOGÍA

Para aspectos concretos del presente proyecto, se aplicaron metodologías que se especifican en los capítulos correspondientes. En términos generales, se ha seguido el siguiente procedimiento:

4.1.- Preparación de las muestras

La metodología general consistió en deshidratar los ejemplares mediante etanol, seguido de un tratamiento con hexametildisilazano (HMDS) tras lo cual se dejaron secar al aire. En la mayoría de los casos para conseguir mayor contraste, y poder diferenciar adecuadamente las estructuras de la anatomía interna, los animales se sometieron a tratamientos de tinción. Bien con alcohol yodado (Alba-Tercedor, 2014) o bien ejemplares vivos se alimentaron en plantas sumergidas en un contraste. Habiéndose utilizado tanto el agente de contraste Iomeron® (iomeprol) (que es un medio de contraste tri-yodado no iónico con una alta concentración de yodo, 400 mg/ml que se observó que se absorbía muy bien por las plantas, y que incluso cuando se diluía al 1% causaba el marchitamiento, por lo que fue necesario diluirlo al 0,1%), como el denominado BAPCs (**B**ranched **A**mphiphilic **P**eptide **C**apsules) que va unido a Hg como medio de contraste (Alba-Alejandre *et al.*, 2018).

4.2.- Escaneado de las muestras

Para realizar el escaneo de los ejemplares, éstos se fijaron con cianoacrilato al extremo de un hilo de pescar de nylon de 200 µm de diámetro, como se ha descrito previamente (Alba-Tercedor, 2014; Alba-Tercedor *et al.*, 2017) o en el caso de las cerezas del café, estas se colocaron en el material Basotec® (una espuma de melamina ligera, con poca densidad a los rayos X).

Para la obtención de imágenes de micro-CT se utilizó el microtomógrafo Bruker SkyScan 1172 (Bruker-micro CT, Kontich, Bélgica) del departamento de Zoología de la Universidad de Granada. Este instrumento posee una fuente de rayos X Hamamatsu L702 y una cámara Ximea de 11 megapíxeles, y permite obtener imágenes 3D con un tamaño de voxel de hasta 480 nm. Los parámetros

de configuración se detallan para cada una de las muestras en su capítulo correspondiente.

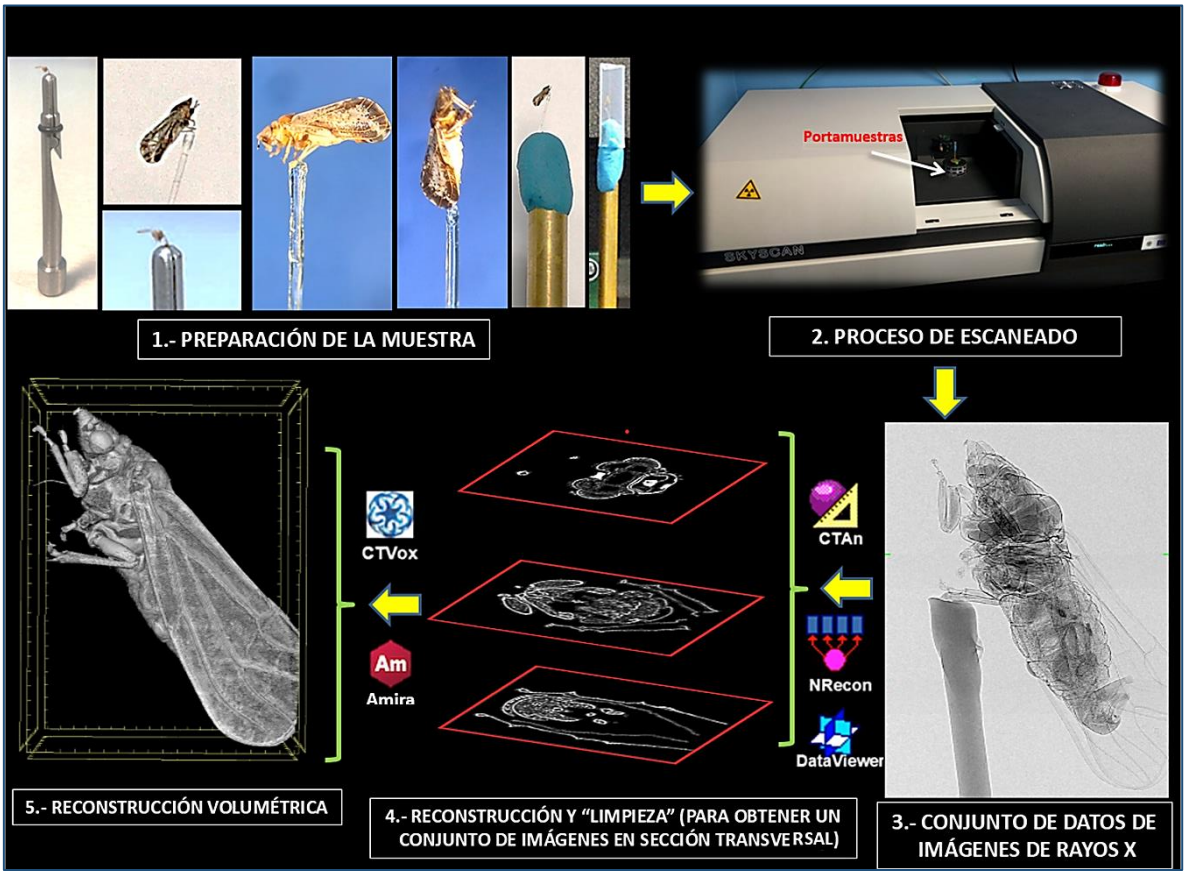

Figura 1.-Esquema de los pasos necesarios desde la preparación de la muestra hasta la reconstrucción volumétrica (renderización) de las imágenes. Se indica el software implicado en cada proceso.

4.3.- Tratamiento y reconstrucción volumétrica de las imágenes

Las versiones más recientes del software Skyscan de Bruker micro-CT (NRecon, DataViewer, CTAnalyser, https://www.bruker.com/products/microtomography.html) se utilizaron para las reconstrucciones preliminares y para el proceso de "limpieza" y obtener los conjuntos de datos de los diferentes "cortes", siguiendo la metodología descrita anteriormente (Alba-Tercedor, 2014). La reconstrucción volumétrica de las imágenes se hizo con los programas CTVox y Amira (Thermo Fisher Scientific, Waltham, MA)(Stalling *et al.*, 2005; Thermo Fisher Scientific, 2017). Los cuales realizan la reconstrucción de forma diferente, CTVox apila las imágenes obtenidas (como si fueran rodajas de la muestra); mientras que el programa Amira® lo hace mediante una triangulación de nubes de puntos. El proceso desde la preparación de la muestra, hasta la obtención de imágenes 3D

mediante microtomografía, al igual que el software implicado en cada proceso se esquematiza en la Fig. 1. Una vez obtenida la reconstrucción (transformación de imágenes de rayos X, en cortes, a modo de “rodajas”), se realiza una “segmentación” (separación individual de las estructuras de interés) manual, en cada una de las imágenes obtenidas (varios miles), véase Fig. 2.

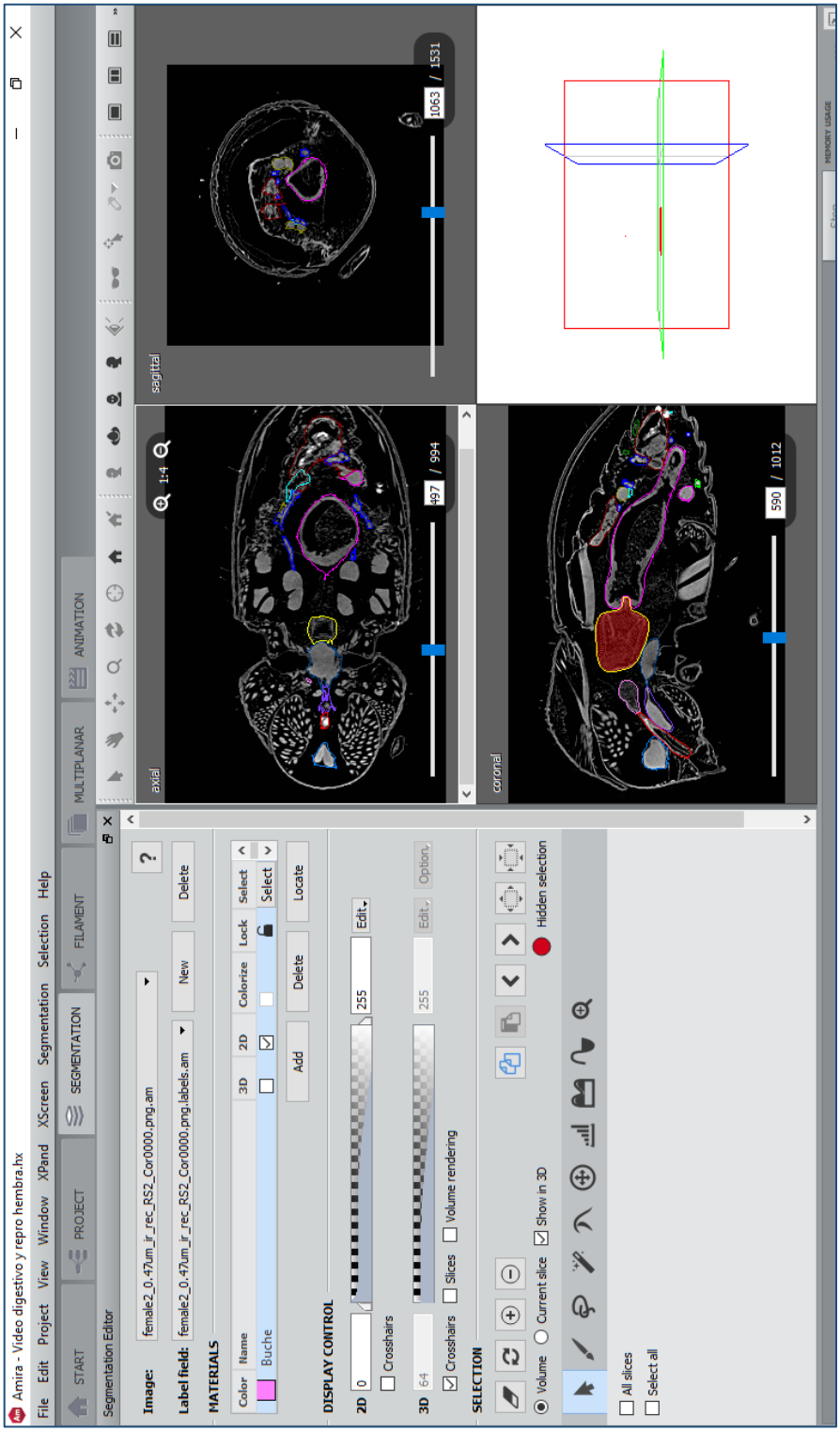

Figura 2.- Ejemplo de ”segmentación” manual de las diferentes estructuras y órganos de una hembra de *Hypothenemus hampei* mediante el software Amira

Mediante el software Amira®, a cada una de las estructuras individualizadas (segmentadas) se le aplicó posteriormente un color artificial, con el objeto de poder identificarlas fácilmente tanto en las fotos como videos. Del mismo modo con el software CTVox alterando las curvas de transferencia de colores primarios, se obtuvieron colores de acuerdo con la diferente transparencia de las estructuras a los rayos X (desde el rojo al azul en un gradiente de poca, a alta opacidad frente a los rayos X), según se explica en un trabajo anterior (Alba-Tercedor, 2014). En el caso del estudio del sistema traqueal de la broca del café, se le proporcionó un color según el diámetro de la luz de los tubos traqueales, tal y como se explica en detalle (como material suplementario) en la publicación correspondiente del sistema respiratorio (Alba-Tercedor & Alba-Alejandre, 2019) que se expone en el apartado 5.6.

4.4.- Bibliografía

Alba-Alejandre, I., Hunter, W. B., & Alba-Tercedor, J. (2018). Micro-CT study of male genitalia and reproductive system of the Asian citrus psyllid, Diaphorina citri Kuwayama, 1908 (Insecta: Hemiptera, Liviidae). *PLoS ONE*, *13*(8), 1–11.

Alba-Tercedor, J. (2014). From the sample preparation to the volume rendering images of small animals : A step by step example of a procedure to carry out the micro-CT study of the leafhopper insect <i>Homalodisca vitripennis<i/> (Hemiptera: Cicadellidae). In *Bruker Micro-CT Users Meeting 2014* (pp. 260–288). Bruker Micro-CT-Skyscan. http://bruker-microct.com/company/UM2014/000_AbstractBook2014.pdf

Alba-Tercedor, J., Hunter, W. B., Cicero, J. M., & Sáinz-Bariáin, M. (2017). Use of micro-CT to elucidate details of the anatomy and feeding of the Asian Citrus Psyllid Diaphorina citri Kuwayama , 1908 (Insecta : Hemiptera , Lividae). In *Bruker Micro-CT Users Meeting 2017* (pp. 270–285). Bruker microCT-Skyscan. http://bruker-microct.com/company/UM2017/AbstractBook2017.pdf

Stalling, D., Westerhoff, M., & Hege, H.-C. (2005). Amira: a highly interactive system for visual data analysis. In *Visualization Handbook* (pp. 749–767). Elsevier. https://doi.org/10.1016/B978-012387582-2/50040-X

Thermo Fisher Scientific. (2017). *Amira 3D visualization and analysis software* (6.7.0). FEI. http://www.thermofisher.com/amira-avizo

5.- RESULTADOS Y DISCUSIÓN

5.1.- "El uso de la microtomografía computarizada para desvelar la anatomía del adulto de *Diaphorina citri* Kuwayama, (Insecta: Hemiptera, Liviidae) y ver cómo perfora las hojas y se alimenta"

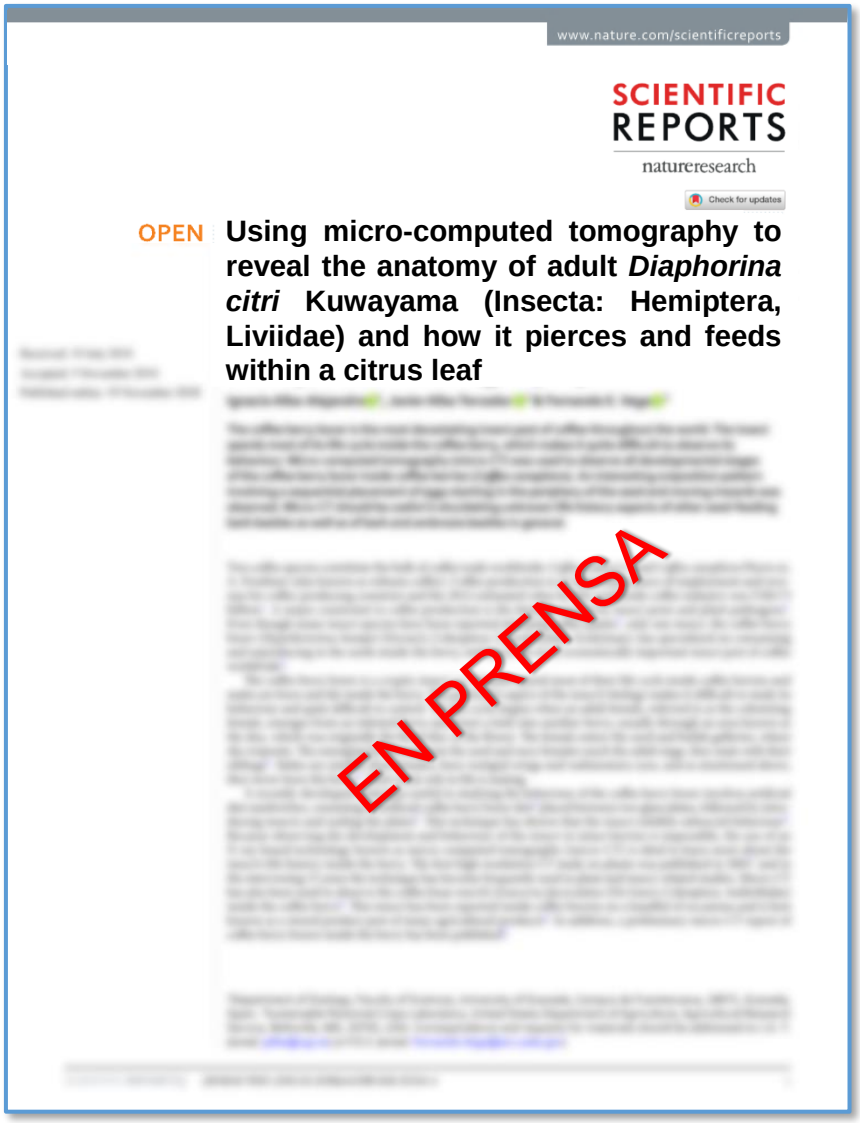

Artículo en prensa en la revista *Scientific Reports*.

Alba-Tercedor J., Hunter WB, **Alba-Alejandre I**, (-in print-) Using micro-computed tomography to reveal the anatomy of adult *Diaphorina citri* Kuwayama (Insecta: Hemiptera, Liviidae) and how it pierces and feeds within a citrus leaf. *Scientific Reports*

5.1.1.- Resumen

El psílido asiático de los cítricos (PAC), Diaphorina citri, representa una plaga dañina para cítricos al transmitir bacterias que causan la enfermedad de Huanglongbing (HLB) (también conocida como enfermedad del enverdecimiento de los cítricos), considerada la enfermedad bacteriana más grave de los cítricos. Dentro de un proyecto multidisciplinar sobre el ACP (www.citrusgreening.org), se presenta un estudio anatómico detallado de la anatomía externa e interna (excepto el sistema reproductor previamente publicado), que incluye una reconstrucción en 3D de un adulto alimentándose de la hoja de un cítrico, utilizando microtomografía computarizada (micro-CT). El primer descubrimiento de las glándulas coxales y escapo-antenales, tras el renderizado de imágenes y videos en detalle, y se reportan las primeras diferencias sexuales en la anatomía interna (en el recto, del intestino posterior y diferente forma y tamaño del ganglio mesotorácico y el cerebro). Este trabajo representa la primera reconstrucción completa en 3D con micro-CT de la anatomía de un insecto psiloideo, siendo el primer estudio anatómico completo realizado del ACP. Representa un avance significativo en el conocimiento de la anatomía del ACP y de los psílidos en general. Imágenes renderizadas de alta calidad, videos complementarios adicionales y un modelo 3D de un macho adulto alimentándose de una hoja de naranjo (apto para usarse con dispositivos móviles), constituyen un atlas anatómico único y son herramientas útiles para futuras investigaciones y como material didáctico.

5.1.2.- Abstract

The Asian citrus psyllid (ACP), *Diaphorina citri*, is a harmful pest of citrus trees that transmits the bacterial disease, Huanglongbing (HLB) (a.k.a. citrus greening disease); this is considered to be the most serious bacterial disease of citrus plants. Within a multidisciplinary project on ACP (www.citrusgreening.org), here we detail an anatomical study of the external and internal anatomy (excluding the reproductive system) using micro-computed tomography (micro-CT). This is the first complete 3D micro-CT reconstruction of the anatomy of a psylloid insect and includes a 3D reconstruction of an adult feeding on a citrus leaf that can be used

on mobile devices. Detailed rendered images and videos support first descriptions of coxal and scapus antennal glands and sexual differences in the internal anatomy (hindgut rectum, mesothoracic ganglion and brain). This represents a significant advance in our knowledge of ACP anatomy, and of psyllids in general. Together the images, videos and 3D model constitute a unique anatomical atlas and are useful tools for future research and as teaching aids.

5.1.3.- Introduction

Since it was first discovered in Taiwan in 1907 (Kuwayama, 1907), the Asian citrus psyllid (ACP) *Diaphorina citri* (Hemiptera: Liviidae) has become the most significant vector of *Candidatus* Liberibacter spp. (Huanglongbing [HLB] or citrus greening disease) in citrus orchards. HLB is the most serious disease threatening the citrus industry (Mead & Fasulo, 2017). To date, HLB has spread to over 40 countries in Asia, Oceania and both North and South America (Halbert & Manjunath, 2004; Shen *et al.*, 2013).

After Witlaczil 's pioneering work at the end of the 19th century (Macloskie, 1886; Witlaczil, 1885) a number of studies have described aspects of the anatomy of psyllid species (Alba-Alejandre, Alba-Tercedor, *et al.*, 2018; Ammar *et al.*, 2015, 2017; Arras *et al.*, 2012; Barcellos *et al.*, 2017; Bitsch, 1979; Blowers & Moran, 1967; Brittain, 1922; Brown *et al.*, 2016; Cicero *et al.*, 2015; Cicero, Alba-Tercedor, *et al.*, 2018; Cicero, 2017, 2020; Cicero & Brown, 2009; Cicero & Stansly, 2019; Dossi & Cônsoli, 2014; Dossi & Cônsoli, 2010; Drohojowska *et al.*, 2013; Garzo *et al.*, 2012; Ghanim *et al.*, 2016; E. Głowacka & Maryańska-Nadachowska, 1993, 1998; Elzbieta Głowacka *et al.*, 1995; Grove, 1919; Hall *et al.*, 2013; Heslop-Harrison, 1952; Kruse *et al.*, 2017; Kuznetsova *et al.*, 2012; Liang *et al.*, 2013; Macharashvili & Kuznetsova, 1997; Mally, 1894; Marchini *et al.*, 2012; Matsuda, 1970, 1976b, 1976a; Morgan *et al.*, 2013; Muir, 1930; Onagbola *et al.*, 2008; Ossiannilsson, 1992; Ouvrard *et al.*, 2002; Pesson, 1951; Prophetou-Athanasiadou & Tzanakakis, 1998; Saunders, 1921; Schlee, 1969; Snodgrass, 1935; Weber, 1929; Yen & Burckhardt, 2017; Zheng *et al.*, 2020; Zucht, 1972). The majority of these descriptions and illustrations are based on

various microscopy techniques that require insect-dissection to enhance visibility of internal structures and organs. While dissection techniques are very useful, they have limitations because they distort the spatial arrangement of internal structures. A relatively recent technique, known as micro-computed tomography (micro-CT), which is based on X-rays, allows visualization of the internal anatomy *in situ*, without the need to dissect the insect; results have been validated by comparing them with classical destructive methodologies (Alba-Tercedor & Alba-Alejandre, 2019; Wipfler *et al.*, 2016). Thus, micro-CT has now been used to elucidate insect anatomy; for ACP, a preliminary publication on the opportunities that micro-CT offers (Alba-Tercedor *et al., 2017*), and two detailed studies of the male (*Alba-Alejandre et al., 2018*) and female (Alba-Alejandre *et al.*, 2020)) reproductive system have already been published, including a revision of the reproductive system of psyllids in general.

Thus, the main aim of the current study was to fill any knowledge gaps by extending anatomical studies of ACP to the entire anatomy (external and internal), and configure a 3D anatomical atlas. Here we present an extensive application of the micro-CT techniques to reveal, in detail, the entire anatomy (excluding the reproductive systems and external abdominal terminalia of both sexes that we have already published (Alba-Alejandre *et al.*, 2018, 2020)) and a 3D reconstruction of an adult feeding on a leaf.

We also present videos as supplementary information; these provide an accurate view of the actual position and internal components of the organs and structures. We present spinning animations, using different rotation axes, that permit detailed observation of the structures from different 3D perspectives (Supplementary Videos S1-S11), and a 3D model that can be used on mobile devices (Supplementary 3D model S12).

Together, this increases current knowledge and helps us understand the morphology and functional anatomy of structures in their natural anatomical position, avoiding deformations that typically occur using standard dissection and/or slide preparation techniques. The high-quality rendered images and the supplementary information (videos and 3D model) represent a unique anatomical atlas of ACP and are useful tools for future research and as teaching aids.

5.1.4.- Materials and Methods

Six adult female and five adult male ACP specimens were scanned for evaluation in this study. They were from the rearing facilities at the United States Department of Agriculture, Agriculture Research Service, Fort Pierce, Florida (USA). Four different staining/contrast methods were used:

1. Live psyllids were prepared by overnight fixation in 4% glutaraldehyde with 2.5% paraformaldehyde in sodium cacodylate buffer pH 6.5; the fixed samples were rinsed three times (10 min each) in 30% ethanol, then dehydrated in an ethanol series (30 min per step; 50%,70%, 80%, 90%, 95%) ending with three steps in 100% ethanol; finally, the samples were chemically dried by placing in 2 ml of 100% hexamethyldisilazane (HDMDS) for 2 h, followed by drying overnight at 35ºC. These specimens are visualized in Figs. 1, 2, 4e-g.

2. Live psyllids were killed and preserved in 70% ethanol, then submerged in a 1% solution of iodine in 100% ethanol for 48 h; samples were transferred to HDMDS for 3 h and dried overnight at room temperature. These specimens are visualized in Figs. 3, 4a-d, 5, 9, 10, 15, 19 and Supplementary videos S1, S2, S11.

3. Psyllids were fed for 72 h on an orange sprig that had been submerged in Iomeron® (iomeprol) contrast agent. This is a tri-iodinated non-ionic contrast media with a high concentration of iodine (400 mgI/mL). We observed that the contrast medium was significantly absorbed into plant cuttings but that, even when diluted at 1%, it caused plant wilting, so it was necessary to dilute it to 0.1%. While in the act of feeding on citrus leaves the psyllids were flash frozen in liquid nitrogen, and then processed as described previously (Alba-Tercedor *et al.*, 2017). Finally, a small drop of fingernail polish placed on the posterior end of the psyllid and the leaf, was used to hold them in place after processing and drying. These specimens are visualized in Figs. 6-8, 17, Supplementary videos S3, S4, and Supplementary 3D model S12).

4. Adult psyllids were fed for three days on an orange tree sprig submerged in BAPC (***B****ranched* ***A****mphiphilic* ***P****eptide* ***C****apsules*) linked to Hg as a contrast agent

(Sukthankar *et al.*, 2014). The insects were rinsed three times in 30% ethanol (10 min for each rinse), dehydrated in an ethanol series (30 min per step, 50%, 70%, 80%, 90%, 95%, and three times at 100%), chemically dried by submersion in 2 ml of 100% HMDS for 2 hours, and dried overnight at 35ºC. These specimens were visualized in Figs. 11-14, 17, 18 and Supplementary videos S5-S10.

Finally the specimens were prepared for scanning by gluing them to the tip of a nylon fishing line (200 µm in diameter) with cyanoacrylate, as previously described (Alba-Tercedor, 2014; Alba-Tercedor *et al., 2017*). The prepared insects were scanned with a SkyScan 1172 desktop high-resolution micro-CT, with a Hamamatsu L702 source and a Ximea 11Mp camera. We used the following setting parameter ranges; isotropic voxel size = 0.52-0.54µm per pixel; source voltage = 44-50KV, source current = 43-68µA, image rotation step=0.2-0.5º, 360º rotation scan, binning 1x1, and no filter.

Recent versions of the Bruker micro-CT's Skyscan software (NRecon v.1.7.4.6, DataViewer v.1.5.6.2, CTAnalyser v.1.18.8.0) were used for primary reconstructions and the 'cleaning' process to obtain datasets on 'slices' through the insect as described previously(Alba-Tercedor, 2014). The most recent version of the software CTVox v.3.3.1 (Bruker micro-CT's Skyscan) was used to obtain the volume-rendered images seen in Figs. 1, 2, 6 and 7. Amira software, v. 2019.3 (Stalling *et al.*, 2005; Thermo Fisher Scientific, 2017), with the built-in 'volrenRed.col' colour filter, was used to obtain the volume-rendered images seen in Figs. 3-5, 9, 11-19 and Supplementary Videos S1-S11; the built-in 'volrenGreen.col' colour filter was used for Figs. 8, 16b, 16d-i. Different anatomical parts were independently segmented to obtain the final rendered colorized images seen in Figs. 11-13, 15, 16b, 16d, and Supplementary Videos S5-S8 and S9. To observe the actual texture of structures after segmentation, and in desired colours, each structure was subjected to the following arithmetic operation: A*(B > 0), where A represents the whole animal and B the segmented structure.

To reconstruct the spaces inside the filter chamber shown in Figs. 14h, i and Supplementary video S9, a task list was conducted within CTAn software as

described previously for reconstruction of the air-filled tracheal system of the coffee berry borer beetle (Alba-Tercedor *et al.*, 2019).

In accordance with the micro-CT results (as seen in the Figs.), standard anatomical positions are used to describe structures.

For consistency, and to avoid poor or misleading descriptions of any structure or form as a result of undesired deformation, the structures visualized and described in this study were checked and found to exist and maintain their shape and position in each of the specimens that were scanned and reconstructed.

5.1.5.- Results

External anatomy. (Figs. 1-8, 9a, Supplementary Videos S1-S4 and Supplementary 3D model S12).

Head. (male: Figs. 1a-d, 6 and 7a; female: Figs. 3a, 3c and Supplementary Video S1). The head has characteristic genal cones (conical lateral structures; each elongated, ca. twice as long as wide). There is a depression each side of the vertex (Figs. 1b, 2b). The antennae (Figs. 3b, 6 and 7a) with broad scapus and pedicel, and a flagellum comprised of eight articles (ca. ¼ narrower than pedicel). Openings of olfactory sensilla (rhinaria) are visible in the 2nd, 4th, 6th and 7th flagellar articles, and on the 8th are two apical setae (the length of the inner one is half the length of the outer) (Fig. 3c); The compound eyes are found laterally, each with a characteristic post-orbital ridge; three ocelli (one frontal, situated dorsally, and two lateral, are situated in a dorsolateral position above the compound eyes and close to the posterior margin of the head. A conspicuously bulging clypeus (cibarium) appears ventrally (Figs. 2d, 5a, 6c and 7a), with two small rounded protuberances (Fig. 15f). The labium appears ventrally, slightly posterior and between the fore coxae (Figs. 1c, 2c, 3a, 3b, 6c, 7a and 7b). The labium has three segments, the 1st segment is the longest, the 3rd segment has a conical shape, with a long anterior slit and a short posterior apical slit and apical setae (Figs. 1c, 2c, 2d, 5a, 5b, 6b, 6c, 7a, 7b, 8a, 15, 16e and Supplementary Videos S3, S4).

Thorax. (male: Figs. 1, 6 and 7; female: Figs. 2, 3a, 5, and Supplementary Video S1). The pronotum has two lateral 'dimples' on each side The mesothorax is well developed. The scutum and scutellum in divisions are very conspicuous in the mesonotum and the prescutum. The metathorax appears narrower. The thoracic pleurae with clearly visible sclerites, including the episternal and epimeral ones, and one spiracular opening on the pleural side of each segment (Figs. 3a, 6a, 6d and Supplementary Video S1). The legs are arranged forwards, the hind ones are clearly longer with enlarged/ longer coxae and conspicuous metatibial saltatorial spines. The tarsi have two claws and a ventral bilobed enlarged pad-like pulvillus (Figs. 6a, 6b). Meta-coxae are prolonged in a pointed structure, and the meracanthi (from a ventral view) appear divergent Figs. 1c, 2c).

Axillary sclerites of the wings are clearly visible on the base of the wing attachments on the thorax wall (Fig. 3a), as well as the parapterum and tegula (Figs.1a, 2a, 3a, 6a, 6b, 6d and Supplementary video S1).

Wings: Wings have reduced venation (Figs. 3a, 4a, 4b, 4g, 6a, 6b, 6d and Supplementary video S1). The costal and subcostal veins end together in the distal marginal third, forming a costal break, similarly on the posterior margin the anal vein interrupts forming an anal break. A narrow pterostigma on the anterior distal margin of the forewings. On the basal posterior margin of the fore wing the anal vein A1 delimits the clavus area. On the basal fore margin of the hind wings there are ca. ten stout setae (Fig. 4b, 4c) and a hook, the hamulus (Fig. 4d) permitting attachment to the fore wing for synchronized flight movements. The dorsal surface of the fore wings is covered with microtrichia giving a sandpaper appearance (see Figs. 4e-g).

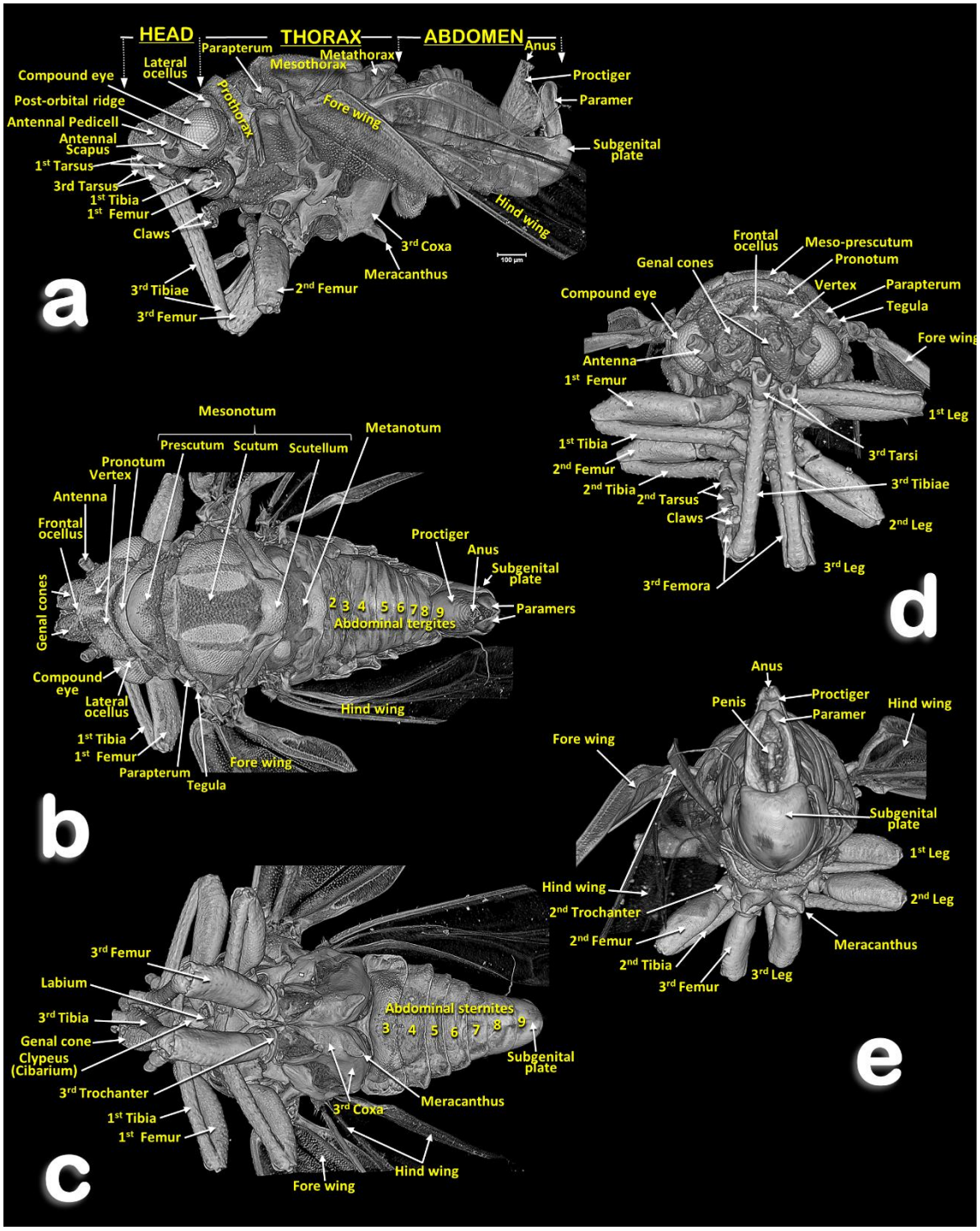

Figure 1.- Volume-rendered images of the general external anatomy of a male *Diaphorina citri* in different views. Left-lateral (**a**), dorsal (**b**), ventral (**c**), frontal (**d**) and posterior (**e**).

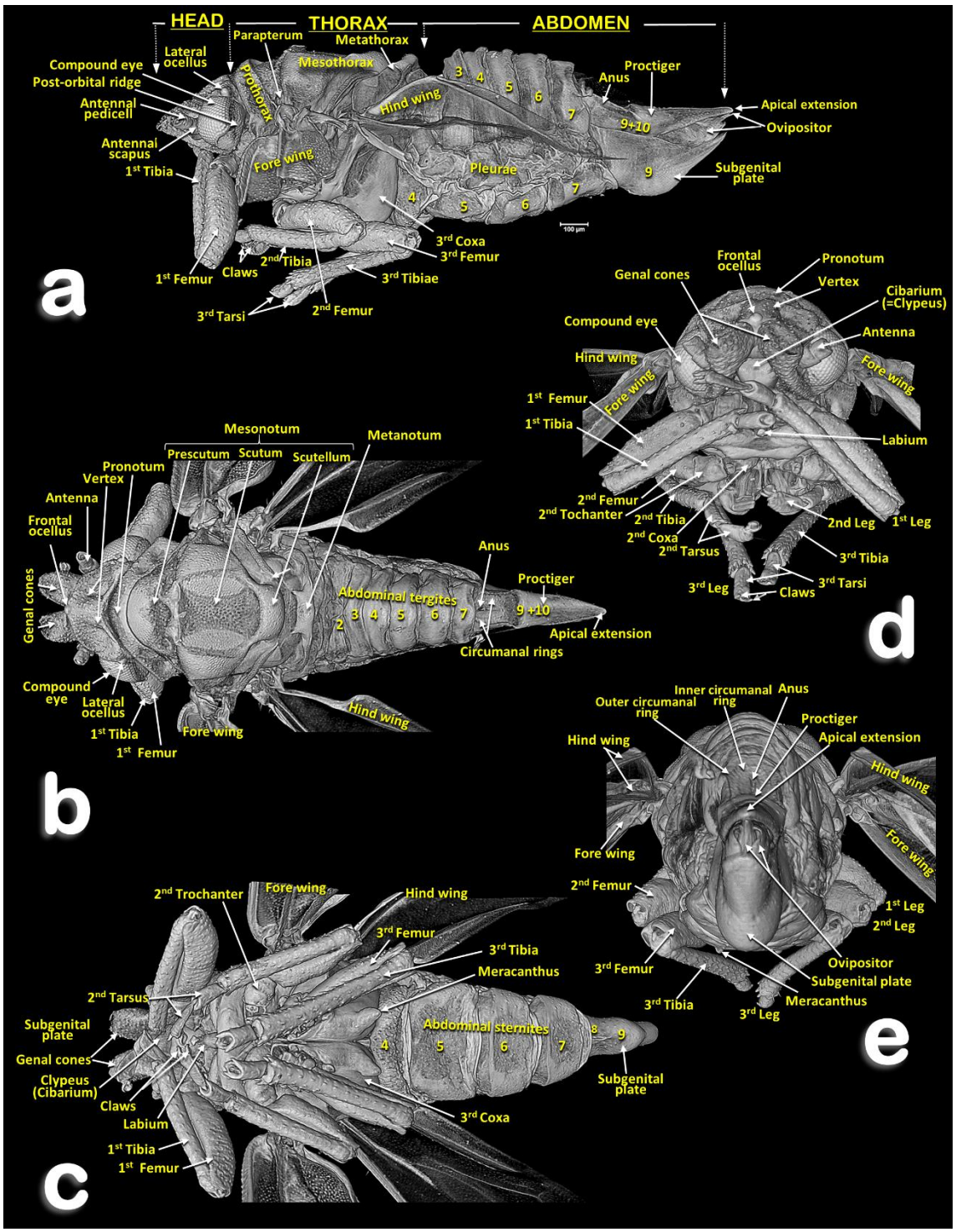

Figure 2.- Volume-rendered images of the general external anatomy of a female *Diaphorina citri* in different views. Left-lateral (**a**), dorsal (**b**), ventral (**c**), frontal (**d**) and posterior (**e**).

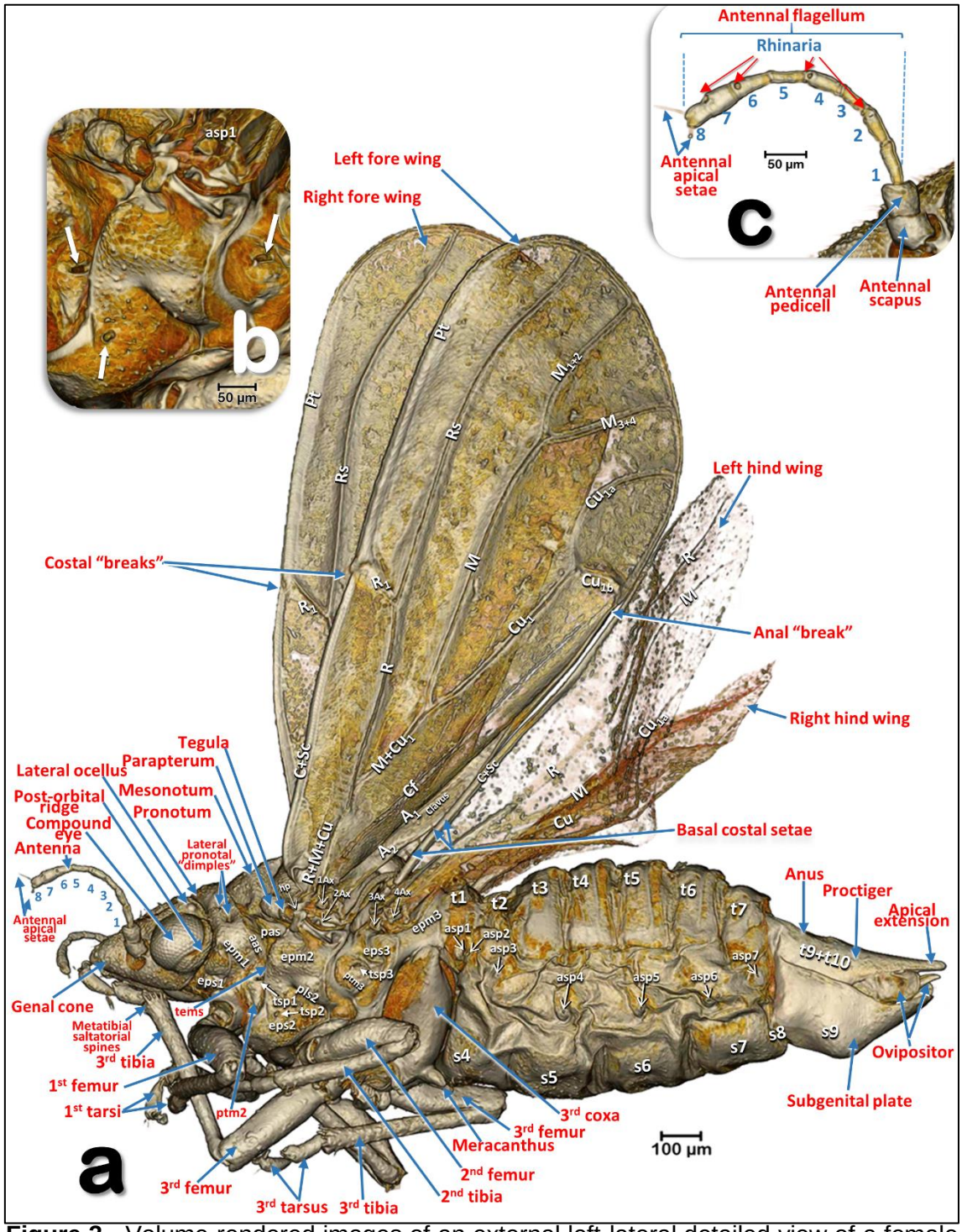

Figure 3.- Volume-rendered images of an external left-lateral detailed view of a female (**a**) and a close-up detail of the pleural región of the thorax (**b**) (with arrows are pointed the spiracular openings), and the antenna (**c**). Abbreviations: A = Anal vein; aas = anterior accessory sclerite; asp = abdominal spiracle; Ax =Axillary sclerite; C = costa vein; Cf = cubital fold; Cu = cubital vein; epm = epimeron; eps = episternum; hp = humeral plate; M = median vein; pas = posterior accessory sclerite; pls = pleural sulcus; Pt = pterostigma; ptm2 = mesothoracic peritreme; ptm3 = metathoracic peritreme; R = radius vein; Rs = radial sector vein; s = abdominal sternite; t = abdominal tergite; tems = transepimeral sulcus; tsp1 = prothoracic spiracle; tsp2= mesothoracic spiracle; tsp3= metathoracic spiracle. Abdominal tergites and sternites are labelled sequentially with the letter 't' and 's', respectively.

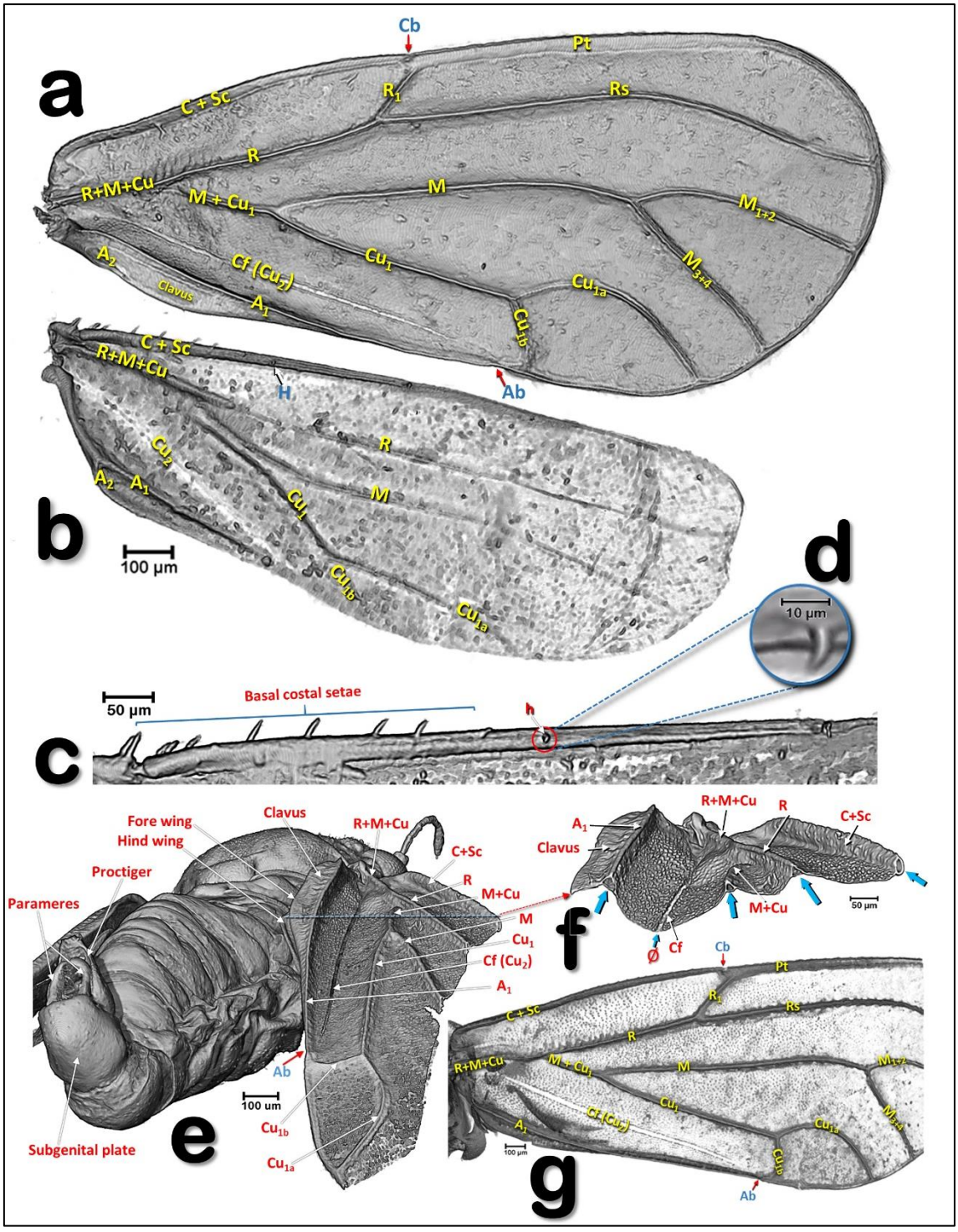

o

Figure 4.- Volume-rendered images of the wings and veins: left wings of a female in a ventral view (**a**-**d**) and right fore wing of a male (**g**)**,** in different perpective views showing the dorsal surface (**e**-**g**). General shape of the wings and veins (**a**-**b**). Details of the dorsal fore basal margin of the hind wing (**c**). Detail of the hamulus (**d**). Right-lateral posterior view of a male showing veins and folds of the right wing (**e**). Details of the basal right fore wing (**f**)**,** as result of a virtual cut marked with a red dashed line in **e** (blue arrows point to show the transversal cut of the vein tubes, with the symbol "Ø" is pointed the non-tubular structure of the cubital fold. Abbreviations: A = Anal vein; An = anal break; C = costa vein; Cb = costal break; Cf = cubital fold; Cu = cubital vein; H = hamulus; M = median vein; R = radius vein; Rs = radial sector vein.

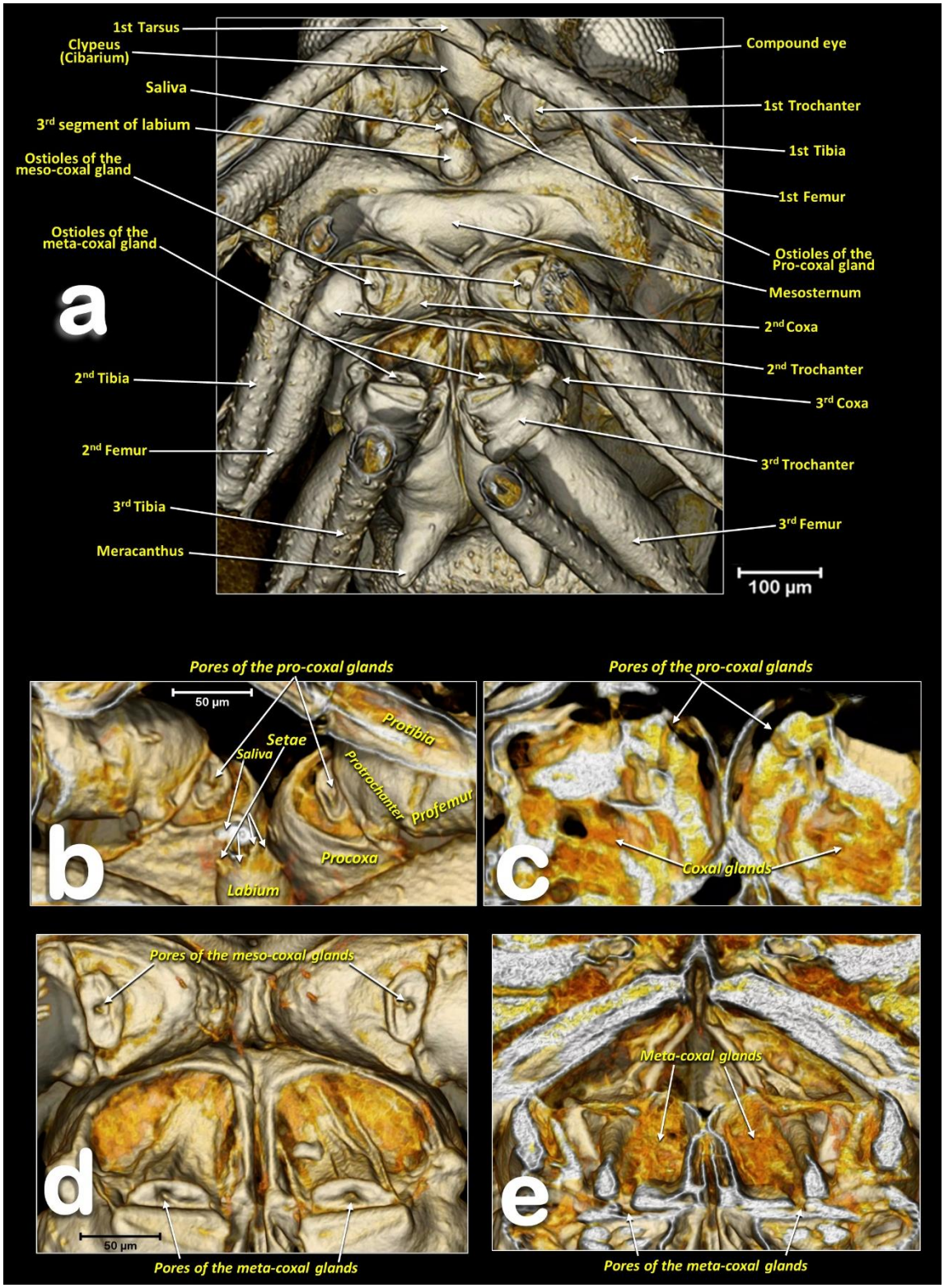

Figure 5.- Volume-rendered images of the anterior half of a female, in a ventral view, showing the main anatomical structures and the ostioles of the coxal glands (**a**). Close-up of the ostioles of the coxal glands (**b**-**d**), and antero-posterior oblique virtual cuts showing the coxal gland tissue inside the coxae (**c**-**e**).

Coxal glands: On the distal membrane of each coxa (between the coxa and the trochanter) is an oval sclerite, with a central hole (ostium) corresponding to the external mouth of the coxal gland (Figs. 5a, 5b, 5d and 6c).

Abdomen. The abdominal tergites/sternites are shown in Figs. 1b,c, 2b,c, 3a. On the pleurae of abdominal segments 2-7 there are six pairs of respiratory spiracles (Fig. 3a, 9a and Supplementary Video S1). The posterior abdominal segments (terminalia) show clear sexual differences: the male terminalia (Fig. 1a-c, 1e) have two parameres (the penis is located interiorly and between them, Fig. 1e) and an elevated proctiger that includes the anus (see more details of the male terminalia in our previous paper(Alba-Alejandre *et al., 2018*)); the female terminalia (Figs. 2a-c, 2e, 3a and Supplementary Video S1) have a pointed appearance, especially in the dorsal view. Due to an apical extension (Fig. 2b), the anus is on the base of the proctiger and it is surrounded by double concentric circum-anal rings, with pori corresponding to the external mouth of the wax glands (see more details of the female terminalia in our previous paper(Alba-Alejandre *et al.*, 2020)).

Internal anatomy (Figs. 5c, 5e, 9b, 9e, 10-19 and Supplementary Videos S1-S11). The internal anatomical details are shown in Figs. 5c, 5d, 9b, 9d, 10-19 and Supplementary Videos S1-S11.

The respiratory system. This opens externally via three pairs of thoracic spiracles and seven pairs of abdominal spiracles (situated on the pleural region of the thoracic segments and the 1st-7th abdominal segments; the 1st and 2nd are very close to each other; Figs. 3a, 6a, 6d, 9a and Supplementary video S1). Using software to achieve transparency it was possible to highlight the abdominal tracheal tubular system of a female (Figs. 9b, 9c and Supplementary Video S1). This is organized as: a pair of dorsal longitudinal tracheal trunks, situated in parallel and following the dorsal vessel (Fig. 10b, 10c); a pair of lateral longitudinal tracheal trunks (located in the dorsal abdominal third), each with a double tube branching anteriorly and entering into the thorax; and ventrally a pair of longitudinal tracheal trunks. The dorsal longitudinal tracheal trunks and the lateral longitudinal tracheal trunks are interconnected by dorso-lateral segmental tracheae. The lateral longitudinal tracheal trunks and the ventral longitudinal -

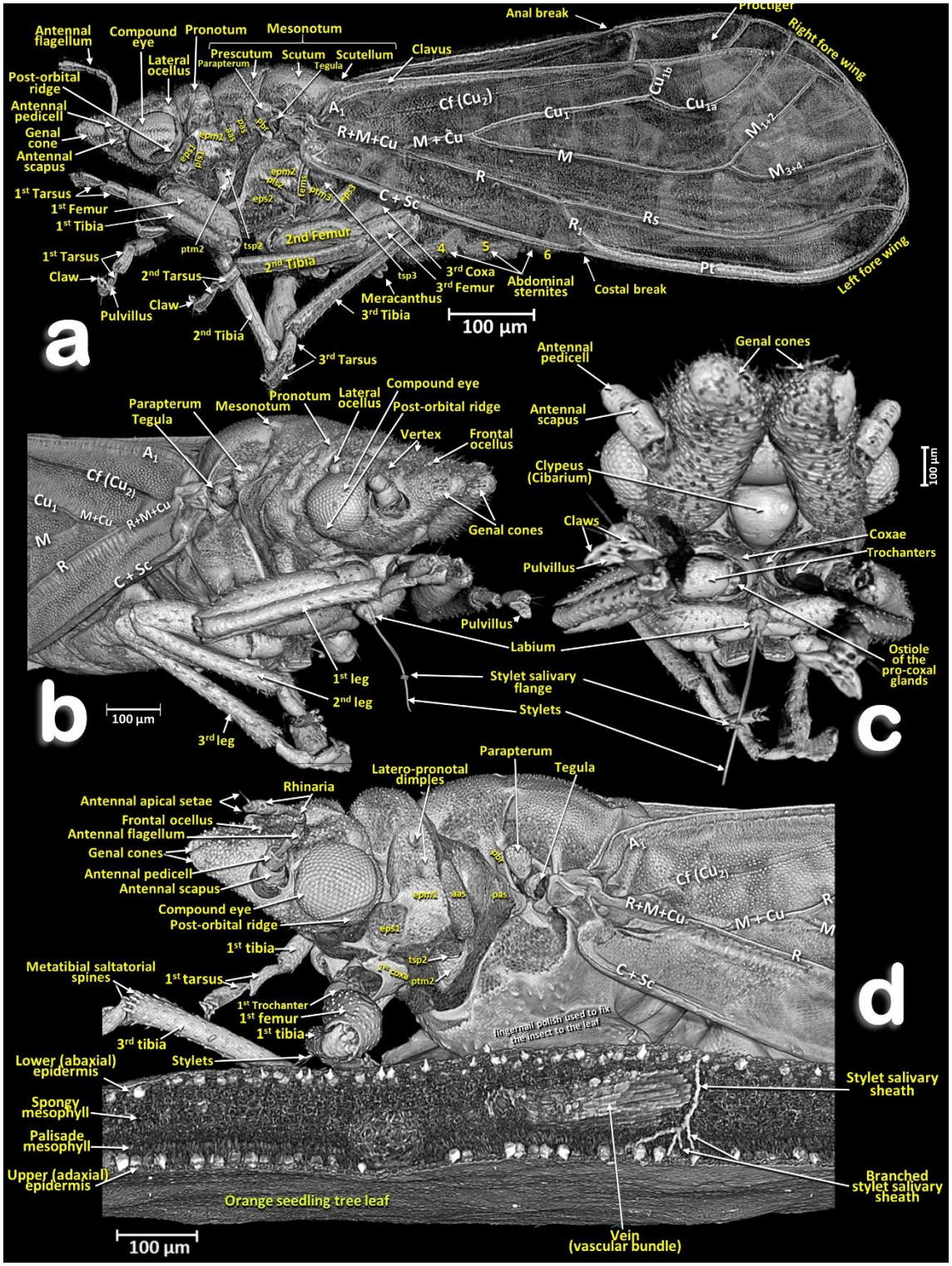

Figure 6.- Volume-rendered images of male adult in different perspective views. Left-lateral (**a**), right-frontal (**b**), ventro-frontal (**c**), and a left-fore half of an individual feeding on an orange seedling tree leaf (**d**). Abbreviations: A = Anal vein; aas = anterior accessory sclerite; C = costa vein; Cb = costal break; Cf = cubital fold; Cu = cubital vein; epm = epimeron; eps = episternum; M = median vein; pas = posterior accessory sclerite; pbr = prealar bridge; pls = pleural sulcus; Pt = pterostigma; ptm2 = mesothoracic peritreme; ptm3 = metathoracic peritreme; R = radius vein; Rs = radial sector vein; tems = transepimeral sulcus; tsp2= mesothoracic spiracle; tsp3= metathoracic spiracle.

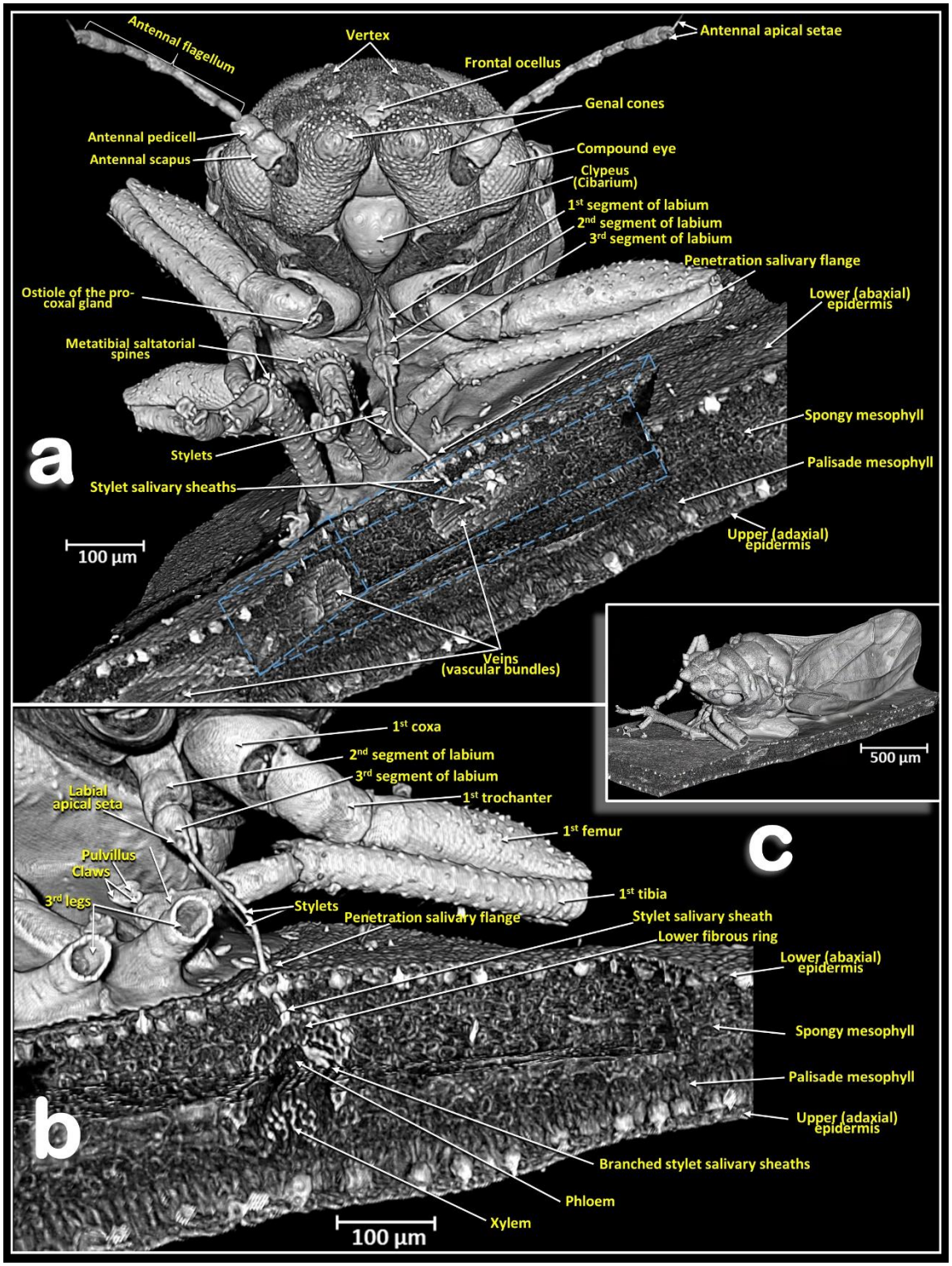

Figure 7.- Volume-rendered close-up images (**a**, **b**) of a male *Diaphorina citri* feeding on an orange seedling tree leaf (**c**) in two perspective views: frontal (**a**) right-frontal (**b**). In (**a**) the virtual box-cut made to visualize the stylets and salivary sheaths inside the leaf and vascular bundle is indicated with a dotted blue line.

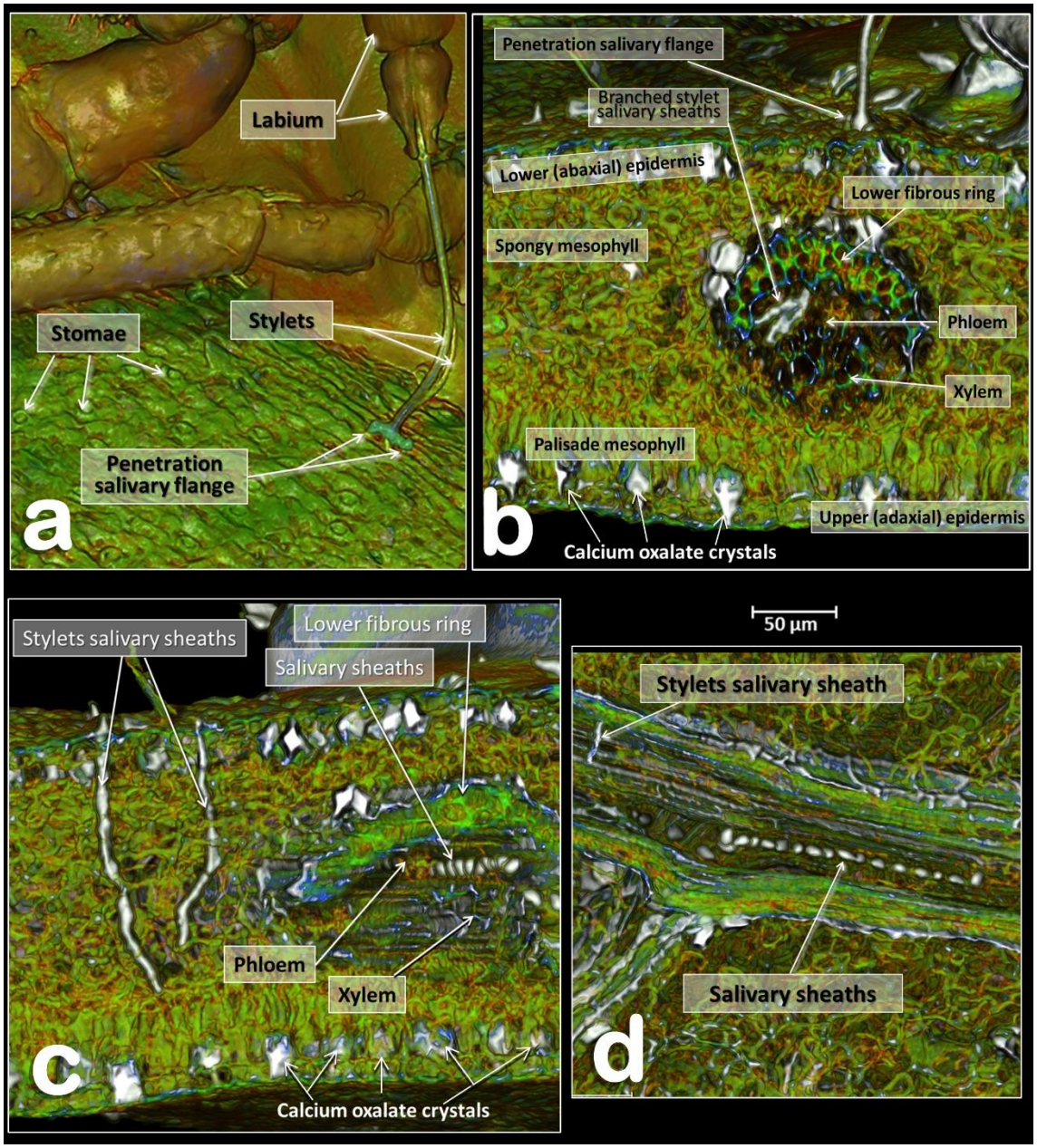

Figure 8.- Volume-rendered images of details of an orange seedling tree leaf where a male *Diaphorina citri* was feeding on the abaxial surface of the leaf. Detail of the stylets and penetration point (**a**). Transverse cut of the leaf showing the penetration point of the stylets, different anatomical structures of the leaf and the tip of the stylets as branched stylet salivary sheaths inside the phloem (**b**). Transverse cut of the leaf showing abandoned stylets and salivary sheaths inside the phloem of a vein (**c**). Middle plane-cut, between the lower and upper surface of the leaf, at the level of the vein shown in (**c)** and (**d**).

tracheal trunks are interconnected by latero-ventral segmental and spiracular tracheae.

The dorsal vessel (heart). This is located in a dorsal-medial abdominal position, and situated immediately below the 4^{th}-7^{th} abdominal tergites (Fig. 10a). It has four dilated heart chambers each opened by a pair of lateral ostia (Figs. 9a, 10c and Supplementary Video S2). The dorsal vessel is extended forwards into an aorta located in an anterior position, starting at the third abdominal segment, (Fig. 10b, 10c). Lateral to each heart chamber are fascicles of alary muscles, (delta-wing-shaped, Fig. 10b).

The digestive system and associated structures. The ACP has a rather complex piercing and pumping feeding apparatus (labium, mandibular/maxillary stylets and a cibarial pump). The digestive system *sensu stricto* (Figs. 11-15 and Supplementary Videos S5-S9) opens to a pharynx running anteriorly inside the cibarium (clypeus) (Figs. 15f-h); the pharynx crosses the ventral nerve cord between the brain and the subesophageal ganglion and has a precibarial-pump (the salivary pump) (Figs. 17c-d and Supplementary Video S4) and also a cibarial pump (Fig. 15c,h) with an internal flapping diaphragmatic cibarial valve (Figs. 15d). The cibarial pump is connected to four pairs of cibarial dilator muscles. Dorsally each pair of cibarial dilator muscles join medially and appear v-shaped; the first pair of muscles are clearly the largest, decreasing in size from the 1^{st} to the 4^{th} (Fig. 15g and Supplementary Video S7).

The esophagus. The pharynx continues into the esophagus which, after a large loop, turn backwards, passing on and close to the ventral nerve cord (Figs. 11a, 11c, 12b and Supplementary Video S5), and then dilates slightly before connecting with the filter chamber (Figs. 15d, 15e and Supplementary Videos S5, S10).

The midgut. The esophagus connects with a dilated afferent midgut (crop), runs backwards to the right and immediately down to form the medial descending midgut arm. After a ventral midgut loop the ascending midgut arm goes left and dorsally, and, after a fore dorsal midgut loop, a right fore midgut dorsal arm runs backwards and down to a right descending dorsal middle arm; from here and after a right midgut middle loop, is the start of the right ascending midgut dorsal

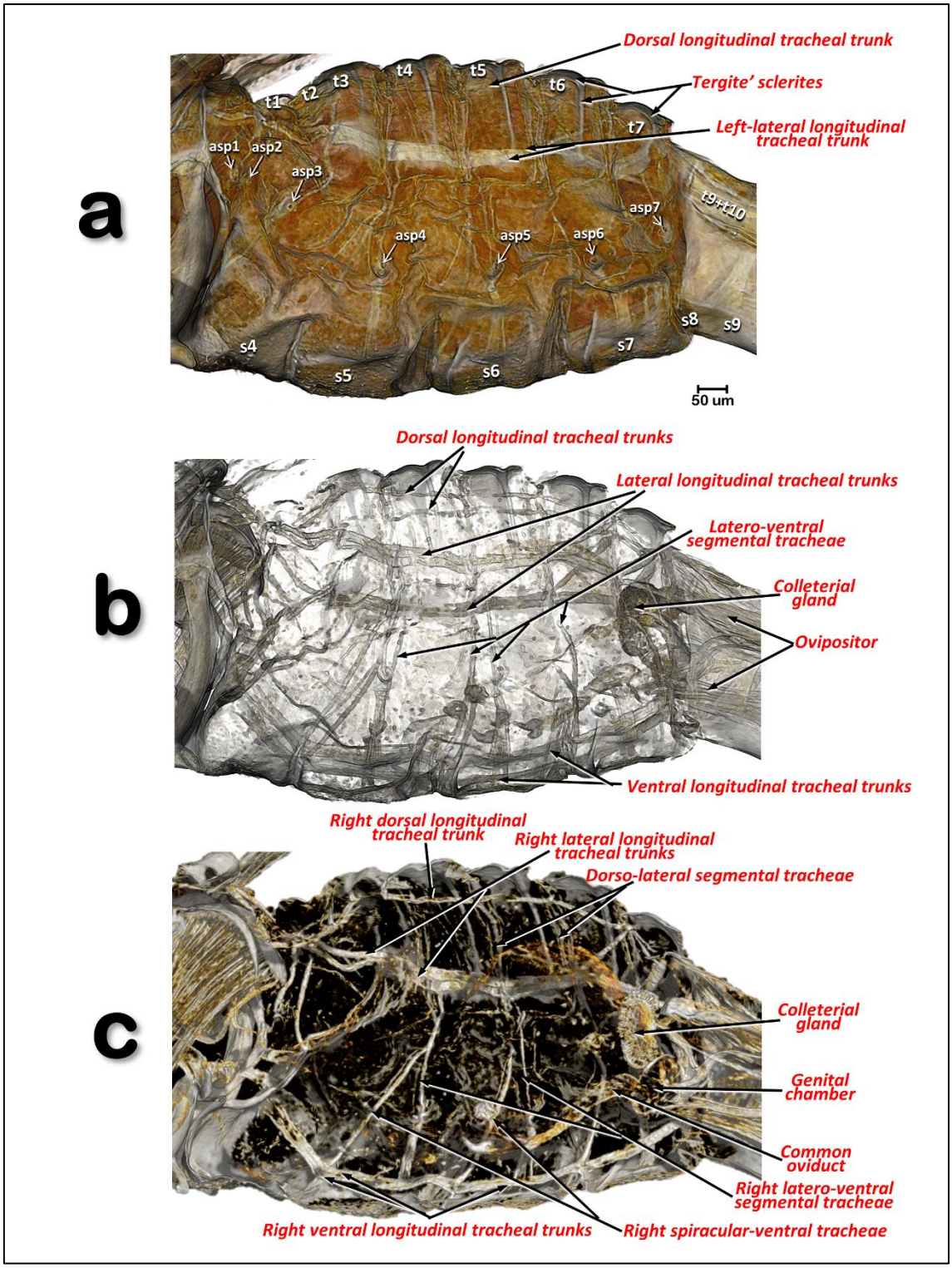

Figure 9.- Volume-rendered images of a left-lateral view of the abdomen of a female, virtually cleared to show the respiratory system. Slightly cleared (**a**) and cleared (**b**, **c**), permitting observation of the tracheal tubular system. Internal view of the right lateral half (**c**). Abbreviations: asp = abdominal spiracle; the abdominal tergites and sternites are labelled sequentially with the letter 't' and 's', respectively.

middle arm in which the 1st midgut appendage is inserted (located in a right-fore position); after this, the right hind midgut dorsal arm continues and joins the 2nd midgut appendage (located in a right-hind position); after this, the left hind midgut dorsal arm continues forwards (the 3rd midgut appendage connects to it and is located in a left-hind position immediately after the connection of the 2nd midgut appendage), and immediately turns down, forming a short left descending midgut dorsal arm which, after a left midgut middle loop, turns upwards forming a short left ascending midgut dorsal middle arm, and then the afferent midgut; the midgut connects to the filter chamber in a posterior dorsal position. The walls of the midgut have very conspicuous rhomboid cells (Fig. 13a and Supplementary Video S8)

The appendages of the midgut. The four appendages show a parallel symmetrical arrangement in pairs, with the 1st and 4th directed forward and the 2nd and 3rd directed backwards (Figs. 11, 12, 13a-c and Supplementary videos S5, S6, S8). They show a tubular structure; the walls are formed from a single layer of cells delimiting an internal lumen (Figs. 11d, 11e, 13, and Supplementary Videos S5, S6, S8).

The inner hindgut. After the midgut, a narrower inner hindgut continues inside the filter chamber; it turns one way and forms a U-turn on the right side, makes two complete turns and exits the filter chamber on the front left side, just behind the esophagus insertion. The inner hindgut progressively increases in diameter; by the last turn it has doubled in diameter, but then thins out as it leaves the filter chamber to form the outer hindgut (Fig. 14 and Supplementary Video S9).

The filter chamber. This is located in the third of the abdomen, in a dorsal-central position and partially extending into the 3rd abdominal segment (Fig. 12 and Supplementary Video S6). It is inclined at an angle of circa 45º with the anterior part (where the esophagus joins) at the same level as where the thorax separates from the abdomen, and lower than the posterior part (Figs. 11, 12, Supplementary Videos S5 and S6). Within the chamber there are three separate regions, or spaces, enclosed in a sheath and surrounded by the inner hindgut. The three regions can be distinguished from each other: the anterior region is spongy, pyriform (1, bulb) and more voluminous than the others; then there is an

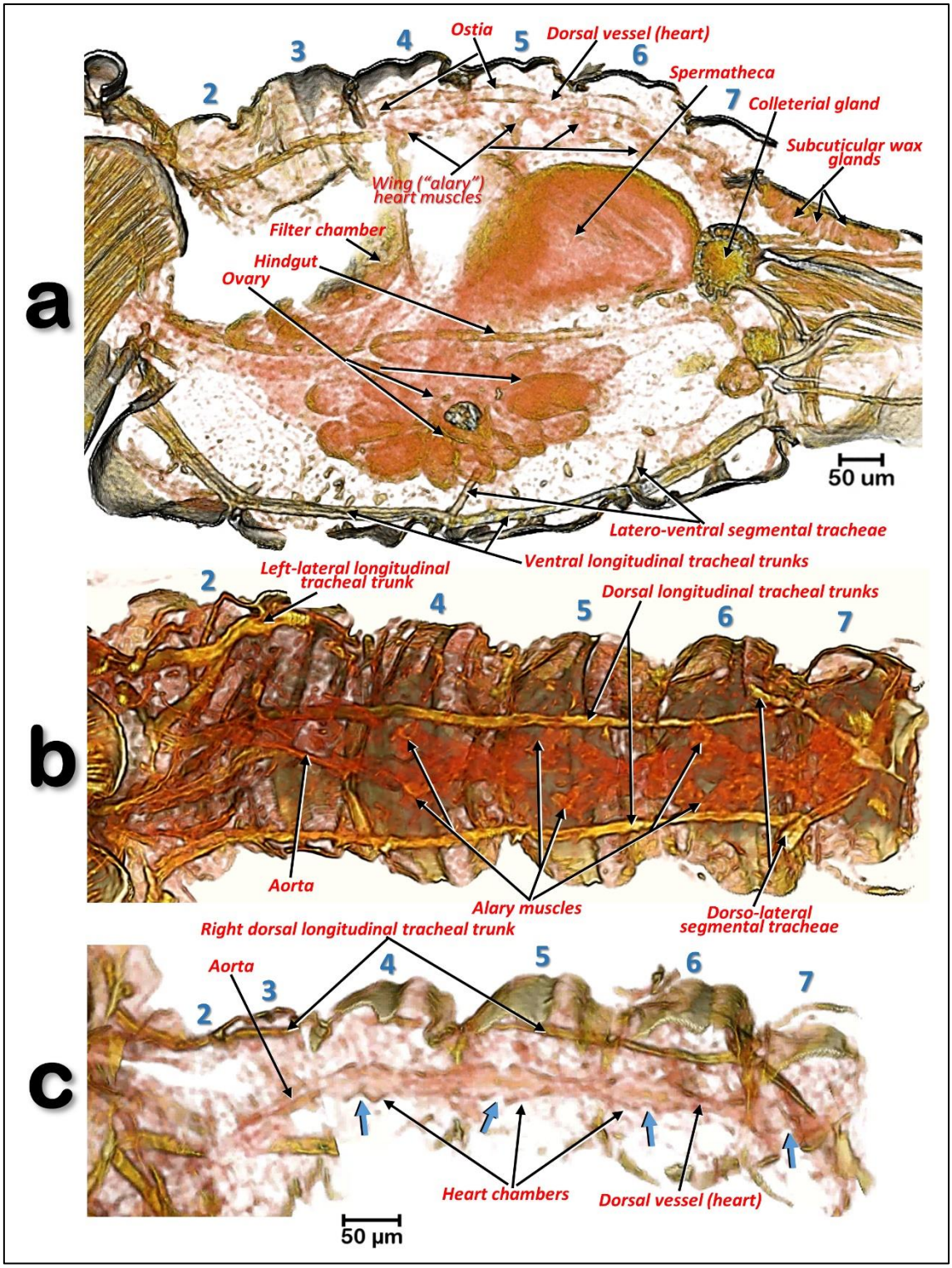

Figure 10.- Volume-rendered images of different slice cuts of the abdomen of a female *Diaphorina citri.* Abdominal oblique sagittal slice, at the level of the dorsal vessel and left ventral tracheal trunk (**a**). Internal view of the dorsal abdominal region (**b**). External view of the dorsal vessel (tergites have been virtually removed by software) (**c**). In (**c**) the blue arrows indicate the ostia of the heart chambers. Abdominal segments are numbered sequentially.

Intermediate region (2) and a posterior region (3) that are of progressively smaller volumes Figs. 14c, d and Supplementary Video S9).

The outer hindgut. The outer hindgut begins at the upper left side of the filter chamber very close behind the point where the esophagus joins (Figs. 13b, d, e, 14a, b, g, h and Supplementary Video S9). It runs above the nerve cord along the length of the abdomen ultimately connecting with the anus (Figs. 11a, 12a and Supplementary Videos S4, S5). The hindgut is posteriorly differentiated into a rectum that, in males, is configured as a long, flared tube; in females it forms a small rectal ampulla, just below the anus (Figs. 11a-c, 12, 17a-d and Supplementary Videos S6, S5).

Salivary glands. The salivary glands are located anteriorly and on both sides of the thorax (Figs. 11a-c, 16a and Supplementary Videos S5-S6). They are vertically arranged in a 'C'-shaped configuration (concave anteriorly) each with three main lobes; each lobe has an acinar configuration with converging bunches of acini (Figs. 16f and Supplementary Video S10).

Cibarial structures. The internal anatomical details of the cibarial structures are shown in Fig. 17 and Supplementary Videos S3, S4. The cibarial space has three large openings, or fenestrations (one dorsal and two laterals), and the walls are reinforced dorsally by the tentorial bridge bar and posteriorly by prolongations of the tentorial arms, forming an oblique bar and a cross-bar. Moreover, there are two ventral ridges giving support posteriorly to the cibarial-pump bed.

The maxillary and mandibular structures. The maxillary and mandibular cones are inside the cibarium (Figs. 17a-c, 17f, 17g and Supplementary Video S3). The maxillary cones are dorsal to the mandibular ones, and connected to the cibarial cross-bar. The maxillary/mandibular retractor/protractor muscles are shown in Fig. 17a. The mandibular cones have a crown-shaped cap (Figs. 17f, 17g and Supplementary Video S3). Stylets emerge from the basal apex of the cones, meeting together in a stylet bundle. Close to the base of the cones, where the stylets emerge, is a small precibarial salivary pump (Fig.17c-e). The stylet bundle can be retracted back and stored in the crumenal pouch; when stored, this forms a characteristic crumenal loop (Fig. 11a, 12b, 15 and Supplementary Videos S5,

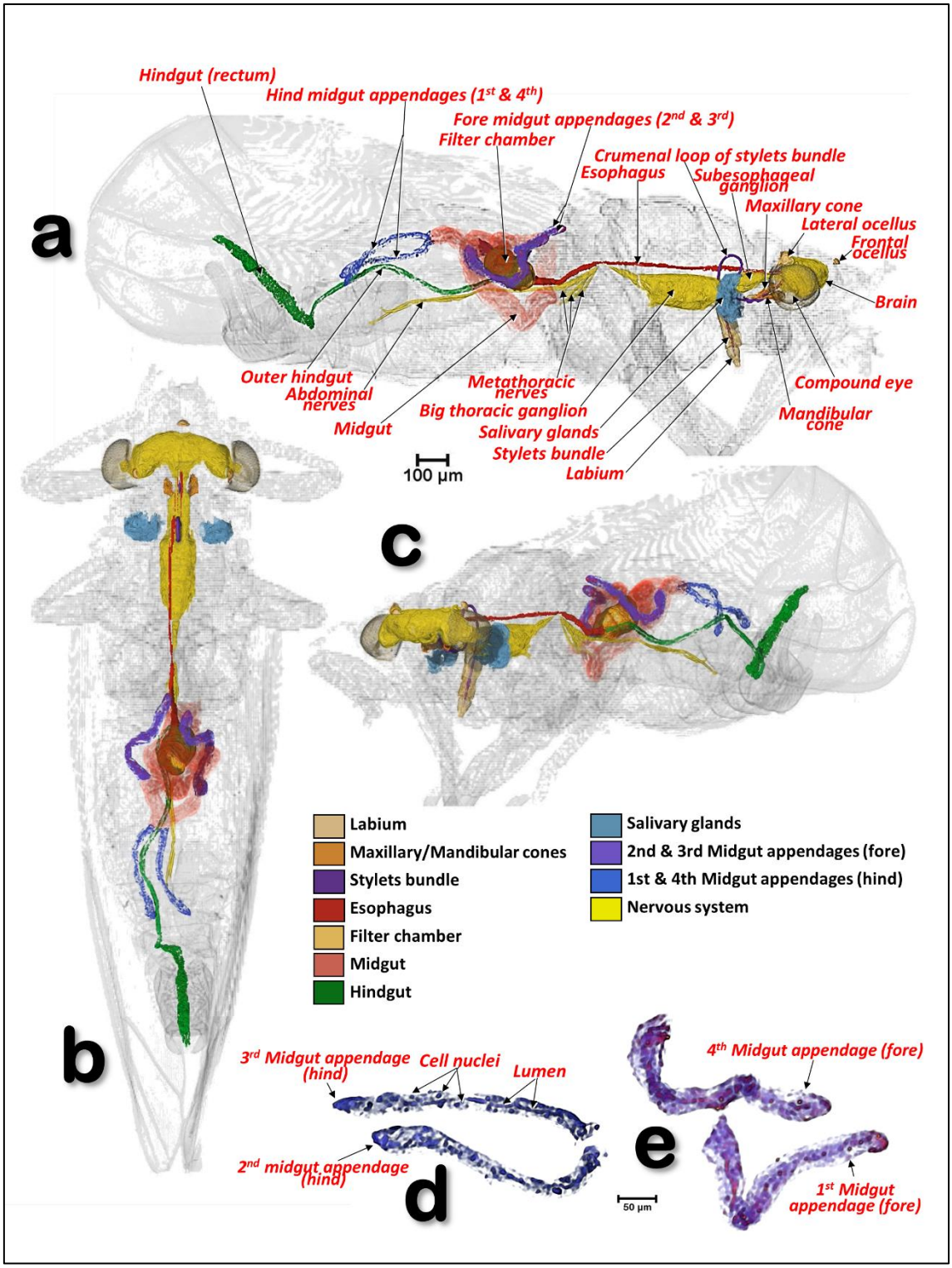

Figure 11.- Volume-rendered images of a male *Diaphorina citri* showing the general position of the nervous system, and the digestive system (including the salivary glands), in different perspective views. Right-lateral (**a**), dorsal (**b**), and left-frontal (**c**). Details of the midgut appendages (**d**, **e**).

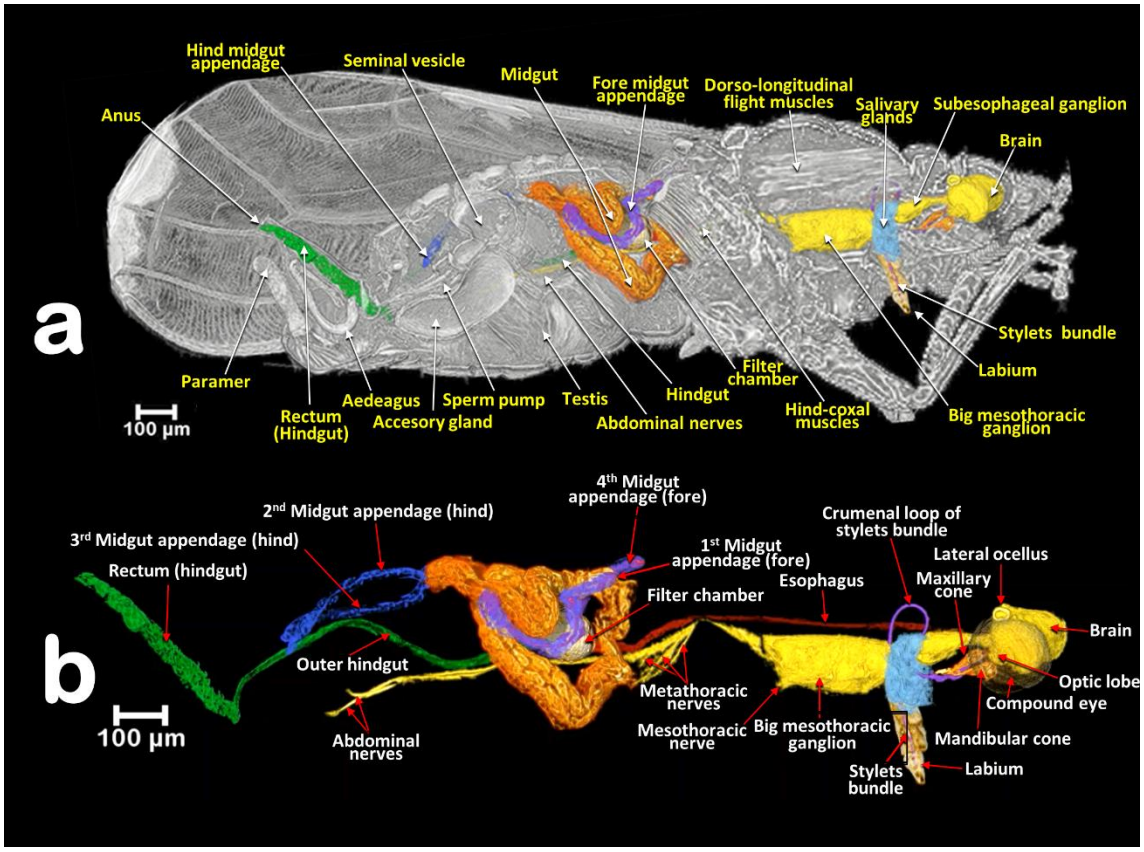

Figure 12.- Volume-rendered images of a male *Diaphorina citri* in a right-lateral view, showing the feeding apparatus, the digestive system (including the salivary glands) and nervous system. Medial sagittal view (**a**). Isolated segmented organs and structures (**b**).

S7). This loop passes through the nerve cord behind the subesophageal ganglion (Figs. 11a, 12b and Supplementary Videos S5-S7).

The nervous system. The nervous system and its spatial relationship with the digestive system is shown in Figs. 11, 12, 15a-c and Supplementary Videos S5, S6. Detailed views of the nervous system in both sexes are shown in Fig. 18, and detailed views of the brain within the head are shown in Fig. 19. The brain has two lateral lobes (each consists of three successive neuropiles: the lamina, the medulla and the lobula complex) forming the optic nerves that connect with the compound eyes (Figs. 18b-d, 18g, 19 and Supplementary Video S11). Anteriorly within the brain there is one central and two lateral mushroom bodies with poorly marked calyces (Figs. 19c, 19d, 19g and 19h). Two circumpharyngeal connectives surround the pharynx and connect with a subesophageal ganglion (Figs. 11a, 12a, 12b, 18b, 18c and 18g). The subesophageal ganglion is connec-

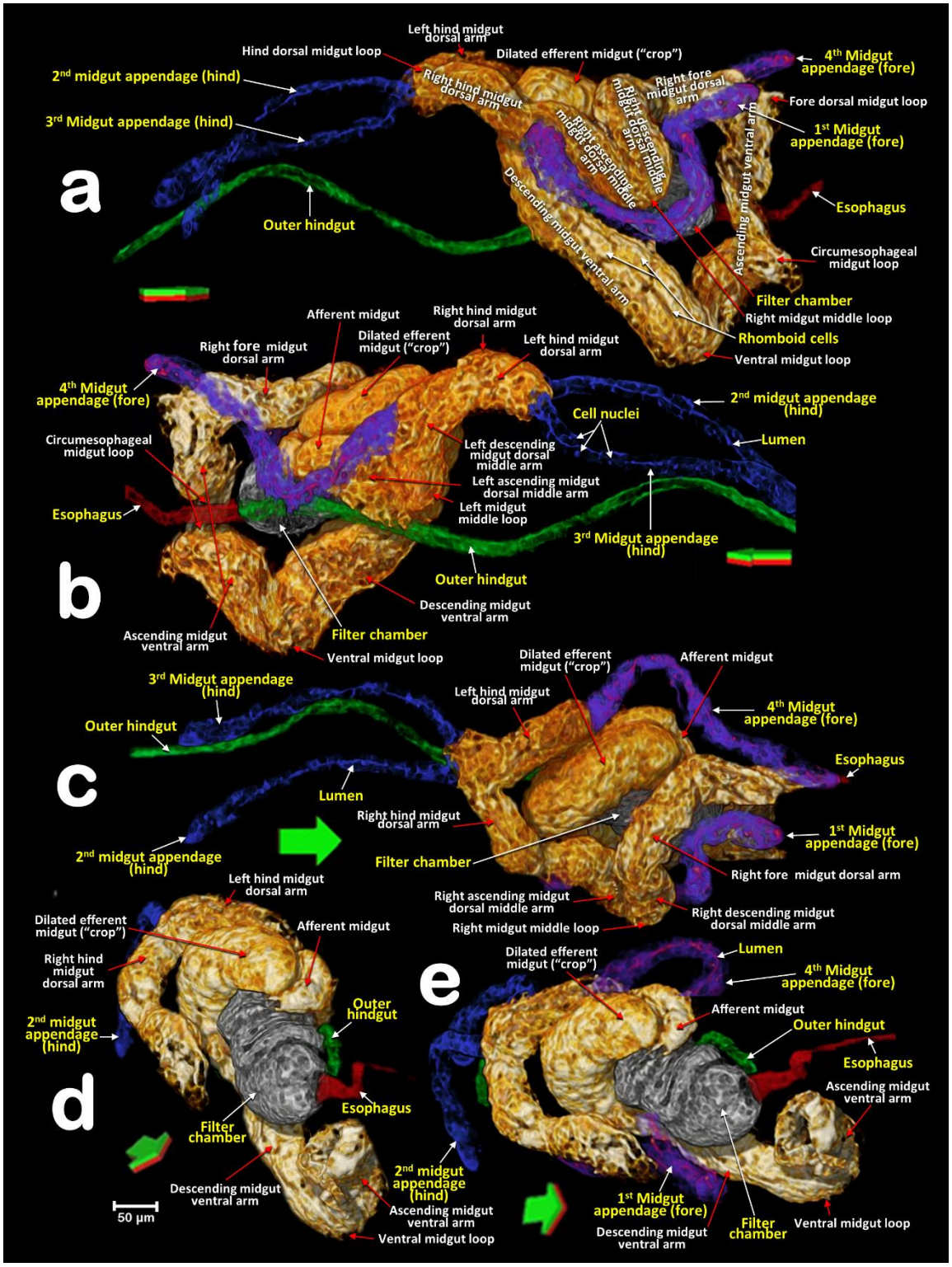

Figure 13.- Volume-rendered close-up images of the digestive system of a male *Diaphorina citri* in different perspectives. Right-lateral (**a**), left-lateral (**b**), dorsal (**c**), right-frontal (**d**) and right-oblique-dorsal (**e**). Arrows indicate the anatomical positions. Green/red surfaces correspond with dorsal/ventral positions.

ted by circumcrumenal connectives to a large, mesothoracic ganglion. Exiting at each side of the mesothoracic ganglion are a pair of prothoracic nerves (anteriorly), and a pair of mesothoracic nerves (posteriorly) (Figs. 12b and 18a-c, 18f, 18g). The large meso-thoracic ganglion is connected to a ventral cord that becomes narrower at the junction of the meso and metathoracic segments. In the metathorax, at the level of the meta-coxae, several ventral meta-thoracic nerves appear, and continue via two abdominal nerves along the length of the abdomen (Figs. 11a, 12b, 18a-c and Supplementary Videos S5, S6).

Tentorium. The cephalic endoskeleton (tentorium) is shown in Figs. 17a-e, 19b-h, Supplementary Videos S3 and S4.

Antennal glands. This is inside the cephalic capsule (head) and there is a sac-like antennal gland connected to each antennal scapus (Figs. 19b-g). Details of the interior of the cephalic capsule including the brain and eyes are shown in Fig. 19 and Supplementary Video S11.

Feeding apparatus. A male feeding on a citrus (orange) leaf is shown in Figs. 6d, 7, 8a and Supplementary Video S3). Penetration of the salivary flange is clearly visible (Figs. 7a, 7b, 8a and 8b), as well as the stylets and salivary sheaths that are inside a vascular bundle of the leaf and reaching the phloem (Figs. 7a, 7b, 8a and Supplementary Video S3). Three different shaped salivary sheaths were observed: branched (Figs. 6d, 7a, 7b, 8b and Supplementary Video S3), rosary-beads (Figs. 8c, 8d) and linear (Fig. 8c). The presence of salivary sheaths resulting from failed piercing/ sucking attempts are shown in Figs. 6d and 8c).

Structure of the citrus leaf. Anatomical structural details of the citrus leaf can be observed in Figs. 6d, 7a, 7b, 8 and Supplementary Video S3).

5.1.6.- Discussion

The terminology we have used for external anatomy maintains the terms most widely used and follows classical entomological papers (Bitsch, 1979; Chapman, 2013; Gillott, 2005; Gullan & Cranston, 2010; Matsuda, 1976a; Pesson, 1951; Snodgrass, 1935; Triplehorn & Johnson, 2005) and specific psylloid publications (Cicero, 2020; Drohojowska *et al.*, 2013; Hodkinson & White, 1979; Ossiannilsson, 1992; Ouvrard *et al.*, 2002). The adult antennal olfatori sensillae

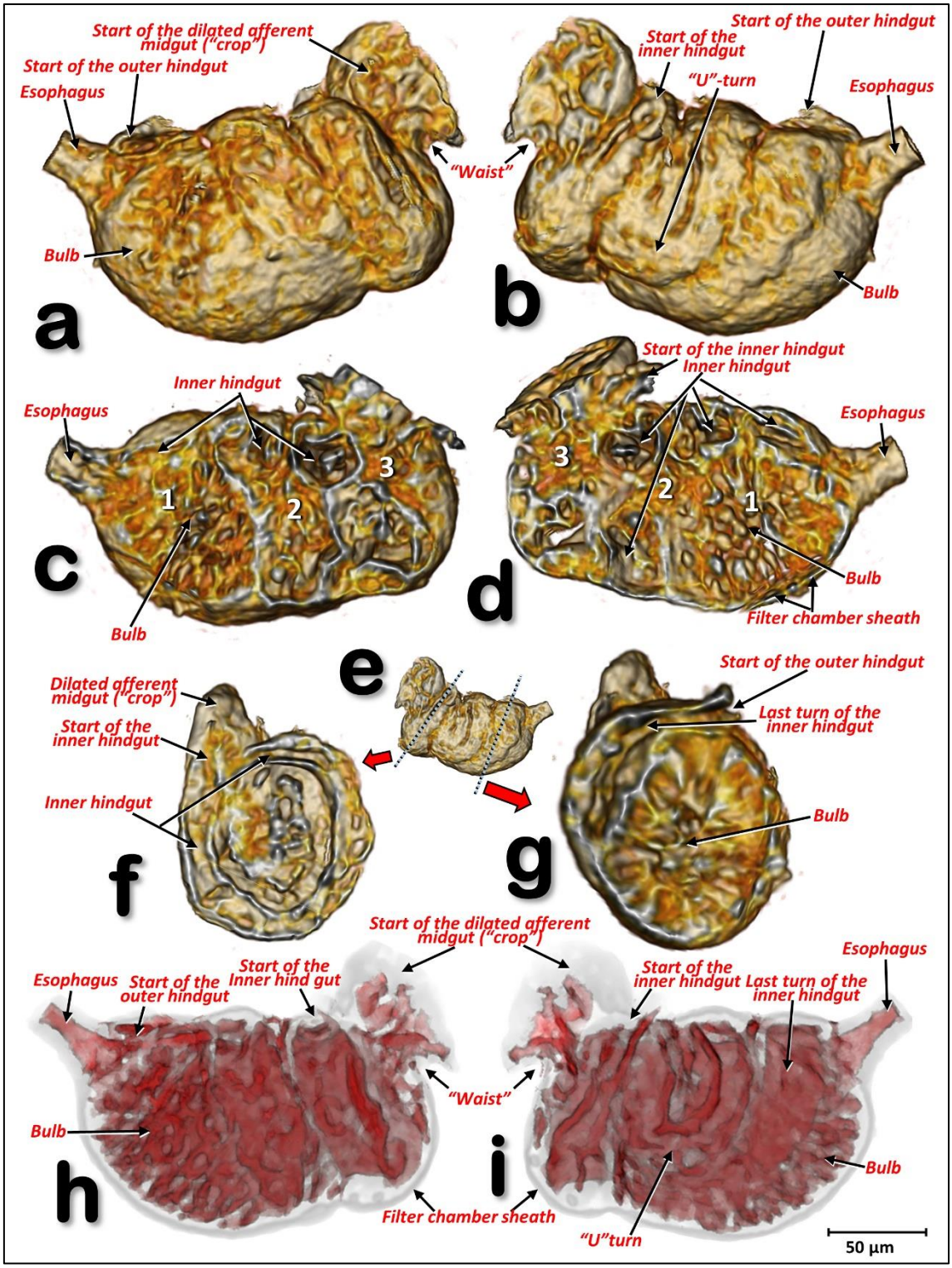

Figure 14.- Volume-rendered close-up images of the filter chamber of a male *Diaphorina citri*, in different perspective views: left-lateral (**a**, **c**, **h**), right-lateral (**b**, **e**, **i**). Internal structure views after virtual cuts: sagittal (**c**, **d**), transverse (**f**, **g**) through positions marked with blue dotted lines in (**e**), and reconstruction of the cavities (spaces) inside the filter chamber (**h**, **i**).

of *Homotoma ficus* were recorded in the XIXth century as 'odour pits' (*Geruchsgruben*) (Witlaczil, 1885), and described as present in the flagellar articles, just as we, and other authors(Arras *et al.*, 2012; Zheng *et al.*, 2020), have observed them in the ACP. The olfatory function of these structures was assumed and, therefore, the term rhinaria frequently used to describe them (e.g. (Burckhardt, 1987; Hodkinson & White, 1979; Onagbola *et al.*, 2008; Ossiannilsson, 1992; Zheng *et al.*, 2020)). Using SEM it has been possible to confirm that these rhinaria correspond to campaniform sensillae (Arras *et al.*, 2012; Zheng *et al.*, 2020) and by investigating odorant-binding proteins, odor receptors and odour-degrading enzymes, their function as odour receptors has been demonstrated (Arras *et al.*, 2012).

Within the feeding apparatus, the labium of *Psyllopsis fraxinicola* has been described and visualized previously by Witlaczil (Witlaczil, 1885) as a three segmented structure. This author also drew schematics of the maxillary/mandibular cones inside the cibarium and the associated protractor/ retractor muscles; his findings fit with our results for the ACP and also with a detailed SEM study (Garzo *et al.*, 2012) describing the existence of a posterior slit on the 3rd labial segment. In another study an association between this posterior slit and a dorsal groove was described (Cicero, 2020). However, we observed a long anterior (dorsal) dividing slit, rather than a groove (Cicero, 2020). The 3rd segment of the ACP's labium has a configuration very similar to that seen by SEM in *Cacopsylla chinensis* (Liang *et al.*, 2013) and the melaleuca psyllid, *Boreioglycaspis melaleucae* (Ammar *et al.*, 2015).

in Hemiptera the labium is also known as the rostrum(Chapman, 2013). As a simplification, the term rostrum has also been used by Cicero and colleagues (Cicero, 2020; Cicero *et al.*, 2015) to describe the external, ventral aspect of the ventralized portion of the head, i.e. a consolidation of the clypeus, postclypeus, anteclypeus, and labrum described by classical authors. In this sense, to simplify descriptions and to avoid uncertainty inherent in attempt to homologize structures (Dmitriev, 2010) and avoid confusion, we have used the term clypeus, rather than rostrum, to refer to the ventral bulging structure of the head which encloses the cibarium. We have chosen this because is the term most commonly

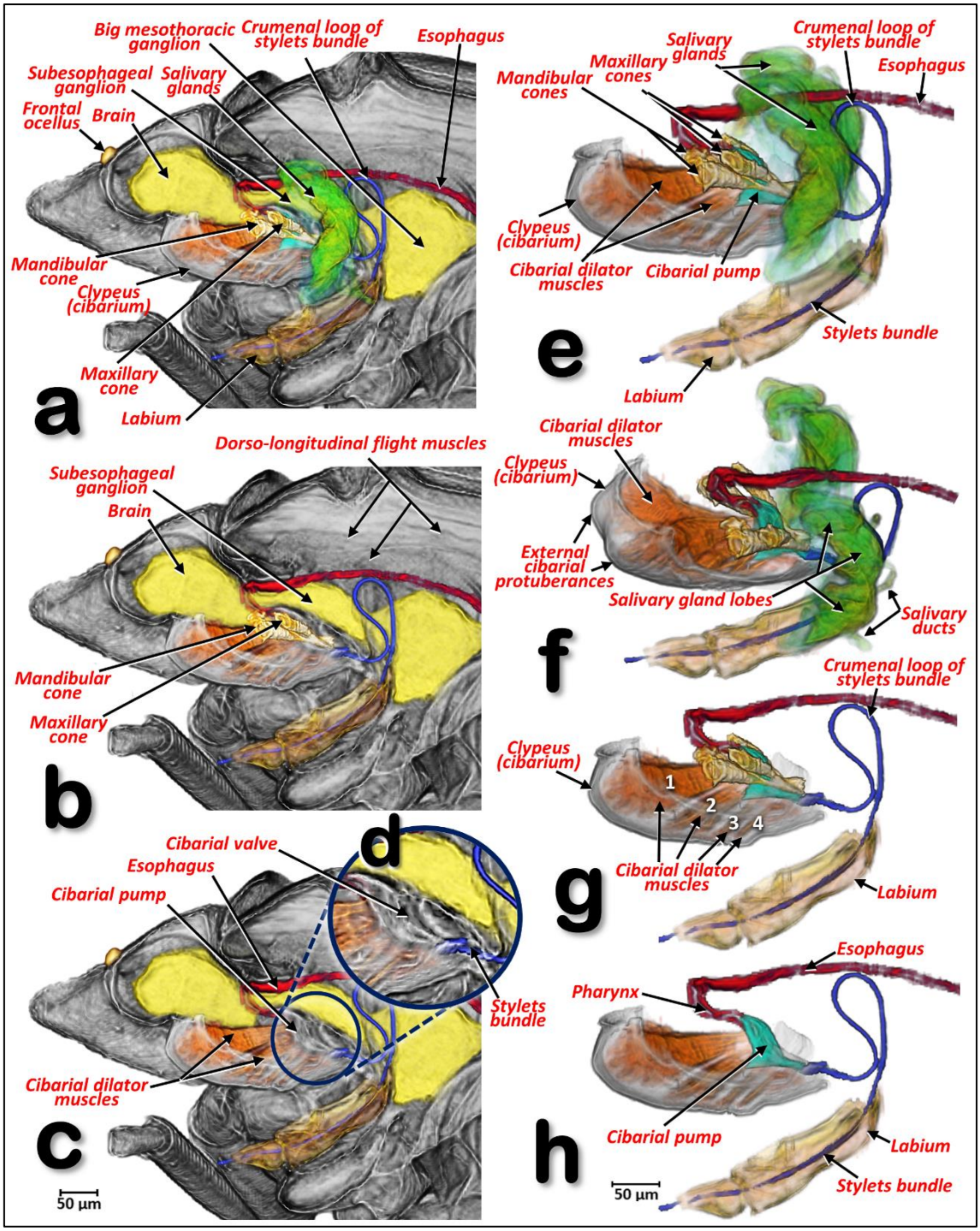

Figure 15.- Volume-rendered images, in a left-lateral view, of the fore region of a female *Diaphorina citri*. In the left-hand column (**a**-**d**) the nervous system, the feeding apparatus, the anterior part of digestive (including the salivary glands) and cibarium are shown. The salivary glands were virtually removed using software in (**a-c)**, and the mandibular and maxillary cones were virtually removed in (**c**). Close-up detail of the cibarial pump (**d**). In the right-hand column, the segmented structures are shown separately from the rest of the animal (**e**-**h**) (**a**, **g**, **h** = left-lateral; **f** = left-lateral, slightly dorsal-oblique). The salivary glands were virtually removed using software from (**f**-**h**), and the mandibular and maxillary cones were virtually removed from (**h**).

used for that structure in homopteran insects (Pesson, 1951; Snodgrass, 1935) and specifically in psyllids (Ammar *et al*., 2015; Brittain, 1922; Grove, 1919; Hodkinson & White, 1979; Liang *et al*., 2013; Saunders, 1921; Weber, 1929).

For *Psylla mali*, a number of studies have included realistic drawings of the feeding apparatus and the maxillary/mandibular cones inside the cibarium(Grove, 1919; Saunders, 1921; Brittain, 1922; Weber, 1929); these have a very similar configuration to that which we describe here for ACP. More recently, there have been several studies on the structures inside the cibarium of several species (Brown *et al.*, 2016; Cicero, 2017; Cicero *et al.*, 2015; Cicero & Brown, 2009; Liang *et al.*, 2013), including ACP (Cicero, 2020; Cicero, Alba-Tercedor, *et al.*, 2018; Garzo *et al.*, 2012). Although all these studies were impressive, they were limited because the structures described had to be dissected from the insect and subjected to preparation processes such as transparency digestion with KOH; this caused distortion and influenced the results obtained. For instance, the typical crown-shaped cap of the mandibular cones (observed also in other species e.g. *P. mali* (Weber, 1929)) were missing in SEM images, appearing only as a medial expansion of the cap that the authors termed the auricle (Brown *et al.*, 2016; Cicero, 2017; Cicero *et al.*, 2015; Cicero, Alba-Tercedor, *et al.*, 2018).

Detailed studies of the thorax of various psylloid species have been published (Brittain, 1922; Drohojowska *et al.*, 2013; Ouvrard *et al.*, 2002; Saunders, 1921; Weber, 1929) but, to our knowledge, there have been no detailed studies of the thorax of ACP .

Leg glands, and particularly coxal glands, have been described in other insect species, e.g. hymenopterans (Billen, 1997, 2009; Billen & Ito, 2006; Da Cruz-Landim *et al.*, 1988; Nijs & Billen, 2015) but, to our knowledge, not for any psylloid species. However, in published SEM images of species in the genus *Cacopsylla* (Drohojowska *et al.*, 2013) coxal orifices (ostioles) are clearly visible, just as we observed them in ACP.

Antennal glands have been reported in other insect species including ants (Bin, 1986; Keil, 1999; Renthal *et al.*, 2008); Dams observed antennal glands in the

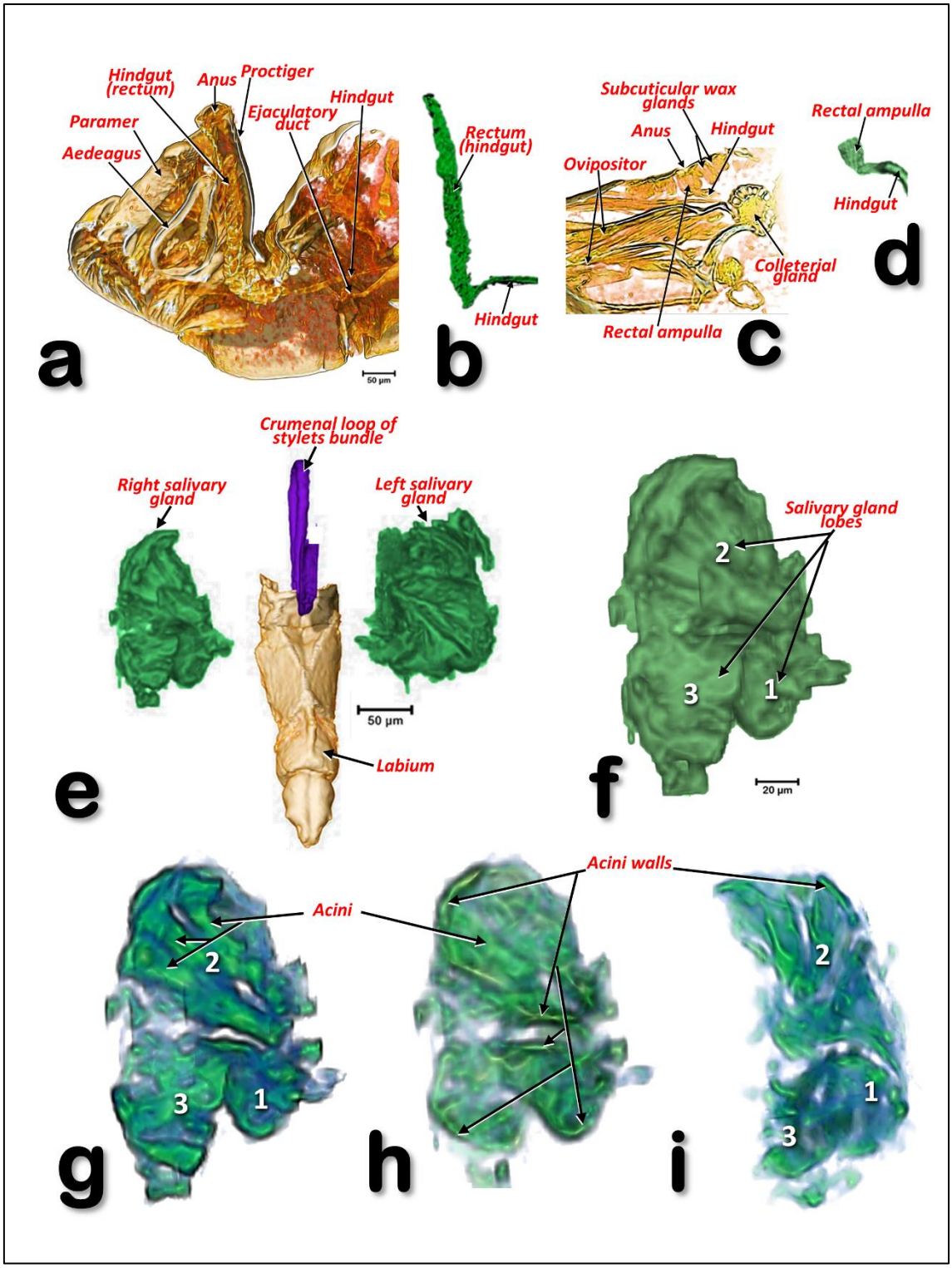

Figure 16.- Volume-rendered images of the abdominal tips of a male *Diaphorina citri* (**a**, **b**) and afemale *D. citri* (**c**, **d**), showing the rectal differences (**b**, **d**). Volume-rendered images of the salivary glands of a male *D. citri* in a frontal (**e**-**h**), and in an inner right-lateral views (**i**). Un-cleared (**e**, **f**), and cleared volume-rendered images (**g**-**i**). Slice ca. 7 µm thick (**h**).

scapus of males from the hymenopteran species *Melittobia australica* and concluded: “Presumably males rely on chemical and tactile stimuli for locating females and for precopulatory behaviour. Chemical information appears to play an important role in the behaviour of both sexes. The size of the complex gland in the male scape and the role of this segment during precopulatory behaviour suggests that the female receives a considerable chemical input during antennation” (Dahms, 1984). Moreover, males of ACP are known to be attracted to a volatile pheromone produced by females, and to colonize citrus plants that were colonized, or had been previously, colonized by females (Wenninger, 2008). However, the location for pheromone production has not been identified. Considering the basal location of the coxal glands, it is quite plausible that, if they produced pheromones, they would be readily transferred to plant surfaces during colonization. It is also possible that the antennal glands could be involved in the production of chemicals that aid recognition during close-range courtship. In fact, in the recent revision of ACP mating behaviour by Mankin and Rhode (Mankin & Rohde, 2020), short-range semiochemicals were shown to play a role in mate-finding in several, but not all, psylloid species. Future research should investigate the secretory role of these structures and, where appropriate, the chemical composition, function and use of the compounds produced as attractants.

There are some discrepancies in the literature concerning the interpretation of wing venation (e.g. between the general publication on psyllids by Hodkinson and White (Hodkinson & White, 1979) with the publication of Ossianilson(Ossiannilsson, 1992)). We followed Yen and Burckhardt (Yen & Burckhardt, 2017) for assigning names to the veins of the fore wings and Ossianilson(Ossiannilsson, 1992) for the hind wings. Venations of the wings are characteristically tubular structures, clearly visible in cross-section. The structure generally known as the Cu_2 (Brown & Hodkinson, 1988; Hodkinson & White, 1979; Ossiannilsson, 1992) is not tubular and cannot be considered as a vein; it is in fact a fold on the cubital area. In fact, at the end of the XIXth century Mally (Mally, 1894) considered it to be a suture, the ‘claval suture’. We name it the cubital fold but, to aid recognition in the figures we have retained the abbreviation Cu_2 in parenthesis.

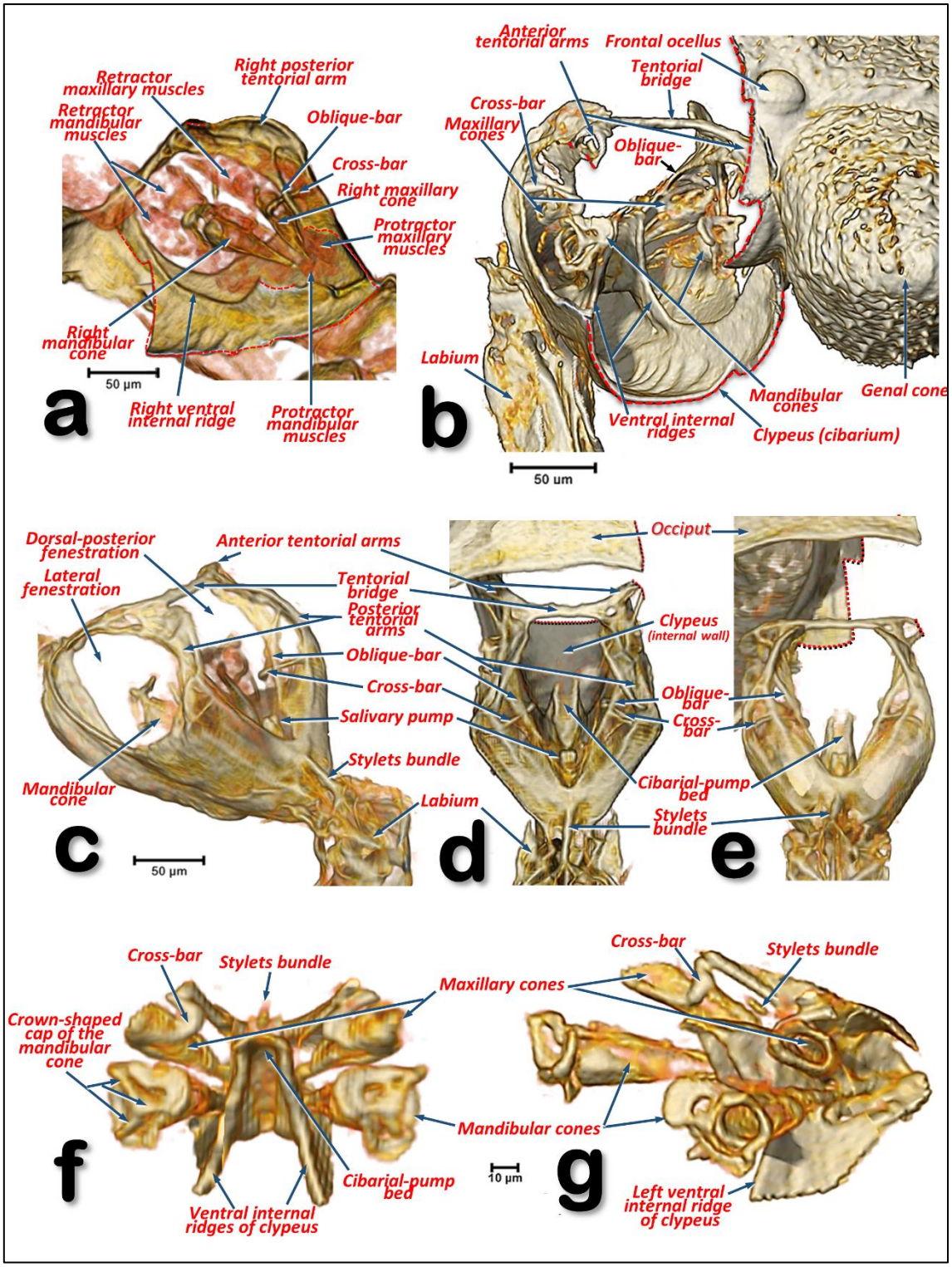

Figure 17.- Volume-rendered detailed images of the feeding apparatus and tentorium of a male Diaphorina citri in different perspective views. Left-lateral (a, g), right-frontal (a, b), left-posterior (c), dorsal (d), posterior (e), frontal (f), and. Volume close-up images of the cibarium: internal right-side view, with the maxillary and mandibular cones rendered (a), and only the 'harder' structures (b-g). Details of the mandibular and maxillary cones (f, g). To be able to see inside the cibarium, different virtual cuts were made using software (cuts are indicated with dotted red lines).

In psyllids the first abdominal segments are reduced, and are joined to the segments of the thorax or abdomen. This makes it difficult to determine how many of them there are. Thus, to date there has been no consensus concerning the visible sclerites of the abdominal segments (Bitsch, 1979; Matsuda, 1976b; Muir, 1930; Pesson, 1951; Zucht, 1972). In fact, many publications on psyllids avoid the controversy and do not number these segments e.g. (Brown & Hodkinson, 1988; Hodkinson & White, 1979).

There are issues with interpretation of the abdominal segment sclerites but, as this is not the focus of this paper, we have adopted the numbering system for tergites and sternites that fits a (difficult) general consensus, but particularly Matsuda's interpretation (Matsuda, 1976b). The results we present here complement those we have already published of the abdominal anatomy and genitalia (terminalia) of male (*Alba-Alejandre et al., 2018*) and female ACP (Alba-Alejandre *et al.*, 2020).

In psylloids, the small size, and sometimes cryptic position, of some respiratory spiracles has resulted in controversy about their number and location (Muir, 1930), (Heslop-Harrison, 1952) but, after an extensive revision, the conclusion was that all psyllids have three pairs of thoracic spiracles (Heslop-Harrison, 1952) and specifically: "so far as can now be ascertained, no psyllid possesses more than seven functional pairs of abdominal spiracles, although the possibility of an eighth pair, particularly in the male, is not overlooked". This agrees with our observation of seven pairs of abdominal spiracles in ACP; we did not find an eighth pair. Moreover the 1st and 2nd abdominal pairs of spiracles are very close to each, as previously observed for *P. mali* (Muir, 1930).

The tubular tracheal system of psylloid species has not previously been studied and described in detail, particularly for adults. Witlaczil (Witlaczil, 1885) described and presented images of it in a nymph of *Trioza rhamni*, but recorded that it was difficult to observe in adults; he also included a schematic diagram of the dorsal view the thoracic tracheal tubes of *P. fraxinicola*, and a lateral view of the thoracic tracheal trunks of *Rhinocola speciosa*. Similarly, a recent paper using the lactic acid clearing technique provided visual evidence, but not details, of tracheal tubes in a nymph of *Cyamophila willieti*(Ruan *et al.*, 2018). To our knowledge, our

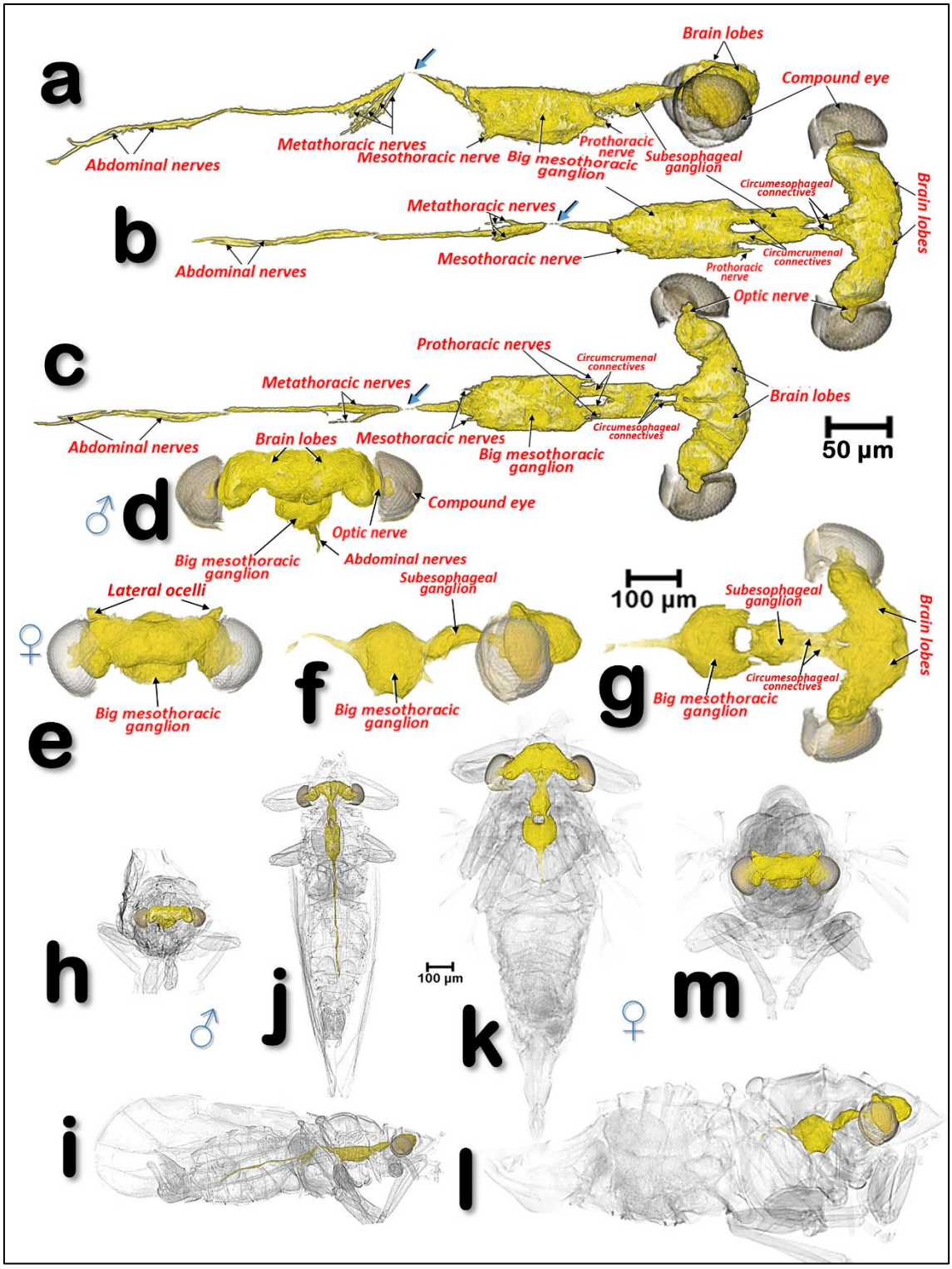

Figure 18.- Volume-rendered images of the nervous system of a male *Diaphorina citri* (**a**-**d, h**-**i**), and a female *D. citri* (**e**-**g**, **k**-**m**). Views are: right-lateral (**a**, **f**, **i**, **l**), dorsal (**b**, **g**, **j**, **k**), ventral (**c**) and frontal (**d**, **e**, **h**, **m**). Blue arrows indicate a narrowing of the ventral cord just as it passes through the wall between the meso- and metathorax (**a**-**c**). Note that in the upper images (**a-g**) the scale for the male and female are not the same, and that in the female only the beginning of the abdominal nerves are rendered.

results on the abdominal tracheal tubular system of ACP represent the most detailed study to date. In the future the micro-CT technique described for coffee berry borer beetle(Alba-Tercedor *et al.*, 2019) could be used to study the ACP respiratory system in even greater detail. However, the micro-CT technique scans specimens that are either anesthetised or have just been killed, i.e. requiring work on living insects; as ACP is an invasive pest and there is a potential risk of escape, this would represent a difficulty for us in Spain.

The circulatory system of insects is responsible for movement of the haemolymph into the haemocoel spaces where organs are immersed. The haemolymph enters various contractile chambers of a dorsal vessel (heart) and is pumped out through an anterior aorta. This is considered as an open circulatory system; it does not play an important role in the transport of gases which is achieved by an aero-vascular system formed from a complex of tubes (i.e. the tracheal system) (Chapman, 2013; Gillott, 2005; Snodgrass, 1935; Wigglesworth, 1930). The heart and anterior aorta was first studied and images presented by Witlaczil(Witlaczil, 1885) in two psyllid species; even though his drawings were largely schematic, descriptions of the abdominal position and extension of the heart in *R. speciose*, and the extension and lateral ostioles of *Psylla buxi*, are in full agreement with our results for ACP. Thus, to date, our results represent the most detailed study of the tracheal system of psylloids, and the only one for ACP.

The alimentary canal (digestive canal *sensu stricto*) of psylloids including ACP, is, with the external anatomy, the most studied and visualised organ (Ammar *et al.*, 2011, 2016; Brittain, 1922; Brown *et al.*, 2016; Cicero, 2020; Cicero, Hunter, *et al.*, 2018; Cicero & Brown, 2009; Ghanim *et al.*, 2016, 2017; Kruse *et al.*, 2017; Witlaczil, 1885). Until the present study, the most detailed studies on adult ACP were those of Cicero *et al.*, (Brown *et al.*, 2016; Cicero, 2020; Cicero & Brown, 2009) based on dissections and images taken using optical and electronic microscopy, which allowed the production of schematic drawings that summarized the general organisation of the alimentary canal.

Snodgrass (Snodgrass, 1935) described the typical homopteran alimentary canal as having a ventriculus consisting of three parts: 1st ventriculus (an anterior enlargement lying immediately posterior to the stomodaeal valve and enclosed in

the filter chamber); 2nd ventriculus (a croplike sac serving as a storage reservoir); and the 3rd ventriculus (a long, tubular section, the functional stomach of the insect, which turns anteriorly to re-enter the filter chamber). Psylloids including ACP all show this organisation, specifically we found: the 1st ventriculus comprised of a bulb and two spongy spaces inside the filter chamber; the 2nd ventriculus comprised of the dilated efferent midgut ('crop'), with a transitional descending midgut ventral arm (in which the rhomboid cells are very conspicuous as they are in the efferent dilated midgut); and the 3rd ventriculus after the ventral midgut loop and continuing on to the inner hindgut inside the filter chamber. This was similar to previous descriptions and figures (Brown *et al.*, 2016; Cicero, 2020; Cicero & Brown, 2009). However, dissection and associated manipulation, some the anatomical positions of structures in these earlier studies do not correspond with the actual arrangement inside the insect as we observed using micro-CT. For instance, it is stated that "the esophagus enters the filter chamber vertically", but with micro-CT we see that the esophagus descends and turns almost horizontally at the dilated end before entering the filter chamber. Similarly, earlier studies found that the 1st ventriculus (inside the filter chamber) was formed from an 'upper' (the bulb) and a 'lower' ventriculus, but micro-CT shows that the bulb is anterior and situated in a lower position compared with the posterior part of the 1st ventriculus.

In general, the alimentary canal of insects starts with the mouth, ends with the anus and consists of three main parts: foregut (stomodaeum), midgut (mesenteron) and hindgut (proctodaeum). In contrast with the midgut, the foregut and hindgut are ectodermic derivates and are chitinized. The foregut consists of the preoral cavity, the mouthparts, the pharynx and the esophagus. From here, food enters the midgut and eventually the hindgut. Waste is excreted through the posterior opening (anus) of the alimentary canal (Chapman, 2013; Gillott, 2005; Snodgrass, 1935). If we follow this general scheme with the corresponding terms for the ACP, the mouthparts correspond to the mandibular and maxillary stylets that are protected inside the labium and together form an alimentary canal (Cicero, 2020; Garzo *et al.*, 2012). Adaptation to a piercing/ sucking feeding strategy means that what should strictly be considered as the preoral cavity and mouth is controversial in homopterans (Cicero, 2020). The pharynx corresponds

to the anterior part of the alimentary canal, it has a small enlargement, containing the precibarial salivary pump (our observation of this in ACP had a similar configuration to that described and visualised for *P. mali* by Grove (Grove, 1919) and Weber(Weber, 1929), and for *Bactericera cockerelli* by Cicero *et al.,* (Cicero *et al.*, 2015)), and a further bigger enlargement which, together with the dilator muscles, formed the cibarial pump. The midgut extends from the esophagus and dilates just before connecting with the filter chamber; after the filter chamber the midgut continues ultimately diminishing in diameter and re-entering the filter chamber as the hindgut (inner hindgut). The hindgut then exits the filter chamber as the outer hindgut, which then dilates into a rectum just before the anus.

The structure of the rectum varies between the sexes. In males the rectum is a long uniformly dilated tube while in females it ends in a rectal ampulla. This could be explained by variation on defecation behavior between the sexes, as has been described previously for the melaleuca psyllid, *Boreioglycaspis melaleucae*. In *B. melaleucae*, adult females produce whitish honeydew balls that are powerfully propelled away from the body, probably to ensure these sticky excretions do not adhere to their nearby eggs and newly-hatched nymphs. In contrast, adult males produce clear droplets of honeydew that are not propelled away from them (Ammar *et al.*, 2015). It is likely that ACP females also propel their droppings away from themselves to avoid contaminating progeny; the rectal ampulla observed in females would facilitate it much better than the more voluminous long rectum seen in males.

Ammar *et al* .(Ammar *et al.,* 2017) distinguished three sections in the midgut of ACP and we observed the same: an anterior-midgut extending from the point of contact with the filter chamber until the position where the 1st abdominal appendage connects (we have termed this the dilated efferent midgut); a middle-midgut that extends from where the 1st abdominal appendage connects until the point at which the 4th abdominal appendage connects; and a posterior-midgut that extends from the insertion of the 4th abdominal appendage until connection with the filter chamber (we have termed this the afferent midgut).

The filter chamber occurs in most homopteran insects and is a modification of the alimentary canal in which two ordinarily distant parts of the digestive tube (the

stomodeum/mesenteron and the proctodaeum) are bound adjacent to each other by a connective tissue sheath. The constituent parts of the filter chamber are usually the two extremities of the mesenteron and the anterior end of the proctodaeum. Thus, the organ formed is considered to be a device for allowing some of the excess water and soluble carbohydrates from food to be eliminated by diffusion directly from the anterior part of the digestive into the posterior; the protein and fatty materials are retained to be digested and absorbed in the stomach (Snodgrass, 1935). The alimentary tract within the filter chamber consists of two connected sections with luminal flows moving in an antiparallel direction that, together, represent a counter-current filter (Hamilton, 2015). To function this filter requires the liquid within to be under high pressure, which explains why the esophagus is dilated just before it enters the filter chamber, as we observed, and has been described previously (Cicero, 2020; Cicero, Hunter, *et al.*, 2018; Cicero & Brown, 2009); according to the Bernoulli principle an increased pipe diameter means a decrease in velocity and kinetic energy and an increase in pressure (Bajpai, 2018). Thereafter, the liquid food is forced under pressure into the filter chamber where the speed slows to facilitate transfer of excess water into the inner hindgut that surrounds the filter chamber. It seems that dilation of the esophagus before entry into the filter chamber occurs in many sap-sucking homopterans, thus this enlargement is clearly visible in the figures in numerous publications e.g. (Pesson, 1951; Snodgrass, 1935; Wigglesworth, 1942).

The filter chamber has been studied in detail in a range of homopteran species, and more than 50 papers on its anatomy and physiology have been published (e.g. (Cicero, Hunter, *et al.*, 2018), (Cecil, 1930; Goodchild, 1963; Hubert *et al.*, 1989; Kershaw, 1914; Lindsay & Marshallt, 1980)). In psylloids the hind-gut and oesophagus are spirally wound round one another (Pesson, 1951; Wigglesworth, 1942), and have been described previously for *P. mali* (Saunders, 1921), (Brittain, 1922) and *P. fraxinicola*(Witlaczil, 1885). With respect to ACP light microscopic images of the digestive tract, including the filter chamber, have been published and there are general schematic anatomical interpretative drawings with a SEM image (Cicero & Brown, 2009), and a micrograph of the filter chamber of one last instar nymph (Brown *et al.*, 2016). Moreover, the anatomy of the alimentary canal

of ACP, including the filter chamber, of ACP has been recently summarised as animated schematic drawings (Cicero, Hunter, *et al.*, 2018).

The four abdominal appendages that end at different points along the midgut are widely considered as Malpighian tubules with an excretory function (Ammar *et al.,* 2011, 2012, 2017; Hamilton, 2015; Kruse *et al.*, 2017; Pesson, 1951; Saunders, 1921; Witlaczil, 1885). From an anatomical point of view, the insertion of Malpighian tubules should be coincident with the end of the mesodeum (midgut) and beginning of the proctodaeum (hindgut) (Chapman, 2013; Gillott, 2005; Snodgrass, 1935). However, the appendages of the midgut flow into the midgut consecutively and are widely separated from each other. This is why we decided to follow Cicero's terminology and use the term abdominal appendages rather than Malpighian tubules, until any potential excretory function is elucidated (Brown *et al.*, 2016; Cicero, 2020; Cicero & Brown, 2009). Micrograph figures of the Malpighian tubules of the bee *Melipona scutellaris* (Nocelli *et al.*, 2016) are fully comparable with our micro-CT volume-rendered images of the midgut appendages of ACP, and also similar to structures described for the psyllids *Psylla alni,* and *T. rhamni* (Witlaczil, 1885) and termed Malpighian tubules.

There are several papers that describe and/or provide images of the salivary glands of potato psyllid *B. cockerelli* (Cicero *et al.*, 2015) and ACP (Ammar *et al.*, 2011, 2017; Cicero, 2020; Cicero & Brown, 2009, 2011). The salivary glands of adult ACP are described as each being comprised of two principal salivary glands and a smaller accessory salivary gland. Comparing these descriptions and micrographs with our results we find that what were described as principal salivary glands are equivalent to the salivary lobes we observed with micro-CT and numbered lobe 1 and lobe 2; what we describe as lobe 3 corresponds with what was previously described as a separate accessory salivary gland. Independently of any observed structural/content differences (see (Ammar *et al.*, 2017; Cicero & Brown, 2009)), all three lobes together form a lateral salivary gland, and we see no reason to separate the 3rd lobe as a different separate accessory salivary gland. Using micro-CT we observed bunches of acini

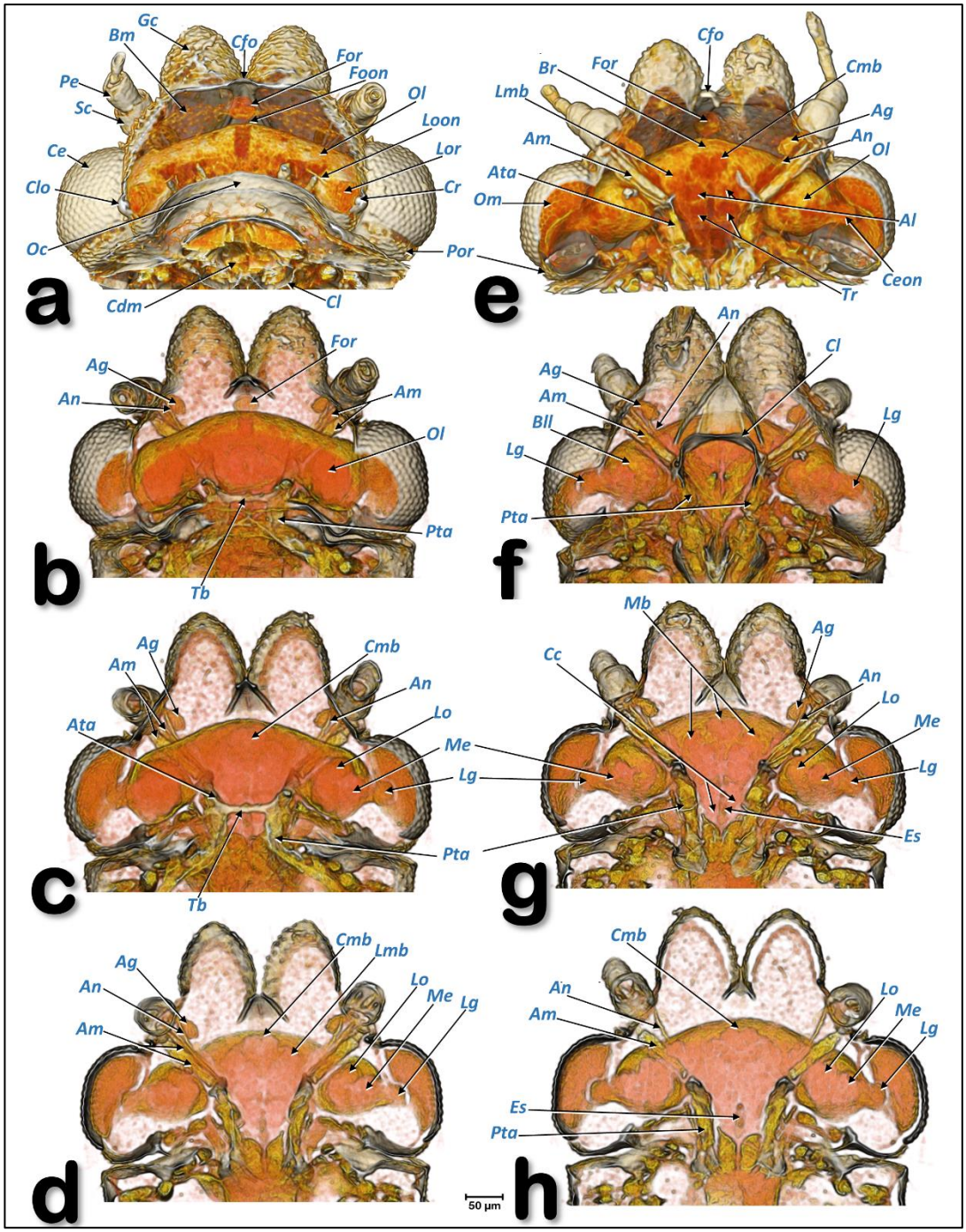

Figure 19.- Volume-rendered images of the head of a female *Diaphorina citri* showing the brain and other internal structures. Dorsal views in the left-hand column (**a**-**d**) and ventral views in the right-hand column (**e**-**h**). From the top to the bottom successive dorsal/ventral cuts were made to obtain virtual slices. Abbreviations: Ag = antennal gland; Al = antennal lobe (deutocerebrum); Am = antennal muscles; An = antennal nerve; Ata = anterior tentorial arms; Bll = lateral lobe of brain; Bm = basal membrane; Br = brain (protocerebrum); Cc = circumesophageal connectives; Ce = compound eye; Cdm = cibarial dilator muscles; Ceon = compound eye optic nerve; Cl = clypeus; Cfo = cornea of the frontal ocellus; Clo = cornea of the lateral ocellus; Cmb = central mushroom body; Cr = crystalline lens; Es = esophagus; Foon = frontal ocellar optic nerve; For = frontal ocellar retina; Lg = lamina ganglionaris; Lmb = lateral mushroom body; Lo = lobulla; Loon =lateral ocellar optic nerve; Lor = lateral ocellar retina; Mb= mushroom bodies; Me = medulla; Oc = occiput; Ol = optic lobe; Om = ommatidia; Pe = pedicell; Pta = posterior tentorial arm; Sc = scapus; Tb = tentorial bridge; Tr = tritocerebrum.

in each lobe and this is in full agreement with previously published images taken from a semithin section (stained with toluidine blue) of the principal salivary gland which showed at least three differentially stained acini/groups of secretory cells (Ammar *et al.,* 2017).

The anatomy of the nervous system in insects has been widely studied, including diagrams made more than 400 years ago by Aldrovandi (Aldrovandi, 1602) and Malpighi (Malpighi, 1669). Since then, many general descriptions of insect nervous systems have been published e.g. (Chapman, 2013; Gillott, 2005; Grassé, 1975; Snodgrass, 1935; Wigglesworth, 1942), including for homopterans (Pesson, 1951). Recently micro-CT has been used to study the anatomy of the nervous system e.g. (Alba-Alejandre *et al.,* 2019; Alba-Tercedor, 2013; Alba-Tercedorv *et al.*, 2017; Alba-Tercedor & Alba-Alejandre, 2019; Alba-Tercedor & Bartomeus, 2016; Greco *et al.*, 2012; Ribi *et al.*, 2008; Rybak *et al.*, 2010; Smith *et al.*, 2016; Sombke *et al.*, 2015; Wipfler *et al.*, 2016). Anatomical studies with images of the nervous system have been made for a range of psylloid species (Austin, 2016; Brittain, 1922; Mally, 1894; Saunders, 1921; Weber, 1929; Witlaczil, 1885; Zucht, 1972), including ACP (Alba-Tercedor *et al.*, 2017; Ammar *et al.*, 2011, 2017). The results we describe here are the first complete study of the nervous system of ACP, and the general organisation conforms with existing descriptions for psylloids.

The ACP brain has the same general organisation as other insects where the brain (considered as derived from the ganglia of three segments) forms the major association centre of the nervous system. It includes the protocerebrum, deutocerebrum and tritocerebrum. The protocerebrum, the largest and most complex region of the brain, contains both neural and endocrine (neurosecretory) elements. Anteriorly it forms the proximal part of the ocellar nerves, and laterally is fused with the optic lobes. A pair of corpora pendunculata are within the protocerebrum which are also known as the mushroom bodies. The mushroom bodies are important association centres, receiving sensory inputs, especially olfactory and visual, and relaying the information to other protocerebral centres They play a central role in learning and memory and their size can be broadly correlated with the development of complex behaviour patterns (as in social Hymenoptera). The median central body is another important association centre,

one function of which appears to be the coordination of segmental motor activities. Each optic lobe contains three neuropilar masses (lobulla, medulla and lamina ganglionaris) in which light stimuli, including those generated by polarized light, are assessed and forwarded to other brain centres. The deutocerebrum is largely composed of the paired antennal lobes. Together with the mushroom bodies, the antennal lobes are essential in learned olfactory behaviour. The tritocerebrum is a small region of the brain located beneath the deutocerebrum and comprises a pair of neuropiles that contain axons, both sensory and motor, leading to and from the frontal ganglion and labrum (Chapman, 2013; Gillott, 2005; Snodgrass, 1935).

Previously, the big (large) mesothoracic ganglion has been called the thoracic ganglion (Brittain, 1922; Saunders, 1921). We have named this the big mesothoracic ganglion, to distinguish it from the subesophageal ganglion, and we agree that this ganglion is likely to be an amalgamation of thoracic and abdominal ganglia, as has been reported for other hemipterans (Ammar *et al.,* 2017). In fact in other insects the abdominal ganglion is fused with ganglia of the thorax, to form a single ganglion; this has been named the thoraco-abdominal ganglion (Chapman, 2013).

Sexual differences in the nervous system of insects have been reported, both in morphology and size, and in structural neuron connections (e.g. in social insects (Beani *et al.*, 2014), flies (Cachero *et al.*, 2010) and beetles (Alba-Alejandre *et al.*, 2019)). Here we report on sexual differences in the nervous system of ACP for the first time. Males have a slender configuration of the brain and almost parallel margins of the subesophageal and large mesothoracic ganglion, while in females both brain and ganglia are more voluminous, and the large mesothoracic ganglion is almost spherical in shape.

The ACP is a phloem-feeding, sap-sucking hemipteran species. Its feeding behaviour has been investigated using the electrical penetration graph (EPG) technique(Bonani *et al.*, 2010; Luo *et al.*, 2015) and light microscopy has been used to confirm that the stylets reach the phloem (this also included observations of the salivary sheath tracks) (Bonani *et al.*, 2010). Different methodologies have been used to study homopteran salivary sheaths inside the plant tissues (e.g.

(Ammar *et al.*, 2014; Ammar & Hall, 2012; Backus *et al.*, 1988; Morgan *et al.*, 2013)). The micro-CT technique has been used to visualise stylet penetration and the salivary sheaths of the meadow spittlebug *Philaenus spumarius* (Cornara *et al.*, 2018) and the aphid species *Myzus persicae* (Jiménez *et al.*, 2020). The present study on ACP obtained rendered images that were fully comparable to previous images obtained using a variety of different techniques; our images include observations of the different configuration and typologies described previously and benefited from being high quality 3D images and videos.

All stain/contrast methodologies we used in the present study enhanced our views of structures. However, the best results were obtained by first feeding animals with orange plant material that had been submerged in BAPC (***B****ranched* ***A****mphiphilic* ***P****eptide* ***C****apsules*) linked to Hg as a contrast agent (Sukthankar *et al.*, 2014); using iodine enabled us to achieve the highest contrasted samples.

5.1.7.- Conclusions

The use of micro-CT techniques for elucidation of the anatomical structures and organs of ACP has enabled us to make a complete reconstruction of the anatomy of this insect, indicating the actual position of internal structures and organs without distortion resulting from dissection. We also include detailed rendered images and videos. This work represents the first complete micro-CT reconstruction of the anatomy of *D. citri*, which, together with our previous study on the male(*Alba-Alejandre et al., 2018*) and female (Alba-Alejandre *et al.*, 2020) reproductive systems and bacteriome, is the first complete, detailed anatomical study of a psylloid. In general, it is the first micro-CT anatomical study of a hemipteran studied as a whole. Together with our previous paper on the coffee berry borer beetle (Alba-Alejandre *et al.*, 2019) these studies represent anatomical reconstructions of the smallest insects carried out to date using micro-CT. Moreover, this is the first report of coxal and antennal glands with a plausible pheromone secretions role, and the first report of differences between the sexes in internal anatomy (i.e. the hindgut, rectum, large mesothoracic ganglion and brain). Additionally, this is the first time a male feeding within an orange leaf has been reconstructed which enabled us to see the arrangement of the feeding

apparatus (labium, stylets bundle), salivary flange, salivary sheaths; we were also able to see how the stylet bundle appears inside the cells of the citrus leaf, the penetration point of the salivary flange at the leaf surface, intact salivary sheaths and abandoned salivary sheaths that resulted from failed piercing attempts.

With the supplementary videos and 3D model of a male feeding on a citrus leaf (suitable for use on mobile devices), this package is useful for future research and/or for teaching insect anatomy to students and the general public. Together this constitutes a unique atlas of the anatomy of the ACP.

5.1.8.- Supplementary Information

Supplementary Videos (mp4):

S1. Animated, volume-rendered images showing the external anatomy and abdominal tracheal tubular system of a female *Diaphorina citri*.

S2. Animated, volume-rendered images of a left-lateral view of the abdomen of an adult female *Diaphorina* citri, with progressive bilateral erosive-slices, from the external surface to the median line, showing several structures and the dorsal vessel (heart) in sagittal view.

S3. Animated, volume-rendered images of an adult male *Diaphorina citri* feeding of a citrus leaf, with detail of the leaf structure, stylets, salivary sheaths and feeding apparatus.

S4. Spinning, animated, volume-rendered images of the feeding apparatus, showing the labium and the internal structures of the cibarium and tentorium of an adult male *Diaphorina citri*.

S5. Spinning, animated, volume-rendered images of an adult male *Diaphorina citri* showing the general position of the nervous system and the digestive (including the salivary glands).

S6. Spinning, animated, volume-rendered images of an adult male *Diaphorina citri* showing the feeding apparatus, the digestive system (including the salivary glands) and the nervous system.

S7. Spinning, animated, volume-rendered images of the anterior body of an adult female *Diaphorina citri* showing the digestive, nervous system, salivary glands, labium, stylets bundle, cibarium, cibarial dilator muscles, cibarial pump and maxillary/mandibular cones.

S8. Spinning, animated, volume-rendered images of the digestive of an adult male *Diaphorina citri*.

S9. Spinning, animated, volume-rendered images of an adult male of *Diaphorina citri* with details of the filter chamber structure and its connections with the esophagus and the outer hindgut.

S10. Spinning, animated, volume-rendered images of an adult male of *Diaphorina citri* with details of the right salivary glands.

S11. Spinning, animated, volume-rendered images of an adult female of *Diaphorina citri* with internal details of the brain and other structures such as the antennal glands and tentorium.

Supplementary 3D model for use on mobile devices (vxm):

S12. Adult male *Diaphorina citri* feeding on the abaxial surface of an orange leaf.

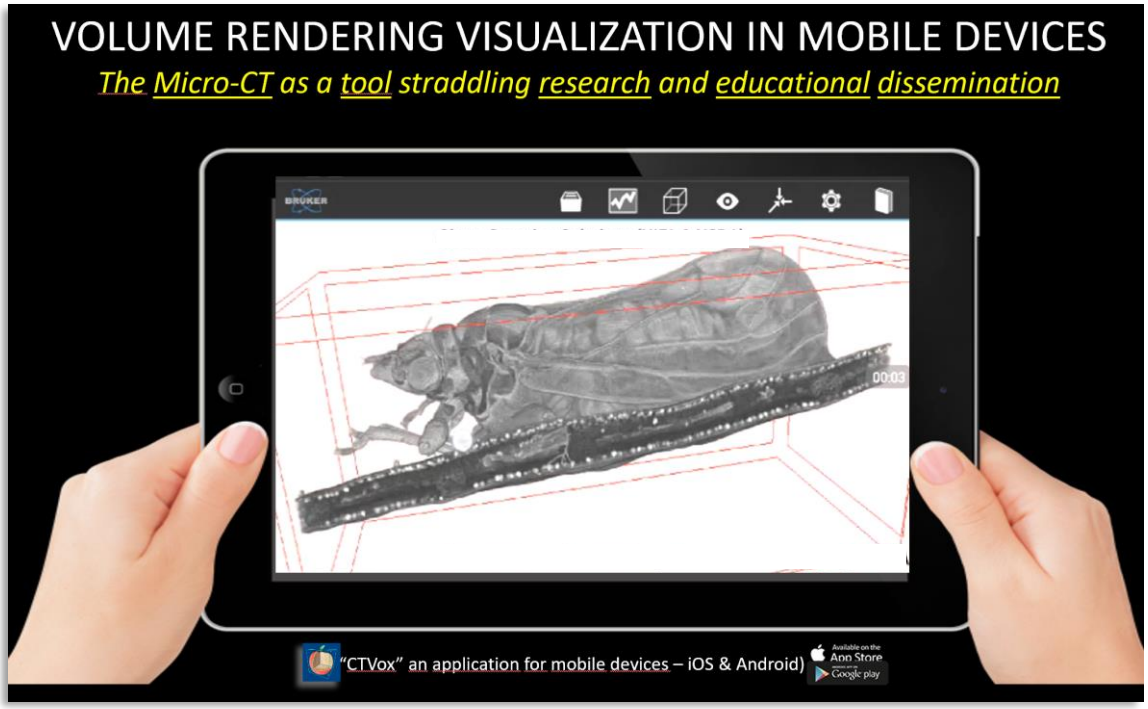

To be visualized with the CTvox app for mobile devices (smartphones and tablets, either with iOS or Android systems). To install CTvox on your device, go through Apple's App Store/Google Play Store, in the usual fashion (the app is free of charge). Instructions can be downloaded in the following links:

1.- For iOS devices:

a) For Ipad:

https://www.bruker.com/fileadmin/user_upload/8-PDF-Docs/Microtomography/CTvoxForIpad.pdf

b) For Iphone:

https://www.bruker.com/fileadmin/user_upload/8-PDF-Docs/Microtomography/CTvoxForIPhone.pdf

2.- For Android devices:

https://www.bruker.com/fileadmin/user_upload/8-PDF-Docs/Microtomography/CTvoxForAndroid.pdf

5.1.9.- References

Alba-Alejandre, I., Alba-Tercedor, J., & Hunter, W. B. (2020). Anatomical study of the female reproductive system and bacteriome of *Diaphorina citri* Kuwayama, (Insecta: Hemiptera, Liviidae) using micro-computed tomography. *Scientific Reports*, *10*(1), 1–14. https://doi.org/10.1038/s41598-020-64132-y

Alba-Alejandre, I., Alba-Tercedor, J., & Vega, F. E. (2019). Anatomical study of the coffee berry borer (*Hypothenemus hampei*) using micro-computed tomography. *Scientific Reports*, *9*(17150), 1–16. https://doi.org/10.1038/s41598-019-53537-z

Alba-Alejandre, I., Hunter, W. B., & Alba-Tercedor, J. (2018). Micro-CT study of male genitalia and reproductive system of the Asian citrus psyllid, *Diaphorina citri* Kuwayama, 1908 (Insecta: Hemiptera, Liviidae). *PLoS ONE*, *13*(8), 1–11. https://doi.org/https://doi.org/10.1371/journal.pone.0202234 Editor:

Alba-Tercedor, J. (2013). Study of the anatomy of the common housefly *Musca domestica* Linnaeus, 1758 (Insecta: Diptera, Muscidae) scanned with the Skyscan 1172 high resolution micro-CT. *Bruker Micro-CT Users Meeting 2013*, 275–289.

Alba-Tercedor, J. (2014). From the sample preparation to the volume rendering images of small animals : A step by step example of a procedure to carry out the micro-CT study of the leafhopper insect *Homalodisca vitripennis* (Hemiptera: Cicadellidae). In *Bruker Micro-CT Users Meeting 2014* (pp. 260–288). Bruker- microCT-Skyscan.

Alba-Tercedor, J., & Alba-Alejandre, I. (2019). Comparing micro-CT results of insects with classical anatomical studies: The European honey bee (*Apis mellifera* Linnaeus, 1758) as a benchmark (Insecta: Hymenoptera, Apidae). *Microscopy and Analysis*, *3*(1), 12-15 EU. https://microscopy-analysis.com/article/january_19/comparing_classical_anatomical_studies_of_insects

Alba-Tercedor, J., Alba-Alejandre, I., & Vega, F. E. (2019). Revealing the respiratory system of the coffee berry borer (*Hypothenemus hampei*; Coleoptera: Curculionidae: Scolytinae) using micro-computed tomography. *Scientific Reports*, *9*(17753), 1–17. https://doi.org/10.1038/s41598-019-54157-3

Alba-Tercedor, J., & Bartomeus, I. (2016). Micro-CT as a tool straddling scientist research, art and education. Study of *Osmia* sp., a mason bee (Insecta, Hymenoptera: Megachilidae). In *Bruker Micro-CT Users Meeting 2016* (pp. 74–91).

Alba-Tercedor, J., Hunter, W. B., Cicero, J. M., & Sáinz-Bariáin, M. (2017). Use of micro-

CT to elucidate details of the anatomy and feeding of the Asian Citrus Psyllid *Diaphorina citri* Kuwayama , 1908 (Insecta : Hemiptera , Lividae). In *Bruker Micro-CT Users Meeting 2017* (pp. 270–285). Bruker micro-CT-Skyscan.

Aldrovandi, U. (1602). *De Animalibus Insectis Libri*.

Ammar, E.-D., & Hall, D. G. (2012). New and Simple Methods for Studying Hemipteran Stylets, Bacteriomes, and Salivary Sheaths in Host Plants. *Annals of the Entomological Society of America*, *105*(5), 731–739. https://doi.org/10.1603/AN12056

Ammar, E.-D., Hall, D. G., & Shatters Jr, R. (2017). Ultrastructure of the salivary glands, alimentary canal and bacteria-like organisms in the Asian citrus psyllid, vector of citrus huanglongbing disease bacteria. *Journal of Microscopy and Ultrastructure*, *5*(1), 9. https://doi.org/10.1016/j.jmau.2016.01.005

Ammar, E.-D., Hall, D. G., & Shatters, R. G. (2015). Ultrastructure and Development of the New Stylets Inside Pre-molting First Instar Nymphs of the Asian Citrus Psyllid *Diaphorina citri* (Hemiptera: Liviidae). *Florida Entomologist —*, *98*(1). https://doi.org/10.1653/024.098.0163

Ammar, E.-D., Hall, D. G., & Shatters, R. G. (2017). Ultrastructure of the salivary glands, alimentary canal and bacteria-like organisms in the Asian citrus psyllid, vector of citrus huanglongbing disease bacteria. *Journal of Microscopy and Ultrastructure*, *5*(1), 9–20. https://doi.org/10.1016/j.jmau.2016.01.005

Ammar, E.-D., Hentz, M., Hall, D. G., & Shatters, R. G. (2015a). Ultrastructure of Wax-Producing Structures on the Integument of the Melaleuca Psyllid Boreioglycaspis melaleucae (Hemiptera: Psyllidae), with Honeydew Excretion Behavior in Males and Females. *PLOS ONE*, *10*(3), e0121354. https://doi.org/10.1371/journal.pone.0121354

Ammar, E.-D., Hentz, M., Hall, D. G., & Shatters, R. G. (2015b). Ultrastructure of Wax-Producing Structures on the Integument of the Metaleuca Psyllid *Boreioglycaspis melaleucae* (Hemiptera: Psyllidae), with Honeydew Excretion Behavior in Males and Females. *PLOS ONE*, *10*(3), e0121354. https://doi.org/10.1371/journal.pone.0121354

Ammar, E.-D., Ramos, J. E., Hall, D. G., Dawson, W. O., & Shatters, R. G. (2016). Acquisition, Replication and Inoculation of *Candidatus* Liberibacter asiaticus following Various Acquisition Periods on Huanglongbing-Infected Citrus by Nymphs and Adults of the Asian Citrus Psyllid. *PLOS ONE*, *11*(7), e0159594. https://doi.org/10.1371/journal.pone.0159594

Ammar, E.-D., Richardson, M. L., Abdo, Z., Hall, D. G., & Shatters, R. G. (2014). Differences in Stylet Sheath Occurrence and the Fibrous Ring (Sclerenchyma) between xCitroncirus Plants Relatively Resistant or Susceptible to Adults of the Asian Citrus Psyllid *Diaphorina citri* (Hemiptera: Liviidae). *PLoS ONE*. https://doi.org/10.1371/journal.pone.0110919

Ammar, E., Shatters, R., Lynch, C., & Hall, D. G. (2011). Detection and relative titer of Candidatus Liberibacter asiaticus in the salivary glands and alimentary canal of *Diaphorina citri* (Hemiptera: Psyllidae) vector of citrus. *Annals of the Entomological Society of America*, *104*(3), 526–533. http://aesa.oxfordjournals.org/content/104/3/526.abstract

Arras, J., Hunter, W., & Bextine, B. (2012). Comparative analysis of antennae sensory arrays in Asian citrus psyllid, *Diaphorina citri*, and potato psyllid, *Bactericera cockerelli* (Hemiptera). *Southwestern Entomologist*. https://doi.org/http://dx.doi.org/10.3958/059.037.0101

Austin, C. (2016). *Morphology of Acercaria: investigations of the ovipositor and internal anatomy*. University of Illinois at Urbana-Champaign.

Backus, E., Hunter, W. B., & Arne, C. N. (1988). Technique for staining Leafhopper (Homoptera: Cicadellidae) salivary sheaths and eggs within unsectioned plant tissue View project. *J. Econ. Entomol.*, *81*(6), 1819–1823. https://doi.org/10.1093/jee/81.6.1819

Bajpai, P. (2018). Hydraulics. In *Biermann's Handbook of Pulp and Paper* (pp. 455–482). Elsevier. https://doi.org/10.1016/B978-0-12-814238-7.00023-4

Barcellos, M. S., Fernanda, J., Cossolin, S., Dias, G., & Lino-Neto, J. (2017). Sperm morphology of the leafhopper *Diaphorina citri* Kuwayama (Hemiptera: Sternorrhyncha: Psylloidea: Liviidae). *Micron*, *99*, 49–55. https://doi.org/10.1016/j.micron.2017.03.017

Beani, L., Dessì-Fulgheri, F., Cappa, F., & Toth, A. (2014). The trap of sex in social insects: From the female to the male perspective. *Neuroscience and Biobehavioral Reviews*, *46*, 519–533. https://doi.org/10.1016/j.neubiorev.2014.09.014

Billen, J. (1997). Morphology and ultrastructure of the metatibial gland in the army ant *Norylus molestus* (Hymenoptera, formicidae). *Belg. J. Zool*, *127*(2), 159–166.

Billen, J. (2009). Occurrence and structural organization of the exocrine glands in the legs of ants. *Arthropods Structure and Development*, *38*, 2–15. https://doi.org/10.1016/j.asd.2008.08.002

Billen, J., & Ito, F. (2006). The basicoxal gland, a new exocrine structure in poneromorph ants (Hymenoptera, Formicidae). *Acta Zoologica (Stockholm)*, *87*, 291–296.

Bin, F. (1986). Morphology of of the antennal sex-gland in male *Trissolcus basalis* (Woll.) (Hymenoptera: Scelionidae), an egg parasitoid of the green stink Bug, *Nezara viridula* (Hemiptera: Pentatomida). *Int. J. Insect Morphol. & Embryol.*, *15*(3), 129–138.

Bitsch, J. (1979). Morphologie Abdominale des Insectes. Ordre des Homoptères, B.-Psylles. In P.-P. Grassé (Ed.), *Traité de Zoologie. Anatomie, Systématique, Biologie. T. VIII, Insectes Thorax, Abdomen. Fasc. II* (pp. 420–429). Masson et Cie.

Blowers, J. R., & Moran, V. C. (1967). Notes on the female reproductive system of the South African Citrus Psylla, *Trioza erytreae* (Del Guercio) (Homoptera : Psyllidae). *Journal of the Entomological Society of Southern Africa*, *30*(1), 75–81. http://journals.co.za/docserver/fulltext/JESSA/30/1/2701.pdf?expires=1506671192&id=id&accname=guest&checksum=3A2E414A6D93326F9DCB5EE541F23E2A

Bonani, J. P., Fereres, A., Garzo, E., Miranda, M. P., Appezzato-Da-Gloria, B., & Lopes, J. R. S. (2010). Characterization of electrical penetration graphs of the Asian citrus psyllid, *Diaphorina citri*, in sweet orange seedlings. *Entomologia Experimentalis et Applicata*, *134*(1), 35–49. https://doi.org/10.1111/j.1570-7458.2009.00937.x

Brittain, W. H. (1922). The morphology and synonymy of *Psylla mali* Schmidberger. *Proceeding Acadian Entomological Society (Fredericton)*, *8*, 23–51.

Brown, J. K., Cicero, J. M., & Fisher, T. W. (2016). Psyllid-Transmitted Candidatus Liberibacter Species Infecting Citrus and Solanaceous Hosts. In J. K. Brown (Ed.), *Vector-Mediated Transmission of Plant Pathogens* (pp. 399–422). The American Phytopathological Society. https://doi.org/10.1094/9780890545355.028

Brown, R. G., & Hodkinson, I. D. (1988). *Taxonomy and Ecology of the Jumping Plant-lice of Panama: Homoptera, Psylloidea*. E. J. Brill/Scandanavian Science Press Ltd.,.

https://books.google.es/books?id=W9942XjeV44C&pg=PA4&lpg=PA4&dq=90-04-08893-8&source=bl&ots=557oIKp3ll&sig=ACfU3U1MfU-KaHESNrmTW00iop7rIg0ogQ&hl=es&sa=X&ved=2ahUKEwikrdL-9onlAhULAWMBHdEtDhkQ6AEwB3oECAkQAQ#v=onepage&q=citri&f=false

Burckhardt, D. (1987). Jumping plant lice (Homoptera: Psylloidea) of the temperate neotropical region. Part 2: Psyllidae (subfamilies Diaphorininae, Acizziinae, Ciriacreminae and Psyllinae). *Zoological Journal of the Linnean Society*, *90*, 145–205. https://onlinelibrary.wiley.com/doi/pdf/10.1111/j.1096-3642.1987.tb01353.x

Cachero, S., Ostrovsky, A. D., Yu, J. Y., Dickson, B. J., & Jefferis, G. S. X. E. (2010). Sexual Dimorphism in the Fly Brain. *Current Biology*, *20*(18), 1589–1601. https://doi.org/10.1016/j.cub.2010.07.045

Cecil, R. (1930). The alimentary canal of *Philaenus leucophthalmus* L. *The Ohio Journal of Science*, *30*(2), 120–130. http://hdl.handle.net/1811/2443

Chapman, R. F. (2013). *The Insects Structure and Function.* (S. J. Simpson & A. E. Douglas (eds.); 5th ed.). Cambridge University Press. Chapman 5 th edition The Insects structure and function.pdf - ResearchGate

Cicero, J. M. (2017). Stylet biogenesis in *Bactericera cockerelli* (Hemiptera: Triozidae). *Arthropod Structure & Development*, *46*(4), 644–661. https://doi.org/10.1016/j.asd.2016.12.007

Cicero, J. M. (2020). Functional Anatomy of the Asian Citrus Psyllid. In J. A. Qureshi & P. A. Stansly (Eds.), *Asian Citrus Psyllid: Biology, Ecology and Management of the Huanglongbing Vector* (pp. 12–29). CABI.

Cicero, J. M., Alba-Tercedor, J., Hunter, W. B., Cano, L. M., Saha, S., Mueller, L. A., & Brown, S. J. (2018). Asian citrus psyllid stylet morphology and applicability to the model for inter-instar stylet replacement in the potato psyllid. *Arthropod Structure & Development*, *47*(5), 542–551. https://doi.org/10.1016/j.asd.2018.06.007

Cicero, J. M., & Brown, J. (2009). The digestive system of *Diaphorina citri* and *Bactericera cockerelli* (Hemiptera: Psyllidae). *Entomological Society of America*, *102*(4), 650–665. http://aesa.oxfordjournals.org/content/102/4/650.abstract

Cicero, J. M., & Brown, J. (2011). Anatomy of accessory salivary glands of the whitefly *Bemisia tabaci* (Hemiptera: Aleyrodidae) and correlations to Begomovirus transmission. *Annals of the Entomological Society …*. http://aesa.oxfordjournals.org/content/104/2/280.abstract

Cicero, J. M., Hunter, W. B., Cano, L. M., Saha, S., Mueller, L. A., & Brown, S. J. (2018). *An animated detailing of the alimentary canal of the Asian citrus psyllid, with special reference to the configuration and function of the filter chamber (online only)* (pp. 1–9). Figshare media. https://figshare.com/articles/An_Animated_Detailing_of_the_Alimentary_Canal_of_the_Asian_Citrus_Psyllid_with_Special_Reference_to_the_Configuration_and_Function_of_the_Filter_Chamber/7599269/3

Cicero, J. M., & Stansly, P. A. (2019). New Anatomical Evidence from the Male Asian Citrus Psyllid (Hemiptera: Liviidae) Invokes Controversy Over the Accepted Function of Some Male Reproductive Organs in Psylloidea. *Journal of Insect Science*, *19*(3). https://doi.org/10.1093/jisesa/iez048

Cicero, J. M., Stansly, P. A., & Brown, J. K. (2015). Functional anatomy of the oral region of the potato psyllid (Hemiptera: Psylloidea: Triozidae). *Annals of the Entomological Society of America*, *108*(5), 743–761. https://doi.org/10.1093/aesa/sav059

Cornara, D., Garzo, E., Morente, M., Moreno, A., Alba-Tercedor, J., & Fereres, A. (2018).

EPG combined with micro-CT and video recording reveals new insights on the feeding behavior of *Philaenus spumarius*. *PLOS ONE*, *13*(7), e0199154: 1-20. https://doi.org/10.1371/journal.pone.0199154

Da Cruz-Landim, C., Morelli, R. L., De Moraes, S., Salles, H. C., & Reginato, R. D. (1988). Note on glands present in Meliponinae (Hymenoptera, Apidae) bees legs. *Revta Bras. Zool.*, *15*(2), 159–155.

Dahms, E. D. (1984). An interpretation of the structure and function of the antennal sense organs of *Melittobia australica* (Hymenoptera: Eulophidae) with the discovery of a large dermal gland in the male scape. *Mem. Qd Mus.*, *21*(2), 361–385.

Dmitriev, D. A. (2010). Homologies of the head of Membracoidea based on nymphal morphology with notes on other groups of Auchenorrhyncha (Hemiptera). *European Journal of Entomology*, *107*(4), 597–613. https://doi.org/10.14411/eje.2010.069

Dossi, Fabio C. A., & Cônsoli, F. L. F. (2014). Gross morphology and ultrastructure of the female reproductive system of *Diaphorina citri* (Hemiptera: Liviidae). *Zoologia*, *31*(2), 162–169. https://doi.org/10.1590/S1984-46702014000200007

Dossi, Fábio C A, & Cônsoli, F. L. (2010). Desenvolvimento ovariano e influência da cópula na maturação dos ovários de *Diaphorina citri* Kuwayama (Hemiptera: Psyllidae). *Neotropical Entomology*, *39*(3), 414–419. https://doi.org/10.1590/S1519-566X2010000300015

Drohojowska, J., Kalandyk-Kołodziejczyk, M., & Simon, E. (2013). Thorax morphology of selected species of the genus Cacopsylla (Hemiptera, Psylloidea). *ZooKeys*, *319*, 27–35. https://doi.org/10.3897/zookeys.319.4218

Garzo, E., Bonani, J. P., Lopes, J. R. S., & Fereres, A. (2012). Morphological description of the mouthparts of the Asian citrus psyllid, *Diaphorina citri* Kuwayama (Hemiptera: Psyllidae). *Arthropod Structure & Development*, *41*(1), 79–86. https://doi.org/10.1016/j.asd.2011.07.005

Ghanim, M., Achor, D., Ghosh, S., Kontsedalov, S., Lebedev, G., & Levy, A. (2017). '*Candidatus* Liberibacter asiaticus' Accumulates inside Endoplasmic Reticulum Associated Vacuoles in the Gut Cells of Diaphorina citri. *Scientific Reports*, *7*(1), 16945. https://doi.org/10.1038/s41598-017-16095-w

Ghanim, M., Fattah-Hosseini, S., Levy, A., & Cilia, M. (2016). Morphological abnormalities and cell death in the Asian citrus psyllid (*Diaphorina citri*) midgut associated with Candidatus Liberibacter asiaticus. *Scientific Reports*, *6*(1), 33418. https://doi.org/10.1038/srep33418

Gillott, C. (2005). Entomology. In *Entomology* (3rd ed.). Springer. www.springeronline.com

Głowacka, E., & Maryańska-Nadachowska, A. (1993). Anatomy of male reproductive system of the Psylla Geoffr. s. 1.(Homoptera, Psyllodea)-Validity for the systematic relations within the Genus. *Folia Biologica (Kraków)*, *41*(3–4), 55–64. https://books.google.es/books?id=c3296OYP72UC&pg=PA55&lpg=PA55&dq=Anatomy+of+Male+Reproductive+System+of+the+Psylla+Geoffr.+s.+1.(Homoptera,+Psyllodea)-Validity+for+the+Systematic+Relations+within+the+Genus&source=bl&ots=3AYvVsTdTJ&sig=OL8ufud_a_jGrMxOUrx

Głowacka, E., & Maryańska-Nadachowska, A. (1998). Male reproductive system and karyotype of *Mycopsylla fici* (Tryon) (Homoptera, Psylloidea). *Folia Biologica (Kraków)*, *46*(1–2), 17–21.

Głowacka, Elzbieta, Kuznetsova, V. G., & Maryańska-Nadachowska, A. (1995). Testis

follicle number in Psyllids (Psylloidea, Homoptera) as an anatomical feature in studies of systematic relations within the group. *Folia Biologica (Kraków)*, *43*(3–4), 115–124.

Goodchild, A. J. P. (1963). Some new observations on the intestinal structures concerned with water disposal in sap-sucking Hemiptera. *Transactions of the Royal Entomological Society of London*, *115*(88), 217–237. https://doi.org/10.1111/j.1365-2311.1963.tb00820.x

Grassé, P.-P. (1975). Le Système Nerveux des Insectes. In *Traité de Zoologie. Anatomie, Systématique, Biologie. T.VIII, Insectes. Splachnologie, Phonation, Vie Aquatique, Rapports avec les Plantes. Fasc. IV Systematique, Biologie. T. VIII, fasc. III: Vol. VIII (III)* (pp. 321–510).

Greco, M. K., Tong, J., Soleimani, M., Bell, D., & Schäfer, M. O. (2012). Imaging live bee brains using minimally-invasive diagnostic radioentomology. *Journal of Insect Science (Online)*, *12*, 89. https://doi.org/10.1673/031.012.8901

Grove, A. J. (1919). The anatomy of the head and mouth parts of *Psylla mali*, the Apple sucker, with some remarks on the function of the labium. *Parasitology*, *11*(3–4), 456–488. https://doi.org/https://doi.org/10.1017/S0031182000004388

Gullan, P. J., & Cranston, P. S. (2010). *Insects: An Outline of Entomology* (4th ed.). Willey-Blackwell.

Halbert, S. S. E. S., & Manjunath, K. K. L. (2004). Asian Citrus Psyllids (Sternorrhyncha: Psyllidae) and Greening Disease of Citrus: a Literature Review and Assessment of Risk in Florida. *Florida Entomologist*, *87*(3), 330–353. https://doi.org/10.1653/0015-4040(2004)087[0330:ACPSPA]2.0.CO;2

Hall, D. G., Richardson, M. L., Ammar, E.-D., & Halbert, S. E. (2013). Asian citrus psyllid, *Diaphorina citri*, vector of citrus huanglongbing disease. *Entomologia Experimentalis et Applicata*, *146*(2), 207–223. https://doi.org/10.1111/eea.12025

Hamilton, K. G. A. (2015). Anatomy: The poor cousin of morphology? *American Entomologist*, *61*(2), 88–95. https://doi.org/10.1093/ae/tmv003

Heslop-Harrison, G. (1952). XXVII.—The number and distribution of the spiracles of the adult psyllid. *Annals and Magazine of Natural History*, *5*(51), 248-260 + plates XIV-XVI. https://doi.org/10.1080/00222935208654288

Hodkinson, I. D., & White, I. M. (1979). *Homoptera Psylloidea* (A. Watson (ed.)). Royal Entomological Society of London.

Hubert, J.-F., Thomas, D., Cavalier, A., & Gouranton, J. (1989). Structural and biochemical observations on specialized membranes of the “filter chamber”, a water-shunting complex in sap-sucking homopteran insects. In *Biology of the Cell* (Vol. 66).

Jiménez, J., Garzo, E., Alba-Tercedor, J., Moreno, A., Fereres, A., & Walker, G. P. (2020). The phloem-pd: a distinctive brief sieve element stylet puncture prior to sieve element phase of aphid feeding behavior. *Arthropod-Plant Interactions*, *14*, 67–78. https://doi.org/10.1007/s11829-019-09708-w

Keil, T. A. (1999). Morphology and Development of the Peripheral Olfactory Organs. In *Insect Olfaction* (pp. 5–47). Springer Berlin Heidelberg. https://doi.org/10.1007/978-3-662-07911-9_2

Kershaw, J. (1914). The alimentary canal of a Cercopid. *Psyche (New York)*, *21*(2), 65–72. https://doi.org/10.1155/1914/82321

Kruse, A., Fattah-Hosseini, S., Saha, S., Johnson, R., Warwick, E., Sturgeon, K.,

Mueller, L., MacCoss, M. J., Shatters, R. G., & Cilia Heck, M. (2017). Combining 'omics and microscopy to visualize interactions between the Asian citrus psyllid vector and the Huanglongbing pathogen Candidatus Liberibacter asiaticus in the insect gut. *PLOS ONE*, *12*(6), e0179531. https://doi.org/10.1371/journal.pone.0179531

Kuwayama, S. (1907). Die Psylliden Japanese. *Transactions of the Sapporo Natural History Society*, *2*, 149-189. (D. citri: p. 160-161, Plate III,Fig. 16). https://www.hemiptera-databases.org/psyllespdf/25.pdf

Kuznetsova, V. G., Labina, E. S., Shapoval, N. A., Maryańska-Nadachowska, A., & Lukhtanov, V. A. (2012). *Cacopsylla fraudatrix* sp.n. (Hemiptera: Psylloidea) recognised from testis structure and mitochondrial gene COI. *Zootaxa*, *63*(3547), 55–63.

Liang, X., Zhang, C., Li, Z., Xu, L., & Dai, W. (2013). Fine structure and sensory apparatus of the mouthparts of the pear psyllid, *Cacopsylla chinensis* (Yang et Li)(Hemiptera: Psyllidae). *Arthropod Structure & Development*, *42*(6), 495–506. http://www.sciencedirect.com/science/article/pii/S1467803913000765

Lindsay, K. L., & Marshallt, A. T. (1980). Ultrastructure of the filter chamber complex in the alimentary canal of *Eurymela distincta* Signoret (Homoptera, Eurymelidae). In *Int. J. Insect Morphol. & Embryol* (Vol. 9).

Luo, X., Yen, A. L., Powell, K. S., Wu, F., Wang, Y., Zeng, L., Yang, Y., & Cen, Y. (2015). Feeding Behavior of *Diaphorina citri* (Hemiptera: Liviidae) and Its Acquisition of "Candidatus Liberibacter Asiaticus", on Huanglongbing-Infected Citrus reticulata Leaves of Several Maturity Stages. *Florida Entomologist*, *98*(1), 186–192. https://doi.org/10.1653/024.098.0132

Macharashvili, I. D., & Kuznetsova, V. G. (1997). Karyotypes, Spermatogenesis, and Morphology of the Internal Reproductive System in Males of Some Psyllid Species (Homoptera, Psylloidea) of the Fauna of Georgia: I. Karyotypes and Spermatogonial Meiosis. *Entomological Review*, *77*(1), 12–20. https://s3.amazonaws.com/academia.edu.documents/39487107/Karyotypes_spermatogenesis_and_morpholog20151028-28433-1pw66oj.pdf?AWSAccessKeyId=AKIAIWOWYYGZ2Y53UL3A&Expires=1508150605&Signature=CzdGVvNgbta89lAvwfvbqYpcBBA%3D&response-content-disposition=inline

Macloskie, G. (1886). Entomology. Witlaczil on Psyllidae. *American Naturalist*, *20*(3), 283–287.

Mally, C. W. (1894). Psyllidae found at Ames. *Proceedings of the Iowa Academy of Science*, *2*(1), 152–171.

Malpighi, M. (1669). *Dissertatio epistolica de bombyce*. J. Martyn & J. Allestry, regiæ societatis typographos.

Mankin, R. W., & Rohde, B. (2020). Mating behavior of the Asian Citrus Psyllid. In J. A. Qureshi & P. A. Stansly (Eds.), *Asian Citrus Psyllid: Biology, Ecology and Management of the Huanglongbing Vector* (pp. 30–42).

Marchini, D., Del Bene, G., Viscuso, R., & Dallai, R. (2012). Sperm Storage by Spermatodoses in the Spermatheca of *Trioza alacris* (Flor, 1861) Hemiptera, Psylloidea, Triozidae: A Structural and Ultrastructural Study. *Journal of Morphology*, *273*, 195–210.

Matsuda, R. (1970). Morphology and evolution of the insect throrax. *Memoirs of the Entomological Society of Canada*, *102*(S76), 5–431.

https://doi.org/10.4039/entm10276fv

Matsuda, R. (1976a). The female efferent duct and associated structures. In *Morphology and Evolution of the Insect Abdomen* (pp. 97–104). Pergamon Press Ltd. https://doi.org/10.1016/B978-0-08-018753-2.50018-6

Matsuda, R. (1976b). The Homoptera. In *Morphology and Evolution of the Insect Abdomen* (pp. 280–299). Pergamon Press Ltd. https://doi.org/10.1016/B978-0-08-018753-2.50040-X

Mead, F. W., & Fasulo, T. R. (2017). Asian Citrus Psyllid, *Diaphorina citri* Kuwayama (Insecta : Hemiptera : Psyllidae). *Series of the Entomology and Nematology Department, UF/IFAS Extension*, *EENY-033*, 1–8. http://entnemdept.ifas.ufl.edu/creatures/.

Morgan, J. K., Luzio, G. A., Ammar, E.-D., Hunter, W. B., Hall, D. G., & Shatters Jr, R. G. (2013). Formation of Stylet Sheaths in āere (in air) from Eight Species of Phytophagous Hemipterans from Six Families (Suborders: Auchenorrhyncha and Sternorrhyncha). *PLoS ONE*, *8*(4), e62444. https://doi.org/10.1371/journal.pone.0062444

Muir, F. (1930). LIII.—Notes on certain controversial points of morphology of the abdomen and genitalia of Psyllidæ. *Annals and Magazine of Natural History, Series 10*, *5*(29), 545–552. https://doi.org/10.1080/00222933008673163

Nijs, C., & Billen, J. (2015). Exocrine glands in the legs of the social wasp *Vespula vulgaris*. *Arthropods Structure and Development*, *44*, 433–443. https://doi.org/10.1016/j.asd.2015.08.011

Nocelli, R. C., Cintra-Socolowski, P., Roat, T. C., Silva-Zacarin, elaine C., & Malaspina, O. (2016). *Comparative physiology of Malpighian tubules: form and function*. https://doi.org/10.2147/OAIP.S72060

Onagbola, E. O. E., Meyer, W. W. L., Boina, R., Stelinski, L. L., Boina, D., & Stelinski, L. L. (2008). Morphological characterization of the antennal sensilla of the Asian citrus psyllid, *Diaphorina citri* Kuwayama (Hemiptera: Psyllidae), with reference to their probable. *Micron*, *39*, 1184–1191. https://doi.org/10.1016/j.micron.2008.05.002

Ossiannilsson, F. (1992). *The Psylloidea (Homoptera) of Fennoscandia and Demark*. E.J. Brill. https://books.google.es/books?id=X_fgWnvLS2gC&pg=PA7&lpg=PA7&dq=ossiannilson+psylloidea+fennoscandian&source=bl&ots=4V0spLX1n1&sig=ACfU3U3D5VxM6vzpdIdJy7VIf5s11DGSrw&hl=es&sa=X&ved=2ahUKEwiumePoq5HlAhVOAWMBHVwbCKgQ6AEwCnoECAgQAQ#v=onepage&q&f=false

Ouvrard, D., Bourgoin, T., & Campbell, B. C. (2002). Comparative Morphological Assessment of the Psyllid Pleuron (Insecta, Hemiptera, Sternorrhyncha). *J. Morphol*, *252*, 276–290. https://doi.org/10.1002/jmor.1105

Pesson, P. (1951). Ordre des Homoptères (Homoptera Leach, 1815). In P.-P. Grassé (Ed.), *Traité de zoologie. Anatomie, systématique, biologie. Tome X. Fascicule II. Insectes supérieurs et Hémipteróides* (Editions M, pp. 1390–1656). Masson et Cie.

Prophetou-Athanasiadou, D. A., & Tzanakakis, M. E. (1998). The Reproductive System and Ovarian Development of the Adult Olive Psylla *Euphyllura phillyreae* Foerster (Homoptera: Aphalaridae). *Entomologia Hellenica*, *12*, 37–45. https://doi.org/http://dx.doi.org/10.12681/eh.14018

Renthal, R., Velasquez, D., Olmos, D., & Vinson, S. B. (2008). Occurrence of antennal glands in ants. *Microscopy Research and Technique*, *71*(11), 787–791. https://doi.org/10.1002/jemt.20620

Ribi, W., Senden, T. J., Sakellariou, A., Limaye, A., & Zhang, S. (2008). Imaging honey bee brain anatomy with micro-X-ray-computed tomography. *Journal of Neuroscience Methods*, *171*(1), 93–97. http://www.sciencedirect.com/science/article/pii/S0165027008001179

Ruan, Y., Y., L., Zhang, M., Chen, X., Liu, Z., Wang, S., & Jiang, S. (2018). Visualisation of insect tracheal systems by lactic acid immersion. *Journal of Microscopy*, *271*(2), 230–236. https://doi.org/10.1111/jmi.12711

Rybak, J., Kuß, A., Lamecker, H., Zachow, S., Hege, H.-C., Lienhard, M., Singer, J., Neubert, K., & Menzel, R. (2010). The Digital Bee Brain: Integrating and Managing Neurons in a Common 3D Reference System. *Frontiers in System Neuroscience*, *4*, *article*(July), 1–15. https://doi.org/10.3389/fnsys.2010.00030

Saunders, L. G. (1921). *The Anatomy of* Psyllia mali *Schmidberger. Manuscript Thesis (M. Sc.) McGill University. Montreal.*

Schlee, D. (1969). Sperma-übertragung (und andere merkmale) in ihrer bedeutung für das phylogenetische system der sternorrhyncha (insecta, hemiptera) Phylogenetische studien an hemiptera I. psylliformes (psyllina und aleyrodina) als monophyletische gruppe. *Z. Morph. Tiere*, *64*, 95–138. https://doi.org/https://doi.org/10.1007/BF00391783

Shen, W., Halbert, S. E., Dickstein, E., Manjunath, K. L., Shimwela, M. M., & Bruggen, A. H. C. van. (2013). Occurrence and in-grove distribution of citrus huanglongbing in north Central Florida. In *Journal of Plant Pathology* (Vol. 95, pp. 361–371). Società Italiana di Patologia Vegetale (SIPaV). https://doi.org/10.2307/23721526

Smith, D. B., Bernhardt, G., Raine, N. E., Abel, R. L., Sykes, D., Ahmed, F., Pedroso, I., & Gill, R. J. (2016). Exploring miniature insect brains using micro-CT scanning techniques. *Scientific Reports*, *6*, 21768. https://doi.org/10.1038/srep21768

Snodgrass, R. E. (1935). *Principles of Insect Morphology*. McGraw-Hill Book Company, Inc. https://doi.org/0801428831

Sombke, A., Lipke, E., Michalik, P., Uhl, G., & Harzsch, S. (2015). Potential and limitations of X-Ray micro-computed tomography in arthropod neuroanatomy: a methodological and comparative survey. *The Journal of Comparative Neurology*, *523*(8), 1281–1295. https://doi.org/10.1002/cne.23741

Stalling, D., Westerhoff, M., & Hege, H.-C. (2005). Amira: a highly interactive system for visual data analysis. In *Visualization Handbook* (pp. 749–767). Elsevier. https://doi.org/10.1016/B978-012387582-2/50040-X

Sukthankar, P., Avila, L. A., Whitaker, S. K., Iwamoto, T., Morgenstern, A., Apostolidis, C., Liu, K., Hanzlik, R. P., Dadachova, E., & Tomich, J. M. (2014). Branched amphiphilic peptide capsules: Cellular uptake and retention of encapsulated solutes. *Biochimica et Biophysica Acta (BBA) - Biomembranes*, *1838*(9), 2296–2305. https://doi.org/10.1016/J.BBAMEM.2014.02.005

Thermo Fisher Scientific. (2017). *Amira 3D visualization and analysis software* (6.7.0). FEI. http://www.thermofisher.com/amira-avizo

Triplehorn, C. A., & Johnson, N. F. (2005). *Borror and De Long's Introduction to the Study of Insects, 7th edition*.

Weber, H. (1929). Kopf und thorax von *Psylla mali* Schmidb. (Hemiptera-Homoptera). Eine morphogenetische studie. *Z. Morph. Ökol. Tiere*, *14*, 59–165. https://link.springer.com/content/pdf/10.1007/BF00419345.pdf

Wenninger, E. (2008). Behavioral evidence for a female-produced sex attractant in

Diaphorina citri. *Entomologia Experimentalis et Applicata*, *128450–459*. http://onlinelibrary.wiley.com/doi/10.1111/j.1570-7458.2008.00738.x/full

Wigglesworth, V. B. (1930). A Theory of Tracheal Respiration in Insects. *Proceedings of the Royal Society B: Biological Sciences*, *106*(743), 229–250. https://doi.org/10.1098/rspb.1930.0024

Wigglesworth, V. B. (1942). *The principles of insect physiology* (2nd ed.). Methuen & CO. LTD. https://archive.org/details/principlesofinse033321mbp/page/n7

Wipfler, B., Pohl, H., Yavorskaya, M. I., & Beutel, R. G. (2016). A review of methods for analysing insect structures — the role of morphology in the age of phylogenomics. In *Current Opinion in Insect Science* (Vol. 18, pp. 60–68). Elsevier Inc. https://doi.org/10.1016/j.cois.2016.09.004

Witlaczil, E. (1885). Die Anatomie der Psylloden. *Zeitschrift Für Wissenschaftliche Zoologie*, *42*, 569-638 + 3 tafeln. https://archive.org/details/zeitschriftfurwi4218unse/page/624/mode/2up?q=psyll

Yen, A., & Burckhardt, D. (2017). *Diagnostic protocol for the detection of the tomato potato Psyllid,* Bactericera cockerelli *(Šulc) prepared for the Subcommittee on Plant Health Diagnostic Standards (SPHDS)*. http://plantbiosecuritydiagnostics.net.au/resource-hub/priority-pest-diagnostic-resources/

Zheng, L., Liang, Q., Yu, M., Cao, Y., & Chen, W. (2020). Morphological characterization of antennae and antennal sensilla of *Diaphorina citri* Kuwayama (Hemiptera: Liviidae) nymphs. *PLOS ONE*, *15*(6), e0234030. https://doi.org/10.1371/journal.pone.0234030

Zucht, B. (1972). Bau und Entwicklung der äußeren Genitalorgane bei Psyllinen (Homopteren). *Zool. Jb. Anat. Bd.*, *231*, 167–231.

5.2.- "Estudio microtomográfico de la genitalia y sistema reproductor del macho del psílido asiático de los cítricos, *Diaphorina citri* Kuwayama, 1908 (Insecta: Hemiptera, Liviidae)"

PLOS ONE

RESEARCH ARTICLE

Micro-CT study of male genitalia and reproductive system of the Asian citrus psyllid, *Diaphorina citri* Kuwayama, 1908 (Insecta: Hemiptera, Liviidae)

Ignacio Alba-Alejandre[1☯], Wayne B. Hunter[2], Javier Alba-Tercedor[1☯*]

1 Department of Zoology, Faculty of Sciences, University of Granada, Campus de Fuentenueva, Granada, Spain, **2** U.S. Dept. Agriculture, Agricultural Research Service, Fort Pierce, Florida, United States of America

☯ These authors contributed equally to this work.
* jalba@ugr.es

Check for updates

OPEN ACCESS

Citation: Alba-Alejandre I, Hunter WB, Alba-Tercedor J (2018) Micro-CT study of male genitalia and reproductive system of the Asian citrus psyllid, *Diaphorina citri* Kuwayama, 1908 (Insecta: Hemiptera, Liviidae). PLoS ONE 13(8): e0202234. https://doi.org/10.1371/journal.pone.0202234

Editor: Ulrich Melcher, Oklahoma State University, UNITED STATES

Received: May 11, 2018

Accepted: July 30, 2018

Published: August 16, 2018

Data Availability Statement: All relevant data are within the paper and its Supporting Information files. Other Videos of ACP Anatomy are at: www.citrusgreening.org and www.youtube.com/albatercedor.

Funding: This work was supported by USDA-NIFA Award 2014-70016-23028 "Developing an Infrastructure and Product Test Pipeline to Deliver Novel Therapies for Citrus Greening Disease", 2015-2020; https://portal.nifa.usda.gov/web/crisprojectpages/1005600-developing-an-

Abstract

The Asian citrus psyllid (ACP), *Diaphorina citri*, is a major vector of the bacteria *Candidatus* Liberibacter asiaticus and *C*.L. americanus, which cause Huanglongbing disease (HLB) (aka Citrus greening disease), considered the most serious bacterial disease of citrus trees. As part of a multidisciplinary project on psyllid biology (www.citrusgreening.org), the results presented here concern a detailed anatomical study of the male reproductive system (testes, seminal vesicles, accessory glands, sperm pump, connecting ducts, and aedeagus) using micro-computed tomography (micro-CT). The study summarizes current knowledge on psyllids male reproductive system and represents significant advances in the knowledge of ACP anatomy.

Introduction

The Asian citrus psyllid (ACP) *Diaphorina citri* (Hemiptera: Liviidae) was first discovered in Shinchiku (Taiwan) in 1907 [1]. Since then, it has become a major vector of citrus in agriculture, transmitting the bacteria *Candidatus* Liberibacter spp. to citrus crops (e.g. lemons, limes, oranges, grapefruit, tangerines, and kumquats), causing Huanglongbing (HLB), also called citrus greening disease. HLB is considered the most serious disease threatening the citrus industry. HLB causes yield loss as well as small, bitter, unpalatable fruit, and eventually tree death. This pathogen is transmitted to the psyllid vector mainly during nymphal feeding on infected citrus trees [2]. *Diaphorina citri* infected with *C.* Liberibacter reportedly increases in fecundity, producing a greater number of offspring [3]. Today HLB has spread to over 40 different countries in Asia, Oceania, and North as well as South America [4,5].

Studies on psyllid anatomy have been published on: general anatomy [6–11], sperm morphology [12,13], testes structure [14–16], biology on different hosts, effects of temperature

Artículo publicado (bajo licencia de dominio público "Creative Commons CC0"):

Alba-Alejandre I, Hunter WB., & Alba- Tercedor J (2018) Micro-CT study of male genitalia and reproductive system of the Asian citrus psyllid, *Diaphorina citri* Kuwayama, 1908 (Insecta: Hemiptera, Liviidae). *PLoS ONE* 13(8), e0202234: 1-16. https://doi.org/10.1371/journal.pone.0202234

5.2.1.- Resumen

El psílido asiático de los cítricos (PAC), *Diaphorina citri*, es un importante vector de la bacteria *Candidatus* Liberibacter asiaticus y *C*.L. americanus, que causan la enfermedad de Huanglongbing (HLB) (también conocida como enfermedad de enverdecimiento de los cítricos), considerada la enfermedad bacteriana más grave de los cítricos. Como parte de un proyecto multidisciplinar sobre biología psílida (www.citrusgreening.org), los resultados presentados aquí se refieren a un estudio anatómico detallado del sistema reproductor masculino (testículos, vesículas seminales, glándulas accesorias, bomba espermática, conductos de conexión y edeago) usando microtomografía computarizada (micro-CT). El estudio resume el conocimiento actual sobre el sistema reproductor masculino de los psílidos y representa avances significativos en el conocimiento de la anatomía del PAC.

5.2.2.- Abstract

The Asian citrus psyllid (ACP), *Diaphorina citri*, is a major vector of the bacteria *Candidatus* Liberibacter asiaticus and *C.*L. americanus, which cause Huanglongbing disease (HLB) (aka Citrus greening disease), considered the most serious bacterial disease of citrus trees. As part of a multidisciplinary project on psyllid biology (www.citrusgreening.org), the results presented here concern a detailed anatomical study of the male reproductive system (testes, seminal vesicles, accessory glands, sperm pump, connecting ducts, and aedeagus) using micro-computed tomography (micro-CT). The study summarizes current knowledge on psyllids male reproductive system and represents significant advances in the knowledge of ACP anatomy.

5.2.3.- Introduction

The Asian citrus psyllid (ACP) *Diaphorina citri* (Hemiptera: Liviidae) was first discovered in Shinchiku (Taiwan) in 1907 (Kuwayama, 1907). Since then, it has become a major vector of citrus in agriculture, transmitting the bacteria *Candidatus* Liberibacter spp. to citrus crops (e.g. lemons, limes, oranges, grapefruit, tangerines, and kumquats), causing Huanglongbing (HLB), also called

citrus greening disease. HLB is considered the most serious disease threatening the citrus industry. HLB causes yield loss as well as small, bitter, unpalatable fruit, and eventually tree death. This pathogen is transmitted to the psyllid vector mainly during nymphal feeding on infected citrus trees (Inoue *et al.*, 2009). *Diaphorina citri* infected with *C.* Liberibacter reportedly increases in fecundity, producing a greater number of offspring (Pelz-Stelinski & Killiny, 2016). Today HLB has spread to over 40 different countries in Asia, Oceania, and North as well as South America (Halbert & Manjunath, 2004; Shen *et al.*, 2013).

Studies on psyllid anatomy have been published on: general anatomy (Alba-Tercedor *et al., 2017*; Bitsch, 1979; Brittain, 1922; Muir, 1930; Saunders, 1921; Zucht, 1972), sperm morphology (Barcellos *et al.*, 2017; Labina & Maryańska-Nadachowska, 2014), testes structure (Głowacka *et al.*, 1995; Valentina G. Kuznetsova *et al.*, 2012; Maryańska-Nadachowska & Głowacka, 2005), biology on different hosts, effects of temperature (Liu & Tsai, 2000; Nava *et al.*, 2007), genetics (V. G. Kuznetsova, Nokkala, & Maryańska-Nadachowska, 1997; Macharashvili & Kuznetsova, 1997; Maryańska-Nadachowska *et al.*, 1996; Wang *et al.*, 2017; Wu *et al.*, 2016), communication between sexes (Wenninger, Hall, *et al.*, 2009), abdominal color, and reproductive potential (Wenninger, Stelinski, *et al.*, 2009) as well as even daily timing of mating and age at reproductive maturity (Wenninger & Hall, 2009). Moreover, a preliminary micro-CT anatomical study is available (Alba-Tercedor *et al.*, 2017). Although different studies have been conducted specifically on the male reproductive system of different Psylloidea species (Conci & Tamanini, 1988; E. Głowacka & Maryańska-Nadachowska, 1993, 1998; Hodkinson & White, 1979; Ibanez *et al.*, 2014; V. G. Kuznetsova, Nokkala, Maryańska-Nadachowska, *et al.*, 1997; Maryanska-Nadachowska *et al.*, 2001; Maryańska-Nadachowska *et al.*, 2001; Maryańska-Nadachowska & Głowacka, 1997; Park & Taylor, 2003; Prophetou-Athanasiadou & Tzanakakis, 1998), studies on ACP are lacking, with only one classical study of the sperm pump by Schlee using light microscopy to examine different species of Psyllina and Aleyrodina, and briefly commenting on *Diaphorina citri* (Schlee, 1969). Also, Stockton *et al.* investigated the possible reasons why females prefer mating with orange males over blue males, providing schematics of reproductive systems from dissected specimens (Stockton *et al.*, 2017).

The main aim of this work was to expand the understanding of the ACP male reproductive system, to fill gaps regarding the anatomical morphology. The study presents the first extensive application of the micro-CT techniques on the male reproductive system in psyllids. This is a non-destructive method, which enhances the viewing and understanding of structures in their natural anatomical position, avoiding additional deformation that often occurs during dissections and/or slide preparation.

5.2.4.- Materials and Methods

The ACP specimens for this study come from the rearing facilities at the United States Department of Agriculture, Agriculture Research Service, Fort Pierce, Florida (USA). Adult specimens shown in Figs 1 to 8 (except that of Fig 7a) were fed for three days on an orange tree sprig submerged in BAPC (***B****ranched* ***A****mphiphilic* ***P****eptide* ***C****apsules*) linked to Hg as a contrast agent (Sukthankar *et al.*, 2014). The insects were rinsed three times, 10 min each, with 30% ethanol, dehydrated in an ethanol series (30 min per step, 50%, 70, 80, 90, 95, three times at 100%), and chemically dried by submersion in 2 ml of 100% hexamethyldisilazane (HMDS) for 2 hours, and drying overnight at 35ºC. Finally they were glued with cyanoacrylate to the tip of a nylon fishing line 200 µm in diameter, as previously described (Alba-Tercedor, 2014; Alba-Tercedor *et al., 2017*). The prepared insects were scanned with a SkyScan 1172 desktop high-resolution micro-CT, with a Hamamatsu L702 source and a Ximea 11Mp camera. Using the following setting parameters: isotropic voxel size=0.54µm per pixel; source voltage=56KV, source current=43µA, image rotation step=0.3º, 360º rotation scan, and no filter. The Fig 7a corresponds to a psyllid taken live and prepared by overnight fixation in 4% glutaraldehyde with 2.5% formaldehyde containing sodium cacodylate buffer pH 6.5, dehydrated as above, and scanned with the following setting parameters: isotropic voxel size=0.52µm per pixel; source voltage=47KV, source current=51µA, image rotation step=0.2º, 360º of rotation scan, and no filter.

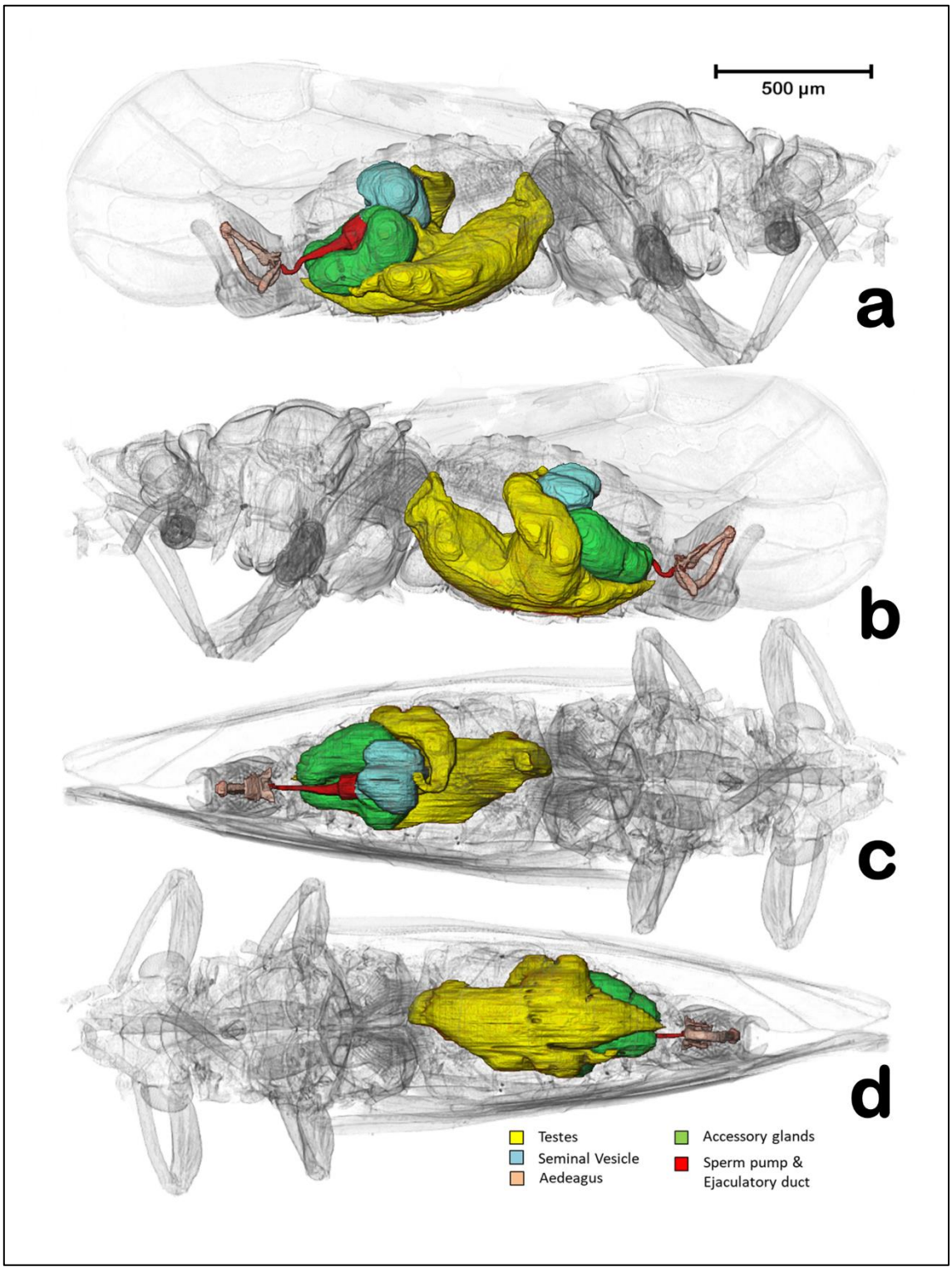

Figure 1.- Volume rendering reconstructions of the male reproductive system in its anatomical position, in different perspective views: (**a**) Right lateral, (**b**) Left lateral, (**c**) Dorsal, (**d**) Ventral.

For primary reconstructions and the cleaning process to compile the datasets of cross-sectional images (slices), we used the Skyscan (www.skyscan.be) software (NRecon, DataViewer, CTAnalyser). We reconstructed, re-oriented, and eliminated noise of the images as previously described (Alba-Tercedor, 2014). Volume renderings of the images were made using FEI's Amira software v.6.4, (using the built-in "volenRed.col" color filter) (FEI, 2017), except for Fig 7a, which was made with Skyscan's software CTVox (colors were applied by varying the color-transfer function curves, in conjunction with the lighting and shading options). For a more detailed explanation of the process, see the previous paper (Alba-Tercedor, 2014).

The images of the aedeagus visualized by microtomography were compared with those made after routine light-microscope slide preparation, using one aedeagus dissected from a male terminalia mounted on a slide in Hoyer's liquid with a cover slip (Fig 7g). In accordance with the micro-CT results (as in the figures), the standard anatomical position is used to describe structures.

5.2.5.- Results

In the specimens studied, the reproductive system appears voluminous, occupying more than 50% of the abdominal volume (Fig 1). It consists of

two lateral testes, appearing to have a single spindle-shaped structure narrow and elongated at both the fore and hind ends, appearing as narrow lobes (Figs 2, 3 and 5a). A vas deferens extends from the medial zone to the posterior ventral surface of the seminal vesicle (Figs 3b,c and 5a). Seminal vesicles appear globose, close to each other and, together with the long, ovoid accessory glands, connect to the sperm pump through short ducts (Figs 1a-d, 3, 4 and 5a-f).

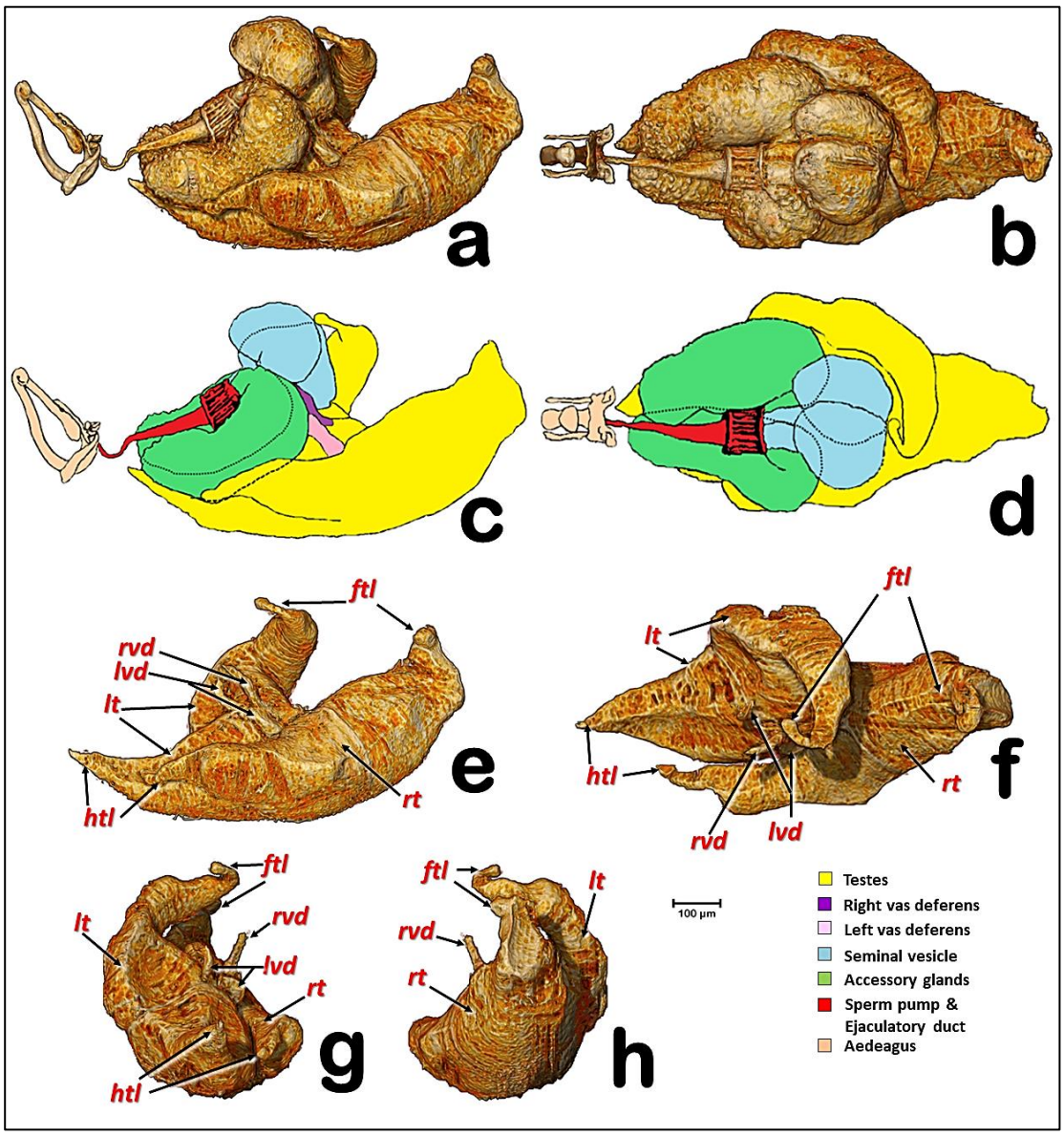

Figure 2.- Volume rendering reconstructions of the male reproductive system in different perspective views: (**a, c**) Right lateral; (**b, d**) Dorsal; (**e**) Testes, lateral; (**f**) Testes, dorsal; (**g**) Testes, postero-anterior; (**h**) Testes, antero-posterior; (**ftl**) Fore testicular lobe; (**htl**) Hind testicular lobe; (**lvd**) Left vas deferens; (**lt**) Left testis; (**rt**) Right testis; (**rvd**) Right vas deferens.

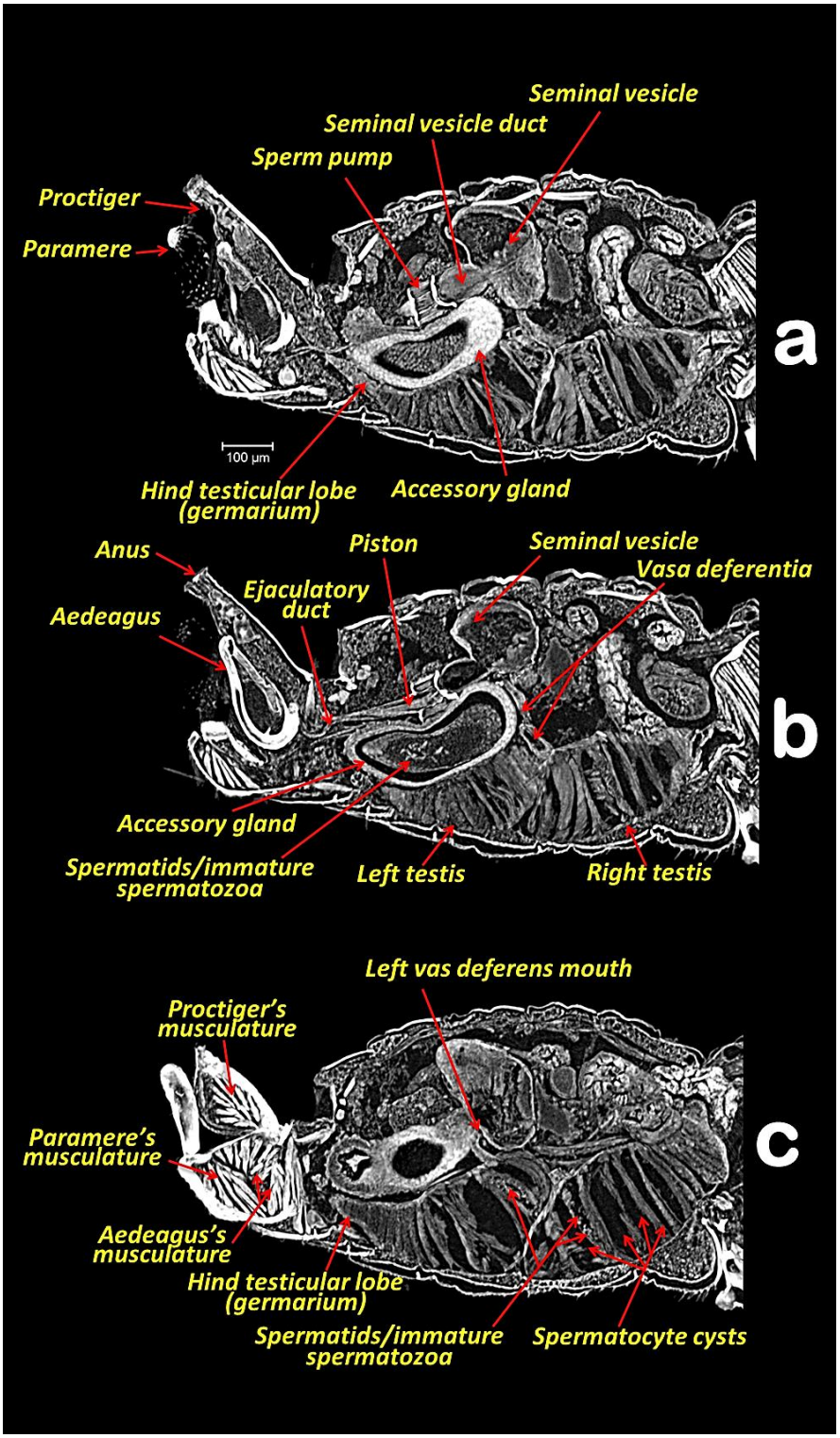

Figure 3.- Abdominal middle-left sagittal section views with Amira Multiplanar slicing. (**a**, **b**, **c**) Consecutive slices (23 µm thick) from the right towards the left side.

Each testis has an anterior (frontal) and posterior (hind) lobe (Figs 2 and 3a,c). In section, the spermatocyte cysts are visible, clearly separated by dorso-ventral walls forming a single row (Figs 3, 4a and 5f). In the middle zone appear

spermatocyte cysts containing spermatozoa in their final developmental stages (Figs 3b,c and 4b). Vasa deferentia appear as long narrow ducts (ca. 20 µm in diameter) (Figs 2, 3b,c, and 5a).

Two globose seminal vesicles touch each other but remain discrete (no interconnection is visible; Figs 1-3 and 5), and from the ventral-hind surface of each a vas deferens extends from the corresponding testis (Figs 3b,c and 5a). From the hind ventral part stems a short wide duct (ca. 50 µm in diameter) that comes together with the accessory gland duct and connects to the sperm pump (Figs 2d,3,4c and 5b-f).

The accessory glands, situated lateroventrally to the sperm pump (Figs 1, 2a-c, 3, 4a, 5f, and 6d), have external and internal walls (Figs3, 4a, 5c-f, and 6d). Inside, dense structures are visible (Figs 3b, 4a,c, and 5f) with the size and shape of the spermatozoa described for *D. citri* (Barcellos *et al.*, 2017). From the inner hind dorsal end of each accessory gland extends a short duct, ovoidal in section (ca. 23 x 40 µm; Figs 2a-d and 5b-e).

Known classically as the sperm pump (Figs 1, 2a-d, 3a-b, 4c, and 5a-b, f-n), this organ is composed of a cylindrical fore part and a long-narrow conical hind part that connects with the sperm duct. The cylindrical part consists of an anterior sclerotized, slightly oval, concave plate (ca. 63 x 87 µm) with two middle foramina separated by a dorso-ventrally aligned ridge (Fig 5j-l). On each side of the ridge are the connections of both seminal vesicles, and accessory-gland ducts. A conical structure is connected to the fore plate through a series of longitudinal muscles appearing as parallel bands, forming a pumping chamber (ca. 50 µm in length; Figs 1a-d, 3a-b, 5b,f-i,k, and 6d). The conical part contains a long piston structure fixed to the anterior part by a muscle, appearing as an attachment filament (Figs 3b, 5f,h). This connects the fore tip of the piston at the center of the longitudinal ridge in the inner-posterior central surface of the concave plate (Fig 5m).

A narrow ejaculatory duct (ca. 15 µm in diameter) extends from the posterior tip of the sperm pump (Figs 1, 2a-d, 3b, 5b,f, and 6d), connected to the aedeagus

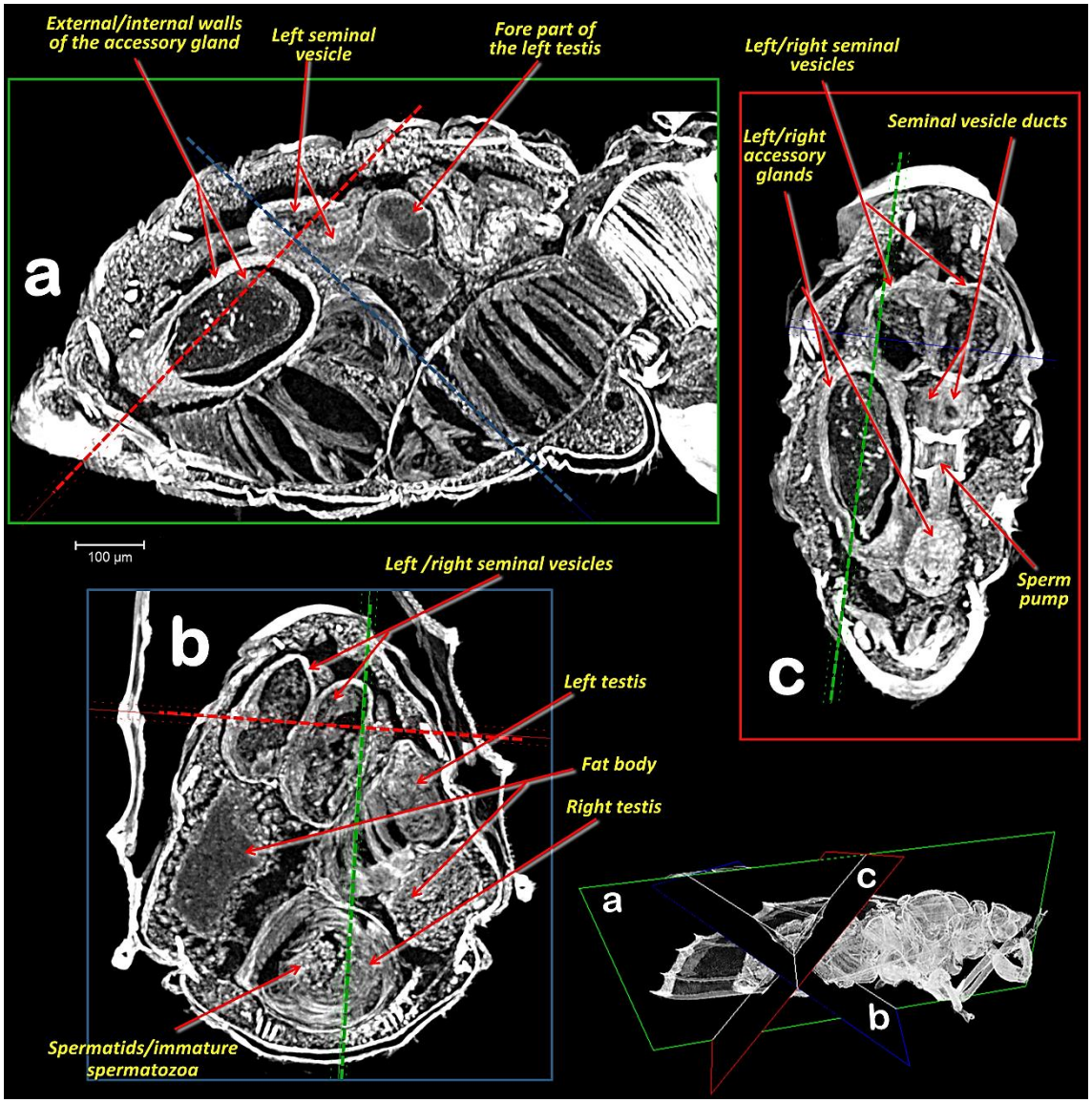

Figure 4. Abdominal Amira Multiplanar sections (**a**, **b**, **c**) slices (23 µm thick) according to plane views shown in the right-bottom view.

and passing through it (Fig 7f) by a foramen situated at its basal fore plate (Fig 8b,k).

The external genitalia (abdominal terminalia) consist of a proctiger plate (also called as anal tube (Ammar *et al.*, 2013)) with the anus opening on the dorsal tip, a subgenital plate, and two parameres (also called lateral plates (Ammar *et al.*, 2013)), acting as forceps or gonostyles (Figs 1, 3, 6, and 7a-d). Each has a small pointed end, and numerous trichoid sensillae along the inner margins (Fig 6b-d).

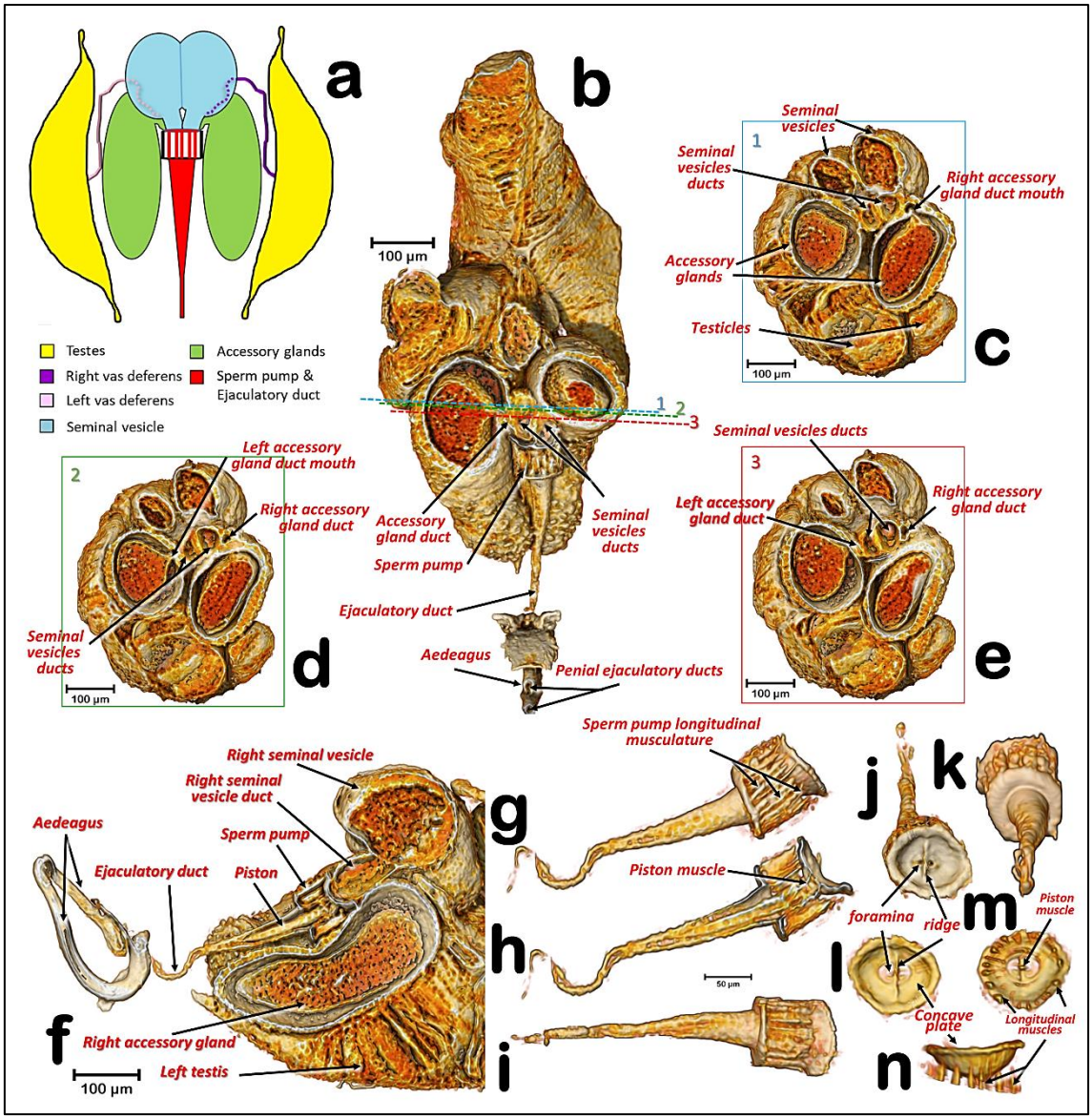

Figure 5. General configuration, sections, and details of the reproductive structures. (**a**) Schematic structure of the male reproductive system, showing the connection between the testes and seminal vesicles (via vasa deferentia) as well as the connection of seminal vesicles and accessory glands to the sperm pump; (**b**) Dorso-ventral (coronal) section at the level of the accessory glands and seminal vesicles ducts. (**c**, **d**, **e**) Antero-posterior (axial) sections of planes shown with blue, green, and red lines numbered as 1, 2, & 3, respectively; (**f**) Sagittal section; (**g**-**k**) sperm pump and ejaculatory duct (**g**: right lateral view, **h**: sagittal section **i**: ventral view, **j**: antero-posterior view, **k**: postero-anterior view); (**l**-**n**) Detail of the anterior plate on the sperm pump showing the foramens **(l**: antero-posterior view, **m**: postero-anterior view, **n**: dorsal view).

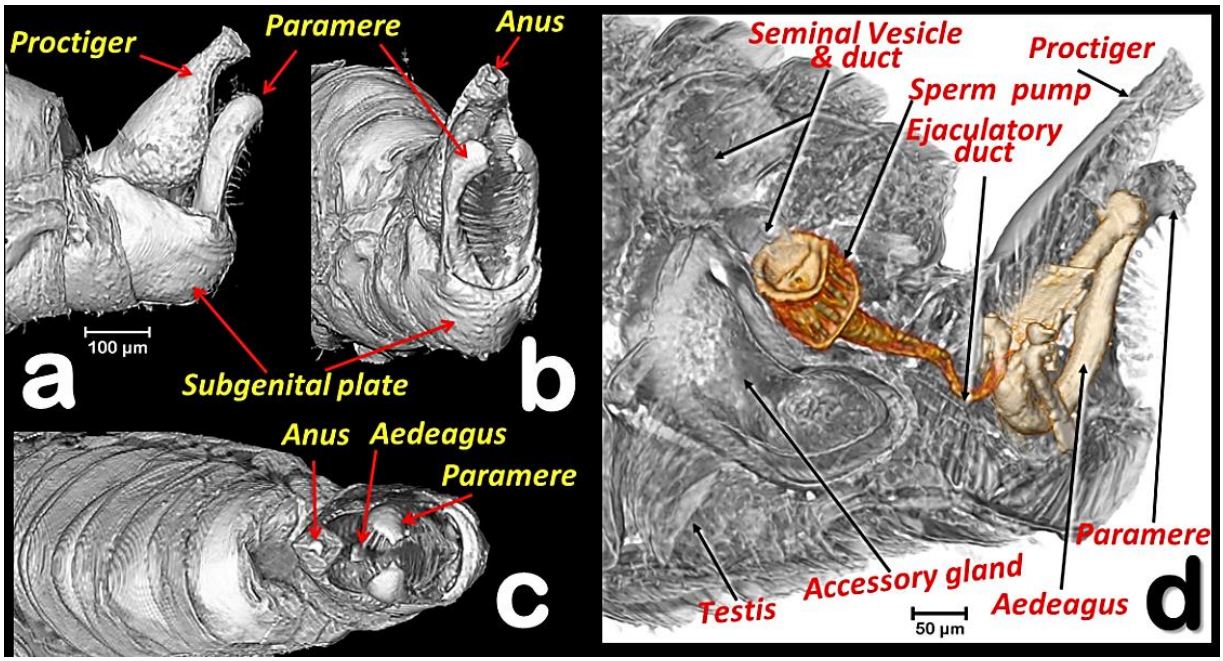

Figure 6. Volume rendering reconstruction of the male abdominal genital terminalia in different perspective views (a-c) and a sagittal right section (d). (**a**) Left lateral, (**b**) Left latero-posterior, (**c**): Apico-dorsal, (**d**) Testis, seminal vesicle, accessory gland, sperm pump, ducts, and aedeagus structures superimposed over a sagittal section of the hind abdominal segments.

Dorsally and externally the elbow joint of the first and second segment of the aedeagus is visible (Fig 6c). The internal musculature are pictured in Figs3, 6d, and 7a-d.

The internal genitalia (Figs 1, 3a-b, 5f, 6d, 7, and 8), consist of a three segmented aedeagus with two long initial segments articulated by a dorsal joint, and an enlarged 3rd distal-end segment, convex on the inner side and flattened on the external side, with a concavity, forming at margins two ridges that are Y shaped (Fig 8b,d-f), and with a rounded tip pierced by two small apical foramina (Fig 8f).

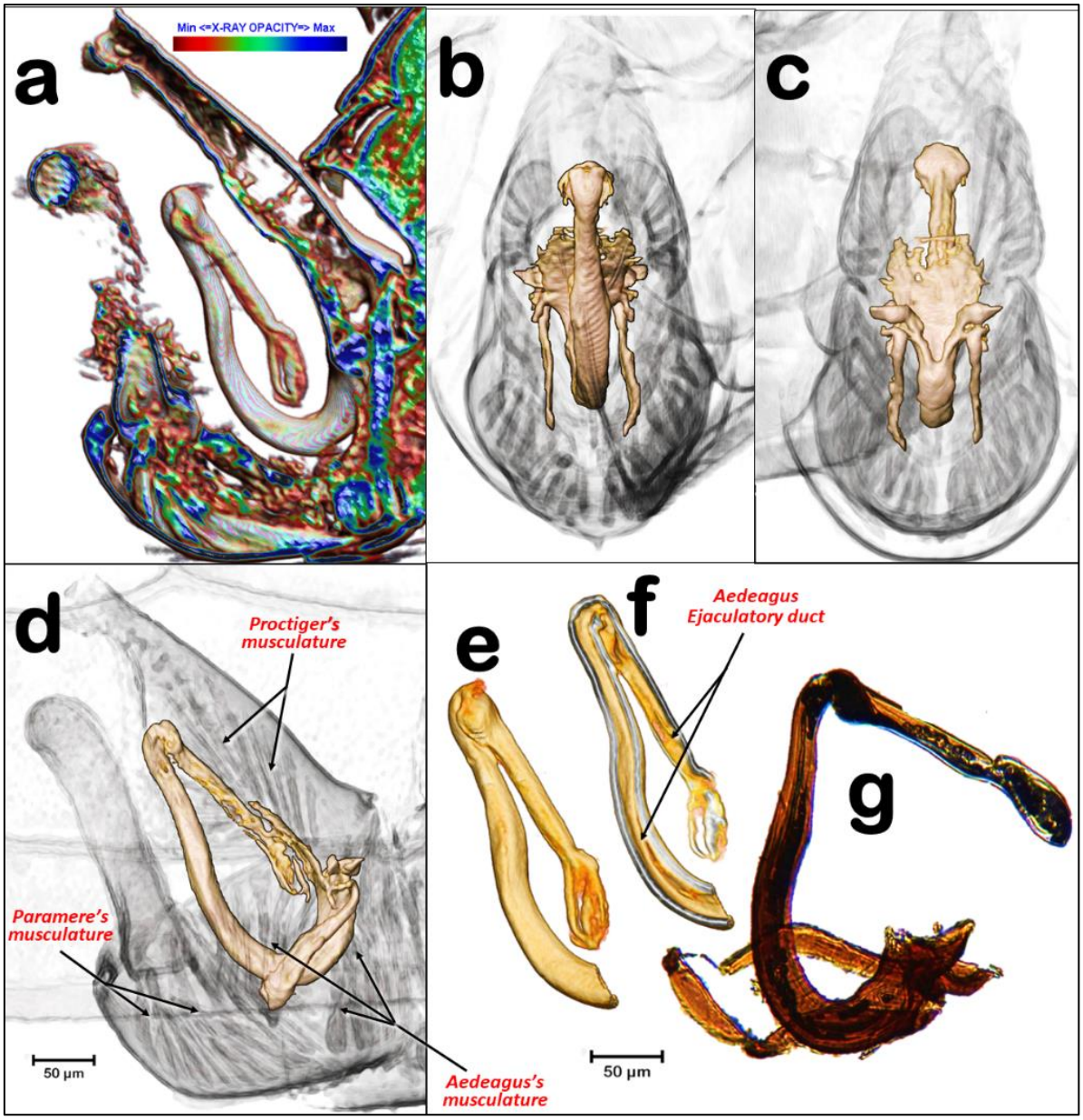

Figure 7. Internal details of the terminalia and aedeagus. (**a**) CTVox volume rendering, (**b-f**) Amira volume renderings, **(g)** light-microscope right lateral view of the aedeagus, mounted in a slide. Volume renderings with details of the male hind abdominal segments showing the anatomical position of the aedeagus structures and associated musculature. (**a**, **d**) right-lateral, (**b**) postero-anterior, (**c**) antero-posterior, transparented to display the sclerotized structures of the aedeagus.

The 1st segment is hook-shaped, with a rectangular (longer than wider) basal fore plate, which is basally pierced by the foramen of the ejaculatory duct. This has two antero-posterior long lateral basal apophyses, two short postero-latero-basal apophyses, and two short antero-latero-basal apophyses. The margin behind the 1st segment is slightly concave on the distal third.

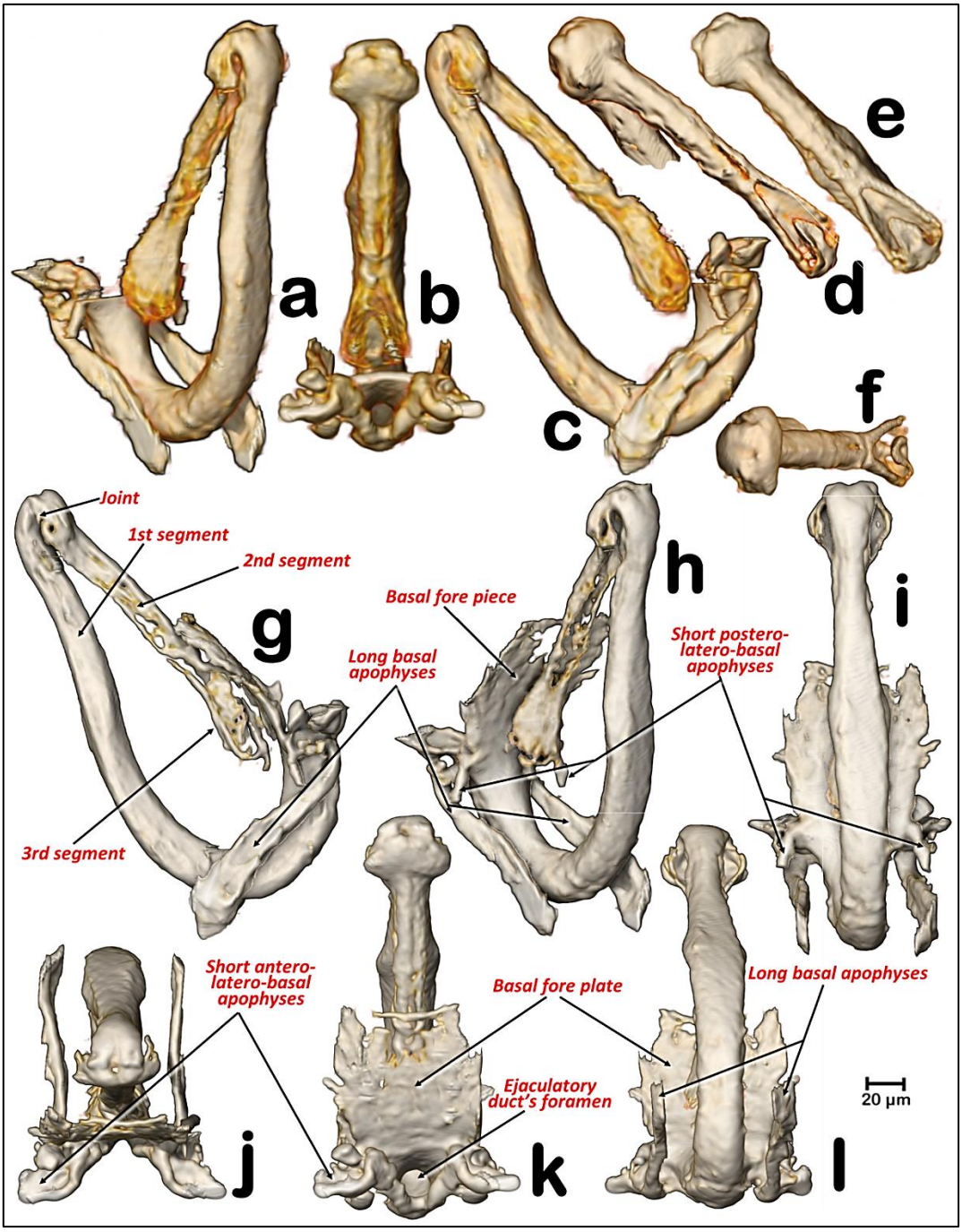

Figure 8. Details of the aedeagus in different perspective views. (**a, h**) angled left-lateral posterior view, (**d**) angled right latero-anterior view, (**b**, **e**, **k**) dorsal, (**c**, **g**) right-lateral, (**i**) postero-anterior, (**f**, **j**) angled dorsal, (**l**) ventral. (**d-l**) For visualization, the renderings have been transparented with Amira software to eliminate soft tissues and enhance harder-sclerotized structures.

Internally, in a resting position, the 1st segment of the aeadeagus appears parallel to the paramers, while the 2nd segment is parallel to dorsal edge of the proctiger and runs from a dorsal position pointing ventralwards to join the 3rd segment.

Different animated perspective views can be visualised as supplementary video files (S1, S2).

5.2.6.- Discussion

Głowacka *et al.* (Głowacka *et al.*, 1995) reported that the testes of *Diaphorina citri* have spermatocyte cysts arranged in one row, in agreement with our observations (Figs 3, 4, and 5f). Moreover, according to these authors each testis has two follicles, while for *Bactericera albiventris* they described and figured an almost complete fusion (but with a slight vestigial separation) of follicles. At first sight, each testis of the ACP appears to consist of a spindle-shaped single lobe. However, a detailed examination clearly reveals narrow lobes at both ends of each testis, and in sagittal sections these unequivocally correspond to the germinal zone of testes (germarium). Thus, what appears to be a single structure, actually consists of two follicles, fused into a single external structure, with a common vas deferens. This agrees with the view in sagittal sections. From each germarium, towards the vas deferens connection, spermatozoa inside spermatocyte cysts are formed and progressively mature. Spermatids/immature spermatozoa are clearly visible in the middle part of each testis (Figs 3c and 4a,b), similar to the description of *Aphalara polygoni* by Głowacka *et al.* (Głowacka *et al.*, 1995).

Although it may seem strange to find spermatozoa in the accessory glands, the seminal vesicles and accessory gland ducts connect to the sperm pump very close together, in a small area of the concave plate, just before the seminal pump chamber (Figs 2b,d and 5a), so that spermatozoa could easily reach the accessory glands.

The structure classically interpreted as a sperm pump has received different names. Witlaczil (Witlaczil, 1885) called it "*kolbenförmiges Organ*"

(literally, “piston-shaped organ”), but it was not until Saunders (Saunders, 1921) that the function of this structure was accurately interpreted and this researcher referred to it as an "ejaculatory pump", as did Brittain (Brittain, 1922). While Qadri (Qadri, 1949) called it a “seminal pump”, Schlee used the term “sperm pump” (Schlee, 1969) and so did Prophetou (Prophetou-Athanasiadou & Tzanakakis, 1998). We adopt the term “sperm pump” as the most accurate name because it refers to its apparent function. The detailed structure revealed by micro-CT appears to have all the impellent suction elements of such a pump. The 3D examination provides new information to explain how the pumping functions to avoid sperm reflux. Thus, by the contraction of the longitudinal muscles surrounding the cylindrical pumping chamber (Fig 5g,m, and n), the sperm would be pressed out of the chamber and into the ejaculatory duct. Simultaneously, the piston’s muscle (attached between the fore tip of the piston and the internal central surface of the inner-posterior side of the concave plate) would contract, preventing sperm reflux. Thus, the dorso-ventral fore ridge of the concave plate apparently reinforces the plate against bending during the muscle contraction.

The observed micro-CT sperm pump structure matches prior descriptions for other closely related Psyllinae species (Brown & Hodkinson, 1988; Schlee, 1969; Zucht, 1972) as well as what Matsuda summarized (Matsuda, 1976). Thus the new visualization improves on the previous drawing of the ACP sperm pump by Mathur (Mathur, 1975).

The genus *Diaphorina* has a characteristic 3-segmented aedeagus. In papers, the male genitalia of *D. citri* are depicted with a “spoon”-shaped, dilated 3rd segment, (Burckhardt (Burckhardt, 1987), Mathur (Mathur, 1975)). In light-microscope slides the 3rd segment looks more enlarged, and spoon shaped (Fig 7g) than in a previous micro-CT study (Alba-Tercedor *et al., 2017*), or in the present study (Figs 7 and 8). This is because in light-microscope slide the 3rd segment results compressed under the cover slip and therefore deformed. In fact, Ammar *et al.* (Ammar *et al.*, 2013) published a picture from a light microscope slide of the male terminalia where the tip of the aedeagus appears unusually enlarged and spoon shaped (as in Fig 7g), but in a SEM image (where the genitalia were not compressed), the 3rd segment has a shape similar to that in our micro-CT volume rendering reconstructions. The most precise anatomical

descriptions of the genitalia and aedeagus of a psyllid species has been published for *Psylla crataegi* by Zucht (Zucht, 1972), and later included in classic works, such as the one by Bitsch (Bitsch, 1979), and the one for *P. mali* by Muir (Muir, 1930) where (after microscopic slide preparation, and threafter compression) the basal fore plate (called the “basal plate”) and the long basal apophyses (called the “basal prolongations”) were depicted. However, no observations have been made on the details described above and summarised in Fig 8, and no similar study has described and/or depicted psyllids, including *D. citri*.

During dissection, certain animal organs such as testes, which are tethered, can spin on the tether and change their position when viewed in the open. However, inside the animal they maintain a fixed position. In fact, by micro-CT, we studied several specimens and in all of them the structures remained in similar positions, as described.

Micro-CT volume rendering images offer quality comparable to low-magnification scanning (SEM), with the additional advantage that viewing is possible from any angle or perspective, in a way not possible with electron microscopy. The rapid advance on micro-CT and nano-CT technology, with constant magnification and resolution improvements, are approaching the power of electron microscopy, representing a promising future for new discoveries.

5.2.7.- Supplementary Information

Videos:

S1.- Video of the ACP male reproductive system. Spinning animation of a micro-CT volume rendering reconstruction of the male reproductive structures, permitting to observe them from different angles. Components (testes, accessory glands, seminal vesicles, sperm pump, ejaculatory duct and aedeagus) are dissembled, rotated and assembled to their actual anatomical position. https://journals.plos.org/plosone/article/file?type=supplementary&id=info:doi/10.1371/journal.pone.0202234.s001

S2.- Video with cut views of the ACP male reproductive system. Spinning animation of a micro-CT volume rendering reconstruction of the male reproductive structures, with progressive sagittal and transversal cut views. https://journals.plos.org/plosone/article/file?type=supplementary&id=info:doi/10.1371/journal.pone.0202234.s002

5.2.8.- References

Alba-Tercedor, J. (2014). From the sample preparation to the volume rendering images of small animals : A step by step example of a procedure to carry out the micro-CT study of the leafhopper insect *Homalodisca vitripennis* (Hemiptera: Cicadellidae). *Bruker Micro-CT Users Meeting 2014*, 260–288. http://www.skyscan.be/company/UM2014/008_Javier_Alba_Tercedor.pdf

Alba-Tercedor, J., Hunter, W. B., Cicero, J., & Brown, S. (2017). Micro-CT Scanning of Asian Citrus Psyllid, *Diaphorina citri*, Anatomy and Feeding. *Journal of Citrus Pathology*, *4*(1), 1–2.

Alba-Tercedor, J., Hunter, W. B., Cicero, J. M., & Sáinz-Bariáin, M. (2017). Use of micro-CT to elucidate details of the anatomy and feeding of the Asian Citrus Psyllid *Diaphorina citri* Kuwayama , 1908 (Insecta : Hemiptera , Lividae). In *Bruker Micro-CT Users Meeting 2017* (pp. 270–285). Bruker microCT-Skyscan. http://bruker-microct.com/company/UM2017/AbstractBook2017.pdf

Ammar, E.-D., Alessandro, R., Shatters Jr, R. G., & Hall, D. G. (2013). Behavioral, Ultrastructural and Chemical Studies on the Honeydew and Waxy Secretions by Nymphs and Adults of the Asian Citrus Psyllid *Diaphorina citri* (Hemiptera: Psyllidae). *PLoS ONE*, *8*(6), e64938. https://doi.org/10.1371/journal.pone.0064938

Barcellos, M. S., Fernanda, J., Cossolin, S., Dias, G., & Lino-Neto, J. (2017). Sperm morphology of the leafhopper *Diaphorina citri* Kuwayama (Hemiptera: Sternorrhyncha: Psylloidea: Liviidae). *Micron*, *99*, 49–55. https://doi.org/10.1016/j.micron.2017.03.017

Bitsch, J. (1979). Morphologie Abdominale des Insectes. Ordre des Homoptères, B.- Psylles. In *Traité de Zoologie. Anatomie, Systématique, Biologie. T. VIII, Insectes Thorax, Abdomen. Fasc. II (P.P. Grassé)* (pp. 420–425).

Brittain, W. H. (1922). The morphology and synonymy of *Psylla mal*i Schmidberger. *Proceeding Acadian Entomological Society (Fredericton)*, *8*, 23–51.

Brown, R. G., & Hodkinson, I. D. (1988). *Taxonomy and Ecology of the Jumping Plant-lice of Panama: Homoptera, Psylloidea*. E. J. Brill/Scandanavian Science Press Ltd.,.

Burckhardt, D. (1987). Jumping plant lice (Homoptera: Psylloidea) of the temperate neotropical region. Part 2: Psyllidae (subfamilies Diaphorininae, Acizziinae, Ciriacreminae and Psyllinae). *Zoological Journal of the Linnean Society*, *90*, 145–205. https://onlinelibrary.wiley.com/doi/pdf/10.1111/j.1096-3642.1987.tb01353.x

Burckhardt, D. (1994). Generic key to chilean jumping plant·lice (Homoptera: Psylloidea) with inclusion of potential exotic pests. *Rev. Chilena Ent.*, *21*, 57–67.

Conci, C., & Tamanini, L. (1988). Seven Species of *Psylloidea* new for Italy (Homoptera). *Annali Dei Musei Civici Di Rovereto*, *4*, 307–320. http://www.museocivico.rovereto.tn.it/UploadDocs/699_Annali4_1988_art15_conci etal.pdf

FEI. (2017). *Amira 3D Visualization and Analysis Software* (6.4). FEI.

Głowacka, E., & Maryańska-Nadachowska, A. (1993). Anatomy of male reproductive system of the *Psylla* Geoffr. s. 1.(Homoptera, Psyllodea)-Validity for the systematic relations within the Genus. *Folia Biologica (Kraków)*, *41*(3–4), 55–64. https://books.google.es/books?id=c3296OYP72UC&pg=PA55&lpg=PA55&dq=Anatomy+of+Male+Reproductive+System+of+the+Psylla+Geoffr.+s.+1.(Homoptera, +Psyllodea)-

Validity+for+the+Systematic+Relations+within+the+Genus&source=bl&ots=3AYv VsTdTJ&sig=OL8ufud_a_jGrMxOUrx

Głowacka, E., & Maryańska-Nadachowska, A. (1998). Male reproductive system and karyotype of *Mycopsylla fici* (Tryon) (Homoptera, Psylloidea). *Folia Biologica (Kraków)*, *46*(1–2), 17–21.

Głowacka, E., Kuznetsova, V. G., & Maryańska-Nadachowska, A. (1995). Testis follicle number in Psyllids (Psylloidea, Homoptera) as an anatomical feature in studies of systematic relations within the group. *Folia Biologica (Kraków)*, *43*(3–4), 115–124.

Halbert, S. S. E. S., & Manjunath, K. K. L. (2004). Asian Citrus Psyllids (Sternorrhyncha: Psyllidae) and Greening Disease of Citrus: a Literature Review and Assessment of Risk in Florida. *Florida Entomologist*, *87*(3), 330–353. https://doi.org/10.1653/0015-4040(2004)087[0330:ACPSPA]2.0.CO;2

Hodkinson, I. D., & White, I. M. (1979). *Homoptera Psylloidea* (A. Watson (ed.)). Royal Entomological Society of London.

Ibanez, F., Hancock, J., & Tamborindeguy, C. (2014). Identification and expression analysis of aquaporins in the potato psyllid, Bactericera cockerelli. *PLoS ONE*, *9*(10). https://doi.org/10.1371/journal.pone.0111745

Inoue, H., Ohnishi, J., Ito, T., Tomimura, K., Miyata, S., Iwanami, T., & Ashihara, W. (2009). Enhanced proliferation and efficient transmission of *Candidatus* Liberibacter asiaticus by adult *Diaphorina citri* after acquisition feeding in the nymphal stage. *Annals of Applied Biology*, *155*(1), 29–36. http://onlinelibrary.wiley.com/doi/10.1111/j.1744-7348.2009.00317.x/full

Kuwayama, S. (1907). Die Psylliden Japanese. *Transactions of the Sapporo Natural History Society*, *2*, 149-189. (*D. citri*: p. 160-161, Plate III,Fig. 16). https://www.hemiptera-databases.org/psyllespdf/25.pdf

Kuznetsova, V. G., Nokkala, S., & Maryańska-Nadachowska, A. (1997). Karyotypes, sex chromosome systems, and male meiosis in Finnish psyllids (Homoptera: Psylloidea). *Folia Biologica (Kraków)*, *45*(3–4), 143–152.

Kuznetsova, V. G., Nokkala, S., Maryańska-Nadachowska, A., & Macharashvili, I. D. (1997). Karyotypes, Spermatogenesis, and Morphology of the Internal Reproductive System in Males of Some Species of Psyllids (Homoptera, Psylloidea) from Georgia: II. Peculiarities of the Reproductive System and Initial Stages of Spermiogenesis. *Entomological Review*, *1*(77), 21–30.

Kuznetsova, Valentina G., Labina, E. S., Shapoval, N. A., Maryańska-Nadachowska, A., & Lukhtanov, V. A. (2012). *Cacopsylla fraudatrix* sp.n. (Hemiptera: Psylloidea) recognised from testis structure and mitochondrial gene *COI*. *Zootaxa*, *63*(3547), 55–63.

Labina, E., & Maryańska-Nadachowska, A. (2014). Variation in sperm formation patterns in jumping plant-lice (Hemiptera: Psylloidea): a light microscopic study. *Folia Biologica (Kraków)*, *62*(4), 321–333. https://doi.org/10.3409/fb62_4.321

Liu, Y., & Tsai, J. (2000). Effects of temperature on biology and life table parameters of the Asian citrus psyllid, *Diaphorina citri* Kuwayama (Homoptera: Psyllidae). *Annals of Applied Biology*, *137*, 201–206. http://onlinelibrary.wiley.com/doi/10.1111/j.1744-7348.2000.tb00060.x/full

Macharashvili, I. D., & Kuznetsova, V. G. (1997). Karyotypes, Spermatogenesis, and Morphology of the Internal Reproductive System in Males of Some Psyllid Species (Homoptera, Psylloidea) of the Fauna of Georgia: I. Karyotypes and Spermatogonial Meiosis. *Entomological Review*, *77*(1), 12–20.

Maryańska-Nadachowska, A., & Głowacka, E. (1997). Remarks on chromosomal numbers and anatomy of male reproductive system in Triozidae (Psylloidea, Homoptera). *Folia Biologica (Kraków)*, *45*(3–4), 125–131.

Maryańska-Nadachowska, A., & Głowacka, E. (2005). Meiotic karyotypes and structure of testes of nineteen species of jumping-lice (Hemiptera, Psylloidea) from South Africa. *Folia Biologica*, *53*(3–4), 143–148. https://doi.org/10.3409/173491605775142710

Maryanska-Nadachowska, A., Kuznetsova, V. G., & Taylor, G. S. (2001). Meiotic karyotypes and structure of testes in males of 12 species of Psyllidae: Acizziinae, Carsidaridae and Triozidae (Hemiptera: Psylloidea) from Australia. *Australian Journal of Entomology*, *40*(4), 357–364. https://doi.org/10.1046/j.1440-6055.2001.00231.x

Maryańska-Nadachowska, A., Kuznetsova, V. G., Yang, C.-T., Woudstra, I. H., & Maryanska-Nadachowska, A. (1996). New data on karyotypes and the number of testicular follicles in the psyllid families Aphalaridae, Psyllidae, Carsidaridae and Triozidae (Homoptera, Psylloidea). *Caryologya*, *49*(3–4), 279–285. https://doi.org/10.1080/00087114.1996.10797372

Maryańska-Nadachowska, A., Taylor, G. S., & Kuznetsova, V. G. (2001). Meiotic karyotypes and structure of testes in males of 17 species of Psyllidae: Spondyliaspidinae (Hemiptera: Psylloidea) from Australia. *Australian Journal of Entomology*, *40*(4), 349–356. https://doi.org/10.1046/j.1440-6055.2001.00230.x

Mathur, R. N. (1975). *Psyllidae of the Indian subcontinent* (U. S. Jain (ed.)). Indian Council of Agricultural Research, New Delhi.

Matsuda, R. (1976). The Homoptera. In *Morphology and Evolution of the Insect Abdomen* (pp. 280–299). Pergamon Press Ltd. https://doi.org/10.1016/B978-0-08-018753-2.50040-X

Muir, F. (1930). LIII.—Notes on certain controversial points of morphology of the abdomen and genitalia of Psyllidæ. *Annals and Magazine of Natural History, Series 10*, *5*(29), 545–552. https://doi.org/10.1080/00222933008673163

Nava, D., Torres, M., Bento, J., & Parra, J. (2007). Biology of *Diaphorina citri* (Hem., Psyllidae) on different hosts and at different temperatures. *Journal of Applied Entomology*, *131*(9–10), 709–715. https://doi.org/10.1111/j.1439-0418.2007.01230.x

Park, H. C., & Taylor, K. R. (2003). Evolutionary Pattern and Taxonomy of Psyllid (Homoptera: Psylloidea) 1. On the Subfamily Spondyliaspidinae. *The Korena Journal of Systematic Zoology*, *19*(1), 139–147. http://ocean.kisti.re.kr/downfile/volume/kssyz/DMBRBT/2003/v19n1/DMBRBT_2003_v19n1_139.pdf

Pelz-Stelinski, K. S., & Killiny, N. (2016). Better Together: Association with "*Candidatus* Liberibacter Asiaticus" Increases the Reproductive Fitness of Its Insect Vector, *Diaphorina citri* (Hemiptera: Liviidae). *Annals of the Entomological Society of America*, *109*(3), 371–376. https://doi.org/10.1093/aesa/saw007

Prophetou-Athanasiadou, D. A., & Tzanakakis, M. E. (1998). The Reproductive System and Ovarian Development of the Adult Olive Psylla *Euphyllura phillyreae* Foerster (Homoptera: Aphalaridae). *Entomologia Hellenica*, *12*, 37–45. https://doi.org/http://dx.doi.org/10.12681/eh.14018

Qadri, M. A. H. (1949). On the morphology and post-embryonic development of the male genitalia and their ducts in Hemiptera. *Journal of the Zoological Society of India*, *1*,

129--143.

Saunders, L. G. (1921). *The Anatomy of Psyllia mali Schmidberger. Manuscript Thesis (M. Sc.) McGill University. Montreal.*

Schlee, D. (1969). Sperma-übertragung (und andere merkmale) in ihrer bedeutung für das phylogenetische system der sternorrhyncha (insecta, hemiptera) Phylogenetische studien an hemiptera I. psylliformes (psyllina und aleyrodina) als monophyletische gruppe. *Z. Morph. Tiere*, *64*, 95–138. https://doi.org/https://doi.org/10.1007/BF00391783

Shen, W., Halbert, S. E., Dickstein, E., Manjunath, K. L., Shimwela, M. M., & Bruggen, A. H. C. van. (2013). Occurrence and in-grove distribution of citrus huanglongbing in north Central Florida. In *Journal of Plant Pathology* (Vol. 95, pp. 361–371). Società Italiana di Patologia Vegetale (SIPaV). https://doi.org/10.2307/23721526

Stockton, D. G., Pescitelli, L. E., Martini, X., & Stelinski, L. L. (2017). Female mate preference in an invasive phytopathogen vector: how learning may influence mate choice and fecundity in *Diaphorina citri*. *Entomologia Experimentalis et Applicata*, *164*(1), 16–26. https://doi.org/10.1111/eea.12590

Sukthankar, P., Avila, L. A., Whitaker, S. K., Iwamoto, T., Morgenstern, A., Apostolidis, C., Liu, K., Hanzlik, R. P., Dadachova, E., & Tomich, J. M. (2014). Branched amphiphilic peptide capsules: Cellular uptake and retention of encapsulated solutes. *Biochimica et Biophysica Acta (BBA) - Biomembranes*, *1838*(9), 2296–2305. https://doi.org/10.1016/J.BBAMEM.2014.02.005

Wang, Y., Xu, C., Tian, M., Deng, X., Cen, Y., & He, Y. (2017). Genetic diversity of *Diaphorina citri* and its endosymbionts across east and south-east Asia. *Pest Management Science*, *73*(10), 2090–2099. https://doi.org/10.1002/ps.4582

Wenninger, E. J., & Hall, D. G. (2009). Daily Timing of Mating and Age at Reproductive Maturity in *Diaphorina citri* (Hemiptera: Psyllidae). *Florida Entomologist*, *90*(4), 715–722. https://doi.org/https://doi.org/10.1653/0015-4040(2007)90[715:DTOMAA]2.0.CO;2

Wenninger, E. J., Hall, D. G., & Mankin, R. W. (2009). Vibrational Communication Between the Sexes in *Diaphorina citri* (Hemiptera: Psyllidae). *Annals of the Entomological Society of America*, *102*(3), 547–555. https://doi.org/10.1603/008.102.0327

Wenninger, E. J., Stelinski, L. L., & Hall, D. G. (2009). Relationships Between Adult Abdominal Color and Reproductive Potential in *Diaphorina citri* (Hemiptera: Psyllidae). *Annals of the Entomological Society of America*, *102*(3), 476–483. https://doi.org/10.1603/008.102.0318

Witlaczil, E. (1885). Die Anatomie der Psylloden. *Zeitschrift Für Wissenschaftliche Zoologie*, *42*, 569–638.

Wu, F., Cen, Y., Deng, X., Zheng, Z., Chen, J., & Liang, G. (2016). The complete mitochondrial genome sequence of *Diaphorina citri* (Hemiptera: Psyllidae). *Mitochondrial DNA Part B*, *1*(1), 239–240. https://doi.org/10.1080/23802359.2016.1156491

Zucht, B. (1972). Bau und Entwicklung der äußeren Genitalorgane bei Psyllinen (Homopteren). *Zool. Jb. Anat. Bd.*, *231*, 167–231.

5.3.- "Estudio anatómico del sistema reproductor y bacterioma de la hembra de *Diaphorina citri* Kuwayama (Insecta: Hemiptera, Liviidae) usando microtomografía computarizada"

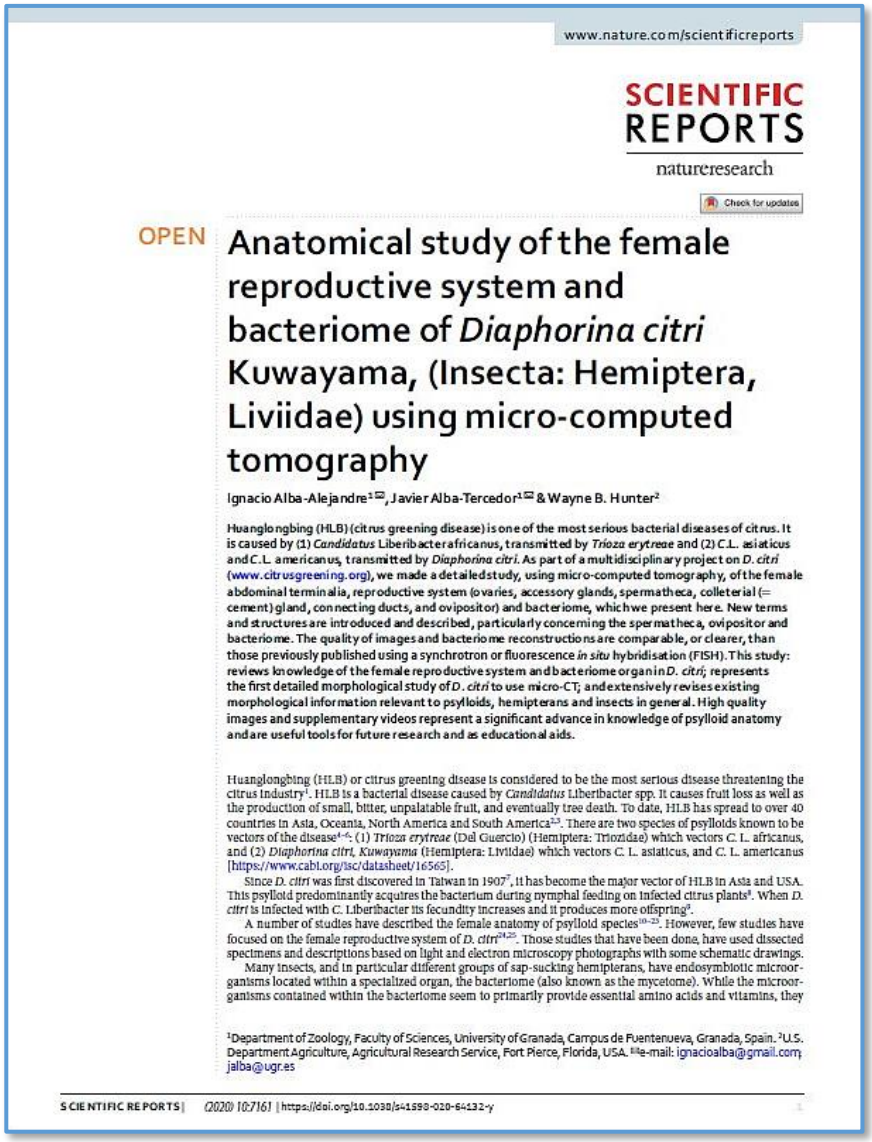

www.nature.com/scientificreports

SCIENTIFIC REPORTS
nature research

Check for updates

OPEN

Anatomical study of the female reproductive system and bacteriome of *Diaphorina citri* Kuwayama, (Insecta: Hemiptera, Liviidae) using micro-computed tomography

Ignacio Alba-Alejandre[1✉], Javier Alba-Tercedor[1✉] & Wayne B. Hunter[2]

Huanglongbing (HLB) (citrus greening disease) is one of the most serious bacterial diseases of citrus. It is caused by (1) *Candidatus* Liberibacter africanus, transmitted by *Trioza erytreae* and (2) C.L. asiaticus and C.L. americanus, transmitted by *Diaphorina citri*. As part of a multidisciplinary project on *D. citri* (www.citrusgreening.org), we made a detailed study, using micro-computed tomography, of the female abdominal terminalia, reproductive system (ovaries, accessory glands, spermatheca, colleterial (= cement) gland, connecting ducts, and ovipositor) and bacteriome, which we present here. New terms and structures are introduced and described, particularly concerning the spermatheca, ovipositor and bacteriome. The quality of images and bacteriome reconstructions are comparable, or clearer, than those previously published using a synchrotron or fluorescence *in situ* hybridisation (FISH). This study: reviews knowledge of the female reproductive system and bacteriome organ in *D. citri*; represents the first detailed morphological study of *D. citri* to use micro-CT; and extensively revises existing morphological information relevant to psylloids, hemipterans and insects in general. High quality images and supplementary videos represent a significant advance in knowledge of psylloid anatomy and are useful tools for future research and as educational aids.

Huanglongbing (HLB) or citrus greening disease is considered to be the most serious disease threatening the citrus industry[1]. HLB is a bacterial disease caused by *Candidatus* Liberibacter spp. It causes fruit loss as well as the production of small, bitter, unpalatable fruit, and eventually tree death. To date, HLB has spread to over 40 countries in Asia, Oceania, North America and South America[2,3]. There are two species of psylloids known to be vectors of the disease[4–6]: (1) *Trioza erytreae* (Del Guercio) (Hemiptera: Triozidae) which vectors *C.* L. africanus, and (2) *Diaphorina citri, Kuwayama* (Hemiptera: Liviidae) which vectors *C.* L. asiaticus, and *C.* L. americanus [https://www.cabi.org/isc/datasheet/16565].

Since *D. citri* was first discovered in Taiwan in 1907[7], it has become the major vector of HLB in Asia and USA. This psylloid predominantly acquires the bacterium during nymphal feeding on infected citrus plants[8]. When *D. citri* is infected with *C.* Liberibacter its fecundity increases and it produces more offspring[9].

A number of studies have described the female anatomy of psylloid species[10–23]. However, few studies have focused on the female reproductive system of *D. citri*[24,25]. Those studies that have been done, have used dissected specimens and descriptions based on light and electron microscopy photographs with some schematic drawings.

Many insects, and in particular different groups of sap-sucking hemipterans, have endosymbiotic microorganisms located within a specialized organ, the bacteriome (also known as the mycetome). While the microorganisms contained within the bacteriome seem to primarily provide essential amino acids and vitamins, they

[1]Department of Zoology, Faculty of Sciences, University of Granada, Campus de Fuentenueva, Granada, Spain. [2]U.S. Department Agriculture, Agricultural Research Service, Fort Pierce, Florida, USA. ✉e-mail: ignacioalba@gmail.com; jalba@ugr.es

Alba-Alejandre, I., Alba-Tercedor, J., & Hunter, W. B. (2020). Anatomical study of the female reproductive system and bacteriome of *Diaphorina citri* Kuwayama, (Insecta: Hemiptera, Liviidae) using micro-computed tomography. *Scientific Reports* 10 (1), 1–14. https://doi.org/10.1038/s41598-020-64132-y

5.3.1.- Resumen

Huanglongbing (HLB) (enfermedad de enverdecimiento de los cítricos) es una de las enfermedades bacterianas más graves de los cítricos. Es causada por (1) *Candidatus* Liberibacter africanus, transmitida por *Trioza erytreae* y (2) *C*.L. asiaticus y *C*.L. americanus, transmitido *por Diaphorina citri*. Como parte de un proyecto multidisciplinar sobre *D. citri* (www.citrusgreening.org), realizamos un estudio detallado, mediante microtomografía computarizada (micro-CT), de la terminalia del abdomen femenino, sistema reproductor (ovarios, glándulas accesorias, espermateca, glándula colectora/cementante, conductos de conexión y el ovipositor) y bacterioma, que presentamos aquí. Se introducen y describen nuevos términos y estructuras, particularmente en relación con la espermateca, el ovipositor y el bacterioma. La calidad de las imágenes y las reconstrucciones del bacterioma son comparables o más claras que las publicadas previamente utilizando un sincrotrón o hibridación fluorescente in situ (FISH). Este estudio: revisa el conocimiento del sistema reproductor femenino y del bacterioma en *D. citri*; representa el primer estudio morfológico detallado de *D. citri* en usar micro-CT; y revisa ampliamente la información morfológica existente relevante para los psiloides, hemípteros e insectos en general. Las imágenes de alta calidad y los videos complementarios representan un avance significativo en el conocimiento de la anatomía psiloide y son herramientas útiles para futuras investigaciones y como ayudas educativas.

5.3.2.- Abstract

Huanglongbing (HLB) (citrus greening disease) is one of the most serious bacterial diseases of citrus. It is caused by (1) *Candidatus* Liberibacter africanus, transmitted by *Trioza erytreae* and (2) *C.*L. asiaticus and *C.*L. americanus, transmitted by *Diaphorina citri.* As part of a multidisciplinary project on *D. citri* (www.citrusgreening.org), we made a detailed study, using micro-computed tomography, of the female abdominal terminalia, reproductive system (ovaries, accessory glands, spermatheca, colleterial/cement gland, connecting ducts, and ovipositor) and bacteriome, which we present here. New terms and structures are introduced and described, particularly concerning the spermatheca, ovipositor and bacteriome. The quality of images and bacteriome reconstructions are

comparable, or clearer, than those previously published using a synchrotron or fluorescence *in situ* hybridisation (FISH). This study: reviews knowledge of the female reproductive system and bacteriome organ in *D. citri*; represents the first detailed morphological study of *D. citri* to use micro-CT; and extensively revises existing morphological information relevant to psylloids, hemipterans and insects in general. High quality images and supplementary videos represent a significant advance in knowledge of psylloid anatomy and are useful tools for future research and as educational aids.

5.3.3.- Introduction

Huanglongbing (HLB) or citrus greening disease is considered to be the most serious disease threatening the citrus industry (Mead & Fasulo, 2017). HLB is a bacterial disease caused by *Candidatus* Liberibacter spp. It causes fruit loss as well as the production of small, bitter, unpalatable fruit, and eventually tree death. To date, HLB has spread to over 40 countries in Asia, Oceania, North America and South America (Halbert & Manjunath, 2004; Shen *et al.*, 2013). There are two species of psylloids known to be vectors of the disease (Capoor *et al.*, 1967; McClean & Oberholzer, 1965; K. Pelz-Stelinski, 2010): (1) *Trioza erytreae* (Del Guercio) (Hemiptera: Triozidae) which vectors *C.* L. africanus, and (2) *Diaphorina citri, Kuwayama* (Hemiptera: Liviidae) which vectors *C.* L. asiaticus, and *C.* L. americanus [https://www.cabi.org/isc/datasheet/16565].

Since *D. citri* was first discovered in Taiwan in 1907 (Kuwayama, 1907), it has become the major vector of HLB in Asia and USA. This psylloid predominantly acquires the bacterium during nymphal feeding on infected citrus plants(Inoue *et al.*, 2009). When *D. citri* is infected with *C.* Liberibacter its fecundity increases and it produces more offspring (K. S. Pelz-Stelinski & Killiny, 2016).

A number of studies have described the female anatomy of psylloid species (Austin & Dietrich, 2016; Bitsch, 1979; Blowers & Moran, 1967; Brittain, 1922; I.D. Hodkinson & White, 1979; Matsuda, 1976; Muir, 1930; Ossiannilsson, 1992; Pesson, 1951; Prophetou-Athanasiadou & Tzanakakis, 1998; Saunders, 1921; Snodgrass, 1935; Witlaczil, 1885; Zucht, 1972). However, few studies have focused on the female reproductive system of *D. citri* (Dossi & Cônsoli, 2010,

2014). Those studies that have been done, have used dissected specimens and descriptions based on light and electron microscopy photographs with some schematic drawings.

Many insects, and in particular different groups of sap-sucking hemipterans, have endosymbiotic microorganisms located within a specialized organ, the bacteriome (also known as the mycetome). While the microorganisms contained within the bacteriome seem to primarily provide essential amino acids and vitamins, they also have a defensive role. Within the bacteriome there are bacteriocytes which are specialized cells that provide nutrients and shelter for these microorganisms. The bacteriome is clearly visible in juvenile stages but it reduces in size or disappears in mature individuals, once the microorganisms have passed into the eggs (e.g. (Baumann, 2005; Chapman, 2013; Chu *et al.*, 2016; Kuechler *et al.*, 2012; Matsuura *et al.*, 2012; Nakabachi *et al.*, 2013; Subandiyah *et al.*, 2000; Weintraub *et al.*, 2014)). Several studies on the bacteriome of *D. citri* have been made and include: visualization of the bacteriome in nymphs (Ammar & Hall, 2012) and adults (Dan *et al.*, 2017) using fluorescence microscopy; the behaviour of symbionts during transovarial transmission and development (Dan *et al.*, 2017); localization and dynamics of *Wolbachia* microorganisms in nymphs and eggs (Ren *et al.*, 2018); and inter-population variability in endosymbiont densities (Chu *et al.*, 2016).

Traditional insect-dissection techniques were first used more than 400 years ago by Aldrovandi (Aldrovandi, 1602) and Malpighi (Malpighi, 1669). While this technique is useful and has resulted in thousands of papers on the internal anatomy of insects, it has limitations because it distorts the spatial arrangement of internal structures. A relatively recent technique, known as micro-computed tomography (micro-CT), which is based on X-rays, allows visualization of the internal anatomy *in situ*, without the need for dissection; results have been validated by comparing them with classical destructive methodologies (Alba-Tercedor & Alba-Alejandre, 2019; Benjamin Wipfler *et al.*, 2016). Thus, micro-CT has been used to elucidate various aspects of insect anatomy (e.g. (Alba-Alejandre *et al.*, 2019; Alba-Tercedor *et al.*, 2019; Alba-Tercedor, 2012a, 2012b, 2012c, 2013, 2014b, 2016; Alba-Tercedor & Alba-Alejandre, 2019; Alba-Tercedor & Bartomeus, 2016; Alba-Tercedor & Sáinz-Cantero Caparrós, 2010, 2012; Alba-

Tercedor & Sánchez Almazo, 2014, 2013; M. Greco *et al.*, 2014; M. K. Greco *et al.*, 2012; Greenlee *et al.*, 2009; Ha *et al.*, 2017; Helm *et al.*, 2018; Iwan *et al.*, 2015; Jiang *et al.*, 2019; Kypke & Solodovnikov, 2018; D. Li *et al.*, 2011; Y. Li *et al.*, 2018; Lowe *et al.*, 2013; Martín-Vega *et al.*, 2018; Raś *et al.*, 2018; Ribi *et al.*, 2008; Schambach *et al.*, 2010; Shaha *et al.*, 2013; Smith *et al.*, 2016; Sombke *et al.*, 2015; Soriano *et al.*, 2010; Westneat, 2003; B Wipfler *et al.*, 2012, 2016)) and behavioural/ anatomical adaptations (e.g. (Alba-Alejandre, Alba-Tercedor, *et al.*, 2018a, 2018b; Alba-Tercedor *et al.*, 2016; Taylor *et al.*, 2016; Verdú *et al.*, 2012) Synchrotron X-ray tomography has been used to elucidate the general 3D configuration of the bacteriome of *Orosius albicinctus* (Hemiptera: Cicadellidae) (Weintraub *et al.*, 2014), and micro-CT has been used to locate and study the mycangia (cuticular cavities where symbiotic fungi proliferate (Beaver, 1989; Chapman, 2013) of ambrosia beetles (Coleoptera: Curculionidae: Scolytinae) (Jiang *et al.*, 2019; Y. Li *et al.*, 2018).

Use of micro-CT facilitated a very detailed study of the male reproductive system of *D. citri* that included a revision of the male reproductive system of psylloids in general (*Alba-Alejandre et al., 2018*; Alba-Tercedor, Hunter, Cicero, & Brown, 2017). In this context, the main aim of the current study was to use micro-CT to extend these anatomical studies to the female reproductive system of *D. citri*. We present here the extensive use of micro-CT techniques to reveal, in detail, the anatomy of the female reproductive system (terminalia, ovaries, accessory glands, spermatheca, colleterial/cement gland, connecting ducts and ovipositor), and the bacteriome organ. This improvement on current knowledge helps us understand the morphology and functional anatomy of structures in their natural anatomical position, avoiding deformations that typically occur using standard dissection and/or slide preparation techniques. We also present videos as supplementary information to provide an accurate view of the actual position and internal components of the organs and structures. Spinning animations, using different rotational axes, permit exceptional views of the minutiae of structures from different 3D perspectives (Supplementary Videos S1-S3). These are useful tools for future research and as teaching aids (see also www.citrusgreening.org).

5.3.4.- Materials and Methods

The six older mated adult female *D. citri* specimens for this study came from the rearing facilities at the United States Department of Agriculture, Agriculture Research Service, Fort Pierce, Florida (USA). These specimens (shown in Figs. 1, 2, 7, 8; Supplementary Video S3) were fed for three days on an orange tree sprig submerged in BAPC (Branched Amphiphilic Peptide Capsules) linked to Hg as a contrast agent (Sukthankar *et al.*, 2014). They were rinsed three times in 30% ethanol (10 min for each rinse), dehydrated in an ethanol series (30 min per step, 50%, 70%, 80%, 90%, 95%, and three times at 100%), chemically dried by submersion in 2 ml of 100% hexamethyldisilazane (HMDS) for 2 hours and dried overnight at 35ºC. In addition, a young mated adult female from the facilities at the University of Florida, Department of Entomology and Nematology was also processed (Figs. 3-5; Supplementary Videos S1 and S2). It was provided by Dr Joseph M. Cicero who separated the abdomen and removed the apical part to facilitate the entry of chemicals during preparation (fixed with 4% formaldehyde and 1.5% glutaraldehyde, rinsed and then incubated in 1% OsO4 for 20 minutes, then rinsed again and dehydrated in an ethanol series, and critical point dried).

All specimens were glued with cyanoacrylate to the tip of a nylon fishing line 200 µm in diameter, as previously described (Alba-Tercedor, 2014a; Alba-Tercedor *et al., 2017*). The prepared specimens were scanned using a SkyScan 1172 desktop high-resolution micro-CT, with a Hamamatsu L702 source and a Ximea 11Mp camera. The following setting parameters were used: a) for the older adult females: isotropic voxel size = 0.52µm per pixel; source voltage = 48KV, source current = 68µA, image rotation step = 0.2º, 360º rotation scan and no filter, resulting in 1802 X-ray images; b) for the young adult female: isotropic voxel size = 0.99µm per pixel; source voltage = 49KV, source current = 51µA, image rotation step = 0.3º, 360º rotation scan and no filter, resulting in 1202 X-ray images.

The most recent versions of the Bruker micro-CT's Skyscan software (NRecon v.1.7.4.6, DataViewer v.1.5.6.2, CTAnalyser v.1.18.8.0, https://www.bruker.com/products/microtomography.html) were used for primary reconstructions and the 'cleaning' process to obtain datasets on 'slices' through the specimens, as described previously (Alba-Tercedor, 2014a). Amira's

software, v. 6.7.0 (Thermo Fisher Scientific, Waltham, MA) (Stalling *et al.*, 2005; Thermo Fisher Scientific, 2017) (with the built-in 'volrenRed.col' colour filter) was used to obtain volume-rendered images (Figs. 1-7; Supplementary Videos S1-S3). Different anatomical parts were independently segmented to obtain the final rendered images used in Figs. 2–7. After segmentation, each structure was subjected to an arithmetic operation to obtain the actual texture of structures in desired colours. Specifically: A*(B > 0), where A represents the whole specimen and B the segmented structure. The Amira's software, multiplanar slice view was used to obtain the rendered images in Fig. 8.

In accordance with the micro-CT results, standard anatomical positions are used to describe structures. Proximal/distal anatomical terminology for any duct departing from an organ is named according to its proximal or distal position in relation to the organ itself (as for instance in Fig. 1 of Slater (Slater *et al.*, 2017)).

For consistency, and to avoid poor or misleading descriptions of any structure or form as a result of undesired deformation, the structures visualized and described in this study were checked and found to exist and maintain their shape and position in each of the seven females that were scanned and reconstructed.

5.3.5.- Results

The structures of the external female terminalia are shown in Fig. 1. Visible are a dorsal proctiger (a narrow dorsal dome-shaped plate) with a pointed apical extension (Fig. 1a, b). The anus opens dorsally in the basal part of the proctiger, at the end of a longitudinal central depression, and is encircled by double concentric (outer and inner) circum-anal rings. Wax pores are visible in the outer circum-anal ring (Fig. 1b). Ventrally appears: the subgenital plate (with a slightly bi-lobed raised appearance, narrowing and apically rounded); the lateral margins of the proctiger; and some apical parts of the ovipositor (2^{nd} and 3^{rd} valvulae) (Fig. 1d). Laterally, the proctiger and the subgenital plate (with a narrow spoon-shaped appearance) are conspicuous, and are visible between both the apical parts of

2nd and 3rd valvulae of the ovipositor (Fig. 1a). A small latero-apical notch appears on each 3rd valvula (Fig. 7j).

In the specimens studied, the abdominal volume occupied by the female reproductive system increases with maturity and with egg development. Thus, while in the young adult female, it occupies less than ¼ of the abdomen (Fig. 3; Supplementary Video S1), in older adult females (with developed vitellogenic eggs) the abdominal cavity appears to be completely occupied by the reproductive organs, and particularly by the eggs (Fig. 2).

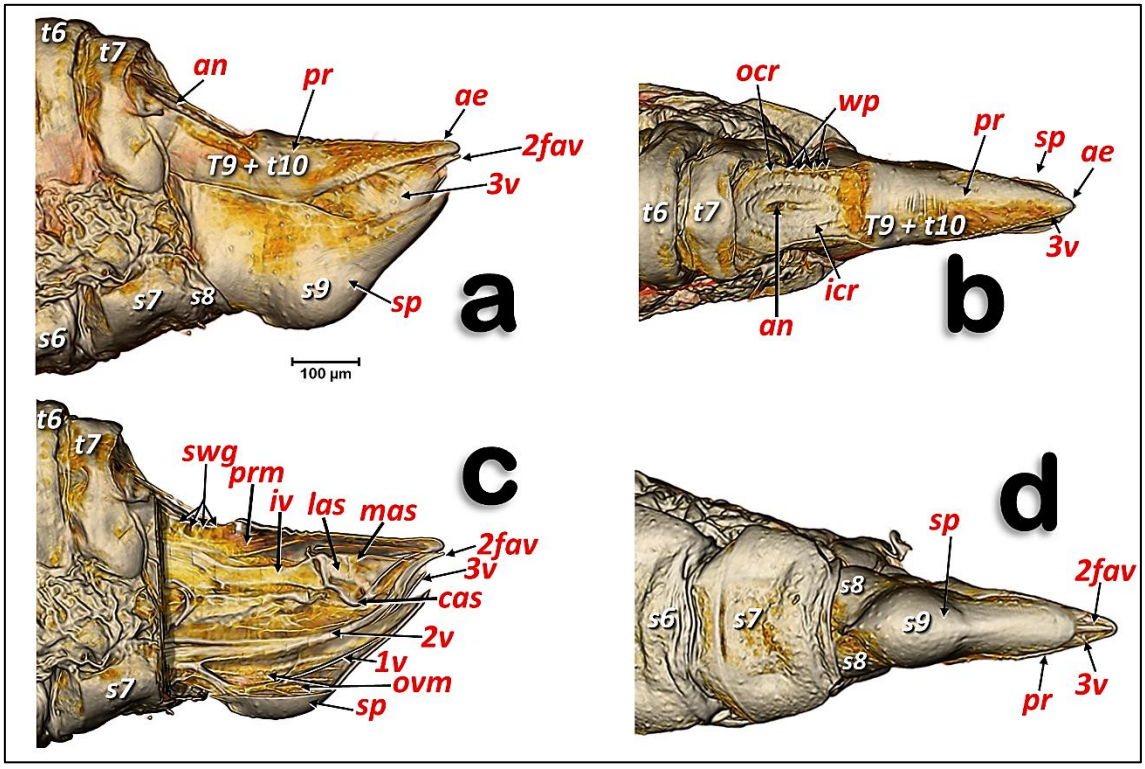

Figure 1.- Volume-rendered images of female terminalia in different views. Left-lateral (**a**, **c**), dorsal (**b**), ventral (**d**) and medial-left virtual box-cut view (**c**). Abbreviations: 2fav = fused apical part of the 2nd valvulae; ae = apical extension: an = anus; cas = centro-apical sclerite; icr = inner circum-anal ring; iv = intervalvular sclerite; las = latero-apical sclerite; mas = medial apical sclerite; ocr = outer circum-anal ring; ovm = ovipositor protractor musculature; pr = proctiger; prm = proctodeal musculature; sp = sub-genital plate; swg = sub-cuticular wax glands; wp = wax pores. Abdominal tergites and sternites are labelled sequentially with the letter 't' and 's', respectively.

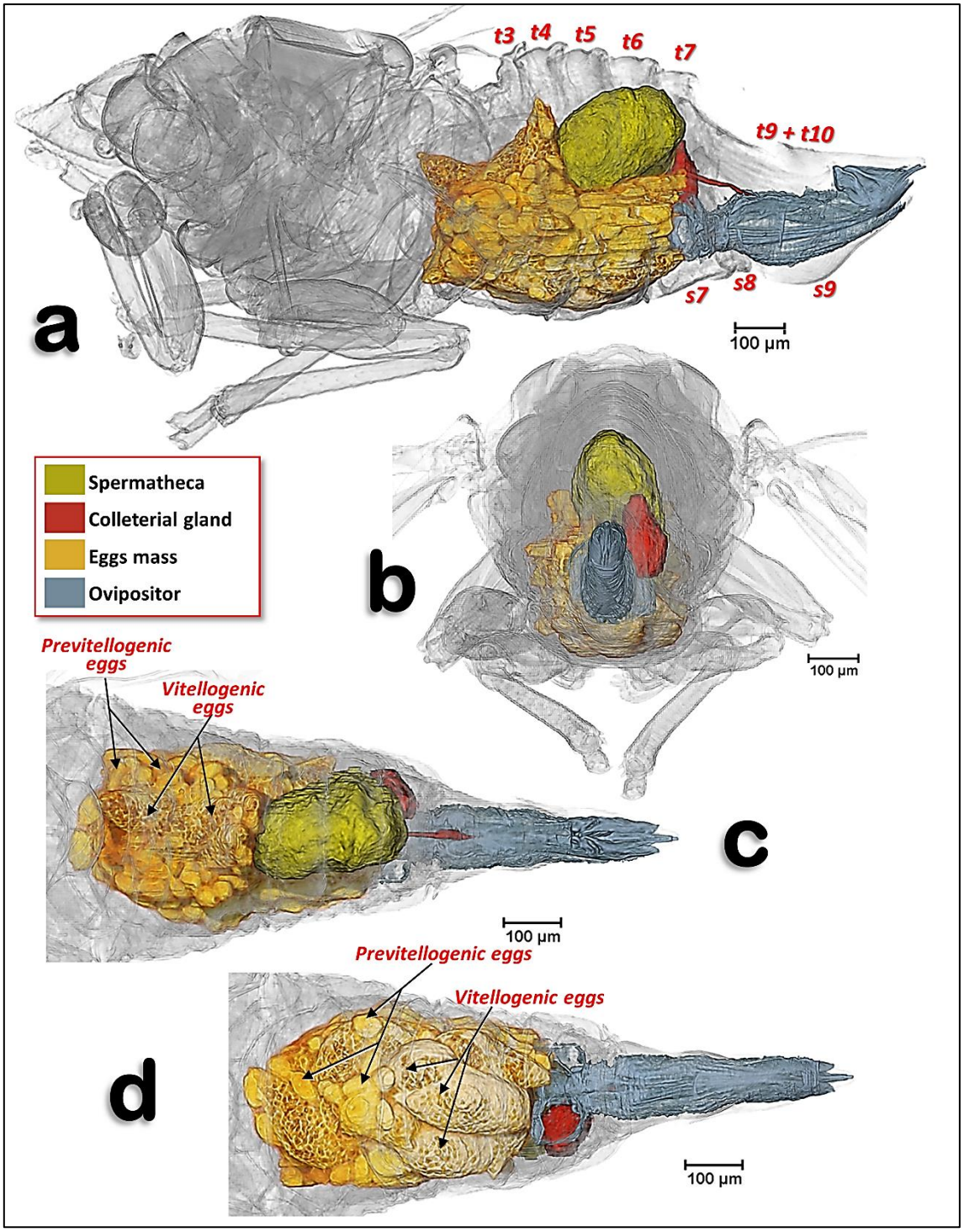

Figure 2.- Volume-rendered images of an older mature adult female showing the reproductive system in its anatomical position, in different views. Left-lateral (**a**), posterior (**b**), dorsal (**c**) and ventral (**d**). Abdominal tergites and sternites are labelled sequentially with the letter 't' and 's', respectively. Note that neither the intervalvular basal sclerite nor the latero-basal plate sclerites of the ovipositor are rendered.

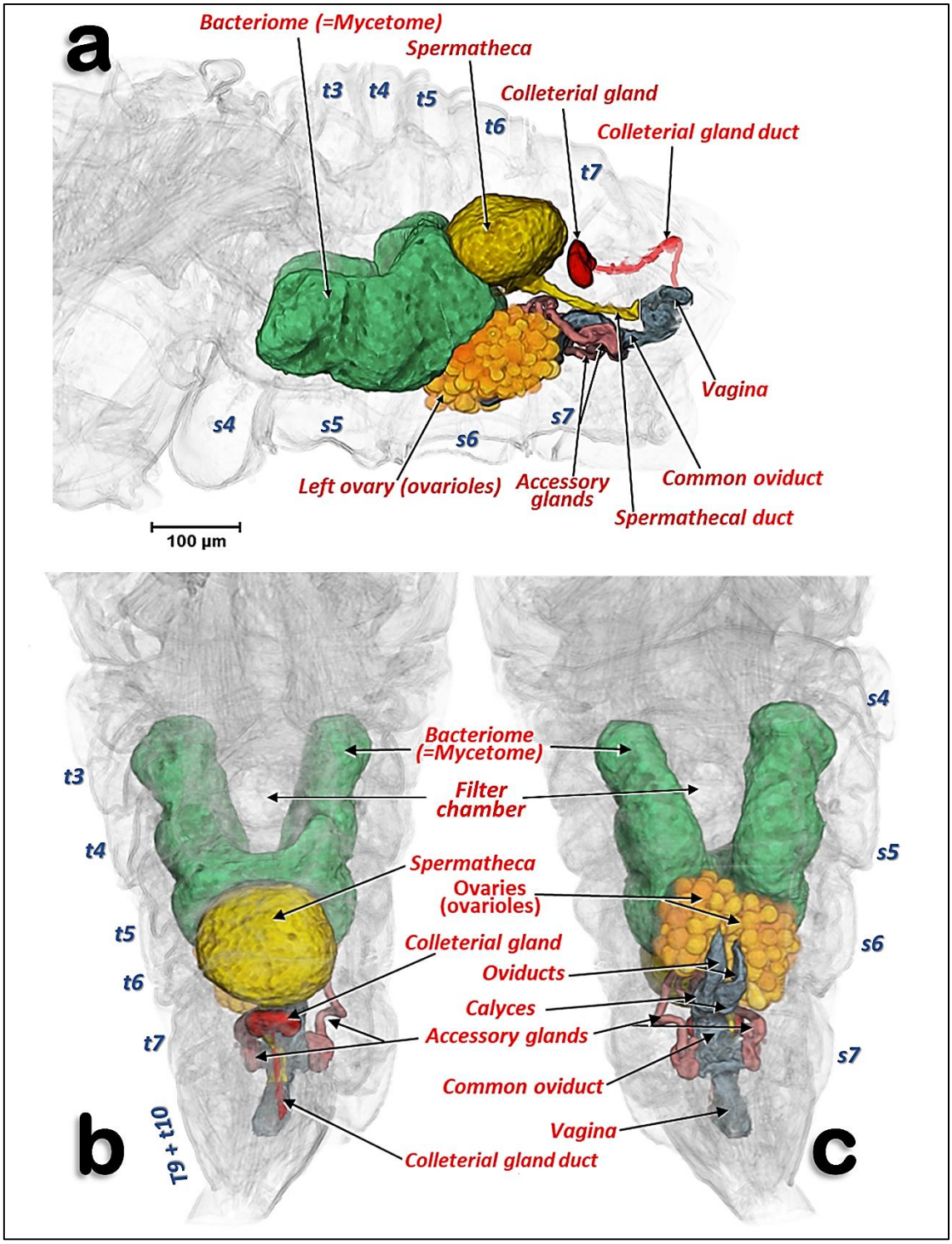

Figure 3.- Volume-rendered images of an adult young female showing the reproductive system organs, bacteriome and the filter chamber, in its anatomical position. Left-lateral (**a**), dorsal (**b**) and ventral (**c**). Note that the ovipositor is not rendered.

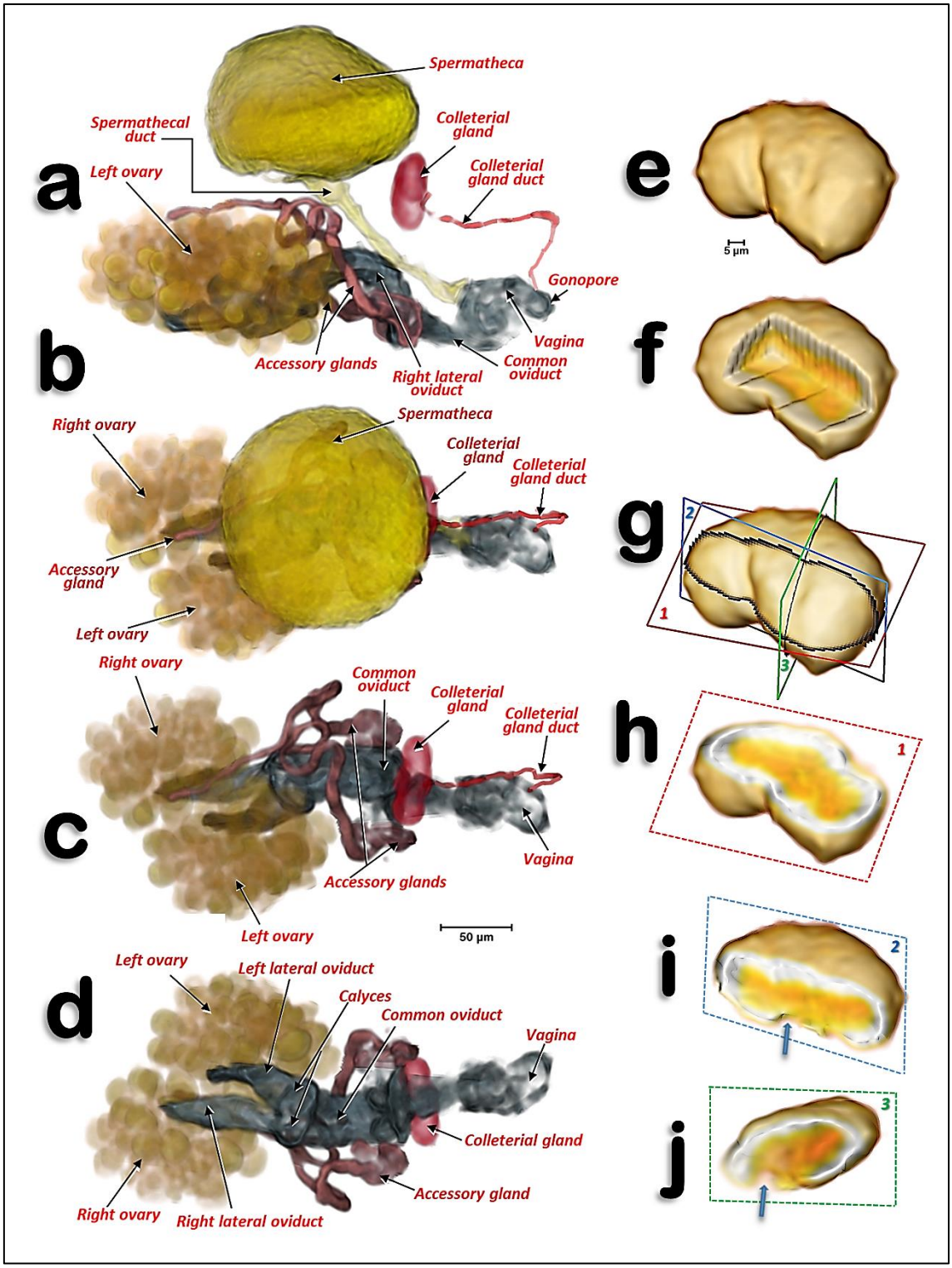

Figure 4.- Volume-rendered images of the reproductive system and organs of a young adult female in different views. Left-lateral (**a**), dorsal (**b**, **c**), and ventral (**d**). For clarity, the spermatheca is not rendered in **c** and **d**. Colleterial gland in left antero-dorsal view (**e**-**i**) and different views of the internal structure after virtual cuts: box-cut (**f**) and different plane cuts (**h**-**j**), as defined in **g**. In **i** and **j** the blue arrows point to the connection of the colleterial gland duct.

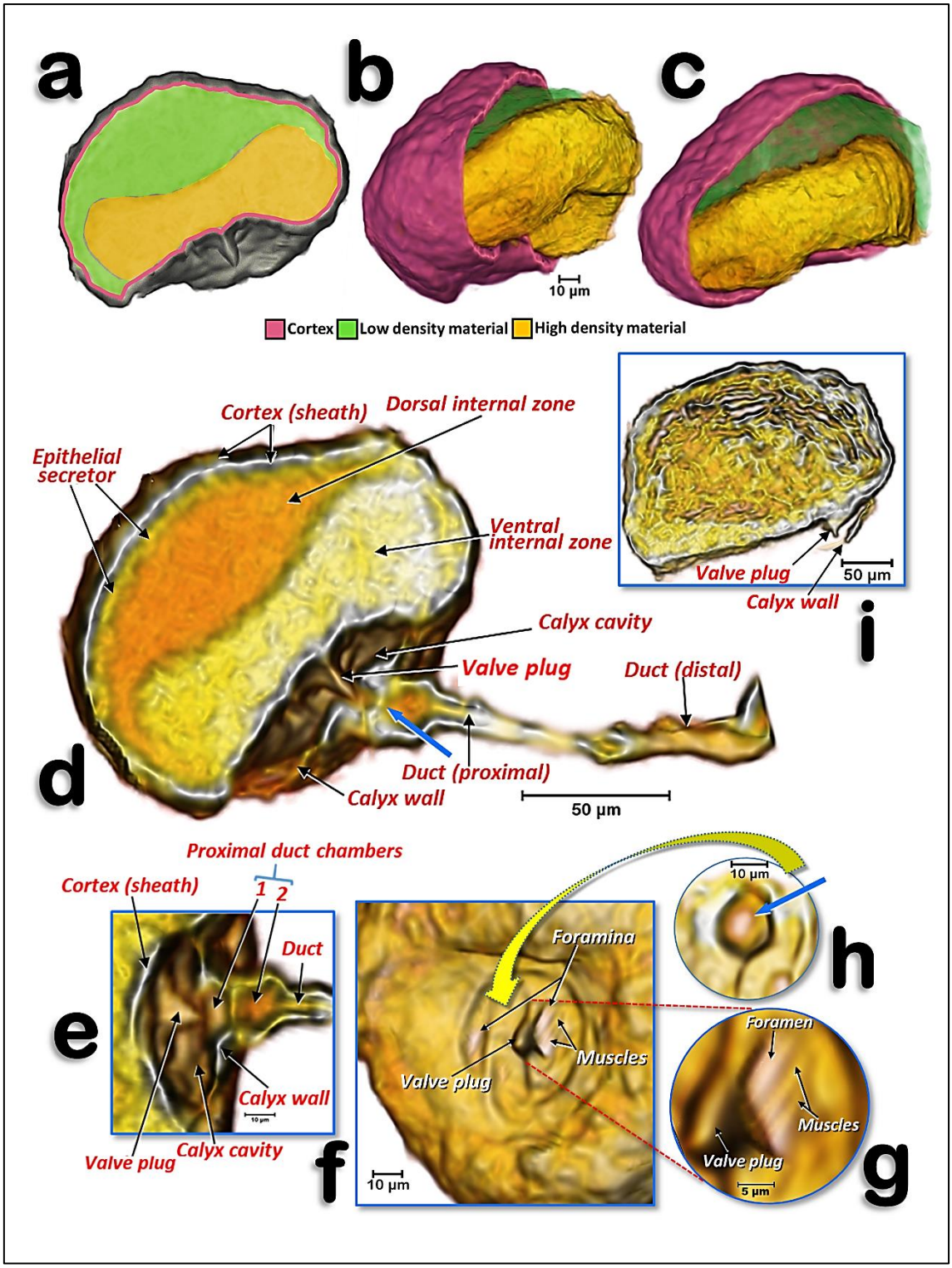

Figure 5.- Volume-rendered images of the spermatheca of a young adult female (**a**-**h**) and of an older adult female, where the calyx is not rendered (**i**). Left-lateral section (**a**,**d**,**e**), details of the structures inside the calyx and proximal spermathecal duct (**e-h**), internal view proximal at the level where the calyx connects (**f**), a detailed view showing the bigger foramen and the closing muscles (**g**), and pierced wall that separates the proximal duct chamber from the interior of the calyx - the blue arrow points to the hole where the valve plug inserts (**h**).

The reproductive organs are at a medio-ventral position in the apical third of the abdominal cavity. This is evident in the young adult female (Fig. 3; Supplementary Video S1), but not in older adult females where the abdomen is

full of eggs (Fig. 2). There are two ovaries, each containing ca. 40-50 ovarioles (we counted 40 in the right and 46 in the left) in a configuration similar to a blackberry fruit (Figs 2a, 2c). The ovarioles of each ovary join in a lateral oviduct that enlarges distally in a calyx. Right and left oviducts come together forming a common oviduct, into which a tubular accessory gland flows on each side, and distally enlarges to form the vagina (Figs 3, 4a-d; Supplementary Video S1). The vagina ends in a gonopore that opens to the genital chamber at the base of the ovipositor (Fig. 8c).

The spermatheca is situated dorsal to the ovaries and in a central position; it is spherical in shape and its surface has small semi-spherical protuberances which give it a rough appearance. The spermatheca is connected to the vagina by a spermathecal duct (Figs. 3a-b, 4a-b). The colleterial (= cement) gland appears situated in a medial position, dorsal to the common oviduct, and posterior to the spermatheca (Figs. 2, 3, 4a-d; Supplementary Video S1). It has a denser external layer (appearing close to white in colour) with less dense internal contents (appearing yellowish in colour) (Figs. 4h-j). From the central posterior side, the colleterial gland is connected to the colleterial gland duct (Figs. 4i-j), through which it releases gland secretions into the space between the valvulae of the ovipositor (Fig. 2a, c).

The structure of the spermatheca is rather complex (Fig. 5; Supplementary Video S2). The main body of it is spherical/ globular and it has an external cortex (sheath) that surrounds an epithelial secretor layer. Internally, it presents as two cavity zones: a dorsal internal zone (less dense in X-ray) and a ventral internal zone (denser in X-ray); these appear as green/ yellow structures (Fig. 5a-c) and orange/ yellow structures (Fig. 5d), respectively. In older adult females, the spermatheca appears laterally compressed (Fig. 2 b-c) and internally lacking the two separate zones (Figs 5i and 8) visible in the young adult female. The connection with the spermathecal duct is through the calyx, a cup-shaped structure that delimits a calyx cavity; within this cavity, the ventral side that is in

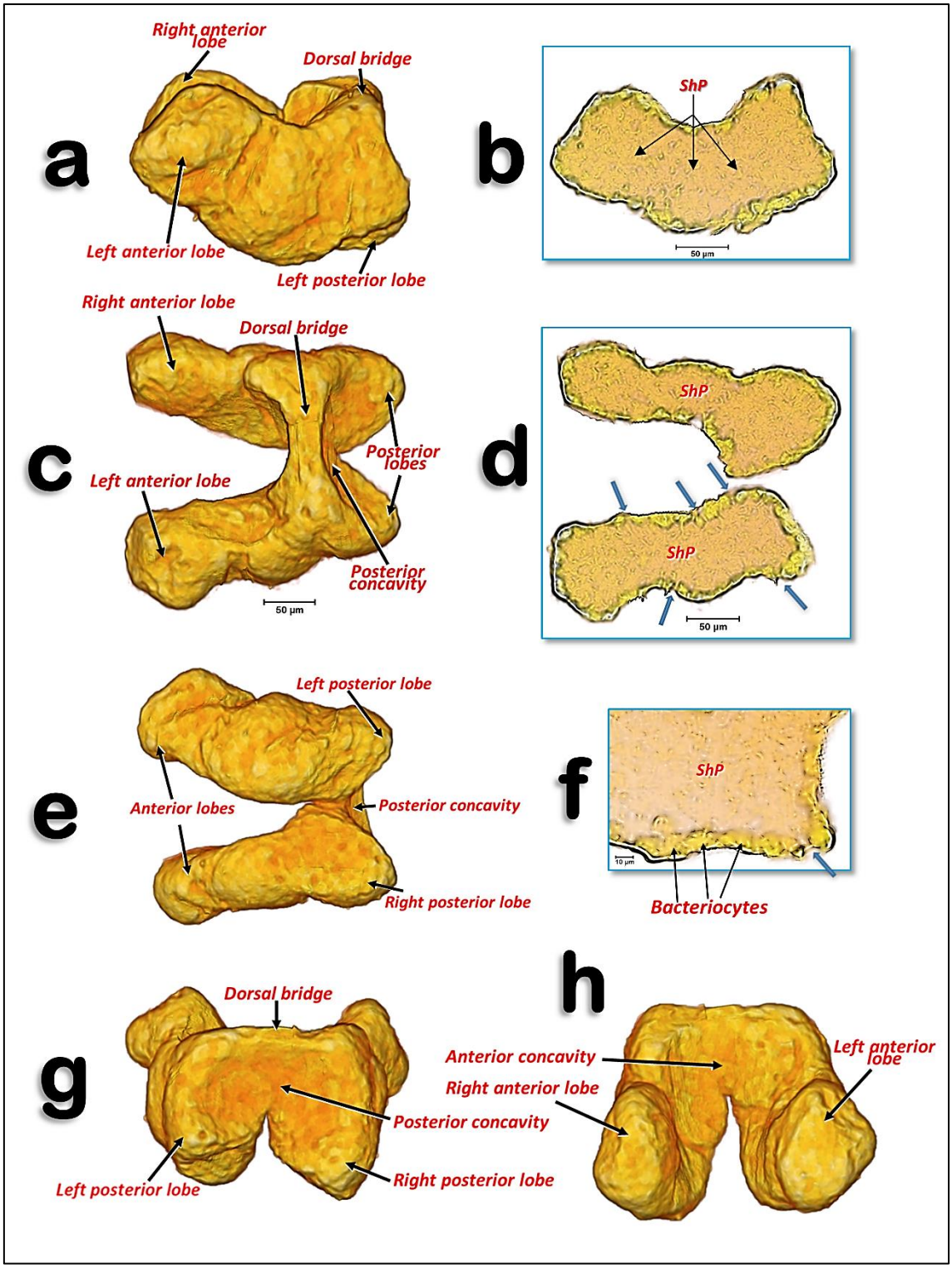

Figure 6.- Volume-rendered images of the bacteriome of a young adult female in different perspective views. Left-lateral (**a**), dorsal (**c**), ventral (**e**), posterior (**g**) and anterior (**h**). Slice sections: left-lateral (**b**), dorsal (**d**) and details of a left-lateral section (**f**). The blue arrows indicate the places where the syncytium reaches the surface of the bacteriome. Abbreviation: ShP = syncytium harbouring *Profftella*.

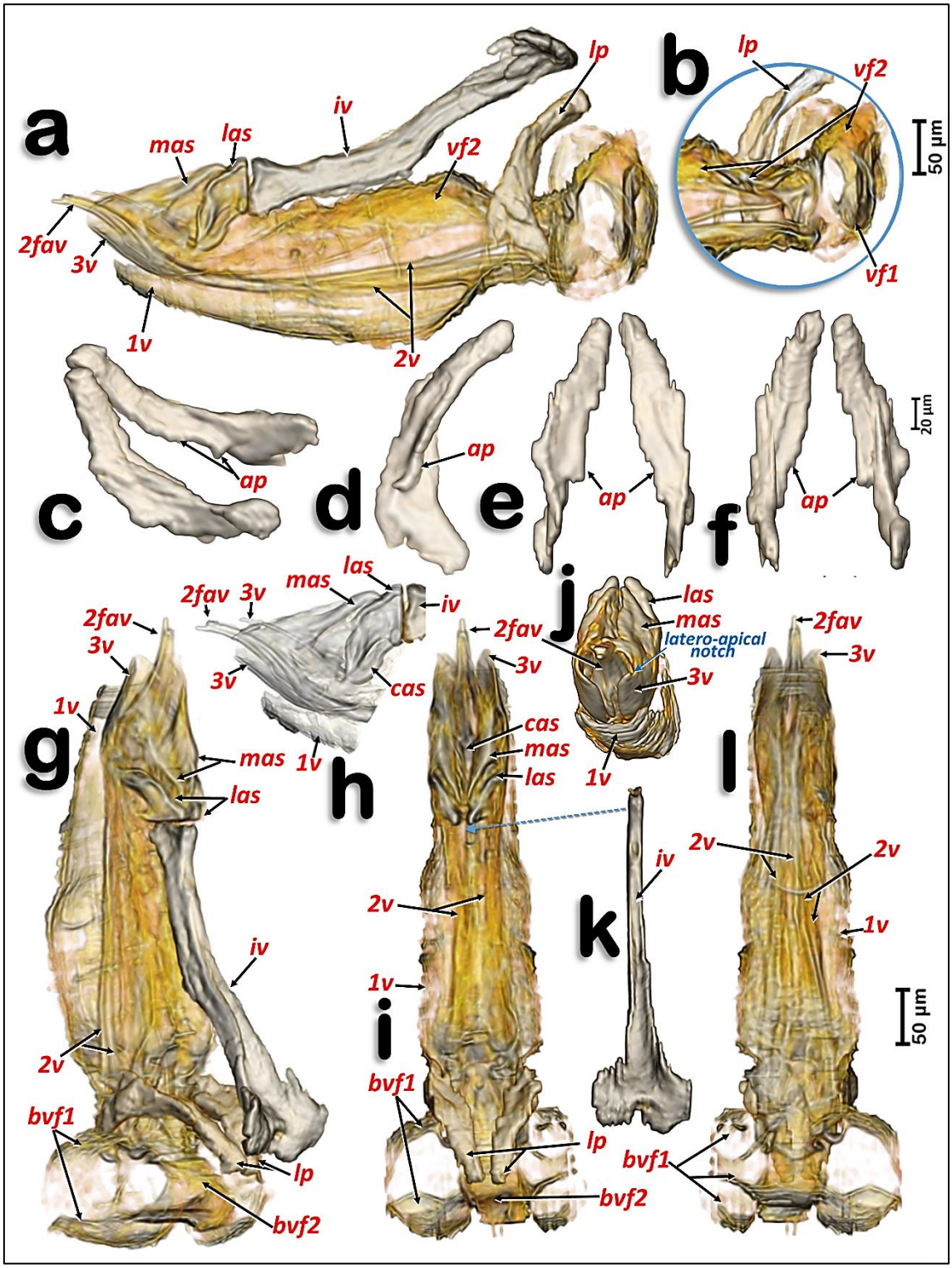

Figure 7.- Volume-rendered images of the ovipositor in different perspective views. Right-lateral (**a**, **b**, **h**)**,** right dorso-lateral (**g**)**,** dorsal (**i**), posterior (**j**) and ventral (**l**). Latero-basal plate sclerites in different views: right dorso-lateral (**c**), internal side of the left sclerite (**d**), posterior (**e**) and frontal (**f**). Detail of a right apical view, using software to show the apical sclerites and valvulae (**h**). Dorsal view of the intervalvular basal sclerite (**k**). Abbreviations: 1v, 2v and 3v = 1st, 2nd and 3rd valvulae; 2fav = fused apical part of the 2nd valvula; ap = latero-basal plate internal apodeme; cas = centro-apical sclerite; iv = basal intervalvular sclerite; las = latero-apical sclerite; lp = latero-basal plate sclerite; mas = medio-apical sclerite; vf1 and vf2 = 1st and 2nd valvifera.

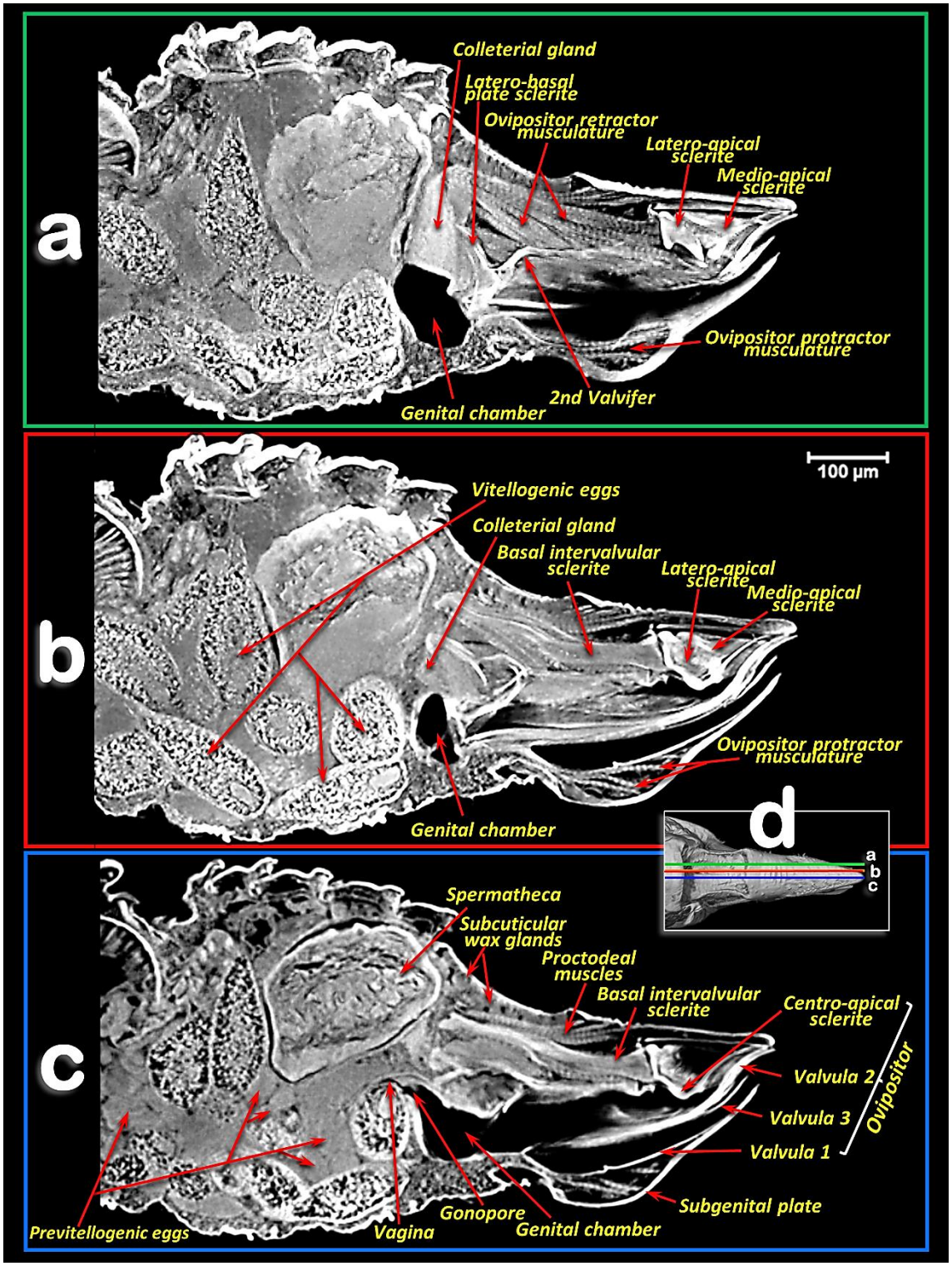

Figure 8.- Amira´s multiplanar sagittal section slices of an older female adult (**a**, **b**, **c**), according to plane cuts shown in **d** (slices **a**, **b**: 23 µm thick and slice **c**: 3 µm thick).

contact with the calyx cavity, presents as a conspicuous cone-shaped structure (valve plug) in the middle of a helical slide-shaped surface that has two little holes (foramina). In the foramina there are small closing muscle fibres (Fig. 5f-g).

The spermathecal duct enlarges proximally, containing two small chambers separated by a central pierced wall (Fig. 5d-e, 5h). Distally the duct connects with the vagina (Fig. 3a-b; Supplementary Video S1).

The ovipositor (Figs. 1c, 2, 7, 8; Supplementary Video S3) is largely hidden inside the apical abdominal segments (Fig. 2a, 2c-d); only some apical parts can be observed externally (Fig. 1a-b, 1d). When segmented and isolated as a whole, three concentrically arranged valvulae (valves) are visible: 1st (ventral), 2nd (dorsal) and 3rd (central) (Fig. 7, particularly 7a, 7g, 7h, 7j). The 1st valvula is configured as a curved blade, forming a spoon-shaped structure that houses the 3rd valvula and this in turn surrounds the 2nd valvula both ventrally and laterally (Fig. 7g, 7j). The ovipositor protractor musculature is attached between the 1st valvula and the inner side of the sub-genital plate (Figs 1c, 8). Valvifer sclerites of the 1st and 2nd valvula are visible. The 1st valvifer appears basally and it seems to enlarge acting as part of the wall of the basal genital chamber; the 2nd valvifer appears as a dorsal broad sclerite extending from the base to 2/3 apical. The 2nd valvula has, on each side, two longitudinal sclerotized reinforcement bars that join in a single lateral bar; from each side, these fuse medially in a pointed apical end (Figs. 7a, g-l)

Dorsally, a conspicuous longitudinal bar, the basal intervalvular sclerite (Fig. 7a, 7g, 7k), serves as an attachment for the ovipositor retractor musculature (Fig. 8a). The basal intervalvular sclerite articulates apically with three small vertical pointed plate sclerites: two lateral (latero-apical sclerites), two medial (medio-apical sclerites) and a single central one (centro-apical sclerite) (Figs. 7a, 7g-l, 8).

Basally at both sides of the ovipositor there are two vertical lateral plates that, dorsally, are curved forwards (Figs. 7a-g, 7i) with a conspicuous longitudinal apodemal ridge on the internal side (Figs. 7c-f).

The bacteriome organ (Figs. 3, 6; Supplementary Video S1) is situated dorsal to the ovaries and anterior to the spermatheca. It is well developed in the young adult female, extending along the anterior abdominal half (Fig. 3). The bacteriome is not visible in older adult females (Figs. 2, 8). It is roughly ‘H’ shaped, with two lateral lobes that have rounded ends. The two lateral lobes are united

dorsally in the anterior third by a dorsal bridge which permits separation of each lateral lobe into a long anterior lobe and a short posterior lobe (Fig. 6a, 6c, 6e, 6g-h). The posterior side of the dorsal bridge, together with the posterior lobes, forms a concavity where the spermatheca fits. In a similar way, there is an anterior concavity in the anterior side of the dorsal bridge. The anterior lobes are anteriorly projected on each side of the digestive system. The filter chamber of the digestive system is located dorsally on the anterior concavity (Figs. 3, 6a, 6c, 6g-h; Supplementary Video S1). In section, the bacteriome shows an external layer of bacteriocytes, and an internal syncytium, containing symbiotic microorganisms, which at some points meets the surface of the bacteriome (Fig. 6b, 6d, 6f).

5.3.6.- Discussion

In psylloids the first abdominal segments are reduced, and attached to segments of the thorax or abdomen, so that it is difficult to interpret and number them. Thus, there has been no consensus concerning the visible sclerites of the abdominal segments (Bitsch, 1979; Matsuda, 1976; Muir, 1930; Pesson, 1951; Zucht, 1972). In fact, publications on psylloids generally avoid the controversy and do not number these segments (e.g. (Brown & Hodkinson, 1988; I.D. Hodkinson & White, 1979)). In this study it was possible to clearly distinguish, dorsally, six tergite sclerites plus the proctiger in the abdomen of female *D. citri*. We interpret these as sclerites of the 3rd-7th tergites (the 8th was not visible because it was small and membranous), and the proctiger. Some authors consider that proctigers of psylloids are either the 9th tergite (Muir, 1930), a fusion of the 9th and 10th tergite (Matsuda, 1976; Zucht, 1972), or a fusion of the 9th-11th tergites (Bitsch, 1979). Ventrally, five sternal sclerites plus the subgenital plate were clearly visible. Moreover between the 7th sternite and the subgenital plate two lateral sternites were apparent, which we interpreted as a divided 8th sternite sclerite (Fig. 1d); this seems to be absent in other psylloid species(Crawford, 1914). The sub-genital plate of psylloids was described by Bitsch (Bitsch, 1979) and other authors as the 9th abdominal sternites (Crawford, 1914; Matsuda, 1976). However, Muir (Muir, 1930) and Zucht (Zucht, 1972) working with *Psylla mali* and *P. crataegi*, respectively, interpreted it as the 7th abdominal sternite, and

numbered the visible abdominal sternites from 3-6 and 7 (sub-genital plate). Specifically, Muir (Muir, 1930) wrote: “There is absolutely no evidence to support the idea that the sub-genital plate is formed by the ninth tergite, and there is no need to suppose that such an abnormal dislocation takes place”. As the problems of interpretation of the abdominal segment sclerites is not the main aim of this paper, we have adopted the numbering of the tergites and sternites that best fits with the general consensus, and particularly with Matsuda’s interpretation (Matsuda, 1976) (Figs. 1-3).

In general the organization of the female reproductive system of *D. citri* that we observed agrees with previous descriptions for other psylloid species (e.g. (Blowers & Moran, 1967; Brittain, 1922; Büning & Büning, 1994; Dossi & Cônsoli, 2010, 2014; Prophetou-Athanasiadou & Tzanakakis, 1998; Saunders, 1921)). Pesson (Pesson, 1951) stated that, in psylloids, each ovary has ca. 25 ovarioles. However, other reports have found up to 100 ovarioles (Büning & Büning, 1994; Hodin, 2009). In *D. citri* up to 50 ovarioles have been reported (Dossi & Cônsoli, 2014) which is close to the number we counted, although it varied between ovaries: 40 in the right ovary and 46 in the left ovary.

In general the calyx (a dilatation of the oviduct for the reception of eggs) is located just after the conjunction of the ovarioles in insects (Chapman, 2013; Gillott, 2005; Gullan & Cranston, 2010; Snodgrass, 1935). However, the dilation we report here for *D. citri*, is configured as a dilation of the oviduct tube before it joins the common oviduct.

Various authors consider the female accessory glands to be synonymous with cement glands (Chapman, 2013; Gillott, 2005; Gullan & Cranston, 2010; Snodgrass, 1935). The role of the female accessory glands in insects is not well known. It has been suggested that their secretions may activate pheromone production (Gullan & Cranston, 2010), or interact with proteins derived from the male accessory glands or his sperm (Chapman, 2013). In muscid flies, the accessory gland secretion contains proteolytic enzymes and an esterase that have essential roles in fertilization of the egg; they break down the acrosomal membrane of the sperm, and they lead to digestion of the cap over the micropyle. Whether this also occurs in other insects is not known (Chapman, 2013). *D. citri*

has a pair of tubular, well developed, female accessory glands and, although their structure has been studied previously using electron microscopy, its function has not been elucidated(Dossi & Cônsoli, 2014); currently their role is speculative and requires further research.

Protuberances of the spermathecal surface, which gave it a rough appearance, correspond to individual secretory cells of the epithelial secretor, as described previously for *Trioza alacris* (Marchini *et al.*, 2012) and *D. citri* (Dossi & Cônsoli, 2010, 2014). The spermatheca is not just a storage sac where spermatozoa are stored and/or nourished prior to egg fertilization. It is likely that the two materials with different densities that we observed in the spermatheca are not two separate cavities, but a single one containing a spermatodose. A spermatodose is a reorganization of the male spermatophore which had been previously transferred into the female spermatheca. The spermatodose protects the sperm from hostile spermiolytic activity (e.g. (Marchini *et al.*, 2012; Pascini & Martins, 2017)). Thus, the ventral internal zone, appearing as high-density material, corresponds to the spermatodose. It is possible to distinguish denser filament structures within the spermatodose, which are of comparable size to spermatozoa as described previously for *D. citri* (Barcellos *et al.*, 2017), and similar to micro-CT-rendered images of spermatozoa inside testes (*Alba-Alejandre et al., 2018*). The dorsal internal zone, appearing as low-density material, corresponds to nutritive liquid secretions of the epithelial secretor. In older adult females, which were close to ovipositing, the stored spermatodose in the internal cavity of the spermatheca had disaggregated to release spermatozoa; this explains the lack of two separate zones. The spermatheca appears to have all the impellent suction elements of a pump, which is as it has been described previously for the harlequin bug *Murgantia histrionica* by Stacconi & Romani (Stacconi & Romani, 2011). In fact, the chambers and valve position in Stacconi & Romani's Figs. 3a and 6 resemble the structures we observed in *D. citri* (Fig. 5d-e; Supplementary Video S2). The pumping function of the spermatheca has been reported in other insects as a spermathecal pump, consisting of muscle fibres located either in the spermathecal sac or in the duct wall. The presence of muscle fibres surrounding the entire spermathecal reservoir has been observed in a number of insect species (see revision by

Pascini & Martins (Pascini & Martins, 2017)). The presence of bundles of muscle fibrils in the spermathecal sheath of *D. citri* has also been described using transmission electron microscopy (Dossi & Cônsoli, 2014). To pump the sperm into the spermatheca, the musculature of the spermathecal sheath contracts. It then relaxes and the elasticity of the spermathecal sheath returns the spermathecal sac to its globular shape, as the sperm are absorbed from the vagina through the spermathecal duct and pour into the calyx cavity. Once sperm reach the calyx cavity (the muscles of the foramina are relaxed so the orifices remain open), the calyx wall contracts so that the valve plug fits into the 1st proximal chamber with its tip occluding the central hole in the wall that divides the two chambers (the hole is oblong-shaped to fit with the compressed shape of the valve plug). Thereafter the sperm glide through the two foramina into the lumen of the spermatheca, where they are protected within the spermatodose. When the female oviposits, the spermathecal pump procedure acts in reverse so that sperm are propelled into the spermatheca duct where the eggs are fertilized as they pass through the vagina at the point where the duct of the spermatheca connects.

The colleterial (= cement) gland produces a substance for attaching eggs to substrates, or for sticking them together in a mass as they are laid (Büning & Büning, 1994; Chapman, 2013; Gullan & Cranston, 2010; Snodgrass, 1935). Some detailed studies of the structure of the colleterial gland have been published (e.g. in the lepidopteran *Sesamia nonagrioides* (De Santis *et al.*, 2008)). These glands are present in a number of Hemiptera and Homoptera (Saunders, 1921); its presence has been described in several different psylloid species (including *D. citri* (Dossi & Cônsoli, 2014)) as an unpaired globular structure connected, by a duct, to the distal third of the intervalvular space of the ovipositor (Blowers & Moran, 1967; Brittain, 1922; Prophetou-Athanasiadou & Tzanakakis, 1998; Saunders, 1921). The micro-CT showed a dense superficial layer corresponding to a secretory epithelium, and an internal cavity (lumen) filled with a less-dense material corresponding to the sticky secretions of the gland (Blowers & Moran, 1967; De Santis *et al.*, 2008; Dossi & Cônsoli, 2014). The colleterial gland duct pours its sticky secretion far further than the gonopore. Thus, once fertilized eggs enter the genital chamber and pass through the

intervalvular space, they become coated with the sticky secretions of the colleterial gland just before they leave the ovipositor; this ensures they adhere to the citrus host plant.

For *P. mali*, Saunders described what he called a median accessory gland or parovarium (Brittain, 1922; Saunders, 1921) which most likely corresponds to the bursa copulatrix described in a number of species in the Hemiptera and Homoptera (Pesson, 1951), including psylloid species (i.e.: *Trioza erytreae* (Blowers & Moran, 1967) and *Euphyllura phillyreae* (Prophetou-Athanasiadou & Tzanakakis, 1998)). However, both dissections of females (Dossi & Cônsoli, 2014) and micro-CT confirm the absence of any bursa copulatrix in *D. citri*.

In many pterygote orders of insects, the female has an ovipositor that is highly evolved and well adapted for egg-laying and appears to be formed of the appendages of the 8th and 9th abdominal segment (Snodgrass, 1935). In Hemiptera the ovipositor has rather a complex structure (Pesson, 1951; Scudder, 1959, 1961; Snodgrass, 1935). Indeed, the lateral view of the female terminalia, with the lateral outline view of the ovipositor and ventral valvular, have been used as an additional taxonomic character for identification of female psylloids (e.g. (Brown & Hodkinson, 1988; Burckhardt, 1987, 1994; Ian David Hodkinson, 2017; Ossiannilsson, 1992)). Despite this, Hodkinson & White stated that ovipositor structures were generally of little taxonomic value (Hodkinson & White, 1979). The structure of the ovipositor has been described in detail for different psylloid species (e.g. *P. mali* (Brittain, 1922; Muir, 1930; Saunders, 1921) *P. crataegi* (Bitsch, 1979; Zucht, 1972), *Pachypsylla celtidis* (Austin & Dietrich, 2016)). Moreover, published light microscopy images from slide preparations show partial views of the distal 2/3^{rds} of the ovipositor of *E. phillyreae* (Prophetou-Athanasiadou & Tzanakakis, 1998) and *D. citri* (Dossi & Cônsoli, 2014).

Interpretation of the elements of the ovipositor vary depending on author. Most recognize and number the valvulae, but there are differences in the interpretation of individual structures. Thus, Muir (Muir, 1930) described the lateral plate sclerites as apodemes of the 8th abdominal sternites, and called them lateral plates (a term that we maintain here); later, Zucht (Zucht, 1972) considered them as the 1st valvifers. Recently Austin (Austin & Dietrich, 2016) considered

each lateral plate to represent a gonangulum (the sclerite that acts as a fulcrum, articulating against the 1st valvifer, and coupled with the 2nd and 3rd valvulae), but Matsuda (Matsuda, 1976) interpreted the lateral plates as a fusion of the 1st valvifer and the gonangulum. Homology amongst gonangula from different insect groups remains unclear (Klass *et al.*, 2012). We maintain the general term 'lateral plates', as used by Muir (Muir, 1930), even though they may represent the gonangulum as Austin (Austin & Dietrich, 2016) suggested for *P. celtidis* (Psyllidae). To the best of our knowledge there is no detailed study of the ovipositor in *D. citri*. Therefore, what we present in this paper represents not only the first detailed study of this structure in *D. citri*, but also the most complete detailed view of the ovipositor of any psylloid species using new micro-CT techniques.

The micro-CT-rendered images and 3D reconstructions of the bacteriome that we obtained are completely comparable to, and clearer than, those previously published for the leafhopper O*. albicinctus* which had been obtained using a synchrotron (Weintraub *et al.*, 2014). Moreover, the detailed structure is comparable to confocal micrographs of histological bacteriome sections made using fluorescence *in situ* hybridization (FISH) (Dan *et al.*, 2017; Kuechler *et al.*, 2012; Matsuura *et al.*, 2012; Nakabachi *et al.*, 2013; Ren *et al.*, 2018; Weintraub *et al.*, 2014). In fact, confocal FISH micrographs (Fig. 1A, and D of Dan *et al.*, (Dan *et al.*, 2017)) of the *D. citri* bacteriome look exactly the same as our micro-CT-rendered images (Figs. 6d, 6f). These images showed an external layer of bacteriocytes, harbouring *Candidatus* Carsonella ruddii (β-Proteobacteria), and an internal syncytium, harbouring *Candidatus* Profftella armatura (γ-Proteobacteria) (Dan *et al.*, 2017; Nakabachi *et al.*, 2013; Ren *et al.*, 2018), which extended to the surface of the bacteriome, and was also clearly visible with micro-CT. Recent evidence has reported the presence of *Wolbachia*, another endosymbiotic bacteria, in the *D. citri* bacteriome (Ren *et al.*, 2018).

5.3.7.- References

Alba-Alejandre, I., Alba-Tercedor, J., & Vega, F. E. (2018a). Micro-CT to Document the Coffee Bean Weevil, *Araecerus fasciculatus*(Coleoptera: Anthribidae), Inside Field-Collected Coffee Berries (Coffea canephora). *Insects*, *9*(3, 100), 1–9. https://doi.org/http://dx.doi.org/10.3390/insects9030100

Alba-Alejandre, I., Alba-Tercedor, J., & Vega, F. E. (2018b). Observing the devastating coffee berry borer (*Hypothenemus hampei*) inside the coffee berry using micro-computed tomography. *Scientific Reports*, *8*(1), 17033. https://doi.org/10.1038/s41598-018-35324-4

Alba-Alejandre, I., Alba-Tercedor, J., & Vega, F. E. (2019). Anatomical study of the coffee berry borer (*Hypothenemus hampei*) using micro-computed tomography. *Scientific Reports*, *9*(1), 17150. https://doi.org/10.1038/s41598-019-53537-z

Alba-Alejandre, I., Hunter, W. B., & Alba-Tercedor, J. (2018). Micro-CT study of male genitalia and reproductive system of the Asian citrus psyllid, *Diaphorina citri* Kuwayama, 1908 (Insecta: Hemiptera, Liviidae). *PLoS ONE*, *13*(8), 1–11. https://doi.org/https://doi.org/10.1371/journal.pone.0202234 Editor:

Alba-Tercedor, J. (2012a). *3D micro-CT study of the anatomy of the nymph of the mayfly Baetis alpinus*. http://www.youtube.com/watch?v=TFSAhrDnt5E. http://www.youtube.com/watch?v=TFSAhrDnt5E

Alba-Tercedor, J. (2012b). *Micro-CT study of the anatomy of the nymph of the mayfly Ephemera danica*. 1. Alba-Tercedor, J. Micro-CT study of the anatomy of the nymph of the mayfly Ephemera danica. (www.Youtube.com, 2012). http://www.youtube.com/watch?v=RpzxsSV42yk

Alba-Tercedor, J. (2012c). Studying the anatomy of wet specimens of mayflies of the genus Baetis (Insecta : Ephemeroptera) by scanning them into a liquid with the Skyscan 1172 high resolution micro-CT. *SkyScan Micro-CT Users Meeting 2012*, 192–195.

Alba-Tercedor, J. (2013). Study of the anatomy of the common housefly Musca domestica Linnaeus, 1758 (Insecta: Diptera, Muscidae) scanned with the Skyscan 1172 high resolution micro-CT. *Bruker Micro-CT Users Meeting 2013*, 275–289.

Alba-Tercedor, J. (2014a). From the sample preparation to the volume rendering images of small animals : A step by step example of a procedure to carry out the micro-CT study of the leafhopper insect *Homalodisca vitripennis* (Hemiptera: Cicadellidae). *Bruker Micro-CT Users Meeting 2014*, 260–288. http://www.skyscan.be/company/UM2014/008_Javier_Alba_Tercedor.pdf

Alba-Tercedor, J. (2014b). Microtomografías de invertebrados. *Investigación y Ciencia*, *Mayo*, 42–43.

Alba-Tercedor, J. (2016). Microtomographic study on the anatomy of adult male eyes of two mayfly species. *Zoosymposia*, *11*, 101. https://doi.org/10.11646/zoosymposia.11.1.13

Alba-Tercedor, J., & Alba-Alejandre, I. (2019). Comparing micro-CT results of insects with classical anatomical studies: The European honey bee (*Apis mellifera* Linnaeus, 1758) as a benchmark (Insecta: Hymenoptera, Apidae). *Microscopy and Analysis*, *3*(1), 12-15 EU. https://microscopy-analysis.com/article/january_19/comparing_classical_anatomical_studies_of_insects

Alba-Tercedor, J., Alba-Alejandre, I., & Vega, F. E. (2019). Revealing the respiratory

system of the coffee berry borer (*Hypothenemus hampei*; Coleoptera: Curculionidae: Scolytinae) using micro-computed tomography. *Scientific Reports*, *9*(1), 17753. https://doi.org/10.1038/s41598-019-54157-3

Alba-Tercedor, J., & Bartomeus, I. (2016). Micro-CT as a tool straddling scientist research, art and education. Study of *Osmia* sp., a mason bee (Insecta, Hymenoptera: Megachilidae). In *Bruker Micro-CT Users Meeting 2016* (pp. 74–91).

Alba-Tercedor, J., Hunter, W. B., Cicero, J., & Brown, S. (2017). Micro-CT scanning of Asian Citrus Psyllid, *Diaphorina citri*, Anatomy and Feeding. *Journal of Citrus Pathology*, *4*(1), 1–2.

Alba-Tercedor, J., Hunter, W. B., Cicero, J. M., & Sáinz-Bariáin, M. (2017). Use of micro-CT to elucidate details of the anatomy and feeding of the Asian Citrus Psyllid *Diaphorina citri* Kuwayama , 1908 (Insecta : Hemiptera , Lividae). In *Bruker Micro-CT Users Meeting 2017* (pp. 270–285). Bruker microCT-Skyscan. http://bruker-microct.com/company/UM2017/AbstractBook2017.pdf

Alba-Tercedor, J., Sáinz-Bariáin, M., & Zamora-Muñoz, C. (2016). Changing the pupal–case architecture as a survival strategy in the caddisfly *Annitella amelia* Sipahiler, 1998 (Insecta, Trichoptera). *Animal Biodiversity and Conservation*, *39*(1), 65–75. http://abc.museucienciesjournals.cat/files/ABC_39-1_pp_65-75-color.pdf

Alba-Tercedor, J., & Sáinz-Cantero Caparrós, C. E. (2010). Studying Aquatic Insects Anatomy with the SkyScan 1172 high-resolution micro-CT. *SkyScan User Meeting 2010*, 2: 8-11. http://www.skyscan.be/company/UM2010/abstract_08.pdf

Alba-Tercedor, J., & Sáinz-Cantero Caparrós, C. E. (2012). Volume rendering reconstructions of the anatomy of small aquatic beetles (Insecta : Coleoptera) scanned with the Skyscan 1172 high resolution micro-CT. *SkyScan Micro-CT Users Meeting 2012*, 75–84. http://www.skyscan.be/company/UM2012/01.pdf

Alba-Tercedor, J., & Sánchez Almazo, I. (2014). The use of micro-CT for the study of eggs and development in insects : a comparison of two microtomographs. *Microscopy and Analysis*, *March*, 7–10.

Alba-Tercedor, J., & Sánchez Almazo, I. (2013). Looking beyond the small: micro-CT study of eggs and development in insects: comparison of the results obtained with the Skyscan 1172 and the attachment for SEM microtomographs. *Bruker Micro-CT Users Meeting 2013*, 102–110.

Aldrovandi, U. (1602). *De Animalibus Insectis Libri*.

Ammar, E.-D., & Hall, D. G. (2012). New and Simple Methods for Studying Hemipteran Stylets, Bacteriomes, and Salivary Sheaths in Host Plants. *Annals of the Entomological Society of America*, *105*(5), 731–739. https://doi.org/10.1603/AN12056

Austin, C., & Dietrich, C. H. (2016). *Morphology of Acercaria: investigations of the ovipositor and internal anatomy*.

Barcellos, M. S., Fernanda, J., Cossolin, S., Dias, G., & Lino-Neto, J. (2017). Sperm morphology of the leafhopper *Diaphorina citri* Kuwayama (Hemiptera: Sternorrhyncha: Psylloidea: Liviidae). *Micron*, *99*, 49–55. https://doi.org/10.1016/j.micron.2017.03.017

Baumann, P. (2005). Biology of Bacteriocyte-Associated Endosymbionts of Plant Sap-Sucking Insects. *The Annual Review of Microbiology*, *58*, 155–183. https://doi.org/10.1146/annurev.micro.59.030804.121041

Beaver, R. A. (1989). Insect–fungus relationships in the bark and ambrosia beetles. In

Wilding N, C. NM, H. PM, & W. JF (Eds.), *Insect–Fungus Interactions* (pp. 121–143). Academic Press Inc.

Bitsch, J. (1979). Morphologie Abdominale des Insectes. Ordre des Homoptères, B.-Psylles. In P.-P. Grassé (Ed.), *Traité de Zoologie. Anatomie, Systématique, Biologie. T. VIII, Insectes Thorax, Abdomen. Fasc. II* (pp. 420–429). Masson et Cie.

Blowers, J. R., & Moran, V. C. (1967). Notes on the female reproductive system of the South African Citrus Psylla, *Trioza erytreae* (Del Guercio) (Homoptera : Psyllidae). *Journal of the Entomological Society of Southern Africa*, *30*(1), 75–81. http://journals.co.za/docserver/fulltext/JESSA/30/1/2701.pdf?expires=1509005324&id=id&accname=guest&checksum=9DC141894F063094AFA46312BE35A085

Brittain, W. H. (1922). The morphology and synonymy of *Psylla mali* Schmidberger. *Proceeding Acadian Entomological Society (Fredericton)*, *8*, 23–51.

Brown, R. G., & Hodkinson, I. D. (1988). *Taxonomy and Ecology of the Jumping Plant-lice of Panama: Homoptera, Psylloidea*. E. J. Brill/Scandanavian Science Press Ltd.,. https://books.google.es/books?id=W9942XjeV44C&pg=PA4&lpg=PA4&dq=90-04-08893-8&source=bl&ots=557oIKp3ll&sig=ACfU3U1MfU-KaHESNrmTW00iop7rIg0ogQ&hl=es&sa=X&ved=2ahUKEwikrdL-9onlAhULAWMBHdEtDhkQ6AEwB3oECAkQAQ#v=onepage&q=citri&f=false

Büning, J., & Büning, J. (1994). The ovary of Ectognatha, the Insecta s. str. In *The Insect Ovary* (pp. 31–324). Springer Netherlands. https://doi.org/10.1007/978-94-011-0741-9_3

Burckhardt, D. (1987). Jumping plant lice (Homoptera: Psylloidea) of the temperate neotropical region. Part 2: Psyllidae (subfamilies Diaphorininae, Acizziinae, Ciriacreminae and Psyllinae). *Zoological Journal of the Linnean Society*, *90*, 145–205. https://onlinelibrary.wiley.com/doi/pdf/10.1111/j.1096-3642.1987.tb01353.x

Burckhardt, D. (1994). Generic key to chilean jumping plant·lice (Homoptera: Psylloidea) with inclusion of potential exotic pests. *Rev. Chilena Ent.*, *21*, 57–67.

Capoor, S., Rao, D., & Viswanath, S. (1967). *Diaphorina citri* Kuway., a vector of the greening disease of citrus in India. *Indian J. Agric. Sci.*, *37*(6), 572–579. http://swfrec.ifas.ufl.edu/hlb/database/pdf/00000830.pdf

Chapman, R. F. (2013). *The Insects Structure and Function.* (S. J. Simpson & A. E. Douglas (eds.); 5th ed.). Cambridge University Press. Chapman 5 th edition The Insects structure and function.pdf - ResearchGate

Chu, C.-C., Gill, T. A., Hoffmann, M., & Pelz-Stelinski, K. S. (2016). Inter-Population Variability of Endosymbiont Densities in the Asian Citrus Psyllid (*Diaphorina citri* Kuwayama). *Microbial Ecology*, *71*(4), 999–1007. https://doi.org/10.1007/s00248-016-0733-9

Crawford, D. L. (1914). A monograph of the jumping plant lice or Psyllidae of the New World. *Bull. U.S. Natn.Mus*, *85*, 1–182.

Dan, H., Ikeda, N., Fujikami, M., & Nakabachi, A. (2017). Behavior of bacteriome symbionts during transovarial transmission and development of the Asian citrus psyllid. *PLOS ONE*, *12*(12), e0189779. https://doi.org/10.1371/journal.pone.0189779

De Santis, F., Conti, E., Romani, R., Salerno, G., Parillo, F., & Bin, F. (2008). Colleterial glands of Sesamia nonagrioides as a source of the host-recognition kairomone for the egg parasitoid *Telenomus busseolae*. *Physiological Entomology*, *33*(1), 7–16. https://doi.org/10.1111/j.1365-3032.2007.00593.x

Dossi, Fabio C. A., & Cônsoli, F. L. F. (2014). Gross morphology and ultrastructure of the female reproductive system of *Diaphorina citri* (Hemiptera: Liviidae). *Zoologia*, *31*(2), 162–169. https://doi.org/10.1590/S1984-46702014000200007

Dossi, Fábio C A, & Cônsoli, F. L. (2010). Desenvolvimento ovariano e influência da cópula na maturação dos ovários de *Diaphorina citri* Kuwayama (Hemiptera: Psyllidae). *Neotropical Entomology*, *39*(3), 414–419. https://doi.org/10.1590/S1519-566X2010000300015

Gillott, C. (2005). Entomology. In *Entomology* (3rd ed.). Springer. www.springeronline.com

Greco, M., Bell, D., Woolnough, L., Laycock, S., Corps, N., Mortimore, D., & Hudson, D. (2014). 3-D visualisation, printing, and volume determination of the tracheal respiratory system in the adult desert locust, *Schistocerca gregaria*. *Entomologia Experimentalis et Applicata*, *152*(1), 42–51. https://doi.org/10.1111/eea.12199

Greco, M. K., Tong, J., Soleimani, M., Bell, D., & Schäfer, M. O. (2012). Imaging live bee brains using minimally-invasive diagnostic radioentomology. *Journal of Insect Science (Online)*, *12*, 89. https://doi.org/10.1673/031.012.8901

Greenlee, K. J., Henry, J. R., Kirkton, S. D., Westneat, M. W., Fezzaa, K., Lee, W.-K., & Harrison, J. F. (2009). Synchrotron imaging of the grasshopper tracheal system: morphological and physiological components of tracheal hypermetry. *American Journal of Physiology-Regulatory, Integrative and Comparative Physiology*, *297*(5), R1343–R1350. https://doi.org/10.1152/ajpregu.00231.2009

Gullan, P. J., & Cranston, P. S. (2010). *Insects: An Outline of Entomology* (4th ed.). Willey-Blackwell.

Ha, Y.-R., Yeom, E., Ryu, J., & Lee, S.-J. (2017). Three-dimensional structures of the tracheal systems of Anopheles sinensis and *Aedes togoi* pupae. *Scientific Reports. Nature Publishing Group*. https://doi.org/10.1038/srep44490

Halbert, S. S. E. S., & Manjunath, K. K. L. (2004). Asian Citrus Psyllids (Sternorrhyncha: Psyllidae) and Greening Disease of Citrus: a Literature Review and Assessment of Risk in Florida. *Florida Entomologist*, *87*(3), 330–353. https://doi.org/10.1653/0015-4040(2004)087[0330:ACPSPA]2.0.CO;2

Helm, B. R., Payne, S., Rinehart, J. P., Yocum, G. D., Bowsher, J. H., & Greenlee, K. J. (2018). Micro-computed tomography of pupal metamorphosis in the solitary bee *Megachile rotundata*. *Arthropod Structure & Development*, *47*(5), 521–528. https://doi.org/10.1016/J.ASD.2018.05.001

Hodin, J. (2009). She shapes events as they come: plasticity in female insect reproduction. In D. W. Whitman & T. N. Ananthakrishnan (Eds.), *Phenotypic plasticity of insects: mechanisms and consequences.* Science Publishers, Inc. https://doi.org/Enfield, Science Publishers.

Hodkinson, I.D., & White, I. M. (1979). *Homoptera Psylloidea* (A. Watson (ed.)). Royal Entomological Society of London.

Hodkinson, I.D:. (2017). *Psyllidae (Jumping plant-lice, psyllids) History of ague (vivax malaria) in northern Britain View project Review of Arctic insect biodiversity View project*.

Inoue, H., Ohnishi, J., Ito, T., Tomimura, K., Miyata, S., Iwanami, T., & Ashihara, W. (2009). Enhanced proliferation and efficient transmission of *Candidatus* Liberibacter asiaticus by adult *Diaphorina citri* after acquisition feeding in the nymphal stage. *Annals of Applied Biology*, *155*(1), 29–36. http://onlinelibrary.wiley.com/doi/10.1111/j.1744-7348.2009.00317.x/full

Iwan, D., Kamiński, M. J., & Raś, M. (2015). The Last Breath: A µCT-based method for investigating the tracheal system in Hexapoda. *Arthropod Structure & Development*, *44*(3), 218–227. https://doi.org/10.1016/j.asd.2015.02.002

Jiang, Z.-R., Kinoshita, ichi, Sasaki, O., Cognato, A. I., & Kajimura, H. (2019). *Non-destructive observation of the mycangia of Euwallacea interjectus (Blandford) (Coleoptera: Curculionidae: Scolytinae) using X-ray computed tomography*. https://doi.org/10.1111/ens.12353

Klass, K.-D., Matushkina, N. A., & Kaidel, J. (2012). The gonangulum: A reassessment of its morphology, homology, and phylogenetic significance. *Arthropod Structure & Development*, *41*(4), 373–394. https://doi.org/10.1016/J.ASD.2012.03.001

Kuechler, S. M., Renz, P., Dettner, K., & Kehl, S. (2012). Diversity of symbiotic organs and bacterial endosymbionts of: Lygaeoid bugs of the families blissidae and lygaeidae (Hemiptera:: Heteroptera: Lygaeoidea). *Applied and Environmental Microbiology*, *78*(8), 2648–2659. https://doi.org/10.1128/AEM.07191-11

Kuwayama, S. (1907). Die Psylliden Japanese. *Transactions of the Sapporo Natural History Society*, *2*, 149-189. (*D. citri*: p. 160-161, Plate III,Fig. 16). https://www.hemiptera-databases.org/psyllespdf/25.pdf

Kypke, J. L., & Solodovnikov, A. (2018). Every cloud has a silver lining: X-ray micro-CT reveals *Orsunius rove* beetle in Rovno amber from a specimen inaccessible to light microscopy. *Historical Biology*, 1–11. https://doi.org/10.1080/08912963.2018.1558222

Li, D., Zhang, K., Zhu, P., Wu, Z., & Zhou, H. (2011). 3D configuration of mandibles and controlling muscles in rove beetles based on micro-CT technique. *Analytical and Bioanalytical Chemistry*, *401*(3), 817–825. https://doi.org/10.1007/s00216-011-5088-y

Li, Y., Ruan, Y., Kasson, M. T., Stanley, E. L., Gillett, C. P. D. T., Johnson, A. J., Zhang, M., & Hulcr, J. (2018). Structure of the Ambrosia Beetle (Coleoptera: Curculionidae) Mycangia Revealed Through Micro-Computed Tomography. *Journal of Insect Science*, *18*(5), 13–14. https://doi.org/10.1093/jisesa/iey096

Lowe, T., Garwood, R. J., Simonsen, T. J., Bradley, R. S., & Withers, P. J. (2013). Metamorphosis revealed: time-lapse three-dimensional imaging inside a living chrysalis. *Journal of the Royal Society, Interface / the Royal Society*, *10*(84), 20130304. https://doi.org/10.1098/rsif.2013.0304

Malpighi, M. (1669). *Dissertatio epistolica de bombyce*. J. Martyn & J. Allestry, regiæ societatis typographos.

Marchini, D., Del Bene, G., Viscuso, R., & Dallai, R. (2012). Sperm Storage by Spermatodoses in the Spermatheca of *Trioza alacris* (Flor, 1861) Hemiptera, Psylloidea, Triozidae: A Structural and Ultrastructural Study. *J. Morphol*, *273*, 195–210. https://doi.org/10.1002/jmor.11017

Martín-Vega, D., Garbout, A., Ahmed, F., Ferrer, L. M., Lucientes, J., Colwell, D. D., & Hall, M. J. R. (2018). Micro-computed tomography visualization of the vestigial alimentary canal in adult oestrid flies. *Medical and Veterinary Entomology*, *32*(3), 378–382. https://doi.org/10.1111/mve.12301

Matsuda, R. (1976). The Homoptera. In *Morphology and Evolution of the Insect Abdomen* (pp. 280–299). Pergamon Press Ltd. https://doi.org/10.1016/B978-0-08-018753-2.50040-X

Matsuura, Y., Kikuchi, Y., Hosokawa, T., Koga, R., Meng, X. Y., Kamagata, Y., Nikoh, N., & Fukatsu, T. (2012). Evolution of symbiotic organs and endosymbionts in

lygaeid stinkbugs. *ISME Journal*, *6*(2), 397–409. https://doi.org/10.1038/ismej.2011.103

McClean, A., & Oberholzer, P. (1965). Greening disease of the sweet orange: evidence that it is caused by a transmissible virus. *South African Journal of Agricultural Science* 8(1), 253–276. http://www.cabdirect.org/abstracts/19670500754.html

Mead, F. W., & Fasulo, T. R. (2017). Asian Citrus Psyllid, *Diaphorina citri* Kuwayama (Insecta : Hemiptera : Psyllidae). *Series of the Entomology and Nematology Department, UF/IFAS Extension*, *EENY-033*, 1–8. http://entnemdept.ifas.ufl.edu/creatures/.

Muir, F. (1930). LIII.—Notes on certain controversial points of morphology of the abdomen and genitalia of Psyllidæ. *Annals and Magazine of Natural History, Series 10*, *5*(29), 545–552. https://doi.org/10.1080/00222933008673163

Nakabachi, A., Ueoka, R., Oshima, K., Teta, R., Mangoni, A., Gurgui, M., Oldham, N. J., van Echten-Deckert, G., Okamura, K., Yamamoto, K., Inoue, H., Ohkuma, M., Hongoh, Y., Miyagishima, S., Hattori, M., Piel, J., & Fukatsu, T. (2013). Defensive bacteriome symbiont with a drastically reduced genome. *Current Biology*, *23*(15), 1478–1484. https://doi.org/10.1016/J.CUB.2013.06.027

Ossiannilsson, F. (1992). *The Psylloidea (Homoptera) of Fennoscandia and Demark*. E.J. Brill. https://books.google.es/books?id=X_fgWnvLS2gC&pg=PA7&lpg=PA7&dq=ossiannilson+psylloidea+fennoscandian&source=bl&ots=4V0spLX1n1&sig=ACfU3U3D5VxM6vzpdIdJy7VIf5s11DGSrw&hl=es&sa=X&ved=2ahUKEwiumePoq5HlAhVOAWMBHVwbCKgQ6AEwCnoECAgQAQ#v=onepage&q&f=false

Pascini, T. V., & Martins, G. F. (2017). The insect spermatheca: an overview. *Zoology*, *121*, 56–71. https://doi.org/10.1016/J.ZOOL.2016.12.001

Pelz-Stelinski, K. (2010). Transmission parameters for *Candidatus* Liberibacter asiaticus by Asian citrus psyllid (Hemiptera: Psyllidae). *Journal of Economic …*. http://jee.oxfordjournals.org/content/103/5/1531.abstract

Pelz-Stelinski, K. S., & Killiny, N. (2016). Better Together: Association with "*Candidatus* Liberibacter Asiaticus" Increases the Reproductive Fitness of Its Insect Vector, *Diaphorina citri* (Hemiptera: Liviidae). *Annals of the Entomological Society of America*, *109*(3), 371–376. https://doi.org/10.1093/aesa/saw007

Pesson, P. (1951). Ordre des Homoptères (Homoptera Leach, 1815). In P.-P. Grassé (Ed.), *Traité de zoologie. Anatomie, systématique, biologie. Tome X. Fascicule II. Insectes supérieurs et Hémipteróides* (Editions M, pp. 1390–1656). Masson et Cie.

Prophetou-Athanasiadou, D. A., & Tzanakakis, M. E. (1998). The Reproductive System and Ovarian Development of the Adult Olive Psylla *Euphyllura phillyreae* Foerster (Homoptera: Aphalaridae). *Entomologia Hellenica*, *12*, 37–45. https://doi.org/http://dx.doi.org/10.12681/eh.14018

Raś, M., Iwan, D., & Kamiński, M. J. (2018). The tracheal system in post-embryonic development of holometabolous insects: a case study using the mealworm beetle. *Journal of Anatomy*, *232*(6), 997–1015. https://doi.org/10.1111/joa.12808

Ren, S.-L., Li, Y.-H., Ou, D., Guo, Y.-J., Qureshi, J. A., Stansly, P. A., Qiu, B.-L., & Bao-Li Qiu, C. (2018). Localization and dynamics of Wolbachia infection in Asian citrus psyllid *Diaphorina citri*, the insect vector of the causal pathogens of Huanglongbing. *Microbiology Open*, *7*, 561. https://doi.org/10.1002/mbo3.561

Ribi, W., Senden, T. J., Sakellariou, A., Limaye, A., & Zhang, S. (2008). Imaging honey bee brain anatomy with micro-X-ray-computed tomography. *Journal of*

Neuroscience Methods, *171*(1), 93–97. https://doi.org/10.1016/j.jneumeth.2008.02.010

Saunders, L. G. (1921). *The Anatomy of Psyllia mali Schmidberger. Manuscript Thesis (M. Sc.) McGill University. Montreal.*

Schambach, S. J., Bag, S., Schilling, L., Groden, C., & Brockmann, M. A. (2010). Application of micro-CT in small animal imaging. *Methods (San Diego, Calif.)*, *50*(1), 2–13. https://doi.org/10.1016/j.ymeth.2009.08.007

Scudder, G. G. E. (1959). The female genitalia of the Heteroptera: morphology and bearing on classification. *Transactions of the Royal Entomological Society of London*, *111*(14), 405–467. https://doi.org/10.1111/j.1365-2311.1959.tb02873.x

Scudder, G. G. E. (1961). The comparative morphology of the insect ovipositor. *Transactions of the Royal Entomological Society of London*, *113*(2), 25–40. https://doi.org/10.1111/j.1365-2311.1961.tb00800.x

Shaha, R. K., Vogt, J. R., Han, C.-S., & Dillon, M. E. (2013). A micro-CT approach for determination of insect respiratory volume. *Arthropod Structure & Development*, *42*(5), 437–442. https://doi.org/10.1016/J.ASD.2013.06.003

Shen, W., Halbert, S. E., Dickstein, E., Manjunath, K. L., Shimwela, M. M., & Bruggen, A. H. C. van. (2013). Occurrence and in-grove distribution of citrus huanglongbing in north Central Florida. In *Journal of Plant Pathology* (Vol. 95, pp. 361–371). Società Italiana di Patologia Vegetale (SIPaV). https://doi.org/10.2307/23721526

Slater, A., Prior, M., & Hacking, C. P. (2017). *Anatomical distribution of ureteric calculi in CT KUB studies: a single-centre audit*. https://doi.org/10.1594/ranzcr2017/R-0114

Smith, D. B., Bernhardt, G., Raine, N. E., Abel, R. L., Sykes, D., Ahmed, F., Pedroso, I., & Gill, R. J. (2016). Exploring miniature insect brains using micro-CT scanning techniques. *Scientific Reports*, *6*(1), 21768. https://doi.org/10.1038/srep21768

Snodgrass, R. E. (1935). *Principles of Insect Morphology*. McGraw-Hill Book Company, Inc. https://doi.org/0801428831

Sombke, A., Lipke, E., Michalik, P., Uhl, G., & Harzsch, S. (2015). Potential and limitations of X-Ray micro-computed tomography in arthropod neuroanatomy: a methodological and comparative survey. *The Journal of Comparative Neurology*, *523*(8), 1281–1295. https://doi.org/10.1002/cne.23741

Soriano, C., Archer, M., Azar, D., Creaser, P., Delclòs, X., Godthelp, H., Hand, S., Jones, A., Nel, A., Néraudeau, D., Ortega-Blanco, J., Pérez-de la Fuente, R., Perrichot, V., Saupe, E., Kraemer, M. S., & Tafforeau, P. (2010). Synchrotron X-ray imaging of inclusions in amber. *Comptes Rendus Palevol*, *9*(6–7), 361–368. https://doi.org/10.1016/j.crpv.2010.07.014

Stacconi, M., & Romani, R. (2011). Ultrastructural and functional aspects of the spermatheca in the american harlequin bug, *Murgantia histrionica* (Hemiptera: Pentatomidae). *Neotropical Entomology*, *40*(2), 222–230. https://doi.org/10.1590/S1519-566X2011000200011

Stalling, D., Westerhoff, M., & Hege, H.-C. (2005). Amira: a highly interactive system for visual data analysis. In *Visualization Handbook* (pp. 749–767). Elsevier. https://doi.org/10.1016/B978-012387582-2/50040-X

Subandiyah, S., Nikoh, N., Tsuyumu, S., Somowiyarjo, S., & Fukatsu, T. (2000). Complex Endosymbiotic Microbiota of the Citrus Psyllid *Diaphorina citri* (Homoptera: Psylloidea). *Zoological Science*, *17*(7), 983–989. https://doi.org/10.2108/zsj.17.983

Sukthankar, P., Avila, L. A., Whitaker, S. K., Iwamoto, T., Morgenstern, A., Apostolidis, C., Liu, K., Hanzlik, R. P., Dadachova, E., & Tomich, J. M. (2014). Branched amphiphilic peptide capsules: Cellular uptake and retention of encapsulated solutes. *Biochimica et Biophysica Acta (BBA) - Biomembranes*, *1838*(9), 2296–2305. https://doi.org/10.1016/J.BBAMEM.2014.02.005

Taylor, G. J., Ribi, W., Bech, M., Bodey, A. J., Rau, C., Steuwer, A., Warrant, E. J., & Baird, E. (2016). The dual function of orchid bee ocelli as revealed by X-Ray Microtomography. *Current Biology : CB*, *26*(10), 1319–1324. https://doi.org/10.1016/j.cub.2016.03.038

Thermo Fisher Scientific. (2017). *Amira 3D visualization and analysis software* (6.7.0). FEI. http://www.thermofisher.com/amira-avizo

Verdú, J. R., Alba-Tercedor, J., & Jiménez-Manrique, M. (2012). Evidence of different thermoregulatory mechanisms between two sympatric Scarabaeus species using infrared thermography and micro-computer tomography. *PLoS ONE*, *7*(3), e33914. https://doi.org/10.1371/journal.pone.0033914

Weintraub, P. G., Hoch, H., Mühlethaler, R., & Zchori-Fein, E. (2014). Synchrotron X-ray micro-computed tomography as a tool for in situ elucidation of insect bacteriomes. *Arthropod Structure & Development*, *43*(2), 183–186. https://doi.org/10.1016/j.asd.2013.11.002

Westneat, M. W. (2003). Tracheal respiration in insects visualized with synchrotron X-ray imaging. *Science*, *299*(5606), 558–560. https://doi.org/10.1126/science.1078008

Wipfler, B, Wieland, F., DeCarlo, F., & Hörnschemeyer, T. (2012). Cephalic morphology of *Hymenopus coronatus* (Insecta: Mantodea) and its phylogenetic implications. *Arthropod Structure & Development*, *41*(1), 87–100. https://doi.org/10.1016/j.asd.2011.06.005

Wipfler, Benjamin, Pohl, H., Yavorskaya, M. I., & Beutel, R. G. (2016). A review of methods for analysing insect structures — the role of morphology in the age of phylogenomics. *Current Opinion in Insect Science*, *18*, 60–68. https://doi.org/10.1016/j.cois.2016.09.004

Witlaczil, E. (1885). Die Anatomie der Psylloden. *Zeitschrift Für Wissenschaftliche Zoologie*, *42*, 569–638.

Zucht, B. (1972). Bau und Entwicklung der äußeren Genitalorgane bei Psyllinen (Homopteren). *Zool. Jb. Anat. Bd.*, *231*, 167–231.

5.4.- "Observando la devastadora broca del café (*Hypothenemus hampei*) dentro de la baya del café usando microtomografía computarizada"

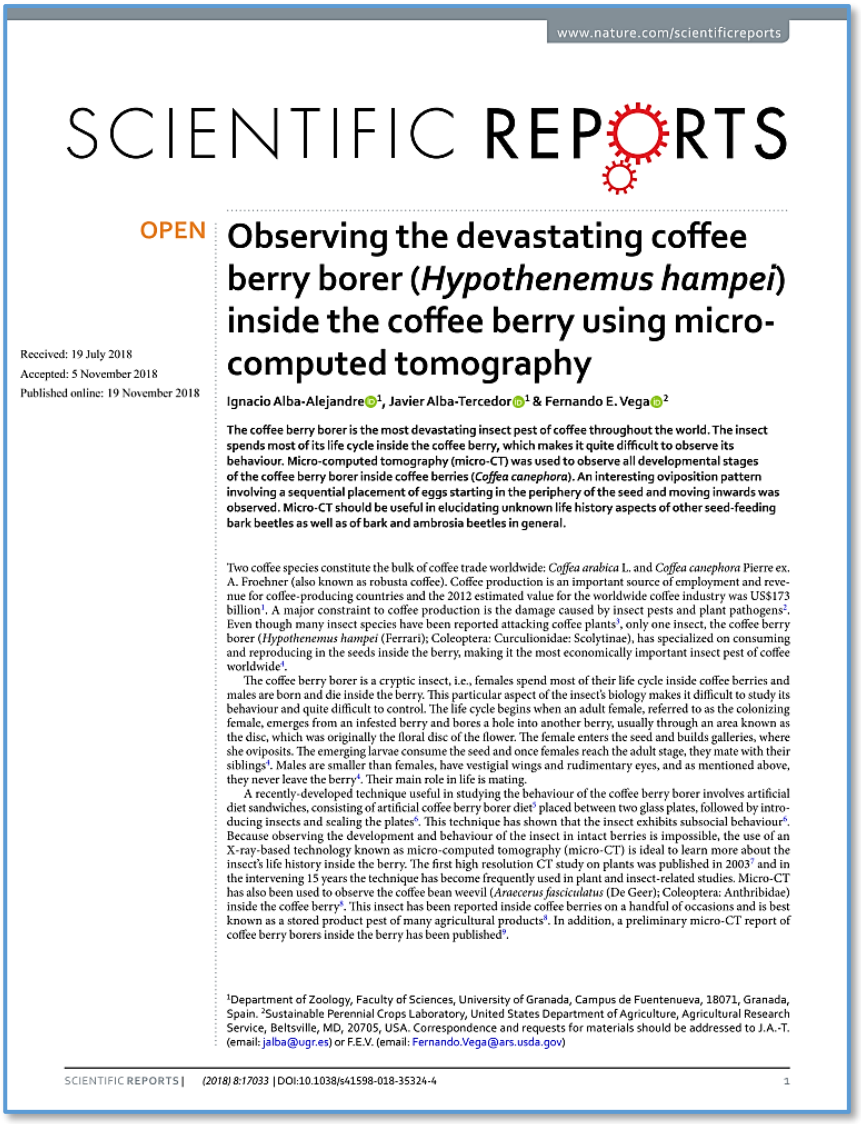

www.nature.com/scientificreports

SCIENTIFIC REPORTS

OPEN

Observing the devastating coffee berry borer (*Hypothenemus hampei*) inside the coffee berry using micro-computed tomography

Received: 19 July 2018
Accepted: 5 November 2018
Published online: 19 November 2018

Ignacio Alba-Alejandre[1], Javier Alba-Tercedor[1] & Fernando E. Vega[2]

The coffee berry borer is the most devastating insect pest of coffee throughout the world. The insect spends most of its life cycle inside the coffee berry, which makes it quite difficult to observe its behaviour. Micro-computed tomography (micro-CT) was used to observe all developmental stages of the coffee berry borer inside coffee berries (*Coffea canephora*). An interesting oviposition pattern involving a sequential placement of eggs starting in the periphery of the seed and moving inwards was observed. Micro-CT should be useful in elucidating unknown life history aspects of other seed-feeding bark beetles as well as of bark and ambrosia beetles in general.

Two coffee species constitute the bulk of coffee trade worldwide: *Coffea arabica* L. and *Coffea canephora* Pierre ex. A. Froehner (also known as robusta coffee). Coffee production is an important source of employment and revenue for coffee-producing countries and the 2012 estimated value for the worldwide coffee industry was US$173 billion[1]. A major constraint to coffee production is the damage caused by insect pests and plant pathogens[2]. Even though many insect species have been reported attacking coffee plants[3], only one insect, the coffee berry borer (*Hypothenemus hampei* (Ferrari); Coleoptera: Curculionidae: Scolytinae), has specialized on consuming and reproducing in the seeds inside the berry, making it the most economically important insect pest of coffee worldwide[4].

The coffee berry borer is a cryptic insect, i.e., females spend most of their life cycle inside coffee berries and males are born and die inside the berry. This particular aspect of the insect's biology makes it difficult to study its behaviour and quite difficult to control. The life cycle begins when an adult female, referred to as the colonizing female, emerges from an infested berry and bores a hole into another berry, usually through an area known as the disc, which was originally the floral disc of the flower. The female enters the seed and builds galleries, where she oviposits. The emerging larvae consume the seed and once females reach the adult stage, they mate with their siblings[4]. Males are smaller than females, have vestigial wings and rudimentary eyes, and as mentioned above, they never leave the berry[4]. Their main role in life is mating.

A recently-developed technique useful in studying the behaviour of the coffee berry borer involves artificial diet sandwiches, consisting of artificial coffee berry borer diet[5] placed between two glass plates, followed by introducing insects and sealing the plates[6]. This technique has shown that the insect exhibits subsocial behaviour[6]. Because observing the development and behaviour of the insect in intact berries is impossible, the use of an X-ray-based technology known as micro-computed tomography (micro-CT) is ideal to learn more about the insect's life history inside the berry. The first high resolution CT study on plants was published in 2003[7] and in the intervening 15 years the technique has become frequently used in plant and insect-related studies. Micro-CT has also been used to observe the coffee bean weevil (*Araecerus fasciculatus* (De Geer); Coleoptera: Anthribidae) inside the coffee berry[8]. This insect has been reported inside coffee berries on a handful of occasions and is best known as a stored product pest of many agricultural products[8]. In addition, a preliminary micro-CT report of coffee berry borers inside the berry has been published[9].

[1]Department of Zoology, Faculty of Sciences, University of Granada, Campus de Fuentenueva, 18071, Granada, Spain. [2]Sustainable Perennial Crops Laboratory, United States Department of Agriculture, Agricultural Research Service, Beltsville, MD, 20705, USA. Correspondence and requests for materials should be addressed to J.A.-T. (email: jalba@ugr.es) or F.E.V. (email: Fernando.Vega@ars.usda.gov)

Alba-Alejandre, I., Alba-Tercedor, J., & Vega, F. E. (2018). Observing the devastating coffee berry borer (*Hypothenemus hampei*) inside the coffee berry using micro-computed tomography. *Scientific Reports*, 8(1), 17033: 1-9. https://doi.org/10.1038/s41598-018-35324-4

5.4.1.- Resumen

La broca del café es la plaga de insectos más devastadora del café en todo el mundo. El insecto pasa la mayor parte de su ciclo de vida dentro de la baya del café, lo que hace que sea bastante difícil observar su comportamiento. La microtomografía computarizada (micro-TC) se utilizó para observar todas las etapas de desarrollo de la broca del café dentro de las bayas de café (*Coffea canephora).* Se observó un patrón de oviposición interesante que involucra una colocación secuencial de huevos que comienza en la periferia de la semilla y se dirige hacia adentro. La micro-TC debería ser útil para dilucidar aspectos desconocidos de la vida de otros escarabajos de la corteza que se alimentan de granos, así como de los escarabajos de la corteza y de ambrosía en general.

5.4.2.- Abstract

The coffee berry borer is the most devastating insect pest of coffee throughout the world. The insect spends most of its life cycle inside the coffee berry, which makes it quite difficult to observe its behaviour. Micro-computed tomography (micro-CT) was used to observe all developmental stages of the coffee berry borer inside coffee berries (*Coffea canephora*). An interesting oviposition pattern involving a sequential placement of eggs starting in the periphery of the seed and moving inwards was observed. Micro-CT should be useful in elucidating unknown life history aspects of other seed-feeding bark beetles as well as of bark and ambrosia beetles in general.

5.4.3.- Introduction

Two coffee species constitute the bulk of coffee trade worldwide: *Coffea arabica* L. and *Coffea canephora* Pierre ex. A. Froehner (also known as robusta coffee). Coffee production is an important source of employment and revenue for coffee-producing countries, and the 2012 estimated value for the worldwide coffee industry was US$173 billion (ICO, 2014). A major constraint to coffee production is the damage caused by insect pests and plant pathogens (Le Pelley, 1968). Even though many insect species have been reported attacking coffee plants

(Waller *et al.*, 2007), only one insect, the coffee berry borer (*Hypothenemus hampei* (Ferrari); Coleoptera: Curculionidae: Scolytinae), has specialized on consuming and reproducing in the seeds inside the berry, making it the most economically important insect pest of coffee worldwide (Vega *et al.*, 2015).

The coffee berry borer is a cryptic insect, i.e., females spend most of their life cycle inside coffee berries and males are born and die inside the berry. This particular aspect of the insect's biology makes it difficult to study its behaviour and quite difficult to control. The life cycle begins when an adult female, referred to as the colonizing female, emerges from an infested berry and bores a hole into another berry, usually through an area known as the disc, which was originally the floral disc of the flower. The female enters the seed and builds galleries, where she oviposits. The emerging larvae consume the seed and once females reach the adult stage, they mate with their siblings (Vega *et al.*, 2015). are smaller than females, have vestigial wings and rudimentary eyes, and as mentioned above, they never leave the berry (Vega *et al.*, 2015). Their main role in life is mating.

A recently-developed technique useful in studying the behaviour of the coffee berry borer involves artificial diet sandwiches, consisting of artificial coffee berry borer diet (Fernando E. Vega *et al.*, 2011) placed between two glass plates, followed by introducing insects and sealing the plates (F. E. Vega *et al.*, 2017). This technique has shown that the insect exhibits subsocial behavior (F. E. Vega *et al.*, 2017). Because observing the development and behaviour of the insect in intact berries is impossible, the use of an X-ray-based technology known as micro-computed tomography (micro-CT) is ideal to learn more about the insect's life history inside the berry. The first high resolution CT study on plants was published in 2003 (Alba-Alejandre *et al.*, 2018) and in the intervening 15 years the technique has become frequently used in plant and insect-related studies. Micro-CT has also been used to observe the coffee bean weevil (*Araecerus fasciculatus* (De Geer); Coleoptera: Anthribidae) inside the coffee berry (Stuppy *et al.*, 2003). This insect has been reported inside coffee berries on a handful of occasions and is best known as a stored product pest of many agricultural

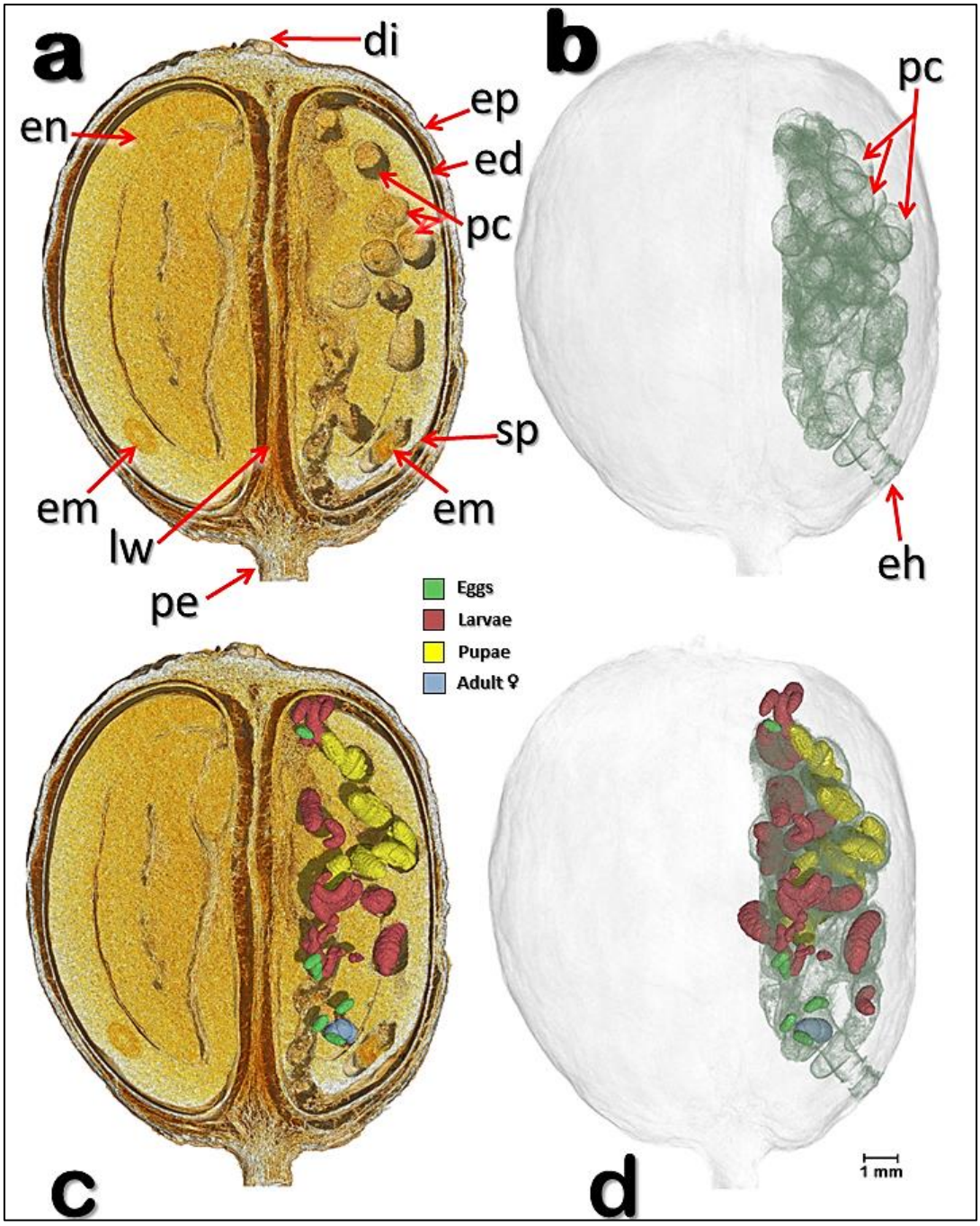

Figure 1.- Volume rendered images of a coffee berry bored-infested. **a**, **c**: meso-sagittal cut at the broadest plane level- perpendicular to the locule wall-, showing both beans and details of the coffee berry structures (**a**: the insects have been removed by software to show details of the galleries and cavities; **e**: different development stages at their actual position); **b**: transparented coffee berry, showing the galleries and cavities inside. **d**: different development stages at their actual position inside the galleries and cavities of the coffee berry. Different development stages have been separately segmented to unveil their location inside the berry (**c**, **d**). Abbreviations**,** di=disc (*style remnant*), ed=endocarp (*parchment*), eh=entrance (penetration hole), m=coffee embryo, en=endosperm *(bean*), ep=epicarp (*outer skin*), lw=locule wall (ovary) me=mesocarp (*mucilage*), pe= pedicel, sp=spermoderm (*silver skin*).

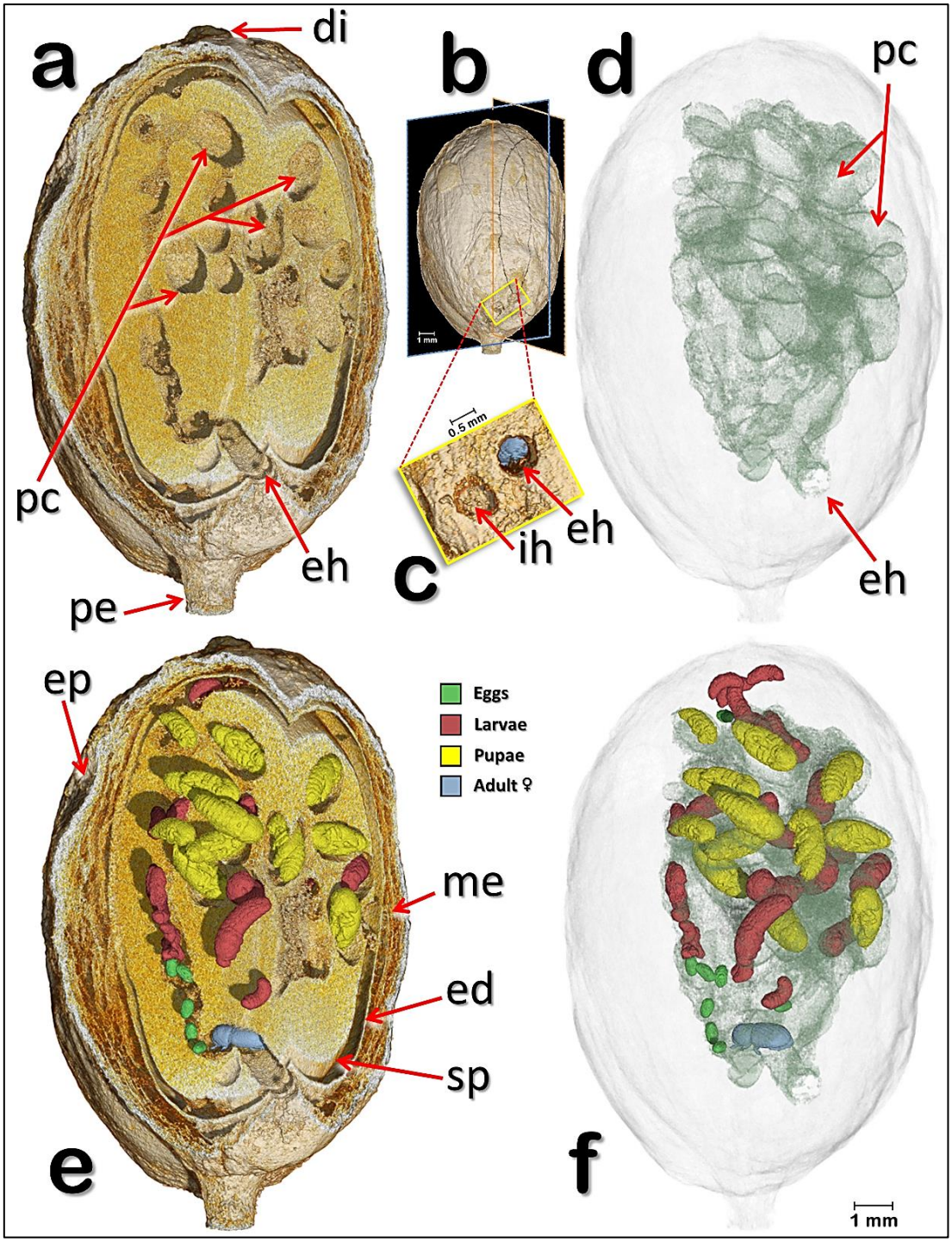

Figure 2.- Volume rendered images of a coffee berry bored-infested berry (berry 1). Oblique-lateral and oblique-apical section views (**a,e**), as shown in (**b**). The insects have been digitally removed to show details of the seed, galleries, and pupal cells (**a,d**). Detail of the latero-basal surface of the coffee berry showing an incomplete hole and the entrance hole bored by the colonizing female, whose posterior can be seen inside the gallery (**c**). Developmental stages of the insect (eggs, larvae, pupae, and adult colonizing female) in different colors (**e,f**). The coffee seed and components of the berry have been made transparent to show the galleries and the specific location of the different developmental stages of the insect (**f**). Abbreviations: di = disc (style remnant); ed = endocarp (parchment); eh = entrance (penetration hole); ep = epicarp (outer skin); ih = incomplete hole; me = mesocarp (mucilage); pc = pupal cell; pe = pedicel; sp = spermoderm (silverskin).

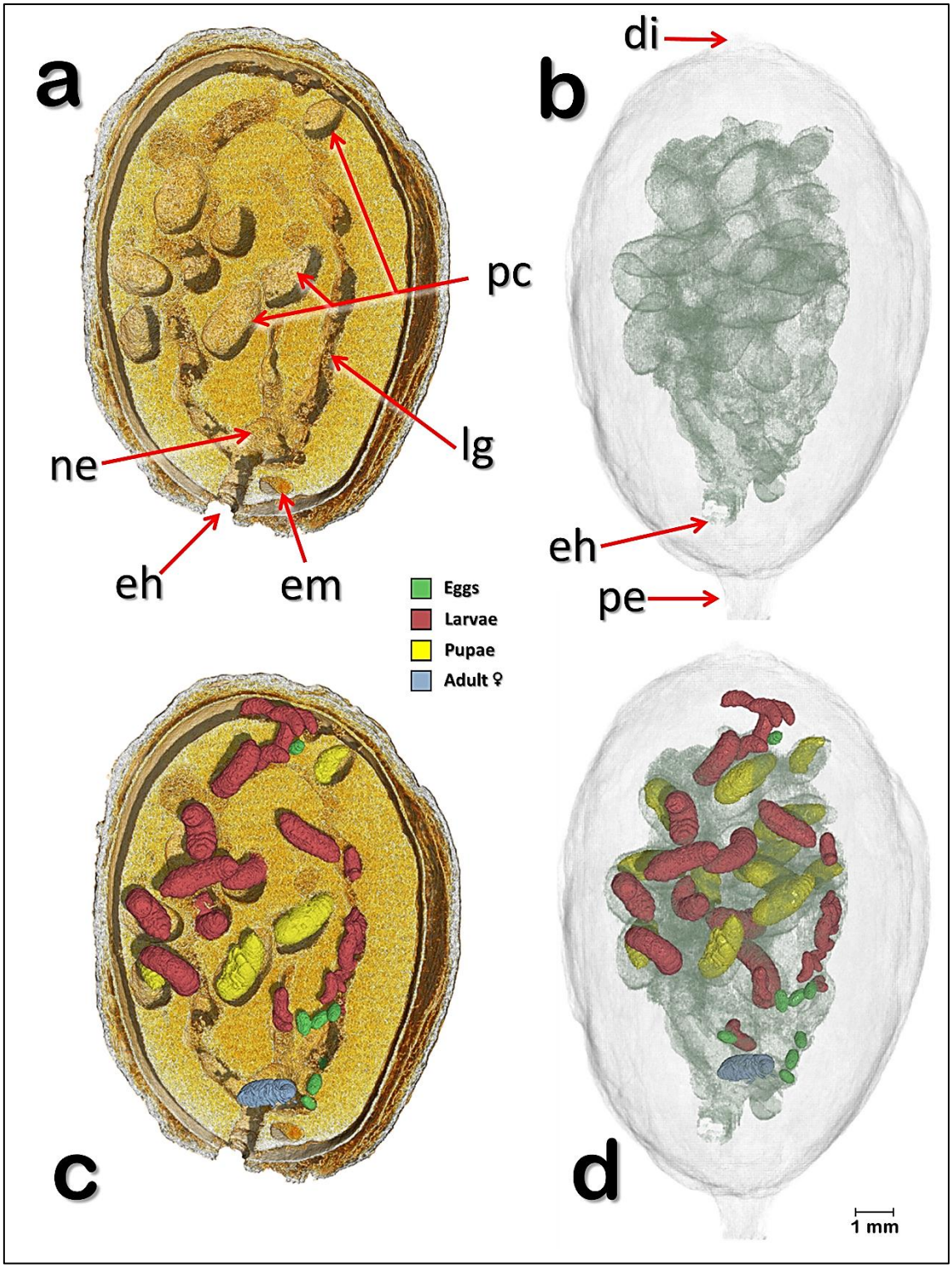

Figure 3.- Volume rendered images of a meso-sagittal section (**a,c**) through an infested coffee berry (berry 1) sectioned at the side opposite to that shown in Fig. 1. The insects have been digitally removed to show details of the galleries and the pupal cells (**a,b**). Developmental stages of the insect (eggs, larvae, pupae, and adult colonizing female) have been separately segmented to unveil their location inside the berry (**c,d**). Abbreviations: di = disc; eh = entrance hole; em = coffee embryo; lg = larval gallery; ne = nest; pc = pupal cell; pe = pedicel.

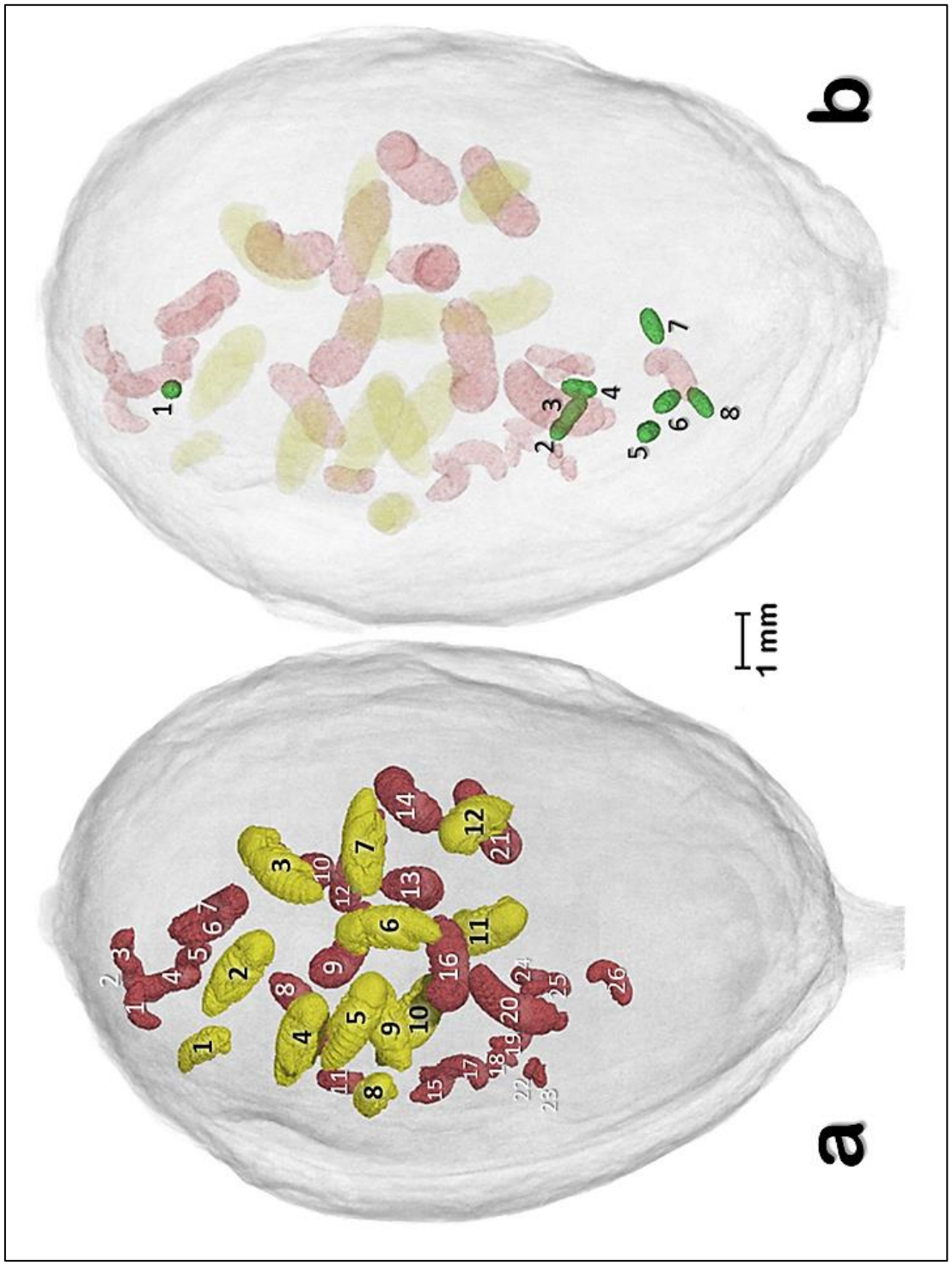

Figure 4.- Volume rendered images of 26 larva and 12 pupae (a) and eight eggs (**b**) (berry 1). Each one has been individually identified. Pupa #1 is a male pupa. Eggs in (**b**) were oviposited in an area of the seed behind the larvae and pupae.

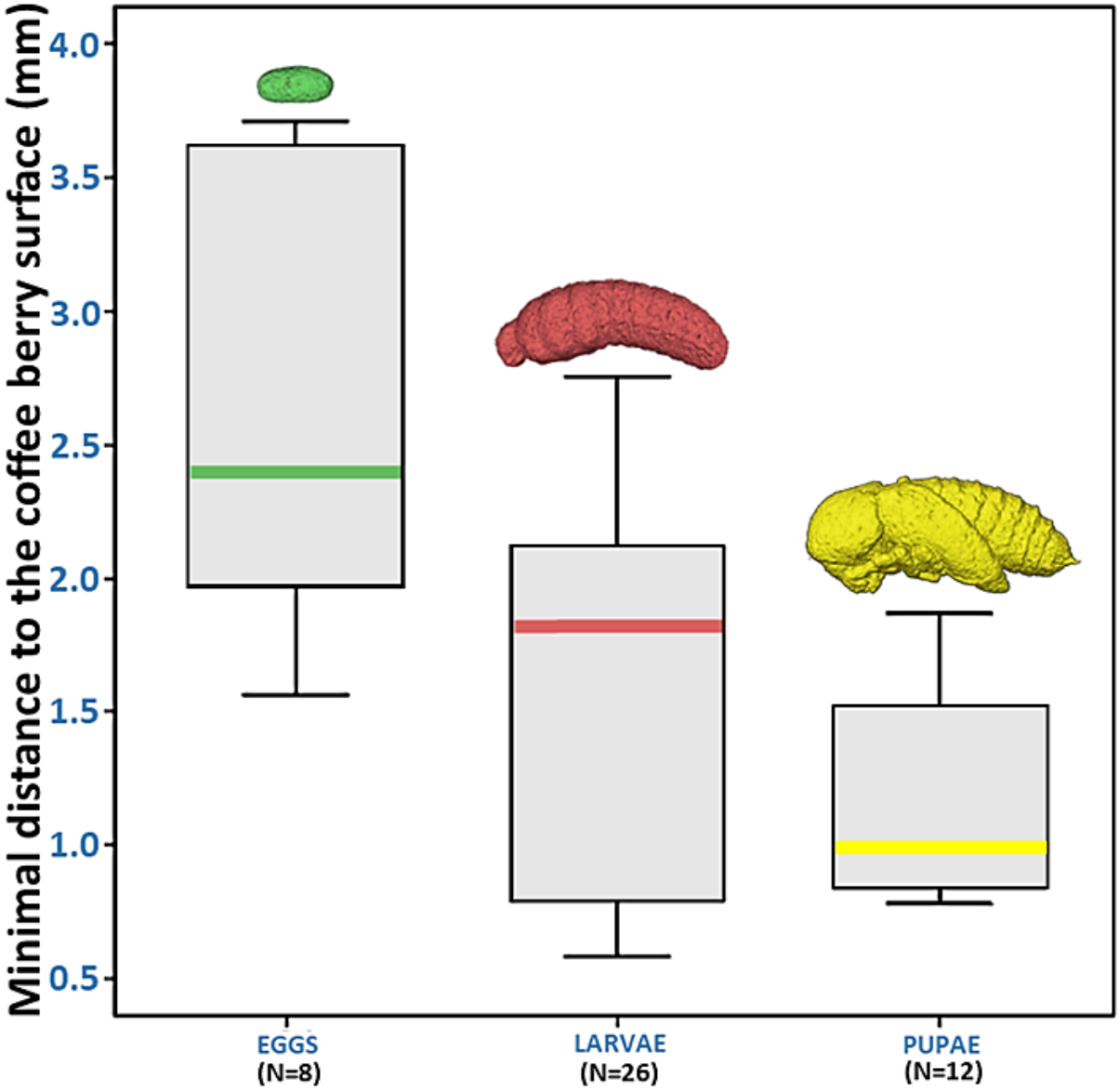

Figure 5.- Minimal distance of eggs, larvae and pupae to the surface of the coffee berry (berry 1). Eggs were further away from the berry surface, followed by larvae and pupae. Differences in location were significantly different based on Kruskwal-Wallis test ($p = 0.004$).

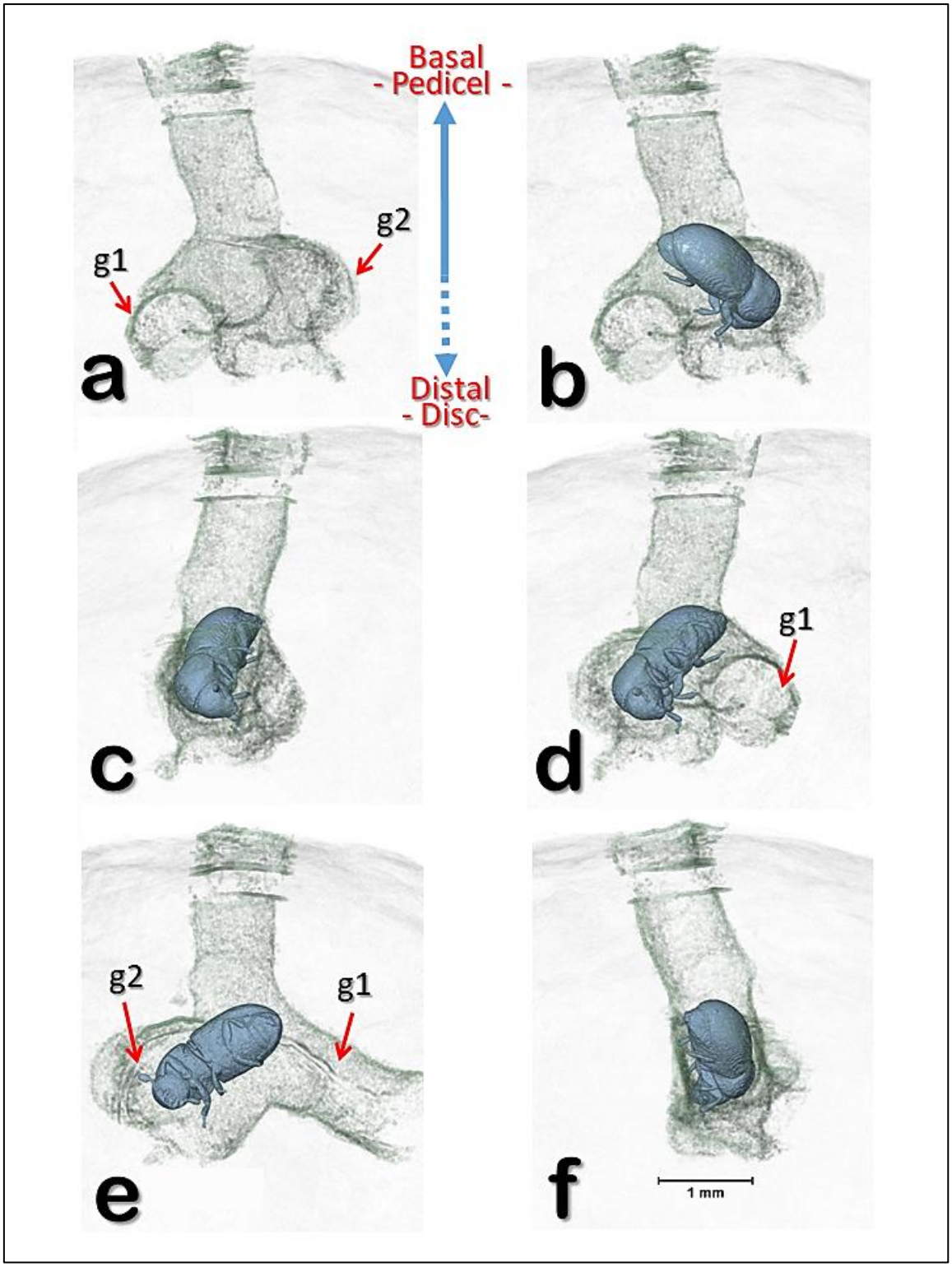

Figure 6.- Volume rendered image reconstructions of the entrance hole and bifurcating galleries (berry 1) at different rotation angles (**a**–**f**). The insect has been digitally removed to show the bifurcating galleries (**a**). The eggs and galleries shown in Figs 1–3 have been digitally removed to focus on the area at the end of the entrance hole. Abbreviations: g1 = 1st gallery; g2 = 2nd gallery.

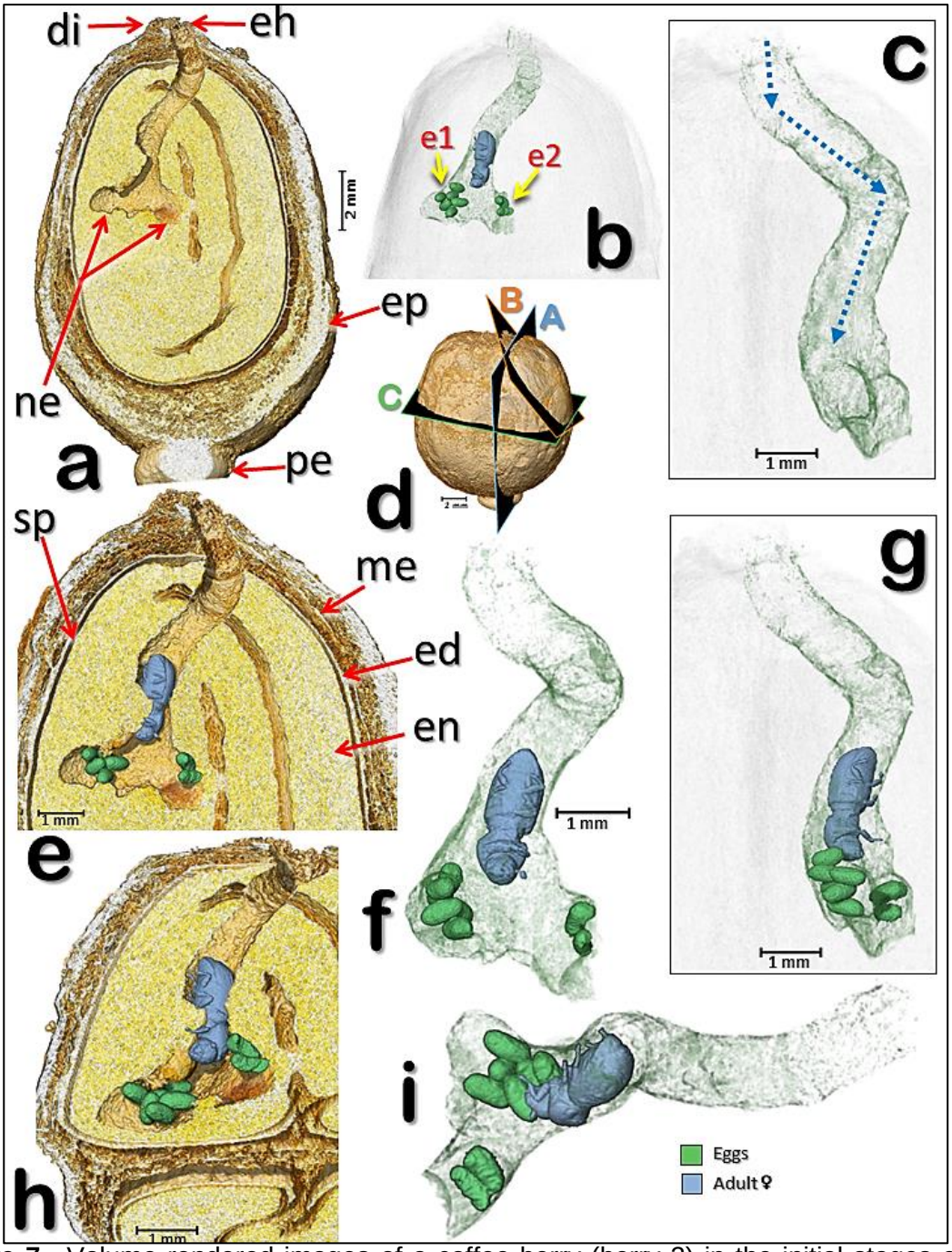

Figure 7.- Volume rendered images of a coffee berry (berry 2) in the initial stages of colonization by a colonizing female. Lateral sections (**a**,**e**,**h**) according to planes "A", "B", and "C" shown in (**d**). The female and eggs have been digitally removed to show the nest and initial gallery following the entrance hole (**a**). The components of the berry have been digitally removed to focus on the entrance hole, gallery, colonizing female, and two batches of eggs (**b**). The female adult and eggs have been digitally removed and the gallery rotated 90° (**c**) in relation to views in (**a**) and (**b**), with the adult and eggs back in place (**g**). The dotted blue arrows (**c**) are helpful in visualizing the alternating angles in the gallery following the entrance hole, and at the end, two nests with eggs (**a**,**b**,**e**–**i**). Detail of the female and eggs inside the galleries and cavities (**f**); visualization has been rotated 45° in relation to (**a**); 45° rotation from the petiole, in a distal view (**i**). Abbreviations: di = disc (style remnant); e1 = 1st egg batch; e2 = 2nd egg batch; ed = endocarp (parchment); eh = entrance hole; en = endosperm (seed); ep = epicarp (outer skin); me = mesocarp (mucilage); ne = nest; pe = pedicel; sp = spermoderm (silverskin).

products (Stuppy *et al.*, 2003). In addition, a preliminary micro-CT report of coffee berry borers inside the berry has been published (Alba-Tercedor *et al.*, 2018).

In this paper, we present results of observations of two coffee berry borer-infested coffee berries using the micro-CT technique. In one of the berries (berry 1) we observed several developmental stages while the second berry (berry 2) had just been colonized by an adult female, and only two batches of eggs had been oviposited.

5.4.4.- Materials and Methods

Coffee berries. J.A.T. collected coffee berries (*Coffea canephora* Pierre ex. A. Froehner; Rubiaceae) at a coffee plantation in Vietnam (*Me Linh Coffee Garden*; 11º53'57.39" N, 108º20'51.16" E; 1043 masl) in November 2017. Out of 55 *C. canephora* berries collected in the field, 12 (22%) were infested with the coffee berry borer. Seven berries (13%) had the insect entrance hole on the disc or very close to it. Five berries (9%) had the entrance hole in the petiole area: two were at a 45º angle through the petiole, and three were next to the petiole.

None of the berries had more than one entrance hole and only one had an incomplete hole next to a complete entrance hole (discussed below).

Micro-CT scans. The berries were kept at room temperature in the laboratory at the University of Granada and were mounted on Basotect® (a light weight melamine foam manufactured by BASF) placed inside a plastic container. A few drops of ethyl acetate were placed on the Basotect® and the plastic container was closed. The emanating vapors produced by the chemical quickly immobilize and kill the insect. Following a 30 min period, micro-CT observations were initiated using a Bruker SkyScan 1172 microtomograph (Bruker-micro CT, Kontich, Belgium) with a Hamamatsu L702 X-ray source and a Ximea 11 megapixels camera. The setting parameters were as follows: voltage = 48 KV; current = 124 µA; isotropic voxel size = 3.25 µm (except for Fig. 7 and Supplementary Video S2, which were 6.7 µm); image rotation step = 0.3º (except for Fig. 7 and Supplementary Video S2, which were 0.2º); 360º of rotation scan, and an Al 0.5 mm filter, resulting in two overlapping connected scans with scan durations of

2h:20min:40s for berry 1 and 1h:24min:58s for berry 2. The most recent versions of the Bruker micro-CT's Skyscan software (NRecon, DataViewer, CTAnalyser) were used for primary reconstructions and the "cleaning" process to obtain the datasets of "slices" as previously described (Alba-Tercedor, 2014). Volume rendered images and videos were obtained with FEI's Amira's software v. 6.5.0 (FEI, 2017) (Thermo Fisher Scientific, Waltham, MA).

5.4.5.- Results

Figures 1-3 show different views of one of two coffee berry borer-infested coffee berries (berry 1) observed with micro-CT technology. Several components of the berry have been identified, including the disc, pedicel, endocarp (parchment), mesocarp (mucilage), spermoderm (silver skin), locule wall (ovary), and coffee embryo.

Figure 1a (berry 1) depicts a meso-sagittal cut of a coffee berry showing the two coffee seeds separated by the locule wall, as well as the galleries and pupal cells created by the insect. We use the term "pupal cell" as used by Hopkins (Hopkins, 1909), Swaine (Swaine, 1918), Dodge (Dodge, 1938), and Browne (Browne, 1973), to describe the enclosed chamber where pupation occurs (Figs. 1–3). According to Hopkins (Hopkins, 1909), "The pupal cell is formed by the prepupal larva or by the pupa itself and is usually located at the end of the larval mine or food burrow of the larva." The pupal cells observed inside the coffee berry were formed by the second larval instar, a developmental stage that includes the prepupa (Gómez *et al.*, 2015) This observation agrees with Bergamin (Bergamin, 1943), who stated the coffee berry borer prepupa is responsible for building the pupal cell.

Figures 1–3 (berry 1) show different section planes through a coffee berry with the location of the different development stages, including the colonizing female. The coffee berry has been made transparent (Fig. 1b) to focus on the insect galleries and pupal cells and on the entrance hole, which is the area through which the coffee berry borer enters the berry, although in this berry the insect entered through the side of the berry, close to the petiole. Figure 1c depicts a meso-sagittal cut that includes the developmental stages of the insect in

different colors, with the components of the berry digitally removed in Fig. 1d to focus on the distribution of the insects within the seed. It is important to note that only one seed has been infested by the insects.

5.4.6.- Discussion

Several bark beetle species from different genera are known to attack seeds, among these, *Araptus*, *Coccotrypes*, *Hypothenemus*, *Pagiocerus*, and *Scolytodes* (Browne, 1973; Schedl, 1960; Wood, 2007). Not much is known about the life history of these bark beetle species inside the seed, including the distribution of eggs as well as the shape of the galleries.

Our visualization of coffee berry borers inside the coffee berry using micro-CT reveals the advantages of using this technology to increase our knowledge on the life history of the insect. For example, the distribution of the developmental stages of the insect at different distances from the surface of the berry suggests that the colonizing females starts ovipositing close to the seed periphery and oviposition then moves inwards, towards the center of the seed. This might be a strategy to disperse the progeny in order to reduce competition. It is important to emphasize that this is purely speculative at this moment and that additional micro-CT observations of coffee berry borer-infested berries are needed to determine if this oviposition pattern holds.

Figures 1-3 show that the insects are only feeding on one of the two coffee seeds, although as the insect population increases, it can be expected for insects as well as the colonizing female to move to the second seed based on the extremely high number of eggs that can be found inside one berry, e.g., 164 (Leefmans, 1924) and 288 (Jaramillo *et al.*, 2009). At the time of analysis, the berry depicted in Figs. 1–3 contained 47 insects, including the colonizing female.

Of the various developmental stages shown in Fig. 4, there are eight unhatched eggs (Fig.4b, Supplementary Video S1) that were oviposited in an area of the seed that is opposite the original batch of eggs resulting in the larvae and pupae seen in Fig. 4a. One of the eggs is in the distal area of the berry, close to the disc (Figs. 1–4). This reveals that the colonizing female does not necessarily place all the eggs in one location. Even though we don't know if these eight eggs would end-up hatching, it is safe to state that there was 100% hatching

in the two previous egg batches resulting in 26 larvae and 12 pupae, as there are no eggs unaccounted for. There are no reports assessing egg fertility inside coffee berries as dissection of a berry with subsequent assessment of hatchability might not be reliable due to the drastic changes in microhabitat experienced by the dissected eggs. Therefore, this is another area that can be further explored using micro-CT.

The two egg batches in Fig. 7 resemble Browne's (Browne, 1973) description of *Coccotrypes*, which as mentioned above, also feeds on seeds: "In fruit and seeds the eggs are placed at the end of a short tunnel, and the larvae enlarge this and also make other irregular tunnels and chambers in all directions." Figure 7 also depicts alternating angles in the gallery following the entrance hole.

Adult coffee berry borer females emerge from the berry using the entrance hole built by the colonizing female. Similarly, "In *Anisandrus* and *Xyleborus*. the brood matures and emerges by way of the entrance gallery" (Dodge, 1938). This is interesting because there is a highway of tunnels and cavities that the new adults have to transit through in order to find the entrance hole, although it is possible that they might use visual cues (e.g., light) and air currents to locate it.

Several papers describe the different types of galleries created by bark beetles (Blackman, 1922; Browne, 1961; Dodge, 1938; Hopkins, 1909; Swaine, 1918). Hopkins (Hopkins, 1909) states that even though different bark beetle genera can make the same or similar type of gallery, "galleries are of taxonomic importance" and the same insect species will construct the same or similar type of gallery in different hosts, thus the shape of the gallery is not determined by the host plant. There are no studies focused on gallery formation by seed boring bark beetles; this fact presents an opportunity to use micro-CT to study gallery form and function in seeds.

As a footnote, in a proceedings paper presenting our preliminary results (Alba-Tercedor *et al.*, 2018), we had stated that a female could be seen grooming an egg. After more detailed analysis including visualization at different angles, it became evident that the female was not grooming the egg and instead had her mouthparts in the proximity of rasped seed material.

In conclusion, the use of micro-CT techniques to study the coffee berry borer has resulted in interesting observations. Future research will expand on these observations to determine if they are the norm. Micro-CT could also be useful for learning more about the cryptic life of other bark beetles, including ambrosia beetles.

5.4.7.- Supplementary Information

Videos:

S1.- Developmental stages inside galleries and cavities of a coffee berry. Volume rendering reconstructions of the galleries and cavities (left), and the different developmental stages in their position inside the coffee berry(right).

https://static-content.springer.com/esm/art%3A10.1038%2Fs41598-018-35324-4/MediaObjects/41598_2018_35324_MOESM2_ESM.mp4

S2.- Entrance gallery of a colonizing female into its nest with eggs inside a coffee berry. Volume rendering reconstructions of the entrance gallery and nest (left), and the female inside the entrance gallery, with two opposite egg laying inside the nest (right).

https://static-content.springer.com/esm/art%3A10.1038%2Fs41598-018-35324-4/MediaObjects/41598_2018_35324_MOESM3_ESM.mp4

5.4.8.- References

Alba-Alejandre, I., Alba-Tercedor, J., & Vega, F. E. (2018). Micro-CT to Document the Coffee Bean Weevil, *Araecerus fasciculatus* (Coleoptera: Anthribidae), Inside Field-Collected Coffee Berries (Coffea canephora). *Insects*, *9*(3, 100), 1–9. https://doi.org/http://dx.doi.org/10.3390/insects9030100

Alba-Tercedor, J. (2014). From the sample preparation to the volume rendering images of small animals : A step by step example of a procedure to carry out the micro-CT study of the leafhopper insect *Homalodisca vitripennis* (Hemiptera: Cicadellidae). In *Bruker Micro-CT Users Meeting 2014* (pp. 260–288). Bruker Micro-CT-Skyscan. http://bruker-microct.com/company/UM2014/000_AbstractBook2014.pdf

Alba-Tercedor, J., Alba-Alejandre, I., & Vega, F. E. (2018). Micro-CT unveils the secret life of the coffee berry borer (*Hypothenemus hampei*; Coleoptera, Curculionidae: Scolytinae) inside coffee berries. In *Bruker Micro-CT Users Meeting 2018* (pp. 165–173). http://bruker-microct.com/company/UM2018/2018_30.pdf

Bergamin, J. (1943). *Contribuição para o conhecimento da biologia da broca do café "Hypothenemus hampei (Ferrari, 1867)" (Col. Ipidae). (São Paulo)*. *14*, 31–72.

Blackman, M. W. (1922). Mississippi bark beetles. *Mississippi Agricultural Experiment Station, Technical Bulletin*, *11*, 1–130.

Browne, F. G. (1961). The biology of Malayan Scolytidae and Platypodidae. *Malayan Forest Records*, *22*, 1–255.

Browne, F. G. (1973). The African species of *Poecilips Schaufuss*. *Revue de Zoologie*

et de Botanique Africaines, *87*, 679–696.

Dodge, H. R. (1938). The bark beetles of Minnesota (Coleoptera: Scolytidae). *University of Minnesota, Agricultural Experiment Station, Technical Bulletin*, *132*, 1–60.

FEI. (2017). *Amira 3D Visualization and Analysis Software* (6.4). FEI.

Gómez, J., Chávez, B. Y., Castillo, A., Valle, F. J., & Vega, F. E. (2015). The coffee berry borer, *Hypothenemus hampei*: How many instars are there? *Annals of the Entomological Society of America*, *108*, 311–315.

Hopkins, A. D. (1909). Contribution towards a monograph of the scolytids beetles. I. The genus *Dendroctonus*. In *Technical series, Bureau of Entomology, U.S. Departament of Agriculture* (Vol. 17).

ICO. (2014). *International Coffee Organization. World coffee trade (1963–2013): a review of the markets, challenges and opportunities facing the sector. International Coffee Organization, London, ICC 111-5 Rev. 1, 29 pp,*.

Jaramillo, J., Chabi-Olaye, A., Poehling, H.-M., Kamonjo, C., & Borgemeister, C. (2009). Development of an improved laboratory production technique for the coffee berry borer *Hypothenemus hampei* , using fresh coffee berries. *Entomologia Experimentalis et Applicata*, *130*(3), 275–281. https://doi.org/10.1111/j.1570-7458.2008.00820.x

Le Pelley, R. H. (1968). *Pests of Coffee*. Longmans, Green and Co., Ltd.

Leefmans, S. (1924). De Koffiebessenboeboek. II. Bestrijding. *Mededeelingen van Het Instituut Voor Plantenziekten*, *62*, 1–99.

Schedl, K. E. (1960). Insectes nuisibles aux fruits et aux graines. *Publications de l'institut National Pour l'étude Agronomique Du Congo Belge, Série Scientifique*, *82*, 1–133.

Stuppy, W. H., Maisano, J. A., Colbert, M. W., Rudall, P. J., & Rowe, T. B. (2003). Three-dimensional analysis of plant structure using high-resolution X-ray computed tomography. In *Trends in Plant Science* (Vol. 8, Issue 1, pp. 2–6). Elsevier Ltd. https://doi.org/10.1016/S1360-1385(02)00004-3

Swaine, J. M. (1918). Canadian bark-beetles. Part II. A preliminary classification with an account of the habits and means of control. (Technical Bulletin). *Dominion of Canada, Department of Agriculture, Entomological Branch, Bulletin No. 14*, 1–143.

Vega, F. E., Simpkins, A., Rodríguez-Soto, M. M., Infante, F., & Biedermann, P. H. W. (2017). Artificial diet sandwich reveals subsocial behaviour in the coffee berry borer *Hypothenemus hampei* (Coleoptera: Curculionidae: Scolytinae). *Journal of Applied Entomology*, *141*(6), 470–476. https://doi.org/10.1111/jen.12362

Vega, Fernando E., Infante, F., & Johnson, A. J. (2015). The genus *Hypothenemus*, with emphasis on *H. hampei*, the coffee berry borer. In *Bark Beetles* (pp. 427–494). Elsevier. https://doi.org/10.1016/B978-0-12-417156-5.00011-3

Vega, Fernando E., Kramer, M., & Jaramillo, J. (2011). Increasing coffee berry borer (Coleoptera: Curculionidae: Scolytinae) female density in artificial diet decreases fecundity. *Journal of Economic Entomology*, *104*(1), 87–93. https://doi.org/10.1603/EC10353

Waller, J. M., Bigger, M., & Hillocks, R. J. (Eds.). (2007). *Coffee Pests, Diseases and Their Management.* CABI.

Wood, S. L. (2007). *Bark and Ambrosia Beetles of South America (Coleoptera, Scolytidae)*. Brigham Young University.

5.5.- "Estudio anatómico de la broca del café (*Hypothenemus hampei*) utilizando microtomografía computarizada"

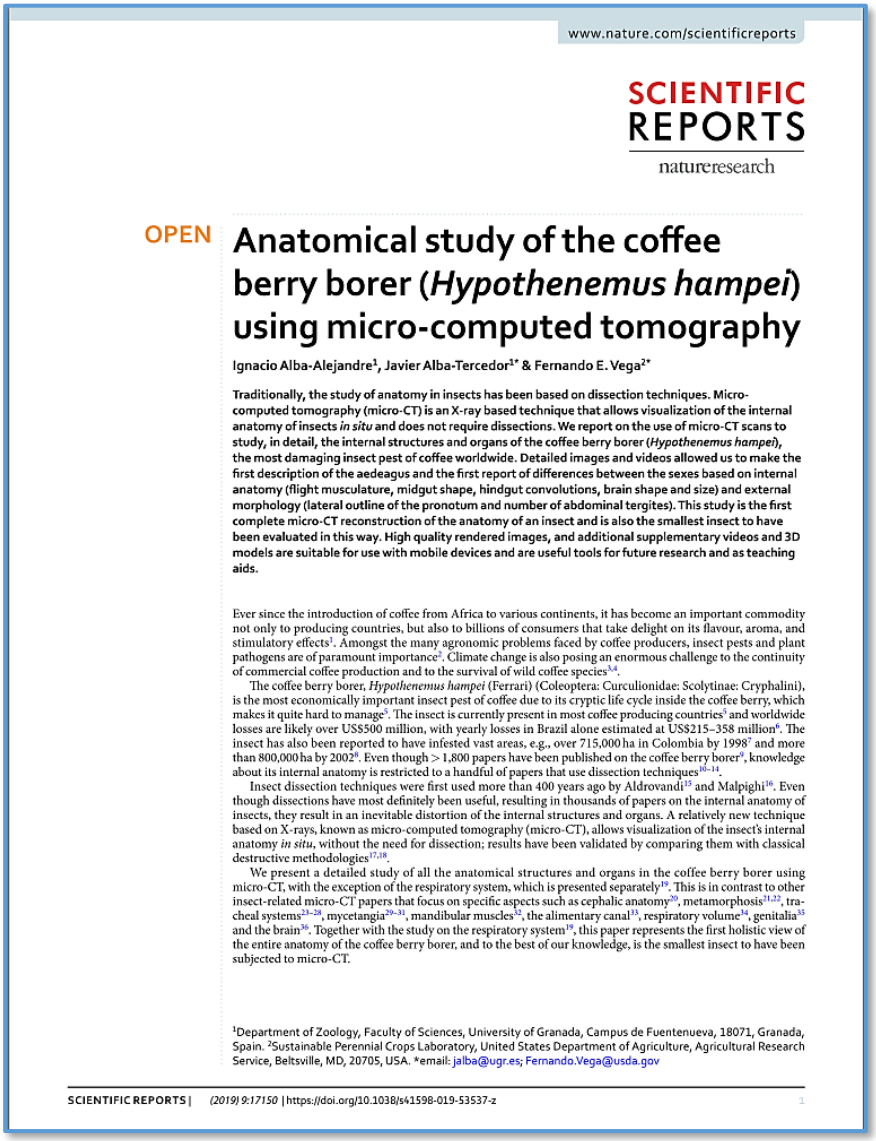

www.nature.com/scientificreports

SCIENTIFIC REPORTS
nature research

OPEN

Anatomical study of the coffee berry borer (*Hypothenemus hampei*) using micro-computed tomography

Ignacio Alba-Alejandre[1], Javier Alba-Tercedor[1*] & Fernando E. Vega[2*]

Traditionally, the study of anatomy in insects has been based on dissection techniques. Micro-computed tomography (micro-CT) is an X-ray based technique that allows visualization of the internal anatomy of insects *in situ* and does not require dissections. We report on the use of micro-CT scans to study, in detail, the internal structures and organs of the coffee berry borer (*Hypothenemus hampei*), the most damaging insect pest of coffee worldwide. Detailed images and videos allowed us to make the first description of the aedeagus and the first report of differences between the sexes based on internal anatomy (flight musculature, midgut shape, hindgut convolutions, brain shape and size) and external morphology (lateral outline of the pronotum and number of abdominal tergites). This study is the first complete micro-CT reconstruction of the anatomy of an insect and is also the smallest insect to have been evaluated in this way. High quality rendered images, and additional supplementary videos and 3D models are suitable for use with mobile devices and are useful tools for future research and as teaching aids.

Ever since the introduction of coffee from Africa to various continents, it has become an important commodity not only to producing countries, but also to billions of consumers that take delight on its flavour, aroma, and stimulatory effects[1]. Amongst the many agronomic problems faced by coffee producers, insect pests and plant pathogens are of paramount importance[2]. Climate change is also posing an enormous challenge to the continuity of commercial coffee production and to the survival of wild coffee species[3,4].

The coffee berry borer, *Hypothenemus hampei* (Ferrari) (Coleoptera: Curculionidae: Scolytinae: Cryphalini), is the most economically important insect pest of coffee due to its cryptic life cycle inside the coffee berry, which makes it quite hard to manage[5]. The insect is currently present in most coffee producing countries[3] and worldwide losses are likely over US$500 million, with yearly losses in Brazil alone estimated at US$215–358 million[6]. The insect has also been reported to have infested vast areas, e.g., over 715,000 ha in Colombia by 1998[7] and more than 800,000 ha by 2002[8]. Even though > 1,800 papers have been published on the coffee berry borer[9], knowledge about its internal anatomy is restricted to a handful of papers that use dissection techniques[10–14].

Insect dissection techniques were first used more than 400 years ago by Aldrovandi[15] and Malpighi[16]. Even though dissections have most definitely been useful, resulting in thousands of papers on the internal anatomy of insects, they result in an inevitable distortion of the internal structures and organs. A relatively new technique based on X-rays, known as micro-computed tomography (micro-CT), allows visualization of the insect's internal anatomy *in situ*, without the need for dissection; results have been validated by comparing them with classical destructive methodologies[17,18].

We present a detailed study of all the anatomical structures and organs in the coffee berry borer using micro-CT, with the exception of the respiratory system, which is presented separately[19]. This is in contrast to other insect-related micro-CT papers that focus on specific aspects such as cephalic anatomy[20], metamorphosis[21,22], tracheal systems[23–28], mycetangia[29–31], mandibular muscles[32], the alimentary canal[33], respiratory volume[34], genitalia[35] and the brain[36]. Together with the study on the respiratory system[19], this paper represents the first holistic view of the entire anatomy of the coffee berry borer, and to the best of our knowledge, is the smallest insect to have been subjected to micro-CT.

[1]Department of Zoology, Faculty of Sciences, University of Granada, Campus de Fuentenueva, 18071, Granada, Spain. [2]Sustainable Perennial Crops Laboratory, United States Department of Agriculture, Agricultural Research Service, Beltsville, MD, 20705, USA. *email: jalba@ugr.es; Fernando.Vega@usda.gov

Alba-Alejandre, I., Alba-Tercedor, J., & Vega, F. E. (2019). Anatomical study of the coffee berry borer (*Hypothenemus hampei*) using micro-computed tomography. *Scientific Reports*, 9(1), 17150: 1-16. https://doi.org/10.1038/s41598-019-53537-z
Publisher Correction: Anatomical study of the coffee berry borer (Hypothenemus hampei) using micro-computed tomography. https://doi.org/10.1038/s41598-019-53537-z

5.5.1.- Resumen

Tradicionalmente, el estudio de la anatomía en los insectos se ha basado en técnicas de disección. La microtomografía computarizada (micro-ct) es una técnica basada en rayos X que permite la visualización de la anatomía interna de los insectos in situ y no requiere disecciones. Informamos sobre el uso de escaneos de micro-ct para estudiar, en detalle, las estructuras internas y los órganos de la broca del café (*Hypothenemus hampei*), la plaga de insectos más dañina del café en todo el mundo. Las imágenes y videos detallados nos permitieron hacer la primera descripción del edeago y el primer informe de las diferencias entre sexos en función de la anatomía interna (musculatura de vuelo, forma del intestino medio, circunvoluciones del intestino posterior, forma y tamaño del cerebro) y morfología externa (contorno lateral del pronoto y número de tergitos abdominales). Este estudio es la primera reconstrucción completa de micro-ct de la anatomía de un insecto y también es el insecto más pequeño que se ha evaluado de esta manera. Las imágenes renderizadas de alta calidad y los videos complementarios y modelos 3D adicionales son adecuados para usar con dispositivos móviles y son herramientas útiles para futuras investigaciones y como material didáctico.

5.5.2.- Abstract

Traditionally, the study of anatomy in insects has been based on dissection techniques. Micro- computed tomography (micro-ct) is an X-ray based technique that allows visualization of the internal anatomy of insects in situ and does not require dissections. We report on the use of micro-ct scans to study, in detail, the internal structures and organs of the coffee berry borer (*Hypothenemus hampei*), the most damaging insect pest of coffee worldwide. Detailed images and videos allowed us to make the first description of the aedeagus and the first report of differences between the sexes based on internal anatomy (flight musculature, midgut shape, hindgut convolutions, brain shape and size) and external morphology (lateral outline of the pronotum and number of abdominal tergites). This study is the first complete micro-ct reconstruction of the anatomy of an insect and is also the smallest insect to have been evaluated in this way. High quality

rendered images, and additional supplementary videos and 3D models are suitable for use with mobile devices and are useful tools for future research and as teaching aids.

5.5.3.- Introduction

Ever since the introduction of coffee from Africa to various continents, it has become an important commodity not only to producing countries, but also to billions of consumers that take delight on its flavor, aroma, and stimulatory effects (Vega, 2008). Among the many agronomic problems faced by coffee producers, insect pests and plant pathogens are of paramount importance (Wintgens, 2004). Climate change is also posing an enormous challenge to the continuity of commercial coffee production as well as to survival of wild coffee species (Davis *et al.*, 2019; Ziska *et al.*, 2018).

The coffee berry borer (*Hypothenemus hampei* (Ferrari); Coleoptera: Curculionidae: Scolytinae: Cryphalini) is the most economically important insect pest of coffee due to its cryptic life habit inside the coffee berry, which makes it quite hard to manage (Vega, Infante, *et al.*, 2015). The insect is currently present in most coffee producing countries (Vega, Infante, *et al.*, 2015) and worldwide losses are likely over US$500 million, with yearly losses in Brazil alone estimated at US$215–358 million (Oliveira *et al.*, 2013). The insect has also been reported to have infested vast areas, e.g., over 715,000 ha in Colombia by 1998 (Duque-Orrego, 2000) and more than 800,000 ha by 2002 (Duque-Orrego *et al.*, 2002). Even though > 1,800 papers have been published on the coffee berry borer (Pérez *et al.*, 2015), knowledge about its internal anatomy is restricted to a handful of papers that use dissection techniques (Constantino *et al.*, 2011; López-Guillén *et al.*, 2011; Román-Ruiz *et al.*, 2017; Rubio-Gómez *et al.*, 2007; Rubio G. *et al.*, 2008).

Insect dissection techniques were first used more than 400 years ago by Aldrovandi (Aldrovandi, 1602) and Malpighi (Malpighi, 1669). Even though dissections have most definitely been useful, resulting in thousands of papers on the internal anatomy of insects, they result in an inevitable distortion of the internal structures and organs. A relatively new technique based on X-rays,

known as micro-computed tomography (micro-CT), allows visualization of the insect's internal anatomy in situ, without the need for dissection; results have been validated by comparing them with classical destructive methologies (Alba-Tercedor & Alba-Alejandre, 2019; Wipfler *et al.*, 2016).

We present a detailed study of all the anatomical structures and organs in the coffee berry borer using micro-CT, with the exception of the respiratory system, which is presented separately (Alba-Tercedor *et al.*, 2019). This is in contrast to other insect-related micro-CT papers that focus on specific aspects such as cephalic anatomy (Richter *et al.*, 2019), metamorphosis (Helm *et al.*, 2018; Lowe *et al.*, 2013), tracheal systems (Greco *et al.*, 2014; Greenlee *et al.*, 2009; Ha *et al.*, 2017; Iwan *et al.*, 2015; Raś *et al.*, 2018; Wasserthal *et al.*, 2018), mycetangia (Jiang *et al.*, 2019; Y. Li, Ruan, *et al.*, 2018; Y. Li, Stanley, *et al.*, 2018), mandibular muscles (D. Li *et al.*, 2011), the alimentary canal(Martín-Vega *et al.*, 2018), respiratory volume (Shaha *et al.*, 2013), genitalia (Simonsen & Kitching, 2014) and the brain (Smith *et al.*, 2016). Together with the study on the respiratory system (Alba-Tercedor *et al.*, 2019), this paper represents the first holistic view of the entire anatomy of the coffee berry borer, and to the best of our knowledge, is the smallest insect to have been subjected to micro-CT.

5.5.4.- Materials and Methods

Insects. Coffee berry borers were reared in artificial diet at the USDA, ARS, Beltsville laboratory (Vega *et al.*, 2011)

Micro-CT scans. The specimens were killed by submerging them in 30% ethanol for 25 minutes. They were then dehydrated in an ethanol series (50%, 70%, 80%, 90%; 25 minutes in each concentration), and stained in 1% iodine in absolute ethanol for three days. Stained insects were placed in a well and submerged in hexamethyldisilazane for 4 h and air-dried overnight. For the scans, specimens were glued with cyanoacrylate to the tip of a nylon fishing line 200 µm in diameter as described by Alba-Tercedor (Alba-Tercedor, 2014) and scanned using a Bruker SkyScan 1172 microtomograph (Bruker-micro CT, Kontich, Belgium) with a Hamamatsu L702 X-ray source and a Ximea 11 megapixels camera. The setting parameters were as follows: voltage = 49 kV; current = 64 µA; isotropic

voxel size = 0.52 µm; image rotation step = 0.5° for the male and 0.4° for the female; 360° of rotation scan, and no filter, resulting in a scan duration of 2 h: 47 min: 55 s and 722 X-ray images for the male, and 3 h: 29 min: 39 s and 902 X-ray images for the female

Coffee berry borers reared at the United States Department of Agriculture, Agriculture Research Service, Beltsville, Maryland (USA) were used for the study.

Image reconstruction, measurements and supplementary videos. Bruker micro-CT's Skyscan software (NRecon, DataViewer, CTAnalyser) was used for primary reconstructions and the 'cleaning' process to obtain datasets for 'slices' as described previously by Alba-Tercedor (Alba-Tercedor, 2014). Volume-rendered images and Supplementary Videos S1–S8 were obtained using Amira's software, v. 6.7.0 (Thermo Fisher Scientific, Waltham, MA) (Stalling *et al.*, 2005) (Thermo Fisher Scientific, 2017). The built-in 'volrenRed.col' colour filter was selected to obtain volume-rendered reconstructions in Figs. 1A,C, 6A–F, 7, 10. Different anatomical parts were independently segmented to finally obtain the rendered colorized images of Figs. 2–10. To be able to obtain the actual texture of structures in desired colours, after segmentation, each structure was subjected to the following arithmetic operation: A*(B > 0), where A represents the whole animal and B the segmented structure. The total length of the alimentary canal was measured manually from the oral opening to the anus using Amira's measuring tool. Figs. 4I,J, Supplementary Video S9 and Supplementary 3D models S10 and S11 for both sexes were obtained using CTVox (a Bruker micro-CT's Skyscan software). Colours were obtained by adjusting the transfer function curves in accordance with the transparency of the structures to X-ray, as described by Alba-Tercedor (Alba-Tercedor, 2014).

Light microscopy study of the proventriculus. A female was cleared by submersion in 10% aqueous KOH for 48 h at room temperature, followed by dissection and subsequent mounting on a slide in a variation of Hoyer's liquid (Alba-Tercedor, 2004). Figure 6G,H were obtained using a Samsung Note 8 smartphone connected to the ocular of an Olympus CH-2 binocular microscope.

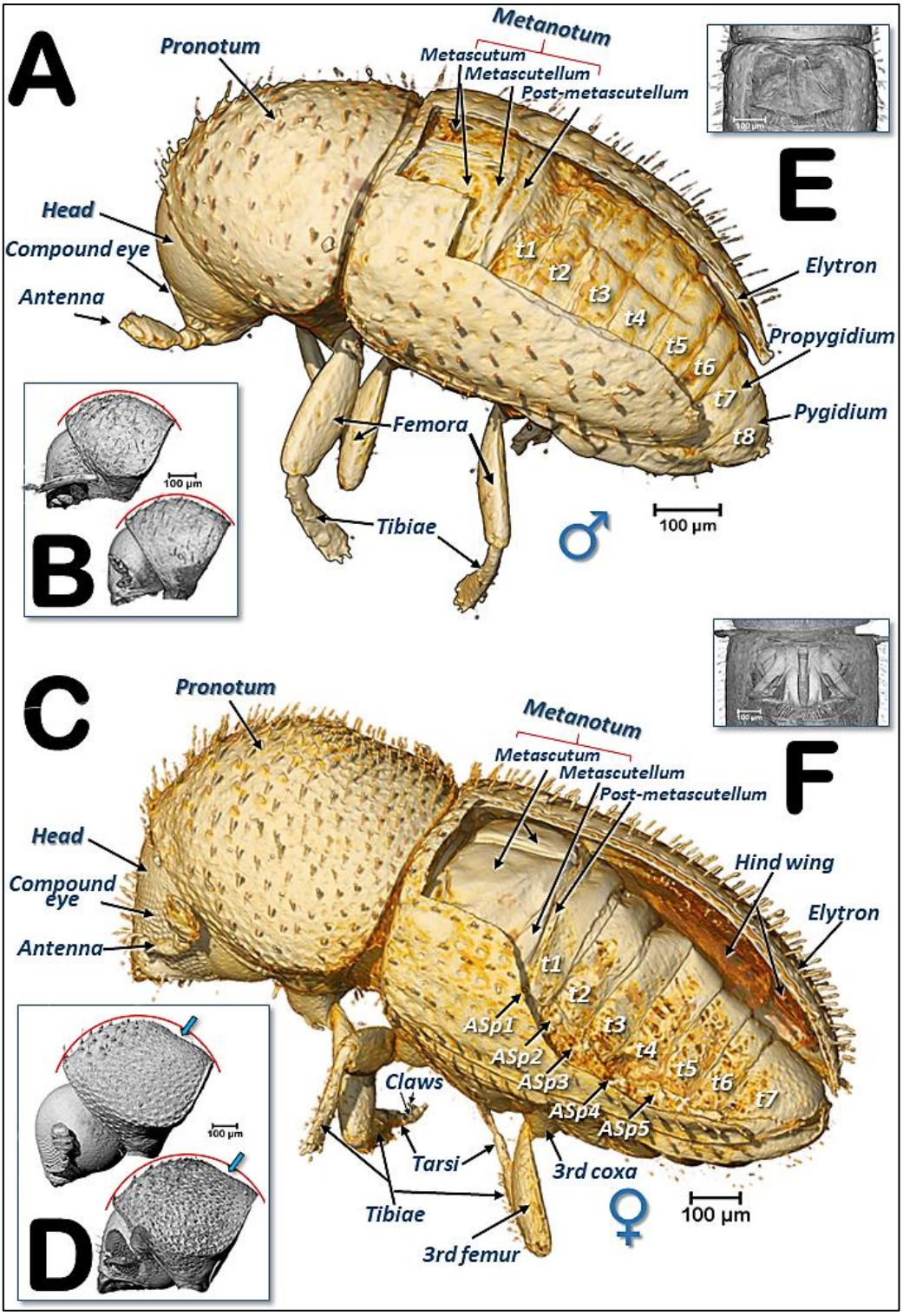

Figure 1.- Left dorso-lateral views of a male (**A**) and a female (**C**) coffee berry borer. Elytra have been removed using software thereby revealing the dorsal part of the thoracic and abdominal segments. Abdominal tergites (t) and the position of the abdominal respiratory spiracles (ASp) are labelled sequentially (terminology after Hopkins (Hopkins, 1909)). Insets (**B**,**D**) show a uniformly curved pronotal disc in males (**B**) in contrast to a concave depression on the posterior pronotal third in females (**D**; blue arrows). Note different scales were used for each sex. The meso- and metanotum were removed by software to observe the reduced flight muscles in the male (**E**) in contrast to conspicuous flight muscles in the female (**F**)

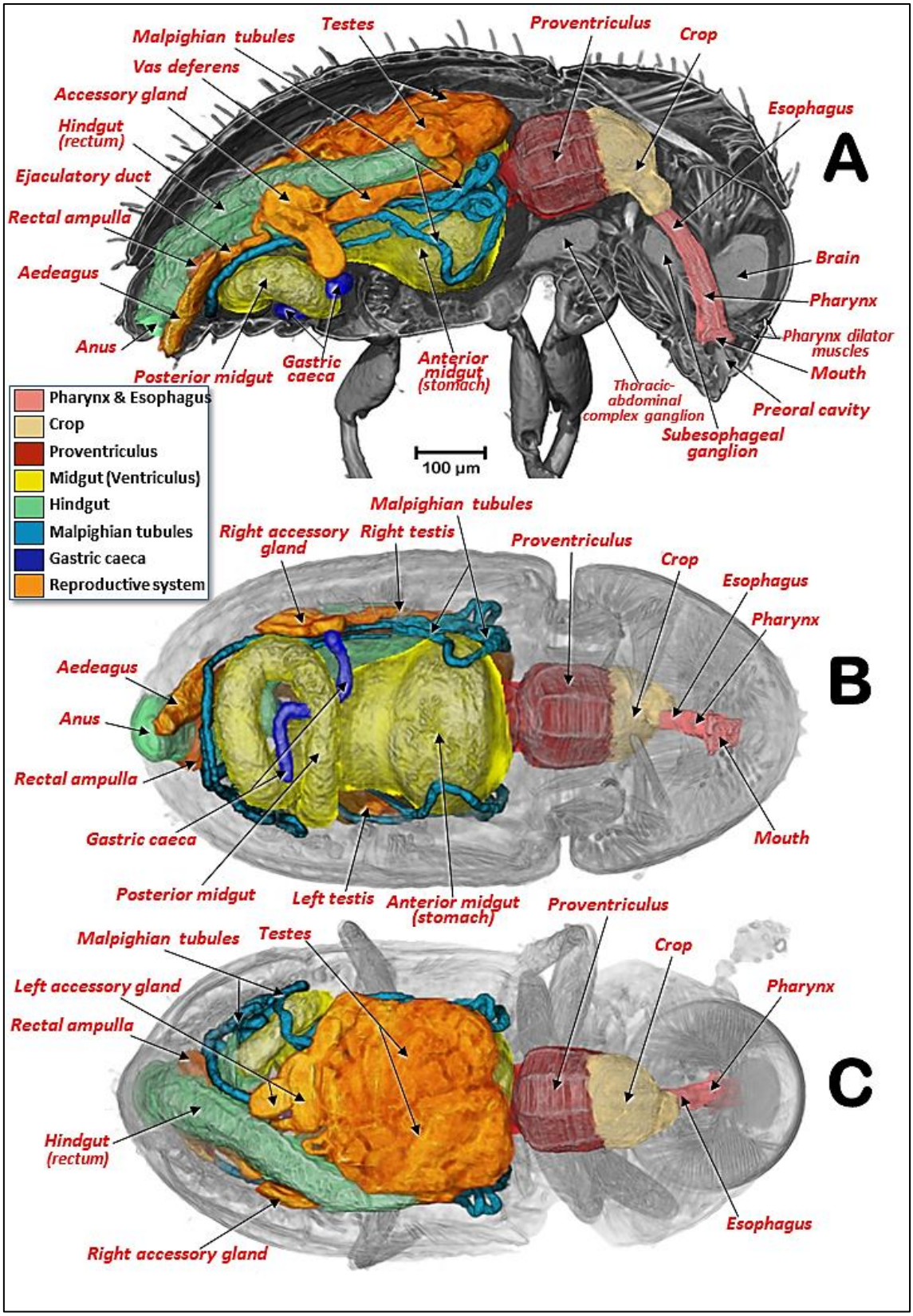

Figure 2.-. Internal anatomy of a male coffee berry borer: right-lateral (**A**), ventral (**B**), and dorsal (**C**) views. To enhance the actual anatomical position of the different organs, the body (except the internal organs) have been rendered transparent (**B**,**C**) by depleting the opacity values using Amira software.

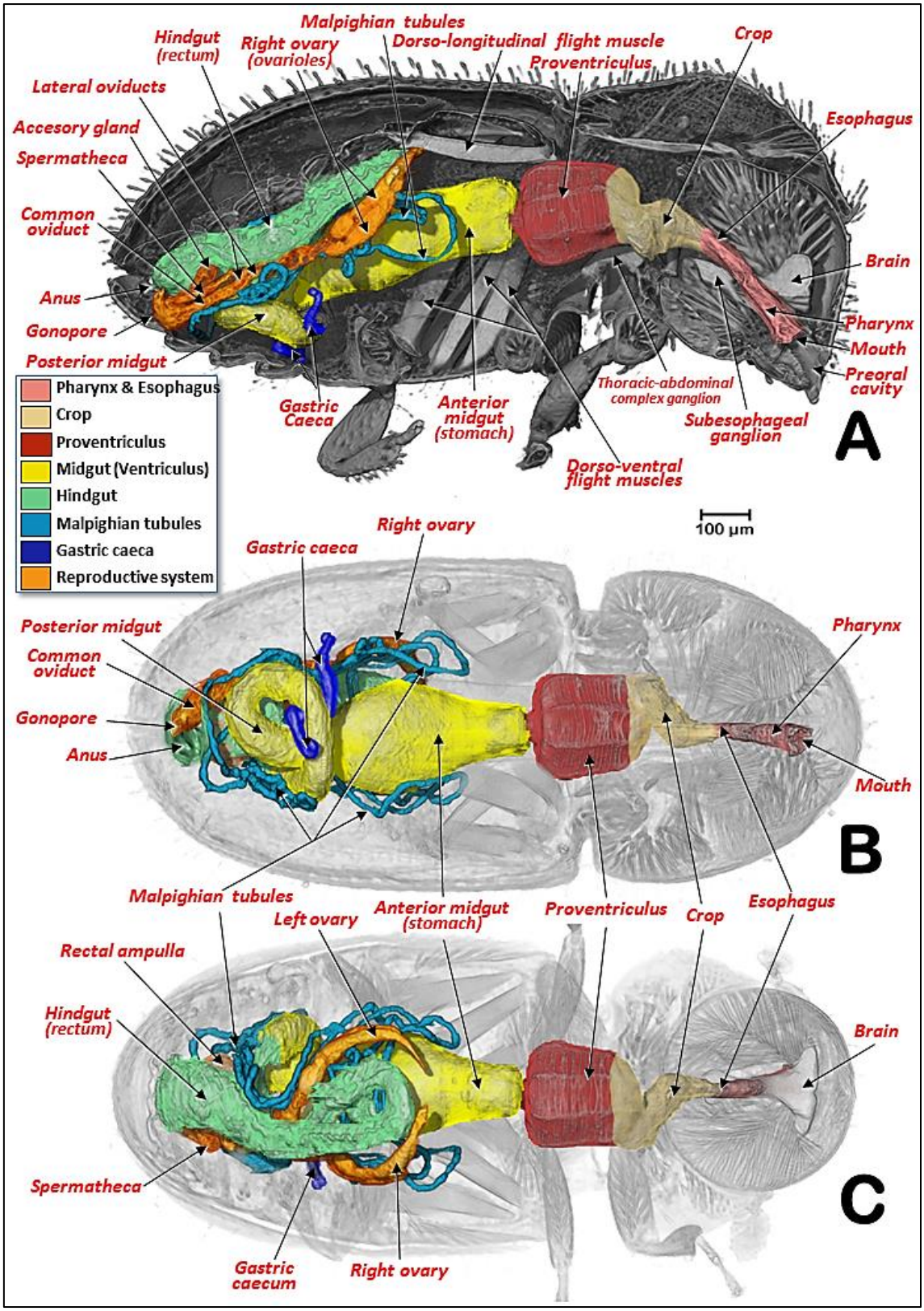

Figure 3.- Internal anatomy of a female coffee berry borer: right-lateral (**A**), ventral (**B**), and dorsal (**C**) views. To enhance the actual anatomical position of the different organs, the body (except the internal organs) has been rendered transparent (**B,C**) by depleting the opacity values using Amira software

5.5.5.- Results

Previously unreported external differences between the sexes were found: males had eight abdominal tergites (Fig. 1A) and, in lateral view, the outline of the pronotal disc appeared uniformly curved (Fig. 1B); the females had seven abdominal tergites (Fig. 1C) and the outline of the pronotal disc had a slight concave depression (Fig. 1D).

The general arrangement of the internal structures and organs of both sexes can be seen in Figs. 2,3, and Supplementary Videos S1, S9. The digestive system, including the excretory system, are shown in Figs. 4, 5, and Supplementary Videos S1–S3, S9. Differences between the sexes in the shape of the midgut and the trajectories of the convolutions that make up the midgut and hindgut are shown in Fig. 4G,H, and Supplementary Video S2. Detailed views of the external and internal structures of the proventriculus, including the musculature are shown in Figs. 6, 7. Light microscopy views are included (Fig. 6G,H) for comparison with the micro-CT reconstructions (Fig. 6A–F; Supplementary Videos S3, S9).

The general internal anatomy of an adult female (with organs and muscles) is shown in Fig. 5A, with the dorsal vessel, aorta, and the nervous system highlighted in different colours. The nervous system and its positional relationship with the digestive system is shown in Fig. 5, and Supplementary Videos S4, S9. Detailed views of the nervous system in both sexes are shown in Figs. 8, 9. The female and male reproductive systems are shown in Fig. 10 and Supplementary Video S5. A study of the aedeagus is shown in Fig. 11 and Supplementary Videos S6, S7

5.5.6.- Discussion

The presence of eight tergites in the male has been described previously (Rubio-Gómez *et al.*, 2007; Rubio G. *et al.*, 2008) (Fig. 1A) but the presence of only seven in the female is new (Fig. 1B). Nüsslin (Nüsslin, 1911) stated that *Hypothenemus* (Cryphalini) females had eight tergites while Wood (Wood, 1954) stated in reference to the 8th tergite that “In all other scolytids and most curculionids it is of reduced size, lacks pubescence and is telescoped beneath

and hidden by tergum 7"; this has been reported for various bark beetle species (Furniss, 2004; Hopkins, 1909; Wood, 1954). As part of this study, we dissected ten females reared in artificial diet and did not find a covered/ obscured 8th tergite. Therefore, it is possible that, either there is variation in the number of tergites amongst the 181 species of *Hypothenemus* (Vega, Infante, *et al.*, 2015), or the 7th and 8th tergites are fused, as was reported in Conophthorus (Scolytini) (Santiago-Blay & Young, 1995). Interestingly, there has been one report of a male coffee berry borer reared on artificial diet that had only seven tergites (Fig. 2C in Vega *et al.* (Vega, Simpkins, *et al.*, 2015)). However, in our study, we dissected ten males from the same colony and all of them had eight tergites

A previously unrecorded external characteristic that varied between the sexes in our study occurred in lateral view, i.e., the outline of the pronotal disc in males was uniformly curved (Fig. 1B) while in females it had a slight concave depression (Fig. 1D). As has been previously described, coffee berry borer males are smaller than females, have vestigial wings (Vega, Infante, *et al.*, 2015; Vega, Simpkins, *et al.*, 2015) and rudimentary compound eyes (Vega *et al.*, 2014) (Figs. 1, 8, 9E,F; Supplementary Videos S1, S4). Other characteristics that vary between sexes in bark and ambrosia beetles are discussed by Kirkendall *et al.* (Kirkendall *et al.*, 2015) and, for *Hypothenemus* in particular by Wood (Wood, 1954) and Vega *et al.*(Vega, Infante, *et al.*, 2015).

The alimentary canal, from mouth to anus, consisted of three main parts: foregut (stomodaeum), midgut (mesenteron) and hindgut (proctodeum). In contrast to the midgut, the foregut and the hindgut were ectodermic derivates and chitinized. The foregut was comprised of the preoral cavity, the mouthparts (where food is masticated), the pharynx, and the esophagus, which was enlarged posteriorly into the crop (where food is temporarily stored before entering the proventriculus, a gizzard-like organ located under the prothorax and whose main function is to grind and filter food particles). From there, food enters the anterior midgut (also referred to as stomach and ventriculus) and eventually the hindgut. Waste is excreted through the posterior opening of the alimentary canal (i.e., the anus). The insertion of Malpighian tubules was coincident with the limit between

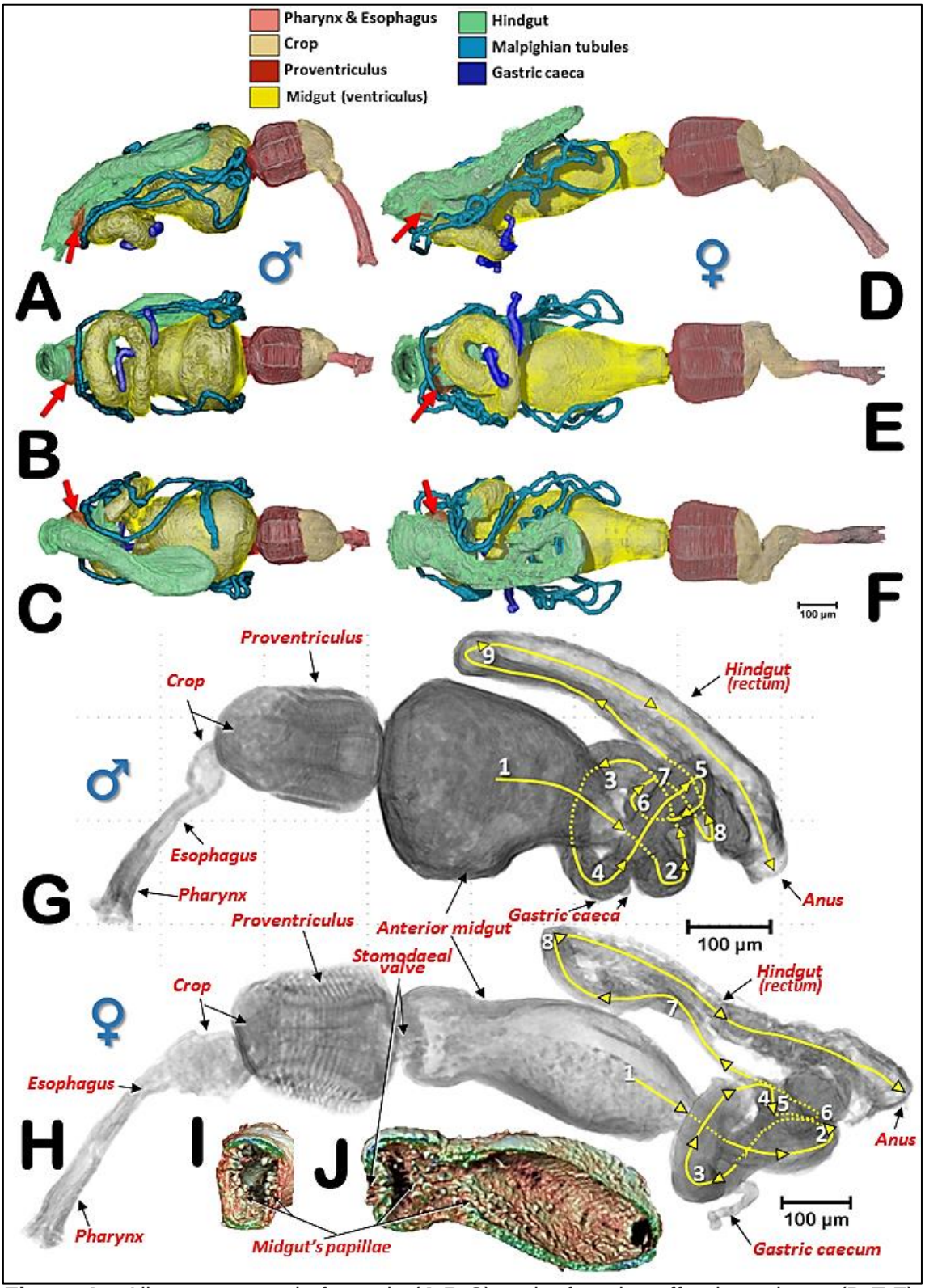

Figure 4.-. Alimentary canal of a male (**A**,**B**,**C**) and a female coffee berry borer (**D**,**E**,**F**): right-lateral (**A**,**D**), ventral (**B**,**E**), and dorsal (**C**,**F**) views. Red arrows indicate the rectal ampulla. Lateral views of the male (**G**) and female (**H**) alimentary canals with the trajectories and convolutions of the midgut and hindgut shown in yellow. Each time the digestive tracts began a new trajectory curve, the new tract is marked with an incremental number. Anterior-transversal (**I**) and sagittal (**J**) cuts close to the stomodaeal valve of the midgut reveal the internal papillae.

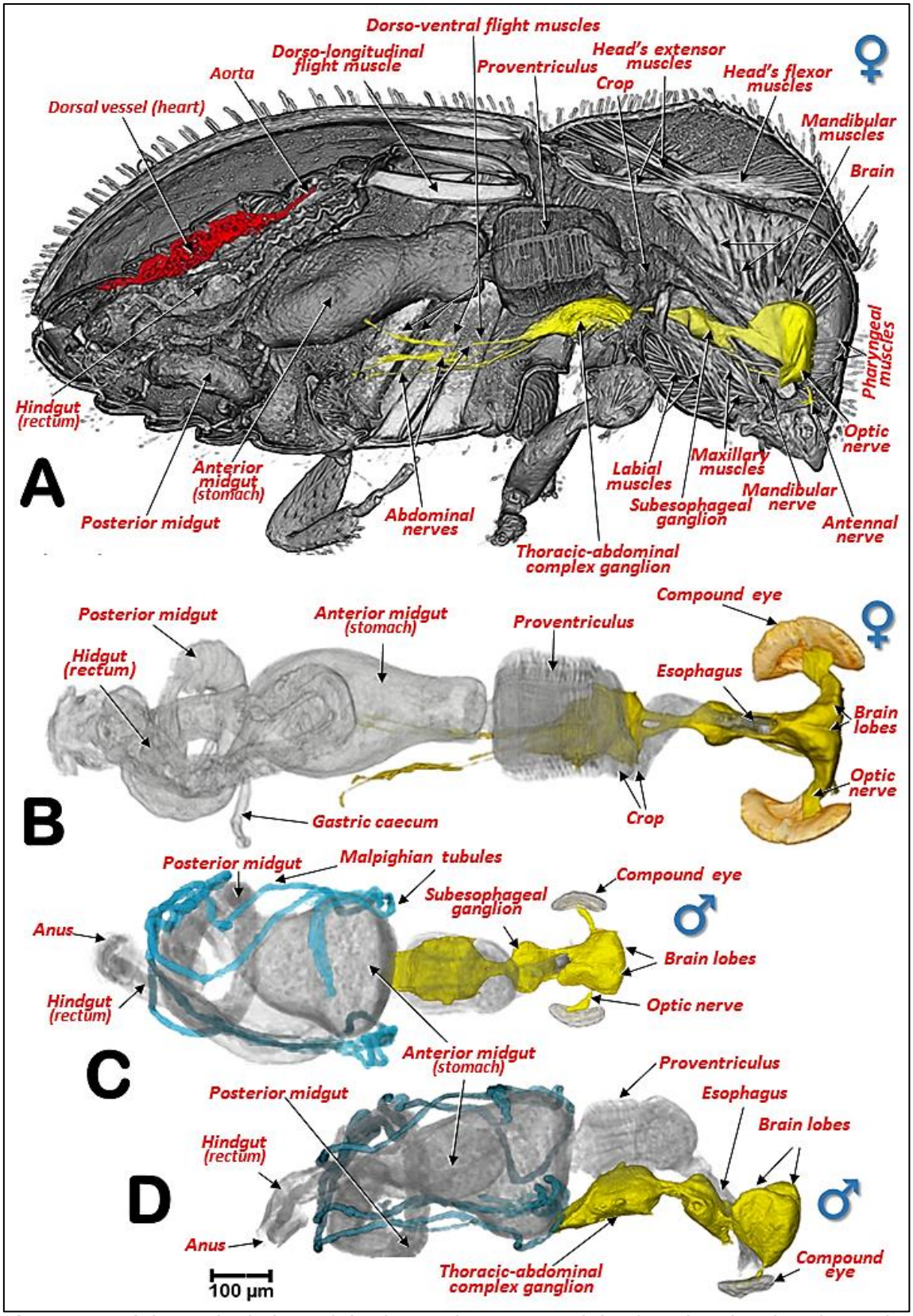

Figure 5.- Right-sagittal view of the internal anatomy of the female, showing the main musculature, dorsal vessel and nervous system (**A**), and a dorsal view of the digestive and nervous systems (**B**). Dorsal (**C**) and right- lateral (**D**) views of a male focusing on the positioning of the nervous system in relation to the digestive system.

the mesodeum (midgut) and the proctodeum (hindgut) separation, as described by others (Chapman, 2013; Gillott, 2005; Snodgrass, 1935).

The pharynx had chitinized ridges, where the pharynx dilator muscles were inserted, and opened into the preoral cavity. The preoral cavity ran across the head, below the brain (Figs. 2, 3, 5; Supplementary Videos S1, S2), through the nervous system (Fig. 5; Supplementary Videos S4, S9), connecting with the crop via a short esophagus. The crop was comprised of two contiguous cavities, one small anterior one and another more voluminous one connected to the proventriculus (Figs. 2, 3, 4, 5, 6A; Supplementary Videos S2, S9).

The proventriculus (Fig. 6, Supplementary Videos S3, S9) was an octagon-shaped organ and once thought to have taxonomic value in Scolytoidea (Beal, 1927; Eaton, 1942; Nobuchi, 1969; Swaine, 1918). A series of outer band muscles surrounded eight heavily sclerotized units (Figs. 6, 7), as previously described by Eaton (Eaton, 1942) for *Ips mexicanus* (=*radiatae*) (Hopkins); these muscles exert a peristaltic function (contraction and relaxation) that grinds and moves food particles through the proventriculus. Another band of inner muscles also have a peristaltic function on the grinding structures, formed by eight plates that appeared as a whole and in cross section with a starry arrangement (Figs. 6C–E, 7E,F). Each of these were formed in two parts, an anterior plate and a posterior plate. Internally these plates formed masticatory teeth, which triturated food particles. The presence of long ‘saber-like bristles’ and masticatory brush-teeth also assist in food grinding and filtering (Figs. 6C–H, 7; Supplementary Videos S2, S3). The general structure agreed with Calders’s (Calder, 1989) ‘Type 7’ Scolytinae.

Eaton (Eaton, 1942) described the grinding-straining mechanism of food moving through the proventriculus of *I. mexicanus* as follows: “Its passage through the proventriculus is probably restricted to the side channels formed by the rows of lamellae, since the obstructing brushes extending into the lumen would prevent direct movement of the food material through the central opening” and indicated this probable passage of food in Fig. 8 (p. 46). However, in our study of the coffee berry borer, it could be clearly seen that the lumen was filled with food particles while the spaces marked by Eaton as possible passageways for food, were devoid of food particles.

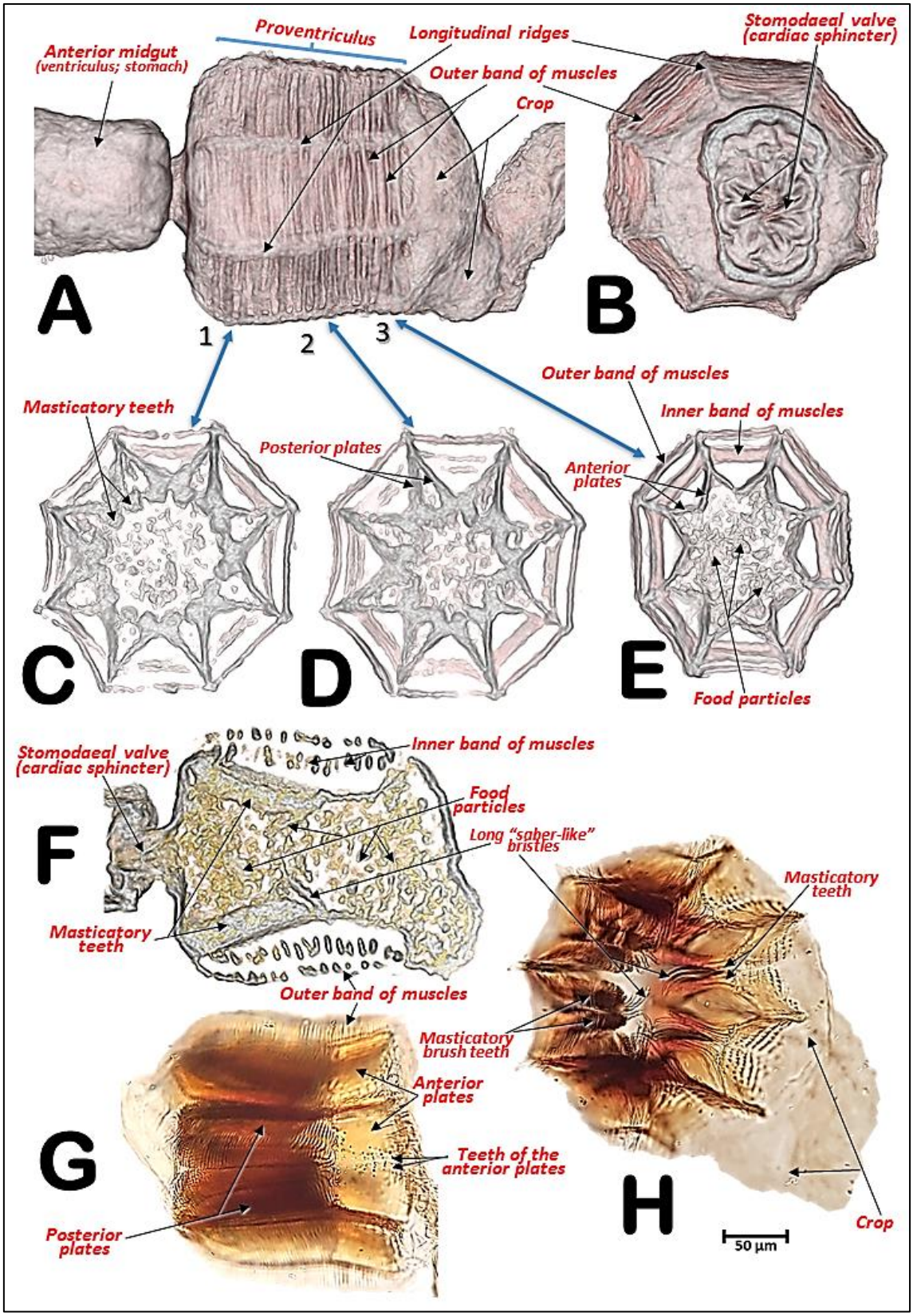

Figure 6.- Details of the proventriculus: micro-CT volume-rendered images (**A**–**F**) and light microscopy photographs (**G**,**H**). Right-lateral view (**A**,**G**); posterior view showing the stomodaeal valve (=cardiac sphincter) (**B**). Progressive transverse slices (thickness ca. 20 µm) from the basal to the apical zone,

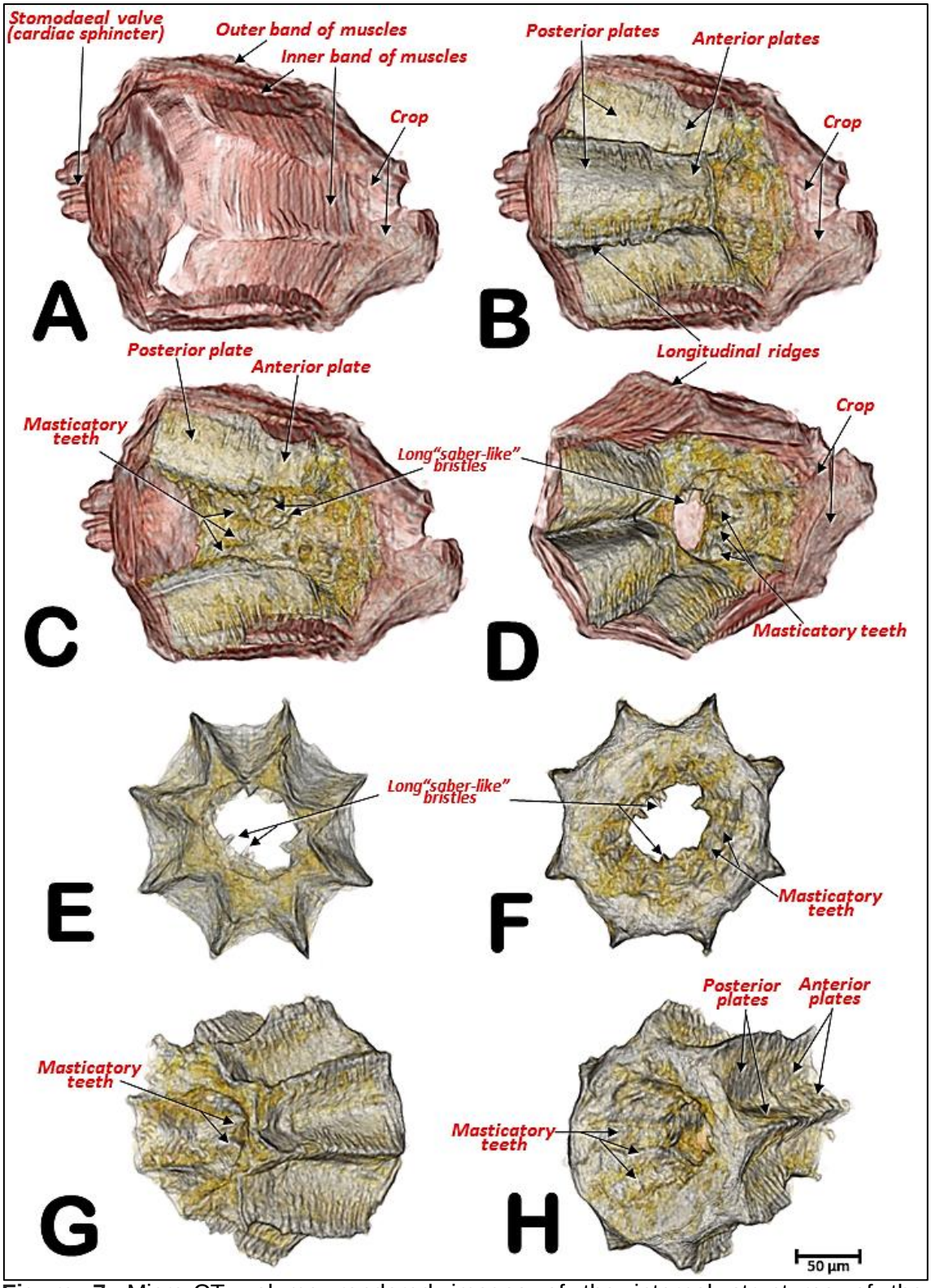

Figure 7.- Micro-CT volume rendered images of the internal structures of the proventriculus from different perspective views: right-lateral (**A,B,C**), right-antero-posterior (**D**), anterior (**E**), posterior (**F**), left antero- posterior (**G**) and right-postero-anterior (**H**). Different perspectives of the grinding sclerotized complex isolated (**E–H**). A: a superficial window was opened, and the grinding sclerotized complex removed; **B,D**: as **A** but including the grinding complex; **C**: as **B** but the grinding complex has been superficially sagittally cut, eliminating one side of the octagonal structure.

From the proventriculus the food moves through the cardiac sphincter (also known as the cardiac or stomodaeal valve; Fig. 6B–F) to the anterior midgut. There were differences between the sexes in the anterior midgut. In the male coffee berry borer, the anterior midgut was much dilated anteriorly (Figs. 2B, 4A–C,G; Supplementary Video S2), which was not apparent in the female (Figs. 3B, 4D–F,H; Supplementary Videos S2, S9). After scanning eight females and two males, it was clear that males had a conspicuously dilated midgut that was not present in females and this was not dependent on how full the cavity was with food. Moreover, we observed that the female (but not in the male) had short papillae covering the entire surface of the anterior part of the midgut, close to the stomodaeal valve; these were also present on 2/3 of the ventral surface (Fig. 4I,J). This arrangement of papillae has not been described previously in curculionids (Calder, 1989).

The midgut has no chitinous lining and is the primary site for secretion of digestive enzymes into the lumen and for absorption of nutrients (Crowson, 1981), although it should be noted that salivary enzymes (e.g., amylases) secreted in the foregut can also initiate digestive action (Klowden, 2007). There is considerable variation in the pH of the foregut, midgut and hindgut of Coleopteran species (Crowson, 1981), with the midgut and hindgut of the coffee berry borer having an acidic pH (4.5–5.2) (Crowson, 1981). Aggregation pheromones in *Dendroctonus* and *Ips* are also produced in the midgut (Blomquist *et al.*, 2010).

The transit of food through the alimentary canal in the coffee berry borer takes ca. 24h (Ceja-Navarro *et al.*, 2015). The anterior midgut of the coffee berry borer has a gradient in oxygen content, with a microaerophilic region close to the surface (0–300 µm depth) followed by an anaerobic region (400–600 µm depth) (Ceja-Navarro *et al.*, 2015). This gradient allows for the activity of oxygen-dependent and anaerobic enzymes. For example, N-demethylases (involved in caffeine metabolism in the coffee berry borer) are oxygen-dependent (Summers *et al.*, 2012), while the fermentation of polysaccharides such as mannan in the coffee bean (Aguilera-Gálvez *et al.*, 2013; Redgwell & Fischer, 2006; Vega, Infante, *et al.*, 2015), is an anaerobic process (Balaman, 2018).

The posterior midgut had two diverticula (right and left), also known as gastric caeca (Figs. 2–4, 5B; Supplementary Videos S2, S9); these increase the surface area of the midgut and are involved in water absorption, digestive activity, and uptake of nutrients (Klowden, 2007).

Insertion of the Malpighian tubules is recognized as the beginning of the hindgut (Chapman, 2013; Gillott, 2005; Romoser, 1981; Snodgrass, 1935). Insertion of six Malpighian tubules has been reported in other Scolytinae (Aslam, 2009; Baker & Estrin, 1974; Bu & Chen, 2009; Calder, 1989; Díaz *et al.*, 2000, 2003) with the distal portion of the Malpighian tubules embedded in the tissues surrounding the rectum (Bu & Chen, 2009; Díaz *et al.*, 2000, 2003). However, after exhaustive visualization of these tubules in both sexes of the coffee berry borer, we only observed four long Malpighian tubules, in contrast with the six reported previously (Rubio G. *et al.*, 2008). They appeared to be folded several times, going forwards and backwards (Figs. 2, 3, 4A–F, 5C,D; Supplementary Videos S1, S2, S4, S9); the distal portions, which were situated at the level of the anterior midgut (stomach), did not surround the rectum. The distal portions are immersed in haemolymph and serve a urinary function (i.e., as excretory organs that remove nitrogenous wastes, mainly uric acid) and also balance water and salt levels in the haemolymph. The anterior part of the hindgut is also referred to as the ileum or intestinum, and the posterior part in some insects is divided into colon and rectum (these three parts are also known as pylorus, ileum and rectum (Chapman, 2013), and are responsible for absorption of solutes such as amino acids, salts and water (Chapman, 2013; Gillott, 2005; Wigglesworth, 1942). The rectum is the most dorsal part of the digestive system, and was slightly displaced to the right side, running backwards to open externally at the anus (Figs. 2–4, 5B–D; Supplementary Videos S1, S2, S4, S9).

It has been reported that the length of the alimentary canal in *Dendroctonus armandi* is almost three times the length of the insect (Bu & Chen, 2009). In the coffee berry borer, the length of the alimentary canal was 2.82 mm for the male and 3.48 mm for the female; the ratio of the length of the alimentary canal to the body of the insect was 2.9 and 2.3, for the male and female, respectively. Moreover, we observed additional differences between the sexes in the number of trajectories of the midgut and hindgut (based on the number of

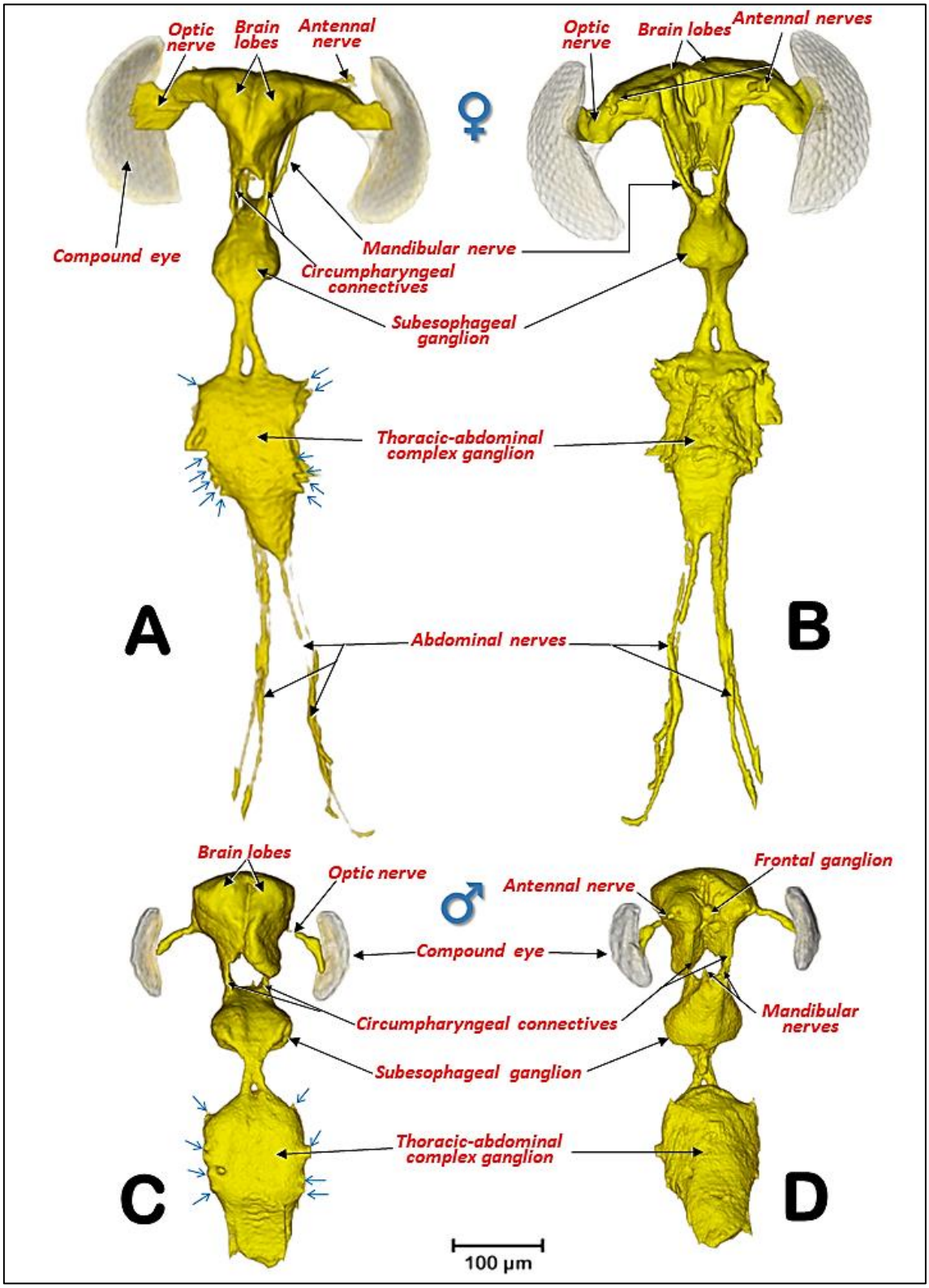

Figure 8.- Nervous systems of a female (**A,B**) and a male (**C,D**) coffee berry borer, showing the main ganglia and nerves (**A,C**: dorsal; **B,D**: ventral). The abdominal nerves are not shown in the male. The nerve insertions in the thoracic-abdominal-complex ganglion are indicated with blue arrows. Terminology after Atkins and Chapman (Atkins & Chapman, 1957) and Snodgrass (Snodgrass, 1935).

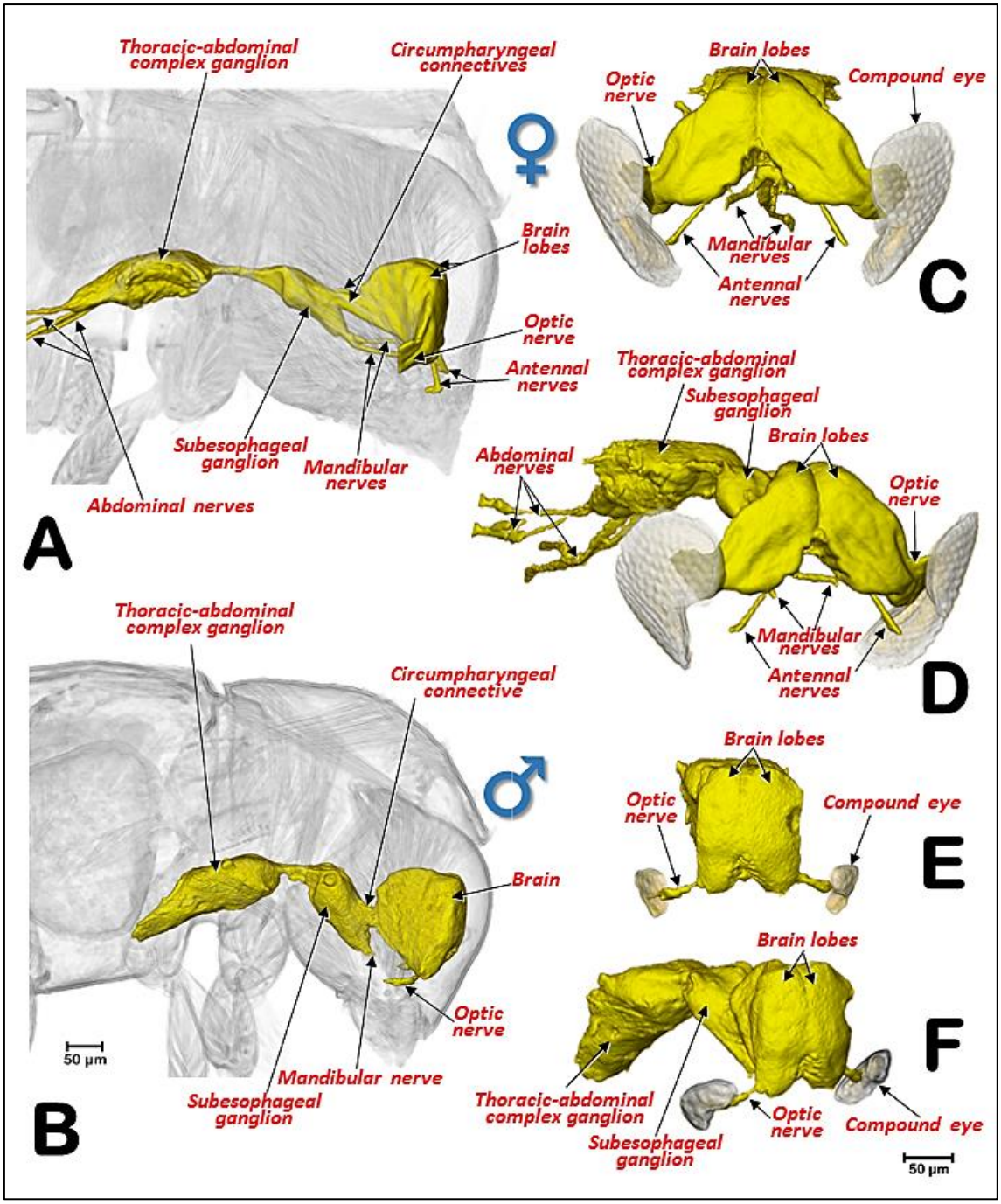

Figure 9.- Lateral views of the nervous system of a female (**A**) and a male (**B**) coffee berry borer allowing comparison of the relative size of the central nervous system in relation to the head. Details in frontal (**C,E**) and latero-frontal (**D,F**) views of the central nervous system of a female (**C,D**) and a male (**E,F**) focusing on the differences between sexes.

times the alimentary canal began a new trajectory curve). We observed nine different trajectories in the male compared with eight in the female (Fig. 4G,H; Supplementary Video S2). Males have a shorter body length than females, suggesting that additional folding of the tubes of mid- and hindgut was necessary to fit into the smaller space.

In both sexes a rectal ampulla was connected to the final tract of the rectum (Figs. 2–3, 4A–F; Supplementary Videos S1, S2); in other Coleoptera this ampulla has a defensive function via secretions (Crowson, 1981).

The male reproductive system (Figs. 2, 10F–I, 11; Supplementary Videos S1, S5) was comprised of two testes touching medially and positioned above the midgut (containing lobular testis follicles where spermatozoa are formed (Chapman, 2013; Gillott, 2005)). Each testis had a vas deferens and a single elongated accessory gland, in contrast to three pairs of accessory glands per pair of testes in *D. monticolae* (Cerezke, 1964). Accessory glands are involved in the production of seminal fluids that mix with sperm to form the ejaculate (Snodgrass, 1935), the vas deferens dilates to form a small seminal vesicle for storage prior to ejaculation (Chapman, 2013). The vasa deferentia on both sides meet to form an ejaculatory duct that is connected to the aedeagus

The structure of the aedeagus in insects was studied in-depth by Snodgrass (Snodgrass, 1935) and updated for Coleoptera by Lindroth and Palmen (Lindroth & Palmen, 1970). The aedeagus is an important taxonomical characteristic used for species identification of insects in general and is of particular relevance in studies of Coleoptera (Zunino, 2012) including bark beetles (Fuchs, 1912). However, to the best of our knowledge, there has been no previous detailed description of the aedeagus in the coffee berry borer. There are only draft schematic drawings and not detailed photographs (Rubio-Gómez *et al.*, 2007; Rubio G. *et al.*, 2008). The micro-CT rendered images of the aedeagus of the coffee berry borer (Figs. 2A,B, 10F–I, 11; Supplementary Videos S6, S7) show two lateral lobes (parameres) and a medial lobe (the intromitting structure, the penis) between them, with a rounded distal part opening called the gonopore. The distal extremity of the aedeagus is armed with apical spines and subapical-dorsal denticles that, as a whole, form anchoring structures (known as titillators (Snodgrass, 1935)) helping ensure the sexes remain connected during

copulation. The general structure of the aedeagus corresponds to the vaginate type described by Lindroth and Palmen (Lindroth & Palmen, 1970) where the parameres are elongated, forming a dorsal channel through which the penis moves.

The female reproductive system (Figs. 3, 10A–E; Supplementary Videos S1, S5) is comprised of two ovaries (located at each side of the body, slightly beneath the hindgut), each containing two ovarioles. Each ovariole had a terminal filament forming the suspensory apparatus of the mature ovary; (Snodgrass, 1935) a germarium in which oocytes are produced from oogonia; a vitellarium in which yolk is deposited into the oocytes through a membranous tube; (Chapman, 2013) and the ovariole pedicel that enlarges to form the calyx for the reception of eggs (Snodgrass, 1935). From each calyx emerged a short lateral oviduct; both lateral oviducts joined to form the common oviduct leading to the female gonopore. Close to the end of the common oviduct, on the right side, in a dorsal position was an ampulla-shaped accessory gland; between the accessory glands (very close to each other) was a hook-shaped spermatheca. The micro-CT rendered images obtained here were totally coincident with light microscopic images obtained following dissection (Román-Ruiz *et al.*, 2017; Rubio-Gómez *et al.*, 2007; Rubio G. *et al.*, 2008). Details of the hooked distal part of the spermatheca, spermatic gland, and the spermathecal muscles described recently (Román-Ruiz *et al.*, 2017) were enhanced using micro-CT (Fig. 10D; Supplementary Video S8). Román-Ruiz *et al.* (Román-Ruiz *et al.*, 2017) first photographed and described the spermatic gland as a “cell agglomeration on the curved distal end of the spermatheca”, but they added that “a further study will be necessary to confirm this finding”. The micro-CT reconstructions allowed us to visualize the structure previously identified as the spermatic gland (Fig. 10A,B,D; Supplementary Video S8) thus confirming its existence and structure.

The circulatory system in insects is responsible for the movement of haemolymph into the haemocoel spaces where organs are immersed. The haemolymph enters various contractile chambers of a dorsal vessel (heart) and is pumped forwards through an anterior aorta. This is what it is considered as an open circulatory system. The circulatory system does not have a key role in the transport of gases as this is achieved by an aero-vascular system formed by a

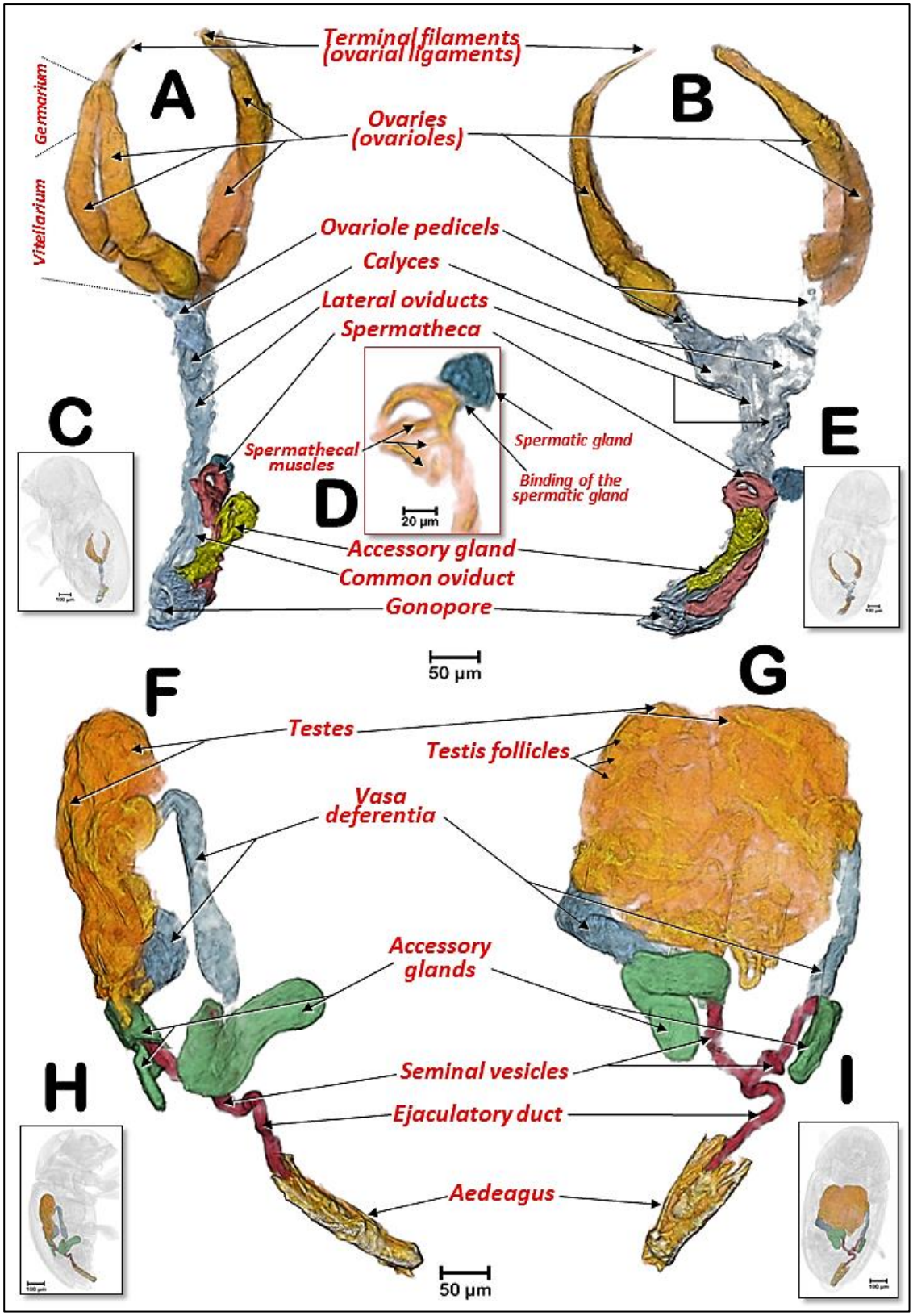

Figure 10.- Female (**A**–**E**) and male (**F**–**I**) coffee berry borer reproductive systems, in latero-dorsal (**A**,**C**), lateral (**E**,**G**) and dorsal (**B**,**D**,**F**,**H**) views. Details of the distal part of the spermatheca, with the spermathecal muscles and the spermatic gland (**D**). Figures (**C**,**E**,**H** and **I**) show the positions of the insect corresponding to figures (**A**,**B**,**F** and **G**), respectively.

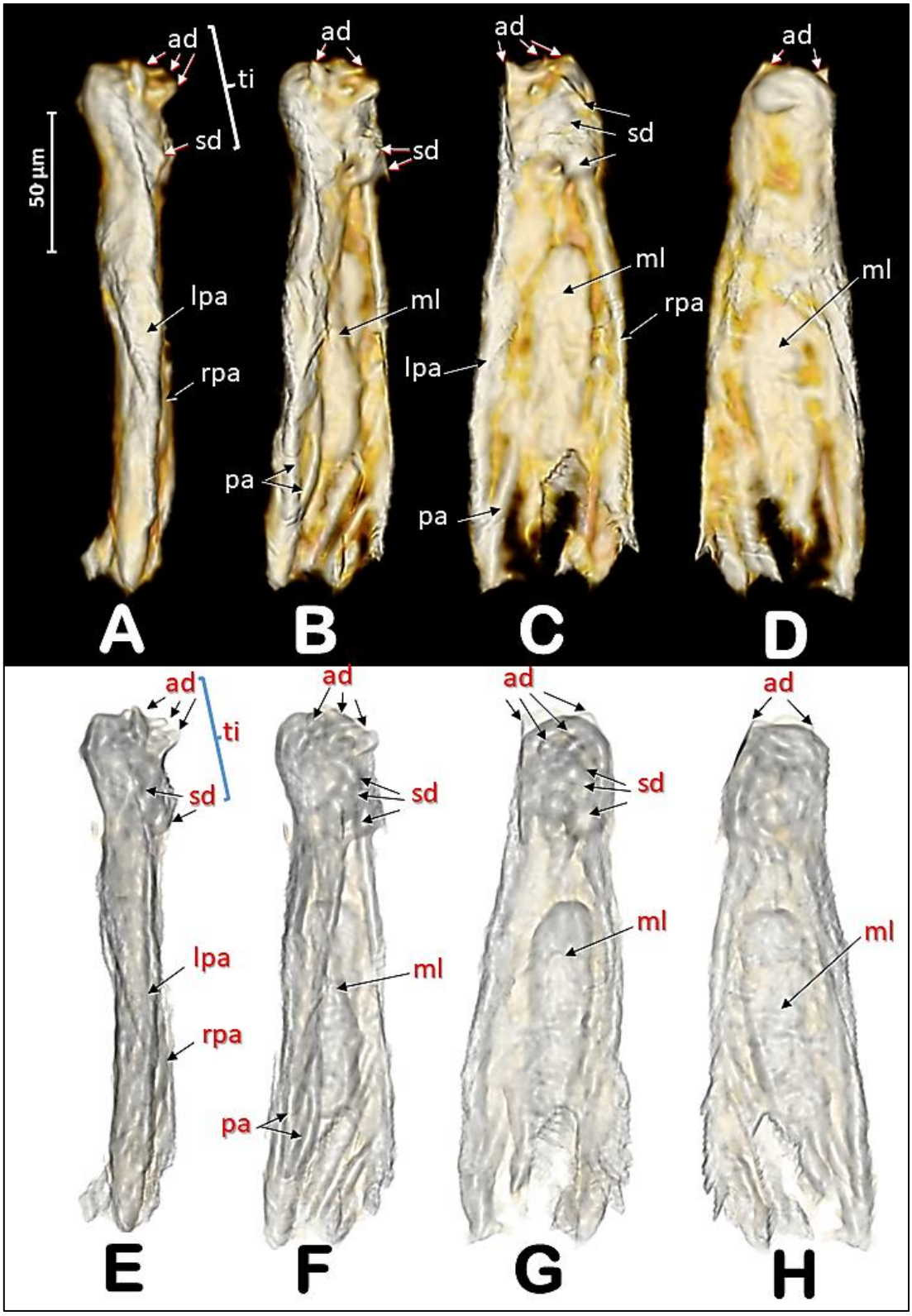

Figure 11.- Rendered images of different views of the aedeagus: left-lateral (**A**,**E**); left-latero-dorsal (**B**,**F**); dorsal (**C**,**G**); and ventral (**D**,**H**). Images at the bottom have been rendered transparent by software to enhance the view of internal structures. Abbreviations: ad = apical denticles (titillators); lpa = left parameres; rpa = right parameres; ml = median lobe ('penis'); pa = paramere apophysys; rpa = right paramere; sd = subapical dorsal denticles; ti = titillators. Terminology after Lindroth and Palmen (Lindroth & Palmen, 1970).

complex of tubes (tracheal system) (Chapman, 2013; Gillott, 2005; Snodgrass, 1935; Wigglesworth, 1930). In the coffee berry borer, as in other insects, the circulatory system is quite simple in contrast with the complexity of the tracheal respiratory system (Alba-Tercedor *et al.*, 2019). The dorsal vessel was segmented in the female; it was in a medial position within the abdomen, just below the tergites. The dorsal vessel had three conspicuous dilated chambers beneath tergites 4–6 which were prolonged anteriorly and posteriorly by aortic vessels.

When observing the musculature (Figs. 1E,F, 2, 3, 5A), it is noteworthy that the dorso-longitudinal and dorso-ventral flight muscles were clearly visible in the female (Figs. 1F, 3A, 5A) and absent in the male (Figs. 1E, 2A). This is likely to be because males have lost their ability to fly as they have vestigial wings, spending their entire life inside the coffee berry (Vega, Infante, *et al.*, 2015; Vega, Simpkins, *et al.*, 2015). The micro-CT rendered images of the flight muscles are completely comparable to, and actually clearer, than those previously published from dissected insects (López-Guillén *et al.*, 2011). Various muscles connected to the pharynx and mouthparts were clearly visible inside the head (mandibular, pharyngeal, maxillary and labial muscles; Figs. 2A, 5A). Head flexor and extensor muscles (Fig. 5A) were clearly visible in the pronotum. While we do not describe here every muscle visible in the micro-CT rendered images and supplementary videos, it will be the subject of a future paper.

The anatomy of the nervous system of insects was described extensively by Snodgrass (Snodgrass, 1935) and summarized and updated by Grassé (Grassé, 1975). There have been several studies on the anatomy of the nervous system in different families and species of Coleoptera (Crowson, 1981; Grassé, 1975). To our knowledge, despite the extensive revision by Calder (Calder, 1989), the most detailed anatomical studies of the nervous system of bark beetles is that of *D. pseudotsugae* by Atkins and Chapman (Atkins & Chapman, 1957), and our own study of the central nervous system of the coffee berry borer (Figs. 2A, 3A, 5,8,9; Supplementary Videos S1, S4, S9); both showed similar general patterns of organisation.

In the coffee berry borer, the brain (Figs. 2A, 3A, 5), located above the anterior end of the foregut, was connected to a ventral cord by two

circumpharyngeal connectives (Figs. 5, 8, 9A,B). Most of the ganglions in the ventral cord were fused, so it was only possible to distinguish a subesophageal ganglion (located beneath the esophagus in a ventral posterior cephalic position; Figs. 5, 8, 9A,B,D,F) and a large thoracic-abdominal complex ganglion (in a ventral thoracic position just below the proventriculus; Figs. 2A, 3A, 5, 8, 9A,B,D–F). Other Scolytinae species have a prothoracic separated ganglion (Atkins & Chapman, 1957; Calder, 1989). In other species, the connectives linking the brain to the ventral cord are known as circumesophageal connectives (Atkins & Chapman, 1957; Chapman, 2013; Gillott, 2005; Snodgrass, 1935). However, it is clear that, in the coffee berry borer, these connectives surround the pharynx and not the esophagus (Figs. 2A, 3A, 5; Supplementary Videos S4, S9). For this reason, we describe them as circumpharyngeal connectives.

Micro-CT also allowed us to visualize different pairs of nerves including optic (to innervate eyes) and antennal (to innervate antennae) nerves in the brain; and mandibular nerves originating in the subesophageal ganglion (to innervate the mandibles) (Figs. 5A, 8A,B,D,9A,B,D). Nerve insertions into the thoracic-abdominal-complex ganglion and long abdominal nerves were also clearly visible (Figs. 8A–C, 9E); together, these innervate the wings, legs and abdominal muscles. Note that the abdominal nerves in the male were not segmented and have not been included in figures. Details of the different ganglia, such as the frontal ganglion (situated ventral to the brain) (Fig. 8D) were also visualized (Figs. 8, 9).

Sexual differences in the nervous system of insects has been reported, both in morphology, size and in the structure of the neural connections, e.g., in social insects (Beani *et al.*, 2014) and flies (Cachero *et al.*, 2010). In the coffee berry borer, there were conspicuous differences both in shape, size and relationship to the head of the nervous system, between the female and the male. The female had a larger, more laterally extended brain lobes, and thicker optic lobes (Fig. 9C,D) than the male (Fig. 9E,F). In relation to the size of the head, the brain of the female is smaller (Figs. 3A, 9A) than the male brain (Figs. 2A, 9B). The smaller brain and thinner optic nerves observed in the male is related to the biology of the species; males remain inside the coffee berry and have rudimentary compound eyes, vestigial wings, and flight muscles, as discussed above.

5.5.7.- Conclusions

The use of micro-CT to elucidate the anatomical structures and organs of the coffee berry borer has facilitated a complete reconstruction of the anatomy of the insect, revealing the actual position of internal structures and organs without the distortions encountered using dissection methods. The technique has also allowed us to obtain detailed rendered images and videos of the aedeagus, which we used to describe it for the first time. This study is the first complete micro-CT reconstruction of the anatomy of an insect and is also the smallest insect to have been evaluated in this way. Moreover, we report previously unreported differences between the sexes with respect to both external morphology (lateral outline of the pronotum and number of abdominal tergites), and internal anatomy (flight musculature, midgut shape, hindgut convolutions and the shape and size of the brain). We have included supplementary videos and a 3D model that is suitable for use with mobile devices and could be a useful tool for scientists working on other insects as well as a teaching aid.

5.5.8.- Supplementary Information

Videos:

S1.- Animated volume rendered images of both sexes of the coffee berry borer (*Hypothenemus hampei*) showing the general anatomy.

https://static-content.springer.com/esm/art%3A10.1038%2Fs41598-019-53537-z/MediaObjects/41598_2019_53537_MOESM2_ESM.mp4

S2.- Comparative animated volume rendered images of the digestive in both sexes of the coffee berry borer (*Hypothenemus hampei*).

https://static-content.springer.com/esm/art%3A10.1038%2Fs41598-019-53537-z/MediaObjects/41598_2019_53537_MOESM3_ESM.mp4

S3.- Animated volume rendered images of the detailed anatomy of the proventriculus of the coffee berry borer (*Hypothenemus hampei*).

https://static-content.springer.com/esm/art%3A10.1038%2Fs41598-019-53537-z/MediaObjects/41598_2019_53537_MOESM4_ESM.mp4

S4.- Animated volume rendered images of a female of the coffee berry borer (*Hypothenemus hampei*) showing the circulatory, digestive and nervous system.

https://static-content.springer.com/esm/art%3A10.1038%2Fs41598-019-53537-z/MediaObjects/41598_2019_53537_MOESM5_ESM.mp4

S5.- Comparative animated volume rendered images of the reproductive system in both sexes of the coffee berry borer (*Hypothenemus hampei*).

https://static-content.springer.com/esm/art%3A10.1038%2Fs41598-019-53537-z/MediaObjects/41598_2019_53537_MOESM6_ESM.mp4

S6.- Animated volume rendered images of the aedeagus of the coffee berry borer (*Hypothenemus hampei*).

https://static-content.springer.com/esm/art%3A10.1038%2Fs41598-019-53537-z/MediaObjects/41598_2019_53537_MOESM7_ESM.mp4

S7.- 3D Animated volume rendered images of the aedeagus of the coffee berry borer (*Hypothenemus hampei*).To be able to visualise the 3D effect use red-cyan anaglyph glasses.

https://static-content.springer.com/esm/art%3A10.1038%2Fs41598-019-53537-z/MediaObjects/41598_2019_53537_MOESM8_ESM.mp4

S8.- Animated volume rendered images of the spermatheca and spermatic gland of the coffee berry borer (*Hypothenemus hampei*).

https://static-content.springer.com/esm/art%3A10.1038%2Fs41598-019-53537-z/MediaObjects/41598_2019_53537_MOESM9_ESM.mp4

S9.- Animated volume rendered images showing the internal organs of the coffee berry borer (*Hypothenemus hampei).*

https://static-content.springer.com/esm/art%3A10.1038%2Fs41598-019-53537-z/MediaObjects/41598_2019_53537_MOESM10_ESM.mp4

5.5.9.- References

Aguilera-Gálvez, C., Vásquez-Ospina, J. J., Gutiérrez-Sanchez, P., & Acuña-Zornosa, R. (2013). Cloning and biochemical characterization of an endo-1,4-β-mannanase from the coffee berry borer *Hypothenemus hampei*. *BMC Research Notes*, *6*(1), 333. https://doi.org/10.1186/1756-0500-6-333

Alba-Tercedor, J. (2004). Efemerópteros. In J. A. Barrientos (Ed.), *Curso Práctico de Entomología* (pp. 511–522). Asociación Española de Entomología. Centro Iberoamericano de la Biodiversidad.

Alba-Tercedor, J. (2014). From the sample preparation to the volume rendering images of small animals : A step by step example of a procedure to carry out the micro-CT study of the leafhopper insect Homalodisca vitripennis (Hemiptera: Cicadellidae). *Bruker Micro-CT Users Meeting 2014*, 260–288. http://www.skyscan.be/company/UM2014/008_Javier_Alba_Tercedor.pdf

Alba-Tercedor, J., & Alba-Alejandre, I. (2019). Comparing micro-CT results of insects with classical anatomical studies: The European honey bee (*Apis mellifera* Linnaeus, 1758) as a benchmark (Insecta: Hymenoptera, Apidae). *Microscopy and Analysis*, *3*(1), 12-15 EU. https://microscopy-analysis.com/article/january_19/comparing_classical_anatomical_studies_of_insects

Alba-Tercedor, J., Alba-Alejandre, I., & Vega, F. E. (2019). Revealing the respiratory system of the coffee berry borer (*Hypothenemus hampei*; Coleoptera: Curculionidae: Scolytinae) using micro-computed tomography. *Scientific Reports*, *9*(1), 17753. https://doi.org/10.1038/s41598-019-54157-3

Aldrovandi, U. (1602). *De Animalibus Insectis Libri*.

Aslam, N. A. (2009). An assessment of some internal characters in the higher classification of the Curculionidae s.l. (Coleoptera). *Transactions of the Royal*

Entomological Society of London, *113*(14), 417–480. https://doi.org/10.1111/j.1365-2311.1961.tb00799.x

Atkins, M. D., & Chapman, J. A. (1957). Studies on nervous nystem anatomy of the Douglas Fir Beetle, *Dendroctonzis pseudotsugae* Hopk. (Scolytidae)'. In *The Canadian Entomologist* (Vol. 89, Issue 2). https://doi.org/https://doi.org/10.4039/Ent8980-2

Baker, W. V., & Estrin, C. L. (1974). The alimentary canal of *Scolytus multistriatu*s (Coleoptera: Scolytidae): a histological study. *The Canadian Entomologist*, *106*(7), 673–686. https://doi.org/10.4039/Ent106673-7

Balaman, S. Y. (2018). *Decision-Making for Biomass-Based Production Chains. The Basic Concepts and Methodologies*. Academic Press.

Beal, J. A. (1927). The Development of the Proventriculus of *Pityogenes Hopkinsi* Swaine. *Annals of the Entomological Society of America*, *20*(4), 522–539. https://doi.org/10.1093/aesa/20.4.522

Beani, L., Dessì-Fulgheri, F., Cappa, F., & Toth, A. (2014). The trap of sex in social insects: From the female to the male perspective. *Neuroscience and Biobehavioral Reviews*, *46*, 519–533. https://doi.org/10.1016/j.neubiorev.2014.09.014

Blomquist, G. J., Figueroa-Teran, R., Aw, M., Song, M., Gorzalski, A., Abbott, N. L., Chang, E., & Tittiger, C. (2010). Pheromone production in bark beetles. *Insect Biochemistry and Molecular Biology*, *40*(10), 699–712. https://doi.org/10.1016/j.ibmb.2010.07.013

Bu, S.-H., & Chen, H. (2009). The Alimentary Canal of *Dendroctonus armandi* Tsai and Li (Coleoptera: Curculionidae: Scolytinae). *The Coleopterists Bulletin*, *63*(4), 485–496. https://doi.org/10.1649/1190.1

Cachero, S., Ostrovsky, A. D., Yu, J. Y., Dickson, B. J., & Jefferis, G. S. X. E. (2010). Sexual Dimorphism in the Fly Brain. *Current Biology*, *20*(18), 1589–1601. https://doi.org/10.1016/j.cub.2010.07.045

Calder, A. A. (1989). The alimentary canal and nervous system of Curculionoidea (Coleoptera): gross morphology and systematic significance. *Journal of Natural History*, *23*(6), 1205–1265. https://doi.org/10.1080/00222938900770671

Ceja-Navarro, J. A., Vega, F. E., Karaoz, U., Hao, Z., Jenkins, S., Lim, H. C., Kosina, P., Infante, F., Northen, T. R., & Brodie, E. L. (2015). Gut microbiota mediate caffeine detoxification in the primary insect pest of coffee. *Nature Communications*, *6*(1), 7618. https://doi.org/10.1038/ncomms8618

Cerezke, H. F. (1964). The morphology and functions of the reproductive systems of *Dendroctonus monticolae* Hopk. (Coleoptera: Scolytidae). *The Canadian Entomologist*, *96*(03), 477–500. https://doi.org/10.4039/Ent96477-3

Chapman, R. F. (2013). *The Insects Structure and Function* (S. J. Simpson & A. E. Douglas (eds.); 5th ed.). Cambridge University Press. Chapman 5 th edition The Insects structure and function.pdf - ResearchGate

Constantino, L. M., Navarro, L., Berrio, A., Acevedo, F. E., Rubio, D., & Benavides, P. (2011). Aspectos biológicos, morfológicos y genéticos de *Hypothenemus obscurus* e *Hypothenemus hampei* (Coleoptera: Curculionidae: Scolytinae). *Revista Colombiana de Entomología*, *37*(2), 173–182.

Crowson, R. A. (1981). The Biology of the Coleoptera. In *The Biology of the Coleoptera*. Academic Press Inc. New York

Davis, A. P., Chadburn, H., Moat, J., O'Sullivan, R., Hargreaves, S., & Nic Lughadha, E.

(2019). High extinction risk for wild coffee species and implications for coffee sector sustainability. *Science Advances*, *5*(1), eaav3473. https://doi.org/10.1126/sciadv.aav3473

Díaz, E., Arciniega, O., Sánchez, L., Cisneros, R., & Zúñiga, G. (2003). Anatomical and histological comparison of the alimentary canal of *Dendroctonus micans, D. ponderosae, D. pseudotsugae pseudotsugae, D. rufipennis,* and *D. terebrans* (Coleoptera: Scolytidae). *Annals of the Entomological Society of America*, *96*(2), 144–152. https://doi.org/10.1603/0013-8746(2003)096[0144:aahcot]2.0.co;2

Díaz, E., Cisneros, R., & Zúñiga, G. (2000). Comparative Anatomical and Histological Study of the Alimentary Canal of the *Dendroctonus frontalis* (Coleoptera: Scolytidae) Complex. *Annals of the Entomological Society of America*, *93*(2), 303–311. https://doi.org/10.1603/0013-8746(2000)093[0303:caahso]2.0.co;2

Duque-Orrego, H. (2000). Economics of coffee berry borer (*Hypothenemus hampei*) in Colombia. *Workshop, Coffee Berry Borer: New Approaches to Integrated Pest Management", Mississippi State University, Starkville, Mississippi*, 14 pp.

Duque-Orrego, H., Márquez-Q, A., & Hernández-S, M. (2002). Estudios de caso sobre costos de manejo integrado de la broca del café en el Departamento de Risaralda. In *Cenicafé* (Vol. 53, Issue 2).

Eaton, C. B. (1942). The Anatomy and Histology of the Proventriculus of *Ips radiatae* Hopkins. *Annals Entomological Society of America*, *35*, 41–49.

Fuchs, G. (1912). Morphologische Studien über Borkenkäfer. II Die Europaischen Hylesinen. In *Verlag von Ernst Reinhard. München*.

Furniss, M. M. (2004). Biology of Trypophloeus striatulus (Coleoptera: Scolytidae) in Feltleaf Willow in Interior Alaska. *Environmental Entomology*, *33*(1), 21–27. https://doi.org/10.1603/0046-225X-33.1.21

Gillott, C. (2005). Entomology. In *Entomology* (3rd ed.). Springer. www.springeronline.com

Grassé, P.-P. (1975). Le Système Nerveux des Insectes. In *Traité de Zoologie. Anatomi, Systematique, Biologie. T. VIII, fasc. III* (pp. 321–510). Masson et Cie.

Greco, M., Bell, D., Woolnough, L., Laycock, S., Corps, N., Mortimore, D., & Hudson, D. (2014). 3-D visualisation, printing, and volume determination of the tracheal respiratory system in the adult desert locust, *Schistocerca gregaria*. *Entomologia Experimentalis et Applicata*, *152*(1), 42–51. https://doi.org/10.1111/eea.12199

Greenlee, K. J., Henry, J. R., Kirkton, S. D., Westneat, M. W., Fezzaa, K., Lee, W.-K., & Harrison, J. F. (2009). Synchrotron imaging of the grasshopper tracheal system: morphological and physiological components of tracheal hypermetry. *American Journal of Physiology-Regulatory, Integrative and Comparative Physiology*, *297*(5), R1343–R1350. https://doi.org/10.1152/ajpregu.00231.2009

Ha, Y.-R., Yeom, E., Ryu, J., & Lee, S.-J. (2017). Three-dimensional structures of the tracheal systems of *Anopheles sinensis* and *Aedes togoi* pupae. *Scientific Reports. Nature Publishing Group*. https://doi.org/10.1038/srep44490

Helm, B. R., Payne, S., Rinehart, J. P., Yocum, G. D., Bowsher, J. H., & Greenlee, K. J. (2018). Micro-computed tomography of pupal metamorphosis in the solitary bee *Megachile rotundata*. *Arthropod Structure & Development*, *47*(5), 521–528. https://doi.org/10.1016/J.ASD.2018.05.001

Hopkins, A. D. (1909). Contribution towards a monograph of the scolytids beetles. I. The genus *Dendroctonus*. In *Technical series, Bureau of Entomology, U.S.*

Departament of Agriculture (Vol. 17).

Iwan, D., Kamiński, M. J., & Raś, M. (2015). The Last Breath: A µCT-based method for investigating the tracheal system in Hexapoda. *Arthropod Structure & Development*, *44*(3), 218–227. https://doi.org/10.1016/j.asd.2015.02.002

Jiang, Z.-R., Kinoshita, ichi, Sasaki, O., Cognato, A. I., & Kajimura, H. (2019). Non-destructive observation of the mycangia of *Euwallacea interjectus* (Blandford) (Coleoptera: Curculionidae: Scolytinae) using X-ray computed tomography. *Entomological. Science.* 22 (2), 173–181 (2019).https://doi.org/10.1111/ens.12353

Kirkendall, L. R., Biedermann, P. H. W., & Jordal, B. H. (2015). Evolution and diversity of bark and ambrosia beetles. In *Bark Beetles* (pp. 85–156). Elsevier. https://doi.org/10.1016/B978-0-12-417156-5.00003-4

Klowden, M. J. (2007). *Physiological systems in insects*. Elsevier/AcademicPress.

Li, D., Zhang, K., Zhu, P., Wu, Z., & Zhou, H. (2011). 3D configuration of mandibles and controlling muscles in rove beetles based on micro-CT technique. *Analytical and Bioanalytical Chemistry*, *401*(3), 817–825. https://doi.org/10.1007/s00216-011-5088-y

Li, Y., Ruan, Y., Kasson, M. T., Stanley, E. L., Gillett, C. P. D. T., Johnson, A. J., Zhang, M., & Hulcr, J. (2018). Structure of the ambrosia beetle (Coleoptera: Curculionidae) mycangia revealed through micro-computed tomography. *Journal of Insect Science*, *18*(5), 13–14. https://doi.org/10.1093/jisesa/iey096

Li, Y., Stanley, E. L., & Skelton, J. (2018). Plasticity of mycangia in *Xylosandrus ambrosi*a beetles Herpetology of Angola View project Taxonomy and Morphology View project. *Insect Science*, *00*, 1–11. https://doi.org/10.1111/1744-7917.12590

Lindroth, C. H., & Palmen, E. (1970). Coleoptera. In S. L. Tuxen (Ed.), *Taxonomist's glossary of genitalia in insects* (pp. 80–88). Scandinavian University Books. http://antbase.org/ants/publications/21060/21060.pdf

López-Guillén, G., Carrasco, J. V., Cruz-López, L., Barrera, J. F., Malo, E. A., & Rojas, J. C. (2011). Morphology and structural changes in flight muscles of *Hypothenemus hampei* (Coleoptera: Curculionidae) Females. *Environmental Entomology*, *40*(2), 441–448. https://doi.org/10.1603/EN10181

Lowe, T., Garwood, R. J., Simonsen, T. J., Bradley, R. S., & Withers, P. J. (2013). Metamorphosis revealed: time-lapse three-dimensional imaging inside a living chrysalis. *Journal of the Royal Society, Interface / the Royal Society*, *10*(84), 20130304. https://doi.org/10.1098/rsif.2013.0304

Malpighi, M. (1669). *Dissertatio epistolica de bombyce*. J. Martyn & J. Allestry, regiæ societatis typographos.

Martín-Vega, D., Garbout, A., Ahmed, F., Ferrer, L. M., Lucientes, J., Colwell, D. D., & Hall, M. J. R. (2018). Micro-computed tomography visualization of the vestigial alimentary canal in adult oestrid flies. *Medical and Veterinary Entomology*, *32*(3), 378–382. https://doi.org/10.1111/mve.12301

Nobuchi, A. (1969). A comparative morphological study of the proventriculus in the adult of the superfamily Scolytoidea (Coleoptera). *Bull. Gov. For. Exp. Stn. (Jpn.)*, *224*, 40–58. https://www.ffpri.affrc.go.jp/pubs/bulletin/201/documents/224-2.pdf

Nüsslin, O. (1911). Phylogenie und System der Borkenkäfer. *Zeitschrift Für Wissenschaftliche Insektenbiologie.*, *7*, 1–5.

Oliveira, C. M., Auad, A. M., Mendes, S. M., & Frizzas, M. R. (2013). Economic impact of exotic insect pests in Brazilian agriculture. *Journal of Applied Entomology*, *137*(1–

2), 1–15. https://doi.org/10.1111/jen.12018

Pérez, J., Infante, F., & Vega, F. E. (2015). A coffee berry borer (Coleoptera: Curculionidae: Scolytinae) Bibliography. *Journal of Insect Science*, *15*(1), 83. https://doi.org/10.1093/jisesa/iev053

Raś, M., Iwan, D., & Kamiński, M. J. (2018). The tracheal system in post-embryonic development of holometabolous insects: a case study using the mealworm beetle. *Journal of Anatomy*, *232*(6), 997–1015. https://doi.org/10.1111/joa.12808

Redgwell, R., & Fischer, M. (2006). Coffee carbohydrates. *Brazilian Journal of Plant Physiology*, *18*(1), 165–174. https://doi.org/10.1590/S1677-04202006000100012

Richter, A., Keller, R. A., Rosumek, B., Economo, E. P., Hita Garcia, F., & Beutel, R. G. (2019). The cephalic anatomy of workers of the ant species *Wasmannia affinis* (Formicidae, Hymenoptera, Insecta) and its evolutionary implications. *Arthropod Structure &. Development. 49, 26–49 (2019).* https://doi.org/10.1016/j.asd.2019.02.002

Román-Ruiz, A. K., Michel, B., Dufour, B. P., Rojas, J. C., Cruz-López, L., & Barrera, J. F. (2017). Description of the sperm and spermatheca of *Hypothenemus hampei* (Coleoptera: Curculionidae: Scolytinae) for the differentiation of mated and unmated females. *Annals of the Entomological Society of America*, *110*(4), 353–359. https://doi.org/10.1093/aesa/sax033

Romoser, W. S. (1981). The Science of Entomology. In *The science of entomology* (Issue Ed. 2). Macmillan Publishing Co. Inc. https://www.cabdirect.org/cabdirect/abstract/19810587640

Rubio-Gómez, J. D., Bustillo-Pardey, Á. E., Vallejo-Espinosa, L. F., Benavides-Machado, P., Acuña-Zornosa, J. R., Rubio, R., & Bustillo, J. D. ; (2007). Morfología del sistema reproductor femenino y masculino de *Hypothenemus hampei* (Ferrari). *Cenicafé*, *58*(1), 75–81.

Rubio G., J. D., Bustillo P., A. E., Vallejo E., L. F., Acuña Z., J. R., & Benavides M., P. (2008). Alimentary canal and reproductive tract of *Hypothenemus hampei* (Ferrari) (Coleoptera: Curculionidae, Scolytinae). *Neotropical Entomology*, *37*(2), 143–151. https://doi.org/10.1590/S1519-566X2008000200006

Santiago-Blay, J. A., & Young, T. L. (1995). Reliable sexing of adult *Conophthorus* (Coleoptera: Scolytidae) beetles. *The Canadian Entomologist*, *127*(4), 605–607. https://doi.org/10.4039/Ent127605-4

Shaha, R. K., Vogt, J. R., Han, C.-S., & Dillon, M. E. (2013). A micro-CT approach for determination of insect respiratory volume. *Arthropod Structure & Development*, *42*(5), 437–442. https://doi.org/10.1016/J.ASD.2013.06.003

Simonsen, T. J., & Kitching, I. J. (2014). Virtual dissections through micro-CT scanning: a method for non-destructive genitalia 'dissections' of valuable Lepidoptera material. *Systematic Entomology*, *39*(3), 606–618. https://doi.org/10.1111/syen.12067

Smith, D. B., Bernhardt, G., Raine, N. E., Abel, R. L., Sykes, D., Ahmed, F., Pedroso, I., & Gill, R. J. (2016). Exploring miniature insect brains using micro-CT scanning techniques. *Scientific Reports*, *6*(1), 21768. https://doi.org/10.1038/srep21768

Snodgrass, R. E. (1935). Principles of Insect Morphology. In *Thorax*. McGraw-Hill Book Company, Inc. https://doi.org/0801428831

Stalling, D., Westerhoff, M., & Hege, H.-C. (2005). Amira: A Highly Interactive System for Visual Data Analysis. *Visualization Handbook*, 749–767.

https://doi.org/10.1016/B978-012387582-2/50040-X

Summers, R. M., Louie, T. M., Yu, C.-L., Gakhar, L., Louie, K. C., & Subramanian, M. (2012). Novel, highly specific N-demethylases enable bacteria to live on caffeine and related purine alkaloids. *Journal of Bacteriology*, *194*(8), 2041–2049. https://doi.org/10.1128/JB.06637-11

Swaine, J. M. (1918). Canadian bark-beetles. Part II. A preliminary classification with an account of the habits and means of control. (Technical Bulletin). *Dominion of Canada, Department of Agriculture, Entomological Branch, Bulletin No. 14*, 1–143.

Thermo Fisher Scientific. (2017). *Amira 3D visualization and analysis software.* (6.7.0). FEI. http://www.thermofisher.com/amira-avizo

Vega, F. E. (2008). The rise of coffee. *American Scientist*, *96*(March-April), 138–145. https://doi.org/10.1093/0195139690.001.0001

Vega, F. E., Infante, F., & Johnson, A. J. (2015). The genus *Hypothenemus*, with emphasis on *H. hampei*, the coffee berry borer. In *Bark Beetles* (pp. 427–494). Elsevier. https://doi.org/10.1016/B978-0-12-417156-5.00011-3

Vega, F. E., Kramer, M., & Jaramillo, J. (2011). Increasing coffee berry borer (Coleoptera: Curculionidae: Scolytinae) female density in artificial diet decreases fecundity. *Journal of Economic Entomology*, *104*(1), 87–93. https://doi.org/10.1603/EC10353

Vega, F. E., Simpkins, A., Bauchan, G., Infante, F., Kramer, M., & Land, M. F. (2014). On the eyes of male coffee berry borers as rudimentary organs. *PloS One*, *9*(1), e85860. https://doi.org/10.1371/journal.pone.0085860

Vega, F. E., Simpkins, A., Bauchan, G., Valdéz-Carrasco, J. M., Castillo, A., & Infante, F. (2015). A mysterious wing spine in male coffee berry borers (Coleoptera: Curculionidae: Scolytinae). *Florida Entomologist*, *98*(1), 352–353. https://doi.org/10.1653/024.098.0155

Wasserthal, L. T., Cloetens, P., Fink, R. H., & Wasserthal, L. K. (2018). X-ray computed tomography study of the flight-adapted tracheal system in the blowfly *Calliphora vicina* , analysing the ventilation mechanism and flow-directing valves. *The Journal of Experimental Biology*, *221*(12), jeb176024. https://doi.org/10.1242/jeb.176024

Wigglesworth, V. B. (1930). A Theory of Tracheal Respiration in Insects. *Proceedings of the Royal Society B: Biological Sciences*, *106*(743), 229–250. https://doi.org/10.1098/rspb.1930.0024

Wigglesworth, V. B. (1942). *The Principles of Insect Physiology* (2nd ed.). Methuen & CO. LTD. ttps://archive.org/details/principlesofinse033321mbp/page/n7

Wintgens, J. N. (2004). *Coffee: Growing, Processing, Sustainable Production* (Jean Nicolas Wintgens (ed.)). Wiley. https://doi.org/10.1002/9783527619627

Wipfler, B., Pohl, H., Yavorskaya, M. I., & Beutel, R. G. (2016). A review of methods for analysing insect structures — the role of morphology in the age of phylogenomics. *Current Opinion in Insect Science*, *18*, 60–68. https://doi.org/10.1016/j.cois.2016.09.004

Wood, S. L. (1954). A revision of North American Cryphalini (Scolytidae: Coleoptera). *Univ. Kansas Sci. Bull*, *36*, 959–1089.

Ziska, L., Bradley, B., Wallace, R., Bargeron, C., LaForest, J., Choudhury, R., Garrett, K., & Vega, F. (2018). Climate change, carbon dioxide, and pest biology, managing the future: coffee as a case study. *Agronomy*, *8*(8), 152. https://doi.org/10.3390/agronomy8080152

Zunino, M. (2012). Cuarenta años de anatomía de las piezas genitales en la taxonomía de los escarabajos (Coleoptera : Scarabaeoidea): el estado del arte. *Dugesiana*, *18*(2), 197–206.

5.6.- "Desvelando el sistema respiratorio de la broca del café (*Hypothenemus hampei*; Coleoptera: Curculionidae: Scolytinae) mediante microtomografía computarizada"

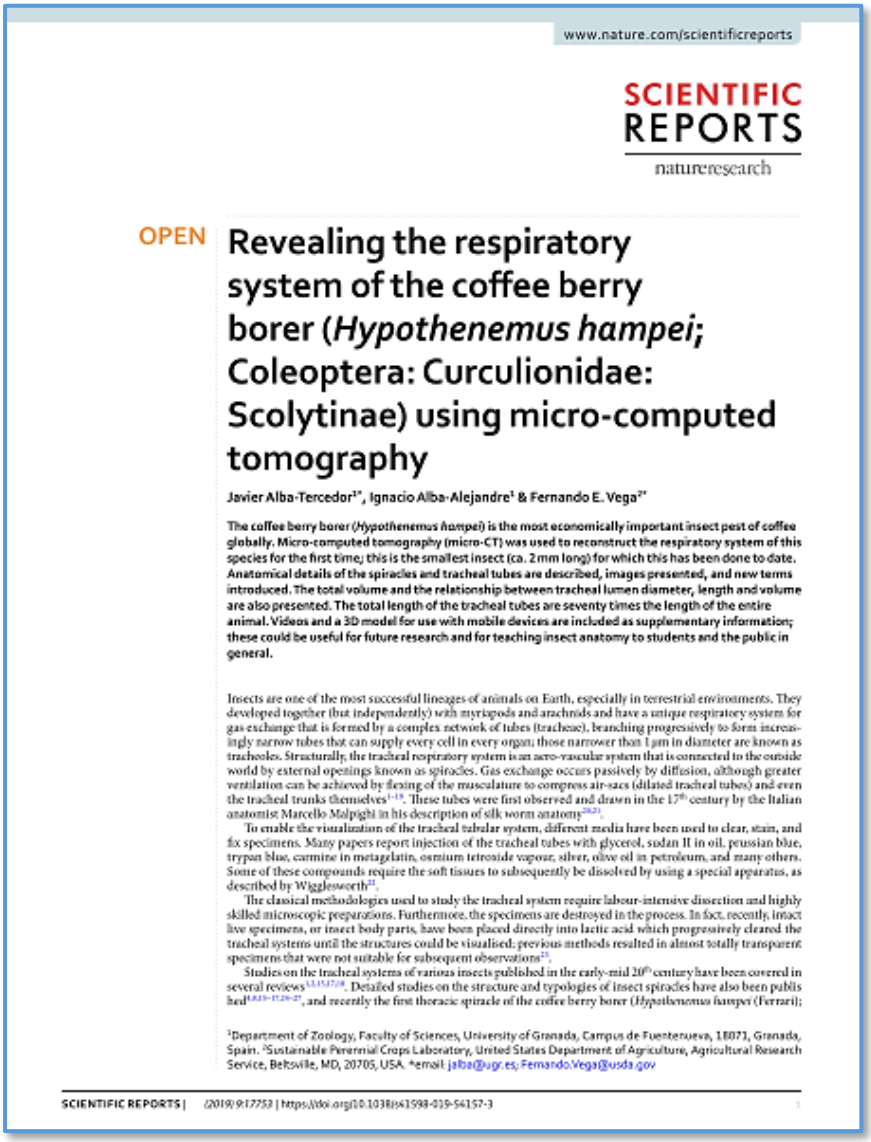

www.nature.com/scientificreports

SCIENTIFIC REPORTS
nature research

OPEN

Revealing the respiratory system of the coffee berry borer (*Hypothenemus hampei*; Coleoptera: Curculionidae: Scolytinae) using micro-computed tomography

Javier Alba-Tercedor[1*], Ignacio Alba-Alejandre[1] & Fernando E. Vega[2*]

The coffee berry borer (*Hypothenemus hampei*) is the most economically important insect pest of coffee globally. Micro-computed tomography (micro-CT) was used to reconstruct the respiratory system of this species for the first time; this is the smallest insect (ca. 2 mm long) for which this has been done to date. Anatomical details of the spiracles and tracheal tubes are described, images presented, and new terms introduced. The total volume and the relationship between tracheal lumen diameter, length and volume are also presented. The total length of the tracheal tubes are seventy times the length of the entire animal. Videos and a 3D model for use with mobile devices are included as supplementary information; these could be useful for future research and for teaching insect anatomy to students and the public in general.

Insects are one of the most successful lineages of animals on Earth, especially in terrestrial environments. They developed together (but independently) with myriapods and arachnids and have a unique respiratory system for gas exchange that is formed by a complex network of tubes (tracheae), branching progressively to form increasingly narrow tubes that can supply every cell in every organ; those narrower than 1 µm in diameter are known as tracheoles. Structurally, the tracheal respiratory system is an aero-vascular system that is connected to the outside world by external openings known as spiracles. Gas exchange occurs passively by diffusion, although greater ventilation can be achieved by flexing of the musculature to compress air-sacs (dilated tracheal tubes) and even the tracheal trunks themselves[1–19]. These tubes were first observed and drawn in the 17th century by the Italian anatomist Marcello Malpighi in his description of silk worm anatomy[20,21].

To enable the visualization of the tracheal tubular system, different media have been used to clear, stain, and fix specimens. Many papers report injection of the tracheal tubes with glycerol, sudan II in oil, prussian blue, trypan blue, carmine in metagelatin, osmium tetroxide vapour, silver, olive oil in petroleum, and many others. Some of these compounds require the soft tissues to subsequently be dissolved by using a special apparatus, as described by Wigglesworth[22].

The classical methodologies used to study the tracheal system require labour-intensive dissection and highly skilled microscopic preparations. Furthermore, the specimens are destroyed in the process. In fact, recently, intact live specimens, or insect body parts, have been placed directly into lactic acid which progressively cleared the tracheal systems until the structures could be visualised; previous methods resulted in almost totally transparent specimens that were not suitable for subsequent observations[23].

Studies on the tracheal systems of various insects published in the early-mid 20th century have been covered in several reviews[3,5,17,19]. Detailed studies on the structure and typologies of insect spiracles have also been published[3,8,13–17,24–27], and recently the first thoracic spiracle of the coffee berry borer (*Hypothenemus hampei* (Ferrari);

[1]Department of Zoology, Faculty of Sciences, University of Granada, Campus de Fuentenueva, 18071, Granada, Spain. [2]Sustainable Perennial Crops Laboratory, United States Department of Agriculture, Agricultural Research Service, Beltsville, MD, 20705, USA. *email: jalba@ugr.es; Fernando.Vega@usda.gov

Artículo publicado (bajo licencia de dominio público "Creative Commons CC0"):

Alba-Tercedor, J., **Alba-Alejandre, I.**, & Vega, F. E. (2019). Revealing the respiratory system of the coffee berry borer (*Hypothenemus hampei*; Coleoptera: Curculionidae: Scolytinae) using micro-computed tomography. *Scientific Reports*, 9(1), 17753: 1-17. https://doi.org/10.1038/s41598-019-54157-3

5.6.1.- Resumen

La broca del café (*Hypothenemus hampei*) es la plaga de insectos de café más importante económicamente a nivel mundial. Se utilizó la microtomografía computarizada (micro-CT) para reconstruir el sistema respiratorio de esta especie por primera vez; Este es el insecto más pequeño (aproximadamente 2 mm de largo) para el que se ha hecho hasta la fecha. Se describen detalles anatómicos de los espiráculos y los tubos traqueales, se presentan imágenes y se introducen nuevos términos. También se presentan el volumen total y la relación entre el diámetro, la longitud y el volumen de la luz traqueal. La longitud total de los tubos traqueales es setenta veces la longitud de todo el animal. Se incluyen videos y un modelo 3D para usar con dispositivos móviles como información complementaria; Estos podrían ser útiles para futuras investigaciones y para enseñar anatomía de insectos a estudiantes y al público en general.

5.6.2.- Abstract

The coffee berry borer (*Hypothenemus hampei*) is the most economically important insect pest of coffee globally. Micro-computed tomography (micro-CT) was used to reconstruct the respiratory system of this species for the first time; this is the smallest insect (ca. 2 mm long) for which this has been done to date. Anatomical details of the spiracles and tracheal tubes are described, images presented, and new terms introduced. The total volume and the relationship between tracheal lumen diameter, length and volume are also presented. The total length of the tracheal tubes are seventy times the length of the entire animal. Videos and a 3D model for use with mobile devices are included as supplementary information; these could be useful for future research and for teaching insect anatomy to students and the public in general.

5.6.3.- Introduction

Insects are one of the most successful lineages of animals on Earth, especially in terrestrial environments. They developed together (but independently) with myriapods and arachnids and have a unique respiratory system for gas exchange

that is formed by a complex network of tubes (tracheae), branching progressively to form increasingly narrow tubes that can supply every cell in every organ; those narrower than 1 µm in diameter are known as tracheoles. Structurally, the tracheal respiratory system is an aero-vascular system that is connected to the outside world by external openings known as spiracles. Gas exchange occurs passively by diffusion, although greater ventilation can be achieved by flexing of the musculature to compress air-sacs (dilated tracheal tubes) and even the tracheal trunks themselves (Boué & Chanton, 1962; Bradley *et al.*, 2009; Chapman, 2013; Crowson, 1981; Gillott, 2005; Grassé, 1976; Harrison, 2009; Klowden, 2007; Nation, 2002; Raś *et al.*, 2018; Richards & Davies, 1977; Snodgrass, 1935; Tonapi, 1978; Wasserthal *et al.*, 2018; Waters *et al.*, 2013; Weis-Fogh, 1964, 1967; Westneat, 2003; Wigglesworth, 1942). These tubes were first observed and drawn in the 17th century by the Italian anatomist Marcello Malpighi in his description of silk worm anatomy (Cobb, 2002; Malpighi, 1669).

To enable the visualization of the tracheal tubular system, different media have been used to clear, stain, and fix specimens. Many papers report injection of the tracheal tubes with glycerol, sudan II in oil, prussian blue, trypan blue, carmine in metagelatin, osmium tetroxide vapour, silver, olive oil in petroleum, and many others. Some of these compounds require the soft tissues to subsequently be dissolved by using a special apparatus, as described by Wigglesworth (Wigglesworth, 1950).

The classical methodologies used to study the tracheal system require labour-intensive dissection and highly skilled microscopic preparations. Furthermore, the specimens are destroyed in the process. In fact, recently, intact live specimens, or insect body parts, have been placed directly into lactic acid which progressively cleared the tracheal systems until the structures could be visualised; previous methods resulted in almost totally transparent specimens that were not suitable for subsequent observations (Ruan *et al.*, 2018).

Studies on the tracheal systems of various insects published in the early-mid 20th century have been covered in several reviews (Crowson, 1981; Grassé, 1976; Richards & Davies, 1977; Snodgrass, 1935; Wigglesworth, 1942). Detailed

studies on the structure and typologies of insect spiracles have also been published (Chapman, 2013; Gillott, 2005; Grassé, 1976; Hassan, 1944; Mbata, 1985; Richards & Davies, 1977; Robertson, 1962; Schmitz & Wasserthal, 1999; Tonapi, 1978), and recently the first thoracic spiracle of the coffee berry borer (*Hypothenemus hampei* (Ferrari); Coleoptera: Curculionidae: Scolytinae) was described (Vega, Bauchan, *et al.*, 2015). A few studies on the coleopteran tracheal system have been conducted using classical methods (i.e., staining and/or dissection) (Hafeez & Gardiner, 1964; Loudon, 1989; Robertson, 1962; Tonapi, 1978). X-ray techniques were valuable in demonstrating forced respiration in beetles by compressive movements of the tracheal tubes (Kaiser *et al.*, 2007; Waters *et al.*, 2013; Westneat, 2003), and also in quantifying aspects of tracheal hypermetry in grasshoppers (Greenlee *et al.*, 2009). Most recently, micro-computed tomography (micro-CT) has become the most important non-destructive technique useful in revealing important anatomical insights on the complex anatomy of tracheal tubular systems in Diptera (Ha *et al.*, 2017; Wasserthal *et al.*, 2018), Orthoptera (Greco *et al.*, 2014; Shaha *et al.*, 2013), Coleoptera (Iwan *et al.*, 2015; Poinapen *et al.*, 2017; Raś *et al.*, 2018) and non-insect arthropods such as camel spiders (Solifugae) (Franz-Guess *et al.*, 2016).

The coffee berry borer is the most devastating insect pest of coffee globally and poses a threat to coffee production due to its cryptic life habit inside the coffee berry, which makes it difficult to manage (Vega, Infante, *et al.*, 2015). We have used modern micro-CT techniques to study this species and revealed various aspects of its biology inside coffee berries (Alba-Alejandre *et al.*, 2018), and the internal anatomy in adults (Alba-Alejandre *et al.*, 2019). In this paper, we present results from a detailed anatomical study of the tubular respiratory system of the coffee berry borer, including its spiracles. The majority of the study relies on micro-CT although additional light microscopic images are included.

5.6.4.- Materials and Methods

Insects. For a previous paper in which we first observed the coffee berry borer inside the coffee berry (Alba-Alejandre *et al.*, 2018), J.A.T. collected coffee berries (*Coffea canephora* Pierre ex. A. Froehner; Rubiaceae) at a coffee

plantation in Vietnam (Me Linh Coffee Garden; 11°53′57.39″N, 108°20′51.16″E; 1043 m.a.s.l.). From this collection, an adult female emerged and was used for the micro-CT study.

Micro-CT scans. The insect was killed by keeping it for 30 min inside a closed plastic container with a piece of cotton impregnated with a few drops of ethyl acetate. It was then glued, using cyanoacrylate, to the tip of a nylon fishing line 200 µm in diameter, as previously described (Alba-Tercedor, 2014), and immediately scanned using a Bruker SkyScan 1172 microtomograph (Bruker-micro CT, Kontich, Belgium) with a Hamamatsu L702 X-ray source and a Ximea 11 megapixels camera. The setting parameters were as follows: voltage = 45 kV; current = 45 µA; isotropic voxel size = 1 µm; image rotation step = 0.3°; 360° of rotation scan with no filter. This resulted in a scan duration of 2 h:11 min:39 s, and 1202 X-ray images. The specimen was air-dried, stored and 14 months later it was scanned again to compare the dry preserved internal anatomical structures of the tracheal system (Supplementary Video S4) with the original images from 'fresh' material. For this latter scan the setting parameters were the same as the first scan except that it was performed with an 180° rotation scan, resulting in a scan duration of 1 h:10 min:33 s, and 642 X-ray images.

Image reconstruction. The most recent versions of the Bruker Micro-CT's Skyscan software (NRecon, DataViewer, CTAnalyser) were used for primary reconstructions and the 'cleaning' process to obtain datasets on 'slices' through the insect as described previously (Alba-Tercedor, 2014). Amira's software, v. 6.7.0 (Thermo Fisher Scientific, Waltham, MA) (Stalling *et al.*, 2005; Thermo Fisher Scientific, 2017) (with the built-in "volrenRed.col" colour filter) was used to obtain volume-rendered images (Figs. 3–5A and 9D; Supplementary Video S4).

To achieve a clean image dataset for the tracheal tubes we modified an existing methodology (Iwan *et al.*, 2015). Briefly, it consisted of scanning the insect immediately after killing it. In insects, the haemolymph fills the internal cavities and it has a similar transparency to the internal structures when viewed by X-ray. Thereafter, whereas the reconstructed image slices hardly showed the internal structures, the empty spaces that were full of gas (such as the interior of the tracheal tubes) were clearly visible. Thus, the process allowed us to

reconstruct these spaces by inverting images from negative to positive and cleaning away the superfluous non-tracheal spaces, to obtain images that contained only the lumen of the tracheae (as described step-by-step in the Supplementary Methods). During the process, the internal spaces in the elytra and hindwing venations were eliminated to facilitate visualisation.

Colour-coded images were created using the 3D analysis plug-in in the CTAnalyser's customised processing tab and saved to determine structure thickness (or separation) as done previously (Alba-Tercedor *et al.*, 2016) and as described in a Bruker microCT method note (Bruker-microCT, 2013). We used CTvox (Bruker' micro-CT's Skyscan software) to obtain images for Fig. 5B,C and the final rendered images, videos and 3D model for mobile devices, with colour code representations of the lumen diameter of the tracheae (Figs. 6–9; Supplementary Videos S1–S3; Supplementary 3D model S5).

Reconstructed images of the two scans (earlier for the tracheal tubular system, and months later for the internal structures) were co-registered with the software DataViewer following the procedure described in a Bruker microCT method note (Bruker-microCT, 2014).

By running the 3D analysis plug-in (in the customised processing tab) of the CTAnalyser software, we could calculate the total volume of the tracheal tubes, as well the ranges according to the lumen diameter (or thickness). Using extrapolation we considered the tracheal tubes as cylinders and from the total calculated volume of each range and thickness it was possible to estimate their length (length = volume/(π(1/2 thickness)^2); adding the calculated lengths for each range we could estimate the total length of all the tracheal tubes in the system (Fig. 10).

Light microscopy study. To study the position and structure of spiracles under light microscopy, a female adult was progressively cleared by submerging it in a 10% KOH water dilution at room temperature. We examined and photographed the coffee berry borer after immersion for 24 h (Fig. 1A) and 48 h (Fig. 1B). Immediately after that, the insect was dissected, and the dorsal (Fig. 2C) and ventral (Fig. 2D) parts of the thorax and abdomen were dissected and mounted on a slide in modified Hoyer's liquid media (Alba-Tercedor, 2004). The position

and structure of the spiracles in Figs. 1 and 2 were obtained using a Samsung Note 8 smartphone connected to the ocular of a Motic SMZ-168 stereo zoom microscope (Fig. 1A [except a], 1B) and to an Olympus CH-2 binocular microscope (Figs. 1Aa,C and 2).

5.6.5.- Results

The external appearance of an adult female coffee berry borer with details of the spiracles obtained using light microscopy is shown in Figs. 1 and 2. As a result of the transparency achieved, in lateral view it is possible to observe a detail of the proventriculus and the mesothoracic spiracle (MsSP; Fig. 1) with two spiracular openings (SpO), and a detail of the fifth abdominal spiracle (Fig. 1Ab) in which dilatations of the lumina of the tracheal tubes can be distinguished as they converge on the spiracle. A lateral view of the thorax (hind part of the pro-thorax, mesothorax, and metathorax), abdomen, location of the metathoracic (MtSp) and abdominal spiracles, abdominal tergites (t1–t7) and sternites (s1–s5) are shown in Fig. 1B.

Details of the five abdominal spiracles (ASp1–ASp5) in their natural position prior to mounting are visible in Fig. 1C, including the spiracle opening (SpO), atrium (Atr), and the elastic bar of the closing apparatus (ClA). Details of the spiracles, including slide-mounted dorsal and ventral segments are shown in Fig. 2. The mesothoracic spiracle in apical view (focused internally with the peritreme) and the two external spiracular openings can be seen in Fig. 2Aa, while the apically focused anterior spiracular opening, and the anterior and posterior lips of the atrium are visible in Fig. 2Ab. The lateral view can be seen in Fig. 2Ac. The spiracular openings and the lips are densely covered with setae (Fig. 2Ab,c). Figure 2B shows the abdominal spiracles, particularly the spiracular openings (SpO), the peritreme (Pe), and the elastic bar of the closing apparatus (ClA). The

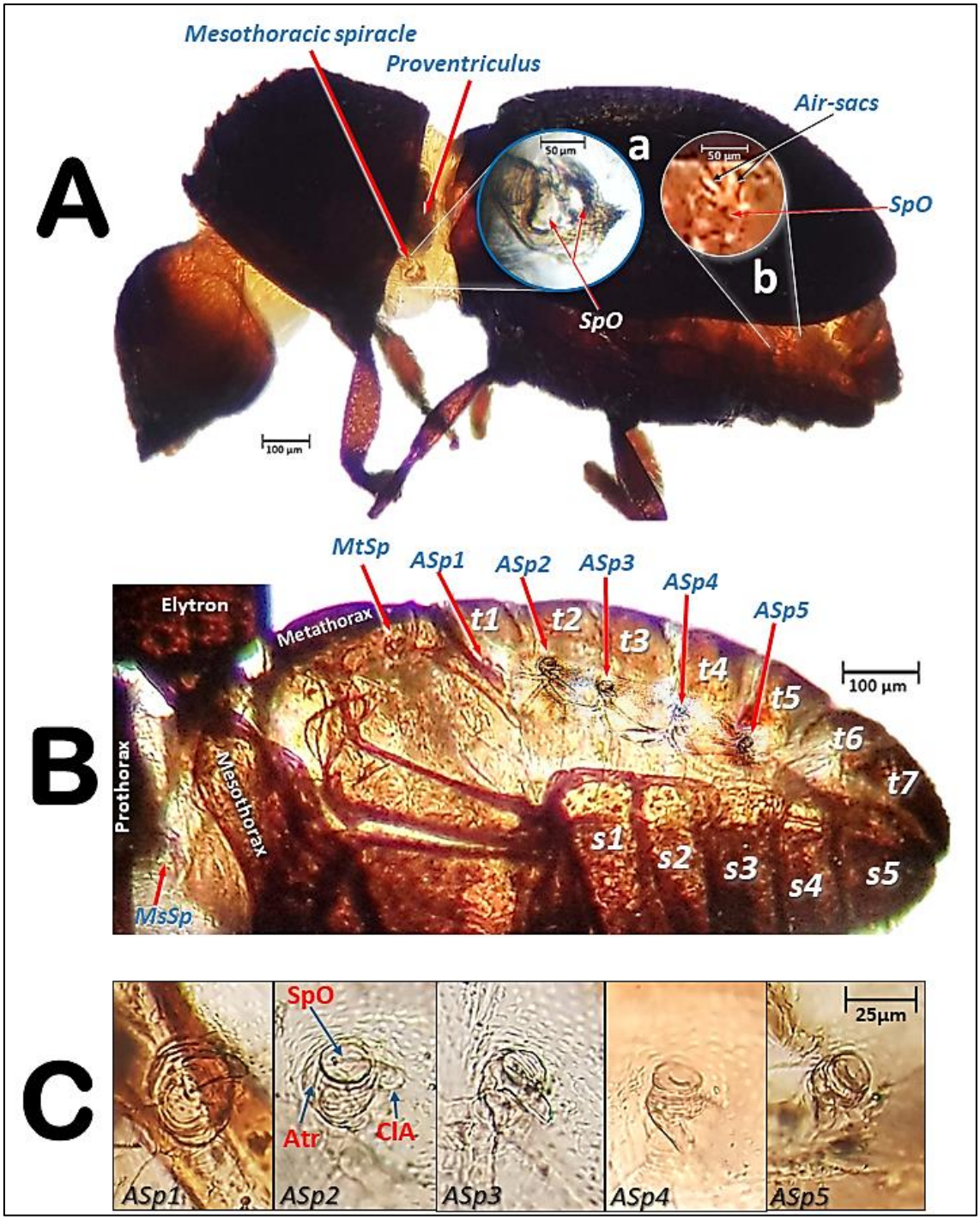

Figure 1.- Lateral view of an adult female coffee berry borer under a stereoscope (**A**, except **A**: a), and under light microscopy (**A**: a; **B**; **C**) after immersion in 10% KOH for 24 (**B**) and 48 h (**C**). Details of the mesothoracic (**A**: a) and 5th abdominal spiracle (**A**: b). Abbreviations: ASp = abdominal spiracle; Atr = spiracular atrium; ClA = elastic bar of the closing apparatus; MsSp = mesothoracic spiracle; MtSp = metathoracic spiracle; s = sternite; SpO = spiracular opening; t = tergite.

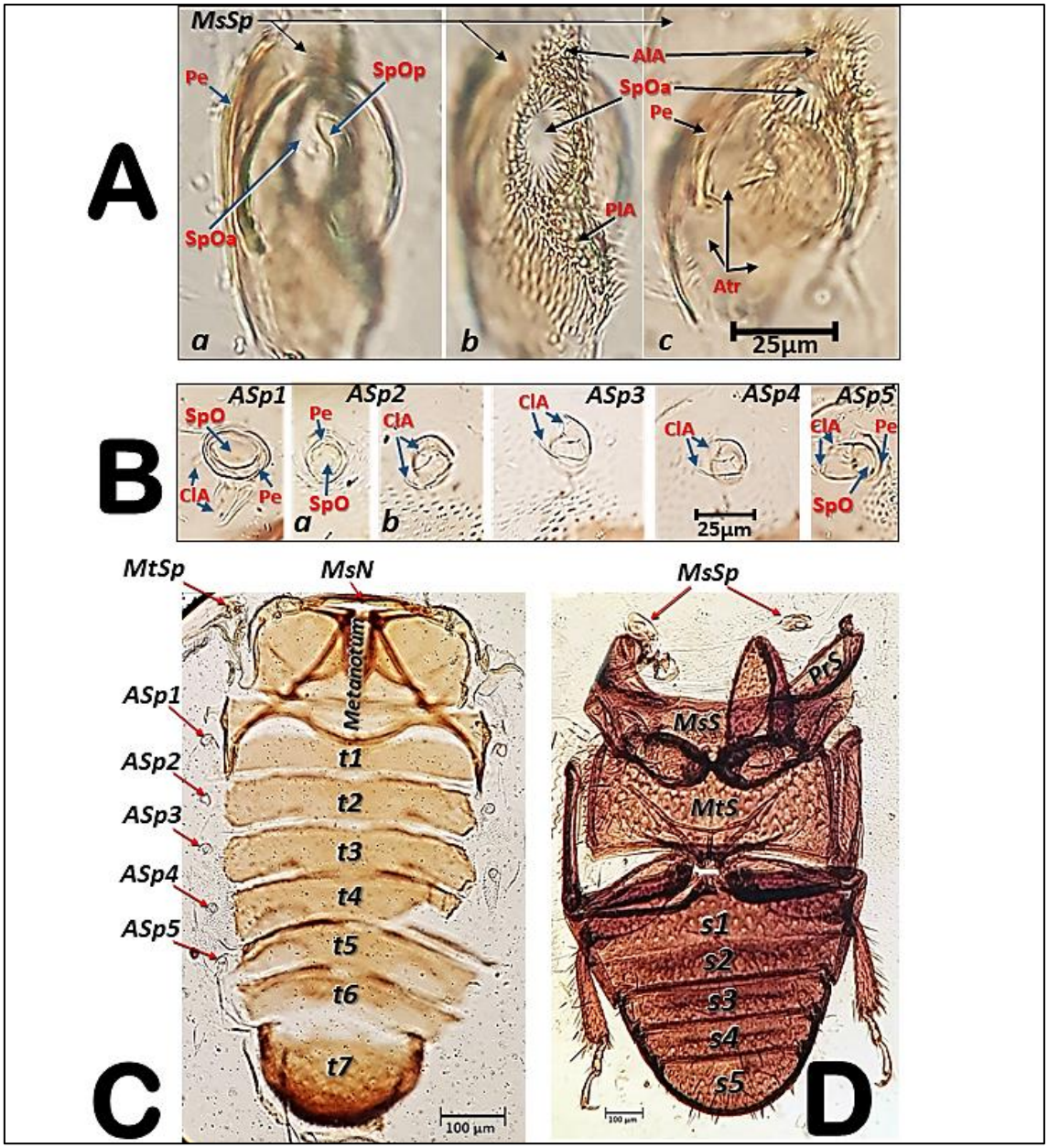

Figure 2.- Light microscopy images of a slide preparation of an adult female coffee berry borer after clarifying in KOH for 48 h and mounting in Hoyer's medium, showing details of the spiracles (**A,B**), with dorsal (**C**) and ventral (**D**) sections separately mounted. Abbreviations: AlA = anterior lip of atrium; ASp = abdominal spiracle (ASp2, in external (a) and internal (b) focused views); Atr = spiracular atrium; ClA = elastic bar of the closing apparatus; MsN = mesonotum; MsSp = mesothoracic spiracle (a: apical inner view; b: apico-external view; c: lateral view); MtSp = metathoracic spiracle; MsS = mesosternite; MtS = metasternite; Pe = peritreme; PlA = posterior lip of atrium; PrS = prosternum; s = sternite; SpOa = anterior spiracular opening; SpOp = posterior spiracular opening; t = tergite.

second abdominal spiracle is shown in detail in an externally focused image of the spiracular opening (SpO) and the peritreme (Pe) sclerite that surrounds it (Fig. 2Ba). The images of the third, fourth, and fifth abdominal spiracles (ASp3-ASp5; Fig. 2B) are internally focused to see the elastic bar of the closing apparatus (ClA). Figure 2C shows the dorsum of a female coffee berry borer with the location of a mesothoracic spiracle (MsSp), metathoracic spiracle (MtSp), the mesonotum (MsN), metanotum (MtN), seven tergites (t1-t7), and five abdominal spiracles (ASp1-ASp5). Figure 2D presents a ventral view with the two prothoracic spiracles (PtSp), mesosternum (MsS), metasternum (MtS), and five sternites (S1-S5).

Figures 6–9 show the complexity of the tubular tracheal respiratory system, viewed from different perspectives. It is important to note that many different, non-repeated angles were chosen in order to observe the positioning of the entire system. The left and right (Fig. 6B) halves are visible in sagittal cuts (Fig. 6), complemented by a left-lateral and a left dorso-ventral view (Fig. 7), and left-lateral, dorsal, and ventral views in Fig. 8. Figure 9 shows close-up views of the tracheal tubes (from the head to the anterior part of the mesothorax) in a left-frontal view (Fig. 9A) and a frontal view (Fig. 9B, and a close-up detail in Fig. 9C). A fronto-posterior view shows the elliptically shaped lumina of the tracheal trunks (Fig. 9D). The left half of a latero-frontal view of the posterior prothorax, mesothorax and anterior metathorax can be seen in Fig. 9E.

The morphological terminology used is summarized in Table 1 and where applicable we cite references that have used each term previously, other terms used with references, and new terms that we have introduced.

Videos are included as Supplementary information (Supplementary Videos S1–S4) and show 3D volume-rendered animations with details of: the complex web of tracheal tubes (Supplementary Videos S1–S3); relationships with the internal anatomy (Supplementary Video S1); the tracheal tubes and their connections to the spiracles (Supplementary Video S3); and a detail of the metathoracic spiracle and the connecting tracheal tubes (Supplementary Video S4).

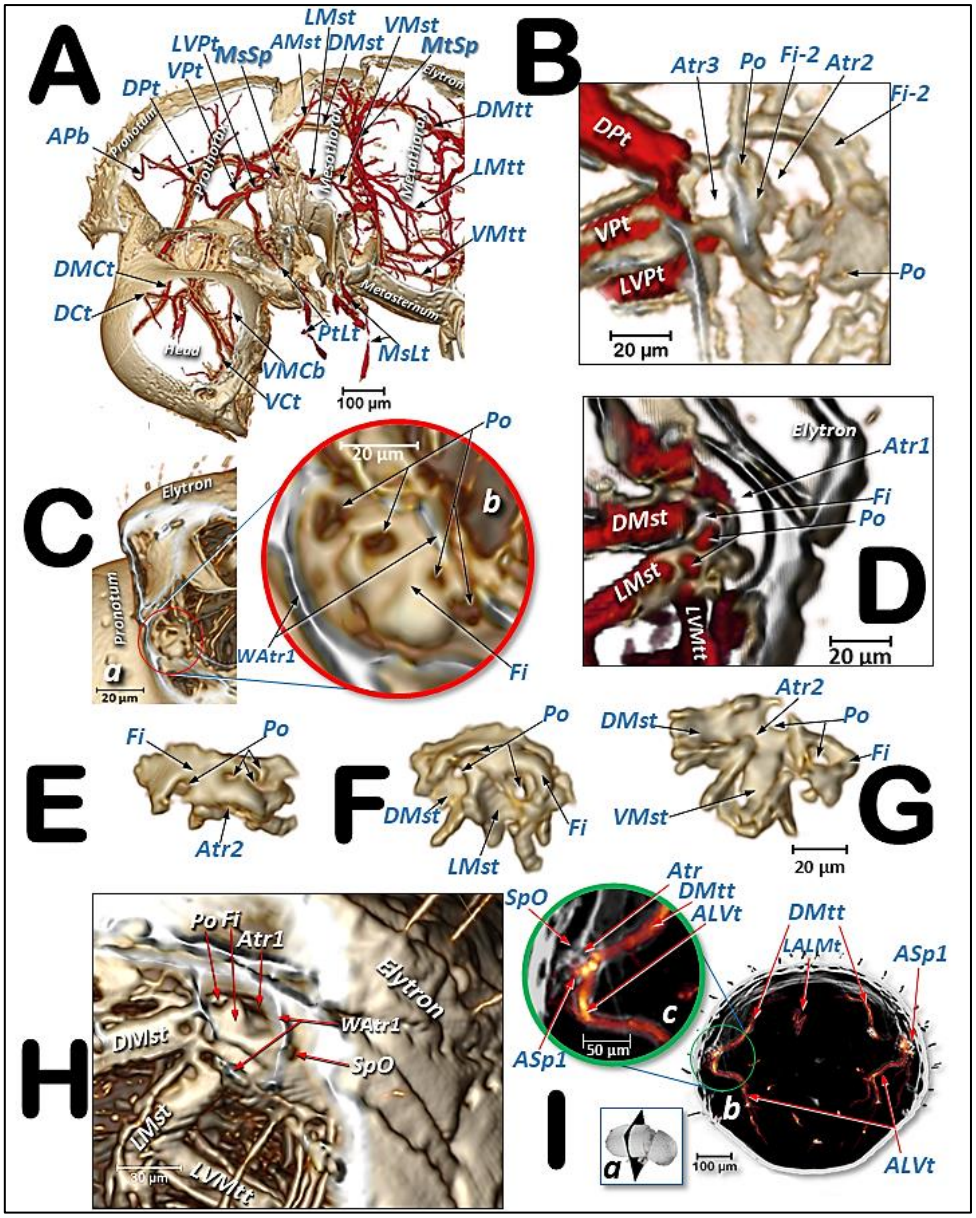

Figure 3.- Volume-rendered images showing the location (**A**) and detailed structures (**B**–**I**) of the spiracles in relation to the tubular tracheal system. Left-sagittal slice section of the head and thorax (**A**); left-lateral slice section of the prothoracic spiracle (**B**); dorso-ventral-oblique left-lateral cut of the body to show the mesothoracic spiracle (**C**, a: in a general view; **b**: detail of the second atrial cavity opened to show the cribellated filtering structure); left-antero-posterior slice section of the mesothoracic spiracle (**D**); details of the filter in different perspectives and with the first spiracular atrium cavity sectioned, in dorso-ventral view and with two progressive rotations to provide a ventro-dorsal view (**E**–**G**); left antero-posterior cut view of the metathoracic spiracle (**H**); and Amira's multiplanar slice section of the abdomen at the level of the first abdominal spiracle (**I**: a: position of the slice section; b: 60 µm thick slice, and c: detail of the right first abdominal spiracle). Abbreviations: ALVt = abdominal latero-ventral trunk; AMst = arc-shaped mesothoracic trunk; ASp = abdominal spiracle; Atr = spiracular atrium; DCt = dorsal cephalic trunk; DMCt = dorsal median cephalic trachea; DMst = dorsal mesothoracic trunk; DMtt = dorsal metathoracic trunk; DPt = dorsal prothoracic trunk; Fi = filter; APb = anterior prothoracic twisted branch; LALMt = long abdominal latero-median tracheae; LMst = lateral mesothoracic trunk; LMtt = lateral metathoracic trunk; LVPt = latero-ventral prothoracic trunk; MsLt = mesothoracic leg trunk; MsSp = mesothoracic spiracle; MtSp = metathoracic spiracle; Po = porus; PtLt = prothoracic leg trunk; SpO = spiracular opening; VCt = ventral cephalic trunk; VMCb = ventral median cephalic branch; VMst = ventral mesothoracic trunk; VMtt = ventral metathoracic trunk; VPt = ventral prothoracic trunk; WAtr = atrial wall.

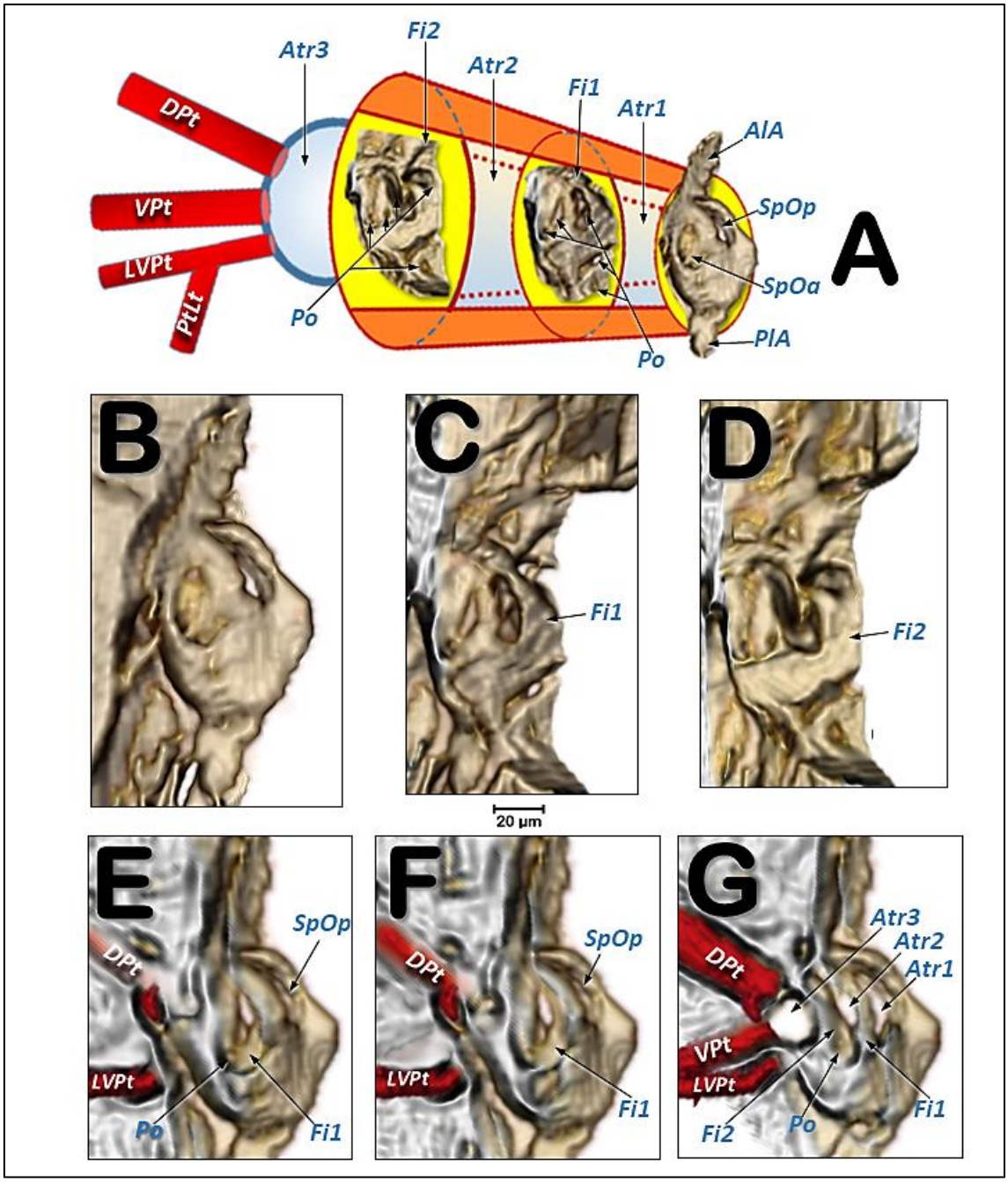

Figure 4.- Volume rendered images of the mesothoracic spiracle (**A**–**G**). Schematic elongated reconstruction (**A**), external left-latero posterior view (**B**), successive virtual erosion of the external wall to show the second filter (**C**), and underneath it the first filter (**D**). Progressive virtual cuts of the left-latero posterior view shown in B, showing the tracheal tubes, atrial cavities, and filters (**E**–**G**). Abbreviations: AlA = anterior lip of atrium; Atr = spiracular atrium; DPt = dorsal prothoracic trunk; Fi = filter; LVPt = latero-ventral prothoracic trunk; Po = porus (opening); PlA = posterior lip of atrium; PtLt = prothoracic leg trunk; SpOa = anterior spiracle opening; SpOp = posterior spiracle opening; VPt = ventral prothoracic trunk.

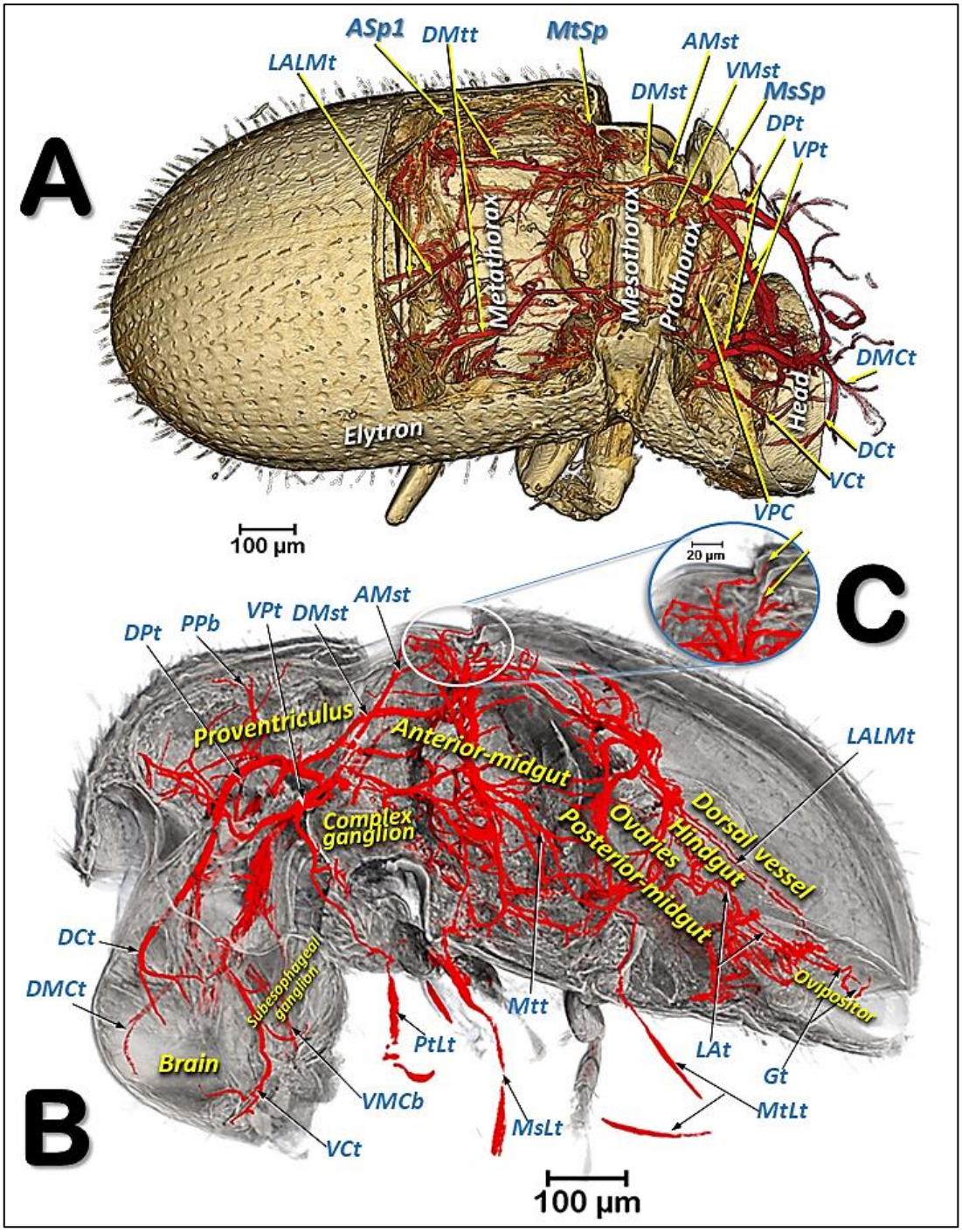

Figure 5.- Volume-rendered images of a right dorso-lateral view where the body wall has been opened with software to show the positions of the tracheal tubes and spiracles (**A**) with a sagittal section showing the tracheal system and the position of the main internal structures (**B**), and a close-up view of the site where the tracheal tubes supply the elytron and hindwing, marked with arrows (**C**). Abbreviations: AMst = arc-shaped mesothoracic trunk; ASp = abdominal spiracle; DCt = dorsal cephalic trunk; DMCt = dorsal median cephalic trachea; DMst = dorsal mesothoracic trunk; DMtt = dorsal metathoracic trunk; DPt = dorsal prothoracic trunk; Gt = genital tracheae; LALMt = long abdominal latero-median tracheae; LAt = latero-abdominal tracheae; MsLt = mesothoracic leg trunk; MsSp = mesothoracic spiracle, MtLt = metathoracic leg trunk; MtSp = metathoracic spiracle; Mtt = metathoracic trunk; PtLt = prothoracic leg trunk; PPb = posterior prothoracic branch; VCt = ventral cephalic trunk; VMCb = ventral median cephalic branch; VMst = ventral mesothoracic trunk; VPC = ventral prothoracic commissure; VPt = ventral prothoracic trunk.

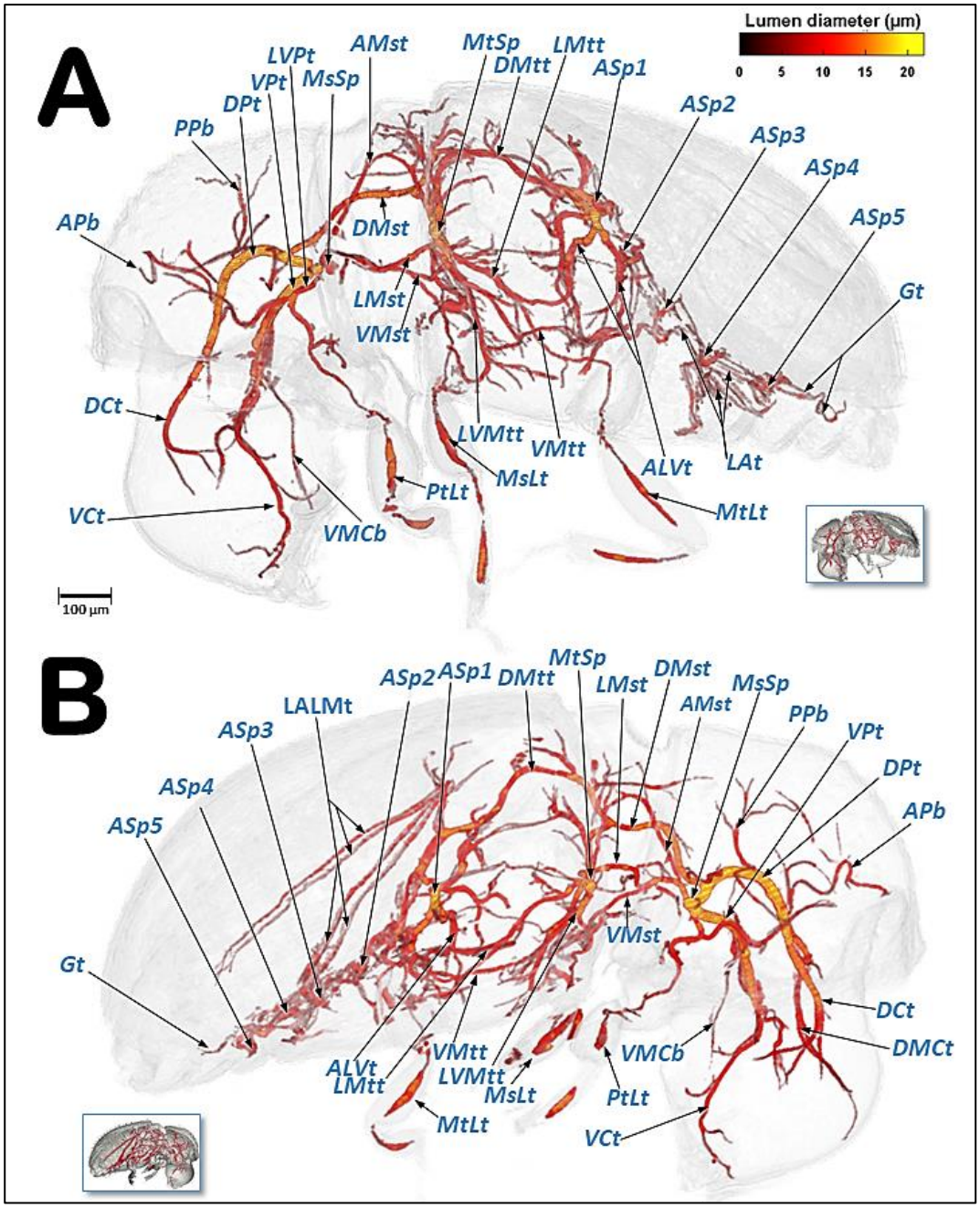

Figure 6.- Volume-rendered images of the left (**A**) and right (**B**) lateral views of the tracheal system (the body has been made transparent). The insets correspond to volume-rendered images of the actual body position. Abbreviations: ALVt = abdominal latero-ventral trunk; AMst = arc-shaped mesothoracic trunk; APb = anterior prothoracic twisted branch; ASp = abdominal spiracle; DCt = dorsal cephalic trunk; DMCt = dorsal median cephalic tracheae; DMst = dorsal mesothoracic trunk; DMtt = dorsal metathoracic trunk; DPt = dorsal prothoracic trunk; Gt = genital tracheae; LALMt = long abdominal latero-median tracheae; LAt = latero- abdominal tracheae; LMst = lateral mesothoracic trunk; LMtt = lateral metathoracic trunk; LVMtt = latero- ventral metathoracic trunk; LVPt = latero-ventral prothoracic trunk; MsLt = mesothoracic leg trunk; MtLt = metathoracic leg trunk; MsSp = mesothoracic spiracle; MtSp = metathoracic spiracle; PPb = posterior prothoracic branch; PtLt = prothoracic leg trunk; VCt = ventral cephalic trunk; VMCb = ventral median cephalic branch; VMst = ventral mesothoracic trunk; VMtt = ventral metathoracic trunk; VPt = ventral prothoracic trunk. Lumen diameter is in accordance with the color scale of the bar shown on the upper right.

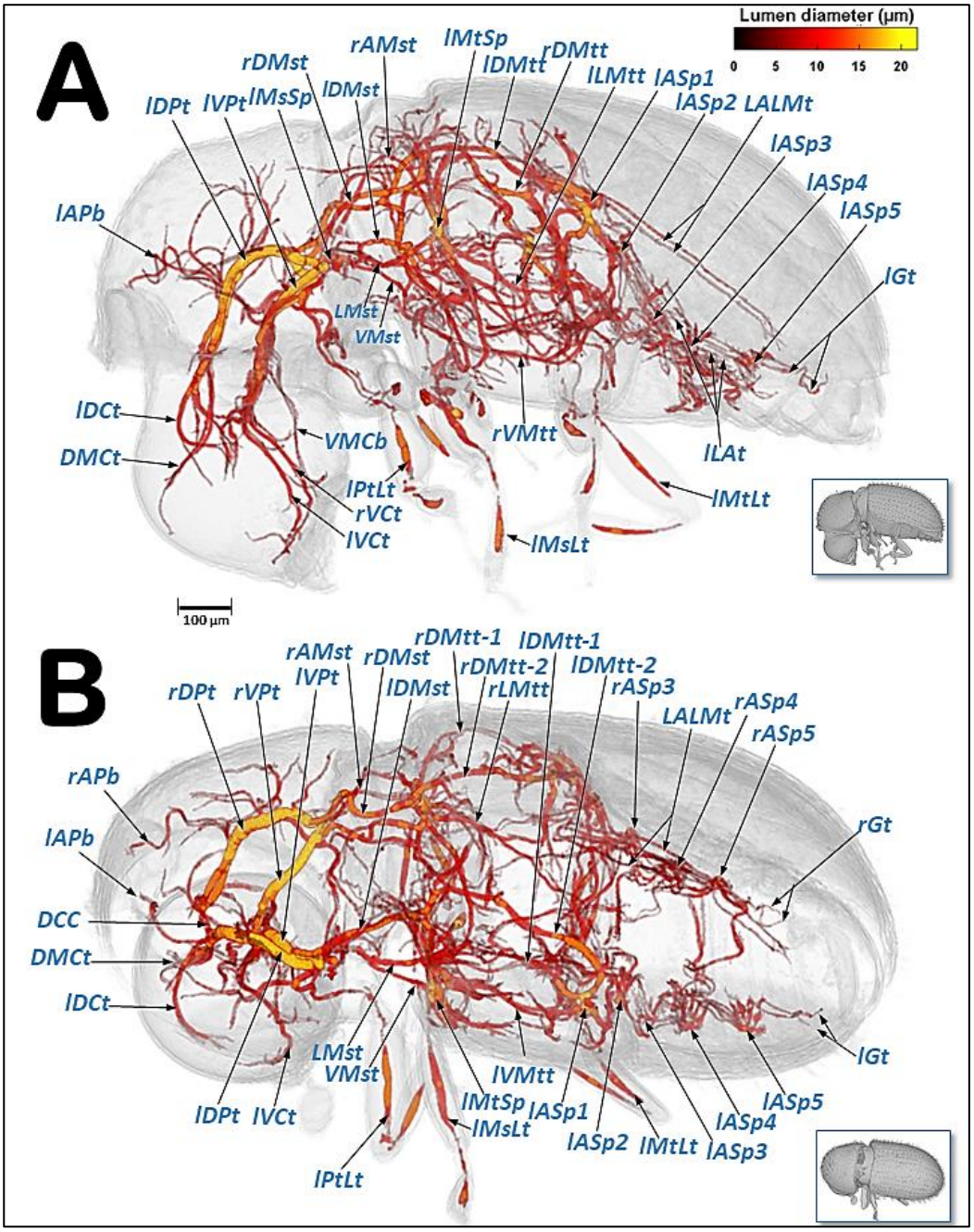

Figure 7.- Volume-rendered images of the tracheal system in a left-lateral (**A**) and a left dorso-ventral view (**B**). The insets correspond to volume-rendered images of the actual body position. Abbreviations: AMst = arc-shaped mesothoracic trunk; APb = anterior prothoracic twisted branch; ASp = abdominal spiracle; DCC = dorsal cephalic commissure; DCt = dorsal cephalic trunk; DMCt = dorsal median cephalic tracheae; DMst = dorsal mesothoracic trunk; DMtt = dorsal metathoracic trunk; DPt = dorsal prothoracic trunk; Gt = genital tracheae; LALMt = long abdominal latero-median tracheae; LAt = latero-abdominal tracheae; LMst = lateral mesothoracic trunk; LMtt = lateral metathoracic trunk; MsLt = mesothoracic leg trunk; MtLt = metathoracic leg trunk; MsSp = mesothoracic spiracle; MtSp = metathoracic spiracle; PtLt = prothoracic leg trunk; VCt = ventral cephalic trunk; VMCb = ventral median cephalic branch; VMst = ventral mesothoracic trunk; VMtt = ventral metathoracic trunk; VPt = ventral prothoracic trunk. Right and left sides are marked with 'r' or 'l', respectively, at the beginning of each label lettering. Lumen diameter is in accordance with the color scale of the bar shown on the upper right.

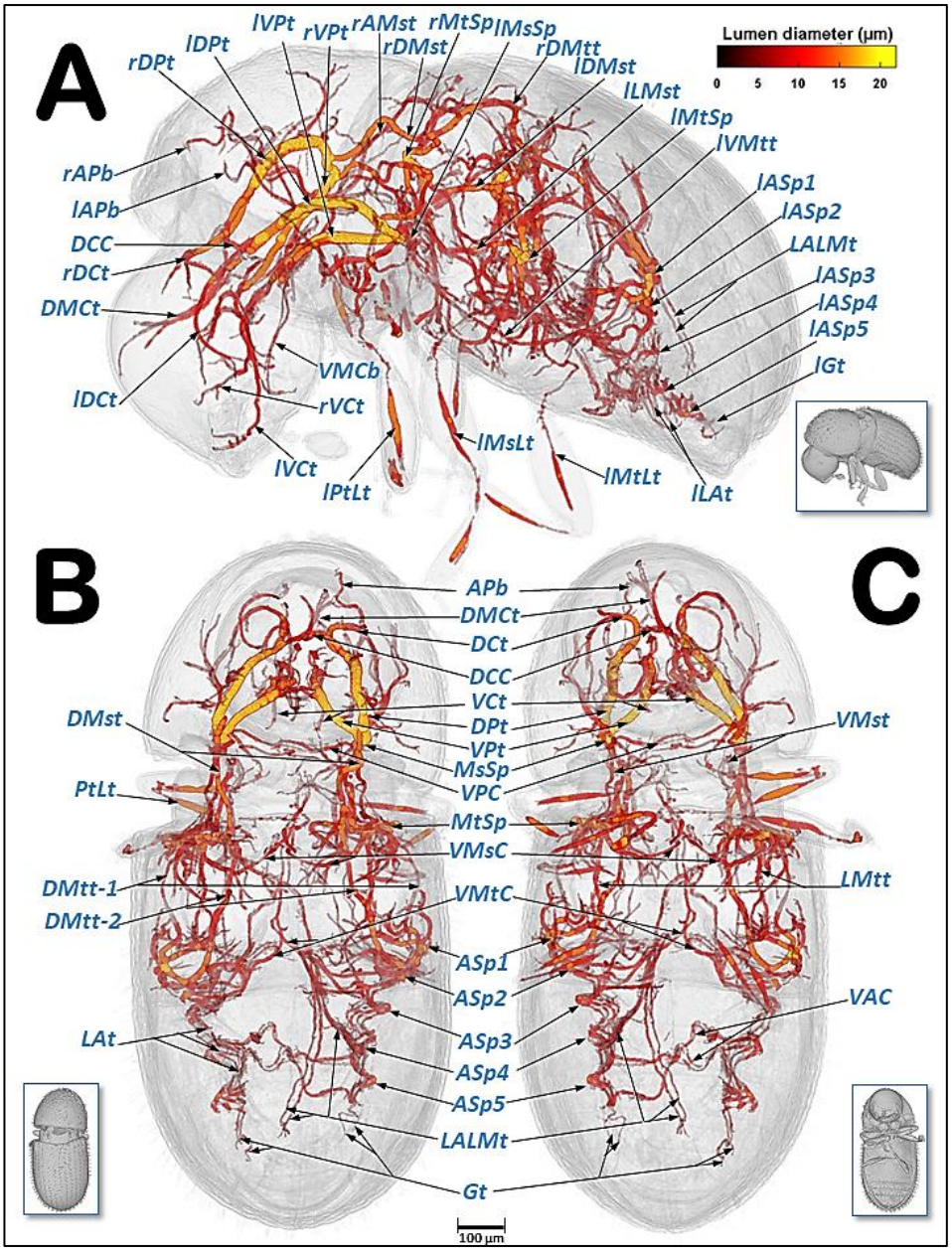

Figure 8.- Volume-rendered images of the tracheal system in a left-lateral (**A**), dorsal (**B**), and ventral (**C**) view. The insets correspond to volume-rendered images of the actual body position. Abbreviations: AMst = arc-shaped mesothoracic trunk; APb = anterior prothoracic twisted branch; ASp = abdominal spiracle; DCC = dorsal cephalic commissure; DCt = dorsal cephalic trunk; DMCt = dorsal median cephalic tracheae; DMst = dorsal mesothoracic trunk; DMtt = dorsal metathoracic trunk; DMtt-1 = lateral branch of the dorsal metathoracic trunk; DMtt-2 = medial branch of the dorsal metathoracic trunk; DPt = dorsal prothoracic trunk; Gt = genital tracheae; LALMt = long abdominal latero-median tracheae; LAt = latero-abdominal tracheae; LMtt = lateral metathoracic trunk; MsLt = mesothoracic leg trunk; MsSp = mesothoracic spiracle; MtLt = metathoracic leg trunk; MtSp = metathoracic spiracle; PtLt = prothoracic leg trunk; VAC = ventral abdominal commissures; VCt = ventral cephalic trunk; VMCb = ventral median cephalic branch; VMsC = ventral mesothoracic commissure; VMtC = ventral metathoracic commissure; VMtt = ventral metathoracic trunk; VPC = ventral prothoracic commissure; VPt = ventral prothoracic trunk. Right and left sides are marked with ‘r’ or ‘l’, respectively, at the beginning of each label lettering. Lumen diameter is in accordance with the color scale of the bar shown on the upper right.

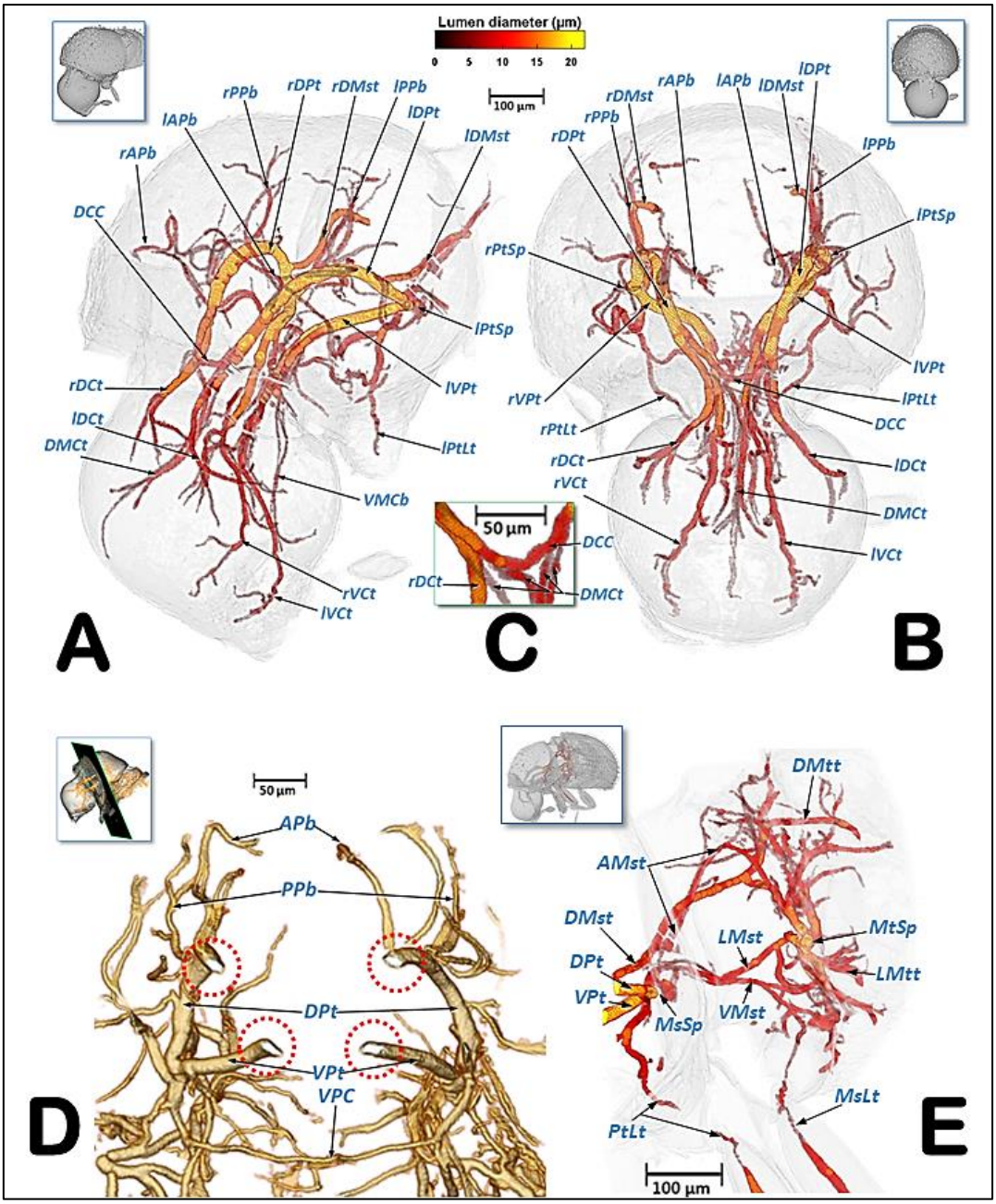

Figure 9.- Volume-rendered images of the cephalic and prothoracic tracheal system in a left-fronto-lateral (**A**), frontal (**B**), and fronto-posterior (**D**, dotted red circles show the elliptic-shaped collapsible lumina of the tracheal trunks) view. Detail close-up of the dorsal cephalic commissure and the dorsal median cephalic tracheae (**C**), the left half of a latero-frontal view of the posterior prothorax, mesothorax and the anterior metathorax (**E**). The insets in (**A**,**B**,**E**), correspond to volume-rendered images of the actual body position, and the one in (**D**) shows the position of the cut. Abbreviations: AMst = arc-shaped mesothoracic trunk; APb = anterior prothoracic twisted branch; DCC = dorsal cephalic commissure; DCt = dorsal cephalic trunk; DMCt = dorsal median cephalic tracheae; DMtt = dorsal metathoracic trunk; DPt = dorsal prothoracic trunk; LMSt = lateral mesothoracic trunk; LMtt = lateral metathoracic trunk; MsSp = mesothoracic spiracle; MtSp = metatoracic spiracle; PPb = posterior prothoracic branch; PtLt = prothoracic leg trunk; VCt = ventral cephalic trunk; VMCb = ventral median cephalic branch; VMst = ventral mesothoracic trunk; VPC = ventral prothoracic commissure; VPt = ventral prothoracic trunk. Right and left sides are marked with 'r' or 'l', respectively, at the beginning of each label lettering. Lumen diameter of (**A**,**B**,**E**) are in accordance with the color scale of the bar shown at the top.

The lumina of the tracheae are shown in Figs. 6–9 and in Supplementary Videos S1– S3, with a colour gradation code, in accordance with their actual lumen diameter range (1.99–21.93 µm). Lumen size distribution ranges of the tracheal tubes and corresponding percentage volume capacities are shown in Fig. 10. The total volume capacity and total length of tubes are also indicated. A vxm file with a model of the tracheal system and teguments for use in mobile devices is included as Supplementary 3D model S5.organization.

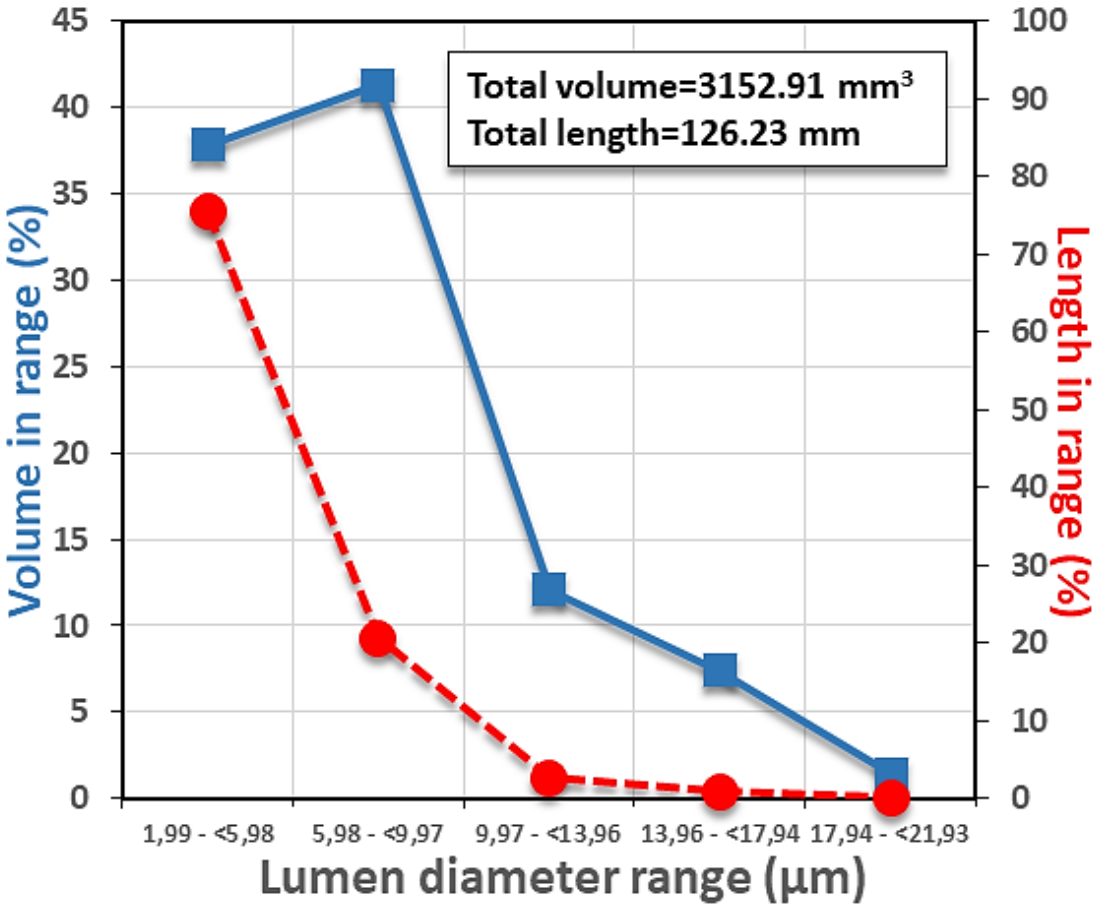

Figure 10.- Lumen diameter (µm) distribution ranges of the tracheal tubes and their corresponding percentage of volume capacity. The total volume capacity and total length of the tracheal tubes is indicated.

Organization of the respiratory spiracles. The tracheal respiratory system opens externally via seven pairs of spiracles (two thoracic [meso- and metathoracic] and five abdominal); these were clearly visible in both light microscopy slide preparations and in micro-CT reconstructed images. The spiracular external openings connect with atrial cavities and tracheal tubes. The mesothoracic spiracles (MsSp) are situated in a latero-ventral position in the

pleural membranous zone, anterior to the mesothorax (Figs. 1A,B, 2D, 3A, 5A, 6, 7A, 8, 9A,B,E; Supplementary Videos S1–S3).

The mesothoracic spiracles protrude and each have two elongated spiracular openings: an anterior opening (SpOa) and a posterior opening (SpOp). The tegument extends to form an anterior lip (AlA) and a posterior lip (PlA). Inside each spiracular opening there is a small cavity called the first atrium (Atr1); this is connected to a second atrial cavity (Atr2) through a cribellated plate of tegument, with two longitudinal openings, several pores, and the first filter (Fi1). The second atrium is connected to a third small atrial cavity (Atr3) through another cribellated plate, housing a second filter (Fi2) (Figs. 2A, 3B and 4).

The methathoracic spiracle (MtSp) are located on the pleura in a latero-dorsal position, beneath the elytra (Figs. 1B, 2C, 3A,H, 5A, 6–8 and 9E, Supplementary Video S4). Each methathoracic spiracle (MtSp) has a small spiracular opening connected to the dome-shaped first atrial cavity (Atr1), through a cribellated curved plate, and with a filter (Fi). The first atrial cavity is connected to a second atrial cavity (Atr2) (Fig. 3C–H; Supplementary Video S4).

The abdominal spiracles (ASp) are laterally located on the fore zone of the uniform membranous pleural region (without any epimeral/episternal differentiation) (Figs. 1B,C, 2C, 5A and 6–8; Supplementary Videos S1–S3).

The abdominal spiracles are simpler structures than the thoracic ones, each with a single spiracular opening surrounded by a circular peritreme sclerite (Pe), opening into a barrel-shaped atrial cavity at the bottom of which is a closing apparatus (ClA) that forms a U-shape elastic bar (flexible rod) that constrains the connection with the tracheae (Figs. 1C, 2B and 3I).

Organization of the tracheal tubes. Three tracheal trunks arise from each mesothoracic spiracle: the latero-ventral prothoracic (LVPt), ventral prothoracic (VPt) and dorsal prothoracic trunks (DPt) (Figs. 3A,B, 4A,E–G, 5–8 and 9A,B,E; Supplementary Videos S1–S3). Each latero-ventral prothoracic trunk is connected through a descendent branch to the prothoracic leg trunk (PtLt) which supplies the prothoracic leg (Figs. 3A, 6–8 and 9A,B,E; Supplementary Videos S1–S3; Supplementary 3D model S5). Descendent branches on both sides are interconnected by a ventral prothoracic commissure (VPC) before supplying the

prothoracic legs (Figs. 5, 8B,C and 9D; Supplementary Videos S1–S3; Supplementary 3D model S5).

The ventral prothoracic trunks run into the head, joining to form the ventral cephalic trunk (VCt). A thin branch is derived from each ventral prothoracic trunk; each branch joins to supply the ventral median cephalic branch (VMCb) which runs ventrally into the head (Figs. 3A, 5–8; Supplementary Videos S1–S3; Supplementary 3D model S5).

The dorsal prothoracic trunks are connected by a dorsal cephalic commissure (DCC) (Figs. 8 and 9A–C; Supplementary Video S1; Supplementary 3D model S5). From each side of the dorsal cephalic commissure two thin tracheae emerge, the dorso-median cephalic tracheae (DMCt) (Fig. 9C; Supplementary Video S1; Supplementary 3D model S5), which run parallel and very close to each other in a median-dorsal position, diverging only at the tip (Figs. 3A, 5, 6B, 7, 8 and 9A–C; Supplementary Videos S1 and S2; Supplementary 3D model S5). The dorsal prothoracic trunks run forward into the head via the dorsal cephalic trunks (DCt). The posterior prothoracic branch (PPb) and the anterior prothoracic twisted branch (APb) are derived dorsally from the dorsal prothoracic trunk (Figs. 3A, 6–8 and 9A,B,D; Supplementary Videos S1–S3; Supplementary 3D model S5).

The dorsal (DMst), lateral (LMst) and ventral (VMst) mesothoracic trunks are derived backwards from the dorsal prothoracic trunk, the ventral prothoracic trunk, and anteriorly and close to the mesothoracic spiracles, respectively (Figs. 3A, 5–8 and 9A,B,E; Supplementary Videos S1–S3; Supplementary 3D model S5). The arc-shaped mesothoracic trunk (AMst) is derived upwards and backwards from the ventral mesothoracic trunk, close to the mesothoracic spiracle. The arc-shaped mesothoracic trunk meets the metathoracic spiracles and from its dorsal arc several branches emerge dorsally (Figs. 3A, 5–7, 8A and 9E; Supplementary Videos S1–S3); one of these branches emerge dorsally and backwards to supply the elytra (Fig. 5B,C). A descendent branch supplying the mesothoracic leg trunk is derived from each ventral mesothoracic trunk (MsLt) (Figs. 3A, 6, 7, 8A and 9E; Supplementary Videos S1–S3; Supplementary 3D model S5).

In the metathorax, the lateral mesothoracic trunk (LMst) and the latero-ventral metathoracic trunk (LVMtt) (which runs laterally from the spiracle towards the ventral section, connecting with the ventral trunk) converge with the metathoracic spiracle, through a short lateral tube (Figs. 3D,H and 6–8; Supplementary Videos S1–S4). There are three main longitudinal tracheal trunks: the dorsal metathoracic trunk (DMtt), derived from the dorsal mesothoracic trunk (DMst); the lateral metathoracic trunk (LMtt); and the ventral metathoracic trunk (VMtt), derived from the latero-ventral metathoracic trunk (LVMtt). A branch that bifurcates to supply the hindwings is derived dorsally and backwards from the dorsal metathoracic trunks (Fig. 5B,C). A descendent branch that supplies the metathoracic leg trunk (MtLt) is derived from the lateral metathoracic trunk (Figs. 3A,F–G,I, 5B, 6–8 and 9E; Supplementary Videos S1–S3; Supplementary 3D model S5). The dorsal metathoracic trunks are divided into a lateral (DMtt-1) and a medial (DMtt-2) parallelised branches (Figs. 7B and 8B; Supplementary Videos S1–S3, Supplementary 3D model S5).

Ventrally, in the mesothorax, the left and right ventral mesothoracic trunks (VMst) meet medially to forma large ventral mesothoracic commissure connecting both sides (VMsC); a similar connection exists in the metathorax, where the latero-ventral metathoracic trunks (LVMtt) converge medially to form a ventral metathoracic commissure (VMtC). Both commissures are medially interconnected by a ventral longitudinal trachea (Fig. 8B,C; Supplementary Videos S1–S3; Supplementary 3D model S5).

The dorsal metathoracic branches (DMtt-1, DMtt-2) converge posteriorly with the lateral metathoracic trunk (LMtt), the ventral metathoracic trunk (VMtt) and the abdominal latero-ventral trunk (ALVt) before connecting with the first abdominal spiracle (ASp1) (Figs. 6–8; Supplementary Videos S1 and S2; Supplementary 3D model S5). The abdominal spiracles are connected by three longitudinal tracheal tubes, the latero-abdominal tracheae (LAt). The ones connecting the first (ASp1) and second (ASp2) spiracles are thicker, and

Table 1.- List of abbreviations used in the paper. The references indicate studies that have previously used the same term. Alternative terms used for the same structure are listed with references, and new terms introduced in this study are noted.

Abreviation	Name	Reference // Other name
AlA/PlA	anterior/posterior lip of atrium	(Snodgrass, 1935)
ALVt	abdominal latero-ventral trunk	newly introduced
AMst	arc-shaped mesothoracic trunk	newly introduced
APb	anterior prothoracic twisted branch	newly introduced
Asp	abdominal spiracle	(Hafeez & Gardiner, 1964; Loudon, 1989; Mbata, 1985; Raś *et al.*, 2018; Richards & Davies, 1977; Robertson, 1962; Snodgrass, 1935; Srivastava, 1976; Tonapi, 1978; Whitten, 1972)
Atr	spiracular atrium	(Hafeez & Gardiner, 1964; Raś *et al.*, 2018; Snodgrass, 1935; Tonapi, 1978) // atrium of the spiracle (Srivastava, 1976)
ClA	elastic bar of the closing apparatus	(Snodgrass, 1935) // closing bar (Tonapi, 1978), occluding apparatus (Richards & Davies, 1977), flexible rod compressing trachea (Wigglesworth, 1942), closing bow(Mbata, 1985), closing apparatus(Srivastava, 1976)
DCC	dorsal cephalic commissure	dorsal tracheal commissure (Snodgrass, 1935), dorsal commissure of the head (Robertson, 1962), dorsal head commissure (Hafeez & Gardiner, 1964), dorsal cervical anastomosis (Whitten, 1972), dorsal commissure (Mbata, 1985), brain commissure (Raś *et al.*, 2018)
DCt	dorsal cephalic trunk	dorsal head trunk (Snodgrass, 1935), superior cephalic tracheae (Robertson, 1962), dorsal cervical trachea (Whitten, 1972), dorsal cephalic trachea (Tonapi, 1978), dorsal head trachea (Boué & Chanton, 1962; Raś *et al.*, 2018)
DMCt	dorsal median cephalic trachea	newly introduced
DPt DMst DMtt	dorsal prothoracic trunk dorsal mesothoracic trunk dorsal metathoracic trunk	lateral plurisegmental tracheal trunk (Snodgrass, 1935), dorsal lateral trunk/lateral trunk (Hafeez & Gardiner, 1964), large lateral longitudinal trunks (Tonapi, 1978), lateral longitudinal trachea (Loudon, 1989), dorsal longitudinal trunk (Raś *et al.*, 2018), dorsal trachea (Mbata, 1985), longitudinal tracheal trunk (Srivastava, 1976)
DMtt-1	lateral branch of the dorsal metathoracic trunk	newly introduced
DMtt-2	medial branch of the dorsal metathoracic trunk	newly introduced
Fi	Filter	filter apparatus (Hassan, 1944; Schmitz & Wasserthal, 1999; Snodgrass, 1935; Srivastava, 1976), sieve (Tonapi, 1978)
Gt	genital tracheae	(Loudon, 1989; Robertson, 1962) // posterior reproductive branch (Hafeez & Gardiner, 1964)
LALMt	long abdominal latero-median tracheae	long median trachea (Hafeez & Gardiner, 1964)
LAt	latero-abdominal tracheae	large lateral longitudinal trunks (Tonapi, 1978), abdominal dorsal longitudinal trunk (Raś *et al.*, 2018)
LMst	lateral mesothoracic trunk	newly introduced
LMtt	lateral metathoracic trunk	newly introduced
LVMtt	latero-ventral metathoracic trunk	newly introduced
LVPt	latero-ventral prothoracic trunk	ventral lateral trunk (Hafeez & Gardiner, 1964), lateral longitudinal trunk (Whitten, 1972)
MsLt	mesothoracic leg trunk	mesothoracic leg tracheae (Robertson, 1962), mesoleg trachea (Raś *et al.*, 2018)
MsSp	mesothoracic spiracle	(Snodgrass, 1935) // anterior thoracic spiracle (Tonapi, 1978; Whitten, 1972)
MtLt	metathoracic leg trunk	metathoracic leg tracheae (Robertson, 1962), metaleg trachea (Raś *et al.*, 2018)
MtSp	metathoracic spiracle	(Hafeez & Gardiner, 1964; Snodgrass, 1935) // posterior thoracic spiracle (Tonapi, 1978)
Pe	peritreme	(Loudon, 1989; Mbata, 1985; Raś *et al.*, 2018; Richards & Davies, 1977; Schmitz & Wasserthal, 1999; Snodgrass, 1935; Srivastava, 1976; Tonapi, 1978)
PPb	posterior prothoracic branch	newly introduced
PtLt	prothoracic leg trunk	prothoracic leg tracheae (Robertson, 1962), proleg trachea (Raś *et al.*, 2018)
SpO	spiracular opening	(Tonapi, 1978) // spiracular aperture (Snodgrass, 1935), atrial orifice (Boué & Chanton, 1962)
SpOa/SpoP	anterior/posterior spiracle opening	spiracular aperture(Richards & Davies, 1977; Snodgrass, 1935)
SpOS	spiracular opening spine	used as taxonomic character in some insects as Coccidae(Hall, 2009)
VAC	ventral abdominal commissure	(Hafeez & Gardiner, 1964) // transverse ventral commissures (Snodgrass, 1935), ventral commissure of abdomen (Robertson, 1962), abdominal ventral commissure (Raś *et al.*, 2018), ventral tracheal commissure (Srivastava, 1976).
VCt	ventral cephalic trunk	ventral head trunk (Snodgrass, 1935), ventral tracheae of the head (Robertson, 1962), ventral cervical trachea (Whitten, 1972), ventral cephalic trachea (Tonapi, 1978), ventral head trachea (Mbata, 1985; Raś *et al.*, 2018)
VMCb	ventral median cephalic branch	labial trachea (Raś *et al.*, 2018)
VMsC	ventral mesothoracic commissure	mesothoracic commissure (Robertson, 1962)
VMtC	ventral metathoracic commissure	metathoracic commissure (Robertson, 1962)
VPC	ventral prothoracic commissure	ventral tracheal commissure (Snodgrass, 1935), prothoracic ventral commissure (Hafeez & Gardiner, 1964), ventral anastomosis (Whitten, 1972)
VPt VMst VMtt	ventral prothoracic trunk ventral mesothoracic trunk ventral metathoracic trunk	ventral plurisegmental tracheal trunk (Snodgrass, 1935), ventral lateral trunk (Hafeez & Gardiner, 1964), lateral longitudinal trunk (Whitten, 1972), ventral thoracic trachea (Tonapi, 1978), ventral longitudinal trunk (Raś *et al.*, 2018)
WAtr	atrial wall	(Hassan, 1944; Snodgrass, 1935; Srivastava, 1976; Tonapi, 1978)

interconnected dorso-ventrally with the abdominal latero-ventral trunks (ALVt). Both sides are connected by a double ventral transversal abdominal commissure (VAC) at the level of the fourth (ASp4) and fifth (ASp5) spiracles. Two parallel genital tracheae (Gt) are derived from the fifth abdominal spiracle (Figs. 1B, 3I, 5B and 6–8; Supplementary Videos S1 and S2; Supplementary 3D model S5).

Two parallel tracheae, the long abdominal latero-median tracheae (LALMt), are derived forwards from the right fourth abdominal spiracle; they ascend dorsally at the level of the first abdominal spiracle, bend backwards and progressively curve to the left to occupy a median position (Figs. 3I, 6B, 7 and 8; Supplementary Videos S1 and S2; Supplementary 3D model S5).

5.6.6.- Discussion

The external openings of the spiracles can represent a risk of water loss and the entry of particulate matter, pathogens, and/or parasites. However, insects have developed hairs, sieve filters and closing mechanisms (such as lips or valves) to minimise these issues (Chiappini & Aldini, 2011; Grassé, 1976; Harrison, 2009; Snodgrass, 1935; Wigglesworth, 1942). Our results show the presence of protective mechanisms in all the spiracles, including filtering sieve plates and the closing apparatus.

Tubular tracheal systems in insects are formed during embryogenesis as a series of segmental invaginations of the integument. Up to three thoracic and nine abdominal pairs of spiracles may exist in embryos, though this number is always reduced prior to hatching; further reductions may occur in endopterygotes during metamorphosis (resulting in a maximum of two thoracic and eight abdominal pairs, in adults). The spiracles of the prothorax disappear during development and those of the mesothorax migrate forward to an antero-lateral position on the prothorax (Chapman, 2013; Crowson, 1981; Gillott, 2005; Grassé, 1976; Richards & Davies, 1977; Snodgrass, 1935; Wigglesworth, 1942). Thus, even when they are originally ‘mesothoracic’ spiracles, due to the acquired new anatomical location, actually they appear situated in a prothoracic position, as shown in Fig. 5A.

In the beginning of the twentieth century, Fuchs (Fuchs, 1912) considered the number of abdominal spiracles as a taxonomical characteristic that varied according to sex. However, in the coffee berry borer we observe that both sexes have the same number of abdominal spiracles.

To assist in ventilation, many insects have air sacs (dilations of the tracheal tubes) that force ventilation when they are compressed by movement of the surrounding muscles (Boué & Chanton, 1962; Chapman, 2013; Gillott, 2005; Grassé, 1976; Harrison, 2009; Mbata, 1985; Miller, 1960; Richards & Davies, 1977; Robertson, 1962; Snodgrass, 1935; Tonapi, 1978; Wasserthal *et al.*, 2018; Weis-Fogh, 1964, 1967). However, some coleopteran species have reduced or no air-sacs at all (Hafeez & Gardiner, 1964; Kaiser *et al.*, 2007; Raś *et al.*, 2018). Our study shows that the coffee berry borer has very small air sacs in the abdominal lateral trunks, close to the spiracles; these were particularly visible close to the third and fifth abdominal spiracles, both with light microscopy (Fig. 1Ab) and micro-CT rendered images of the tracheal lumina, where they appear as small dilations close to these abdominal spiracles (Figs. 6–8).

It has also been shown that compression of the pronotal main tracheal trunks (dorsal and ventral prothoracic trunks) forces ventilation and exchange of gases in the tracheal tubular system (Waters *et al.*, 2013; Westneat, 2003). Cross-sections of these compressible trunks show elliptic-shaped lumina to make them easily collapsible (Chapman, 2013; Cobb, 2002; Robertson, 1962; Snodgrass, 1935) as seen in Fig. 9D. Hence, due to their proximity, the mesothoracic spiracles must have an important functional role in tracheal ventilation, with large volumes of gases passing through them. In fact, the tracheal tubes arising anteriorly to the mesothoracic spiracles supply the prothoracic and proventricular muscles and the forelegs, and via cephalic derivations they also supply the brain, the subesophageal ganglion, and the mouthparts (Fig. 5B).

Confirming their key functional importance, the mesothoracic spiracles are by far the most complex, with three consecutive filter plates and three atrial cavities. Moreover, the external openings have two mobile lips, one anterior and another posterior, to close the anterior and posterior external spiracular openings,

respectively (Fig. 4). Spiracles situated underneath the elytra (mesothoracic and abdominal) are more protected; we did not observe any filters in the abdominal spiracles (Figs. 1C, 2B and 3I). In contrast, the metathoracic spiracles, which are more exposed because the metathorax moves in relation to the abdomen, showed a very small spiracular opening (Fig. 3H) and a filter plate (Fig. 3C–H). Tracheal tubes in the meso- and metathorax surround and supply the anterior midgut, and the middle and hind legs. Extensions from the ventral pro- and mesothoracic commissures, together with anterior prolongations of the meso- and metathoracic commissures, supply the complex ganglion (resulting from the fusion of the thoracic and abdominal ganglions1) (Fig. 5B; Supplementary Video S1; Supplementary 3D model S5).

The U-shaped bar of the closing apparatus of the abdominal spiracles, first described by Snodgrass (Snodgrass, 1935), and observed by many authors (Chapman, 2013; Fuchs, 1912; Gillott, 2005; Wigglesworth, 1942), are almost identical to those described for the whirligig beetle Dineutes indicus (Coleoptera: Gyrinidae)(Waters *et al.*, 2013). Muscles operating the closing apparatus of the abdominal spiracles have been observed previously (Chapman, 2013; Gillott, 2005; Tonapi, 1978; Wigglesworth, 1942), as well as the muscles operating the closing apparatus of the mesothoracic spiracle in the coffee berry borer. The latter was not visible in Fig. 2 because the specimen had been treated with KOH, nor were they observed in micro-CT rendered images.

The general organisation of the tracheal system in the coffee berry borer is similar to that described previously for others coleopteran species, such as two tenebrionids, the flour beetle (*Tribolium anaphe*) (Hafeez & Gardiner, 1964) and the meal- worm beetle (*Tenebrio molitor*) (Richards & Davies, 1977). Thus, the dorsal cephalic commissure is clearly visible in the coffee berry borer (Figs. 7B, 8 and 9A–C) but the ventral cephalic commissure was not visible. Transversal fine tubes, close to each other, were observed in the positions where other species have the ventral commissure, but when observed in detail they did not join to form a continuous commissure (Fig. 9B). Moreover, the long abdominal latero-median trachea (LALMt; also termed the ‘long median trachea’), which is normally located on the left side of the animal (Hafeez & Gardiner, 1964), was on the right side in the coffee berry borer. This may be because the authors (Hafeez

& Gardiner, 1964) drew it from a microscope view and thereafter the position was inverted as a specular image, or the position in that species is different to what we observed in the coffee berry borer. Furthermore, in *T. anaphe* the long abdominal latero-median trachea appears as a single trachea when running anteriorly and is divided into six branches when it runs posteriorly; in the coffee berry borer it appears as two tracheal tubes along its entire length (Figs. 6B, 7 and 8; Supplementary Video S4; Supplementary 3D model S5).

Classically the tracheal system is considered to consist of two dorsal longitudinal trunks, two lateral trunks, and two ventral trunks, connected by transversal tubes (Boué & Chanton, 1962; Chapman, 2013; Crowson, 1981; Gillott, 2005; Grassé, 1976; Harrison, 2009; Richards & Davies, 1977; Wigglesworth, 1942). In the coffee berry borer, it is, more or less, similar to this in the head and thorax. On each side of the abdomen there are three longitudinal latero-abdominal tracheae (LAt) that at first sight, could be interpreted as the dorsal, lateral, and ventral trunks described classically. In fact, previous studies have shown that the dorsal trunks should run along the dorsal vessel (heart) but, in the coffee berry borer, the dorsal latero-abdominal tracheae are situated far away from the dorsal vessel. We observed that the long abdominal latero-median tracheae (LALMt) followed the posterior-midgut and gonads when running forward, while passing over the hindgut (rectum) just below the dorsal vessel when running backwards (Fig. 5B) (Alba-Alejandre *et al.*, 2019). Therefore, the long abdominal latero-median tracheae play an important role in supplying the digestive tract, gonads and heart in coffee berry borer. This would explain the presence of small air sacs close to the spiracles for increasing abdominal ventilation. On both sides, the abdominal tracheal system runs posteriorly as two parallel tracheal tubes (genital tracheae); in females these extend to the reproductive system, supplying the ovipositor musculature.

Although many of the anatomical details have been observed and/or described and named in other insect species, we are the first to describe and name new anatomical details. Of note, despite a recent study renaming the ventral abdominal commissures as abdominal ventral commissures (Richards & Davies, 1977), this terms has been used previously by other authors in different

insect species (Hafeez & Gardiner, 1964; Robertson, 1962; Snodgrass, 1935; Srivastava, 1976) (Table 1).

As identified by Iwan *et al.* (Iwan *et al.*, 2015), using the same microtomography instrument as us, the small voxel size achieved permits visualization of tracheoles. However, as tracheoles are filled with tracheolar fluid, through which interchange of gases occurs (Chapman, 2013; Gillott, 2005; Wigglesworth, 1930, 1942), the methodology is unable to reconstruct the tubes in the same way as gas-filled tube cavities can be reconstructed. In fact, very fine tracheal tubes (up to 1.99 µm diam.) were reconstructed in the coffee berry borer, but nothing narrower could be visualized. Wigglesworth (Wigglesworth, 1930) experienced the same problem when studying the tracheal system of a dragonfly (*Aeschna*) under light microscopy. He observed that when the tracheoles were filled with fluid they were not visible, but by eliminating the tracheolar fluid using a hypertonic solution of potassium lactate, the problem could be solved. Unfortunately, potassium lactate would not solve the problem because it would create other non-tracheolar empty spaces introducing noise into reconstructions.

In recent micro-CT studies of the mealworm beetle tracheal system (Iwan *et al.*, 2015; Raś *et al.*, 2018) the minimum diameter of tracheal tubes that could be reconstructed was 25 µm, which is significantly greater than the smallest lumina we reconstructed (1.99 µm), and also greater that the largest lumina we reconstructed (21.92 µm) in the coffee berry borer, which is ten times smaller. However, the largest tracheal tubes of the mealworm beetle have approximately 20 times larger diameters (400 µm) than those of the coffee berry borer, the largest of which are the dorsal and ventral prothoracic trunks that are collapsible to facilitate ventilation (Fig. 8D). Avoiding large diameter tubes could be an adaptation in such a small insect as the coffee berry borer. In fact, to our knowledge, no collapsible tracheae have been reported in mealworm beetles in any studies of its tracheal system (Kaiser *et al.*, 2007; Raś *et al.*, 2018).

Most of the tracheae we observed have very narrow lumina: the narrowest tubes (lumen diameter range:1.99–6 µm) accounted for more than 75.5% of the total length of tubes and 37.8% of the total volume; all tubes with lumina ≤9.97 µm accounted for 96.6% of the total length and 79.1% of total tracheal volume

capacity. A similar relationship between tracheal diameter and its occurrence as a proportion of the entire tracheal system has been reported for the mealworm beetle, although the frequency of occurrence decreases as the diameter increased, and the diameter only decreases from 200 to 400 µm (Richards & Davies, 1977). However, we observed a much steeper slope for this relationship (Fig. 10).

The total estimated length of the tracheal tubes was 122.23 mm. As the studied female was ca.1.8 mm in length, this means that the tracheal tubes were 70 times the total length of the body. If we transpose this to a human scale, then a 175 cm long insect (the average height for American males (*Height Chart of Men and Women in Different Countries - Disabled World*, 2019)) would have 123 m of tracheal tubes (longer than a football or soccer field).

In conclusion, we have confirmed that the use of micro-CT techniques to reconstruct and study the tracheal tubular system of insects is an extraordinarily useful and reliable technique; the only limitation was the inability to reconstruct the smallest tubes (<1.99 µm). Even though the technique is time consuming (during scanning but especially during reconstruction and visualization), once the software parameter for a particular species have been determined and verified, it is possible to create task list procedures that may speed up the process (Iwan *et al.*, 2015).

This is the first complete study on the tracheal system of the coffee berry borer, the smallest insect to be studied so far using micro-CT. Obtaining similar results using classical dissection methods would have been very difficult, if not impossible. Furthermore, micro-CT allowed to reconstruct the actual position and shape of the anatomical structures without any displacement and/or deformation due to manipulation. It has permitted us to measure, quantify and visualize structures from any perspective. Moreover, videos and a 3D model can be displayed on mobile devices which be used in future research, as well as for teaching insect anatomy to students and the public in general.

5.6.7.- Supplementary Information Videos

S1.- Tracheal system. Part I: a female adult of the coffee berry borer is progressively made transparent, allowing to see the internal tracheal respiratory system and the complexity of tubes-External spinning views and a virtual travel inside the animal is shown. Lumen size of the tracheal tubes is indicated in a gradation of colors in accordance with a color-scale bar shown at the upper right of the video.

https://static-content.springer.com/esm/art%3A10.1038%2Fs41598-019-54157-3/MediaObjects/41598_2019_54157_MOESM2_ESM.mp4

S2.- Tracheal system. Part II: a female adult of the coffee berry borer is progressively made transparent permitting to see the internal tracheal respiratory system and the complexity of tubes, inside the body walls. Lumen size of the tubes is indicated in a gradation of colors in accordance with a color-scale bar shown at the upper right of the video.

https://static-content.springer.com/esm/art%3A10.1038%2Fs41598-019-54157-3/MediaObjects/41598_2019_54157_MOESM3_ESM.mp4

S3.- Tracheal system. Part III. Details of the position of the respiratory spiracles.

https://static-content.springer.com/esm/art%3A10.1038%2Fs41598-019-54157-3/MediaObjects/41598_2019_54157_MOESM4_ESM.mp4

S4.- Close-up view of the metathoracic spiracle structure and its connecting tracheal tubes. To ease the differentiation of the tracheae, in some parts of the video the tracheal lumina appears reconstructed in red colour

https://static-content.springer.com/esm/art%3A10.1038%2Fs41598-019-54157-3/MediaObjects/41598_2019_54157_MOESM5_ESM.mp4

3D model to visualise with mobile devices (vxm)

https://static-content.springer.com/esm/art%3A10.1038%2Fs41598-019-54157-3/MediaObjects/41598_2019_54157_MOESM6_ESM.vxm

S5.- Supplementary 3D model: tracheal tubular system and the teguments to be visualized with the CTvox app for mobile devices (smartphones and tablets, either with iOS or Android systems).To install CTvox on your device, go through Apple's AppStore/Google Play Store, in the usual way (the app is free of charge). Instructions can be downloaded in the following links:

1.-For iOS devices:

a) For Ipad: https://www.bruker.com/fileadmin/user_upload/8-PDF-Docs/Microtomography/CTvoxForIpad.pdf

b) For Iphone: https://www.bruker.com/fileadmin/user_upload/8-PDF-Docs/Microtomography/CTvoxForIPhone.pdf

2.-For Android devices: https://www.bruker.com/fileadmin/user_upload/8-PDF-Docs/Microtomography/CTvoxForAndroid.pdf

5.6.8.- References

Alba-Alejandre, I., Alba-Tercedor, J., & Vega, F. E. (2018). Observing the devastating coffee berry borer (*Hypothenemus hampei*) inside the coffee berry using micro-computed tomography. *Scientific Reports*, *8*(1), 17033. https://doi.org/10.1038/s41598-018-35324-4

Alba-Alejandre, I., Alba-Tercedor, J., & Vega, F. E. (2019). Anatomical study of the coffee berry borer (*Hypothenemus hampei*) using micro-computed tomography. *Scientific Reports*, *9*(1), 17150. https://doi.org/10.1038/s41598-019-53537-z

Alba-Tercedor, J. (2004). *Efemerópteros in Curso Práctico de Entomología (ed. Barrientos, J. A.) 511–522 (Asociación Española de Entomología. Centro Iberoamericano de la Biodiversidad).*

Alba-Tercedor, J. (2014). From the sample preparation to the volume rendering images of small animals : A step by step example of a procedure to carry out the micro-CT study of the leafhopper insect *Homalodisca vitripennis* (Hemiptera: Cicadellidae). In *Bruker Micro-CT Users Meeting 2014* (pp. 260–288). Bruker Micro-CT-Skyscan. http://bruker-microct.com/company/UM2014/000_AbstractBook2014.pdf

Alba-Tercedor, J., Sáinz-Bariáin, M., & Zamora-Muñoz, C. (2016). Changing the pupal–case architecture as a survival strategy in the caddisfly *Annitella amelia* Sipahiler, 1998 (Insecta, Trichoptera). *Animal Biodiversity and Conservation*, *39*(1), 65–75. http://abc.museucienciesjournals.cat/files/ABC_39-1_pp_65-75-color.pdf

Boué, H., & Chanton, R. (1962). 4º L'appareil respiratoire. In *Biologie Animale. Zoologie I. Invertebrés* (2nd ed., pp. 388–397). G. Doin & Cie.

Bradley, T. J., Briscoe, A. D., Brady, S. G., Contreras, H. L., Danforth, B. N., Dudley, R., Grimaldi, D., Harrison, J. F., Kaiser, J. A., Merlin, C., Reppert, S. M., VandenBrooks, J. M., & Yanoviak, S. P. (2009). Episodes in insect evolution. *Integrative and Comparative Biology*, *49*(5), 590–606. https://doi.org/10.1093/icb/icp043

Bruker-microCT. (2013). How to make color-coded 3D models for structure thickness in CTVox. Method note 25. *Bruker-Skyscan Method Notes*, 1–10.

Bruker-microCT. (2014). *Advanced image registration in Dataviewer. Method note MCT-048*. 1–7.

Chapman, R. F. (2013). *The Insects Structure and Function* (S. J. Simpson & A. E. Douglas (Eds.); 5th ed.). Cambridge University Press. Chapman 5 th edition The Insects structure and function.pdf - ResearchGate

Chiappini, E., & Aldini, R. N. (2011). Morphological and physiological adaptations of wood-boring beetle larvae in timber. *Journal of Entomological and Acarological Research*, *43*(2), 47–59. https://doi.org/10.4081/jear.2011.47

Cobb, M. (2002). Malpighi, Swammerdam and the colourful silkworm: replication and visual representation in early modern science. *Annals of Science*, *59*, 111–147. https://doi.org/10.1080/00033790110050759

Crowson, R. A. (1981). The Biology of the Coleoptera. In *The Biology of the Coleoptera*. Academic Press Inc. New York

Franz-Guess, S., Klußmann-Fricke, B.-J., Wirkner, C. S., Prendini, L., & Starck, J. M. (2016). Morphology of the tracheal system of camel spiders (*Chelicerata: Solifugae*) based on micro-CT and 3D-reconstruction in exemplar species from three families. *Arthropod Structure & Development*, *45*(5), 440–451. https://doi.org/10.1016/j.asd.2016.08.004

Fuchs, G. (1912). Morphologische Studien über Borkenkäfer. II Die Europaischen Hylesinen. In *Verlag von Ernst Reinhard. München*.

Gillott, C. (2005). Entomology. In *Entomology* (3rd ed.). Springer. www.springeronline.com

Grassé, P.-P. (1976). L'Appareil Respiratoire. *Traité de Zoologie. Anatomie, Systématique, Biologie. T.VIII, Insectes. Splachnologie, Phonation, Vie Aquatique, Rapports Avec Les Plantes. Fasc. IV*, 93–204.

Greco, M., Bell, D., Woolnough, L., Laycock, S., Corps, N., Mortimore, D., & Hudson, D. (2014). 3-D visualisation, printing, and volume determination of the tracheal respiratory system in the adult desert locust, *Schistocerca gregaria*. *Entomologia Experimentalis et Applicata*, *152*(1), 42–51. https://doi.org/10.1111/eea.12199

Greenlee, K. J., Henry, J. R., Kirkton, S. D., Westneat, M. W., Fezzaa, K., Lee, W.-K., & Harrison, J. F. (2009). Synchrotron imaging of the grasshopper tracheal system: morphological and physiological components of tracheal hypermetry. *American Journal of Physiology-Regulatory, Integrative and Comparative Physiology*, *297*(5), R1343–R1350. https://doi.org/10.1152/ajpregu.00231.2009

Ha, Y.-R., Yeom, E., Ryu, J., & Lee, S.-J. (2017). Three-dimensional structures of the tracheal systems of *Anopheles sinensis* and *Aedes togoi* pupae. *Scientific Reports. Nature Publishing Group*. https://doi.org/10.1038/srep44490

Hafeez, M. A., & Gardiner, B. G. (1964). The internal morphology of the adult of T*ribolium anaphe* Hinton (Coleoptera: Tenebrionidae). *Proceedings of the Royal Entomological Society of London. Series A, General Entomology*, *39*(10–12), 137–145. https://doi.org/10.1111/j.1365-3032.1964.tb00996.x

Hall, W. J. (2009). Observations on the Coccidae of southern Rhodesia. *Proceedings of the Royal Entomological Society of London. Series B, Taxonomy*, *1*(9), 185–195. https://doi.org/10.1111/j.1365-3113.1932.tb01380.x

Harrison, J. F. (2009). Tracheal System. In V. H. Resh & R. T. Cardé (Eds.), *Encyclopedia of Insects* (pp. 1011–1015). Academic Press. https://doi.org/10.1016/B978-0-12-374144-8.00265-4

Hassan, A. A. G. (1944). The structure and mechanism of the spiracular regulatory apparatus in adult Diptera and certain other groups of insects. *Transactions of the Royal Entomological Society of London*, *94*, 103–153. https://doi.org/10.1111/j.1365-2311.1944.tb01214.x

Height Chart of Men and Women in Different Countries - Disabled World. (2019). https://www.disabled-world.com/calculators-charts/height-chart.php

Iwan, D., Kamiński, M. J., & Raś, M. (2015). The Last Breath: A µCT-based method for investigating the tracheal system in Hexapoda. *Arthropod Structure & Development*, *44*(3), 218–227. https://doi.org/10.1016/j.asd.2015.02.002

Kaiser, A., Klok, C. J., Socha, J. J., Lee, W.-K., Quinlan, M. C., & Harrison, J. F. (2007). Increase in tracheal investment with beetle size supports hypothesis of oxygen limitation on insect gigantism. *Proceedings of the National Academy of Sciences*, *104*(32), 13198–13203. https://doi.org/10.1073/pnas.0611544104

Klowden, M. J. (2007). *Physiological systems in insects*. Elsevier/AcademicPress.

Loudon, C. (1989). Tracheal hypertrophy in mealworms: design and plasticity in oxygen supply systems. *Journal of Experimental Biology*, *147*, 217–235. http://jeb.biologists.org/content/jexbio/147/1/217.full.pdf

Malpighi, M. (1669). *Dissertatio epistolica de bombyce*. J. Martyn & J. Allestry, regiæ

societatis typographos.

Mbata, K. J. (1985). The anatomy of the armoured ground cricket, *Acanthoplus speiseri* Brancsik 1895 (Orthoptera: Tettigoniidae, Hetrodinae) [Iowa State University Capstones]. In *Retrospective Theses and Dissertations*. https://lib.dr.iastate.edu/rtd

Miller, P. L. (1960). Respiration in the desert locust: III. Ventilation and the spiracles during flight. *J. Exp. Biol.*, *37*(2), 264–278. http://jeb.biologists.org/content/jexbio/37/2/264.full.pdf

Nation, J. L. (2002). Insect Physiology and Biochemistry. In *Insect Physiology and Biochemistry*. CRC Press. https://doi.org/10.1201/b18758

Poinapen, D., Konopka, J. K., Umoh, J. U., Norley, C. J. D., Mcneil, J. N., & Holdsworth, D. W. (2017). Micro-CT imaging of live insects using carbon dioxide gas-induced hypoxia as anesthetic with minimal impact on certain subsequent life history traits. *BMC Zology*, *2*(9), 2–13. https://doi.org/10.1186/s40850-017-0018-x

Raś, M., Iwan, D., & Kamiński, M. J. (2018). The tracheal system in post-embryonic development of holometabolous insects: a case study using the mealworm beetle. *Journal of Anatomy*, *232*(6), 997–1015. https://doi.org/10.1111/joa.12808

Richards, O., & Davies, R. (1977). The respiratory system. In O. Richards & R. Davies (Eds.), *A General Textbook of Entomology* (pp. 209–233). Chapman and Hall.

Robertson, C. H. (1962). The anatomy of the respiratory system of the Passalus beetle, *Popilius disjunctus* (Illiger). *American Midland Naturalist*, *68*(2), 376–393.

Ruan, Y., Y., L., Zhang, M., Chen, X., Liu, Z., Wang, S., & Jiang, S. (2018). Visualisation of insect tracheal systems by lactic acid immersion. *Journal of Microscopy*, *271*(2), 230–236. https://doi.org/10.1111/jmi.12711

Schmitz, A., & Wasserthal, L. T. (1999). Comparative morphology of the spiracles of the Papilionidae, Sphingidae, and Saturniidae (Insecta: Lepidoptera). *International Journal of Insect Morphology and Embryology*, *28*(1–2), 13–26. https://doi.org/10.1016/S0020-7322(98)00033-6

Shaha, R. K., Vogt, J. R., Han, C.-S., & Dillon, M. E. (2013). A micro-CT approach for determination of insect respiratory volume. *Arthropod Structure & Development*, *42*(5), 437–442. https://doi.org/10.1016/J.ASD.2013.06.003

Snodgrass, R. E. (1935). Principles of insect morphology. In *Thorax*. McGraw-Hill Book Company, Inc. https://doi.org/0801428831

Srivastava, K. P. (1976). On the respiratory system of the lemon-butterfly, *Papilio demoleus* l. (Lepidoptera: Papilionidae). *Australian Journal of Entomology*, *14*(4), 363–370. https://doi.org/10.1111/j.1440-6055.1975.tb02052.x

Stalling, D., Westerhoff, M., & Hege, H.-C. (2005). Amira: a highly interactive system for visual data analysis. In *Visualization Handbook* (pp. 749–767). Elsevier. https://doi.org/10.1016/B978-012387582-2/50040-X

Thermo Fisher Scientific. (2017). *Amira 3D visualization and analysis software.* (6.7.0). FEI. http://www.thermofisher.com/amira-avizo

Tonapi, G. T. (1978). Some adaptive features in the respiratory system of *Dineutes indicus* Aubé (Coleoptera, Gyrinidae). *Zoologica Scripta*, *6*(2), 107–112. https://doi.org/10.1111/j.1463-6409.1978.tb00790.x

Vega, F. E., Bauchan, G., Infante, F., Valdez-Carrasco, J. M., & Beaver, R. (2015). Visualizing the mesothoracic spiracles in a bark beetle: *Hypothenemus hampei* (Coleoptera: Curculionidae). *Annals of the Entomological Society of America*,

108(3), 446–448. https://doi.org/10.1093/aesa/sav016

Vega, F. E., Infante, F., & Johnson, A. J. (2015). The genus *Hypothenemus*, with emphasis on *H. hampei*, the coffee berry borer. In *Bark Beetles* (pp. 427–494). Elsevier. https://doi.org/10.1016/B978-0-12-417156-5.00011-3

Wasserthal, L. T., Cloetens, P., Fink, R. H., & Wasserthal, L. K. (2018). X-ray computed tomography study of the flight-adapted tracheal system in the blowfly *Calliphora vicina*, analysing the ventilation mechanism and flow-directing valves. *The Journal of Experimental Biology*, *221*(12), jeb176024. https://doi.org/10.1242/jeb.176024

Waters, J. S., Lee, W.-K., Westneat, M. W., & Socha, J. J. (2013). Dynamics of tracheal compression in the horned passalus beetle. *American Journal of Physiology-Regulatory, Integrative and Comparative Physiology*, *304*(8), R621–R627. https://doi.org/10.1152/ajpregu.00500.2012

Weis-Fogh, T. (1964). Functional design of the tracheal system of flying insects as compared with the avian lung. *Journal of Experimental Biology*, *41*(2), 207–227. http://jeb.biologists.org/content/jexbio/41/2/207.full.pdf

Weis-Fogh, T. (1967). Respiration and tracheal ventilation in locusts and other flying insects. *Journal of Experimental Biology*, *47*, 561–587. http://jeb.biologists.org/content/47/3/561.short

Westneat, M. W. (2003). Tracheal Respiration in Insects Visualized with Synchrotron X-ray Imaging. *Science*, *299*(5606), 558–560. https://doi.org/10.1126/science.1078008

Whitten, J. M. (1972). Comparative anatomy of the tracheal system. *Annual Review of Entomology*, *17*(1), 373–402. https://doi.org/10.1146/annurev.en.17.010172.002105

Wigglesworth, V. B. (1930). A Theory of Tracheal Respiration in Insects. *Proceedings of the Royal Society B: Biological Sciences*, *106*(743), 229–250. https://doi.org/10.1098/rspb.1930.0024

Wigglesworth, V. B. (1942). *The Principles of Insect Physiology* (2nd ed.). Methuen & CO. LTD. ttps://archive.org/details/principlesofinse033321mbp/page/n7

Wigglesworth, V. B. (1950). A new method for injecting the tracheae and tracheoles of insects. *Journal of Cell Science*, *s3-91*(14). http://jcs.biologists.org/content/s3-91/14/217

5.7.- Material adicional: "Microtomografía computarizada para documentar el gorgojo del café, *Araecerus fasciculatus* (Coleoptera: Anthribidae), dentro de bayas de café recolectadas en el campo (*Coffea canephora*)"

insects

MDPI

Communication

Micro-CT to Document the Coffee Bean Weevil, *Araecerus fasciculatus* (Coleoptera: Anthribidae), Inside Field-Collected Coffee Berries (*Coffea canephora*)

Ignacio Alba-Alejandre [1], Javier Alba-Tercedor [1] and Fernando E. Vega [2,*]

[1] Department of Zoology, Faculty of Sciences, University of Granada, Campus de Fuentenueva, 18071 Granada, Spain; ignacioalba@gmail.com (I.A.-A.); jalba@ugr.es (J.A.-T.)
[2] Sustainable Perennial Crops Laboratory, United States Department of Agriculture, Agricultural Research Service, Beltsville, MD 20705, USA
* Correspondence: Fernando.Vega@ars.usda.gov; Tel.: +1-301-504-5101

Received: 22 June 2018; Accepted: 10 August 2018; Published: 14 August 2018

check for updates

Abstract: The coffee bean weevil, *Araecerus fasciculatus* (De Geer) (Coleoptera: Anthribidae), is a cosmopolitan insect with >100 hosts, and has been reported as a pest of stored coffee. During a study involving the coffee berry borer, we observed coffee bean weevils emerging from field-collected coffee berries and used micro-computerized tomography (micro-CT) scans to observe the insect inside the berry. Two eggs had eclosed inside the berry, resulting in observations of a newly eclosed adult beetle and a 5th instar larva, each feeding on one of the two seeds. This is the first time since 1775, when the insect was first described, that the insect has been observed inside a coffee berry.

Keywords: coffee quality; insect biology; losses; stored coffee; stored product pest

1. Introduction

The genus *Araecerus* Schönherr comprises ca. 75 species [1], with the coffee bean weevil, *Araecerus fasciculatus* (De Geer) (Coleoptera: Anthribidae), being the most economically important. Chittenden [2,3] coined the name coffee bean weevil and Valentine [1] has published a succinct account on the controversy involving the many different scientific names used for the insect.

The coffee bean weevil is ca. 4–5 mm long [4], has a worldwide distribution, over 100 hosts, and is mostly considered a stored product pest [5,6]. The insect has been occasionally reported as a pest of stored coffee beans, into which females insert an egg 1–2 mm deep, followed by larval consumption of the bean [7]. In Brazil, de Figueiredo Jr. [8] reported ca. 30% losses in coffee stored for 6 months, and Abrahão and Bitran [9] reported 20% losses in coffee stored for 9 months. In Colombia, Cabal Concha [7] reported heavy infestation of stored coffee in several locations. Depending on temperatures, there could be 8–10 insect generations per year in stored green coffee [8].

In addition to the losses caused by the insect, green coffee exhibiting insect damage (Figure 1c) is considered a defect and will negatively impact on grading and quality [10]. Furthermore, insect damage could also result in the presence of insect fragments. Locatelli and Viganò [11] determined the presence of insect fragments in 44 *C. arabica* and 27 *C. canephora* green coffee beans samples in Italy and found that 23% and 15% of the samples, respectively, contained coffee bean weevil fragments.

Even though it has been reported that the coffee bean weevil only attacks stored green coffee beans [12,13], the insect also attacks coffee berries in the field. For example, referring to the coffee bean weevil and *Coffea arabica*, Chittenden [3] stated, "the raw berry of which it also infests." In Brazil, Autuori [4] has reported that females oviposit up to six eggs inside berries, but only one, and rarely

Artículo publicado (bajo licencia de dominio público "Creative Commons"):

Alba-Alejandre, I., Alba-Tercedor, J., & Vega, F. E. (2018). Micro-CT to Document the Coffee Bean Weevil, *Araecerus fasciculatus* (Coleoptera: Anthribidae), Inside Field-Collected Coffee Berries (*Coffea canephora*). *Insects*, 9(3, 100), 1–9. https://doi.org/10.3390/insects9030100

5.7.1.- Resumen

El gorgojo del grano de café, *Araecerus fasciculatus* (De Geer) (Coleoptera: Anthribidae), es un insecto cosmopolita con > 100 hospedadores, y ha sido reportado como una plaga del café almacenado. Durante un estudio que involucró a la broca del café, observamos que los gorgojos de los granos de café emergían de las bayas de café recolectadas en el campo y usamos microtomografía computarizada (micro-CT) para observar el insecto dentro de la baya. Dos huevos se habían eclosionado dentro de la baya, lo que resultó en la observación de un escarabajo adulto recién eclosionado y una larva de quinto estadio, cada uno alimentándose de una de las dos semillas. Esta es la primera vez desde 1775, cuando se describió por primera vez el insecto, que el insecto ha sido observado dentro de una baya de café.

5.7.2.- Abstract

The coffee bean weevil, *Araecerus fasciculatus* (De Geer) (Coleoptera:

Anthribidae), is a cosmopolitan insect with >100 hosts, and has been reported as a pest of stored coffee. During a study involving the coffee berry borer, we observed coffee bean weevils emerging from field-collected coffee berries and used micro-computerized tomography (micro-CT) scans to observe the insect inside the berry. Two eggs had eclosed inside the berry, resulting in observations of a newly eclosed adult beetle and a 5th instar larva, each feeding on one of the two seeds. This is the first time since 1775, when the insect was first described, that the insect has been observed inside a coffee berry.

5.7.3.- Introduction

The genus *Araecerus* Schönherr comprises ca. 75 species (Valentine, 2005), with the coffee bean weevil, *Araecerus fasciculatus* (De Geer) (Coleoptera: Anthribidae), being the most economically important. Chittenden (Chittenden, 1896, 1897) coined the name coffee bean weevil and Valentine (Valentine, 2005)

has published a succinct account on the controversy involving the many different scientific names used for the insect.

The coffee bean weevil is ca. 4–5 mm long (Autuori, 1931), has a worldwide distribution, over 100 hosts, and is mostly considered a stored product pest (Mphuru, 1974; Waller *et al.*, 2007). The insect has been occasionally reported as a pest of stored coffee beans, into which females insert an egg 1–2 mm deep, followed by larval consumption of the bean (Cabal Concha, 1956). In Brazil, de Figuereido Jr. (De Figuereido, 1957) reported ca. 30% losses in coffee stored for 6 months, and Abrahão and Bitran (Abrahão & Bitran, 1973) reported 20% losses in coffee stored for 9 months. In Colombia, Cabal Concha (Cabal Concha, 1956) reported heavy infestation of stored coffee in several locations. Depending on temperatures, there could be 8–10 insect generations per year in stored green coffee (De Figuereido, 1957).

In addition to the losses caused by the insect, green coffee exhibiting insect damage (Figure 1c) is considered a defect and will negatively impact on grading and quality (Caspersen, 2016). Furthermore, insect damage could also result in the presence of insect fragments. Locatelli and Viganò (Locatelli & Viganò, 1991) determined the presence of insect fragments in 44 *C. arabica* and 27 *C. canephora* green coffee beans samples in Italy and found that 23% and 15% of the samples, respectively, contained coffee bean weevil fragments.

Even though it has been reported that the coffee bean weevil only attacks stored green coffee beans (Bemelmans, 1930; Cárdenas Murillo & Posada Flórez, 2001), the insect also attacks coffee berries in the field. For example, referring to the coffee bean weevil and *Coffea arabica*, Chittenden (Chittenden, 1897) stated, “the raw berry of which it also infests.” In Brazil, Autuori (Autuori, 1931) has reported that females oviposit up to six eggs inside berries, but only one, and rarely two, eclose. The larva initially feeds on the pulp or on mucilage between the two seeds, followed by penetration into the seed and consumption of the coffee bean (Autuori, 1931). Also in Brazil, da Costa Lima (Da Costa Lima, 1956) mentions that the insect can be found in coffee plantations, although in

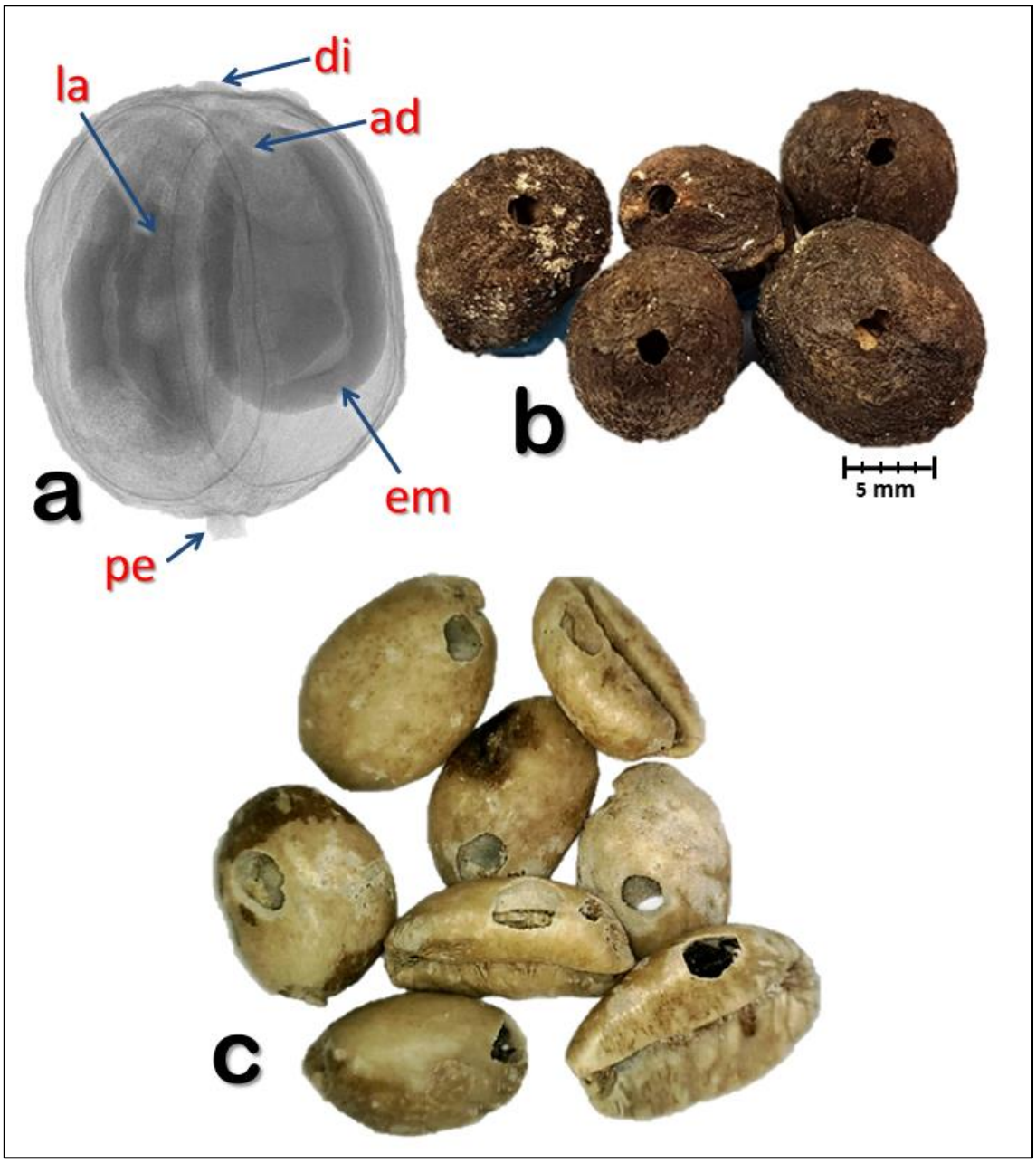

Figure 1.- X-ray image of a coffee bean weevil-infested coffee berry (**a**). Infested coffee berries showing the adult weevil exit hole next to the disc (**b**). Green coffee beans (*Coffea liberica*) from British Guiana damaged by the coffee bean weevil (**c**). Abbreviations: ad = adult; di = disc (style remnant); em = coffee embryo; la = larva; pe = pedicel

small numbers, and Abrahão and Bitran (Abrahão & Bitran, 1973) reported 4.2% infestation in the field. The insect has also been reported in coffee berries in the field in Togo (Mancion & Alibert, 1936) and Ghana (Padi, 1999). Sekhar (Sekhar, 1964) reported infestations in the field in India, which is incorrect based on the

following statement: “Fruits infested by the weevil show circular holes, 0.5–1.0 mm. in diameter.” The size of these holes corresponds to the coffee berry borer (see Results and Discussion). The Directoria de Agricultura (Agricultura, 1923) in Brazil recommended that “When the insect attacks the coffee fruit still on the tree, the fruit should be harvested and burned or disinfected, because otherwise, it will be impossible to avoid that the larvae, which are inside the beans, reach the adult stage”.

As part of our studies aimed at learning more about the behavior of the coffee berry borer (*Hypothenemus hampei* (Ferrari); Coleoptera: Curculionidae: Scolytinae) inside the berry (Alba-Tercedor *et al.*, 2018), we observed coffee bean weevils emerging from coffee berries collected in the field. We report on the use of micro-computerized tomography (micro-CT) scans to observe and record coffee bean weevils inside coffee berries collected in a coffee plantation in Vietnam.

5.7.4.- Materials and Methods

Coffee Berries Fifty coffee berries (Coffea canephora Pierre ex. A. Froehner; Rubiaceae) which were red or starting to turn red, were randomly collected from several coffee plants by the second author in November 2017 at the Me Linh Coffee Garden plantation in southern Vietnam (11º53′57.39″ N, 108º20′51.16″ E; 1043 m above sea level). The berries were kept at ambient temperature in Petri dishes containing moistened filter paper in the laboratory at the Department of Zoology, University of Granada, Spain. While examining the berries 63 days after they were collected, we noticed the presence of coffee bean weevils in the Petri dish (Supplementary Video S1). To determine if berries were still infested with weevils, we visualized the internal parts of the berry (Figure 1a) using X-rays produced by a high-resolution micro-CT system (see below), until movement was detected. The first berry in which movement was detected was used for the micro-CT study.

Micro-CT Scans A coffee bean weevil-infested coffee berry was mounted on a piece of Basotect® (low weight melamine resin foam; BASF, Schwarzheide,

Germany), inside a plastic container. Basotect® has a very low density that makes it transparent to X-rays, thus allowing the material to be digitally removed during the segmentation process (Alba-Tercedor & Alba-Alejandre, 2017). To avoid insect movement during the scans, insects were killed by adding several drops of ethyl acetate to the melamine foam followed by closing the container. Scans were initiated 30 min later with a Bruker SkyScan 1172 high-resolution desk-top microtomograph (Bruker, Kontich, Belgium) upgraded with a Hamamatsu L7902 100/250 X-ray source and a Ximea (SHT) 11 megapixels camera (Ximea GmbH, Münster, Germany). The scanning parameters were as follows: isotropic voxel size = 5.96 µm per pixel; voltage = 48 KV, current = 124 µA; image rotation step = 0.2◦; 360◦ of rotation scan and an Al 0.5 mm filter, resulting in two connected scans and 2400 X-ray raw images. The most recent version of the Bruker micro-CT's Skyscan software (NRecon, DataViewer, CTAnalyser) was used for primary reconstructions and the "cleaning" process to obtain the datasets of "slices" as described by Alba-Tercedor (Alba-Tercedor, 2014). Amira's Software 6.4.0 (Thermo Fisher Scientific, 2017) was used to obtain volume rendering reconstructions images in Figures 2 and 3, to make the Supplementary Video S2, and to measure the width of the larval cephalic capsule and the length of frass.

The macrophotograph of coffee berries shown in Figure 1b and the Supplementary Video S1 were obtained using a Samsung Galaxy Note8 smartphone. The macrophotograph of the coffee bean weevil was taken with an AxioZoom V16 zoom microscopy system (Carl Zeiss Microscopy LLC, Thornwood, NY, USA). The images were observed using a 1.0x/0.25 NA or 2.3x/0.25 NA Plan Neofluar® objective. LED lighting was used for brightfield imaging and a Zeiss AxioCam HRc color camera (Carl Zeiss Light Microscopy, Gottingen, Germany) was used to capture the images. ZEN imaging software (Carl Zeiss Microscopy LLC, Thornwood, NY, USA) was used to capture 60–75 z-stack images using extended depth of focus to produce 2D images. The macrophotograph of *Ptinus sensu stricto* was taken with a Samsung Galaxy Note8 smartphone connected to the ocular of a Motic SMZ168 Stereo Zoom microscope (MoticEurope S.L.U., Barcelona, Spain).

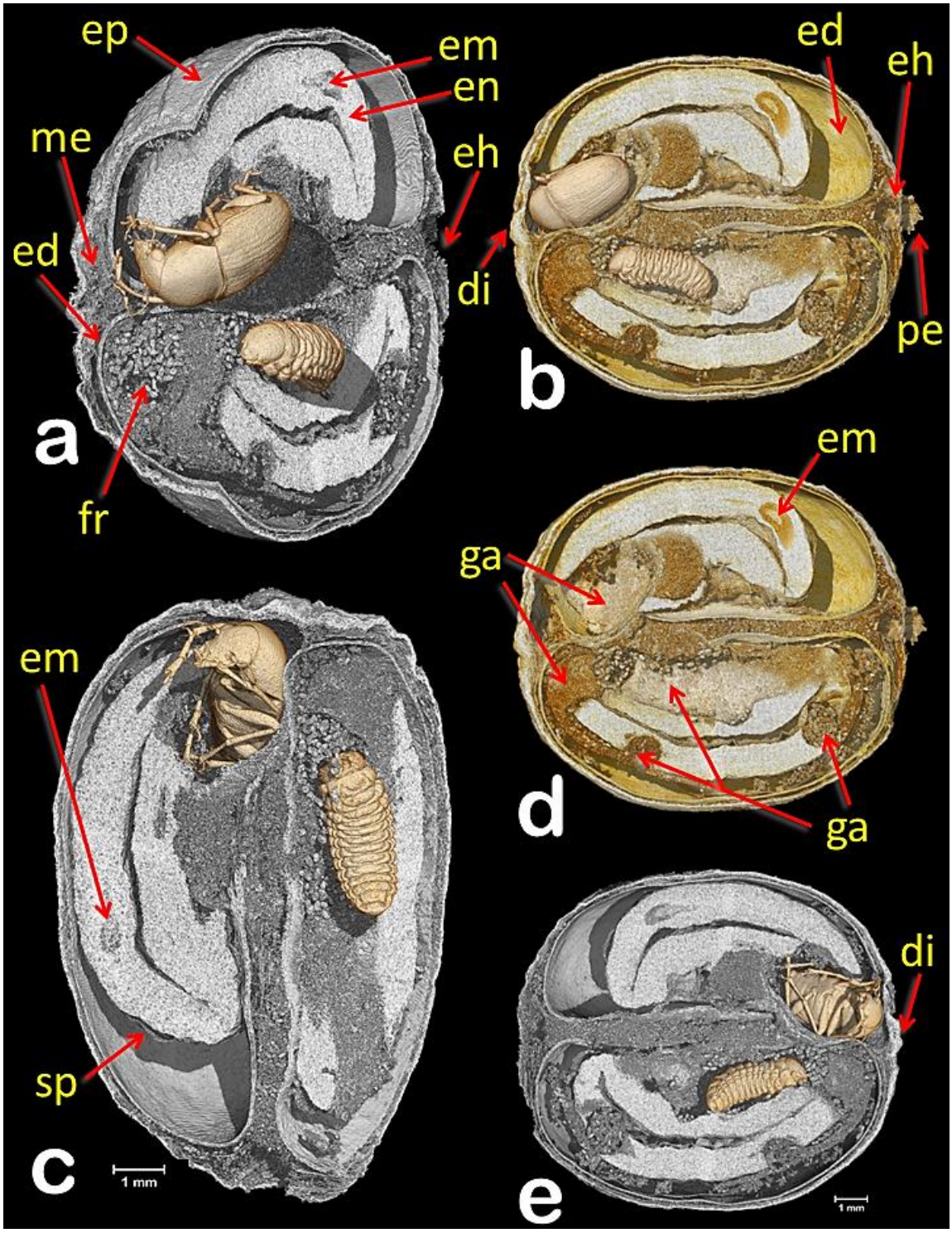

Figure 2.- Micro-CT volume rendering images of a coffee berry infested with a female adult coffee bean weevil and a 5th instar larva that have been separately segmented to unveil their location inside the berry. Latero-apical cut view (**a**). Lateral cut view (**b**). Lateral cut views, at two perpendicular cut planes (**c**). Same view shown in "(**b**)", but the insects have been eliminated with software to enhance the galleries (**d**). Lateral cut view from side opposite to that shown in "(**b**)" (**e**). Abbreviations: di = disc (style remnant); ed = endocarp (parchment); eh = entrance hole; em = coffee embryo; en = endosperm (seed); ep = epicarp (outer skin); fr = frass; ga = galleries; me = mesocarp (mucilage); pe = pedicel; sp = spermoderm (silverskin).

5.7.5.- Results and Discussion

Based on the presence of emergence holes (Figure 1b) 63 days after the berries were collected, six out of 50 berries (12%) were infested with the coffee bean weevil. All exit holes were located next to the disc. Five berries were photographed (Figure 1b); the sixth berry is the one used in the study, which did not yet have an emergence hole, although both the female adult and 5th instar larva (Figures 2–4) have their anterior part positioned towards the disc. The coffee bean weevil has five instars that can be identified using the width of the cephalic capsule (Cabal Concha, 1956; Cotton, 1921); therefore, the larva shown in Figures 2–4 is a 5th instar (0.903 mm wide). Figure 2 reveals three interesting findings: (1) two eggs had eclosed, which according to Autuori (Autuori, 1931) is rare; (2) both seeds are being consumed; and (3) there is a partial entrance hole. It is worth noting that we also collected a male of *Ptinus* s.str. (Ptinidae) that had emerged from a coffee berry (Figure 5i). *Ptinus tectus* has been reported on stored coffee (Archibald & Chalmers, 1983).

As mentioned above, female coffee bean weevils oviposit inside the berry. Therefore, the partial entrance hole in the berry (Figure 2) posed a conundrum. The entrance hole is much too small (ca. 0.95 mm diam.) for a coffee bean weevil, whose width is 2–3 mm (Autuori, 1931) and whose emergence hole can be up to 3 mm diam. (Da Costa Lima, 1956). Despite being close to the petiole and not on the disc, which is where the coffee berry borer colonizing female usually bores into the berry, the partial hole appears to have been bored by a coffee berry borer, whose entrance holes range from 0.6–0.8 mm (Varón *et al.*, 2004) to 1 mm diameter (Wilkinson, 1928). It is possible that the coffee bean weevil oviposited in the partially bored entrance hole, where one egg eclosed. The first instar larvae then bored into the berry, based on the connection between the partial entrance hole and a gallery filled with ca. 175 µm long frass and rasped seed material (Figures 2–4; according to Autuori (Autuori, 1931), larvae gnaw more than they eat), and as the gallery progresses away from the partial entrance hole, the length of the frass increases to ca. 290 µm (Figures 3 and 4), which indicates an older larval instar. Cabal Concha (Cabal Concha, 1956) mentions that 4th and 5th instars are more active and voracious than earlier instars, and that not all the

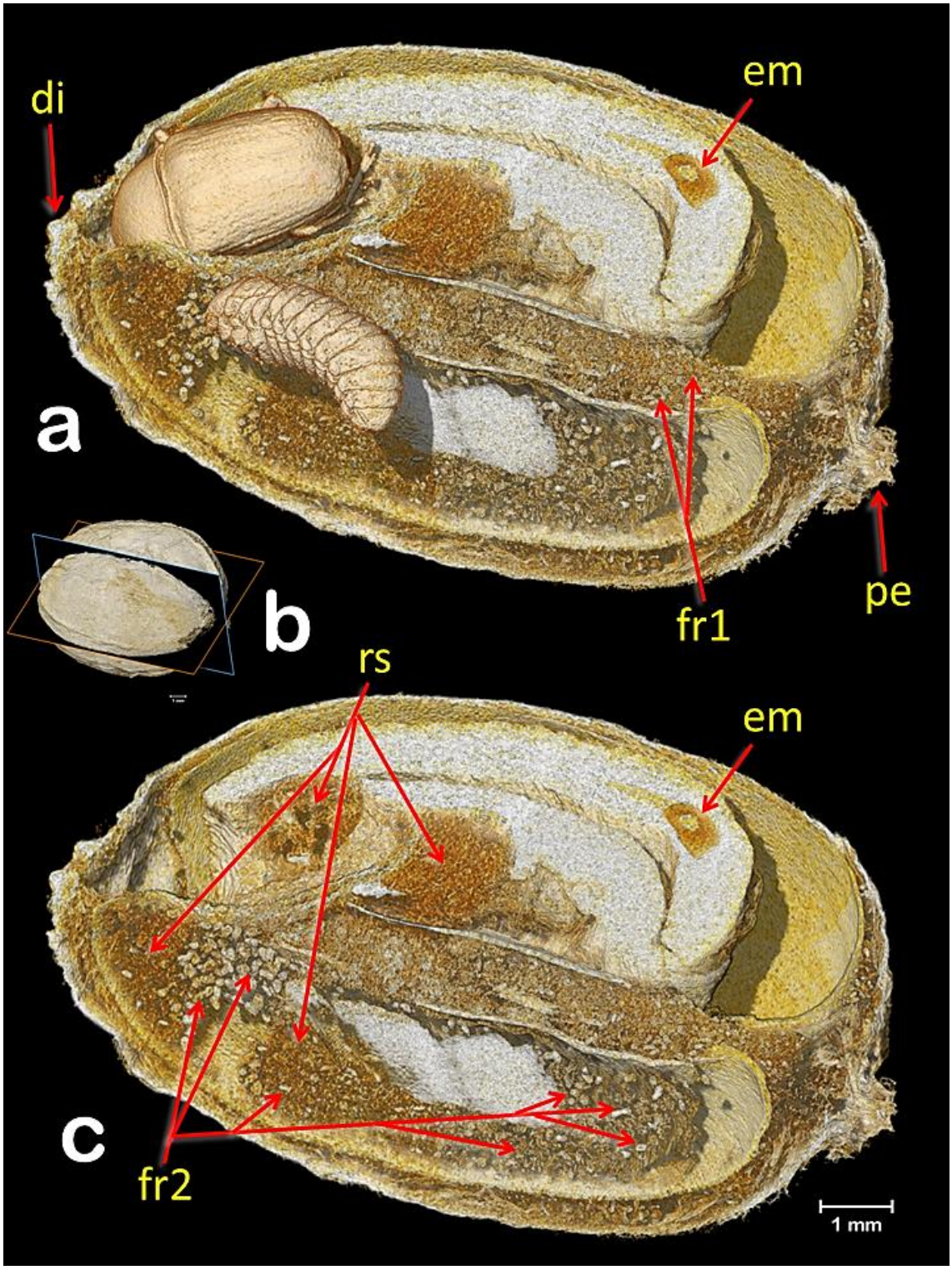

Figure 3.- Volume rendering images of a coffee berry infested with the coffee bean weevil (**a**,**c**), sectioned as shown in (**b**). The female adult and 5th instar larva (**a**) have been separately segmented to unveil their location inside the berry. Digital removal of the insects (**c**) allows to see the cavities and galleries filled with frass (fr1, fr2) and rasped seed material (rs). It is possible to distinguish the older galleries occupied during the time the larva was younger and smaller because they are filled with a smaller frass size (ca. 175 µm long; fr1). Newer galleries have a larger frass size (ca. 290 µm long; fr2). Abbreviations: di = disc (style remnant); em = coffee embryo; pe = pedicel.

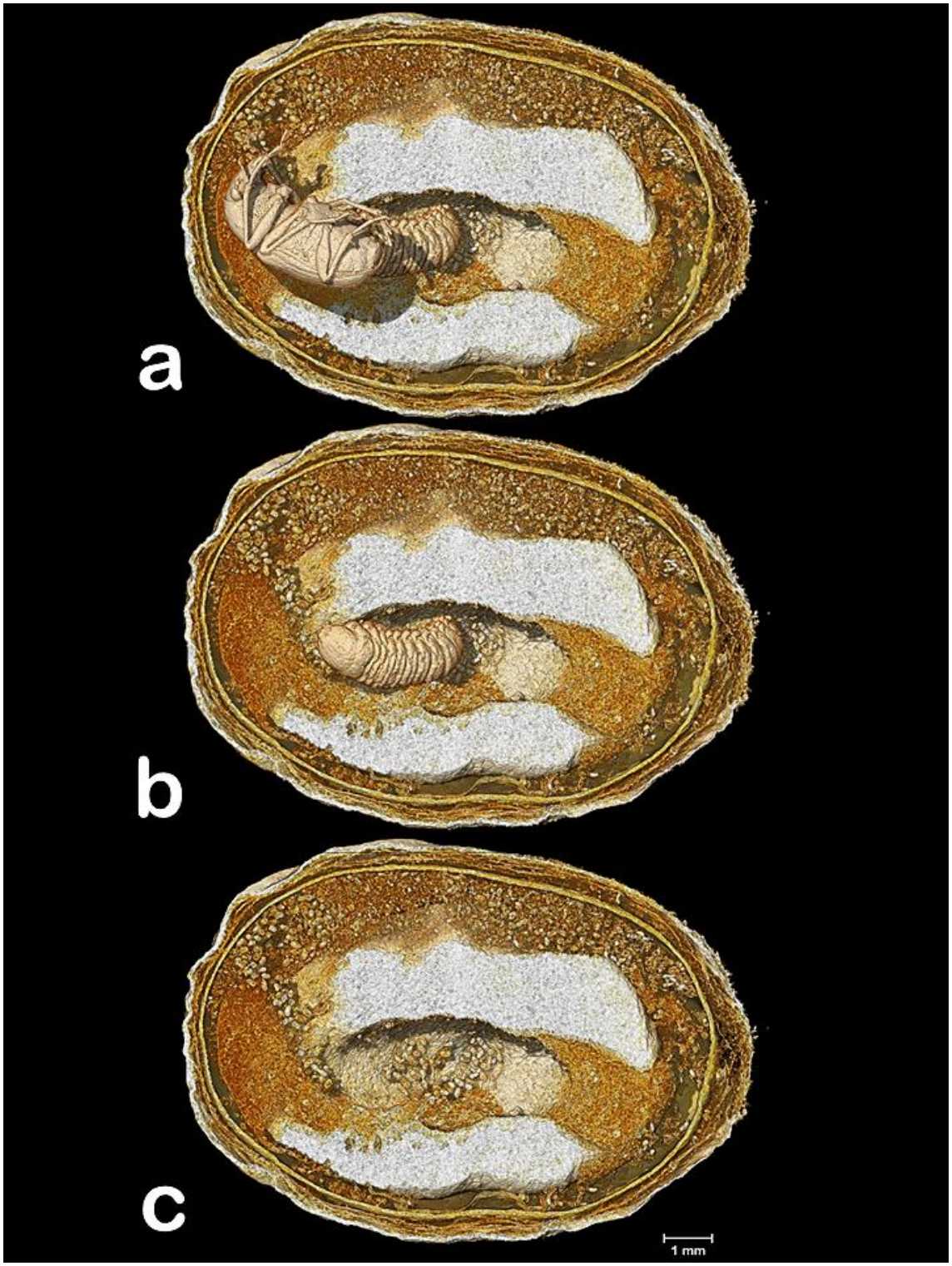

Figure 4.- Volume rendering images of a coffee berry infested with the coffee bean weevil, sectioned in a perpendicular plane in relation to Figure 2b,d. Images show galleries partially filled with frass and rasped seed material. The position of the insects is shown in (**a**). The adult female was digitally removed, leaving the 5th instar larvae (**b**). Both insects have been digitally removed (c).

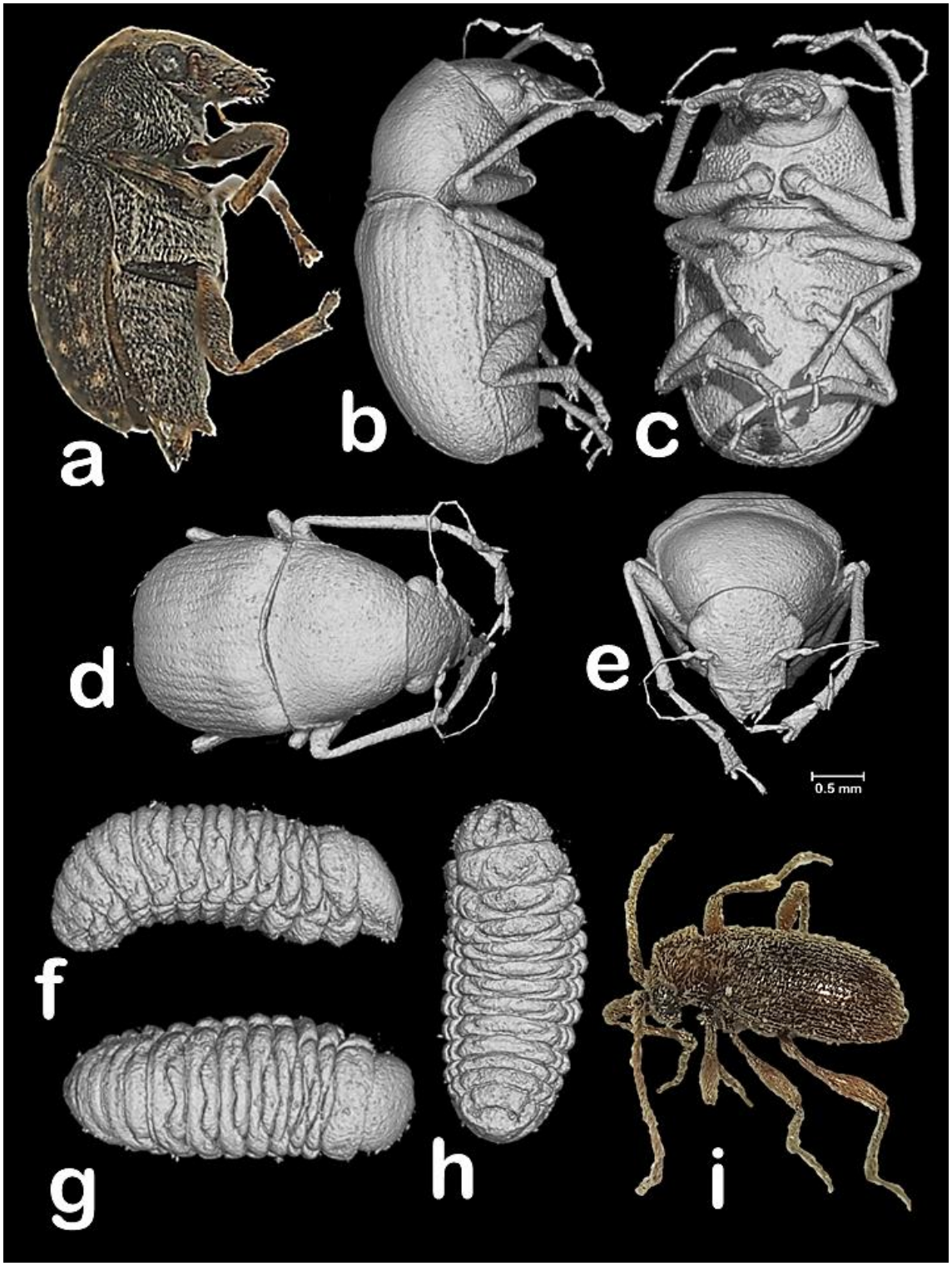

Figure 5.- Female adult and larva of the coffee bean weevil (**a**–**h**), and macro-photography of a male of *Ptinus sensu stricto* (**i**). Macrophotography (a) and micro-CT volume rendering images (**b**–**h**) of the same coffee bean weevil specimens inside the coffee berry shown in Figure 2, but digitally extracted from the berry and visualized with Amira software (Thermo Fisher Scientific, 2017). Female adult (**a**–**e**) and a 5th instar larva (**f**–**h**). Lateral views (**a**,**b**,**f**); ventral views (**c**,**h**); antero-dorsal view (**d**); dorsal view (**g**); and frontal view (**e**).

material they gnaw is consumed (thus supporting Autuori's observation (Autuori, 1931)) and instead, is accumulated. At times of highest heat intensity, they spread it around their body which is hypothesized to (1) create a barrier with the seed wall thus reducing the heat intensity and (2) serve as a defense against parasitoids and predators trying to reach the insect (Cabal Concha, 1956).

5.7.6.- Conclusions

Even though *A. fasciculatus* was first reported by Charles De Geer in 1775 as *Curculio fasciculatus* (De Geer, 1775), this is the first time, in the intervening 242 years, we have been able to "freeze" the activity of the insect inside a coffee berry and study it in detail using modern micro-CT techniques. This study reveals interesting aspects of the biology of the coffee bean weevil inside the coffee berry.

5.7.7.- Supplementary Information

Videos:

S1.- Coffee bean weevil walking over coffee berries inside Petri dish.

https://www.dropbox.com/s/gl59hk3ztjplnn2/S2.-Aracereus%20fasciculatus%20walking.mp4?dl=0

S2.- Micro-CT volume rendering of a coffee bean weevil adult and 5th larval instar inside a coffee berry.

https://www.youtube.com/watch?v=S_ppgGc0I0U

5.7.8.- References

Abrahão, J., & Bitran, E. A. (1973). Caruncho das tulhas atacando lavouras de café. *O Biol.*, *39*, 245–247.

Agricultura, D. de. (1923). Praga do café. *Bol. Agric.*, *24*, 83–88.

Alba-Tercedor, J. (2014). From the sample preparation to the volume rendering images of small animals : A step by step example of a procedure to carry out the micro-CT study of the leafhopper insect *Homalodisca vitripennis* (Hemiptera: Cicadellidae). In *Bruker Micro-CT Users Meeting 2014* (pp. 260–288). Bruker Micro-CT-Skyscan. http://bruker-microct.com/company/UM2014/000_AbstractBook2014.pdf

Alba-Tercedor, J., & Alba-Alejandre, I. (2017). Comparing micro-CT results of insects with classical anatomical studies: The European honey bee (*Apis mellifera* Linnaeus, 1758) as a benchmark (Insecta : Hymenoptera , Apidae). In *Bruker Micro-*

CT Users Meeting 2017 (pp. 147–167). Bruker micro-CT. http://bruker-microct.com/company/UM2017/AbstractBook2017.pdf

Alba-Tercedor, J., Alba-Alejandre, I., & Vega, F. E. (2018). Micro-CT unveils the secret life of the coffee berry borer (*Hypothenemus hampei*; Coleoptera, Curculionidae: Scolytinae) inside coffee berries. In *Bruker Micro-CT Users Meeting 2018* (pp. 165–173). http://bruker-microct.com/company/UM2018/2018_30.pdf

Archibald, R. D., & Chalmers, I. S. (1983). Stored product Coleoptera in New Zealand. *N. Z. Entomol.*, *7*, 371–397.

Autuori, M. (1931). Dados biologicos sobre o *Araecerus fasciculatus* (De Geer) (Col. Anthribiidae). *Revista de Entomología*, *1*, 52–61.

Bemelmans, J. (1930). *Les ennemis du caféier. Ann. Gembloux*. *36*, 418–424.

Cabal Concha, A. (1956). Biología y control del gorgojo del café: *Araecerus fasciculatus* De Geer Fam: (Anthribiidae), en Barranquilla—Colombia. *Rev. Fac. Nac. Agron. Medellín, 18*(49), 49–72.

Cárdenas Murillo, R., & Posada Flórez, F. J. (2001). *Los Insectos y Otros Habitantes de Cafetales y Platanales* (C. D. de C. del Quindío (ed.)).

Caspersen, B. (2016). A focus on flaws. Do you use the SCAA's green arabica coffee classification system? *Roast*, 24–28, 30–32, 34, 36–40.

Chittenden, F. H. (1896). Insects Affecting Cereals and Other Dry Vegetable Foods. *U.S. Department of Agriculture, Division of Entomology, Bulletin No. 4—New Series; Government Printing Office: Washington, DC, USA*, 112–130.

Chittenden, F. H. (1897). An invasion of the coffee-bean weevil. In Some Little-Known Insects Affecting Stored Vegetable Products: A Collection of Articles Detailing Certain Original Observations Made Upon Insects of This Class. *U.S. Department of Agriculture, Division of Entomology, Bulletin No. 8—New Series; Government Printing Office: Washington, DC, USA*, 36–38.

Cotton, R. T. (1921). Four Rhynchophora attacking corn in storage. *J. Agric. Res.*, *20*, 605–614.

Da Costa Lima, A. (1956). *Insetos do Brasil, Volume 10, Coleópteros, Fourth and Last Part; Serie Didática #12* (E. N. de Agronomia (ed.)).

De Figuereido, E. R. (1957). O contrôle do "caruncho" das tulhas. *O Biol.*, *23*, 197–200.

De Geer, C. (1775). *Memoires pour Servir a l'Histoire des Insectes; Volume 5*. Pierre Hesselberg.

Locatelli, D. P., & Viganò, C. A. (1991). Contaminazioni entomatiche in caffe crudo e tostato. *Ind. Aliment.*, *30*, 977–991.

Mancion, J., & Alibert, H. (1936). La production du café au Togo et quelques insectes déprédateurs du caféier. *L'Agron. Coloniale*, *224*, 33–43.

Mphuru, A. N. (1974). *Araecerus fasciculatus* De Geer (Coleoptera: Anthribidae): A review. *Trop. Stored Prod. Inf.*, *26*, 7–15.

Padi, B. (1999). Insects associated with coffee berries in Ghana. *Proceedings of the 18th International Scientific Colloquium on Coffee, Helsinki, Finland, 2–6 August 1999*, 524–528.

Sekhar, P. S. (1964). *Entomology in India*. Entomological Society of India.

Thermo Fisher Scientific. (2017). *Amira 3D visualization and analysis software.* (6.7.0). FEI. http://www.thermofisher.com/amira-avizo

Valentine, B. D. (2005). The scientific name of the coffee bean weevil and some additional bibliography (Coleoptera: Anthribidae: Araecerus Schönherr). *Insecta Mundi*, *19*, 247–253.

Varón, E. H., Hanson, P., Borbón, O., Carballo, M., & Hilje, L. (2004). Potencial de hormigas como depredadores de la broca del café (*Hypothenemus hampei*) en Costa Rica. *Manejo Integr. Plagas Agroecol.*, *73*, 42–50.

Waller, J. M., Bigger, M., & Hillocks, R. J. (2007). *Coffee Pests, Diseases and Their Management*. CABI Publishing.

Wilkinson, H. (1928). *The Coffee Berry Borer Beetle Stephanoderes hampei (Ferr.)*. The Government Printer; Colony and Protectorate of Kenya.

6.- DISCUSIÓN GENERAL

6.1.- Anatomía de *Diaphorina citri* (ACP)

Para la anatomía externa hemos seguido la terminología general clásica (Bitsch, 1979; Chapman, 2013; Gillott, 2005; Gullan & Cranston, 2010; Matsuda, 1976a; Pesson, 1951; Snodgrass, 1935; Triplehorn & Johnson, 2005) y la específica utilizada en homópteros psiloideos (Cicero, 2020; Drohojowska et al., 2013; Hodkinson & White, 1979; Ossiannilsson, 1992; Ouvrard et al., 2002), intentando mantener aquellos términos cuyo uso está más ampliamente aceptado.

Las sensilas antenales olfatorias (rhinaria) que observamos en el ACP, y su presencia alterna en los antenómeros, ha sido también observada por otros autores (Arras et al., 2012; Zheng et al., 2020), y su presencia fue ya puesta de manifiesto para *Homotoma ficus*, como "fosas de olor" (*Geruchsgruben*) a finales del XIX (Witlaczil, 1885). Desde entonces su función olfatoria fue asumida, de ahí el nombre de rhinaria, con que se mencionan frecuentemente (Burckhardt, 1987; Hodkinson & White, 1979; Onagbola *et al.*, 2008; Ossiannilsson, 1992; Zheng *et al.*, 2020). Mediante microscopía electrónica de barrido se ha confirmado que su estructura se corresponde con sensilas de tipo campaniforme (Arras *et al.*, 2012; Zheng *et al.*, 2020). Recientemente, estudiando su contenido en proteínas ligadas a funciones olfativas y la presencia de receptores olfativos y enzimas específicas, se ha demostrado su función como receptores olfativos (Arras *et al.*, 2012).

En relación con el aparato bucal, Witlaczil (Witlaczil, 1885) también describió y dibujó para *Psyllopsis fraxinicola* el labio (con tres segmentos), y de forma esquemática los conos maxilares y mandibulares, así como la musculatura asociada, lo cual concuerda con nuestras observaciones para el ACP. Un estudio reciente de SEM del labio de ACP (Garzo et al., 2012) muestra una hendidura posterior en el tercer segmento labial que también aparece en las figuras de Cicero (Cicero, 2020). Sin embargo nosotros observamos una corte divisorio muy largo en la cara anterior (dorsal) en vez de la hendidura que señala Cicero (Cicero, 2020), con una configuración muy similar a lo observado mediante SEM en otras especies de psílidos: *Cacopsylla chinensis* (Liang *et al.*, 2013) y *Boreioglycaspis melaleucae* (Ammar *et al*., 2015).

El término rostro lo mantenemos como un término genérico que simplifica las descripciones y evita las incertidumbres inherentes a los intentos de homologar terminologías, tal y como señaló Cicero (Cicero, 2020; Cicero *et al.*, 2015) y por ejemplo trató de hacer Dmitriev (Dmitriev, 2010). Así, el labio de los hemípteros se conoce como rostro (Chapman, 2013). Hemos mantenido el término clípeo (que encierra el cibario) en el sentido más ampliamente utilizado para esa estructura en los insectos homópteros psílidos (p.ej.: (Ammar *et al*., 2015; Brittain, 1922; Grove, 1919; Hodkinson & White, 1979; Liang *et al*., 2013; Saunders, 1921; Weber, 1929)).

Para el psílido *Psylla mali*, en las publicaciones iniciales más citadas (Brittain, 1922; Saunders, 1921), en los trabajos de Grove (Grove, 1919) y en el de Weber (Weber, 1929) especialmente, se encuentran dibujos muy realistas del aparato bucal, incluidos los conos mandibulares y maxilares existentes dentro de cibario, y que muestran una configuración muy similar a la que nosotros describimos y figuramos para el ACP. Trabajos más recientes muestran las estructuras, dentro de cibario, en diferentes especies (Brown *et al*., 2016; Cicero, 2017; Cicero *et al*., 2015; Cicero & Brown, 2009; Liang *et al*., 2013), incluido el ACP (Cicero, 2020; Cicero, Alba-Tercedor, *et al.*, 2018; Garzo *et al.*, 2012). La mayoría de esos estudios, aunque con imágenes muy llamativas, tienen la limitación de que las estructuras se obtuvieron mediante disecciones y se sometieron a procesos de preparación (incluyendo digestión con KOH) que claramente han distorsionado y alterado los resultados obtenidos. Así, por ejemplo, la típica capsula en forma de corona de los conos mandibulares (observada también en *P. mali* (Weber, 1929), o que nosotros hemos observado mediante microtomografía en el psíllido del olivo *Euphyllura olivina*, no se observa en ninguna de la imágenes de SEM de los trabajos anteriores, y solo aparece la expansión medial.

Estudios sobre el tórax de diferentes especies de psiloideos han sido publicados por diferentes autores (Brittain, 1922; Drohojowska *et al.*, 2013; Ouvrard *et al.*, 2002; Saunders, 1921; Weber, 1929), pero no tenemos conocimiento de la publicación de ningún estudio detallado del tórax de *D. citri*, y de ahí el valor por su novedad de este trabajo.

La presencia de glándulas en las patas, y particularmente glándulas coxales, ha sido descrita en insectos (p.ej.: (Billen, 1997, 2009; Billen & Ito, 2006; Da Cruz-Landim *et al*., 1988; Nijs & Billen, 2015), pero no tenemos noticias de que hayan sido, hasta ahora, mencionadas en ningún psiloideo. Sin embargo, en publicaciones con imágenes de SEM de diferentes especies del género *Cacopsylla* (Drohojowska *et al.*, 2013) se ven claramente los orificios coxales (ostiolos) que nosotros describimos en el ACP.

Glándulas antenales se han descrito en hormigas y otros insectos (p.ej.: (Bin, 1986; Keil, 1999; Renthal *et al*., 2008)). Dahms (Dahms, 1984) encontró una glándula en el escapo de los machos de la abeja *Melittobia australica* y concluyó que presumiblemente los machos dependen de los estímulos químicos y táctiles para localizar a las hembras y que el comportamiento precopulatorio, con movimiento y contacto de las antenas, sugiere que la hembra recibe un aporte químico considerable por la secreción de esta glándula antenal. Asimismo, se ha demostrado que los machos del ACP son atraídos por feromonas producidas por las hembras, y que los machos son atraídos y colonizan plantas de cítricos que previamente han estado colonizadas por hembras (Wenninger, 2008). Sin embargo, no se ha localizado donde se producen estas feromonas que impregnan las superficies de las plantas y atraen a los individuos. Pero considerando la localización basal de las glándulas coxales que hemos encontrado, resulta bastante plausible que estas segreguen feromonas que impregnen las superficies de las plantas en las que se posan los individuos. Durante el cortejo precopulatorio, en la distancia corta, las glándulas antenales producirán las sustancias químicas que ayudan al reconocimiento de sexos. De hecho en una revisión reciente del comportamiento reproductor del ACP (Mankin & Rohde, 2020) se concluye que en la corta distancia son los "semioquímicos"[1] que juegan un papel importante en el encuentro para la cópula de algunos (no todos) psiloideos. Por tanto, esto abriría una línea muy interesante de investigación para conocer el papel secretor de esas estructuras

[1] **Semioquímico** (del griego "σημεῖον", *semeion*, señal) es una sustancia química o complejo de sustancias químicas emitidas por un organismo que afectan el comportamiento de otros individuos (https://es.wikipedia.org/wiki/Semioqu%C3%ADmico)

y en su caso dilucidar la composición química de las secreciones y su posible papel como feromonas de atracción y reconocimiento sexual.

Respecto de la venación de las alas de los psiloideos existen discrepancias de interpretación. Lo que es fácil de observar cuando se comparan, por ejemplo, la publicación general de Hodkinson y White (Hodkinson & White, 1979) con la de Ossianilson (Ossiannilsson, 1992)). Nosotros hemos seguido a Yen y Burckhardt (Yen & Burckhardt, 2017) para los nombres de la venas del ala anterior y a Ossianilson (Ossiannilsson, 1992) para las del ala posterior. Las venas tienen una estructura tubular, que es claramente visible en sección transversal del ala. Sin embargo, lo que generalmente se interpreta con vena Cu_2 (p.ej.: (Brown & Hodkinson, 1988; Hodkinson & White, 1979; Ossiannilsson, 1992)) no tiene estructura tubular, se corresponde con un pliegue en el área cubital y no es una vena alar. De hecho Mally, a finales del siglo XIX, lo consideró como una “sutura claval” (Mally, 1894). Por ello nosotros lo llamamos pliegue cubital, y entre paréntesis hemos mantenido la abreviatura Cu_2 para ayudar a los lectores acostumbrados a la terminología en uso.

En los psílidos los primeros segmentos abdominales están reducidos y se juntan con los segmentos torácicos o abdominales, lo que dificulta su interpretación y numeración. No existiendo un consenso en la asignación numérica de los segmentos abdominales visibles (Bitsch, 1979; Matsuda, 1976b; Muir, 1930b; Pesson, 1951; Zucht, 1972). De hecho, las obras generales sobre psílidos evitan la controversia y no numeran los segmentos abdominales (p.ej.:(Hodkinson & White, 1979)). En consecuencia, y como la interpretación de los segmentos abdominales no es el principal objetivo de este trabajo, nosotros hemos numerado los terguitos y esternitos siguiendo el difícil consenso general y particularmente la interpretación de Matsuda (Matsuda 1976b).

El pequeño tamaño y la posición críptica de algunos espiráculos respiratorios de los psiloideos explica la controversia que ha existido tanto en cuantos son, como en su localización (ver las discusiones en los trabajos previos de Muir (Muir, 1930b) y Hesslop-Harrison (Heslop-Harrison, 1952)). Después de una extensa revisión, Hesslop-Harrison (Heslop-Harrison, 1952) concluyó que ningún psílido posee más de siete espiráculos abdominales funcionales, aunque

pueda haber un octavo, especialmente en los machos. Lo que concuerda con nuestras observaciones de 7 pares de espiráculos abdominales en el ACP, pero no encontramos un octavo. Además el primero y segundo par de espiráculos están muy próximos, tal y como fue observado en *P. mali* (Muir, 1930b).

Hasta ahora no se había estudiado en detalle el sistema traqueal de ninguna especie de psiloideos, y en especial en los adultos. Witlaczil (Witlaczil, 1885) describió y dibujó el sistema traqueal de la ninfa de *Trioza rhamni*, pero para los adultos señaló que era difícil observarlo. Recientemente, transparentando los ejemplares con ácido láctico se ha publicado una fotografía (sin descripción alguna) en la que se observan tubos traqueales de *Cyamophila willieti* (Ruan *et al.*, 2018). Por tanto, nuestros resultados sobre el sistema traqueal abdominal representan el primer estudio detallado en los adultos. En el futuro utilizando la técnica descrita en el capítulo 5.6 (Alba-Tercedor et al., 2019) sería posible completar el estudio del sistema respiratorio del ACP. Esa técnica necesita escanear los especímenes inmediatamente después de matarlos o anestesiarlos. Siendo esta la causa de que no la hayamos podido aplicar dado lo arriesgado que sería que nos enviaran a nuestro laboratorio ejemplares vivos, que en caso de fuga podrían atacar a los cultivos de cítricos de la península ibérica.

El vaso dorsal (corazón) y la aorta anterior fue descrita y dibujada por primera vez en dos especies de psílidos por Witlatczil (Witlaczil, 1885), y a pesar de que los dibujos son esquemáticos, tanto la posición y extensión del vaso dorsal que estudió en *R speciosa* y la extensión y los ostiolos laterales que estudió en *P. buxi*, concuerdan con lo que nosotros hemos observado en el ACP. Así, el detallado estudio que presentamos representa hasta la fecha el único estudio del circulatorio del ACP y el más detallado de los realizados en psílidos.

Según Snodgrass (Snodgrass, 1935), en los homópteros el canal alimentario típico presenta un ventrículo, que consta de tres partes: ventrículo-1 (un ensanchamiento anterior situado inmediatamente posterior a la válvula estomodeal, encerrado en la cámara filtradora), ventrículo-2 (en forma de saco, a modo de buche de almacenamiento) y ventrículo-3 (una sección tubular del estómago anterior de los insectos, que se curva anteriormente para volver a

entrar en la cámara filtradora). Los homópteros psiloideos, y el ACP muestran una organización acorde con lo descrito por Snodgrass, en donde el ventrículo-1 corresponde con el bulbo, y otros dos espacios espongiformes situados dentro de la cámara filtradora, el ventrículo-2 se corresponde con el intestino medio ("buche") que presenta un tracto ventral descendente (en donde y al igual que en el asa ventral del intestino medio son muy patentes las células romboidales) y el ventrículo-3, después del asa ventral del intestino medio que se prolonga en el intestino posterior interno, dentro de la cámara filtradora. De forma similar a lo ya descrito y figurado (Brown *et al*., 2016; Cicero, 2020; Cicero & Brown, 2009). Sin embargo, debido a las disecciones y manipulaciones, la posición anatómica, y algunas aseveraciones sobre las estructuras, descritas en los trabajos previos, no se corresponden con la posición real dentro del animal. Asi, por ejemplo, se ha mencionado que "el esófago entra verticalmente en la cámara filtradora"; pero la micro-CT muestra que el esófago desciende, se vuelve casi horizontal, justo en el tracto final que además está dilatado. Del mismo modo se habían distinguido dos partes anatómicas dentro del ventrículo-1 (dentro de la cámara filtradora), una "superior" (que se corresponde con el bulbo) y otra "inferior". Sin embargo, las imágenes de micro-CT muestran que el bulbo es anterior y está situado en una posición inferior con respecto a la parte posterior del ventrículo.

En general, en los insectos, el canal alimenticio comienza con la boca y termina en el ano, y consta de tres partes principales: intestino anterior (estomodeo), intestino medio (mesenteron) e intestino posterior (proctodeo). En la parte anterior se distingue una cavidad preoral, las piezas bucales, la faringe y el esófago. Desde aquí el alimento pasa al intestino medio e intestino posterior. Siendo expulsados los desechos a través del orificio anal (Chapman, 2013; Gillott, 2005; Snodgrass, 1935a). Siguiendo este esquema, en el ACP (al igual que en otros homópteros) las piezas bucales se corresponden con los estiletes mandibulares y maxilares que están protegidos dentro del labio, y forman juntos un canal salivar y otro alimenticio (Cicero, 2020; Garzo *et al.*, 2012). Pero debido a las fuertes transformaciones evolutivas que han sufrido los insectos homópteros como succionadores, tanto lo que corresponde a la cavidad preoral en sentido estricto y estructuras adyacentes son aspectos actualmente en discusión (Cicero, 2020). La faringe corresponde a la parte anterior del canal

alimenticio. Tiene una pequeña dilatación que contiene la bomba precibarial salivar (lo que hemos observado en el ACP presenta una configuración similar a lo que dibujó Grove (Grove, 1919), y Weber (Weber, 1929) describió y dibujó para *P. mali*, y Cicero *et al.* (Cicero *et al.*, 2015) para *Bactericera cockerelli*, respectivamente). La faringe posteriormente se dilata, y en ella se insertan músculos para configurar la bomba cibarial. A continuación, el esófago continúa y justo antes de conectar con la cámara filtradora se dilata. El intestino medio continúa después de la cámara filtradora, y continua hasta que vuelve a disminuir de diámetro y vuelve a penetrar en la cámara filtradora como intestino posterior (intestino posterior interno) que sale de la cámara y se dirige posteriormente formando el intestino posterior externo que se dilata en un recto, antes del ano.

Observamos diferencias sexuales en la configuración del recto; mientras que en los machos se presenta como una tubo largo, uniformemente dilatado, en las hembras termina en una ampolla rectal). Esto podría deberse a las diferencias sexuales en la defecación. De hecho, en el psílido *Boreioglycaspis melaleucae* se ha observado que las hembras producen pequeñas bolas blanquecinas de melaza que son expulsadas del cuerpo con fuerza a modo de disparos, lanzando estas pegajosas excreciones lejos de los huevos y de las ninfas recién eclosionadas. Por el contrario, los machos de esa especie depositan gotitas de melaza inmediatamente detrás de ellos (Ammar *et al*., 2015). Así que muy probablemente, igualmente las hembras de ACP lancen lejos pequeñas bolitas de excrementos para evitar contaminar a los huevos y a las ninfas recién eclosionadas. Para ello la existencia de la ampolla rectal facilitaría esta función, en vez del recto largo y voluminoso que aparece en los machos.

En el intestino medio Ammar *et al.* (Ammar *et al.*, 2017) reconocen un intestino medio anterior (que se extiende desde el contacto con la cámara filtradora, lo que nosotros hemos llamado aquí intestino medio dilatado eferente, hasta que desemboca el primer apéndice abdominal), y un intestino medio central (que se extiende desde la conexión del primer apéndice abdominal, hasta la conexión del cuarto apéndice abdominal), y un intestino medio posterior (que se extiende desde la inserción del cuarto apéndice abdominal hasta la conexión con la cámara filtradora, lo que nosotros hemos llamado intestino medio aferente).

La cámara filtradora es una modificación del tubo digestivo que se encuentra en la mayoría de los insectos homópteros, en que dos partes normalmente distantes (estomodeo/mesenteron y proctodeo) se sitúan en íntimo contacto y se rodean de una cubierta de tejido conectivo. El órgano así formado permite que el exceso de agua y los carbohidratos solubles del alimento difundan directamente desde la parte anterior del digestivo a la posterior, mientras que las proteínas y las sustancias grasas se retienen y se absorben (Snodgrass, 1935a). El tubo digestivo dentro de la cámara filtradora consta dos secciones que confluyen entre sí y que tienen flujos que circulan paralelos y en sentido contrario, configurando un filtro contracorriente (Hamilton, 2015). Esto requiere una alta presión del fluido, y esto explicaría el por qué el esófago se dilata justo antes de entrar en la cámara filtradora, como hemos observado en el ACP y se había señalado anteriormente (Cicero, 2020; Cicero *et al*., 2018; Cicero & Brown, 2009), porque según el principio de Bernoulli un aumento del diámetro de la tubería implica una disminución de la velocidad y la energía cinética y un aumento de la presión (Bajpai, 2018). Por tanto, el alimento líquido es forzado por la mayor presión a entrar en la cámara filtradora, mientras que el flujo disminuye su velocidad facilitando la transferencia del exceso de agua al intestino posterior interno que rodea la parte externa dentro de la cámara filtradora. Al parecer, esa dilatación del esófago antes de entrar en la cámara filtradora existe en muchas otras especies, ya que se observa claramente en las figuras del digestivo de diferentes especies de homópteros chupadores de savia, realizadas por diferentes autores (p.ej.: (Pesson, 1951; Snodgrass, 1935; Wigglesworth, 1942)).

La cámara filtradora ha sido estudiada en detalle en diferentes especies de homópteros chupadores de savia, y de acuerdo con Cicero *et al.* (Cicero, Hunter, *et al.*, 2018) más de 50 publicaciones tratan diferentes aspectos sobre la anatomía y fisiología de la cámara filtradora (p.ej.: (Cecil, 1930; Goodchild, 1963; Hubert et al., 1989; Kershaw, 1914; Lindsay & Marshallt, 1980)). En los psiloideos se ha descrito que el intestino posterior y el esófago se unen en espiral uno alrededor del otro (Pesson, 1951; Wigglesworth, 1942a), y fue sucintamente descrito en *P. mali* (Brittain, 1922; Saunders, 1921) y en *P. fraxinicola* (Witlaczil,

1885). Respecto de *D. citri* se han publicado imágenes de microscopia óptica del digestivo, que incluyen a la cámara filtradora, así como dibujos esquemáticos y fotografías de SEM (Cicero & Brown, 2009), y una microtomografía de la cámara filtradora de la ninfa de último estadío (Brown *et al*., 2016). Además, el conocimiento anatómico del tubo digestivo, incluida la cámara filtradora del ACP se ha resumido recientemente mediante dibujos esquemáticos animados. (Cicero *et al.*, 2018). Sin embargo, nuestro trabajo representa el primer estudio de detalle de la anatomía de la cámara filtradora de los adultos del ACP.

Los cuatro apéndices abdominales, que desembocan en diferentes puntos del intestino medio, han sido considerados como túbulos de Malpigio, considerando que tiene una función excretora (Ammar *et al.*, 2011, 2017; Ammar & Hall, 2012; Hamilton, 2015; Kruse *et al.*, 2017; Pesson, 1951; Saunders, 1921; Witlaczil, 1885). Sin embargo, y desde un punto de vista estrictamente anatómico, la inserción de los túbulos de Malpigio debería coincidir con la separación y ser el el límite entre el mesenteron (intestino medio) y el proctodeo (intestino posterior) (Chapman, 2013; Gillott, 2005; Snodgrass, 1935a). Sin embargo, los apéndices del intestino medio desembocan consecutivamente y en puntos alejados unos de otros. Es por eso que decidimos seguir la opinión de Cicero y llamarlos “apéndices abdominales”, en lugar de túbulos de Malpigio, hasta que finalmente se aclare su función excretora. (Brown *et al.*, 2016; Cicero, 2020; Cicero & Brown, 2009). Pero en todo caso las microfotografías recientemente publicadas por Nocelli *et al.* (Nocelli *et al.,* 2016) de los túbulos de Malpigio de la abeja *Melipona scutellari*s son totalmente comparables con las imágenes microtomográficas que nosotros hemos obtenido de los apéndices de intestino medio del ACP (y similares a los dibujos de *P. mali* y *T. rhamni*, realizados por Witlazcil (Witlaczil, 1885)).

Respecto a las glándulas salivales, existen diferentes trabajos con descripciones, o imágenes, que contienen las glándulas salivares de psílido de la patata *B. cockerelli* (Cicero *et al.*, 2015), e inclusive del ACP (Ammar *et al.,* 2011, 2017; Cicero, 2020; Cicero & Brown, 2009, 2011). Las glándulas salivales de los adultos de *D. citri* se han descrito como compuestas a cada lado por dos glándulas principales y una glándula salival accesoria más pequeña. Al comparar estas descripciones y microfotografías con nuestros resultados observamos que:

lo que se ha denominado glándulas salivales principales corresponden a los lóbulos salivales que observamos con microtomografía y que hemos numerado como lóbulos 1 y 2; y el lóbulo 3 corresponde a lo que se ha considerado como una glándula salival accesoria separada. Sin embargo, independientemente de las diferencias estructurales observadas en los trabajos previos (ver: Ammar, *et al.,* 2017; Cicero & Brown, 2009)), los tres lóbulos forman juntos una glándula salival lateral y, por tanto, no consideramos que haya ninguna razón para considerar el tercer lóbulo como una glándula salival accesoria separada diferente. En cada lóbulo los racimos de acinos que observamos con micro-CT son totalmente equiparables a las imágenes publicadas previamente de un corte semifino (teñido con azul de toluidina) de la glándula salival principal, mostrando al menos tres acinos con grupos de células secretoras teñidos diferencialmente (Ammar *et al.*, 2017).

Según Głowacka *et al.* (Głowacka *et al.*, 1995) los testículos de *D. citri* tienen quistes de espermatocitos dispuestos en una sola fila, lo que coincide con nuestras observaciones. Además, según estos autores cada testículo tiene dos folículos, mientras que para *Bactericera albiventris* describieron y publicaron figuras de una fusión casi completa (pero con una ligera separación vestigial) de folículos. A primera vista, cada testículo del ACP parece estar formado por un lóbulo único en forma de huso. Sin embargo, un examen detallado revela claramente lóbulos estrechos en ambos extremos de cada testículo, y en las secciones sagitales, que corresponden inequívocamente a la zona germinal de los testículos (germarium). Así, lo que parece ser una estructura única, en realidad consta de dos folículos, fusionados en una única estructura externa, con un conducto deferente común. Esto concuerda con la vista en secciones sagitales. Desde cada germario, hacia la conexión de los conductos deferentes, se forman espermatozoides dentro de los quistes de espermatocitos y maduran progresivamente. Las espermátidas/espermatozoides inmaduros son claramente visibles en la parte media de cada testículo similar a lo descrito en la especie *Aphalara polygoni* por Głowacka *et al.* (Głowacka *et al.*, 1995).

Aunque pueda parecer extraño encontrar espermatozoides en las glándulas accesorias, sin embargo, es posible dado que las vesículas seminales y los conductos de las glándulas accesorias se conectan muy próximos a la

bomba espermática, en una pequeña área de la placa cóncava, justo antes de la cámara de la bomba espermática. De modo que los espermatozoides pueden llegar fácilmente a las glándulas accesorias.

La estructura clásicamente interpretada como bomba espermática, ha recibido diferentes nombres: Witlaczil (Witlaczil, 1885) la llamó "*kolbenförmiges organ*" (literalmente, “órgano en forma de pistón”), pero no fue hasta comienzos del siglo XX que su función fue interpretada (Saunders, 1921) y se le llamó “bomba eyaculadora” (Brittain, 1922). Quadri (Qadri, 1949) la denominó “bomba seminal” y Schlee usó el término “bomba espermática” (Schlee, 1969), al igual que Prophetou (Prophetou-Athanasiadou & Tzanakakis, 1998). Nosotros usamos el término "bomba espermática" como el nombre más exacto porque alude a su función. La estructura detallada revelada por micro-CT parece tener todos los elementos de una bomba aspirante-impelente. El examen 3D proporciona nueva información para explicar cómo funciona el bombeo para evitar el reflujo de esperma. Mediante la contracción de los músculos longitudinales que rodean la cámara de bombeo cilíndrica, los espermatozoides saldrían de la cámara y entrarían en el conducto eyaculador. Simultáneamente, el músculo del pistón (unido entre la punta delantera del pistón y la superficie central interna de la placa cóncava) se contraería, evitando el reflujo de los espermatozoides. Así, la cresta anterior dorso-ventral de la placa cóncava aparentemente refuerza la placa contra la flexión durante la contracción muscular. Las estructuras observadas mediante micro-CT encajan con descripciones previas de otras especies próximas de Psyllinae (R. G. Brown & Hodkinson, 1988; Schlee, 1969; Zucht, 1972) que recopiló Matsuda (Matsuda, 1976b). Las nuevas visualizaciones completan y mejoran el conocimiento previo de la bomba espermática del ACP realizado por Mathur (Mathur, 1975).

En relación con la genitalia, el género *Diaphorina* se caracteriza por un edeago de tres segmentos. En las publicaciones, el tercer segmento del edeago se presenta dilatado en su extremo y con forma de cuchara (ver (Burckhardt, 1987) y (Mathur, 1975)). Sin embargo cuando se comparan las imágenes obtenidas mediante micro-CT con las obtenidas mediante microscopía óptica, en las de micro-CT el tercer segmento del edeago aparece menos ensanchado (ver cap. 5.2, (Alba-Alejandre et al., 2018) y el trabajo previo CT (Alba-Tercedor et

al., 2017a). Esto se debe sin duda a que en las preparaciones microscópicas el edeago se comprime bajo la presión de la lámina cubreobjetos y por tanto se deforma. De hecho Ammar *et al.* (Ammar *et al.*, 2013) publicaron recientemente una imagen de microscopía óptica en la que el extremo del edeago aparece muy ensanchado, en forma de cuchara; pero en una imagen de SEM (en la que la genitalia no está comprimida) el segmento 3 tiene una forma similar a la de nuestras reconstrucciones mediante micro-CT. Sin duda, hasta ahora, el estudio anatómico más detallado de la genitalia de un psílido fue la publicada por Zucht (Zucht, 1972) de *P. crataegi*, que posteriormente se ha reproducido en trabajos clasicos como el de Bitsch (Bitsch, 1979). Asi como el estudio de *P. mali* realizado por Muir (Muir, 1930a), en donde (a partir de preparaciones microscópicas, y por tanto deformadas por compresión) describió la placa basal anterior ("basal plate") y las apófisis basales largas (que llamó "basal prolongations"). A pesar de ello, no existe un estudio de detalle similar de ninguna especie de psilloideo, incluido el ACP, similar al que hemos realizado a lo largo de presente trabajo.

Respecto al sistema reproductor femenino de *D. citri* lo que hemos observado concuerda a grandes rasgos con las descripciones previas de otras especies de psiloideos (p.ej.: (Blowers & Moran, 1967; Brittain, 1922; Büning & Büning, 1994; Dossi & Cônsoli, 2010, 2014; Prophetou-Athanasiadou & Tzanakakis, 1998; Saunders, 1921)). Según Pesson (Pesson, 1951), en los psiloideos cada ovario consta de alrededor de 25 ovariolas, pero otros autores encontraron más de 100 (Büning & Büning, 1994; Hodin, 2009). En el ACP se han encontrado alrededor de 50 ovariolas (Dossi & Cônsoli, 2014) que coincide con el número que nosotros contamos y que varía entre ovarios (contamos 40 en el ovario derecho y 46 en el izquierdo).

En general en los insectos, el cáliz (una dilatación del oviducto para la recepción de los huevos) se localiza justo en la unión de las ovariolas (ver por ej.: (Chapman, 2013; Gillott, 2005; Gullan & Cranston, 2010; Snodgrass, 1935a)). Sin embargo, la dilatación que nosotros hemos encontrado en *D. citri* corresponde a una dilatación del tubo del oviducto, justo antes de unirse con el oviducto común.

Varios autores consideran que las glándulas accesorias de las hembras son sinónimas de las glándulas del cemento (Chapman, 2013; Gillott, 2005; Gullan & Cranston, 2010; Snodgrass, 1935a). Su papel no se conoce bien, pero se ha sugerido que sus secreciones pueden activar la producción de feromonas (Gullan & Cranston, 2010) o interactuar con proteínas de las glándulas accesorias del macho o su esperma (Chapman, 2013). En múscidos se ha visto que la secreción de las glándulas accesorias contiene enzimas proteolíticas y una estearasa que juegan un papel clave en la fertilización de los huevos; pero no se sabe si esto ocurre en otros insectos (Chapman, 2013). El ACP tiene un par de glándulas accesorias tubulares muy bien desarrolladas, y aunque su estructura se ha estudiado previamente mediante microscopía electrónica, su función aún no se conoce (Dossi & Cônsoli, 2014), por tanto requiere futuras investigaciones.

Las protuberancias que observamos en la superficie de la espermateca del ACP, que le dan un aspecto rugoso, corresponden a las células secretoras del epitelio secretor, tal y como se ha sido descrito previamente en *Trioza alacris* (Marchini et al., 2012) y en *D. citri* (Dossi & Cônsoli, 2010, 2014). La espermateca no es solo un saco de almacenamiento donde se almacenan y/o nutren los espermatozoides antes de la fertilización del óvulo. Es probable que los dos materiales con diferentes densidades que observamos en la espermateca no sean dos cavidades separadas, sino una sola que contiene una espermatodosis (una reorganización del espermatóforo masculino transferido a la espermateca de la hembra). Se ha demostrado que la reorganización en espermatodosis protege a los espermatozoides de la actividad espermiolítica (p.ej.: (Marchini *et al.*, 2012; Pascini & Martins, 2017)). Así, la zona interna ventral, que se observa como un material de alta densidad, correspondería a la espermatodosis. Es posible distinguir estructuras de filamentos más densos dentro de la espermatodosis, que son de tamaño comparable a los espermatozoides como se describió anteriormente para *D. citri* (Barcellos et al., 2017) y similares a la imágenes de micro-CT que obtuvimos en este trabajo de los espermatozoides dentro de los testículos (ver cap. 5.2, (Alba-Alejandre *et al.*, 2018)). La zona interna dorsal, que aparece como material de baja densidad, correspondería a las secreciones líquidas nutritivas del epitelio secretor. En las hembras adultas,

próximas a ovipositar, la espermatodosis almacenada en la cavidad interna de la espermateca se disgrega para liberar espermatozoides; lo que explica el que no se observen dos zonas separadas dentro de la espermateca.

El estudio de micro-CT revela que la espermateca parece tener todos los elementos de una bomba aspirante-impelente, que es como se ha descrito anteriormente para la chinche arlequín *Murgantia histrionica* por Stacconi y Romani (Stacconi & Romani, 2011). De hecho, las cámaras y la posición de la vávula que aparecen en el trabajo de Stacconi y Romani son muy similares a lo que observamos en el ACP.

La función de bombeo de la espermateca se ha visto en otros insectos en los que se ha descrito como una bomba espermática, que contiene fibras musculares ubicadas bien en el saco espermático o en la pared del conducto. La presencia de fibras musculares que rodean todo el reservorio espermáticó se ha observado en varias especies de insectos (ver revisión de Pascini & Martins (Pascini & Martins, 2017)). En el ACP, mediante microscopía electrónica se ha descrito la presencia de estructuras musculares (Dossi & Cônsoli, 2014). Para bombear el esperma hacia la espermateca, la musculatura de la vaina espermática se contrae, luego se relaja y la elasticidad de la vaina espermática devuelve el saco espermático a su forma globular, absorbiendo a los espermatozoides desde la vagina a través del conducto espermático y se vierten en la cavidad del cáliz. Una vez que los espermatozoides llegan a la cavidad del cáliz (los músculos de los orificios de entrada se relajan para que los orificios permanezcan abiertos), la pared del cáliz se contrae de modo que el tapón de la válvula encaje en la primera cámara proximal con su punta ocluyendo el orificio central en la pared que divide los dos cámaras (el orificio tiene forma oblonga para adaptarse a la forma comprimida del tapón de la válvula). A partir de entonces, los espermatozoides se deslizan a través de los dos agujeros hacia el lumen de la espermateca, donde quedan protegidos dentro de la espermatodosis. Cuando la hembra oviposita, el procedimiento de bombeo espermático actúa a la inversa para que los espermatozoides sean impulsados hacia el conducto de la espermateca, donde los óvulos se fertilizan a medida que pasan a través de la vagina en el punto donde se conecta el conducto de la espermateca.

La glándula colleterial (=del cemento) produce una sustancia pegajosa para adherir los huevos al substrato, o para juntarlos en una masa (Büning & Büning, 1994; Chapman, 2013; Gullan & Cranston, 2010; Snodgrass, 1935a). Se han publicado estudios detallados de la glándula del cemento de varios insectos (p. ej. del lepidóptero *Sesamia nonagrioides* (De Santis *et al.*, 2008)). Estas glándulas están presentes tanto en hemípteros como en homópteros (Saunders, 1921) y su presencia ha sido descrita en diferentes especies de psiloideos (incluyendo a *D. citri* (Dossi & Cônsoli, 2014)) como una estructura globular conectada por un conducto al tercio distal del espacio intervalvular del ovipositor (Blowers & Moran, 1967; Brittain, 1922; Prophetou-Athanasiadou & Tzanakakis, 1998; Saunders, 1921). La micro-CT muestra una capa superficial densa correspondiente a un epitelio secretor, y una cavidad interna (lumen) llena de un material menos denso correspondiente a las secreciones pegajosas de la glándula (Blowers & Moran, 1967; De Santis *et al.*, 2008; Dossi & Cônsoli, 2014). El conducto de la glándula coleterial vierte su secreción pegajosa lejos del gonoporo. Así, una vez que los óvulos fecundados entran en la cámara genital y atraviesan el espacio intervalvular, se recubren con las secreciones pegajosas de la glándula coleterial justo antes de que abandonen el ovipositor; esto asegura que se adhieran a la planta huésped de cítricos.

En *P. mali* Saunders describió lo que denominó glándula accesoria mediana o paraovario (Brittain, 1922; Saunders, 1921) que muy probablemente corresponda a la “bursa copulatrix” descrita en diferentes especies de hemípteros y homópteros (Pesson, 1951), incluidas algunas especies de psiloideos (i.e.: *T. erytreae* (Blowers & Moran, 1967) y *E. phillyreae* (Prophetou-Athanasiadou & Tzanakakis, 1998)).Sin embargo, tanto mediante la disección de hembras (Dossi & Cônsoli, 2014) como nuestros estudios mediante micro-CT se confirma la ausencia de bursa copulatryx en *D. citri*.

La estructura del ovipositor ha sido descrita en detalle en varias especies de psiloideos (p.ej.: *P. mali* (Brittain, 1922; Muir, 1930a; Saunders, 1921) *P. crataegi* (Bitsch, 1979; Zucht, 1972), *Pachypsylla celtidis* (Austin, 2016)). Además de haberse publicado imágenes parciales realizadas mediante microscopía óptica de preparaciones del ovipositor, tanto de *E. phillyreae*

(Prophetou-Athanasiadou & Tzanakakis, 1998), como de *D. citri* (Dossi & Cônsoli, 2014).

La interpretación de los elementos del ovipositor varía según el autor. La mayoría reconoce y numera las válvulas, pero existen diferencias en la interpretación de las diferentes estructuras. Así Muir (Muir, 1930a) consideró a las láminas laterales como escleritos del 8º segmento abdominal y las llamó láminas laterales (término que nosotros hemos mantenido). Posteriormente Zucht (Zucht, 1972) consideró que estas corresponden al primer valvífero. Recientemente Austin (Austin, 2016) considera que cada lámina lateral representa el gonángulo (el esclerito que actúa como fulcro, articulándose sobre el primer valvífero y que se acopla con la 2ª y 3ª válvulas). Sin embargo para Matsuda (Matsuda, 1976b) las láminas laterales son la fusión del primer valvífero y el gonángulo. En cualquier caso aún no está clara la homología entre lo que se ha identificado como gonángulo en diferentes insectos (Klass *et al.*, 2012). Nosotros mantenemos el término "láminas laterales", en el sentido de Muir (Muir, 1930), siendo conscientes de que es posible que se corresponda con el gonángulo, tal y como Austin (Austin, 2016) sugiere en *P. celtidis*. Por lo tanto, lo que presentamos en esta tesis representa no solo el primer estudio detallado de esta estructura en *D. citri,* sino también la vista detallada más completa del ovipositor de cualquier especie de psiloideo utilizando nuevas técnicas de micro-CT.

Tanto las imágenes de micro-CT, como las reconstrucciones 3D del bacterioma que hemos obtenido son completamente comparables y más claras que las publicadas previamente de la cigarrilla *O*. *albicinctus*, utilizando un sincrotrón (Weintraub et al., 2014). Además, los detalles estructurales observados son comparables a los estudios mediante microscopía confocal de cortes histológicos del bacterioma, usando técnicas de hibridación de fluorescencia *in situ* (FISH) *(Dan et al., 2017; Kuechler et al., 2012; Matsuura et al.*, 2012; Nakabachi *et al.*, 2013; Ren *et al*., 2018; Weintraub *et al.*, 2014). De hecho, las imágenes confocales obtenidas del bacterioma del ACP (Dan *et al.*, 2017) son prácticamente idénticas a las que hemos obtenido mediante micro-CT. Estas imágenes mostraban una capa externa de bacteriocitos que albergaba *Candidatus Carsonella ruddii* (β-Proteobacteria) y un sincitio interno que

albergaba *Candidatus Profftella armatura* (γ-Proteobacteria) (Dan *et al.*, 2017; Nakabachi *et al.*, 2013; Ren *et al.*, 2018).

La anatomía del sistema nervioso de los insectos ha sido ampliamente estudiada y fue dibujado ya hace más de 400 años por Aldrovandi (Aldrovandi, 1602) y Malpigio (Malpighi, 1669). Desde entonces ha aparecido en una infinidad de publicaciones generales sobre insectos (p.ej.: (Chapman, 2013; Gillott, 2005; Grassé, 1975; Snodgrass, 1935; Wigglesworth, 1942)), incluyendo obras dedicadas a los homópteros (Pesson, 1951). A lo largo de la realización de esta tesis, y recientemente la microtomografía se ha utilizado para estudiar la anatomía del sistema nervioso en insectos (p.ej.: (Alba-Alejandre *et al.*, 2019; Alba-Tercedor, 2013; Alba-Tercedor *et al.*, 2017b; Alba-Tercedor & Alba-Alejandre, 2019; Alba-Tercedor & Bartomeus, 2016; Greco *et al.*, 2012; Ribi *et al.*, 2008; Rybak et al., 2010; Smith et al., 2016; Sombke et al., 2015; Wipfler *et al*., 2016)). Existen estudios anatómicos en que se incluyen vistas del sistema nervioso de diferentes especies de psiloideos (Austin, 2016; Brittain, 1922; Mally, 1894; Saunders, 1921; Weber, 1929; Witlaczil, 1885; Zucht, 1972). En diferentes trabajos se han mencionado o reproducido en figuras algunos aspectos del sistema nervioso del ACP (Alba-Tercedor *et al*., 2017b; Ammar *et al.*, 2011, 2017). Pero nuestros resultados representan el primer estudio completo del sistema nervioso de *D. citri* que a grandes rasgos coincide con la organización general conocida en otros psiloideos.

El cerebro del ACP presenta a grandes rasgos la organización típica de los insectos en general, en la que el cerebro (considerado como derivado de los ganglios de tres segmentos) forma el principal centro de asociación del sistema nervioso. Incluye el protocerebro, deutocerebro y tritocerebro. El protocerebro, la región más grande y compleja del cerebro, contiene elementos tanto neurales como endocrinos (neurosecretores). Anteriormente forma la parte proximal de los nervios ocelares y lateralmente se fusiona con los lóbulos ópticos. Dentro del protocerebro hay un par de cuerpos pedunculados, los cuerpos en forma de seta. Estos son importantes centros de asociación, reciben información sensorial, especialmente olfativa y visual, y transmiten la información a otros centros protocerebrales. Además, juegan un papel central en el aprendizaje y la memoria y su tamaño puede correlacionarse ampliamente con el desarrollo de patrones

de comportamiento complejos (como ocurre en los himenópteros sociales). El cuerpo central es otro importante centro de asociación, cuya función parece ser la coordinación de actividades motoras segmentarias. Cada lóbulo óptico contiene tres masas neuropilares (lóbulo, médula y lámina ganglionaris) en las que los estímulos lumínicos, se evalúan y se envían a otros centros cerebrales. El deutocerebro se compone en gran parte de los lóbulos antenales emparejados. Junto con los cuerpos pedunculados los lóbulos de las antenas son esenciales en el comportamiento olfativo aprendido. El tritocerebro es una pequeña región del cerebro ubicada debajo del deutocerebro y comprende un par de neuropilos que contienen axones, tanto sensoriales como motores, que van hacia / desde el ganglio frontal y el labro (ver por ej.: (Chapman, 2013; Gillott, 2005; Snodgrass, 1935a)).

El gran ganglio mesotorácico ha sido llamado ganglio torácico (Brittain, 1922; Saunders, 1921). Nosotros hemos preferido llamarlo “gran ganglio mesotorácico” para distinguirlo del ganglio subesofágico, ya que coincidimos con la opinión de Ammar *et al.*, de que este gran ganglio procede de la unión de ganglios torácicos y abdominales, como ocurre en otros hemípteros (Ammar *et al.*, 2017). De hecho, en otros insectos el ganglio resultado de la unión de ganglios abdominales y torácicos se ha llamado ganglio toraco-abdominal (Chapman, 2013).

Se han descrito diferencias sexuales en el sistema nervioso de los insectos, tanto en morfología y tamaño, como en las conexiones neuronales estructurales (p.ej. en insectos sociales (Beani *et al.*, 2014), dípteros (Cachero et al., 2010) y en el desarrollo de esta tesis, ver capítulo 5.5. (Alba-Alejandre *et al.*, 2019)). Nuestro trabajo representa la primera evidencia de la existencia de diferencias sexuales en el sistema nervioso de ACP. Hemos observado que los machos tienen un cerebro poco masivo y tanto el ganglio subesófagico como el gran ganglio mesotorácico tienen los márgenes paralelos; mientras que en las hembras tanto el cerebro como los ganglios son más voluminosos, siendo el gran ganglio mesotorácico casi esférico.

D. citri es una especie de hemíptero chupador de savia que succiona del floema. Su picadura ha sido estudiada usando gráficas de penetración eléctrica

(EPG) (Bonani *et al.*, 2010; Luo *et al.*, 2015), ayudada con imágenes de microscopia óptica para confirmar que los estiletes alcanzan el floema (lo que implica observaciones de las pistas que dejan las vainas salivares (Bonani *et al.*, 2010). Se han utilizado diferentes métodos para estudiar las vainas salivares de los homópteros dentro de los tejidos vegetales (i.e: (Ammar *et al*., 2012, 2014; Backus *et al*., 1988; Morgan *et al.,* 2013)). Recientemente la micro-CT se ha utilizado para visualizar la penetración de los estiletes y las vainas salivares de la cigarrilla espumadora *Philaenus spumarius* (Cornara *et al.*, 2018) y el áfido *Myzus persicae* (Jiménez *et al.*, 2020). En el ACP mediante micro-CT obtuvimos imágenes totalmente comparables a otras obtenidas previamente con diferentes técnicas, incluyendo las diferentes configuraciones y tipologías que hemos observado, con la ventaja de obtener imágenes y videos 3D de alta calidad.

6.2.- Anatomía de *Hypothenemus hampei* (broca del café)

La presencia de ocho terguitos abdominales había sido previamente descrita (Rubio-Gómez et al., 2007; Rubio G. et al., 2008), pero resulta una novedad nuestro descubrimiento de que la hembra presenta siete. Nüsslin (Nüsslin, 1911) refiere que las hembras de *Hypothenemus* (Cryphalini) tienen ocho terguitos abdominales, mientras que Wood (Wood, 1954) refiriéndose al 8º terguito abdominal escribió: “En todos los demás escólítidos y en la mayoría de los curculiónidos es de tamaño reducido, carece de pubescencia y está oculto telescópicamente por debajo del tergo 7 ”; lo que ha sido encontrado en diferentes especies de escarabajos de la corteza (“bark beetles”) (Furniss, 2004; Hopkins, 1909; Wood, 1954). Como parte de este estudio, se diseccionaron diez hembras criadas en el laboratorio y no se encontró el octavo terguito. Por lo tanto, es posible que haya variación en el número de terguitos entre las 181 especies del género *Hypothenemus* (Vega, Infante, et al., 2015), o bien que el 7º y 8º terguitos están fusionados, como se vio que ocurre en el género *Conophthorus* (Scolytini) (Santiago-Blay & Young, 1995). Curiosamente, se ha citado un macho de la broca del café que tenía solo siete terguitos (Vega, Simpkins, *et al.*, 2015)). Sin embargo, en este estudio diseccionamos diez machos de una misma colonia y todos tenían ocho terguitos.

Hemos observado una diferencia sexual no descrita: en vista lateral, el contorno del disco pronotal de los machos se muestra uniformemente curvado mientras que en las hembras tiene una ligera depresión cóncava. Como se había descrito anteriormente, los machos de la broca del café son más pequeños que las hembras, y tienen alas vestigiales (Vega, Infante, *et al.*, 2015; Vega, Simpkins, *et al.*, 2015) y ojos compuestos rudimentarios (Vega *et al.*, 2014).

En el digestivo, el proventrículo, con sección octogonal se pensó que en los escolitoideos su forma podría tener valor taxonómico (Beal, 1927; Eaton, 1942; Nobuchi, 1969; Swaine, 1918). La serie de bandas musculares externas y las esclerotizaciones que observamos en la broca del café son comparables a lo que Eaton (Eaton, 1942) describió de la especie *Ips mexicanus* (=*radiatae*) (Hopkins), y su estructura general coincide con el "Tipo 7" descrito por Calder en los escolitinos (Calder, 1989).

Eaton (Eaton, 1942) describió el mecanismo de filtrado y molienda de los alimentos dentro del proventrículo de *I. mexicanus* de la siguiente manera: "Su paso a través del proventrículo probablemente está restringido a los canales laterales formados por las filas de laminillas, ya que los cepillos obstructores que se extienden en el lumen evitaría el movimiento directo del material alimenticio a través de la abertura central" e indicó este probable paso de los alimentos. Sin embargo, en nuestro estudio de la broca del café, vemos claramente que la luz estaba llena de partículas de alimentos, mientras que los espacios marcados por Eaton como posibles pasajes para los alimentos estaban desprovistos de partículas de alimentos.

Encontramos diferencias entre los sexos en el intestino medio anterior. Después de escanear a ocho hembras y dos machos, quedó claro que los machos tenían un intestino medio visiblemente dilatado que no estaba presente en las hembras y esto no dependía de cómo de llena estaba la cavidad con comida. Además, observamos que las hembras (pero no los machos) tienen papilas cortas que cubren toda la superficie de la parte anterior del intestino medio, cerca de la válvula estomodeal; y también se observaron en 2/3 de la superficie ventral). Esta disposición de papilas no se habia descrito previamente en curculiónidos (Calder, 1989).

Se había descrito la existencia de seis túbulos de Malpigio (Rubio G. *et al.*, 2008). Sin embargo, después de una visualización exhaustiva de estos túbulos en ambos sexos, solo observamos cuatro túbulos de Malpighi.

En *Dendroctonus armandi* se ha publicado que la longitud del tubo digestivo es casi tres veces la longitud del insecto (Bu & Chen, 2009). En la broca del café, medimos una longitud del tubo digestivo de 2,82 mm para el macho y de 3,48 mm para la hembra; la relación entre la longitud del tubo digestivo y el cuerpo del insecto fue de 2,9 y 2,3, para el macho y la hembra, respectivamente. Además, observamos diferencias adicionales entre los sexos en el número de trayectorias del intestino medio y posterior (en base al número de veces que el tubo digestivo hace una curva y cambia de trayectoria). Los machos tienen nueve trayectorias diferentes, mientras que las hembras tienen ocho. Los machos tienen una longitud corporal más corta que las hembras, lo que sugiere que se necesite un pliegue adicional de los tubos del intestino medio y posterior para encajar en el espacio más pequeño.

El sistema reproductor masculino está compuesto por dos testículos que se tocan medialmente y situados por encima del intestino medio (contienen folículos testiculares lobulares, donde se forman los espermatozoides (Chapman, 2013; Gillott, 2005)). Cada testículo tiene un conducto deferente y una sola glándula accesoria alargada, en contraste con los tres pares de glándulas accesorias por par de testículos observadas en *D. monticolae* (Cerezke, 1964). Las glándulas accesorias participan en la producción de fluidos seminales que se mezclan con los espermatozoides para formar el eyaculado (Snodgrass, 1935b), que se almacena antes de la eyaculación, en los conductos deferentes que se dilatan para formar una pequeña vesícula seminal (Chapman, 2013). Los conductos deferentes de ambos lados se juntan para formar un conducto eyaculatorio que está conectado al edeago.

El edeago constituye una característica taxonómica de primer orden utilizada para la identificación de especies de insectos en general y es de particular relevancia en estudios de coléopteros (Zunino, 2012). Sin embargo, hasta donde sabemos, no existe una descripción detallada del edeago de la broca del café. Solo hay dibujos esquemáticos y no fotografías detalladas (Rubio-

Gómez *et al.*, 2007; Rubio G. *et al.*, 2008). El edeago de la broca del café presenta dos lóbulos laterales (parámetros) y un lóbulo medio (la estructura intromitente, el pene) entre ellos, con una abertura (gonoporo) de la parte distal. La extremidad distal del edeago está armada con espinas apicales y dentículos subapicales en su cara dorsal que, en su conjunto, forman estructuras de anclaje (conocidas como titiladores (Snodgrass, 1935b)) que ayudan a mantener a los individuos unidos durante la cópula. La estructura del edeago se corresponde con el tipo vaginado descrito por Lindroth y Palmen (Lindroth & Palmen, 1970), en que los parámeros que son alargados forman un canal dorsal a través del cual el pene se desplaza.

Respecto al sistema reproductor femenino, las imágenes de micro-CT obtenidas aquí coinciden totalmente con las imágenes previas de microscopía óptica obtenidas después de diseccionar los individuos (Román-Ruiz *et al.*, 2017; Rubio-Gómez *et al.*, 2007; Rubio G. *et al.*, 2008). Detalles de la parte distal en forma de gancho de la espermateca, la glándula espermática y los músculos espermáticos descritos recientemente (Román-Ruiz *et al.*, 2017) han podido evidenciarse mediante micro-CT. Estos autores fueron los primeros en fotografiar y describir la glándula espermática de la broca del café, como una "aglomeración celular en el extremo distal curvo de la espermateca", y añadieron que "será necesario un estudio adicional para confirmar este hallazgo". Las reconstrucciones de micro-CT de este estudio han permitido visualizar la estructura previamente identificada como la glándula espermática confirmando así su existencia y configuración estructural.

En la broca del café, como en otros insectos, el sistema circulatorio es bastante simple en contraste con la complejidad del sistema respiratorio traqueal (ver capítulo 5.6, (Alba-Tercedor *et al.*, 2019). El vaso dorsal que estudiamos en la hembra; está en una posición medial dentro del abdomen, justo debajo de los terguitos, y está formado por tres cámaras dilatadas situadas debajo de los terguitos 4-6 que se prolongan anterior y posteriormente por vasos aórticos.

Al observar la musculatura se ve que los músculos dorso-longitudinales y dorso-ventrales del vuelo son claramente visibles en la hembra, pero están ausentes en el macho. Con toda probabilidad esto se debe a que los machos

han perdido la capacidad de volar (tienen alas vestigiales) pasando toda su vida dentro de la baya del café (Vega, Infante, *et al.*, 2015; Vega, Simpkins, *et al.*, 2015). Las imágenes de micro-CT de los músculos de vuelo son completamente comparables, y de hecho más claras, que las publicadas anteriormente a partir de disecciones (López-Guillén *et al.*, 2011).

En relación con el sistema respiratorio, las aberturas externas (espiráculos) representan unos riesgos enormes de pérdida de agua y de entrada de partículas, patógenos, y/o parásitos. Sin embargo los insectos han desarrollado mecanismos para minimizar este problema, como son la existencia de pilosidad, filtros, mecanismos de cierre (tales como labios o válvulas) (Chiappini & Aldini, 2011; Grassé, 1976; Harrison, 2009; Snodgrass, 1935b; Wigglesworth, 1942b). Nuestros resultados muestran la presencia de mecanismos protectores en todos los espiráculos de la broca del café, incluyendo placas filtradoras y mecanismos de cierre.

Los sistemas tubulares traqueales de los insectos se forman durante la embriogénesis como una serie de invaginaciones segmentarias del tegumento. En los embriones pueden existir hasta tres pares de espiráculos torácicos y nueve abdominales, aunque este número siempre se reduce antes de la eclosión; pueden ocurrir reducciones adicionales en endopterigotas durante la metamorfosis (resultando en un máximo de dos pares torácicos y ocho abdominales, en adultos). Los espiráculos del protórax desaparecen durante el desarrollo y los del mesotórax migran hacia adelante a una posición antero-lateral en el protórax (Chapman, 2013; Crowson, 1981; Gillott, 2005; Grassé, 1976; Richards & Davies, 1977; Snodgrass, 1935b; Wigglesworth, 1942b). De tal modo, que aunque originalmente son espiráculos "mesotorácicos", debido a la nueva ubicación anatómica adquirida, aparecen situados en una posición protorácica.

A principios del siglo XX Fuchs (Fuchs, 1912) consideraba el número de espiráculos abdominales como una característica taxonómica que variaba según el sexo. Sin embargo, en la broca del café observamos que ambos sexos tienen el mismo número de espiráculos abdominales.

Para ayudar en la ventilación, muchos insectos tienen sacos aéreos (dilataciones de los tubos traqueales) que fuerzan la ventilación cuando son comprimidos por el movimiento de los músculos circundantes (Boué & Chanton, 1962; Chapman, 2013; Gillott, 2005; Grassé, 1976; Harrison, 2009; Mbata, 1985; Miller, 1960; Richards & Davies, 1977; Robertson, 1962; Snodgrass, 1935b; Tonapi, 1978; Wasserthal et al., 2018; Weis-Fogh, 1964, 1967). Sin embargo, algunos coleópteros tienen sacos aéreos muy reducidos o ausentes (Hafeez & Gardiner, 1964; Kaiser et al., 2007; Raś et al., 2018). Nuestro estudio muestra que la broca del café tiene sacos aéreos muy pequeños en los troncos laterales abdominales, cerca de los espiráculos. Estos pudimos observarlos, tanto mediante microscopia óptica como mediante micro-CT, cerca del tercer y quinto espiráculos abdominales.

Se ha demostrado que la compresión de los troncos traqueales principales pronotales (troncos protorácicos dorsal y ventral) fuerzan la ventilación y el intercambio de gases de los tubos traqueales (Waters et al., 2013; Westneat, 2003). En sección transversal estos troncos comprimibles son de sección elíptica para facilitar su compresión (Chapman, 2013; Cobb, 2002; Robertson, 1962; Snodgrass, 1935). Lo cual pudimos observarlo mediante micro-CT en los troncos traqueales pronotales de la broca del café. Por eso, debido a su proximidad, los espiráculos mesotorácicos deben tener un papel funcional importante en la ventilación traqueal, pasando por ellos grandes volúmenes de gases. De hecho, los tubos traqueales que surgen anteriormente a los espiráculos mesotorácicos suplen a los músculos protorácicos y proventriculares y a las patas delanteras, y a través de derivaciones cefálicas también suplen al cerebro, el ganglio subesofágico y a las piezas bucales.

Confirmando su gran importancia funcional, los espiráculos mesotorácicos son, con mucho, los más complejos, y tienen tres filtros consecutivos. Además, las aberturas externas tienen dos labios móviles, uno anterior y otro posterior, para cerrar las aberturas espiraculares externas anterior y posterior, respectivamente. Los espiráculos situados debajo de los élitros (mesotorácicos y abdominales) están más protegidos; no observamos ningún filtro en los espiráculos abdominales. Por el contrario, los espiráculos metatorácicos, que

están más expuestos, presentan una abertura espiracular muy pequeña y una placa filtradora.

La barras del aparato de cierre en forma de U que hay en los espiráculos que fue descrita por vez primera en insectos por Snodgrass (Snodgrass, 1935b), y observada por muchos otros autores (Chapman, 2013; Fuchs, 1912; Gillott, 2005; Wigglesworth, 1942), son muy similares a las encontradas en el coleóptero girínido *Dineustes indicus* por Waters *et al.* (Waters *et al.*, 2013). Del mismo modo los músculos oclusores que hemos observado, habían sido observados en otros insectos (Chapman, 2013; Gillott, 2005; Tonapi, 1978; Wigglesworth, 1942).

La organización general del sistema traqueal en la broca del café es similar a la descrita anteriormente para otras especies de coleópteros, el escarabajo de la harina (*Tribolium anaphe*) (Hafeez & Gardiner, 1964) y el escarabajo gusano de la harina (*Tenebrio molitor*) (Richards & Davies, 1977). Así, la comisura cefálica dorsal es claramente visible en la broca del café, pero la comisura cefálica ventral no es visible. Se observaron tubos finos transversales, cercanos entre sí, en las posiciones donde otras especies tienen la comisura ventral, pero cuando se observaron en detalle no se unen para formar una comisura continua. Además, la tráquea latero-mediana abdominal larga (LALMt; también denominada 'tráquea mediana larga'), que normalmente se encuentra en el lado izquierdo del animal (Hafeez & Gardiner, 1964), se sitúa en el lado derecho en la broca del café. Esto puede deberse a que los autores (Hafeez & Gardiner, 1964) lo dibujaron a través del microscopio y la posición se invirtió, como una imagen especular, o bien la posición en esa especie es diferente a la que observamos en la broca del café. Además, mientras que en *T. anaphe*, la tráquea latero-mediana abdominal larga aparece como una tráquea única al discurrir hacia delante y se divide en seis ramas cuando discurre hacia atrás; en la broca del café aparece como dos tubos traqueales en toda su longitud.

Clásicamente se considera que el sistema traqueal consta de dos troncos longitudinales dorsales, dos troncos laterales y dos troncos ventrales, conectados por tubos transversales (Boué & Chanton, 1962; Chapman, 2013;

Crowson, 1981; Gillott, 2005; Grassé, 1976; Harrison, 2009; Richards & Davies, 1977; Wigglesworth, 1942b). En la broca del café, es más o menos similar a éste en la cabeza y el tórax. A cada lado del abdomen hay tres tráqueas latero-abdominales longitudinales que a primera vista podrían interpretarse como los troncos dorsal, lateral y ventral descritos clásicamente. De hecho, estudios previos han demostrado que los troncos dorsales deben correr a lo largo del vaso dorsal (corazón) pero, en la broca del café, las tráqueas latero-abdominales dorsales están situadas lejos del vaso dorsal. Observamos que las tráqueas latero-medianas abdominales largas siguen a lo largo del intestino medio posterior y las gónadas al dirigirse hacia adelante, mientras que cuando discurren hacia atrás pasan por el intestino posterior (recto) justo debajo del vaso dorsal. Así, las tráqueas latero-medianas abdominales largas deben jugar un papel importante en el suministro del tracto digestivo, las gónadas y el corazón en la broca del café. Esto explicaría la presencia de pequeños sacos aéreos cerca de los espiráculos para aumentar la ventilación abdominal. En ambos lados, el sistema traqueal abdominal discurre posteriormente como dos tubos traqueales paralelos, en las hembras estos se extienden al sistema reproductor, y suplen a la musculatura del ovipositor.

Aunque muchos de los detalles anatómicos evidenciados mediante micro-CT en la broca del café, se habían observado en otras especies de insectos, gracias a nuestro trabajo se han podido describir y nombrar nuevos detalles anatómicos. Es de destacar que, a pesar de un estudio que cambió el nombre de las comisuras abdominales ventrales a comisuras ventrales abdominales (Richards & Davies, 1977), ese término había sido utilizado previamente por otros autores en diferentes especies de insectos (Hafeez & Gardiner, 1964; Robertson, 1962; Snodgrass, 1935; Srivastava, 1976).

Según lo identificado por Iwan *et al.* (Iwan et al., 2015) utilizando el mismo modelo de microtomógrafo que nosotros, el pequeño tamaño de voxel logrado permite la visualización de las traqueolas. Sin embargo, como las traqueolas están llenas de líquido traqueolar, a través del cual se produce el intercambio de gases (Chapman, 2013; Gillott, 2005; Wigglesworth, 1930, 1942b), como la metodología que hemos usado para reconstruir la luz de los tubos traqueales reconstruye espacios llenos de aire, aquellas traqueolas llenas de líquido

traqueolar no fueron reconstruidas en las imágenes renderizadas. De hecho, se reconstruyeron tubos traqueales muy finos (hasta 1,99 µm de diámetro) en este estudio de la broca del café. Wigglesworth (Wigglesworth, 1930) experimentó el mismo problema al estudiar el sistema traqueal de una libélula (*Aeschna*) mediante microscopía óptica. Observó que cuando las traqueolas estaban llenas de líquido no eran visibles, pero al eliminar el líquido traqueolar con una solución hipertónica de lactato de potasio, el problema se podía solucionar. Desafortunadamente, para estudios de micro-CT el lactato de potasio no resolvería el problema porque crearía otros espacios vacíos no traqueolares introduciendo ruido en las reconstrucciones.

En estudios recientes de micro-CT del sistema traqueal del escarabajo del gusano de la harina (Iwan *et al.*, 2015; Raś *et al.*, 2018) el diámetro mínimo de los tubos traqueales que pudieron reconstruir fue de 25 µm, que es significativamente mayor que el diámetro interno más pequeño que nosotros hemos reconstruido (1,99 µm), y también mayor que el diámetro mayor que reconstruimos (21,92 µm) en la broca del café, insecto que es diez veces más pequeño. Sin embargo, los tubos traqueales más grandes del escarabajo del gusano de la harina tienen diámetros aproximadamente 20 veces más grandes (400 µm) que los de la broca del café, siendo los más grandes los troncos protorácicos dorsal y ventral que se pueden plegar para facilitar la ventilación. Evitar los tubos de gran diámetro podría ser una adaptación en un insecto tan pequeño como la broca del café. De hecho, hasta donde sabemos, no se han reportado tráqueas colapsables (en el sentido de su facilidad para comprimirse) en ningún estudio del sistema traqueal del gusano de la harina (Kaiser *et al.*, 2007; Raś *et al.*, 2018).

La mayoría de las tráqueas que observamos tienen una luz muy estrecha: los tubos más estrechos (rango de diámetro de la luz: 1,99–6 µm) representaron más del 75,5% de la longitud total de los tubos y el 37,8% del volumen total; todos los tubos con lumina ≤9,97 µm representaron el 96,6% de la longitud total y el 79,1% de la capacidad de volumen traqueal total. Se ha informado de una relación similar entre el diámetro traqueal y su ocurrencia como proporción de todo el sistema traqueal para el escarabajo del gusano de la harina, aunque la frecuencia de ocurrencia disminuye a medida que aumenta el diámetro, y el

diámetro solo disminuye de 200 a 400 µm (Richards & Davies, 1977). Sin embargo, en la broca del café observamos una pendiente mucho más pronunciada para esta relación.

La longitud total estimada de los tubos traqueales fue de 122,23 mm. Como la hembra estudiada tenía una longitud aproximada de 1,8 mm, esto significa que los tubos traqueales tenían 70 veces la longitud total del cuerpo. Si trasladamos esto a una escala humana, entonces un insecto de 175 cm de largo (la altura promedio para los hombres estadounidenses (*Height Chart of Men and Women in Different Countries - Disabled World*, 2019)) tendría 123 m de tubos traqueales (longitud mayor que la de un campo de fútbol).

La anatomía del sistema nervioso de los insectos fue descrito “in extenso” por Snodgrass (Snodgrass, 1935) y resumida y actualizada por Grassé (Grassé, 1975). Se han realizado varios estudios sobre la anatomía del sistema nervioso en diferentes familias y especies de coleópteros Coleoptera (Crowson, 1981; Grassé, 1975). Pero, hasta donde sabemos, a pesar de la extensa revisión de Calder (Calder, 1989), el estudio anatómico más detallado del sistema nervioso de los escarabajos de la corteza es el de *D. pseudotsugae* por Atkins y Chapman (Atkins & Chapman, 1957), que muestra patrones generales de organización similares a lo que nosotros observamos mediante micro-CT.

En la broca del café, el cerebro ubicado sobre el extremo anterior del intestino anterior, está conectado a la cadena nerviosa ventral por dos conectivos circumfaríngeos. La mayoría de los ganglios de la cadena nerviosa ventral están fusionados, por lo que solo es posible distinguir un ganglio subesofágico (ubicado debajo del esófago en una posición cefálica postero-ventral) y un gran ganglio del complejo torácico-abdominal, en una posición torácica ventral justo debajo del proventrículo. Algunas especies de Scolytinae tienen un ganglio protorácico independiente (Atkins & Chapman, 1957; Calder, 1989). En otras especies, los conectivos que unen el cerebro a la cadena nerviosa ventral se conocen como conectivos circumesofágicos (Atkins & Chapman, 1957; Chapman, 2013; Gillott, 2005; Snodgrass, 1935). Sin embargo, está claro que, en la broca del café, estos conectivos rodean la faringe y no el esófago. Por esta razón, los describimos como conectivos circumfaríngeos.

Al igual que observamos en *D. citri*, en la broca del café hemos descubierto notables diferencias sexuales no conocidas anteriormente, en lo referente a la forma, tamaño y relación de tamaño del cerebro con el tamaño de la cabeza. Las hembras tienen los lóbulos cerebrales más grandes, más extendidos lateralmente, y los lóbulos ópticos más gruesos que el macho. En relación con el tamaño de la cabeza, el cerebro de las hembras es más pequeño que el de los machos. El cerebro más pequeño y los nervios ópticos más delgados que se observan en los machos están relacionados con la biología de la especie; ya que los machos no salen de la baya del café y por eso tienen ojos compuestos rudimentarios, alas vestigiales y músculos de vuelo ausentes, como se discutió anteriormente.

6.3.- La broca del café dentro de las bayas de café

Se sabe que varias especies de escarabajos de la corteza de diferentes géneros atacan las semillas, entre ellas *Araptus, Coccotrypes, Hypothenemus, Pagiocerus y Scolytodes*(Browne, 1973; Schedl, 1960; Wood, 2007). No se sabe mucho sobre la historia de vida de estas especies de escarabajos de la corteza dentro de la semilla, incluida la distribución de los huevos y la forma de las galerías.

Nuestras visualizaciones de la broca del café dentro de la baya del café, utilizando micro-CT, han revelado las ventajas de utilizar esta tecnología para estudiar la vida de estos insectos dentro de la baya del café. Por ejemplo, la distribución de las etapas de desarrollo del insecto a diferentes distancias de la superficie de la baya sugiere que las hembras colonizadoras comienzan a ovipositar cerca de la periferia de la semilla y luego la oviposición se mueve hacia adentro, hacia el centro de la semilla. Esta podría ser una estrategia para dispersar la progenie a fin de reducir la competencia.

De los diversos estadios de desarrollo evidenciados dentro de las bayas del café, observamos ocho huevos sin eclosionar que se ovipositaron en un área de la semilla opuesta a la primera puesta de huevos (que dieron lugar a las larvas y pupas observadas). Se observó uno de los huevos en el área distal de la baya, cerca del disco, lo que revela que la hembra colonizadora no necesariamente coloca todos los huevos en un solo lugar. Aunque no sabemos si estos ocho

huevos terminarían eclosionando, es seguro afirmar que hubo un 100% de eclosión en los dos lotes de huevos anteriores, lo que resultó en 26 larvas y 12 pupas. No hay informes que evalúen la fertilidad de los huevos dentro de las bayas de café, ya que la disección de una baya y una evaluación posterior de porcentaje de eclosiones de huevos podría no ser fiable debido a los cambios drásticos en el microhábitat que experimentan los huevos tras la disección de la baya. Por lo tanto, esta es otra área que habría que investigar más a fondo utilizando micro-CT.

Los dos lotes de huevos observados se asemejan a lo descrito para *Coccotrypes* por Browne (Browne, 1973): “En frutos y semillas, los huevos se colocan al final de un túnel corto y las larvas agrandan y hacen otros túneles y cámaras irregulares en todas direcciones”. Las imágenes reconstruidas de las galerías mediante micro-CT muestras ángulos alternos, en “zig-zag”, en la galería que parte del orificio de entrada, que junto con la disposición de la hembra situándose a modo de tapón, con el extremo abdominal dirigido hacia el orificio de salida, actuarían como barreras dificultando la entrada de patógenos y/o parasitoides.

Las hembras adultas de la broca del café emergen de la baya utilizando el orificio de entrada construido por la hembra colonizadora. Del mismo modo, “En *Anisandrus* y *Xyleborus*. la cría madura y emerge por la galería de entrada ” (Dodge, 1938). Esto es interesante porque hay un gran recorrido de túneles y cavidades por las que los nuevos adultos tienen que transitar para encontrar el orificio de entrada, y muy probablemente utilicen señales visuales (luz) y corrientes de aire para localizarlo.

Hay varios trabajos que describen diferentes tipos de galerías creadas por los escarabajos de la corteza (Blackman, 1922; Browne, 1961; Dodge, 1938; Hopkins, 1909; Swaine, 1918). Hopkins (Hopkins, 1909) afirmó que aunque diferentes géneros de escarabajos de la corteza pueden hacer el mismo tipo de galería o similar, "las galerías son de importancia taxonómica" y la misma especie de insecto construirá el mismo tipo de galería o similar en diferentes hospedadores, por lo que la forma de la galería no está determinada por la planta huésped. No hay estudios centrados en la formación de galerías por los

escarabajos de la corteza perforadores de semillas; este hecho presenta una oportunidad para utilizar micro-CT para estudiar la forma y función de la galería en diferentes semillas, al igual que hemos hecho con este estudio pionero de la broca del café.

6.4.- El gorgojo del café dentro de las bayas del café

Aunque la especie *Araecerus. fasciculatus* fue descrita hace dos siglos y medio (De Geer, 1775), esta es la primera vez, que se ha podido "congelar" la actividad del insecto en el interior de las bayas de café, y estudiarla en detalle utilizando técnicas modernas de micro-CT. La micro-CT ha revelado tres hallazgos interesantes: (1) dos huevos habían eclosionado, lo que según Autuori (Autuori, 1931) es raro; (2) se consumen ambas semillas; y (3) hay un orificio de entrada parcial.

Las hembras de los gorgojos del café ovipositan dentro de la baya. Por lo tanto, el orificio de entrada parcial en la baya observado plantea una incógnita. El orificio de entrada es demasiado pequeño (aprox. 0,95 mm de diámetro) para un gorgojo del grano de café, cuyo ancho es de 2 a 3 mm (Autuori, 1931) y cuyo orificio de emergencia puede tener hasta 3 mm de diámetro (Da Costa Lima, 1956). A pesar de estar cerca del pecíolo y no en el disco, que es donde la hembra colonizadora de la broca del café suele perforar la baya, el agujero parcial parece haber sido perforado por la broca del café, cuyos orificios de entrada oscilan entre 0,6 y 0,8 mm. (Varón et al., 2004) a 1 mm de diámetro (Wilkinson, 1928). Es posible que el gorgojo del café haya desovado en el orificio de entrada parcialmente perforado, donde eclosionó un huevo.

En base a la conexión existente entre el orificio de entrada parcial y una galería llena de excrementos y material procedente del raspado de la semilla de aprox. 175 µm de largo, las larvas del primer estadío debieron perforar la baya hacia el interior. De hecho, según Autuori (Autuori, 1931), las larvas roen más de lo que comen. A medida que la galería se aleja del orificio de entrada parcial, la longitud del excremento aumenta a 290 µm, lo que indica una larva más vieja. Cabal Concha (Cabal Concha, 1956) mencionaron que los estadios 4 y 5 son

más activos y voraces que los estadios anteriores, y que no todo el material que roen con las mandíbulas se consume (apoyando así la observación de Autuori (Autuori, 1931)) y, en cambio, se acumula. En momentos de mayor intensidad de calor, lo esparcen alrededor de su cuerpo, lo que se supone que (1) crea una barrera con la pared de la semilla, reduciendo así la intensidad del calor y (2) sirve como defensa contra parasitoides y depredadores que intentan alcanzar el insecto (Cabal Concha, 1956).

6.5.- Presencia en el café de una especie no descrita de coleóptero (*Ptinus* s.str., Ptinidae)

Por último, señalar que durante la realización de esta tesis también recolectamos un macho de una especie no descrita de *Ptinus* s.str. (Ptinidae) que había emergido de una baya de café. Hasta ahora, solo se había descrito la presencia de otra especie de Ptinidae (*Ptinus tectus*) en café almacenado (Archibald & Chalmers, 1983).

6.6.- Bibliografía

Alba-Alejandre, I., Alba-Tercedor, J., & Vega, F. E. (2019). Anatomical study of the coffee berry borer (*Hypothenemus hampei*) using micro-computed tomography. *Scientific Reports*, *9*(17150), 1–16. https://doi.org/10.1038/s41598-019-53537-z

Alba-Alejandre, I., Hunter, W. B., & Alba-Tercedor, J. (2018). Micro-CT study of male genitalia and reproductive system of the Asian citrus psyllid, *Diaphorina citri* Kuwayama, 1908 (Insecta: Hemiptera, Liviidae). *PLoS ONE*, *13*(8), 1–11. https://doi.org/https://doi.org/10.1371/journal.pone.0202234 Editor:

Alba-Tercedor, J. (2013). Study of the anatomy of the common housefly *Musca domestica* Linnaeus, 1758 (Insecta: Diptera, Muscidae) scanned with the Skyscan 1172 high resolution micro-CT. *Bruker Micro-CT Users Meeting 2013*, 275–289.

Alba-Tercedor, J., & Alba-Alejandre, I. (2019). Comparing micro-CT results of insects with classical anatomical studies: The European honey bee (*Apis mellifera* Linnaeus, 1758) as a benchmark (Insecta: Hymenoptera, Apidae). *Microscopy and Analysis*, *3*(1), 12-15 EU. Retrieved from https://microscopy-analysis.com/article/january_19/comparing_classical_anatomical_studies_of_insects

Alba-Tercedor, J., Alba-Alejandre, I., & Vega, F. E. (2019). Revealing the respiratory system of the coffee berry borer (*Hypothenemus hampei*; Coleoptera: Curculionidae: Scolytinae) using micro-computed tomography. *Scientific Reports*, *9*(17753), 1–17. https://doi.org/10.1038/s41598-019-54157-3

Alba-Tercedor, J., & Bartomeus, I. (2016). Micro-CT as a tool straddling scientist research, art and education. Study of *Osmia* sp., a mason bee (Insecta, Hymenoptera: Megachilidae). In *Bruker Micro-CT Users Meeting 2016* (pp. 74–91).

Alba-Tercedor, J., Hunter, W. B., Cicero, J. M., & Sáinz-Bariáin, M. (2017). Use of micro-CT to elucidate details of the anatomy and feeding of the Asian Citrus Psyllid Diaphorina citri Kuwayama , 1908 (Insecta : Hemiptera , Lividae). In *Bruker Micro-CT Users Meeting 2017* (pp. 270–285). Kontich: Bruker microCT-Skyscan.

Aldrovandi, U. (1602). *De Animalibus Insectis Libri*. Bologna.

Ammar, E.-D., Alessandro, R., Shatters Jr, R. G., & Hall, D. G. (2013). Behavioral, Ultrastructural and Chemical Studies on the Honeydew and Waxy Secretions by Nymphs and Adults of the Asian Citrus Psyllid *Diaphorina citri* (Hemiptera: Psyllidae). *PLoS ONE*, *8*(6), e64938. https://doi.org/10.1371/journal.pone.0064938

Ammar, E.-D., & Hall, D. G. (2012). New and Simple Methods for Studying Hemipteran Stylets, Bacteriomes, and Salivary Sheaths in Host Plants. *Annals of the Entomological Society of America*, *105*(5), 731–739. https://doi.org/10.1603/AN12056

Ammar, E.-D., Hall, D. G., & Shatters, R. G. (2017). Ultrastructure of the salivary glands, alimentary canal and bacteria-like organisms in the Asian citrus psyllid, vector of citrus huanglongbing disease bacteria. *Journal of Microscopy and Ultrastructure*, *5*(1), 9–20. https://doi.org/10.1016/j.jmau.2016.01.005

Ammar, E.-D., Hentz, M., Hall, D. G., & Shatters, R. G. (2015). Ultrastructure of Wax-Producing Structures on the Integument of the Metaleuca Psyllid Boreioglycaspis melaleucae (Hemiptera: Psyllidae), with Honeydew Excretion Behavior in Males and Females. *PLOS ONE*, *10*(3), e0121354. https://doi.org/10.1371/journal.pone.0121354

Ammar, E.-D., Richardson, M. L., Abdo, Z., Hall, D. G., & Shatters, R. G. (2014).

Differences in Stylet Sheath Occurrence and the Fibrous Ring (Sclerenchyma) between xCitroncirus Plants Relatively Resistant or Susceptible to Adults of the Asian Citrus Psyllid *Diaphorina citri* (Hemiptera: Liviidae). *PLoS ONE*. https://doi.org/10.1371/journal.pone.0110919

Ammar, E., Shatters, R., Lynch, C., & Hall, D. G. (2011). Detection and relative titer of Candidatus Liberibacter asiaticus in the salivary glands and alimentary canal of *Diaphorina citri* (Hemiptera: Psyllidae) vector of citrus. *Annals of the Entomological Society of America*, *104*(3), 526–533. Retrieved from http://aesa.oxfordjournals.org/content/104/3/526.abstract

Archibald, R. D., & Chalmers, I. S. (1983). Stored product Coleoptera in New Zealand. *N. Z. Entomol.*, *7*, 371–397.

Arras, J., Hunter, W., & Bextine, B. (2012). Comparative analysis of antennae sensory arrays in Asian citrus psyllid, *Diaphorina citri*, and potato psyllid, *Bactericera cockerelli* (Hemiptera). *Southwestern Entomologist*. https://doi.org/http://dx.doi.org/10.3958/059.037.0101

Atkins, M. D., & Chapman, J. A. (1957). *Studies on Nervous System Anatomy of the Douglas Fir Beetle, Dendroctonzis pseudotsugae Hopk. (Scolytidae)'*. *The Canadian Entomologist* (Vol. 89). https://doi.org/https://doi.org/10.4039/Ent8980-2

Austin, C. (2016). *Morphology of Acercaria: investigations of the ovipositor and internal anatomy*. University of Illinois at Urbana-Champaign.

Autuori, M. (1931). Dados biologicos sobre o *Araecerus fasciculatus* (De Geer) (Col. Anthribiidae). *Revista de Entomología*, *1*, 52–61.

Backus, E., Hunter, W. B., & Arne, C. N. (1988). Technique for staining Leafhopper (Homoptera: Cicadellidae) salivary sheaths and eggs within unsectioned plant tissue View project. *J. Econ. Entomol.*, *81*(6), 1819–1823. https://doi.org/10.1093/jee/81.6.1819

Bajpai, P. (2018). Hydraulics. In *Biermann's Handbook of Pulp and Paper* (pp. 455–482). Elsevier. https://doi.org/10.1016/B978-0-12-814238-7.00023-4

Barcellos, M. S., Fernanda, J., Cossolin, S., Dias, G., & Lino-Neto, J. (2017). Sperm morphology of the leafhopper *Diaphorina citri* Kuwayama (Hemiptera: Sternorrhyncha: Psylloidea: Liviidae). *Micron*, *99*, 49–55. https://doi.org/10.1016/j.micron.2017.03.017

Beal, J. A. (1927). The Development of the Proventriculus of *Pityogenes* Hopkinsi Swaine. *Annals of the Entomological Society of America*, *20*(4), 522–539. https://doi.org/10.1093/aesa/20.4.522

Beani, L., Dessì-Fulgheri, F., Cappa, F., & Toth, A. (2014). The trap of sex in social insects: From the female to the male perspective. *Neuroscience and Biobehavioral Reviews*, *46*, 519–533. https://doi.org/10.1016/j.neubiorev.2014.09.014

Billen, J. (1997). Morphology and ultrastructure of the metatibial gland in the army ant *Norylus molestus* (Hymenoptera, formicidae). *Belg. J. Zool*, *127*(2), 159–166.

Billen, J. (2009). Occurrence and structural organization of the exocrine glands in the legs of ants. *Arthropods Structure and Development*, *38*, 2–15. https://doi.org/10.1016/j.asd.2008.08.002

Billen, J., & Ito, F. (2006). The basicoxal gland, a new exocrine structure in poneromorph ants (Hymenoptera, Formicidae). *Acta Zoologica (Stockholm)*, *87*, 291–296.

Bin, F. (1986). Morphology of of the antennal sex-gland in male *Trissolcus basalis* (Woll.) (Hymenoptera: Scelionidae), an egg parasitoid of the green stink Bug, *Nezara*

viridula (Hemiptera: Pentatomida). *Int. J. Insect Morphol. & Embryol.*, *15*(3), 129–138.

Bitsch, J. (1979). Morphologie Abdominale des Insectes. Ordre des Homoptères, B.-Psylles. In P.-P. Grassé (Ed.), *Traité de Zoologie. Anatomie, Systématique, Biologie. T. VIII, Insectes Thorax, Abdomen. Fasc. II* (pp. 420–429). Paris, New York, Barcelone, Milan: Masson et Cie.

Blackman, M. W. (1922). Mississippi bark beetles. *Mississippi Agricultural Experiment Station, Technical Bulletin*, *11*, 1–130.

Blowers, J. R., & Moran, V. C. (1967). Notes on the female reproductive system of the South African Citrus Psylla, *Trioza erytreae* (Del Guercio) (Homoptera : Psyllidae). *Journal of the Entomological Society of Southern Africa*, *30*(1), 75–81

Bonani, J. P., Fereres, A., Garzo, E., Miranda, M. P., Appezzato-Da-Gloria, B., & Lopes, J. R. S. (2010). Characterization of electrical penetration graphs of the Asian citrus psyllid, *Diaphorina citri*, in sweet orange seedlings. *Entomologia Experimentalis et Applicata*, *134*(1), 35–49. https://doi.org/10.1111/j.1570-7458.2009.00937.x

Boué, H., & Chanton, R. (1962). 4º L'appareil respiratoire. In *Biologie Animale. Zoologie I. Invertebrés* (2nd ed., pp. 388–397). Paris: G. Doin & Cie.

Brittain, W. H. (1922). The morphology and synonymy of *Psylla mali* Schmidberger. *Proceeding Acadian Entomological Society (Fredericton)*, *8*, 23–51.

Brown, J. K., Cicero, J. M., & Fisher, T. W. (2016). Psyllid-Transmitted Candidatus Liberibacter Species Infecting Citrus and Solanaceous Hosts. In J. K. Brown (Ed.), *Vector-Mediated Transmission of Plant Pathogens* (pp. 399–422). St. Paul, Minnesota: The American Phytopathological Society. https://doi.org/10.1094/9780890545355.028

Brown, R. G., & Hodkinson, I. D. (1988). *Taxonomy and Ecology of the Jumping Plant-lice of Panama: Homoptera, Psylloidea*. Lei- den, The Netherlands: E. J. Brill/Scandanavian Science Press Ltd.

Browne, F. G. (1961). The biology of Malayan Scolytidae and Platypodidae. *Malayan Forest Records*, *22*, 1–255.

Browne, F. G. (1973). The African species of Poecilips Schaufuss. *Revue de Zoologie et de Botanique Africaines*, *87*, 679–696.

Bu, S.-H., & Chen, H. (2009). The Alimentary Canal of *Dendroctonus armandi* Tsai and Li (Coleoptera: Curculionidae: Scolytinae). *The Coleopterists Bulletin*, *63*(4), 485–496. https://doi.org/10.1649/1190.1

Büning, J., & Büning, J. (1994). The ovary of Ectognatha, the Insecta s. str. In *The Insect Ovary* (pp. 31–324). Springer Netherlands. https://doi.org/10.1007/978-94-011-0741-9_3

Burckhardt, D. (1987). Jumping plant lice (Homoptera: Psylloidea) of the temperate neotropical region. Part 2: Psyllidae (subfamilies Diaphorininae, Acizziinae, Ciriacreminae and Psyllinae). *Zoological Journal of the Linnean Society*, *90*, 145–205.

Cabal Concha, A. (1956). Biología y control del gorgojo del café: *Araecerus fasciculatus* De Geer Fam: (Anthribiidae), en Barranquilla—Colombia. *Rev. Fac. Nac. Agron. Medellín, 18*(49), 49–72.

Cachero, S., Ostrovsky, A. D., Yu, J. Y., Dickson, B. J., & Jefferis, G. S. X. E. (2010). Sexual Dimorphism in the Fly Brain. *Current Biology*, *20*(18), 1589–1601. https://doi.org/10.1016/j.cub.2010.07.045

Calder, A. A. (1989). The alimentary canal and nervous system of Curculionoidea (Coleoptera): gross morphology and systematic significance. *Journal of Natural History*, *23*(6), 1205–1265. https://doi.org/10.1080/00222938900770671

Cecil, R. (1930). The alimentary canal of *Philaenus leucophthalmus* L. *The Ohio Journal of Science*, *30*(2), 120–130.

Cerezke, H. F. (1964). The morphology and functions of the reproductive systems of *Dendroctonus monticolae* Hopk. (Coleoptera: Scolytidae). *The Canadian Entomologist*, *96*(03), 477–500. https://doi.org/10.4039/Ent96477-3

Chapman, R. F. (2013). *The Insects Structure and Function*. (S. J. Simpson & A. E. Douglas, Eds.) (5th ed.). Cambridge: Cambridge University Press.

Chiappini, E., & Aldini, R. N. (2011). Morphological and physiological adaptations of wood-boring beetle larvae in timber. *Journal of Entomological and Acarological Research*, *43*(2), 47–59. https://doi.org/10.4081/jear.2011.47

Cicero, J. M. (2017). Stylet biogenesis in *Bactericera cockerelli* (Hemiptera: Triozidae). *Arthropod Structure & Development*, *46*(4), 644–661. https://doi.org/10.1016/j.asd.2016.12.007

Cicero, J. M. (2020). Functional Anatomy of the Asian Citrus Psyllid. In J. A. Qureshi & P. A. Stansly (Eds.), *Asian Citrus Psyllid: Biology, Ecology and Management of the Huanglongbing Vector* (pp. 12–29). Boston: CABI.

Cicero, J. M., Alba-Tercedor, J., Hunter, W. B., Cano, L. M., Saha, S., Mueller, L. A., & Brown, S. J. (2018). Asian citrus psyllid stylet morphology and applicability to the model for inter-instar stylet replacement in the potato psyllid. *Arthropod Structure & Development*, *47*(5), 542–551. https://doi.org/10.1016/j.asd.2018.06.007

Cicero, J. M., & Brown, J. (2009). The digestive system of *Diaphorina citri* and *Bactericera cockerelli* (Hemiptera: Psyllidae). *Entomological Society of America*, *102*(4), 650–665.

Cicero, J. M., & Brown, J. (2011). Anatomy of accessory salivary glands of the whitefly *Bemisia tabaci* (Hemiptera: Aleyrodidae) and correlations to Begomovirus transmission. *Annals of the Entomological Society of America, 104(2): 280-286.*

Cicero, J. M., Hunter, W. B., Cano, L. M., Saha, S., Mueller, L. A., & Brown, S. J. (2018). An animated detailing of the alimentary canal of the Asian citrus psyllid, with special reference to the configuration and function of the filter chamber (online only). Figshare media. Retrieved from https://figshare.com/articles/An_Animated_Detailing_of_the_Alimentary_Canal_of_the_Asian_Citrus_Psyllid_with_Special_Reference_to_the_Configuration_and_Function_of_the_Filter_Chamber/7599269/3

Cicero, J. M., Stansly, P. A., & Brown, J. K. (2015). Functional anatomy of the oral region of the potato psyllid (Hemiptera: Psylloidea: Triozidae). *Annals of the Entomological Society of America*, *108*(5), 743–761. https://doi.org/10.1093/aesa/sav059

Cobb, M. (2002). Malpighi, Swammerdam and the colourful silkworm: replication and visual representation in early modern science. *Annals of Science*, *59*, 111–147. https://doi.org/10.1080/00033790110050759

Cornara, D., Garzo, E., Morente, M., Moreno, A., Alba-Tercedor, J., & Fereres, A. (2018). EPG combined with micro-CT and video recording reveals new insights on the feeding behavior of *Philaenus spumarius*. *PLOS ONE*, *13*(7), e0199154: 1-20. https://doi.org/10.1371/journal.pone.0199154

Crowson, R. A. (1981). *The Biology of the Coleoptera. The Biology of the Coleoptera*.

London: Academic Press Inc. Retrieved from New York

Da Costa Lima, A. (1956). *Insetos do Brasil, Volume 10, Coleópteros, Fourth and Last Part; Serie Didática #12*. (E. N. de Agronomia, Ed.). Rio de Janeiro, Brazil.

Da Cruz-Landim, C., Morelli, R. L., De Moraes, S., Salles, H. C., & Reginato, R. D. (1988). Note on glands present in Meliponinae (Hymenoptera, Apidae) bees legs. *Revta Bras. Zool.*, *15*(2), 159–155.

Dahms, E. D. (1984). An interpretation of the structure and function of the antennal sense organs of *Melittobia australica* (Hymenoptera: Eulophidae) with the discovery of a large dermal gland in the male scape. *Mem. Qd Mus.*, *21*(2), 361–385.

Dan, H., Ikeda, N., Fujikami, M., & Nakabachi, A. (2017). Behavior of bacteriome symbionts during transovarial transmission and development of the Asian citrus psyllid. *PLOS ONE*, *12*(12), e0189779. https://doi.org/10.1371/journal.pone.0189779

De Geer, C. (1775). *Memoires pour Servir a l'Histoire des Insectes; Volume 5*. Stockholm, Sweden: Pierre Hesselberg.

De Santis, F., Conti, E., Romani, R., Salerno, G., Parillo, F., & Bin, F. (2008). Colleterial glands of Sesamia nonagrioides as a source of the host-recognition kairomone for the egg parasitoid Telenomus busseolae. *Physiological Entomology*, *33*(1), 7–16. https://doi.org/10.1111/j.1365-3032.2007.00593.x

Dmitriev, D. A. (2010). Homologies of the head of Membracoidea based on nymphal morphology with notes on other groups of Auchenorrhyncha (Hemiptera). *European Journal of Entomology*, *107*(4), 597–613. https://doi.org/10.14411/eje.2010.069

Dodge, H. R. (1938). The bark beetles of Minnesota (Coleoptera: Scolytidae). *University of Minnesota, Agricultural Experiment Station, Technical Bulletin*, *132*, 1–60.

Dossi, Fabio C. A., & Cônsoli, F. L. F. (2014). Gross morphology and ultrastructure of the female reproductive system of *Diaphorina citri* (Hemiptera: Liviidae). *Zoologia*, *31*(2), 162–169. https://doi.org/10.1590/S1984-46702014000200007

Dossi, Fábio C A, & Cônsoli, F. L. (2010). Desenvolvimento ovariano e influência da cópula na maturação dos ovários de *Diaphorina citri* Kuwayama (Hemiptera: Psyllidae). *Neotropical Entomology*, *39*(3), 414–419. https://doi.org/10.1590/S1519-566X2010000300015

Drohojowska, J., Kalandyk-Kołodziejczyk, M., & Simon, E. (2013). Thorax morphology of selected species of the genus *Cacopsylla* (Hemiptera, Psylloidea). *ZooKeys*, *319*, 27–35. https://doi.org/10.3897/zookeys.319.4218

Eaton, C. B. (1942). The Anatomy and Histology of the Proventriculus of *Ips radiatae* Hopkins. *Annals Entomological Society of America*, *35*, 41–49.

Fuchs, G. (1912). *Morphologische Studien über Borkenkäfer. II Die Europaischen Hylesinen*. *Verlag von Ernst Reinhard. München*.

Furniss, M. M. (2004). Biology of *Trypophloeus striatulus* (Coleoptera: Scolytidae) in Feltleaf Willow in Interior Alaska. *Environmental Entomology*, *33*(1), 21–27. https://doi.org/10.1603/0046-225X-33.1.21

Garzo, E., Bonani, J. P., Lopes, J. R. S., & Fereres, A. (2012). Morphological description of the mouthparts of the Asian citrus psyllid, *Diaphorina citri* Kuwayama (Hemiptera: Psyllidae). *Arthropod Structure & Development*, *41*(1), 79–86. https://doi.org/10.1016/j.asd.2011.07.005

Gillott, C. (2005). *Entomology*. *Entomology* (3rd ed.). Dordrecht: Springer. Retrieved

from www.springeronline.com

Głowacka, E., Kuznetsova, V. G., & Maryańska-Nadachowska, A. (1995). Testis follicle number in Psyllids (Psylloidea, Homoptera) as an anatomical feature in studies of systematic relations within the group. *Folia Biologica (Kraków)*, *43*(3–4), 115–124.

Goodchild, A. J. P. (1963). Some new observations on the intestinal structures concerned with water disposal in sap-sucking Hemiptera. *Transactions of the Royal Entomological Society of London*, *115*(88), 217–237. https://doi.org/10.1111/j.1365-2311.1963.tb00820.x

Grassé, P.-P. (1975). Le Système Nerveux des Insectes. In *Traité de Zoologie. Anatomie, Systématique, Biologie. T.VIII, Insectes. Splachnologie, Phonation, Vie Aquatique, Rapports avec les Plantes. Fasc. IV Systematique, Biologie. T. VIII, fasc. III* (Vol. VIII (III), pp. 321–510). Paris: Masson et Cie

Grassé, P.-P. (1976). L'Appareil Respiratoire. *Traité de Zoologie. Anatomie, Systématique, Biologie. T.VIII, Insectes. Splachnologie, Phonation, Vie Aquatique, Rapports Avec Les Plantes. Fasc. IV*, 93–204.

Greco, M. K., Tong, J., Soleimani, M., Bell, D., & Schäfer, M. O. (2012). Imaging live bee brains using minimally-invasive diagnostic radioentomology. *Journal of Insect Science (Online)*, *12*, 89. https://doi.org/10.1673/031.012.8901

Grove, A. J. (1919). The anatomy of the head and mouth parts of *Psylla mali*, the Apple sucker, with some remarks on the function of the labium. *Parasitology*, *11*(3–4), 456–488. https://doi.org/https://doi.org/10.1017/S0031182000004388

Gullan, P. J., & Cranston, P. S. (2010). *Insects: An Outline of Entomology* (4th ed.). Willey-Blackwell.

Hafeez, M. A., & Gardiner, B. G. (1964). The internal morphology of the adult of Tribolium anaphe Hinton (Coleoptera: Tenebrionidae). *Proceedings of the Royal Entomological Society of London. Series A, General Entomology*, *39*(10–12), 137–145. https://doi.org/10.1111/j.1365-3032.1964.tb00996.x

Hamilton, K. G. A. (2015). Anatomy: The poor cousin of morphology? *American Entomologist*, *61*(2), 88–95. https://doi.org/10.1093/ae/tmv003

Harrison, J. F. (2009). Tracheal System. In V. H. Resh & R. T. Cardé (Eds.), *Encyclopedia of Insects* (pp. 1011–1015). Burlington, San Diego, London: Academic Press. https://doi.org/10.1016/B978-0-12-374144-8.00265-4

Height Chart of Men and Women in Different Countries - Disabled World. (2019). Retrieved from https://www.disabled-world.com/calculators-charts/height-chart.php

Heslop-Harrison, G. (1952). XXVII.—The number and distribution of the spiracles of the adult psyllid. *Annals and Magazine of Natural History*, *5*(51), 248-260 + plates XIV-XVI. https://doi.org/10.1080/00222935208654288

Hodin, J. (2009). *She shapes events as they come: plasticity in female insect reproduction.* (D. W. Whitman & T. N. Ananthakrishnan, Eds.), *Phenotypic plasticity of insects: mechanisms and consequences.* Enfield (USA): Science Publishers, Inc. https://doi.org/Enfield, Science Publishers.

Hodkinson, I. D., & White, I. M. (1979). *Homoptera Psylloidea*. (A. Watson, Ed.). London: Royal Entomological Society of London.

Hopkins, A. D. (1909). *Contribution towards a monograph of the scolytids beetles. I. The genus Dendroctonus*. *Technical series, Bureau of Entomology, U.S. Departament of Agriculture* (Vol. 17).

Hubert, J.-F., Thomas, D., Cavalier, A., & Gouranton, J. (1989). *Structural and biochemical observations on specialized membranes of the "filter chamber", a water-shunting complex in sap-sucking homopteran insects*. *Biology of the Cell* (Vol. 66).

Iwan, D., Kamiński, M. J., & Raś, M. (2015). The Last Breath: A µCT-based method for investigating the tracheal system in Hexapoda. *Arthropod Structure & Development*, *44*(3), 218–227. https://doi.org/10.1016/j.asd.2015.02.002

Jiménez, J., Garzo, E., Alba-Tercedor, J., Moreno, A., Fereres, A., & Walker, G. P. (2020). The phloem-pd: a distinctive brief sieve element stylet puncture prior to sieve element phase of aphid feeding behavior. *Arthropod-Plant Interactions*, *14*, 67–78. https://doi.org/10.1007/s11829-019-09708-w

Kaiser, A., Klok, C. J., Socha, J. J., Lee, W.-K., Quinlan, M. C., & Harrison, J. F. (2007). Increase in tracheal investment with beetle size supports hypothesis of oxygen limitation on insect gigantism. *Proceedings of the National Academy of Sciences*, *104*(32), 13198–13203. https://doi.org/10.1073/pnas.0611544104

Keil, T. A. (1999). Morphology and Development of the Peripheral Olfactory Organs. In *Insect Olfaction* (pp. 5–47). Berlin, Heidelberg: Springer Berlin Heidelberg. https://doi.org/10.1007/978-3-662-07911-9_2

Kershaw, J. (1914). The alimentary canal of a Cercopid. *Psyche (New York)*, *21*(2), 65–72. https://doi.org/10.1155/1914/82321

Klass, K.-D., Matushkina, N. A., & Kaidel, J. (2012). The gonangulum: A reassessment of its morphology, homology, and phylogenetic significance. *Arthropod Structure & Development*, *41*(4), 373–394. https://doi.org/10.1016/J.ASD.2012.03.001

Kruse, A., Fattah-Hosseini, S., Saha, S., Johnson, R., Warwick, E., Sturgeon, K., … Cilia Heck, M. (2017). Combining 'omics and microscopy to visualize interactions between the Asian citrus psyllid vector and the Huanglongbing pathogen Candidatus Liberibacter asiaticus in the insect gut. *PLOS ONE*, *12*(6), e0179531. https://doi.org/10.1371/journal.pone.0179531

Kuechler, S. M., Renz, P., Dettner, K., & Kehl, S. (2012). Diversity of symbiotic organs and bacterial endosymbionts of: Lygaeoid bugs of the families blissidae and lygaeidae (Hemiptera:: Heteroptera: Lygaeoidea). *Applied and Environmental Microbiology*, *78*(8), 2648–2659. https://doi.org/10.1128/AEM.07191-11

Liang, X., Zhang, C., Li, Z., Xu, L., & Dai, W. (2013). Fine structure and sensory apparatus of the mouthparts of the pear psyllid, *Cacopsylla chinensis* (Yang et Li)(Hemiptera: Psyllidae). *Arthropod Structure & Development*, *42*(6), 495–506.

Lindroth, C. H., & Palmen, E. (1970). Coleoptera. In S. L. Tuxen (Ed.), *Taxonomist's glossary of genitalia in insects* (pp. 80–88). Copenhagen, Munksgaard: Scandinavian University Books.

Lindsay, K. L., & Marshallt, A. T. (1980). *Ultrastructure of the filter chamber complex in the alimentary canal of* Eurymela distincta *Signoret (Homoptera, Eurymelidae)*. *Int. J. Insect Morphol. & Embryol* (Vol. 9).

López-Guillén, G., Carrasco, J. V., Cruz-López, L., Barrera, J. F., Malo, E. A., & Rojas, J. C. (2011). Morphology and Structural Changes in Flight Muscles of *Hypothenemus hampei* (Coleoptera: Curculionidae) Females. *Environmental Entomology*, *40*(2), 441–448. https://doi.org/10.1603/EN10181

Luo, X., Yen, A. L., Powell, K. S., Wu, F., Wang, Y., Zeng, L., … Cen, Y. (2015). Feeding Behavior of *Diaphorina citri* (Hemiptera: Liviidae) and Its Acquisition of "Candidatus Liberibacter Asiaticus", on Huanglongbing-Infected *Citrus reticulata* Leaves of

Several Maturity Stages. *Florida Entomologist*, *98*(1), 186–192. https://doi.org/10.1653/024.098.0132

Mally, C. W. (1894). Psyllidae found at Ames. *Proceedings of the Iowa Academy of Science*, *2*(1), 152–171.

Malpighi, M. (1669). *Dissertatio epistolica de bombyce*. London: J. Martyn & J. Allestry, regiæ societatis typographos.

Mankin, R. W., & Rohde, B. (2020). Mating behavior of the Asian Citrus Psyllid. In J. A. Qureshi & P. A. Stansly (Eds.), *Asian Citrus Psyllid: Biology, Ecology and Management of the Huanglongbing Vector* (pp. 30–42). Boston.

Marchini, D., Del Bene, G., Viscuso, R., & Dallai, R. (2012). Sperm Storage by Spermatodoses in the Spermatheca of *Trioza alacris* (Flor, 1861) Hemiptera, Psylloidea, Triozidae: A Structural and Ultrastructural Study. *J. Morphol*, *273*, 195–210. https://doi.org/10.1002/jmor.11017

Mathur, R. N. (1975). *Psyllidae of the Indian subcontinent*. (U. S. Jain, Ed.). Madras: Indian Council of Agricultural Research, New Delhi.

Matsuda, R. (1976a). The female efferent duct and associated structures. In *Morphology and Evolution of the Insect Abdomen* (pp. 97–104). Oxford: Pergamon Press Ltd. https://doi.org/10.1016/B978-0-08-018753-2.50018-6

Matsuda, R. (1976b). The Homoptera. In *Morphology and Evolution of the Insect Abdomen* (pp. 280–299). Oxford: Pergamon Press Ltd. https://doi.org/10.1016/B978-0-08-018753-2.50040-X

Matsuura, Y., Kikuchi, Y., Hosokawa, T., Koga, R., Meng, X. Y., Kamagata, Y., … Fukatsu, T. (2012). Evolution of symbiotic organs and endosymbionts in lygaeid stinkbugs. *ISME Journal*, *6*(2), 397–409. https://doi.org/10.1038/ismej.2011.103

Mbata, K. J. (1985). *The anatomy of the armoured ground cricket, Acanthoplus speiseri Brancsik 1895 (Orthoptera: Tettigoniidae, Hetrodinae)*. *Retrospective Theses and Dissertations*. Iowa State University Capstones. Retrieved from https://lib.dr.iastate.edu/rtd

Miller, P. L. (1960). Respiration in the desert locust: III. Ventilation and the spiracles during flight. *J. Exp. Biol.*, *37*(2), 264–278.

Morgan, J. K., Luzio, G. A., Ammar, E.-D., Hunter, W. B., Hall, D. G., & Shatters Jr, R. G. (2013). Formation of Stylet Sheaths in āere (in air) from Eight Species of Phytophagous Hemipterans from Six Families (Suborders: Auchenorrhyncha and Sternorrhyncha). *PLoS ONE*, *8*(4), e62444. https://doi.org/10.1371/journal.pone.0062444

Muir, F. (1930). LIII.—Notes on certain controversial points of morphology of the abdomen and genitalia of Psyllidæ. *Annals and Magazine of Natural History, Series 10*, *5*(29), 545–552. https://doi.org/10.1080/00222933008673163

Nakabachi, A., Ueoka, R., Oshima, K., Teta, R., Mangoni, A., Gurgui, M., Fukatsu, T. (2013). Defensive Bacteriome Symbiont with a Drastically Reduced Genome. *Current Biology*, *23*(15), 1478–1484. https://doi.org/10.1016/J.CUB.2013.06.027

Nijs, C., & Billen, J. (2015). Exocrine glands in the legs of the social wasp *Vespula vulgaris*. *Arthropods Structure and Development*, *44*, 433–443. https://doi.org/10.1016/j.asd.2015.08.011

Nobuchi, A. (1969). A Comparative Morphological Study of the Proventriculus in the Adult of the Superfamily Scolytoidea (Coleoptera). *Bull. Gov. For. Exp. Stn. (Jpn.)*, *224*, 40–58.

Nocelli, R. C., Cintra-Socolowski, P., Roat, T. C., Silva-Zacarin, elaine C., & Malaspina, O. (2016). Comparative physiology of Malpighian tubules: form and function. https://doi.org/10.2147/OAIP.S72060

Nüsslin, O. (1911). Phylogenie und System der Borkenkäfer. *Zeitschrift Für Wissenschaftliche Insektenbiologie.*, *7*, 1–5.

Onagbola, E. O. E., Meyer, W. W. L., Boina, R., Stelinski, L. L., Boina, D., & Stelinski, L. L. (2008). Morphological characterization of the antennal sensilla of the Asian citrus psyllid, *Diaphorina citri* Kuwayama (Hemiptera: Psyllidae), with reference to their probable. *Micron*, *39*, 1184–1191. https://doi.org/10.1016/j.micron.2008.05.002

Ossiannilsson, F. (1992). *The Psylloidea (Homoptera) of Fennoscandia and Demark*. E.J. Brill.

Ouvrard, D., Bourgoin, T., & Campbell, B. C. (2002). Comparative Morphological Assessment of the Psyllid Pleuron (Insecta, Hemiptera, Sternorrhyncha). *J. Morphol*, *252*, 276–290. https://doi.org/10.1002/jmor.1105

Pascini, T. V., & Martins, G. F. (2017). The insect spermatheca: an overview. *Zoology*, *121*, 56–71. https://doi.org/10.1016/J.ZOOL.2016.12.001

Pesson, P. (1951). Ordre des Homoptères (Homoptera Leach, 1815). In P.-P. Grassé (Ed.), *Traité de zoologie. Anatomie, systématique, biologie. Tome X. Fascicule II. Insectes supérieurs et Hémipteróides* (Editions M, pp. 1390–1656). Paris: Masson et Cie.

Prophetou-Athanasiadou, D. A., & Tzanakakis, M. E. (1998). The Reproductive System and Ovarian Development of the Adult Olive Psylla *Euphyllura phillyreae* Foerster (Homoptera: Aphalaridae). *Entomologia Hellenica*, *12*, 37–45. https://doi.org/http://dx.doi.org/10.12681/eh.14018

Qadri, M. A. H. (1949). On the morphology and post-embryonic development of the male genitalia and their ducts in Hemiptera. *Journal of the Zoological Society of India*, *1*, 129--143.

Raś, M., Iwan, D., & Kamiński, M. J. (2018). The tracheal system in post-embryonic development of holometabolous insects: a case study using the mealworm beetle. *Journal of Anatomy*, *232*(6), 997–1015. https://doi.org/10.1111/joa.12808

Ren, S.-L., Li, Y.-H., Ou, D., Guo, Y.-J., Qureshi, J. A., Stansly, P. A., … Bao-Li Qiu, C. (2018). Localization and dynamics of Wolbachia infection in Asian citrus psyllid *Diaphorina citri*, the insect vector of the causal pathogens of Huanglongbing. *Microbiology Open*, *7*, 561. https://doi.org/10.1002/mbo3.561

Renthal, R., Velasquez, D., Olmos, D., & Vinson, S. B. (2008). Occurrence of antennal glands in ants. *Microscopy Research and Technique*, *71*(11), 787–791. https://doi.org/10.1002/jemt.20620

Ribi, W., Senden, T. J., Sakellariou, A., Limaye, A., & Zhang, S. (2008). Imaging honey bee brain anatomy with micro-X-ray-computed tomography. *Journal of Neuroscience Methods*, *171*(1), 93–97.

Richards, O., & Davies, R. (1977). The respiratory system. In O. Richards & R. Davies (Eds.), *A General Textbook of Entomology* (pp. 209–233). London: Chapman and Hall.

Robertson, C. H. (1962). The anatomy of the respiratory system of the *Passalus* beetle, Popilius disjunctus (Illiger). *American Midland Naturalist*, *68*(2), 376–393.

Román-Ruiz, A. K., Michel, B., Dufour, B. P., Rojas, J. C., Cruz-López, L., & Barrera, J. F. (2017). Description of the sperm and spermatheca of *Hypothenemus hampe*i

(Coleoptera: Curculionidae: Scolytinae) for the differentiation of mated and unmated females. *Annals of the Entomological Society of America*, *110*(4), 353–359. https://doi.org/10.1093/aesa/sax033

Ruan, Y., Y., L., Zhang, M., Chen, X., Liu, Z., Wang, S., & Jiang, S. (2018). Visualisation of insect tracheal systems by lactic acid immersion. *Journal of Microscopy*, *271*(2), 230–236. https://doi.org/10.1111/jmi.12711

Rubio-Gómez, J. D., Bustillo-Pardey, Á. E., Vallejo-Espinosa, L. F., Benavides-Machado, P., Acuña-Zornosa, J. R., Rubio, R., & Bustillo, J. D. ; (2007). Morfología del sistema reproductor femenino y masculino de *Hypothenemus hampe*i (Ferrari). *Cenicafé*, *58*(1), 75–81.

Rubio G., J. D., Bustillo P., A. E., Vallejo E., L. F., Acuña Z., J. R., & Benavides M., P. (2008). Alimentary canal and reproductive tract of *Hypothenemus hampei* (Ferrari) (Coleoptera: Curculionidae, Scolytinae). *Neotropical Entomology*, *37*(2), 143–151. https://doi.org/10.1590/S1519-566X2008000200006

Rybak, J., Kuß, A., Lamecker, H., Zachow, S., Hege, H.-C., Lienhard, M., … Menzel, R. (2010). The Digital Bee Brain: Integrating and Managing Neurons in a Common 3D Reference System. *Frontiers in System Neuroscience*, *4*, *article*(July), 1–15. https://doi.org/10.3389/fnsys.2010.00030

Santiago-Blay, J. A., & Young, T. L. (1995). Reliable sexing of adult *Conophthorus* (Coleoptera: Scolytidae) beetles. *The Canadian Entomologist*, *127*(4), 605–607. https://doi.org/10.4039/Ent127605-4

Saunders, L. G. (1921). *The Anatomy of* Psyllia mali *Schmidberger. Manuscript Thesis (M. Sc.) McGill University. Montreal.*

Schedl, K. E. (1960). Insectes nuisibles aux fruits et aux graines. *Publications de l'institut National Pour l'étude Agronomique Du Congo Belge, Série Scientifique*, *82*, 1–133.

Schlee, D. (1969). Sperma-übertragung (und andere merkmale) in ihrer bedeutung für das phylogenetische system der sternorrhyncha (insecta, hemiptera) Phylogenetische studien an hemiptera I. psylliformes (psyllina und aleyrodina) als monophyletische gruppe. *Z. Morph. Tiere*, *64*, 95–138. https://doi.org/https://doi.org/10.1007/BF00391783

Smith, D. B., Bernhardt, G., Raine, N. E., Abel, R. L., Sykes, D., Ahmed, F., … Gill, R. J. (2016). Exploring miniature insect brains using micro-CT scanning techniques. *Scientific Reports*, *6*, 21768. https://doi.org/10.1038/srep21768

Snodgrass, R. E. (1935). *Principles of Insect Morphology*. New York & London: McGraw-Hill Book Company, Inc. https://doi.org/0801428831

Sombke, A., Lipke, E., Michalik, P., Uhl, G., & Harzsch, S. (2015). Potential and limitations of X-Ray micro-computed tomography in arthropod neuroanatomy: a methodological and comparative survey. *The Journal of Comparative Neurology*, *523*(8), 1281–1295. https://doi.org/10.1002/cne.23741

Srivastava, K. P. (1976). On the respiratory system of the lemon-butterfly, *Papilio demoleus* l. (Lepidoptera: Papilionidae). *Australian Journal of Entomology*, *14*(4), 363–370. https://doi.org/10.1111/j.1440-6055.1975.tb02052.x

Stacconi, M., & Romani, R. (2011). Ultrastructural and functional aspects of the spermatheca in the american harlequin bug, *Murgantia histrionica* (Hemiptera: Pentatomidae). *Neotropical Entomology*, *40*(2), 222–230. https://doi.org/10.1590/S1519-566X2011000200011

Swaine, J. M. (1918). Canadian bark-beetles. Part II. A preliminary classification with an

account of the habits and means of control. (Technical Bulletin). *Dominion of Canada, Department of Agriculture, Entomological Branch, Bulletin No. 14*, 1–143.

Tonapi, G. T. (1978). Some adaptive features in the respiratory system of *Dineutes indicus* Aubé (Coleoptera, Gyrinidae). *Zoologica Scripta*, *6*(2), 107–112. https://doi.org/10.1111/j.1463-6409.1978.tb00790.x

Triplehorn, C. A., & Johnson, N. F. (2005). *Borror and De Long's Introduction to the Study of Insects, 7th edition*.

Varón, E. H., Hanson, P., Borbón, O., Carballo, M., & Hilje, L. (2004). Potencial de hormigas como depredadores de la broca del café (*Hypothenemus hampei*) en Costa Rica. *Manejo Integr. Plagas Agroecol.*, *73*, 42–50.

Vega, F. E., Infante, F., & Johnson, A. J. (2015). The genus *Hypothenemus*, with emphasis on H. hampei, the coffee berry borer. In *Bark Beetles* (pp. 427–494). Elsevier. https://doi.org/10.1016/B978-0-12-417156-5.00011-3

Vega, F. E., Simpkins, A., Bauchan, G., Infante, F., Kramer, M., & Land, M. F. (2014). On the eyes of male coffee berry borers as rudimentary organs. *PloS One*, *9*(1), e85860. https://doi.org/10.1371/journal.pone.0085860

Vega, F. E., Simpkins, A., Bauchan, G., Valdéz-Carrasco, J. M., Castillo, A., & Infante, F. (2015). A mysterious wing spine in male coffee berry borers (Coleoptera: Curculionidae: Scolytinae). *Florida Entomologist*, *98*(1), 352–353. https://doi.org/10.1653/024.098.0155

Wasserthal, L. T., Cloetens, P., Fink, R. H., & Wasserthal, L. K. (2018). X-ray computed tomography study of the flight-adapted tracheal system in the blowfly *Calliphora vicina* , analysing the ventilation mechanism and flow-directing valves. *The Journal of Experimental Biology*, *221*(12), jeb176024. https://doi.org/10.1242/jeb.176024

Waters, J. S., Lee, W.-K., Westneat, M. W., & Socha, J. J. (2013). Dynamics of tracheal compression in the horned passalus beetle. *American Journal of Physiology-Regulatory, Integrative and Comparative Physiology*, *304*(8), R621–R627. https://doi.org/10.1152/ajpregu.00500.2012

Weber, H. (1929). Kopf und thorax von *Psylla mali* Schmidb. (Hemiptera-Homoptera). Eine morphogenetische studie. *Z. Morph. Ökol. Tiere*, *14*, 59–165.

Weintraub, P. G., Hoch, H., Mühlethaler, R., & Zchori-Fein, E. (2014). Synchrotron X-ray micro-computed tomography as a tool for in situ elucidation of insect bacteriomes. *Arthropod Structure & Development*, *43*(2), 183–186. https://doi.org/10.1016/j.asd.2013.11.002

Weis-Fogh, T. (1964). Functional design of the tracheal system of flying insects as compared with the avian lung. *Journal of Experimental Biology*, *41*(2), 207–227. Retrieved from http://jeb.biologists.org/content/jexbio/41/2/207.full.pdf

Weis-Fogh, T. (1967). Respiration and tracheal ventilation in locusts and other flying insects. *Journal of Experimental Biology*, *47*, 561–587. Retrieved from http://jeb.biologists.org/content/47/3/561.short

Wenninger, E. (2008). Behavioral evidence for a female-produced sex attractant in *Diaphorina citri*. *Entomologia Experimentalis et Applicata*, *128450–459*.

Westneat, M. W. (2003). Tracheal Respiration in Insects Visualized with Synchrotron X-ray Imaging. *Science*, *299*(5606), 558–560. https://doi.org/10.1126/science.1078008

Wigglesworth, V. B. (1930). A Theory of Tracheal Respiration in Insects. *Proceedings of the Royal Society B: Biological Sciences*, *106*(743), 229–250.

https://doi.org/10.1098/rspb.1930.0024

Wigglesworth, V. B. (1942). *The principles of insect physiology* (2nd ed.). London: Methuen & CO. LTD.

Wilkinson, H. (1928). *The Coffee Berry Borer Beetle Stephanoderes hampei (Ferr.)*. Nairobi, Kenya: The Government Printer; Colony and Protectorate of Kenya.

Wipfler, B., Pohl, H., Yavorskaya, M. I., & Beutel, R. G. (2016, December 1). A review of methods for analysing insect structures — the role of morphology in the age of phylogenomics. *Current Opinion in Insect Science*. Elsevier Inc. https://doi.org/10.1016/j.cois.2016.09.004

Witlaczil, E. (1885). Die Anatomie der Psylloden. *Zeitschrift Für Wissenschaftliche Zoologie*, *42*, 569-638 + 3 tafeln.

Wood, S. L. (1954). A revision of North American Cryphalini (Scolytidae: Coleoptera). *Univ. Kansas Sci. Bull*, (36), 959–1089.

Wood, S. L. (2007). *Bark and Ambrosia Beetles of South America (Coleoptera, Scolytidae)*. Brigham Young University.

Yen, A., & Burckhardt, D. (2017). *Diagnostic protocol for the detection of the tomato potato Psyllid,* Bactericera cockerelli *(Šulc) prepared for the Subcommittee on Plant Health Diagnostic Standards (SPHDS)*. resources/

Zheng, L., Liang, Q., Yu, M., Cao, Y., & Chen, W. (2020). Morphological characterization of antennae and antennal sensilla of *Diaphorina citri* Kuwayama (Hemiptera: Liviidae) nymphs. *PLOS ONE*, *15*(6), e0234030. https://doi.org/10.1371/journal.pone.0234030

Zucht, B. (1972). Bau und Entwicklung der äußeren Genitalorgane bei Psyllinen (Homopteren). *Zool. Jb. Anat. Bd.*, *231*, 167–231.

Zunino, M. (2012). Cuarenta años de anatomía de las piezas genitales en la taxonomía de los escarabajos (Coleoptera : Scarabaeoidea): el estado del arte. *Dugesiana*, *18*(2), 197–206.

7.- CONCLUSIONES

7.1.- En términos generales:

1. Los resultados aquí obtenidos confirman que las técnicas de micro-CT constituyen una excelente alternativa a los métodos tradicionales basados en la disección. Al no ser destructivas permiten observar las estructuras (externas e internas) en su posición anatómica real, desde cualquier perspectiva, tantas veces como se requiera, sin riesgo de deformarlas o romperlas. Se evitan los inconvenientes de las deformaciones producidas durante las manipulaciones que requiere la disección. Asimismo, durante el estudio microtomográfico de ambas especies se han podido completar detalles de estructuras ya descritas por otros autores y al mismo tiempo se han descubierto otras que nunca habían sido descritas, y que de no ser por la micro-CT difícilmente podrían haberse puesto de manifiesto.
2. Esta tesis representa la primera reconstrucción completa mediante micro-CT de la anatomía (externa e interna) de *D. citri,* y de *H.* hampei. Representando los primeros estudios anatómicos completos de un insecto homóptero Psylloidea, y de un coleóptero, realizados en detalle con estas técnicas. Del mismo modo, son las reconstrucciones anatómicas de los insectos más pequeños realizadas hasta la fecha con micro-CT.
3. En su conjunto, los resultados obtenidos constituyen unos atlas anatómicos únicos (con imágenes 3D de alta resolución, completadas con videos de las estructuras en 3D y modelos 3D, para utilizarlos con dispositivos móviles) que constituyen en su conjunto una base sólida en la que realizar nuevas investigaciones y pueden ser de gran ayuda en las tareas docentes y de divulgación.

7.2.- Respecto del psílido asiático de los cítricos (*Diaphorina citri*):

1. Por primera vez se ha reconstruido en detalle: **a)** el digestivo, en su posición real anatómica y en especial la cámara filtradora, **b)** el sistema traqueal abdominal, el vaso dorsal, aorta y músculos aliformes, **c)** el bacterioma, **d)** las estructuras internas de la cámara cibarial (incluida la

bomba cibarial y su musculatura), **e)** los órganos reproductores de ambos sexos, destacando por su novedad el estudio de los segmentos genitales, del edeago y ovipositor (con las estructuras asociadas) y la musculatura, **f)** se describen las estructuras implicadas en la acción como bombas aspirante-impelentes, tanto de la bomba espermática de los machos, como de la espermateca en las hembras, y **g)** el sistema nervioso (cerebro y cadena nerviosa ventral).

2. Por vez primera se han evidenciado diferencias sexuales en función de la conformación de estructuras internas diferentes de los órganos reproductores. Asi, mientras el recto en los machos es alargado y grueso, en las hembras es corto y en forma de pequeña ampolla rectal, lo que facilitaría la expulsión de las heces a cierta distancia (a modo de "disparo"), para evitar que contaminen a la puesta y a los juveniles recién eclosionados. Del mismo modo en las hembras, tanto el cerebro como los ganglios de la cadena ventral son más masivos, y con el gran ganglio mesotorácico casi esférico (mientras que en los machos tiene los bordes laterales casi paralelos).
3. Se ha puesto de manifiesto la existencia de glándulas coxales y antenales (no descritas hasta ahora en Psylloidea) con un posible papel secretor de feromonas de atracción y reconocimiento de sexos.
4. Se ha reconstruido por primera vez a un individuo alimentándose de una hoja de naranjo, lo que ha permitido ver la disposición y conformación del aparato bucal (labio y haz de estiletes) en el momento de la "picadura" (con el reborde salival en el punto de penetración de la superficie de la hoja, sus vainas salivales, así como vainas salivales abandonadas tras intentos fallidos de perforación para alcanzar los vasos), visualizándose el haz de estiletes atravesando las estructuras de la hoja, y como éste penetra en el floema.

7.3.- Respecto de la broca del café (*Hypothenemus hampei*):

1. Se ha puesto de manifiesto por primera vez la actividad de estos insectos en el interior de la cereza del café, concluyendo que: **a)** la hembra excava

los primeros tramos de túneles en “ziz-zag” para dificultar la entrada de parasitoides, y **b)** la oviposición se realiza en cámaras que se disponen secuencialmente desde la periferia hacia el interior, maximizando el uso del recurso y así dispersar la progenie para reducir la competencia.

2. Por primera vez se ha reconstruido en detalle: **a)** el digestivo, en su posición real anatómica, con un estudio detallado del proventrículo, **b)** el vaso dorsal y aorta, **c)** los tubos de Malpigio (que son 4, frente a los 6 señalados anteriormente en Scolytidae), **d)** los órganos reproductores de ambos sexos, destacando por su novedad el estudio tanto de los segmentos genitales, como del edeago (no descrito hasta ahora), estructuras asociadas y la musculatura, y **e)** el sistema nervioso central (cerebro y cadena nerviosa ventral).
3. Se ha reconstruido por vez primera el sistema traqueal y se ha podido calcular la longitud total de tubos (que es 70 veces la longitud del cuerpo). La gran mayoría de los tubos traqueales son muy finos y en general los tubos con una luz ≤9.97 µm constituyen el 96,6% de la longitud total de tubos traqueales y el 79,1% de la capacidad total del volumen traqueal.
4. Se han reconstruido por primera vez los espiráculos respiratorios. Estos, para evitar que las partículas finas (fruto de su actividad) penetren en los tubos traqueales, tienen un complejo sistema de filtración. Destacando por su peculiaridad los espiráculos mesotorácicos que presentan una triple barrera desde el exterior, hasta el atrio, del que parten los troncos traqueales. Asimismo, los espiráculos metatorácicos, además de presentar una placa filtradora, se encuentran protegidos bajo la base de los élitros.
5. Salvo minúsculas dilataciones (en las tráqueas que desembocan en las inmediaciones de los espiráculos respiratorios abdominales) no presentan sacos aéreos desarrollados. Son los troncos traqueales del pronoto los que tienen el papel principal en la ventilación traqueal. Por ello, son mucho más gruesos que el resto y presentan una sección elíptica que facilita su compresión al contraerse los músculos del pronoto.

6. Se han encontrado nuevas diferencias sexuales:
    - Externamente, y en vista lateral: el contorno del pronoto de los machos aparece uniformemente curvo, mientras que en las hembras hay una pequeña depresión posterior. Del mismo modo, los machos poseen ocho terguitos mientras las hembras tienen siete.
    - Internamente: **a)** en los machos el digestivo medio anterior esta dilatado, y tienen 9 circunvoluciones en el digestivo medio y posterior, mientras que en las hembras tienen 8, **b)** los machos presentan alas vestigiales músculos del vuelo ausentes, y **c)** los lóbulos cerebrales de la hembra son mayores y están más extendidos lateralmente, y con lóbulos ópticos más gruesos que en los machos.

7.4.- Respecto del gorgojo del grano de café (*Araecerus fasciculatus*):

1. Se ha podido "congelar" la actividad del insecto en el interior de una baya de café y estudiarla en detalle. Habiéndose reconstruido adultos hembras y larvas de 5º estadio dentro de la cereza del café.
2. Se reporta como hecho inusual que en cada cereza de café se encontraron dos larvas.
3. Las larvas consumen las dos semillas.
4. En las cerezas de café, los orificios de salida de los adultos se localizan en la proximidad del disco de la cereza de café.

8.- OTROS: informes y documentos

INDICIOS DE CALIDAD DE LAS REVISTAS EN QUE SE HAN PUBLICADO LOS ARTICULOS CON LOS RESULTADOS DE LA PRESENTE TESIS DOCTORAL

A) PLoS One

1.- Alba-Alejandre, I., Hunter, W.B. & Alba-Tercedor J. (2018). Micro-CT study of male genitalia and reproductive system of the Asian citrus psyllid, *Diaphorina citri* Kuwayama, 1908 (Insecta: Hemiptera, Liviidae).*PLoS ONE* 13(8), e0202234: 1-16. https://doi.org/10.1371/journal.pone.0202234.

La revista PLOS ONE, aparece en el JCR-2018 con un factor de impacto de 2.776 en la categoría MULTIDISCIPLINARY SCIENCES (en el Q2, posición 24 de 69).

B) Scientific Reports

2.- Alba-Alejandre, I., Alba-Tercedor, J., & Vega, F. E. (2018). Observing the devastating coffee berry borer (*Hypothenemus hampei*) inside the coffee berry using micro-computed tomography. *Scientific Reports*, 8(1), 17033: 1-9. https://doi.org/10.1038/s41598-018-35324-4

3.- Alba-Alejandre, I., Alba-Tercedor, J., & Vega, F. E. (2019). Anatomical study of the coffee berry borer (*Hypothenemus hampei*) using micro-computed tomography. *Scientific Reports*, 9(1), 17150: 1-16. https://doi.org/10.1038/s41598-019-53537-z

4.- Alba-Tercedor, J., **Alba-Alejandre, I**., & Vega, F. E. (2019). Revealing the respiratory system of the coffee berry borer (*Hypothenemus hampei*; Coleoptera: Curculionidae: Scolytinae) using micro-computed tomography. *Scientific Reports*, 9(1), 17753: 1-17. https://doi.org/10.1038/s41598-019-54157-3

5.- Alba-Alejandre, I., Alba-Tercedor, J., & Hunter, W. B. (2020). Anatomical study of the female reproductive system and bacteriome of *Diaphorina citri* Kuwayama, (Insecta: Hemiptera, Liviidae) using micro-computed tomography. *Scientific Reports* 10 (1), 1–14. https://doi.org/10.1038/s41598-020-64132-y

Publisher Correction: Anatomical study of the coffee berry borer (Hypothenemus hampei) using micro-computed tomography. https://doi.org/10.1038/s41598-019-53537-z

6.- Alba-Tercedor J., Hunter WB, **Alba-Alejandre I**, (2020). Using micro-computed tomography to reveal the anatomy of adult *Diaphorina citri* Kuwayama (Insecta: Hemiptera, Liviidae) and how it pierces and feeds within a citrus leaf. *Scientific Reports* (en revisión).

La revista SCIENTIFIC REPORTS, aparece:

- En el JCR-2018 con un factor de impacto de 4.011 en la categoría MULTIDISCIPLINARY SCIENCES (en el Q1, posición 15 de 69).

- En el JCR-2019 con un factor de impacto de 3.998 en la categoría MULTIDISCIPLINARY SCIENCES (en el Q1, posición 17 de 71).

C) Insects

7.- Alba-Alejandre, I., Alba-Tercedor, J., & Vega, F. E. (2018). Micro-CT to Document the Coffee Bean Weevil, *Araecerus fasciculatus* (Coleoptera: Anthribidae), Inside Field-Collected Coffee Berries (*Coffea canephora*). *Insects*, 9(3, 100), 1–9. https://doi.org/10.3390/insects9030100

La revista INSECTS, aparece en el JCR-2018 con un factor de impacto de 2.139 en la categoría ENTOMOLOGY (en el Q1, posición 18 de 98).